ISSN 1949-8470 (online)

World Journal of *Radiology*

World J Radiol 2014 June 28; 6(6): 223-391

Published by Baishideng Publishing Group Inc

WJR World Journal of Radiology

A peer-reviewed, online, open-access journal of Radiology

Editorial Board

2014-2017

The *World Journal of Radiology* Editorial Board consists of 365 members, representing a team of worldwide experts in radiology. They are from 36 countries, including Afghanistan (1), Argentina (2), Australia (5), Austria (7), Belgium (2), Brazil (8), Canada (6), Chile (1), China (43), Croatia (1), Denmark (4), Egypt (6), France (5), Germany (22), Greece (10), India (12), Iran (6), Ireland (2), Israel (3), Italy (47), Japan (13), Netherlands (1), New Zealand (1), Pakistan (1), Poland (2), Portugal (1), Serbia (1), Singapore (3), Slovakia (1), South Korea (18), Spain (4), Sweden (2), Switzerland (4), Thailand (1), Turkey (26), United Kingdom (11), and United States (82).

EDITORS-IN-CHIEF

Kai U Juergens, *Bremen*
Edwin JR van Beek, *Edinburgh*
Thomas J Vogl, *Frankfurt*

GUEST EDITORIAL BOARD MEMBERS

Wing P Chan, *Taipei*
Chung-Huei Hsu, *Taipei*
Chin-Chang Huang, *Taipei*
Tsong-Long Hwang, *Taoyuan*
Jung-Lung Hsu, *Taipei*
Chia-Hung Kao, *Taichung*
Yu-Ting Kuo, *Tainan*
Hon-Man Liu, *Taipei*
Hui-Lung Liang, *Kaohsiung*
Chun Chung Lui, *Kaohsiung*
Sen-Wen Teng, *Taipei*
Yung-Liang (William) Wan, *Taoyuan*

MEMBERS OF THE EDITORIAL BOARD

Afghanistan

Takao Hiraki, *Okayama*

Argentina

Patricia Carrascosa, *Vicente Lopez*
Maria C Ziadi, *Rosario*

Australia

Lourens Bester, *Sydney*
Gemma A Figtree, *Sydney*
Stuart M Grieve, *Sydney*
Wai-Kit Lee, *Fitzroy*
Prabhakar Ramachandran, *Melbourne*

Austria

Herwig R Cerwenka, *Graz*
Gudrun M Feuchtner, *Innsbruck*
Benjamin Henninger, *Innsbruck*
Rupert Lanzenberger, *Vienna*
Shu-Ren Li, *Vienna*
Veronika Schopf, *Vienna*
Tobias De Zordo, *Innsbruck*

Belgium

Steve Majerus, *Liege*
Kathelijne Peremans, *Merelbeke*

Brazil

Clerio F Azevedo, *Rio de Janeiro*
Patrícia P Alfredo, *São Paulo*
Eduardo FC Fleury, *São Paulo*
Edward Araujo Júnior, *São Paulo*
Wellington P Martins, *Ribeirao Preto*
Ricardo A Mesquita, *Belo Horizonte*
Vera MC Salemi, *São Paulo*
Claudia Szobot, *Porto Alegre*
Lilian YI Yamaga, *São Paulo*

Canada

Marie Arsalidou, *Toronto*
Otman A Basir, *Waterloo*
Tarik Zine Belhocine, *Toronto*
James Chow, *Toronto*
Tae K Kim, *Toronto*
Anastasia Oikonomou, *Toronto*

China

Hong-Wei Chen, *Wuxi*
Feng Chen, *Hangzhou*
Jian-Ping Chu, *Guangzhou*
Guo-Guang Fan, *Shenyang*
Bu-Lang Gao, *Shijiazhuang*
Qi-Yong Gong, *Chengdu*
Ying Han, *Beijing*
Xian-Li Lv, *Beijing*
Yi-Zhuo Li, *Guangzhou*
Xiang-Xi Meng, *Harbin*
Yun Peng, *Beijing*
Jun Shen, *Guangzhou*
Ze-Zhou Song, *Hangzhou*
Wai Kwong Tang, *Hong Kong*
Gang-Hua Tang, *Guangzhou*
Jie Tian, *Beijing*
Lu-Hua Wang, *Beijing*
Xiao-bing Wang, *Xi'an*
Yi-Gen Wu, *Nanjing*
Kai Wu, *Guangzhou*
Hui-Xiong Xu, *Shanghai*
Zuo-Zhang Yang, *Kunming*
Xiao-Dan Ye, *Shanghai*
David T Yew, *Hong Kong*
Ting-He Yu, *Chongqing*
Zheng Yuan, *Shanghai*
Min-Ming Zhang, *Hangzhou*
Yudong Zhang, *Nanjing*
Dong Zhang, *ChongQing*
Wen-Bin Zeng, *Changsha*

Yue-Qi Zhu, *Shanghai*

Croatia

Goran Kusec, Osijek

Denmark

Poul E Andersen, *Odense*
Lars J Petersen, *Aalborg*
Thomas Z Ramsoy, *Frederiksberg*
Morten Ziebell, *Copenhagen*

Egypt

Mohamed F Bazeed, *Mansoura*
Mohamed Abou El-Ghar, *Mansoura*
Reem HA Mohamed, *Cairo*
Mohamed R Nouh, *Alexandria*
Ahmed AKA Razek, *Mansoura*
Ashraf A Zytoon, *Shebin El-Koom*

France

Sabine F Bensamoun, *Compiègne*
Romaric Loffroy, *Dijon*
Stephanie Nougaret, *Montpellier*
Hassane Oudadesse, *Rennes*
Vincent Vinh-Hung, *Fort-de-France*

Germany

Henryk Barthel, *Leipzig*
Peter Bannas, *Hamburg*
Martin Beeres, *Frankfurt*
Ilja F Ciernik, *Dessau*
A Dimitrakopoulou-Strauss, *Heidelberg*
Peter A Fasching, *Erlanegn*
Andreas G Schreyer, *Regensburg*
Philipp Heusch, *Duesseldorf*
Sonja M Kirchhoff, *Munich*
Sebastian Ley, *Munich*
Adel Maataoui, *Frankfurt am Main*
Stephan M Meckel, *Freiburg*
Hans W Muller, *Duesseldorf*
Kay Raum, *Berlin*
Dirk Rades, *Luebeck*
Marc-Ulrich Regier, *Hamburg*
Alexey Surov, *Halle*
Martin Walter, *Magdeburg*
Axel Wetter, *Essen*
Christoph Zilkens, *Düsseldorf*

Greece

Panagiotis Antoniou, *Thessaloniki*
Nikos Efthimiou, *Athens*
Dimitris Karnabatidis, *Patras*
George Latsios, *Athens*
Stylianos Megremis, *Iraklion*
Alexander D Rapidis, *Athens*
Kiki Theodorou, *Larissa*
Ioannis A Tsalafoutas, *Athens*
Evanthia E Tripoliti, *Ioannina*
Athina C Tsili, *Ioannina*

India

Ritesh Agarwal, *Chandigarh*
Chandan J Das, *New Delhi*
Prathamesh V Joshi, *Mumbai*
Naveen Kalra, *Chandigarh*
Chandrasekharan Kesavadas, *Trivandrum*
Jyoti Kumar, *New Delhi*
Atin Kumar, *New Delhi*
Kaushala P Mishra, *Allahabad*
Daya N Sharma, *New Delhi*
Binit Sureka, *New Delhi*
Sanjay Sharma, *New Delhi*
Raja R Yadav, *Allahabad*

Iran

Majid Assadi, *Bushehr*
SeyedReza Najafizadeh, *Tehran*
Mohammad Ali Oghabian, *Tehran*
Amir Reza Radmard, *Tehran*
Ramin Sadeghi, *Mashhad*
Hadi Rokni Yazdi, *Tehran*

Ireland

Tadhg Gleeson, *Wexford*
Frederik JAI Vernimmen, *Cork*

Israel

Dafna Ben Bashat, *Tel Aviv*
Amit Gefen, *Tel Aviv*
Tamar Sella, *Jerusalem*

Italy

Adriano Alippi, *Rome*
Dante Amelio, *Trento*
Michele Anzidei, *Rome*
Filippo F Angileri, *Messinas*
Stefano Arcangeli, *Rome*
Roberto Azzoni, *San Donato milanese*
Tommaso V Bartolotta, *Palermo*
Tommaso Bartalena, *Imola*
Livia Bernardin, *San Bonifacio*
Federico Boschi, *Verona*
Sergio Casciaro, *Lecce*
Emanuele Casciani, *Rome*
Musa M Can, *Napoli*
Alberto Cuocolo, *Napoli*
Michele Ferrara, *Coppito*
Mauro Feola, *Fossano*
Giampiero Francica, *Castel Volturno*
Luigi De Gennaro, *Rome*
Giulio Giovannetti, *Pisa*
Francesca Iacobellis, *Napoli*
Formato Invernizzi, *Monza Brianza*
Francesco Lassandro, *Naples*
Lorenzo Livi, *Florence*
Pier P Mainenti, *Napoli*
Laura Marzetti, *Chieti*
Giuseppe Malinverni, *Crescentino*
Enrica Milanesi, *Turin*
Giovanni Morana, *Treviso*
Lorenzo Monti, *Milan*
Silvia D Morbelli, *Genoa*
Barbara Palumbo, *Perugia*
Cecilia Parazzini, *Milan*
Stefano Pergolizzi, *Messina*
Antonio Pinto, *Naples*
Camillo Porcaro, *Rome*
Carlo C Quattrocchi, *Rome*
Alberto Rebonato, *Perugia*
Giuseppe Rizzo, *Rome*
Roberto De Rosa, *Naples*
Domenico Rubello, *Rovigo*
Andrea Salvati, *Bari*
Sergio Sartori, *Ferrara*
Luca M Sconfienza, *Milano*
Giovanni Storto, *Rionero*
Nicola Sverzellati, *Parma*
Alberto S Tagliafico, *Genova*
Nicola Troisi, *Florence*

Japan

Yasuhiko Hori, *Chiba*
Hidetoshi Ikeda, *Koriyama*
Masahito Kawabori, *Sapporo*
Tamotsu Kamishima, *Sapporo*
Hiro Kiyosue, *Yufu*
Yasunori Minami, *Osaka-sayama*
Yasuhiro Morimoto, *Kitakyushu*
Satoru Murata, *Tokyo*
Shigeki Nagamachi, *Miyazaki*
Hiroshi Onishi, *Yamanashi*
Morio Sato, *Wakayama Shi*
Yoshito Tsushima, *Maebashi*
Masahiro Yanagawa, *Suita*

Netherlands

Willem Jan van Rooij, *Tilburg*

New Zealand

W Howell Round, *Hamilton*

Pakistan

Wazir Muhammad, *Abbottabad*

Poland

Maciej S Baglaj, *Wroclaw*

Piotr Czauderna, *Gdansk*

Portugal

Joao Manuel RS Tavares, *Porto*

Serbia

Olivera Ciraj-Bjelac, *Belgrade*

Singapore

Gopinathan Anil, *Singapore*
Terence KB Teo, *Singapore*
Cher Heng Tan, *Singapore*

Slovakia

Stefan Sivak, *Martin*

South Korea

Ki Seok Choo, *Busan*
Seung Hong Choi, *Seoul*
Dae-Seob Choi, *Jinju*
Hong-Seok Jang, *Seoul*
Yong Jeong, *Daejeon*
Chan Kyo Kim, *Seoul*
Se Hyung Kim, *Seoul*
Joong-Seok Kim, *Seoul*
Sang Eun Kim, *Seongnam*
Sung Joon Kwon, *Seoul*
Jeong Min Lee, *Seoul*
In Sook Lee, *Busan*
Noh Park, *Goyang*
Chang Min Park, *Seoul*
Sung Bin Park, *Seoul*
Deuk Jae Sung, *Seoul*
Choongsoo Shin, *Seoul*
Kwon-Ha Yoon, *Iksan*

Spain

Miguel A De Gregorio, *Zaragoza*
Antonio Luna, *Jaén*
Enrique Marco de Lucas, *Santander*
Fernando Ruiz Santiago, *Granada*

Sweden

Dmitry Grishenkov, *Stockholm*
Tie-Qiang Li, *Stockholm*

Switzerland

Nicolau Beckmann, *Basel*
Christian Boy, *Bern*
Giorgio Treglia, *Bellinzona*

Stephan Ulmer, *Kiel*

Thailand

Sirianong Namwongprom, *Chiang Mai*

Turkey

Kubilay Aydin, *Istanbul*
Ramazan Akdemir, *Sakarya*
Serhat Avcu, *Ankara*
Ayse Aralasmak, *Istanbul*
Oktay Algin, *Ankara*
Nevbahar Akcar, *Meselik*
Bilal Battal, *Ankara*
Zulkif Bozgeyik, *Elazig*
Nazan Ciledag, Aakara
Fuldem Y Donmez, *Ankara*
Gulgun Engin, *Istanbul*
Ahmet Y Goktay, *Izmir*
Oguzhan G Gumustas, *Bursa*
Kaan Gunduz, *Ankara*
Pelin Ozcan Kara, *Mersin*
Kivanc Kamburoglu, *Ankara*
Ozgur Kilickesmez, *Istanbul*
Furuzan Numan, *Istanbul*
Cem Onal, *Adana*
Ozgur Oztekin, *Izmir*
Seda Ozbek (Boruban), *Konya*
Selda Sarikaya, *Zonguldak*
Figen Taser, *Kutahya*
Baran Tokar, *Eskisehir*
Ender Uysal, *Istanbul*
Ensar Yekeler, *Istanbul*

United Kingdom

Indran Davagnanam, *London*
M DC Valdés Hernández, *Edinburgh*
Alan Jackson, *Manchester*
Suneil Jain, *Belfast*
Long R Jiao, *London*
Miltiadis Krokidis, *Cambridge*
Pradesh Kumar, *Liverpool*
Peter D Kuzmich, *Derby*
Georgios Plataniotis, *Brighton*
Vanessa Sluming, *Liverpool*

United States

Garima Agrawal, *Saint Louis*
James R Brasic, *Baltimore*
Rajendra D Badgaiyan, *Buffalo*
Ulas Bagci, *Bethesda*
Anat Biegon, *Stony Brook*
Ramon Casanova, *Winston Salem*
Wenli Cai, *Boston*
Zheng Chang, *Durham*
Corey J Chakarun, *Long Beach*
Kai Chen, *Los Angeles*
Hyun-Soon Chong, *Chicago*
Marco Cura, *Dallas*
Ravi R Desai, *Bensalem*
Delia DeBuc, *Miami*
Carlo N De Cecco, *Charleston*
Timm-Michael L Dickfeld, *Baltimore*
Subba R Digumarthy, *Boston*
Huy M Do, *Stanford*
Todd A Faasse, *Grand Rapids*
Salomao Faintuch, *Boston*
Girish M Fatterpekar, *New York*
Dhakshinamoorthy Ganeshan, *Houston*
Robert J Griffin, *Little Rock*
Andrew J Gunn, *Boston*
Sandeep S Hedgire, *Boston*
Timothy J Hoffman, *Columbia*
Mai-Lan Ho, *San Francisco*
Juebin Huang, *Jackson*
Abid Irshad, *Charleston*
Matilde Inglese, *New York*
El-Sayed H Ibrahim, *Jacksonville*
Paul R Julsrud, *Rochester*
Pamela T Johnson, *Baltimore*
Ming-Hung Kao, *Tempe*
Sunil Krishnan, *Houston*
Richard A Komoroski, *Cincinnati*
Sandi A Kwee, *Honolulu*
King Kim, *Ft. Lauderdale*
Guozheng Liu, *Worcester*
Yiyan Liu, *Newark*
Venkatesh Mani, *New York*
Lian-Sheng Ma, *Pleasanton*
Rachna Madan, *Boston*
Zeyad A Metwalli, *Houston*
Yilong Ma, *Manhasset*
Hui Mao, *Atlanta*
Feroze B Mohamed, *Philadelphia*
Gul Moonis, *Boston*
John L Nosher, *New Brunswick*
Rahmi Oklu, *Boston*
Aytekin Oto, *Chicago*
Bishnuhari Paudyal, *Philadelphia*
Rajul Pandya, *Youngstown*
Chong-Xian Pan, *Sacramento*
Jay J Pillai, *Baltimore*
Neal Prakash, *Duarte*
Reza Rahbar, *Boston*
Ali S Raja, *Boston*
Gustavo J Rodriguez, *El Paso*
David J Sahn, *Portlsand*
Steven Schild, *Scottsdale*
Ali R Sepahdari, *Los Angeles*
Li Shen, *Indianapolis*
JP Sheehan, *Charlottesville*
Atul B Shinagare, *Boston*
Sarabjeet Singh, *Boston*
Charles J Smith, *Columbia*
Kenji Suzuki, *Chicago*
Monvadi Srichai-Parsia, *Washington*
Sree H Tirumani, *Boston*
Hebert A Vargas, *New York*
Sachit Verma, *Philadelphia*
Yoichi Watanabe, *Minneapolis*
Li Wang, *Chapel Hill*
Carol C Wu, *Boston*
Shoujun Xu, *Houston*
Min Yao, *Cleveland*
Xiaofeng Yang, *Atlanta*
Qingbao Yu, *Albuquerque*
Aifeng Zhang, *Chicago*
Chao Zhou, *Bethlehem*
Hongming Zhuang, *Philadelphia*

WJR World Journal of Radiology

Contents

Monthly Volume 6 Number 6 June 28, 2014

FRONTIER

223 White matter abnormalities: Insights into the pathophysiology of major affective disorders
Serafini G, Gonda X, Rihmer Z, Girardi P, Amore M

TOPIC HIGHLIGHT

230 Effectiveness of chest radiography, lung ultrasound and thoracic computed tomography in the diagnosis of congestive heart failure
Cardinale L, Priola AM, Moretti F, Volpicelli G

238 Application of fluorodeoxyglucose positron emission tomography in the management of head and neck cancers
Siddiqui F, Yao M

252 Congenital hyperinsulinism: Role of fluorine-18L-3, 4 hydroxyphenylalanine positron emission tomography scanning
Gopal-Kothandapani JS, Hussain K

261 Sustained attention in psychosis: Neuroimaging findings
Sepede G, Spano MC, Lorusso M, De Berardis D, Salerno RM, Di Giannantonio M, Gambi F

274 Rotator cuff disorders: How to write a surgically relevant magnetic resonance imaging report?
Tawfik AM, El-Morsy A, Badran MA

REVIEW

284 A handy review of carpal tunnel syndrome: From anatomy to diagnosis and treatment
Ghasemi-rad M, Nosair E, Vegh A, Mohammadi A, Akkad A, Lesha E, Mohammadi MH, Sayed D, Davarian A, Maleki-Miyandoab T, Hasan A

301 Neuroimaging in Huntington's disease
Niccolini F, Politis M

313 Imaging of the small bowel: Crohn's disease in paediatric patients
Casciani E, De Vincentiis C, Polettini E, Masselli G, Di Nardo G, Civitelli F, Cucchiara S, Gualdi GF

329 Comparative review of vertebroplasty and kyphoplasty
Ruiz Santiago F, Santiago Chinchilla A, Guzmán Álvarez L, Pérez Abela AL, Castellano García MM, Pajares López M

Contents

World Journal of Radiology
Volume 6 Number 6 June 28, 2014

344 Diffusion-weighted magnetic resonance imaging in management of bladder cancer, particularly with multimodal bladder-sparing strategy
Yoshida S, Koga F, Kobayashi S, Tanaka H, Satoh S, Fujii Y, Kihara K

355 Multi-detector computed tomography in the diagnosis and management of acute aortic syndromes
Hallinan JTPD, Anil G

MINIREVIEWS

366 Use of stereotactic radiosurgery in the treatment of gynecologic malignancies: A review
Long B, Eskander RN, Tewari KS

CLINICAL TRIALS STUDY

374 Feasibility study of computed *vs* measured high b-value (1400 s/mm²) diffusion-weighted MR images of the prostate
Bittencourt LK, Attenberger UI, Lima D, Strecker R, de Oliveira A, Schoenberg SO, Gasparetto EL, Hausmann D

PROSPECTIVE STUDY

381 Coronary artery calcium score on low-dose computed tomography for lung cancer screening
Arcadi T, Maffei E, Sverzellati N, Mantini C, Guaricci AI, Tedeschi C, Martini C, La Grutta L, Cademartiri F

CASE REPORT

388 Myotendinous rupture of temporalis muscle: A rare injury following seizure
Naffaa LN, Tandon YK, Rubin M

World Journal of Radiology
Volume 6 Number 6 June 28, 2014

Contents

APPENDIX	I-V	Instructions to authors
ABOUT COVER		Editorial Board Member of *World Journal of Radiology*, Georgios Plataniotis, MD, PhD, Doctor, Department of Oncology, Sussex Cancer Centre, Royal Sussex County Hospital, Brighton BN2 5 BE, United Kingdom
AIM AND SCOPE		*World Journal of Radiology* (*World J Radiol*, *WJR*, online ISSN 1949-8470, DOI: 10.4329) is a peer-reviewed open access academic journal that aims to guide clinical practice and improve diagnostic and therapeutic skills of clinicians. *WJR* covers topics concerning diagnostic radiology, radiation oncology, radiologic physics, neuroradiology, nuclear radiology, pediatric radiology, vascular/interventional radiology, medical imaging achieved by various modalities and related methods analysis. The current columns of *WJR* include editorial, frontier, diagnostic advances, therapeutics advances, field of vision, mini-reviews, review, topic highlight, medical ethics, original articles, case report, clinical case conference (clinicopathological conference), and autobiography. We encourage authors to submit their manuscripts to *WJR*. We will give priority to manuscripts that are supported by major national and international foundations and those that are of great basic and clinical significance.
INDEXING/ABSTRACTING		*World Journal of Radiology* is now indexed in PubMed Central, PubMed, Digital Object Identifier, and Directory of Open Access Journals.
FLYLEAF	I-III	Editorial Board

EDITORS FOR THIS ISSUE

Responsible Assistant Editor: *Xiang Li*
Responsible Electronic Editor: *Dan-Ni Zhang*
Proofing Editor-in-Chief: *Lian-Sheng Ma*
Responsible Science Editor: *Fang-Fang Ji*
Proofing Editorial Office Director: *Jin-Lei Wang*

NAME OF JOURNAL
World Journal of Radiology

ISSN
ISSN 1949-8470 (online)

LAUNCH DATE
December 31, 2009

FREQUENCY
Monthly

EDITORS-IN-CHIEF
Kai U Juergens, MD, Associate Professor, MRT und PET/CT, Nuklearmedizin Bremen Mitte, ZE-MODI - Zentrum für morphologische und molekulare Diagnostik, Bremen 28177, Germany

Edwin JR van Beek, MD, PhD, Professor, Clinical Research Imaging Centre and Department of Medical Radiology, University of Edinburgh, Edinburgh EH16 4TJ, United Kingdom

Thomas J Vogl, MD, Professor, Reader in Health Technology Assessment, Department of Diagnostic and Interventional Radiology, Johann Wolfgang Goethe University of Frankfurt, Frankfurt 60590, Germany

EDITORIAL OFFICE
Jin-Lei Wang, Director
Xiu-Xia Song, Vice Director
World Journal of Radiology
Room 903, Building D, Ocean International Center,
No. 62 Dongsihuan Zhonglu, Chaoyang District,
Beijing 100025, China
Telephone: +86-10-59080039
Fax: +86-10-85381893
E-mail: editorialoffice@wjgnet.com
Help Desk: http://www.wjgnet.com/esps/helpdesk.aspx
http://www.wjgnet.com

PUBLISHER
Baishideng Publishing Group Inc
8226 Regency Drive,
Pleasanton, CA 94588, USA
Telephone: +1-925-223-8242
Fax: +1-925-223-8243
E-mail: bpgoffice@wjgnet.com
Help Desk: http://www.wjgnet.com/esps/helpdesk.aspx
http://www.wjgnet.com

PUBLICATION DATE
June 28, 2014

COPYRIGHT
© 2014 Baishideng Publishing Group Inc. Articles published by this Open-Access journal are distributed under the terms of the Creative Commons Attribution Non-commercial License, which permits use, distribution, and reproduction in any medium, provided the original work is properly cited, the use is non commercial and is otherwise in compliance with the license.

SPECIAL STATEMENT
All articles published in journals owned by the Baishideng Publishing Group (BPG) represent the views and opinions of their authors, and not the views, opinions or policies of the BPG, except where otherwise explicitly indicated.

INSTRUCTIONS TO AUTHORS
Full instructions are available online at http://www.wjgnet.com/1949-8470/g_info_20100316162358.htm.

ONLINE SUBMISSION
http://www.wjgnet.com/esps/

World Journal of Radiology

Submit a Manuscript: http://www.wjgnet.com/esps/
Help Desk: http://www.wjgnet.com/esps/helpdesk.aspx
DOI: 10.4329/wjr.v6.i6.223

World J Radiol 2014 June 28; 6(6): 223-229
ISSN 1949-8470 (online)
© 2014 Baishideng Publishing Group Inc. All rights reserved.

FRONTIER

White matter abnormalities: Insights into the pathophysiology of major affective disorders

Gianluca Serafini, Xenia Gonda, Zoltan Rihmer, Paolo Girardi, Mario Amore

Gianluca Serafini, Paolo Girardi, Department of Neurosciences, Mental Health and Sensory Organs, Suicide Prevention Center, Sant'Andrea Hospital, Sapienza University of Rome, 00189 Rome, Italy
Xenia Gonda, Zoltan Rihmer, Department of Clinical and Theoretical Mental Health, Kutvolgyi Clinical Center, 1125 Budapest, Hungary
Mario Amore, Department of Neuroscience, Rehabilitation, Ophthalmology, Genetics, Maternal and Child Health, Section of Psychiatry, University of Genova, I-16146 Genova, Italy
Author contributions: Serafini G designed the study and wrote the manuscript; Amore M, Girardi P and Rihmer Z provided the intellectual impetuous and supervised the search strategy; Gonda X contributed in reviewing the literature and provided help in selecting papers in the present manuscript.
Correspondence to: Gianluca Serafini, MD, PhD, Department of Neurosciences, Mental Health and Sensory Organs, Suicide Prevention Center, Sant'Andrea Hospital, Sapienza University of Rome, 1035-1039, Via di Grottarossa, 00189 Rome, Italy. gianluca.serafini@uniroma1.it
Telephone: +39-06-33775675 Fax: +39-06-33775342
Received: January 23, 2014 Revised: April 13, 2014
Accepted: May 16, 2014
Published online: June 28, 2014

Abstract

The presence of white matter hyperintensities (WMHs) has been commonly associated with poor outcome in subjects with major affective disorders. Unfortunately, WMHs may be frequently confounded by the use of psychoactive medications and duration of illness. Although findings from the current literature are quite conflicting, we proposed that subjects with WMHs may be at higher suicidal risk when compared to other subgroups without. Based on the Fazekas modified scale, the severity of WMHs may serve as a trait marker of disease. Interestingly, the presence of WMHs may represent a neurobiological marker between the underlying vulnerability and clinical presentation of major affective disorders.

© 2014 Baishideng Publishing Group Inc. All rights reserved.

Key words: White matter hyperintensities; Major affective disorders; Suicidal behaviour; Neuroimaging; Outcome

Core tip: Understanding neural correlates underlying psychiatric morbidity over time is critical but, to date, structural magnetic resonance imaging studies identified only not stable risk predictors of unfavourable outcome in psychiatric populations. The presence of white matter hyperintensities (WMHs) has been commonly associated with a poor outcome in individuals with major affective disorders. Based on our studies, subjects with WMHs may be considered at higher suicidal risk than those without and the severity of WMHs as assessed by the Fazekas modified scale may serve as a trait marker of disease. WMHs may represent an interesting neurobiological marker between the underlying vulnerability and clinical presentation of major affective disorders.

Serafini G, Gonda X, Rihmer Z, Girardi P, Amore M. White matter abnormalities: Insights into the pathophysiology of major affective disorders. *World J Radiol* 2014; 6(6): 223-229 Available from: URL: http://www.wjgnet.com/1949-8470/full/v6/i6/223.htm DOI: http://dx.doi.org/10.4329/wjr.v6.i6.223

INTRODUCTION

Major affective disorders are chronic and disabling diseases that are associated with significant functional impairment. Patients with major affective disorders commonly experience long-term negative outcomes, frequent relapses, incomplete recovery between episodes, residual symptoms, persistent psychosocial impairment and high suicide risk[1,2]. Among all major affective disorders, bipolar disorder (BD), including both BD type I and type Ⅱ, is a serious mental illness that affects approximately

1%-3% of the adult population. However, if subthreshold cases are also considered, the lifetime prevalence of bipolar disorders is around 6%[3]. White matter hyperintensities (WMHs) are, no doubt, the most common neuroimaging finding in patients with BD, regardless of age[4]. However, WMHs are also frequent in other major affective disorders (for details see Table 1 in the recent study of Serafini *et al*[5]).

WMHs are hyperintense signals on T2-weighted magnetic resonance images (MRI) identifying ependymal loss and altered brain myelination. According to their localization, WMHs may be classified in periventricular white matter hyperintensities (PWMHs) having a debated origin and deep white matter hyperintensities (DWMHs) with a predominant vascular aetiology[6].WMHs are known to be commonly associated with older age and several risk factors such as arterial hypertension and diabetes mellitus (Figure 1).

WMHs are frequently associated with demyelinating disorders, in particular multiple sclerosis, an illness involving the presence of different causative mechanisms[7,8]. As suggested[7,8], distinct patterns of demyelination have been documented over time and subcortical WMHs have been repeatedly recorded in patients with multiple sclerosis. MRI may be commonly used to monitor disease progress in the white matter of patients with multiple sclerosis[9]. However, MRI techniques may be considered as not sufficiently sensitive to detect purely cortical MS lesions[10] and their sensitivity can be improved using higher field strength or voxel-based morphometry.

Several studies suggested that WMHs are consistently associated with major affective disorders and suicidal behaviour in children as well as in young adults[11,12]. Overall, the association between WMHs and major affective disorders has been confirmed by several lines of evidence, not only in patients with major depressive disorder (MDD) but also in those with bipolar disorder (BD)[13], respectively. This manuscript aimed to selectively review our research studies that have been published to date about the association between white matter hyperintensities assessed by MRI, major affective disorders, and suicidal behaviour.

A critical review of the eight studies that have been published by our research group about white matter abnormalities, major affective disorders, and suicidal behaviour has been conducted.

This is, in summary, an educational commentary reviewing the evidence derived by our research studies concerning the presence and significance of white matter abnormalities in subjects with major affective disorders.

MAIN FINDINGS

Eight research articles have been performed by our research group about the association between WMHs, major affective disorders, and suicidal behaviour. The presence of WMHs was assessed by a neuroradiologist blind to all clinical information, using the modified Fazekas four-point rating scale describing MRI hyperintensities on an ascending scale of intensity and frequency[14]. A second neuroradiologist, blind to all clinical information and previous ratings, usually reviewed all MRI films.

STUDIES CONDUCTED ON SAMPLES OF SUBJECTS WITH BOTH UNIPOLAR AND BIPOLAR DISORDERS

Pompili *et al*[12] initially suggested that WMHs in patients with major affective disorders might be useful biological markers of suicidality. The authors investigated a sample of 65 subjects of which 44.6% had a history of at least one suicide attempt. After logistic regression analyses they reported that the prevalence of WMHs was significantly higher in subjects with past suicide attempts and elevated suicide risk.

Subsequently, Pompili *et al*[15] analyzed 99 patients of which 40.4% were diagnosed as BD- Ⅰ, 21.2% were diagnosed as BD- Ⅱ and 38.4% as unipolar MDD. They found that 27.3% of patients showed evidence of PWMHs, 36.4% presented DWMHs whereas 14.1% had hyperintensities in both periventricular and deep locations. Interestingly, the presence of PWMHs was the only variable significantly associated with attempted suicide even after controlling for age. Subjects with PWMHs were 8 times more likely to have attempted suicide when compared to individuals without PWMHs. Therefore, patients with major affective disorders and PWMHs are more likely to have a history of suicide attempts even after controlling for potential confounding variables such as cardiovascular risk factors and age.

In 2011, Serafini *et al*[16] reported that differences among temperament groups as measured by the Temperament Evaluation of Memphis, Pisa, Paris and San Diego-autoquestionnaire (TEMPS-A) are supported by differences at the MRI indicating that different temperament profiles are associated with differences in the subcortical brain structures of 247 patients with major affective disorders (specifically 143 with BD type Ⅰ, 42 with BD type Ⅱ, and 62 with MDD). TEMPS-A is a self-report questionnaire designed to measure temperamental variations in psychiatric patients and healthy volunteers and has been used by the authors on the basis of the diagnostic criteria for affective temperaments (cyclothymic, dysthymic, irritable, hyperthymic, and anxious). They found that 48% of patients had PWMHs (specifically, more than 15% had PWMHs of 2 or higher on the Fazekas modified scale), and 39% had DWMHs (in particular, more than 7% had DWMHs of 2 or higher on the Fazekas modified scale). Patients in the high- dysthymic, cyclothymic, irritability, and anxiety group were more likely to have higher Beck Hopelessness Scale (BHS), more DWMHs, higher Mini International Neuropsychiatric Interview (MINI) suicidal risk, and more recent suicide attempts when compared with patients in the hyperthymia group. BHS is a 20-item psychometric instrument designed to measure negative attitudes about the future whereas MINI is a short structured interview developed

Table 1 Salient publications of our research group about white matter hyperintensities in affective disorders

Ref.	Sample characteristics	Study type	Location of WMHs	Main findings	Limitations of the study	Conclusion
Serafini *et al*[5]	148 patients (77 men, 71 women) with BD-Ⅰ having a mean age of 47.9 yr	Research article	Centrum semiovale (24.4%) and corona radiata (20.2%) regions, cortical and subcortical deep frontal (17.6%), parietal (15.1%), and temporal (8.4%) areas	A total of 73 subjects (49.3%) reported PWMHs and 59 (39.9%) had DWMHs. Overall, 41 (27.7%) subjects had both PWMHs and DWMHs. Patients with BD-I and lower insight for mania had significantly more PWMHs (54.6% *vs* 22.2%; $P < 0.05$), significantly higher scores on the $HDRS_{17}$ (27.05 ± 6.54 *vs* 23.67 ± 8.64; $t_{146} = -1.98$; $P < 0.05$), and more frequent BHS score ≥ 9 (66.2% *vs* 38.9%; $P < 0.05$) when compared to those with higher insight for mania	All participants were inpatients (a potential confounder). The present study did not include a formal measure of insight. The effects of psychoactive medications on insight ratings and image processing were not analyzed	Patients with PWMHs were more likely to have impaired insight than those without. Different insight levels reflected different MRI findings
Serafini *et al*[19]	85 adult outpatients (16 men and 69 women) with CH and having a mean age of 50.1	Research article	Not specified	Above 40% of patients had PWMHs and almost 98% had DWMHs. Patients with PWMHs differed from those without periventricular lesions on depression severity (t 77.76 = 2.30; $P < 0.05$). Patients with PWMHs had lower CES-D scores (13.79 ± 7.51 *vs* 18.19 ± 9.68) than patients without PWMHs. Patients with more severe DWMHs were older (53.89 ± 13.26 *vs* 47.40 ± 11.91) and reported lower scores on the drive dimension (9.97 ± 2.86 *vs* 11.14 ± 2.52) than patients with mild lesions or without any deep lesion	Different mechanisms may be considered in the emergence of WMHs and it is possible that WMHs may represent only the 'tip of the iceberg' in terms of structural white matter lesions	Patients with PWMHs were 1.06 times more likely to have lower CES-D scores ($P < 0.05$) than patients without PWMHs. Patients with more severe DWMHs were 1.04 times more likely to be older ($P < 0.05$) than patients with mild or without any DWMHs
Serafini *et al*[16]	247 patients (118 men, 129 women) with major affective disorders, specifically 143 BD-I, 42 BD-Ⅱ, and 62 with MDD	Research article	Centrum semiovale (24.4%) and corona radiata (20.2%) regions, cortical and subcortical deep frontal (17.6%), parietal (15.1%), and temporal (8.4%) areas	48% of patients had PWMHs (more than 15% had PWMHs of 2 or higher on the Fazekas modified scale), and 39% had DWMHs (more than 7% had DWMHs of 2 or higher on the Fazekas modified scale). Patients in the high dysthymic, cyclothymic, irritability, and anxiety group were more likely to have higher BHS ≥ 9 = 77% *vs* 52%; $P > 0.001$), more DWMHs (46% *vs* 29%; $\chi^2_{n=3} = 9.90$; $P < 0.05$), higher MINI suicidal risk (54% *vs* 42%; $P < 0.05$), and more recent suicide attempts (24% *vs* 14%; $P < 0.05$), than patients in the hyperthymia group	The small sample size did not allow to generalize findings. The association between the lethality or number of suicide attempts and the presence, severity, or number of hyperintensities was not assessed. The study lacks of accounting for the cognitive effects of medications	Differences among temperament groups as measured by the TEMPS-A are supported by differences at the MRI indicating that different temperament profiles are associated with differences in subcortical brain structures
Serafini *et al*[20]	A 76-year-old woman with BD hospitalized for a mixed state	Case report with a 2-yr follow-up	Not specified	Patient had severe WMHs, she took lithium and haloperidol during the hospitalization. She was euthymic at discharge as well as after two-years of follow-up. Her nutrition had a high concentration of Vitamin-D	A second MRI was not performed	Although WM lesions were persistent, the patient improved in both mood and quality of life. Lithium and Vitamin-D may have exerted possible protective effects
Serafini *et al*[18]	54 patients (30 men and 24 women) with LOBD (≥ 60 yr old) having a mean age of 68 yr. 76% had a diagnosis of BD-I, and 24% had a diagnosis of BD-Ⅱ	Letter to the Editor including research data	Centrum semiovale (22%), corona radiata (15%), paratrigonal regions (6%), cortical, subcortical deep frontal (46%), parietal (24%) areas	Confluence of DWMH lesions were found in 17% of the patients (modified Fazekas scale ≥ 2) whereas in 28% PWMH confluent lesions (modified Fazekas scale ≥ 2) were reported. No significant association resulted between diagnosis and PWMHs or DWMHs. BD-Ⅱ with DWMHs had a poorer quality of life than BD-Ⅰ subjects	The link between clinical features of bipolar disorders and deep brain lesions on MRI remains quite unknown	MRI findings of DWMHs could be a useful biological predictor of severity in patients with BD-Ⅱ
Pompili *et al*[17]	47 LOBD patients (55.3% men and 44.7% women)	Review article including research data	Frontal (26.1) and centrum semiovale areas (26.1%), corona radiata (17.4%), parietal (17.4%), and paratrigonal regions (8.7%)	55.3% of these patients had periventricular WMHs, 46.4% had WMHs of mild severity, 50% WMHs of moderate severity, and only 3.6 WMHs of high severity. 34% of LOBD patients had both deep and periventricular WMHs. A significant relationship between older age with LOBD and WMHs was reported	Vascular-related mechanisms cannot be the only factors implicated in the pathophysiology of the WMHs in LOBD subjects. The study did not assess how cerebro-vascular risk factors are related to the type / intensity of medications, and the progression of WMHs	MRI findings of WMHs could be a useful biological predictor of severity in patients with LOBD

Pompili *et al*[15]	99 patients having a mean age of 46.5 yr. 40.4% were diagnosed as BD-I, 21.2% as BD-Ⅱ, and 38.4% as unipolar MDD	Research article	Corona radiate (n = 10), centrum semiovale (n = 6), and frontal subcortical white matter (n = 18)	It has been suggested that 27.3% of patients showed evidence of PWMHs and 36.4% of DWMHs whereas 14.1% of patients had hyperintensities in both locations. The presence of PWMHs was the only variable significantly associated with attempted suicide even after controlling for age. Subjects with PWMHs were 8 times more likely to have attempted suicide than individuals without PWMHs [OR = 8.08 (95%CI: 2.67-24.51)]	The small sample size may affect the generalization of results. PWMHs were able to explain only a small part of the variability of suicide attempt risk, indicating that one single variable is not sufficient to predict suicidality	Patients with affective disorders and PWMHs are more likely to have a history of suicide attempts even after controlling for potential confounding variables such as cardiovascular risk factors and age
Pompili *et al*[12]	65 subjects, 29 (44.6%) with a history of at least one suicide attempt, and 36 (65.4%) without. Subjects had a mean age of 44.61 yr	Research article	Not specified	After logistic regression analyses, the prevalence of WMHs was significantly higher in subjects with past suicide attempts (P = 0.01) and other clinical indicators of elevated suicide risk	The association between WMHs and suicidality holds true for both unipolar and bipolar depressed patients	WMHs in patients with major affective disorders might be useful biological markers of suicidality

AD: Affective disorders; BD-I: Bipolar disorder type I; BD-Ⅱ: Bipolar disorder type Ⅱ; BHS: Beck Hopelessness Scale; CES-D: Center for Epidemiologic Studies Depression Scale; CH: Chronic headache; DWMHs: Deep WMHs; LO: Late-onset; LOBD: Late-onset bipolar disorder; Mini: Mini International Neuropsychiatric Interview; MDD: Major depressive disorder; MRI: Magnetic resonance imaging; PWMHs: Periventricular WMHs; SA: Suicide attempts; WMHs: White matter hyperintensities; TEMPS-A: Temperament Evaluation of Memphis, Pisa, Paris and San Diego-autoquestionnaire. WMHs that usually appear as hyperintense signals on T2-weighted MRI, are characterized by ependymal loss and differing degrees of myelination and can be related to several clinical conditions such as major depressive disorders (BDI, BDⅡ, MDD), and CH. The mentioned Table reported the most relevant publications of our research group about WMHs and their significance in major affective disorders.

to explore psychiatric disorders according to DSM-Ⅲ-R; importantly, one section of this instrument is developed to assess suicidal risk with questions about past and current suicidality.

STUDIES CONDUCTED ON SAMPLES OF PATIENTS WITH BIPOLAR AFFECTIVE DISORDERS

Pompili *et al*[17] conducted an overview of the literature (including research data) in which reported that 55.3% of patients had periventricular WMHs (46.4% of them of mild severity, 50% of moderate severity, and only 3.6 of high severity, respectively). They also found that 34% of late-onset bipolar disorder (LOBD) patients had both deep and periventricular WMHs and a significant relationship has been suggested between older age with LOBD and WMHs. The authors concluded that MRI findings of WMHs could be a useful biological predictor of severity in patients with LOBD.

Subsequently, Serafini *et al*[18] reported that in a sample of 54 patients (30 men and 24 women) with LOBD (≥ 60 years old) 76% had a diagnosis of BD type Ⅰ, 24% a diagnosis of BD type Ⅱ whereas confluence of deep lesions (modified Fazekas scale ≥ 2) was found in 17% of the patients and in 28% periventricular confluent lesions (modified Fazekas scale ≥ 2). The authors suggested that no significant association between diagnosis and PWMHs/DWMHs emerged but, interestingly, subjects with BD type Ⅱ and DWMHs had a poorer quality of life compared to paients with BD type Ⅰ.

Finally, Serafini *et al*[5] suggested that in a sample of 148 patients with BD type Ⅰ (having a mean age of 47.9 years) a total of 49.3% reported PWMHs and 39.9% had DWMHs. Overall, 27.7% of subjects had both PWMHs and DWMHs. They reported that patients with BD type Ⅰ and lower insight for mania had significantly more PWMHs (54.6% *vs* 22.2%; $P < 0.05$), significantly higher scores on the $HDRS_{17}$ (27.05 ± 6.54 *vs* 23.67 ± 8.64; t146 = -1.98; $P < 0.05$), and more frequent BHS scores ≥ 9 (66.2% *vs* 38.9%; $P < 0.05$) when compared to patients with BD type Ⅰ and higher insight for mania. Importantly, different insight levels reflected different MRI findings. The authors concluded that patients with PWMHs were more likely to have impaired insight than those without.

STUDIES ON SAMPLES OF PATIENTS WITH CHRONIC MIGRAINE

Serafini *et al*[19] found that in a sample of 85 adult outpatients with a chronic headache above 40% of patients had PWMHs and almost 98% DWMHs, respectively. Patients

Figure 1 White matter hyperintensities as assessed by magnetic resonance images. White matter hyperintensities (WMHs) appear as hyperintense signals on T2-weighted magnetic resonance images and represent ependymal loss and differing degrees of myelination. These lesions can be related to a wide variety of clinical conditions and pathophysiological processes. WMHs, depending on the localization, are commonly classified as periventricular hyperintensities (PWMHs) or deep white matter hyperintensities (DWMHs). DWMHs were identified as having mainly a vascular aetiology whereas PWMHs could be due to ependymal loss, differing degrees of myelination and cerebral ischemia. WMHs are reported to be commonly associated with older age, and cardiovascular risk factors such as hypertension and diabetes.

with PWMHs significantly differed from those without periventricular lesions on depression severity. Patients with PWMHs had lower Center for Epidemiologic Studies Depression Scale (CES-D) scores (13.79 ± 7.51 *vs* 18.19 ± 9.68) when compared with patients without PWMHs. Also, patients with more severe DWMHs were older (53.89 ± 13.26 *vs* 47.40 ± 11.91) and reported lower scores on the drive dimension (9.97 ± 2.86 *vs* 11.14 ± 2.52) than patients with mild or without any deep lesion.

Overall, patients with PWMHs were 1.06 times more likely to have lower CES-D scores compared to patients without PWMHs. Patients with more severe DWMHs were 1.04 times more likely to be older than patients with mild or without DWMHs.

CASE REPORTS

Based on a case report study of a 76-year-old woman with BD hospitalized for a mixed state and having severe WMHs treated with lithium and haloperidol during the hospitalization, Serafini *et al*[20] found that she was euthymic at discharge as well as after two-years of follow-up. The authors suggested that, although WM lesions were persistent, the patient improved in both mood and quality of life. Lithium and Vitamin-D (highly present in her nutrition) may have exerted possible neuroprotective effects.

DISCUSSION AND CLINICAL IMPLICATIONS

Patients with WMHs, particularly those with abnormalities in the white matter of prefrontal cortex, amygdala-hippocampus complex, thalamus and basal ganglia whose integrity implicates adequate mood regulation may be at higher risk for developing mood disorders because of possible alterations of neuroanatomic pathways[21]. Also, volumetric studies clearly indicated the possible involvement of the frontal cortex, temporal lobes, basal ganglia and cerebellum in BD and, recently, subgenual cingulate cortex in adolescents with BD type I [22].

Understanding the nature and significance of white matter abnormalities in major affective disorders is critical as these lesions may represent neurobiological markers able to indicate the risk for subsequent development of more aggressive illness subtypes and the need of more targeted interventions[23].

WMH location may be critical in the expression of certain affective dysfunctions (*e.g.*, cognitive/emotional impairments). Periventricular lesions seem to be more common in BD type I compared to BD-type Ⅱ, and healthy controls[5,12,18]. This may indicate that these neuroimaging findings are sensitive and even subtype selective diagnostic tools in bipolar patients whereas DWMHs are predictors of a less favourable outcome being associated with a poorer response to treatment, and recurrent illness episodes[24].

A relevant association between increased rates of WMHs and a history of suicide attempts has also been suggested in both unipolar and bipolar patients[12]. This finding has been replicated in a sample of 99 consecutively admitted inpatients with major affective disorders where neuroimaging measures were found to be markers of risk for suicidal attempts. Specifically, attempters and nonattempters differed only for the presence of PWMHs, with the former who were more likely to have PWMHs[15]. Moreover, a significant association between older age and WMHs[17], and between DWMHs and poor prognosis was reported in a sample of patients with late-onset bipolar Ⅱ disorder[18] demonstrating that WMHs could be useful biological predictors of illness severity.

Differences in MRI profiles were also found to be associated with differences among temperament groups measured by the TEMPS-A[16]. Specifically, patients with higher scores for dysthymic and lower scores for hyperthymic temperament were more likely to have higher BHS scores, more DWMHs, higher MINI suicidal risk, and more recent suicide attempts than patients with higher scores for hyperthymic and lower scores for dysthymic temperament. The presence of a dysthymic temperament profile together with DWMHs may presumably play a critical role in the emergence of hopelessness as assessed by BHS. These differential characteristics may be used for grouping subjects with mood disorders potentially helping in optimizing reliable treatment strategies.

It has also been found that in contrast to hyperthymic temperament the short allele of the serotonin transporter gene was significantly related to depressive, cyclothymic, irritable and anxious temperaments[25] and with violent suicidal behavior in nonclinical populations. A study on elderly depressed patients showed that individuals with the short allele of the serotonin transporter gene had more microstructural white matter abnormalities in the frontolimbic and other brain regions[26] compared to

those without. These findings indicate that the short allele of the serotonin transporter gene, DWMHs, affective temperaments containing more or less depressive component, and suicidal behaviour (in chronological order) are strongly related to each other and the presence of the first three in the same subject could serve as a powerful marker for predicting future suicidal behaviour.

However, also negative associations have been reported[5,19,20]. In particular, patients with chronic migraine and PWMHs reported fewer depressive symptoms as assessed by the Center for Epidemiologic Studies Depression Scale (CES-D) than those with chronic migraine without PWMHs[19]. In contrast with the generally poor outcome related to the presence of WMHs in patients with affective disorders, the possible protective effect of lithium and Vitamin-D in ameliorating mood and psychosocial functioning in a patient with BD has also been suggested[20].

Additionally, our last study found that subjects with PWMHs were more likely to have impaired insight compared to those without, but any association between PWMHs and suicidal behaviour as assessed using BHS has been found[5].

These latter findings[5] seem to contradict our previous results regarding the association between WMHs and poor outcome including suicidality in both unipolar and bipolar depressed individuals. However, in these studies we recruited a sample of subjects with chronic migraine and a sample of patients with BD type I respectively, whereas the previous results were reported in mixed samples (including both bipolar and unipolar depressed patients)[12,15] or other specific subgroups[5,16-20]. It's possible to speculate that the association between PWMHs and suicidal behaviour is significant only in some specific subgroups of patients with major affective disorders in which WMHs may serve as a marker of disease. WMHs could not be a risk factor for suicide among inpatients with other predominant conditions (*e.g.*, chronic migraine) or in those with certain specific illness subtypes.

Another consideration needs to be critically addressed. WMHs were in most cases able to explain only a small part of the variability related to suicide attempt risk, indicating that one single variable is not sufficient to predict a complex behaviour such as suicide[15]. Table 1 summarized the most relevant findings of our studies.

LIMITATIONS

MRI studies investigating the presence of WMHs should be considered in the light of the following limitations. First, the small sample size of the studies did not allow for generalization of the present findings. In addition, samples are often mixed including inpatients admitted to a psychiatric hospital for more severe affective symptoms that were compared to outpatients usually exhibiting less severe/more stable illness episodes. Also, in most cases the absence of a direct comparison between patients with major depression and other subjects with different mood disorders limited the clinical relevance of the findings.

Not all studies evaluated the presence, severity, or number of hyperintense lesions and most of them used visual scales such as the Fazekas modified rating scale that is a less objective evaluation method than many volumetric methods available.

Moreover, most studies recruited patients treated with psychoactive medications or having a history of substance abuse, but not all analyzed the effects of these variables on insight ratings and image processing. The lack of accounting for the cognitive effects of medications may be considered an important limitation. In order to comprehensively examine the effect of different medications on the neurobiology of clinical symptoms, studies should investigate patients with early affective symptoms or first illness episodes. Also, not all studies include an healthy comparison group and this may limit conclusive statements about the specificity of results.

Other methodological issues concern the procedure. MRI studies were of quite low spatial resolution especially if performed using a 1.5 T scanner. Studies using 3 T scanner and/or higher resolution techniques would likely yield a much higher number and extent of WMHs than studies using a 1.5 T scanner. An analysis quantifying total white matter lesion volume would strengthen the findings of most studies. In addition, diffusion tensor imaging techniques may be more sensitive for detecting white matter abnormalities associated with mood disorders. Finally, although some studies reported that WMHs were predominant in some brain regions, not all analyzed WMHs using regional analyses.

CONCLUSION

In summary, although it is possible that WMHs may represent only the 'tip of the iceberg' and an extreme consequence of underlying microstructural processes that affect brain connectivity, we believe that they may represent relevant biological markers of poor outcome in patients with major affective diseases. The presence of WMHs may be used for grouping subjects who will manifest more severe illness impairments from those who will present a better outcome, potentially helping clinicians in optimizing the best treatment strategy. WMHs may be considered as a proxy for identifying subgroups of patients with more severe illness subtypes requiring more targeted interventions. For example, the early identification of individuals at risk for highly lethal suicide attempts through the assessment of WMHs may help to closely monitor this clinical subgroup of subjects with poor outcome.

Based on our studies, it has been demonstrated that WMHs are a useful biological marker of poor outcome including suicidality in the specific subpopulations of patients which were investigated. However, as studies using MRI techniques are biased by several limitations, further prospective studies are needed in order to provide a better understanding of the biological processes involved in WMH progression as well as to elucidate the nature of the association between WMHs and major affective disorders.

ACKNOWLEDGMENTS

Xénia Gonda is recipient of the Janos Bolyai Research Fellowship of the Hungarian Academy of Sciences.

REFERENCES

1 **Cho DY**, Lee WY, Chen CC. Limbic leukotomy for intractable major affective disorders: a 7-year follow-up study using nine comprehensive psychiatric test evaluations. *J Clin Neurosci* 2008; **15**: 138-142 [PMID: 18068369 DOI: 10.1016/j.jocn.2006.10.017]
2 **Rihmer Z**. Suicide risk in mood disorders. *Curr Opin Psychiatry* 2007; **20**: 17-22 [PMID: 17143077 DOI: 10.1097/YCO.0b013e3280106868]
3 **Rihmer Z**, Angst J. Epidemiology of bipolar disorder. In: Kasper S, Hirschfeld RMA. Handbook of bipolar disorder. New York: Taylor and Francis, 2005; 21-35
4 **Vasudev A**, Thomas A. 'Bipolar disorder' in the elderly: what's in a name? *Maturitas* 2010; **66**: 231-235 [PMID: 20307944 DOI: 10.1016/j.maturitas.2010.02.013]
5 **Serafini G**, Pompili M, Innamorati M, Girardi N, Strusi L, Amore M, Sher L, Gonda X, Rihmer Z, Girardi P. The impact of periventricular white matter lesions in patients with bipolar disorder type I. *CNS Spectr* 2014 Jan 10; 1-12 Epub ahead of print [PMID: 24411553]
6 **Thomas AJ**, Perry R, Barber R, Kalaria RN, O'Brien JT. Pathologies and pathological mechanisms for white matter hyperintensities in depression. *Ann N Y Acad Sci* 2002; **977**: 333-339 [PMID: 12480770]
7 **Morris G**, Maes M. Myalgic encephalomyelitis/chronic fatigue syndrome and encephalomyelitis disseminata/multiple sclerosis show remarkable levels of similarity in phenomenology and neuroimmune characteristics. *BMC Med* 2013; **11**: 205 [PMID: 24229326]
8 **Kanekar S**, Devgun P. A pattern approach to focal white matter hyperintensities on magnetic resonance imaging. *Radiol Clin North Am* 2014; **52**: 241-261 [PMID: 24582339 DOI: 10.1016/j.rcl.2013.11.010]
9 **Neema M**, Stankiewicz J, Arora A, Guss ZD, Bakshi R. MRI in multiple sclerosis: what's inside the toolbox? *Neurotherapeutics* 2007; **4**: 602-617 [PMID: 17920541]
10 **Bö L**, Geurts JJ, Mörk SJ, van der Valk P. Grey matter pathology in multiple sclerosis. *Acta Neurol Scand Suppl* 2006; **183**: 48-50 [PMID: 16637929]
11 **Ehrlich S**, Breeze JL, Hesdorffer DC, Noam GG, Hong X, Alban RL, Davis SE, Renshaw PF. White matter hyperintensities and their association with suicidality in depressed young adults. *J Affect Disord* 2005; **86**: 281-287 [PMID: 15935248 DOI: 10.1016/j.jad.2005.01.007]
12 **Pompili M**, Ehrlich S, De Pisa E, Mann JJ, Innamorati M, Cittadini A, Montagna B, Iliceto P, Romano A, Amore M, Tatarelli R, Girardi P. White matter hyperintensities and their associations with suicidality in patients with major affective disorders. *Eur Arch Psychiatry Clin Neurosci* 2007; **257**: 494-499 [PMID: 17901999 DOI: 10.1007/s00406-007-0755-x]
13 **Kempton MJ**, Geddes JR, Ettinger U, Williams SC, Grasby PM. Meta-analysis, database, and meta-regression of 98 structural imaging studies in bipolar disorder. *Arch Gen Psychiatry* 2008; **65**: 1017-1032 [PMID: 18762588 DOI: 10.1001/archpsyc.65.9.1017]
14 **Coffey CE**, Figiel GS, Djang WT, Weiner RD. Subcortical hyperintensity on magnetic resonance imaging: a comparison of normal and depressed elderly subjects. *Am J Psychiatry* 1990; **147**: 187-189
15 **Pompili M**, Innamorati M, Mann JJ, Oquendo MA, Lester D, Del Casale A, Serafini G, Rigucci S, Romano A, Tamburello A, Manfredi G, De Pisa E, Ehrlich S, Giupponi G, Amore M, Tatarelli R, Girardi P. Periventricular white matter hyperintensities as predictors of suicide attempts in bipolar disorders and unipolar depression. *Prog Neuropsychopharmacol Biol Psychiatry* 2008; **32**: 1501-1507 [PMID: 18572296 DOI: 10.1016/j.pnpbp.2008.05.009]
16 **Serafini G**, Pompili M, Innamorati M, Fusar-Poli P, Akiskal HS, Rihmer Z, Lester D, Romano A, de Oliveira IR, Strusi L, Ferracuti S, Girardi P, Tatarelli R. Affective temperamental profiles are associated with white matter hyperintensity and suicidal risk in patients with mood disorders. *J Affect Disord* 2011a; **129**: 47-55 [PMID: 20708276 DOI: 10.1016/j.jad.2010]
17 **Pompili M**, Serafini G, Innamorati M, Serra G, Forte A, Lester D, Ducci G, Girardi P, Tatarelli R. White matter hyperintensities, suicide risk and late-onset affective disorders: an overview of the current literature. *Clin Ter* 2010; **161**: 555-563 [PMID: 21181087]
18 **Serafini G**, Pompili M, Innamorati M, De Rossi P, Ferracuti S, Girardi P, Tatarelli R. Deep white matter hyperintensities as possible predictor of poor prognosis in a sample of patients with late-onset bipolar II disorder. *Bipolar Disord* 2010; **12**: 755-756 [PMID: 21040293 DOI: 10.1111/j.1399-5618.2010.00867.x]
19 **Serafini G**, Pompili M, Innamorati M, Negro A, Fiorillo M, Lamis DA, Erbuto D, Marsibilio F, Romano A, Amore M, D'Alonzo L, Bozzao A, Girardi P, Martelletti P. White matter hyperintensities and self-reported depression in a sample of patients with chronic headache. *J Headache Pain* 2012; **13**: 661-667 [PMID: 23080079 DOI: 10.1007/s10194-012-0493-y]
20 **Serafini G**, Pompili M, Angelone M, Lester D, Girardi P, Tatarelli R. Clinical and functional outcome in a subject with bipolar disorder and severe white matter hyperintensities. *Eur J Psychiatry* 2011b; **25**: 41-45
21 **Rigucci S**, Serafini G, Pompili M, Kotzalidis GD, Tatarelli R. Anatomical and functional correlates in major depressive disorder: the contribution of neuroimaging studies. *World J Biol Psychiatry* 2010; **11**: 165-180 [PMID: 19670087]
22 **Singh MK**, Chang KD, Chen MC, Kelley RG, Garrett A, Mitsunaga MM, Bararpour L, Howe M, Reiss AL, Gotlib IH. Volumetric reductions in the subgenual anterior cingulate cortex in adolescents with bipolar I disorder. *Bipolar Disord* 2012; **14**: 585-596 [PMID: 22938166 DOI: 10.1111/j.1399-5618.2012.01043.x]
23 **Borgwardt S**, Fusar-Poli P. White matter pathology--an endophenotype for bipolar disorder? *BMC Psychiatry* 2012; **12**: 138 [PMID: 22970986 DOI: 10.1186/1471-244X-12-138]
24 **Moore PB**, Shepherd DJ, Eccleston D, Macmillan IC, Goswami U, McAllister VL, Ferrier IN. Cerebral white matter lesions in bipolar affective disorder: relationship to outcome. *Br J Psychiatry* 2001; **178**: 172-176 [PMID: 11157432 DOI: 10.1192/bjp.178.2.172]
25 **Gonda X**, Fountoulakis KN, Rihmer Z, Lazary J, Laszik A, Akiskal KK, Akiskal HS, Bagdy G. Towards a genetically validated new affective temperament scale: a delineation of the temperament phenotype of 5-HTTLPR using the TEMPS-A. *J Affect Disord* 2009; **112**: 19-29 [PMID: 18455241 DOI: 10.1016/j.jad.2008.03.012]
26 **Alexopoulos GS**, Murphy CF, Gunning-Dixon FM, Glatt CE, Latoussakis V, Kelly RE, Kanellopoulos D, Klimstra S, Lim KO, Young RC, Hoptman MJ. Serotonin transporter polymorphisms, microstructural white matter abnormalities and remission of geriatric depression. *J Affect Disord* 2009; **119**: 132-141 [PMID: 19375170 DOI: 10.1016/j.jad]

P- Reviewers: Brasic JR, Yang YK **S- Editor**: Wen LL
L- Editor: A **E- Editor**: Zhang DN

World Journal of Radiology

Submit a Manuscript: http://www.wjgnet.com/esps/
Help Desk: http://www.wjgnet.com/esps/helpdesk.aspx
DOI: 10.4329/wjr.v6.i6.230

World J Radiol 2014 June 28; 6(6): 230-237
ISSN 1949-8470 (online)
© 2014 Baishideng Publishing Group Inc. All rights reserved.

TOPIC HIGHLIGHT

WJR 6th Anniversary Special Issues (6): CT

Effectiveness of chest radiography, lung ultrasound and thoracic computed tomography in the diagnosis of congestive heart failure

Luciano Cardinale, Adriano Massimiliano Priola, Federica Moretti, Giovanni Volpicelli

Luciano Cardinale, Adriano Massimiliano Priola, Federica Moretti, Institute of Radiology, University of Turin, AOU San Luigi Gonzaga, 10043 Orbassano, Torino, Italy
Giovanni Volpicelli, Department of Emergency Medicine, University of Turin, AOU San Luigi Gonzaga, 10043 Orbassano, Torino, Italy
Author contributions: Cardinale L and Volpicelli G planned the research and collected the materials; Priola AM and Moretti F were involved in the collection of clinical data; Moretti F wrote the paper assisted by Priola AM and Volpicelli G; Volpicelli G and Cardinale L reviewed this commentary and supervised its publication; Volpicelli G was involved in the language translation.
Correspondence to: Luciano Cardinale, MD, PhD, Institute of Radiology, University of Turin, AOU San Luigi Gonzaga, Regione Gonzole 10, 10043 Orbassano, Torino, Italy. luciano.cardinale@gmail.com
Telephone: +39-1-1902601 Fax: +39-1-19026303
Received: December 28, 2013 Revised: April 22, 2014
Accepted: May 15, 2014
Published online: June 28, 2014

Abstract

Hydrostatic pulmonary edema is as an abnormal increase in extravascular water secondary to elevated pressure in the pulmonary circulation, due to congestive heart failure or intravascular volume overload. Diagnosis of hydrostatic pulmonary edema is usually based on clinical signs associated to conventional radiography findings. Interpretation of radiologic signs of cardiogenic pulmonary edema are often questionable and subject. For a bedside prompt evaluation, lung ultrasound (LUS) may assess pulmonary congestion through the evaluation of vertical reverberation artifacts, known as B-lines. These artifacts are related to multiple minimal acoustic interfaces between small water-rich structures and alveolar air, as it happens in case of thickened interlobular septa due to increase of extravascular lung water. The number, diffusion and intensity of B lines correlates with both the radiologic and invasive estimate of extravascular lung water. The integration of conventional chest radiograph with LUS can be very helpful to obtain the correct diagnosis. Computed tomography (CT) is of limited use in the work up of cardiogenic pulmonary edema, due to its high cost, little use in the emergencies and radiation exposure. However, a deep knowledge of CT signs of pulmonary edema is crucial when other similar pulmonary conditions may occasionally be in the differential diagnosis.

© 2014 Baishideng Publishing Group Inc. All rights reserved.

Key words: Dyspnea; Ultrasonography; Emergency department; Lung diseases; Interstitial/ultrasonography; Pulmonary edema/radiography; Pulmonary edema/ultrasonography; Heart failure/complications; Heart Failure/ultrasonography

Core tip: Acute decompensated heart failure (ADHF) is a frequent emergency condition that represents a diagnostic challenge for the emergency physicians. Imaging has a fundamental role in the diagnosis of heart failure, but the efficacy of the diagnostic process is highly dependent from the ability to integrate information drawn from lung ultrasound (LUS), chest radiography and computed tomography (CT). Chest radiography and LUS are the most used diagnostic tools: the first one combining relative low cost with the panoramic view that allows exclusion of many pulmonary conditions that comes into the differential diagnosis; otherwise the second one has higher sensitivity in the diagnosis of the early signs of pulmonary congestion and permit to perform the examination at bedside during the first clinical approach. CT scan is the best method to have a panoramic thoracic view and CT scan is a powerful method but it has many limitations due to costs, availability in emergency situations and relatively high

radiation exposure. The modern clinician and radiologist should be aware of the potential and limitations of these diagnostic tools and be prepared to integrate information derived from a correct use of ultrasound, conventional radiology and CT.

Cardinale L, Priola AM, Moretti F, Volpicelli G. Effectiveness of chest radiography, lung ultrasound and thoracic computed tomography in the diagnosis of congestive heart failure. *World J Radiol* 2014; 6(6): 230-237 Available from: URL: http://www.wjgnet.com/1949-8470/full/v6/i6/230.htm DOI: http://dx.doi.org/10.4329/wjr.v6.i6.230

INTRODUCTION

Acute decompensated heart failure (ADHF) is a frequent emergency condition that, often represents a diagnostic challenge for the emergency physicians. Accurate assessment of effectiveness of medical treatment on reducing pulmonary congestion, which is the consequence of elevated cardiac filling pressure, is a basic step for a correct management of patients with ADHF. Most patients hospitalized for ADHF are not submitted to invasive hemodynamic measurements, and clinical improvement relies on change in physical findings, radiologic imaging, and hormone levels. Physical findings of elevated filling pressure are often inadequate and rarely decisive to assess real clinical improvement when considered alone[1-3].

Chest X-ray (CXR) is the traditional first line procedure to assess pulmonary congestion, but interpretation of radiologic signs, such as vascular opacity redistribution and interstitial edema, are often questionable and subjective, while different levels of expertize of the readers may cause high inter-observer variability.

In doubtful cases, lung ultrasound (LUS) has been shown to be of value in assessing pulmonary congestion by the evaluation of vertical comet tail artifacts, named B-lines. These artifacts represent easy-to-acquire and highly reproducible bedside signs of diffuse interstitial syndrome, but their limitation is the low specificity[4,5].

B-lines are caused by a change of the normal balance between the air and fluid pulmonary content, when air is lost and fluid are increased. The multiple and small air-fluid interfaces due to small water-rich structures surrounded by air presenting in the lung periphery, create a reverberation phenomenon represented on the screen by multiple B-lines[6]. However, this phenomenon is irrespective of the cardiogenic or pulmonary origin of the condition.

Concerning thoracic computed tomography (CT) scan, it is rarely used for diagnosing pulmonary congestion, unless highly selected cases where other pulmonary interstitial conditions come into the differential. Signs of hydrostatic pulmonary edema on high-resolution CT should always be recognized, even if edema may sometimes be misdiagnosed and the differential diagnosis not always is easily read by the radiologist. Indeed, sometimes signs of pulmonary congestion on CT imaging represent an unexpected condition on patients investigated for other diseases[7].

This review describes the specific signs of cardiogenic pulmonary edema of these three main imaging techniques and discuss their role in the diagnostic process.

CHEST X-RAY

In the acute phase of decompensated heart failure, the early pulmonary alteration is congestion of the vascular bed due to progressive increase of capillary hydrostatic pressure. When pressure increases further and the lymphatic vessels become congested, fluids begin to accumulate in the interstitium around arteries, veins, and airways, and particularly in the interlobular septa. In the early phase, this mechanism protects the lung against the final stage of congestion, that is leakage of fluids into the alveolar spaces, the alveolar edema. The radiologic findings at chest radiography reflect the anatomo-pathologic alterations.

As severity of congestion increases, the sequence of signs visible on chest radiographs are: (1) vascular opacity "redistribution" towards the upper lobes and distention of the upper pulmonary veins; (2) enlargement and loss of definition of hilar structures; (3) septal lines in the lower lung, indicated as Kerley A and B lines; (4) peribronchial and perivascular cuffing with widening and blurring of the margins; and (5) thickening of interlobar fissures with subpleural fluid accumulation (Figure 1)[8,9].

Redistribution, known also as cephalization, occurs only in the setting of chronic pulmonary venous hypertension, very often encountered in mitral stenosis (Figure 2). Cardiomegaly and pleural effusions are adjunctive radiologic findings quite frequently detected in cardiogenic pulmonary congestion. When congestion increases and becomes alveolar edema, chest radiography shows bilateral and usually symmetric parenchymal opacities, with a central or basilar distribution, without air bronchogram[10] (Figure 3).

The distribution of alveolar edema may be influenced by gravity. In this case performing the examination in supine or orthostatic position and right or left decubitus, may consistently change the radiologic pattern. Moreover, a coexistent condition of chronic obstructive lung disease may influence irregular distribution of edema as fluids tend to leak in the area of the lung where the structure of the organ is less subverted.

In the emphysematous lung, edema of the alveolar spaces will not be imaged because of alveolar destruction in over-inflated areas, while accentuation of interstitial signs of congestion may still being detected at CXR.

In case of large, acute myocardial infarction (MI) that involves the function of the mitral valve, a regional asymmetric distribution of pulmonary edema may produce atypical radiologic patterns that mimic non-cardiogenic edema or, in some cases, even pneumonia (Figure 4).

This pattern is caused by the flow vector due to mitral regurgitation, which may be massively directed toward the right superior pulmonary vein[11]. However, opacities

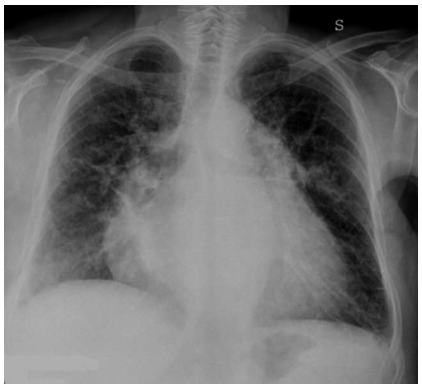

Figure 1 Posterior-anterior chest X-ray in a patient with congestive heart failure and interstitial pulmonary edema. In the figure are shown radiographic signs that suggest interstitial pulmonary edema including enlarged and loss of definition of large pulmonary vessels, both Kerley's A and Kerley's B lines associated with cardiomegaly.

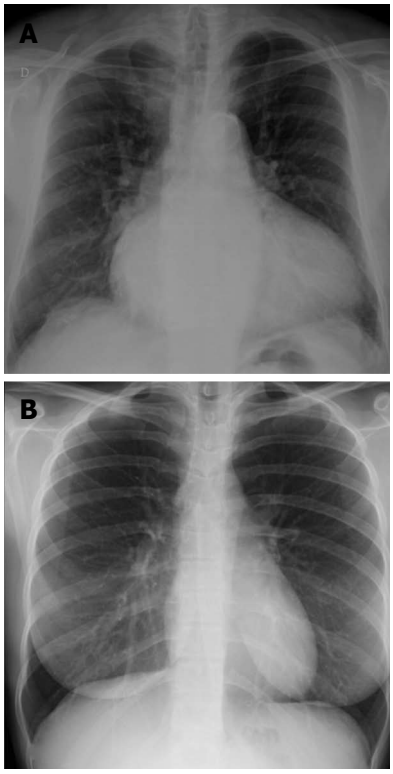

Figure 2 Posterior-anterior chest X-ray demonstrating enlargement of atrial and left ventricles, with redistribution of lung circulation from bases to apex suggestive to pulmonary congestion (A), note the blood vessels are more prominent in the upper lung fields compared to the lung bases, just the opposite of normal (B).

due to alveolar edema may rapidly change their dimension and even dissolve on the effect of treatment. Thus, radiologic follow-up may sometimes contribute to resolve the diagnostic dilemma.

Signs of pulmonary congestion at chest radiography may even precede clinical symptoms. Conversely, pulmonary edema may be still visible radiographically for hours or even days after hemodynamic recovery[12].

To date, CXR represents the first line imaging exam in patients presenting to the emergency department (ED)

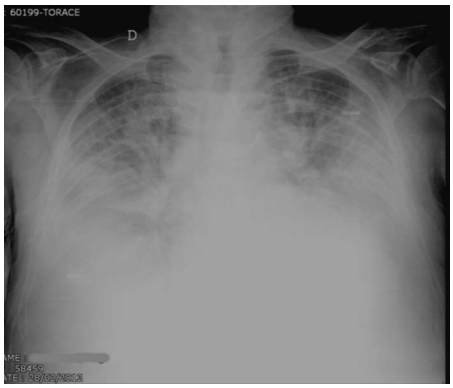

Figure 3 Supine radiogram in a patient with cardiogenic alveolar edema. Note that the vascular perihilar structures are not defined because of the presence of confluent peripheral and gravitational consolidations, with large pleural effusion. Cardiomegaly is also present.

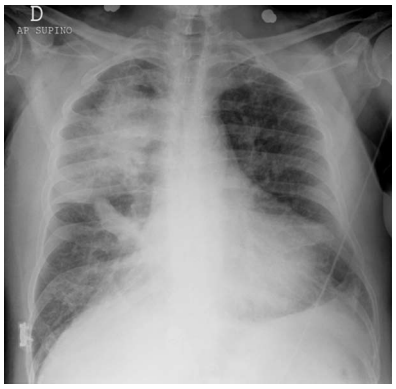

Figure 4 Antero-posterior chest radiograph with asymmetric pulmonary edema with grade 3 mitral insufficiency shows pulmonary edema predominantly within the right upper lobe.

complaining of acute dyspnea. The possibility of correct diagnosis at CXR is greater the more severe and prolonged will be pulmonary congestion, because the radiologic signs are more accurate and clearly visible. Relating the diagnosis of cardiogenic pulmonary congestion, CXR is moderately specific (specificity 76%, 83%), but not very sensitive (50%-68%)[13].

Therefore, CXR does not have a direct role in the pathway for the diagnosis of heart failure, where the standard of care is cardiac and LUS. The main reason of this limitation is that CXR is not sensitive enough, because heart failure cannot be ruled out with certainty in the presence of a normal radiologic pattern. However, our opinion is that CXR is highly useful to diagnose alternative diagnoses when they are, together with decompensated heart failure in the differential.

LUNG ULTRASOUND

Quite recently, LUS opened new perspectives in the bedside evaluation of pulmonary congestion. Many authors produced a growing number of papers showing the power of LUS in diagnosing pulmonary diseases[14-20].

Rather than from technologic progress, development

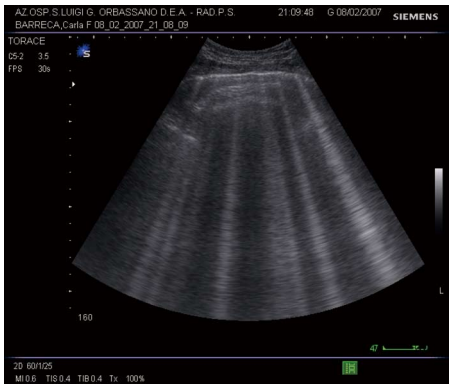

Figure 5 Lung ultrasound scan showing multiple B-lines from a case of cardiogenic pulmonary oedema. When a similar pattern is visualised on multiple locations in the anterior and lateral chest, it is diagnostic of the interstitial syndrome.

of modern LUS is mainly based on discovering the significance of sonographic artifacts[21]. Particularly, some vertical echogenic linear artifacts, known as B-lines, are simple, noninvasive signs of pulmonary interstitial fluid that can be easily evaluated at bedside. B-lines originate from multiple small subpleural air/fluid acoustic interfaces, due to the fact that air and water are two elements with opposite values of acoustic impedance[22]. This phenomenon is related to the contrast between air-filled and water-rich structures, which generate multiple reverberation of the ultrasound beam that is visualized on the screen as linear vertical artifacts, the B-lines (Figure 5).

In the normally aerated lung, only a very few B-lines can be detected by sonography[23].

When the water content increases and air decreases due to disease, the thickened interlobular septa and fluid into the alveolar spaces cause the appearance of multiple and diffuse B-lines (Figure 6)[4,5].

Any condition of the lung where alveolar air is partially lost and interstitial fluids or cellularity are diffusely increased, causes the appearance of B-lines at LUS. B-lines underlines the so called interstitial syndrome.

The fundamental technique for diagnosing interstitial syndrome consists of examining the anterior and lateral chest using four intercostal scans per side, corresponding to the upper and inferior areas anteriorly and the upper and basal areas laterally. A positive scan is characterized by a minimum of three B-lines, whereas a positive examination is defined by at least two positive areas per side[5,17] (Figure 6).

Simple detection of B-lines does not allow differentiation of the disease involving the lung interstitium, but other organ ultrasound signs can be used to confirm the diagnosis of pulmonary congestion in decompensated heart failure. For convenience a focused cardiac sonography can be performed using the same probe used for lung examination, looking for global left ventricle function impairment, which will be detected in about 50% of cases with acute decompensated heart failure[24].

Regarding LUS, other signs than B-lines may be evaluated for differentiating similar patterns of interstitial syndrome from cardiogenic and non-cardiogenic causes. These includes evaluation of pleural sliding and irregularities, distribution of B-lines and sub-pleural consolidations. Some studies showed the reliability of these signs in differentiating signs of cardiogenic pulmonary edema from ARDS and pulmonary fibrosis[25].

The primary diagnosis of pulmonary interstitial fluid in the emergency setting is crucial for the differential diagnosis between a cardiogenic and non-cardiogenic respiratory failure. Some studies showed the usefulness of B-lines as a primary diagnostic test in acute respiratory failure patients[20,26]. Lung ultrasound appears to be particularly useful in differentiating between exacerbation of chronic obstructive pulmonary disease (COPD), a condition that does not show B-lines, and decompensated heart failure. In a study performed in dyspneic patients in the emergency department, diffuse B-lines were detected in 100% of patients with cardiogenic pulmonary oedema but was absent in 92% of cases with exacerbation of COPD and 98.75% of those with normal lungs[26]. Conclusion of the study was that sonographic detection of B-lines might help distinguish pulmonary edema from exacerbation of COPD.

Other studies showed the correlation between B-lines and natriuretic peptides in the primary evaluation of acute decompensated heart failure in the Emergency department[27]. Pulmonary interstitial fluid, sonographically demonstrated by B-lines, was strictly correlated with natriuretic hormones level. Conclusions of these studies was that LUS can be used alone or can provide additional predictive power to natriuretic peptides in the immediate evaluation of dyspneic patients to diagnose the cardiac origin of the symptom.

Another great potential of LUS is that B-lines are highly sensitive to the resolution of lung congestion in patients admitted to the hospital for acute decompensated heart failure. Clearance of B-lines represents a direct sign of effective treatment, but also may be useful to specify the diagnosis in cases where the origin of B-lines cannot be differentiated at a first examination[28].

Finally, LUS may be also useful to diagnose unsuspected conditions when it is performed in combination with other tools, showing similar performances as compared to other more panoramic chest diagnostic imaging tools[29-32].

COMPUTED TOMOGRAPHY

On high resolution computed tomography (HRCT), signs of hydrostatic edema generally results in a combination of septal thickening and ground-glass opacities. Incidence and predominance of these signs is individually variable[33-39] (Figure 7).

Crazy paving and consolidation are also frequently imaged. In some patients, ill-defined perivascular and centrilobular opacities may also be detected, or ground-glass opacity may appear lobular and patchy with a tendency to have a parahilar and gravitational distribution (Figure 8)[40].

There is some evidence that a parahilar or bat wing

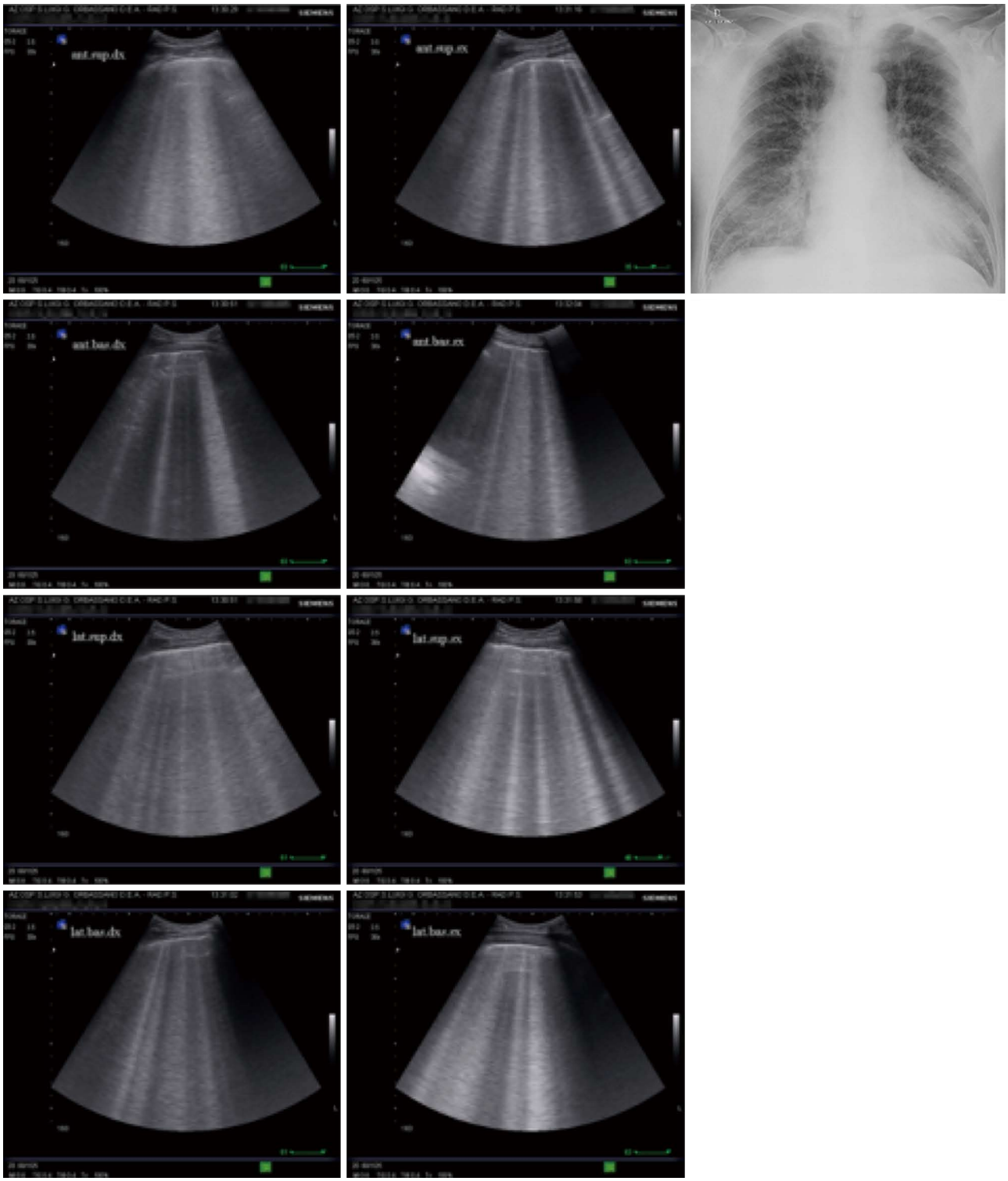

Figure 6 A typical sonographic pattern of diffuse alveolar-interstitial syndrome (left side) and corresponding chest radiograph (right side) in a case of acute cardiogenic pulmonary oedema. In the sonographic images on either side of the radiogram, the presence of multiple adjacent comet-tail artefacts (at least three per scan and in all chest areas examined) can be easily distinguished. The images illustrate the sonographic B+ pattern corresponding to the radiological finding of pulmonary oedema.

distribution of edema is typically found in patients who have a rapid accumulation of fluid[40]. Occasionally edema may have unilateral distribution, as may happen in patients with a prolonged lateral decubitus, or asymmetric and even with bizarre distribution in patients with regional emphysema[29]. In studies on hydrostatic edema in dog lungs, high resolution CT patterns showed predominantly central, peribronchovascular, and posterior distribution of edema, associated with an apparent increased thickness of bronchial walls[30,31].

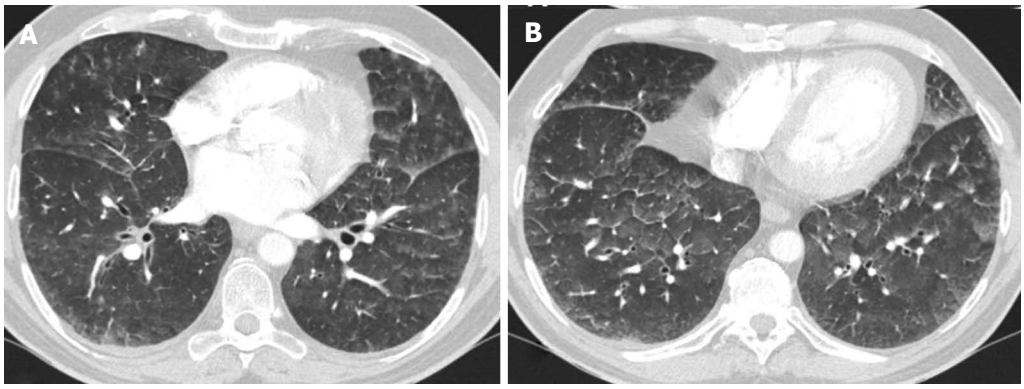

Figure 7 Computed tomography scan through lower lobes shows, limited areas of ground-glass opacity, with thickening of major fissures reflecting subpleural interstitial edema. Is also present interlobular septal and peribronchovascular interstitial thickening.

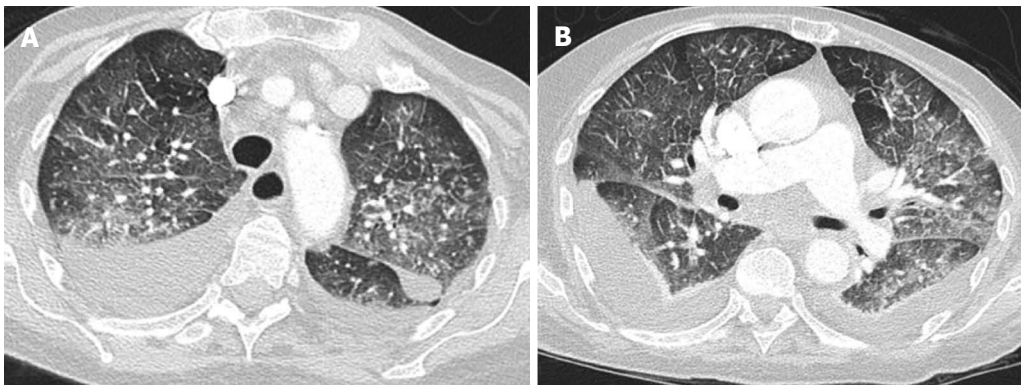

Figure 8 Computed tomography scan through aortic arch and pulmonary arteries planes shows ground-glass opacity with geographic distribution and partial sparing of the lung periphery. Thickening of interlobular septa and sub-pleural edema and bilateral pleural effusion with passive atelectasis of lower lobes is also present.

Table 1 A proposed diagnostic alghoritm for the diagnosis of pulmonary edema

Lung ultrasound	Chest X-ray	Chest CT
First line in emergency and critically ill monitoring and to assess pulmonary congestion in typical clinical presentation	Second line to confirm doubtful cases in emergency or critically ill after haemodynamic recovery	Third step differential diagnosis of Pulmonary Embolism

CT: Computed tomography.

Table 2 Diagnostic accuracy of chest X-ray and ultrasound in patients with heart failure

	Sensitivity
X-ray	56%
US	100%

Difference of patients showing radiologic and ultrasound (US) signs of congestive heart faliure (personal data not pubblished).

STRENGTHS AND WEAKNESSES OF INTEGRATED USE OF LUS, CHEST X-RAY AND CT FOR THE DIAGNOSIS OF CARDIOGENIC PULMONARY EDEMA

Imaging has a fundamental role in the diagnosis of heart failure, but the efficacy of the diagnostic process is highly dependent from the ability to integrate information drawn from LUS, chest radiography and CT (Table 1).

Chest radiography has the great advantage of combining relative low cost with the panoramic view that allows exclusion of many pulmonary conditions that comes into the differential diagnosis. CT scan is the best method to have a panoramic thoracic view, and much more sensitive than chest radiography for the first diagnosis of many conditions, like pulmonary embolism and early phase of cardiogenic pulmonary edema. However, it has many limitations due to costs, availability in emergency situations and relatively high radiation exposure. However, in recent years technological advances have made it possible to improve the modulation of dose exposure to follow the principles of radiological protection. Besides radiation exposure, low availability and feasibility are other fundamental limitations. CT scan cannot be performed as routine technique in heart failure because of the high prevalence of this disease and high costs of use.

However, while LUS and chest radiography are the first choice imaging technique in most cases, in selected cases where multiple conditions are in the differential, CT

scan may become the method of reference. This is the case in acutely dyspneic patients when the differential diagnosis with pulmonary embolism is a challenge. In other cases, when the differential diagnosis includes diffuse parenchymal lung diseases, the high-resolution CT of the chest may be useful to rule-out or confirm pulmonary congestion.

Lung ultrasound has the limitation of being a surface imaging technique far less panoramic than chest radiography and CT scan. However, the great advantages of LUS are a higher sensitivity than chest radiography in the diagnosis of the early signs of interstitial thickening due to pulmonary congestion, and the possibility to perform the examination at bedside during the first clinical approach (Table 2).

CONCLUSION

In the diagnostic imaging of pulmonary congestion due to decompensated heart failure, LUS and CXR are the most used diagnostic tools. Lung ultrasound does not fully replace CXR but may be of great help in some specific situations, like in the emergency setting when a prompt diagnostic evaluation of dyspneic patients at bedside is needed and also for monitoring clinical evolution. Moreover, LUS outperforms conventional radiology for the diagnosis of early signs of pulmonary congestion and should always be considered when radiologic signs are not detected on CXR but heart failure is still considered a possibility. However, LUS standing alone has a limited specificity for cardiogenic pulmonary congestion. Indeed, the main ultrasound signs of the interstitial syndrome, the B lines, are also detected in other pulmonary conditions, even chronic, characterized by loss of aeration and increase in fluids. Moreover, CXR is superior to LUS as a panoramic imaging modality that allows an immediate and comprehensive evaluation of the thoracic structures. CT scan is a powerful method for the evaluation of the thorax and even more panoramic, but is of limited use in the first diagnosis of decompensated heart failure in comparison to CXR and LUS. However, in selected cases it may be of help in the differential diagnosis of interstitial lung diseases or other causes of respiratory failure. Very often, in cases when a CT study is performed to investigate other conditions, the diagnosis of pulmonary congestion is incidental.

Integration of information obtained by the correct use of these three thoracic imaging, may improve the accuracy of the diagnostic process for cardiogenic pulmonary edema. The modern clinician and radiologist should be aware of the potential and limitations of these diagnostic tools and be prepared to integrate information derived from a correct use of ultrasound, conventional radiology and CT.

ACKNOWLEDGMENTS

We thanks for his support Professor Andrea Veltri, Chief of Radiology Unit, AOUS Luigi Gonzaga, Orbassano (TO)/IT.

REFERENCES

1 **Stevenson LW**, Perloff JK. The limited reliability of physical signs for estimating hemodynamics in chronic heart failure. *JAMA* 1989; **261**: 884-888 [PMID: 2913385 DOI: 10.1001/jama.261.6.884]
2 **Chakko S**, Woska D, Martinez H, de Marchena E, Futterman L, Kessler KM, Myerberg RJ. Clinical, radiographic, and hemodynamic correlations in chronic congestive heart failure: conflicting results may lead to inappropriate care. *Am J Med* 1991; **90**: 353-359 [PMID: 1825901 DOI: 10.1016/0002-9343(91)80016-F]
3 **Badgett RG**, Lucey CR, Mulrow CD. Can the clinical examination diagnose left-sided heart failure in adults? *JAMA* 1997; **277**: 1712-1719 [PMID: 9169900 DOI: 10.1001/jama.277.21.1712]
4 **Lichtenstein D**, Mézière G, Biderman P, Gepner A, Barré O. The comet-tail artifact. An ultrasound sign of alveolar-interstitial syndrome. *Am J Respir Crit Care Med* 1997; **156**: 1640-1646 [PMID: 9372688 DOI: 10.1164/ajrccm.156.5.96-07096]
5 **Volpicelli G**, Mussa A, Garofalo G, Cardinale L, Casoli G, Perotto F, Fava C, Frascisco M. Bedside lung ultrasound in the assessment of alveolar-interstitial syndrome. *Am J Emerg Med* 2006; **24**: 689-696 [PMID: 16984837 DOI: 10.1016/j.ajem.2006.02.013]
6 **Lichtenstein D**, Mezière G, Biderman P, Gepner A. The comet-tail artifact: an ultrasound sign ruling out pneumothorax. *Intensive Care Med* 1999; **25**: 383-388 [PMID: 10342512 DOI: 10.1007/s001340050862]
7 **Storto ML**, Kee ST, Golden JA, Webb WR. Hydrostatic pulmonary edema: high-resolution CT findings. *AJR Am J Roentgenol* 1995; **165**: 817-820 [PMID: 7676973 DOI: 10.2214/ajr.165.4.7676973]
8 **Heitzman ER**, Ziter FM. Acute interstitial pulmonary edema. *Am J Roentgenol Radium Ther Nucl Med* 1966; **98**: 291-299 [PMID: 5925099 DOI: 10.2214/ajr.98.2.291]
9 **Milne EN**, Pistolesi M, Miniati M, Giuntini C. The radiologic distinction of cardiogenic and noncardiogenic edema. *AJR Am J Roentgenol* 1985; **144**: 879-894 [PMID: 3872571 DOI: 10.2214/ajr.144.5.879]
10 **Maffessanti M**, Lucangelo U, Pellegrin A. Radiologia toracica in terapia intensiva. *Radiol Med* 2010; **115**: S34-S44
11 **Cardinale L**, Volpicelli G, Lamorte A, Martino J. Revisiting signs, strengths and weaknesses of Standard Chest Radiography in patients of Acute Dyspnea in the Emergency Department. *J Thorac Dis* 2012; **4**: 398-407 [PMID: 22934143]
12 **Pistolesi M**, Miniati M, Milne EN, Giuntini C. The chest roentgenogram in pulmonary edema. *Clin Chest Med* 1985; **6**: 315-344 [PMID: 3907943]
13 **Mant J**, Doust J, Roalfe A, Barton P, Cowie MR, Glasziou P, Mant D, McManus RJ, Holder R, Deeks J, Fletcher K, Qume M, Sohanpal S, Sanders S, Hobbs FD. Systematic review and individual patient data meta-analysis of diagnosis of heart failure, with modelling of implications of different diagnostic strategies in primary care. *Health Technol Assess* 2009; **13**: 1-207, iii [PMID: 19586584 DOI: 10.3310/hta13320]
14 **Lichtenstein DA**. Ultrasound in the management of thoracic disease. *Crit Care Med* 2007; **35**: S250-S261 [PMID: 17446785 DOI: 10.1097/01.CCM.0000260674.60761.85]
15 **Volpicelli G**, Silva F, Radeos M. Real-time lung ultrasound for the diagnosis of alveolar consolidation and interstitial syndrome in the emergency department. *Eur J Emerg Med* 2010; **17**: 63-72 [PMID: 20945542 DOI: 10.1097/MEJ.0b013e3283101685]
16 **Volpicelli G**. Lung sonography. *J Ultrasound Med* 2013; **32**: 165-171 [PMID: 23269722]

17 **Volpicelli G**, Elbarbary M, Blaivas M, Lichtenstein DA, Mathis G, Kirkpatrick AW, Melniker L, Gargani L, Noble VE, Via G, Dean A, Tsung JW, Soldati G, Copetti R, Bouhemad B, Reissig A, Agricola E, Rouby JJ, Arbelot C, Liteplo A, Sargsyan A, Silva F, Hoppmann R, Breitkreutz R, Seibel A, Neri L, Storti E, Petrovic T. International evidence-based recommendations for point-of-care lung ultrasound. *Intensive Care Med* 2012; **38**: 577-591 [PMID: 22392031 DOI: 10.1007/s00134-012-2513-4]

18 **Bouhemad B**, Zhang M, Lu Q, Rouby JJ. Clinical review: Bedside lung ultrasound in critical care practice. *Crit Care* 2007; **11**: 205 [PMID: 17316468 DOI: 10.1186/cc5668]

19 **Picano E**, Frassi F, Agricola E, Gligorova S, Gargani L, Mottola G. Ultrasound lung comets: a clinically useful sign of extravascular lung water. *J Am Soc Echocardiogr* 2006; **19**: 356-363 [PMID: 16500505 DOI: 10.1016/j.echo.2005.05.019]

20 **Volpicelli G**, Cardinale L, Garofalo G, Veltri A. Usefulness of lung ultrasound in the bedside distinction between pulmonary edema and exacerbation of COPD. *Emerg Radiol* 2008; **15**: 145-151 [PMID: 18236088 DOI: 10.1007/s10140-008-0701-x]

21 **Lichtenstein DA**, Mezière G, Lascols N, Biderman P, Courret JP, Gepner A, Goldstein I, Tenoudji-Cohen M. Ultrasound diagnosis of occult pneumothorax. *Crit Care Med* 2005; **33**: 1231-1238 [PMID: 15942336 DOI: 10.1097/01.CCM.0000164542.86954.B4]

22 **Soldati G**, Copetti R, Sher S. Sonographic interstitial syndrome: the sound of lung water. *J Ultrasound Med* 2009; **28**: 163-174 [PMID: 19168766]

23 **Volpicelli G**, Caramello V, Cardinale L, Mussa A, Bar F, Frascisco MF. Detection of sonographic B-lines in patients with normal lung or radiographic alveolar consolidation. *Med Sci Monit* 2008; **14**: CR122-CR128 [PMID: 18301355]

24 **Vasan RS**, Larson MG, Benjamin EJ, Evans JC, Reiss CK, Levy D. Congestive heart failure in subjects with normal versus reduced left ventricular ejection fraction: prevalence and mortality in a population-based cohort. *J Am Coll Cardiol* 1999; **33**: 1948-1955 [PMID: 10362198 DOI: 10.1016/S0735-1097(99)00118-7]

25 **Copetti R**, Soldati G, Copetti P. Chest sonography: a useful tool to differentiate acute cardiogenic pulmonary edema from acute respiratory distress syndrome. *Cardiovasc Ultrasound* 2008; **6**: 16 [PMID: 18442425 DOI: 10.1186/1476-7120-6-16]

26 **Lichtenstein D**, Mezière G. A lung ultrasound sign allowing bedside distinction between pulmonary edema and COPD: the comet-tail artifact. *Intensive Care Med* 1998; **24**: 1331-1334 [PMID: 9885889 DOI: 10.1007/s001340050771]

27 **Gargani L**, Frassi F, Soldati G, Tesorio P, Gheorghiade M, Picano E. Ultrasound lung comets for the differential diagnosis of acute cardiogenic dyspnoea: a comparison with natriuretic peptides. *Eur J Heart Fail* 2008; **10**: 70-77 [PMID: 18077210 DOI: 10.1016/j.ejheart.2007.10.009]

28 **Volpicelli G**, Caramello V, Cardinale L, Mussa A, Bar F, Frascisco MF. Bedside ultrasound of the lung for the monitoring of acute decompensated heart failure. *Am J Emerg Med* 2008; **26**: 585-591 [PMID: 18534289 DOI: 10.1016/j.ajem.2007.09.014]

29 **Maffessanti M**, Dalpiaz G. Pulmonary Edema in Diffuse Lung Disease: Clinical Features, Pathology, HRCT. Milan: Springer, 2004: 186-189

30 **Forster BB**, Müller NL, Mayo JR, Okazawa M, Wiggs BJ, Paré PD. High-resolution computed tomography of experimental hydrostatic pulmonary edema. *Chest* 1992; **101**: 1434-1437 [PMID: 1582313 DOI: 10.1378/chest.101.5.1434]

31 **Scillia P**, Delcroix M, Lejeune P, Mélot C, Struyven J, Naeije R, Gevenois PA. Hydrostatic pulmonary edema: evaluation with thin-section CT in dogs. *Radiology* 1999; **211**: 161-168 [PMID: 10189466 DOI: 10.1148/radiology.211.1.r99ap07161]

32 **Volpicelli G**, Melniker LA, Cardinale L, Lamorte A, Frascisco MF. Lung ultrasound in diagnosing and monitoring pulmonary interstitial fluid. *Radiol Med* 2013; **118**: 196-205 [PMID: 22744356 DOI: 10.1007/s11547-012-0852-4]

33 **Ketai LH**, Godwin JD. A new view of pulmonary edema and acute respiratory distress syndrome. *J Thorac Imaging* 1998; **13**: 147-171 [PMID: 9671417 DOI: 10.1097/00005382-199807000-00001]

34 **Gluecker T**, Capasso P, Schnyder P, Gudinchet F, Schaller MD, Revelly JP, Chiolero R, Vock P, Wicky S. Clinical and radiologic features of pulmonary edema. *Radiographics* 1999; **19**: 1507-1531; discussion 1507-1531 [PMID: 10555672 DOI: 10.1148/radiographics.19.6.g99no211507]

35 **Todo G**, Herman PG. High-resolution computed tomography of the pig lung. *Invest Radiol* 1986; **21**: 689-696 [PMID: 3580031 DOI: 10.1097/00004424-198609000-00003]

36 **Webb WR**, Stein MG, Finkbeiner WE, Im JG, Lynch D, Gamsu G. Normal and diseased isolated lungs: high-resolution CT. *Radiology* 1988; **166**: 81-87 [PMID: 3336706]

37 **Bessis L**, Callard P, Gotheil C, Biaggi A, Grenier P. High-resolution CT of parenchymal lung disease: precise correlation with histologic findings. *Radiographics* 1992; **12**: 45-58 [PMID: 1734481 DOI: 10.1148/radiographics.12.1.1734481]

38 **Malagari K**, Nikita A, Alexopoulou E, Brountzos E, Papathanasiou M, Mitromaras J, Zakynthinos E, Papiris S, Kelekis DA. Cirrhosis-related intrathoracic disease. Imaging features in 1038 patients. *Hepatogastroenterology* 2005; **52**: 558-562 [PMID: 15816477]

39 **Tanaka N**, Matsumoto T, Miura G, Emoto T, Matsunaga N. HRCT findings of chest complications in patients with leukemia. *Eur Radiol* 2002; **12**: 1512-1522 [PMID: 12042962 DOI: 10.1007/s003300101112]

40 **Mukhopadhyay P**, Rezzoug F, Webb CL, Pisano MM, Greene RM. Suppression of chondrogenesis by Id helix-loop-helix proteins in murine embryonic orofacial tissue. *Differentiation* 2009; **77**: 462-472 [PMID: 19349107]

P- Reviewers: Tripoliti EE, Yew DT **S- Editor**: Ji FF
L- Editor: A **E- Editor**: Zhang DN

World Journal of Radiology

Submit a Manuscript: http://www.wjgnet.com/esps/
Help Desk: http://www.wjgnet.com/esps/helpdesk.aspx
DOI: 10.4329/wjr.v6.i6.238

World J Radiol 2014 June 28; 6(6): 238-251
ISSN 1949-8470 (online)
© 2014 Baishideng Publishing Group Inc. All rights reserved.

TOPIC HIGHLIGHT

WJR 6th Anniversary Special Issues (7): PET

Application of fluorodeoxyglucose positron emission tomography in the management of head and neck cancers

Farzan Siddiqui, Min Yao

Farzan Siddiqui, Department of Radiation Oncology, Henry Ford Health System, Detroit, MI 48202, United States
Min Yao, Department of Radiation Oncology, University Hospitals Case Medical Center, Cleveland, OH 44106, United States
Author contributions: Both authors contributed to review of literature and manuscript preparation.
Correspondence to: Min Yao, MD, PhD, Department of Radiation Oncology, University Hospitals Case Medical Center, 11100 Euclid Avenue, Cleveland, OH 44106, United States. min.yao@uhhospitals.org
Telephone: +1-216-8443103 Fax: +1-216-8442005
Received: January 3, 2014 Revised: February 16, 2014
Accepted: March 7, 2014
Published online: June 28, 2014

Abstract

The use of fluorodeoxyglucose positron emission tomography (FDG PET) scan technology in the management of head and neck cancers continues to increase. We discuss the biology of FDG uptake in malignant lesions and also discuss the physics of PET imaging. The various parameters described to quantify FDG uptake in cancers including standardized uptake value, metabolic tumor volume and total lesion glycolysis are presented. PET scans have found a significant role in the diagnosis and staging of head and neck cancers. They are also being increasingly used in radiation therapy treatment planning. Many groups have also used PET derived values to serve as prognostic indicators of outcomes including loco-regional control and overall survival. FDG PET scans are also proving very useful in assessing the efficacy of treatment and management and follow-up of head and neck cancer patients. This review article focuses on the role of FDG-PET computed tomography scans in these areas for squamous cell carcinoma of the head and neck. We present the current state of the art and speculate on the future applications of this technology including protocol development, newer imaging methods such as combined magnetic resonance and PET imaging and novel radiopharmaceuticals that can be used to further study tumor biology.

© 2014 Baishideng Publishing Group Inc. All rights reserved.

Key words: Fluorodeoxyglucose; Positron emission tomography; Squamous cell carcinoma; Head and neck cancer; Radiation therapy planning

Core tip: Fluorodeoxyglucose positron emission tomography (FDG PET) computed tomography (CT) scans should be obtained for patients for squamous cell carcinoma of the head and neck whenever clinically indicated and feasible. Pre-treatment scans are helpful in detecting the sites of primary cancer, staging the tumor and ruling out the presence of distant metastases. For patients undergoing radiation therapy, PET/CT scans provide anatomic as well as functional information to aid in treatment planning. After completion of radiotherapy, PET scans should be obtained approximately 12 wk after treatment to assess treatment response and to determine if any salvage therapy is required for persistent, recurrent or metastatic disease.

Siddiqui F, Yao M. Application of fluorodeoxyglucose positron emission tomography in the management of head and neck cancers. *World J Radiol* 2014; 6(6): 238-251 Available from: URL: http://www.wjgnet.com/1949-8470/full/v6/i6/238.htm DOI: http://dx.doi.org/10.4329/wjr.v6.i6.238

INTRODUCTION

Head and neck cancers (HNC) account for approximately 650000 new cancers each year across the world and result in about 350000 deaths, representing 6% of all cancer cases[1,2]. In the United States, approximately 52000 new

cases of oral cavity, pharyngeal and laryngeal cancers are diagnosed every year with approximately 11000 deaths[3]. Approximately 95% of these are squamous cell carcinomas (HNSCC) and they often present in locally advanced stages. The treatment of head and neck cancers involves a multi-disciplinary approach and includes surgery, radiation therapy and chemotherapy. Traditional staging approaches for head and neck cancers include clinical examination and surgical pathologic staging. The advent of concurrent radiation and chemotherapy for organ preservation in head and neck cancers has reduced the incidence of surgical resection especially in locally advanced larynx cancers and oropharynx cancers[4,5]. However, this has also brought forth the need to have detailed non-invasive imaging techniques to accurately identify tumor size and location, cervical lymph node involvement and presence or absence of distant metastases. The use of computed tomography (CT) scans and magnetic resonance imaging (MRI) scans allowed structural and anatomical information to be obtained and vastly improved the ability of oncologists to clinically stage these patients appropriately. However, the use of fluorine-18-fluorodeoxyglucose positron-emission tomography (FDG-PET) has added a new biologic and functional end-point to these imaging techniques and opened a whole new arena for research and development in management of head and neck cancers. Additionally, PET/CT and PET/MRI combinations are now able to provide both anatomic and functional information in co-registered images.

The review will focus on the current applications of FDG PET/CT scans in management of squamous cell cancers of the head and neck. The use of PET/MRI and FDG PET/CT for other head and neck cancers (*e.g.*, salivary gland, thyroid cancers *etc.*) is beyond the scope of this review.

BIOLOGY OF FDG-UPTAKE

Rapidly proliferating cancers cells utilize glucose as a source of energy and metabolism. Glucose undergoes glycolysis after intracellular transportation. This transportation is mediated by a family of glucose transporter proteins (GLUTs)[6-8]. These trans-membrane proteins allow energy independent transport of glucose across the hydrophobic cell membrane. Thirteen GLUTs have been identified of which GLUT1, GLUT3, and GLUT4 have high affinity for glucose. The expression of GLUTs is induced by hypoxia-inducible factor, growth factors and various oncogenes[9]. Increased expression of GLUT1 has been found in many cancers, including head and neck cancer[9]. The degree of expression of GLUT1 has also been shown to be associated with aggressiveness of the cancer. Elevated glycolytic activity and increased expression of GLUT1 are found in advanced cancer stages and predict significantly poorer treatment outcomes[10-13].

Fluorine^{18}-FDG (^{18}F-FDG) is an analog of glucose with ^{18}F occupying the position of oxygen on carbon-2. Similar to glucose, GLUTs facilitate the transport of ^{18}F-FDG into the cell. In the next step, both glucose and FDG are phosphorylated by the hexokinase enzyme. Glucose, upon phosphorylation, enters the glycolytic pathway for energy production. FDG, on the other hand, cannot undergo glycolysis and is trapped as FDG-6-phosphate in the intracellular environment. This trapped FDG can then be imaged to spatially locate the metabolically active cancer cells. FDG uptake in cancer cells of HNSCC was shown to be significantly correlated with cell proliferation by flow cytometry[14,15].

PHYSICS OF PET IMAGING

A detailed description of the physics of FDG-PET scanning is beyond the scope of this review. However, in brief, at the heart of this imaging technique is the radioisotope ^{18}F. It is produced using a cyclotron and has a half-life of 110 min allowing it to be transported for use in PET scanner facilities.

^{18}F decays by positron (β^+) emission 97% of the time and is converted to oxygen-18. The emitted positron travels a short distance in soft tissue, decelerates rapidly and interacts with an electron near the end of its track. This interaction is called the annihilation reaction and mass is converted to energy with the release of two 0.511MeV photons which travel outwards at 180° to each other. These annihilation photons are detected by scintillators and a simultaneous or coincident detection of these photons makes it possible to spatially localize the point of origin. The information is collected on a multitude of such coincident events and processed to generate a PET image.

Nowadays, most PET scans are co-registered with simultaneously obtained CT scans to produce PET/CT images which give functional information along with anatomic co-localization. For areas like the head and neck a smaller area can be scanned with intravenous contrast administration to obtain further normal tissue anatomy and tumor extent.

QUANTITATIVE IMAGE INTERPRETATION

In order to be used as a valid imaging biomarker, accurate and reproducible quantification of FDG uptake is necessary. A simplified measurement using standardized uptake value (SUV), given by the following formula, is now the most widely used method for the quantification of FDG up take.

$$SUV = \frac{\text{Tissue activity } (\mu Ci / ml)}{\text{Injected Dose } (mCi) \Big/ \text{Body weight } (kg)}$$

In this formula, tissue activity is the radioactivity measured by the PET scanner within a region of interest (ROI) or the maximal value; injected dose is the dose of ^{18}F-FDG administered, corrected for physical decay. The SUV in this formula represents the activity of ^{18}F-FDG within the tumor measured over a certain interval after ^{18}F-FDG

injection and normalized to the dose of ^{18}F-FDG administered and to the body weight[16].

There are many different factors that can affect ^{18}F-FDG uptake and its subsequent quantification. The biologic factors include blood glucose level, interval between injection and start of PET study, patient motion and breathing, patient comfort, and inflammatory process near or at the tumor. There are also many technical and physical factors such as attenuation correction, calibration, image reconstruction, data analysis, *etc*, which are beyond the scope of this review and have been discussed by others[17-20]. Despite these, it has been shown that there is a good correlation between SUV and glucose utilization rate in various cancers including HNSCC[21].

Various forms of SUV-based parameters have been described in literature. These include: (1) SUVmax- This measures the highest (maximal) SUV in a region of interest. This has been the most common used parameter in clinical practice as it is thought to be the most reproducible and independent of how the ROI is defined. However, it represents only a single point within the tumor/lesion and may not be representative of the entire tumor volume; (2) SUVmean or SUVaverage- This value may provide a more global picture of the tumor activity as it averages the intensity of uptake in a region of interest (ROI). This, however, suffers from the subjectivity and variability of the definition of this ROI which may differ between individuals and institutions; (3) Metabolic tumor volume (MTV)- This is measured in cubic centimeters and represents the tumor volume with active FDG uptake. There is no standard way for tumor segmentation from PET images (For further discussion, refer to Chapter 4 on PET in radiotherapy treatment planning). Threshold-based method is often used. Some authors used a threshold of SUV > 2.5. Others used 40% or 50% SUVmax as a threshold. The MTV is measured as the tumor volume with SUV above the threshold selected. However, the volumes vary significantly depending on the threshold selected; and (4) Total lesion glycolysis (TLG) - This is a product of the tumor volume, determined by CT - scan or MRI, and SUVmean.

USE OF PET/CT IN THE DIAGNOSIS AND STAGING OF HEAD AND NECK CANCERS

Primary cancers of the head and neck are mainly diagnosed by clinical examination in the office and supplemented by imaging studies such as CT scans and MRI. Staging of the primary tumor, *i.e*., T-stage in the American Joint Committee on Cancer (AJCC) staging system, mainly depends on the tumor size and invasion of the primary tumor, which is better assessed by CT and MRI imaging.

Occasionally, in about 2%-9% of cases, patients may present with a lymph node in the neck with no obvious primary site visible on clinical or routine diagnostic imaging tests[22]. Such cases are labeled as unknown or occult primary head and neck cancers. Pathologic evaluation of the nodes, usually by fine needle aspiration, may reveal a diagnosis of squamous cell carcinoma or adenocarcinoma. Squamous cell histology indicates that the primary site is likely in the head and neck while adenocarcinomas mainly arise below the clavicle (*e.g*., lung cancer, gastric cancer). The traditional method for detection of the primary site in cases of squamous cell histology involves examination under anesthesia and random biopsies from the nasopharynx, oropharynx, hypopharynx, larynx and any mucosal areas which appear abnormal. Tonsillectomy is often performed. These maneuvers are able to detect the primary site in about half of the cases initially labeled as unknown primary head and neck cancers[23].

FDG-PET scans have been proven to be an invaluable tool in these cases. Rusthoven *et al*[24] summarized the results of 16 published studies with a combined total of 302 patients to evaluate the role FDG-PET in unknown primary head and neck cancers. They reported that FDG-PET was able to detect primary tumors in 24.5% (range, 5% to 73% in various studies) cases where conventional methods were unsuccessful. The primary site was found at the base of tongue in 27 patients (24.3%), tonsils in 20 patients (18.0%) and below the clavicle in 27 patients (24.3%). The sensitivity, specificity, and accuracy of FDG-PET in the detection of primary tumors were 88.3%, 74.9%, and 78.8%, respectively. Interestingly, PET scans were able to identify an additional 16% regional nodal metastases and 11% distant metastases previously undiscovered. Several prospective studies have confirmed these findings[22,25]. Rudmik *et al*[25] recently reported results of 30 patients who underwent PET/CT. PET/CT was performed after conventional workup and prior to operative panendoscopy. The surgeons were blinded to the results. Patients had routine examination under anesthesia and directed biopsies, and the PET/CT results were then revealed to the surgeon intraoperatively. Additional biopsies were taken if the PET/CT was positive. The traditional work-up identified tumors in 25% of patients, whereas PET/CT-directed biopsies revealed the primary lesion in 55% of patients. The sensitivity, specificity, positive predictive value, and negative predictive value of PET/CT in detection of primary tumor were 92%, 63%, 79%, and 83%, respectively.

Detection of the site of primary cancer allows directed therapy to the tumor (surgery or radiation therapy) while sparing or minimizing the toxicity to uninvolved mucosal areas or tissues. The current paradigm for diagnosis and staging work-up for unknown primary cancers involves obtaining a PET/CT and then obtaining directed biopsies from the suspicious areas. Figure 1 illustrates a patient who presented with multiple left neck nodes. Conventional workup failed to identify the primary tumor but PET showed the primary tumor in left base of tongue.

As noted above, PET scans have also helped in identification of previously unidentified involved cervical

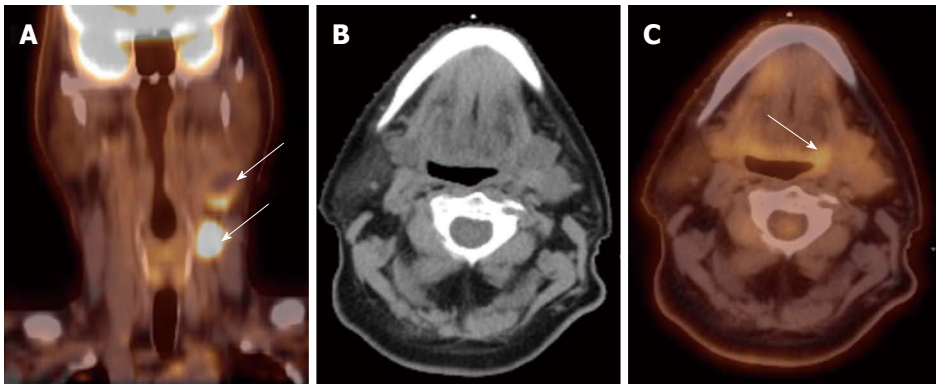

Figure 1 Computed tomography. A: A patient presented with multiple left neck nodes (arrows); B: The conventional methods as well as the computed tomography (CT) imaging could not identify the primary tumor; C: A positron emission tomography/CT scan showed increased fluorodeoxyglucose uptake in the left base of tongue (arrow) and a directed biopsy of this area confirmed the primary site.

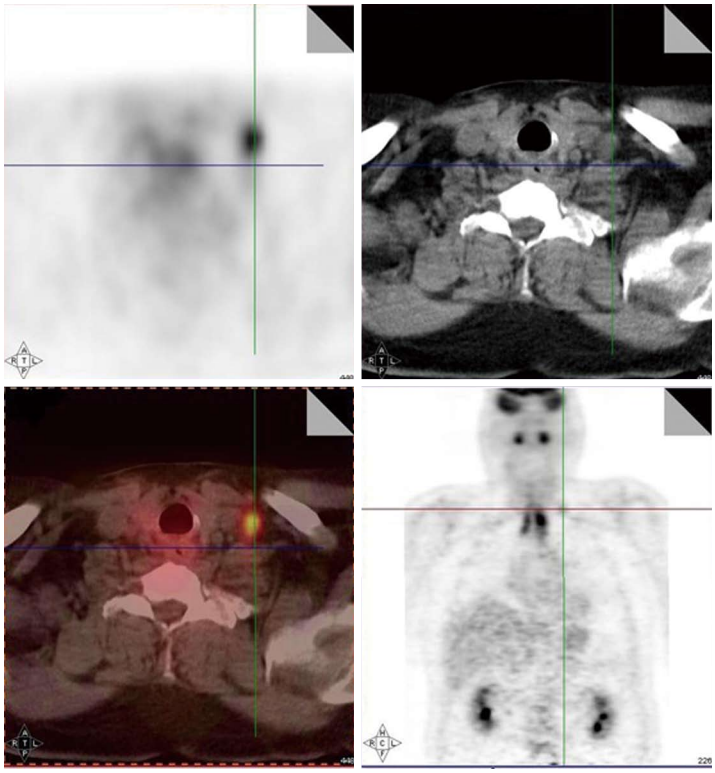

Figure 2 Increased fluorodeoxyglucose positron-uptake in the low neck revealed a metastatic lymph node which would otherwise be difficult to detect because of the presence of muscular and vascular structures in this region of the neck.

lymph nodes. Various CT and MRI based criteria have been developed to label lymph nodes are being involved by cancer or not[26]. However, this may still result in 20%-30% rate of false-positive and false-negative results. Various reports comparing FDG-PET with other imaging modalities including ultrasound, CT and MRI have consistently reported a much higher sensitivity and specificity for PET scans when compared with the gold-standard, surgical lymph node dissection[27,28]. This has specially been helpful in detecting lymph nodes which are at a distance from the primary or in the contralateral neck, especially when the lymph node has not reached size criteria by CT/MRI. PET is also very helpful in detecting involved lymph nodes in the lower neck where there are complex muscular and vascular structures (Figure 2). The average sensitivity and specificity for PET scan to detect involved nodes are reported to be 90% or higher[27].

Local-regionally advanced head and neck cancers metastasize to mediastinal lymph nodes, lungs, bone and liver. PET scans are also helpful in ruling out presence of distant metastases as PET images in head and neck cancer are often obtained from skull base to hips and PET are more sensitive in small metastasis than CT. Various reports have documented the incidence of distant metastases as detected by PET scans ranging from 6% to 25% for stage Ⅲ/Ⅳ head and neck cancers[29-34]. The sensitivity and specificity of PET scans for the detection of metastases are 77% and 94%, respectively. Hearle *et al*[35] noted distant metastases in 10% of 299 patients evaluated with 97% sensitivity and 96% specificity. These PET findings resulted in a change in the management plan in 8% to 15% of cases[30,36]. Figure 3 shows a head and neck

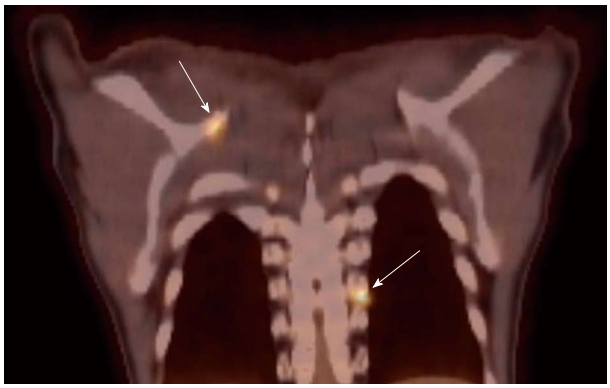

Figure 3 Small bone metastases detected in a patient with head and neck squamous cell carcinoma (arrow). These lesions were not visible on the computed tomography scan.

cancer patient with small bone metastases detected by PET scan but these lesions were missed in the CT scan.

The use of tobacco products (chewing and smoking) and alcohol have been associated with the development of head and neck cancers. This risk extends to other sites of the aero-digestive tract including lung and esophageal cancers. Synchronous primary cancers have been noted in approximately 10% of head and neck cancer patients. Strobel *et al*[37] reported 69 synchronous primary cancers in 62 patients among 589 consecutive patients imaged with PET scans. Most (80%) of these were in the upper aero-digestive tract. A recent report from Japan noted a higher rate (18%) of second primary cancers among 230 head and neck cancer patients[38]. Evaluation of the diagnostic sensitivity showed that PET scans were most likely to detect second primaries in other head and neck sites and lungs while the sensitivity for finding gastric and esophageal cancers was much lower at 25% and 7.6%, respectively. Needless to say, the discovery of these second primary cancers resulted in a change in the management plan for these patients. Figure 4 shows a patient who presented with right oral tongue cancer and PET was obtained as part of the workup that revealed he also had a cancer in the soft palate as well in the upper esophagus. Figure 5 is an example of a patient with a synchronous laryngeal and lung squamous cell carcinomas.

RADIATION THERAPY PLANNING

Radiation treatment plays an important role in the management of head and neck cancer. Radiotherapy is given as a definitive treatment when the tumor is not resectable or when organ preservation is preferable[5,39]. Radiotherapy is also given to patients who have high risk pathology features after surgery[40,41]. Chemotherapy is often administrated concurrently with radiotherapy in locally advanced disease.

In the past decade, intensity-modulated radiotherapy (IMRT) has become a standard radiation technique in head and neck cancer[42,43]. IMRT is a highly conformal radiation technique which allows delivery of different radiation dose to different adjacent structures, also called dose painting, thus enabling delivery of high dose to the tumor targets while sparing the normal tissues. The use of IMRT has led to a reduction in xerostomia and improvements in quality of life following treatment[44-46]. However, highly conformal treatments can lead to disease not being included in the high-dose radiation treatment volume, resulting in locoregional failures. On the other hand, over-drawing the target volumes can result in high-dose radiation being unnecessarily delivered to normal tissues that may lead to increased toxicities. Therefore, accurate delineation of the tumor volume and regions at risk are critical in order to achieve the best treatment outcomes.

Since FDG PET scan has a high sensitivity in detecting tumor, it plays an important role in radiation treatment planning especially in IMRT planning. FDG PET scan is routinely obtained and co-registered with treatment planning CT images for treatment planning. Currently there are following several practical applications of PET in radiation treatment planning: (1) Detecting small lymph nodes that are not size criteria in CT and including these nodes in high dose target. In general, lymph nodes less than 1.0 cm in CT or MRI are usually called benign. However, PET scan has higher resolution and can detect malignant node as small as 0.5 to 0.6 cm. As mentioned above, PET has a high sensitivity for malignant lymph node, reported being up to 90%. Therefore, PET avid nodes are included in the high dose radiation targets especially when biopsy confirmed to be malignant. Figure 6 shows a patient with nasopharyngeal cancer, initially staged as T1N0 after conventional workup. However, FDG PET revealed hypermetabolic foci in the primary tumor in the nasopharynx and in bilateral level II lymph nodes which were small and were not called as lymphadenophy in the CT and MRI (Figure 6B). Fine needle biopsies of the right level II lymph node was obtained and confirmed to contain metastatic disease. Therefore, these lymph nodes were included in the high dose area in the IMRT plan (Figure 6C); (2) Detecting the primary tumor in patients who present with "unknown primary" and including the primary tumor in the high dose target. As mentioned above, in head and neck cancer with unknown primary, FDG PET can detect primary tumor in 25% of patients where conventional work up were unsuccessful. Most of these primary tumors are in the oropharynx, such as tonsil and the base of the tongue. When the primary tumor is detected, the patient is treated with radiation field tailored to the primary tumor, thus avoiding radiating the whole pharyngeal axis which is the standard radiation technique in patients with unknown primary. Figure 7 illustrates the IMRT plan for the patient with the primary tumor detected in PET. The left base of tongue tumor detected by PET was included in the high dose field while the larynx and nasopharynx were spared; (3) Accurate delineation of the edge of the primary tumor. Accurate delineation of the edge of tumor to generate gross tumor volume (GTV) is the first step in target de-

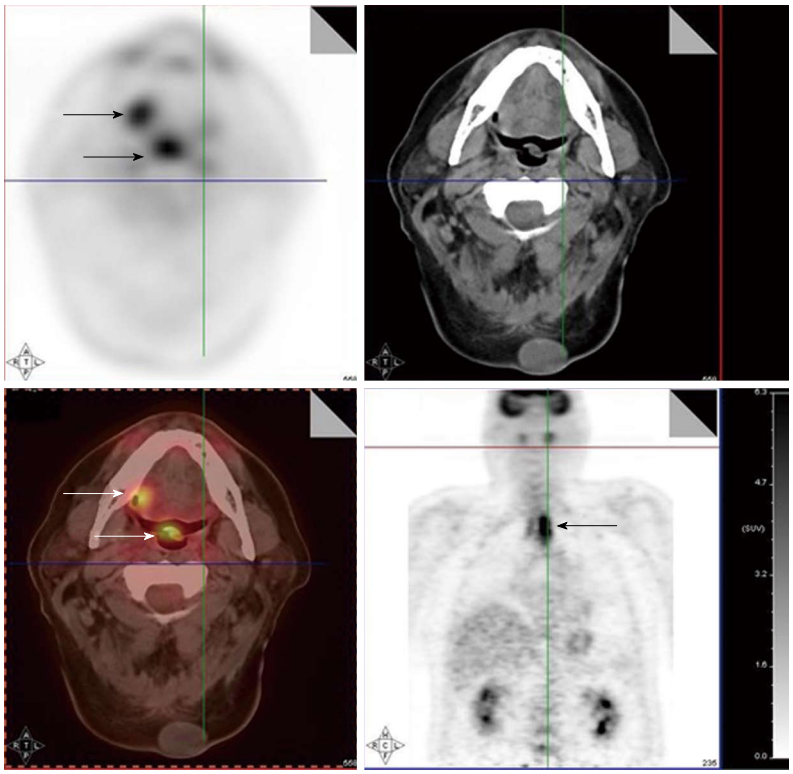

Figure 4 A positron emission tomography scan was obtained in a patient with a diagnosis of right oral tongue cancer (anterior arrow in axial views). The positron emission tomography/computed tomography revealed two additional primary cancers, one in the soft palate and the other in the upper esophagus.

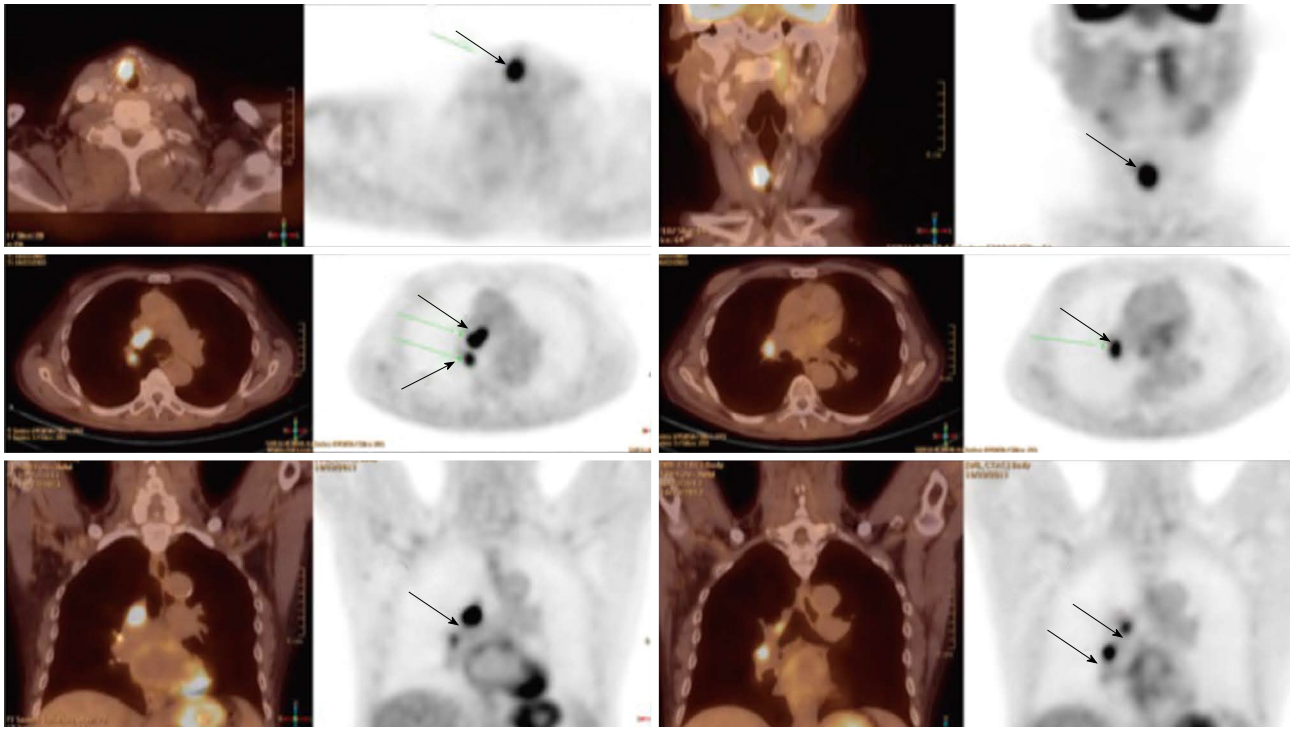

Figure 5 A patient with a synchronous laryngeal and lung squamous cell carcinomas. A 70-year-old male with diagnosis of squamous cell carcinoma of the glottic larynx T3N0M0 (A and B; arrow). He underwent a positron emission tomography/computed tomography scan which revealed additional lesions in the right lung which were biopsied endobronchial and shown to be a second primary lung cancer with mediastinal lymphadenopathy (C and D; arrows).

lineation for IMRT planning. It is often difficult to separate the tumor from surrounding soft tissue and muscle in CT imaging which is the primary imaging modality in radiation treatment planning, especially for tumor in the oral tongue and oropharynx. Figure 8 shows a patient with oral tongue cancer, comparing CT (Figure 8A) *vs* PET (Figure 8B). The border of the tumor in the CT was not very clear, difficult to separate from the tongue

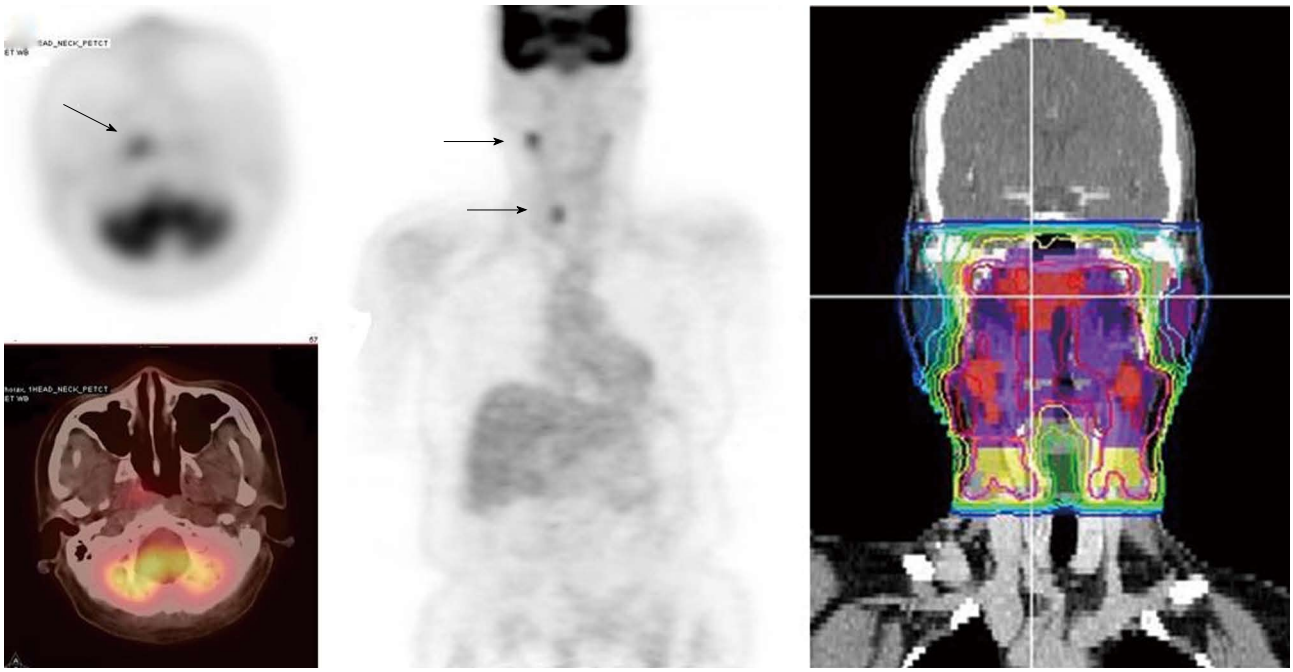

Figure 6 A patient with nasopharyngeal cancer. A: Initial stage was T1N0 when the patient was referred to our institution after conventional workup (arrow in axial image); B: Fluorodeoxyglucose positron emission tomography revealed hypermetabolic foci in the primary tumor in the nasopharynx and in bilateral level Ⅱ lymph nodes which were small and were not called as lymphadenophy in her computed tomography and magnetic resonance imaging. Fine needle biopsies of these lymph nodes were obtained. The right level Ⅱ node (arrows) was confirmed to contain metastatic disease, while the left level Ⅱ lymph node was not diagnostic; C: Intensity modulated radiotherapy plan for this patient. The right level Ⅱ node was treated to a high dose of radiation. The lower neck was treated with an anterior-posterior field (From Woods C, Sohn J, Machtay M, Yao M. Radiation treatment planning for head and neck cancer with PET. *PET Clinics* 2012; **7**: 396; with permission).

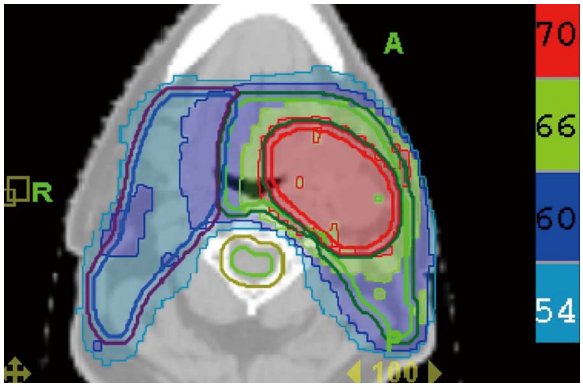

Figure 7 Treatment plan for the patient described in Figure 1. The base of tongue was found to be the primary cancer site and this area was included in the high dose intensity-modulated radiotherapy plan while sparing uninvolved mucosal areas.

muscle. Yet, the PET showed sharp contrast between the tumor and sounding tissue. The GTV based on CT (Figure 8C) is much larger than that based on PET (Figure 8D). Several studies have published comparing GTV generated by CT *vs* those when PET was incorporated, and noted a trend for decreasing GTVs when PET was used[47-52]. Some studies also showed that the interobserver variability deceased when PET was used for target delineation[47]; and (4) In postoperative radiation, detecting recurrent tumor even before radiation and including the recurrent tumor in high dose target. Patients with high risk pathology features are treated with adjuvant chemoradiation for better local regional control and survival. Postoperative radiotherapy is often given 4 to 6 wk after surgery when the surgical wound is fully healed. However, some patients may have local regional recurrences even before radiation. Because of the anatomical distortion and fibrotic changes after surgery, and flap reconstruction, these recurrences are difficult to be detected by physical examination and CT imaging. FDG PET is ideal imaging modality at this setting. Shintani *et al*[53] reported 91 consecutive patients referred to postoperative adjuvant radiation after complete surgical resection. These patients had FDG PET obtained at a median time of 28 d after surgery. They reported 27 patients with suspicious PET findings. Further biopsies led to changes in adjuvant treatment in 14 patients (15.4%), including increasing the radiation therapy dose in 6 patients, and extending the radiation therapy treatment volume and increasing the dose in 1 patient. Liao *et al*[54] also reported 29 patients who had a PET scan obtained before postoperative radiation. They found 7 patients with positive PET studies, 3 with distant metastases and 4 with local regional recurrences. For those who had local regional disease detected by the PET, the radiation volumes and radiation dose have to be changed, with higher dose delivered to the recurrent tumor. Thus, for patients with high risk features, especially for those who have a prolonged interval from surgery to radiation, a post-surgery and pre-radiation FDG PET will be valuable in treatment decision and radiation treatment planning.

Following are some active investigations in further ex-

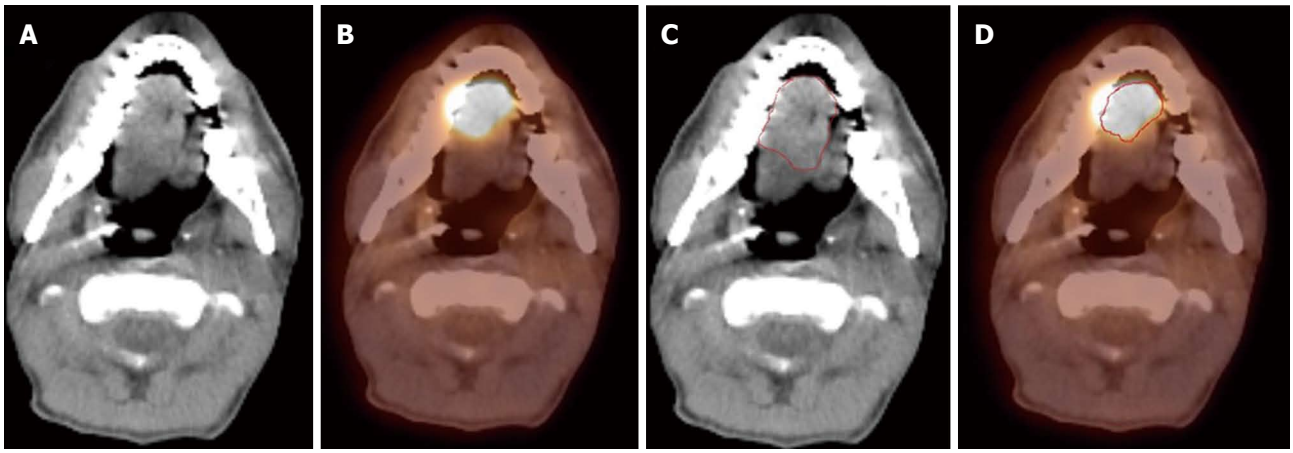

Figure 8 A patient with oral tongue cancer. The edge of the tumor was not very clear in the computed tomography (CT) image (A), but more obvious in the PET image (B). Gross tumor volume was outlined based on CT scan (C) *vs* with fluorodeoxyglucose positron emission tomography/CT (D). The volume included is larger with CT alone.

ploration how to use PET in radiation treatment in head and neck cancer: (1) Subvolume delineation and dose escalation. Tumors are not homogeneous. Since FDG uptake is correlated with tumor aggressiveness, the region of the tumor with higher FDG uptake may harbor more aggressive cancer cells and may require higher radiation dose to eradicate. Indeed, FDG-avid regions in the tumor have been shown to be correlated with hypoxia that is associated with tumor radioresistance[55,56]. With the dose painting capability of IMRT, a higher radiation dose can be delivered to these tumor subvolumes to achieve potentially better tumor control. Schwartz *et al*[57] studied theoretical IMRT models using PET derived volumes in 20 patients with head and neck cancer. They found that a mean dose of 74.9 Gy (range, 71.53-80.98 Gy) could be delivered to the PET-avid volume without overdosing the adjacent critical structures. Madani *et al*[58] conducted a Phase I study of dose escalation to FDG-avid subvolmes. They reported it was feasible to deliver a radiation boost of 30 Gy in 10 fractions to the PET tumor volume before standard IMRT treatment, and they are planning a randomized phase II trial comparing this treatment regimen with standard IMRT; and (2) Adaptive radiation therapy. During the course of radiation treatment, the patient can have significant physical/anatomical changes due to tumor response. A second CT simulation and replanning are required in order to ensure the tumor is being dosed appropriately. Changes also occur in the FDG uptake of the tumor during the course of radiotherapy and some investigators have explored adaptive radiotherapy and planning techniques to alter the plan based on the changes in PET imaging[59,60].

ASSESSMENT OF TREATMENT EFFICACY, FURTHER MANAGEMENT AND FOLLOW-UP

FDG PET/CT scans have been proven to be a useful technology in assessing treatment response in patients treated with definitive radiation and chemotherapy and for detecting residual and recurrent disease. PET/CT scans are usually performed 2 to 3 mo after treatment completion. The optimal timing of obtaining the scan has been debated in literature and based on many reports it has been determined that the 12-wk time point after completion of therapy may be the most appropriate[31,61,62]. Scans obtained at earlier time-points (< 8 wk) have a high rate of false-positive FDG uptake in the radiation treatment field due to inflammatory changes. Scans done too late (> 16 wk) may allow residual loco-regional disease to grow and metastasize. If increased FDG uptake is noted at the primary site, patients should undergo a biopsy followed by a surgical resection for residual disease. Figure 9 shows a serial PET/CT scans in a patient treated for oropharyngeal squamous cell carcinoma.

The role of FDG PET/CT in decision making for neck dissection after chemoradiation has also been extensively investigated. Yao *et al*[63] reported a 100% negative predictive value (NPV) and 43% positive predictive value (PPV) for PET scans done 12 wk after radiation in 53 patients who were noted to have a complete response at the primary site. A prospective study in 112 consecutive patients reported by Porceddu *et al*[64] also noted the utility of the 12-wk post radiochemotherapy PET scan in decision making for neck dissection. Patients who had equivocal PET results underwent another scan 4 to 6 wk later. Patients who had CT abnormalities but were PET-negative were observed and no subsequent neck node failures were noted in these patients. Nine patients continued to have PET-positive disease in the neck of which 8 underwent surgery. Residual disease was noted pathologically in 6 of these 8. Another prospective study from MD Anderson Cancer Center reported on 98 patients[65]. They stratified patients into low-risk and high-risk groups based on tumor stage, nodal stage, overall stage, tumor site, smoking history and HPV status. The most significant benefit of FDG PET/CT over CT scans was noted in detecting residual disease among high-risk patients. The NPV of PET/CT was 75% as compared to 37.5%

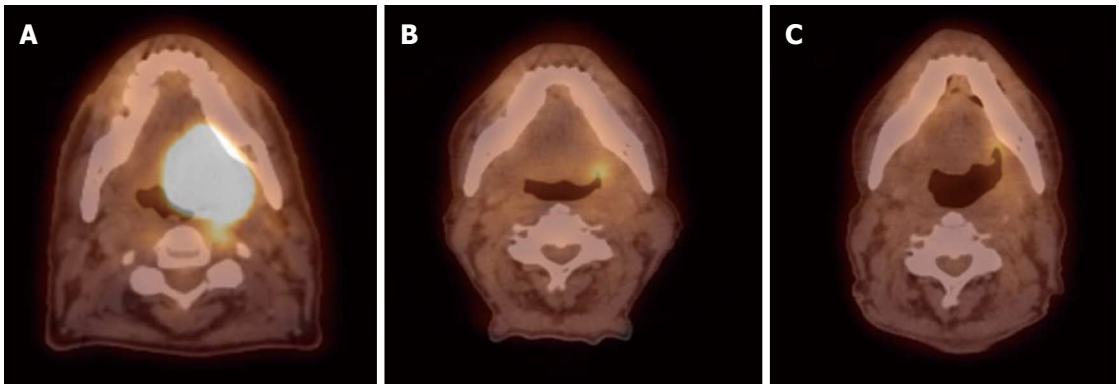

Figure 9 Sixty-six year old male was diagnosed with squamous cell carcinoma of the left base of tongue T4aN1M0. He received external beam radiation therapy (70 Gy in 35 fractions) with concurrent cisplatin 100 mg/m^2 (3 cycles). Positron emission tomography/computed tomography scans were done pre-treatment (A) and at 3-mo (B) and 8 mo (C) post-radiation therapy. Follow-up images show good response to treatment with sustained response at least 8 mo from treatment.

for CT alone.

The role of FDG-PET scans for long term follow-up surveillance for detection of loco-regional and distant metastatic recurrence has also been extensively investigated. Gupta *et al*[66] conducted a meta-analysis of 51 studies involving 2,335 patients. They reported a NPV of approximately 95% for both primary and neck disease for response assessment and surveillance. A recent report analyzed the role of long-term surveillance PET/CT scans in 214 patients with negative scans after completion of therapy[67]. Nine percent of these patients recurred on follow-up. This suggested a NPV for surveillance PET/CT of 91%. Based on these data the authors recommended that radiologic surveillance can be stopped early in those patients who are noted to have two consecutive negative PET/CT scans within 6 mo of each other.

PROGNOSIS

Many attempts have been made to establish PET/CT scan derived parameters as prognostic indicators. These studies have looked at pre-treatment, post-treatment and during treatment scans to obtain SUV and metabolic tumor volume (MTV) to serve as prognostic indices. Most of these studies have been retrospective. However, some prospective trials have also been reported. A recent review article summarizes these studies[68].

Allal *et al*[69] conducted a prospective study in 120 patients with HNSCC to evaluate the role of pre-treatment SUV in predicting for local control and disease-free survival. Seventy-three patients underwent radiation therapy with or without concurrent chemotherapy and 47 had surgery with or without adjuvant radiation therapy. At a median follow-up of 48 mo, 46 patients had recurrent and/or distant metastatic disease. In these patients the SUV was noted to be 5.8 *vs* 3.6 for those with disease controlled ($P = 0.002$). On the other hand, Vernon *et al*[70] reviewed 42 patients receiving PET/CT guided definitive radiotherapy and found that neither SUV of the primary tumor nor SUV of the lymph node was predictive of tumor recurrence.

In another prospective study, FDG PET was obtained 4 wk prior to chemoradiotherapy and 8 wk after completion of treatment in 98 patients[71]. Primary tumor and nodal SUVmax was calculated for both time points. The only prognostic factor for disease-specific survival was found to be the post-treatment primary tumor SUVmax. The mean SUVmax for those who failed was 7.2, compared to 4.2 for those who did not fail ($P < 0.01$). Pre-treatment SUVmax of primary tumor and lymph node were not found to be significantly associated with treatment outcomes. The conclusions from these studies are not consistent, partly due to the inherent problems with SUV measurement as it represents only a single point within the tumor but not represent the entire tumor. Additionally, there is heterogeneity in the patient population, heterogeneity in treatment modalities, small patient samples and the use of different endpoints.

In recent years, PET-based tumor volumes, *i.e.*, metabolic tumor volume (MTV), are being explored. La *et al*[72] from Stanford University evaluated the prognostic value of MTV in 85 patients. A threshold of 50% maximal intensity was used to define the metabolic tumor volumes. They found that MTV had a significant relationship with disease-free survival ($P < 0.001$) and with overall survival ($P < 0.001$) on univariate analysis. An increase in MTV of 17.4 mL was significantly associated with an increased hazard of first event (recurrence or death). SUVmax did not show a significant relationship with either of these endpoints. Another report from the same group of investigators validated these findings in an additional 83 patients[73]. Recently the results of a sub-group of patients enrolled on the RTOG 0522 trial were presented[74]. Seventy-four patients underwent baseline and 8-wk post treatment PET scans. Baseline SUVmax or SUVpeak of the primary or nodal disease were not predictive for outcomes. However, patients having a primary tumor MTV above the cohort median had a significantly worse loco-regional control and progression free survival.

Some groups have also evaluated the utility of PET scans done during therapy. PET scans were done after neoadjuvant chemotherapy in 16 patients. These patients

then underwent surgical resection and histopathologic responses were correlated with SUVmax. Comparisons between pathologic responders and non-responders revealed that there was significant difference in post-chemotherapy SUVmax and percent decrease in SUVmax[75].

The applicability of PET scans during the course of radiation therapy is harder to evaluate because of difficulty in image interpretation with inflammatory changes due to radiation and the cost of additional imaging. Such a study has, however, been done and reported on by Hentschel *et al*[76]. This prospective study evaluated the role of serial PET scans during early phase of radiation therapy and the ability of these scans to predict treatment outcomes. Patients were divided into two groups and all of them underwent 4 PET scans. In one group, PET scans were obtained before treatment, at 10 Gy, 30 Gy and 50 Gy. In the other group, PET scans were obtained before treatment, at 20 Gy, 40 Gy, and 60 Gy. Patients who had a rapid early response with > 50% decline in SUVmax at 10 Gy or 20 Gy as compared to the pre-treatment SUVmax had a significantly higher overall survival, loco-regional control and disease-free survival at 2 years. The 2-year overall survival was 88% for those who had more than 50% decline in SUVmax compared to 38% for those with less than 50% decline ($P = 0.02$). The 2-year disease-free survival was 75% and 31%, respectively for those with > 50% decline as compared to < 50% decline in SUVmax. And the 2-year local-regional control rate was 88% *vs* 40% for those with > 50% decline *vs* to those < 50% decline in SUVmax ($P = 0.06$).

There is currently no consensus on what time points to use for PET scan based prognostication and what parameters are the most useful. There may be value in combining traditional prognostic factors with PET based parameters. Yao *et al*[77] showed that T-stage, N-stage and pretreatment SUV of the lymph node were significantly associated with distant metastasis. However, the combination of these factors can better predict distant metastasis-free survival. The 3-year distant metastasis-free survival was 98.1% for no factors, 88.6% for one factor, 68.3% for two factors, and 41.7% for three factors. Similarly, Moeller *et al*[65] incorporated HPV status in their mortality risk assessment in addition to post-treatment tumor SUVmax. They noted FDG PET/CT was predictive for outcomes in HPV-negative and non-oropharyngeal primaries.

FUTURE DIRECTIONS

FDG PET/CT scan has been proven to be a useful technology on many fronts in head and neck cancer and has significant impact on the management as discussed above. Currently, there are many exciting new areas of research and development that are being actively investigated and will continue to expand the role of this imaging modality in the future. These efforts can be broadly categorized as follows: (1) Protocol development and standardization: a: Head and neck cancer staging - There may be a possibility of combining anatomical information, which forms the basis of the current AJCC system, with functional information obtained from PET scans; b: Standardized uptake value (SUV) - Even though SUV is a widely used and reported parameter it suffers from some drawbacks that make it difficult to compare values between different institutions[19,78,79]. Further standardization in the way SUV is determined would allow inter-institutional collaboration and co-operative group clinical trials. Additional objectively measurable parameters which allow cross-platform and cross-hardware comparisons also need to be developed; c: PET/CT simulators - PET/CT scans are often co-registered with CT scans obtained for radiation therapy planning. PET/CT simulators are also available at some institutions which facilitate this. Consensus guidelines need to be developed for tumor and target volume delineation when using PET information for radiation treatment planning; d: PET as a prognostic indicator - The use of PET/CT scans as prognostic indicators in head and neck cancers and for follow-up and surveillance requires further research and investigation; and e: Economic analyses - Cost-benefit analyses suggest that PET/CT scans are cost-effective for diagnosis, staging and therapeutic decision making in head and neck cancers[80,81]. Common availability and decreasing costs of this technology will allow greater use and acceptance; (2) Newer imaging technology - Magnetic resonance imaging (MRI) offers superior imaging for soft-tissue delineation but offers little functional information unless MR spectroscopy is performed. MR spectroscopy can be performed in a limited volume. Recently MR/PET hybrid technologies have been developed for used in the clinic. This offers the advantages of high-quality soft tissue imaging from MR with whole-body and functional imaging from the PET component[82-84]. A recent review article highlights the potential for this new hybrid technology, the technical challenges and its use in clinical situations[85]; and (3) Newer radiopharmaceuticals - Many new radioisotopes and radiotracers are being developed to image further functional characteristics of tumors including hypoxia, tumor proliferation, amino acid metabolism and presence of EGFR on tumor cells. An excellent review on this topic has been provided by Wang *et al*[86]. As outlined in this review, a large number of efforts are being focused on hypoxia imaging. Hypoxia poses a major radiobiological disadvantage and confers radioresistance to the tumor. Hypoxic cells are not killed in response to radiation therapy and may be responsible for treatment failure, either locally or as distant metastasis. Some of the newer radiopharmaceuticals being used to image the hypoxic portion of the tumor include [^{18}F]fluoromisonidazole (FMISO), copper-diacetyl-bis (N4-methylthiosamicarbazone) (Cu-ATSM) and [^{18}F]fluoroazomycin arabinoside (FAZA). Once identified using PET scans, these hypoxic areas of the tumor can be preferentially targeted to receive a higher dose of radiation using IMRT technique.

The applications of FDG PET/CT scanning mentioned in this article highlight the extensive work done

by groups across the world to the study the usefulness and application of this technology in various scenarios. Future work will continue to highlight the importance of this imaging modality in head and neck cancers.

REFERENCES

1 **Jemal A**, Bray F, Center MM, Ferlay J, Ward E, Forman D. Global cancer statistics. *CA Cancer J Clin* 2011; **61**: 69-90 [PMID: 21296855 DOI: 10.3322/caac.20107]
2 **Parkin DM**, Bray F, Ferlay J, Pisani P. Global cancer statistics, 2002. *CA Cancer J Clin* 2005; **55**: 74-108 [PMID: 15761078 DOI: 10.3322/canjclin.55.2.74]
3 **Siegel R**, Naishadham D, Jemal A. Cancer statistics, 2013. *CA Cancer J Clin* 2013; **63**: 11-30 [PMID: 23335087 DOI: 10.3322/caac.21166]
4 Induction chemotherapy plus radiation compared with surgery plus radiation in patients with advanced laryngeal cancer. The Department of Veterans Affairs Laryngeal Cancer Study Group. *N Engl J Med* 1991; **324**: 1685-1690 [PMID: 2034244 DOI: 10.1056/NEJM199106133242402]
5 **Forastiere AA**, Goepfert H, Maor M, Pajak TF, Weber R, Morrison W, Glisson B, Trotti A, Ridge JA, Chao C, Peters G, Lee DJ, Leaf A, Ensley J, Cooper J. Concurrent chemotherapy and radiotherapy for organ preservation in advanced laryngeal cancer. *N Engl J Med* 2003; **349**: 2091-2098 [PMID: 14645636 DOI: 10.1056/NEJMoa031317]
6 **Vander Heiden MG**, Cantley LC, Thompson CB. Understanding the Warburg effect: the metabolic requirements of cell proliferation. *Science* 2009; **324**: 1029-1033 [PMID: 19460998 DOI: 10.1126/science.1160809]
7 **Vander Heiden MG**, Locasale JW, Swanson KD, Sharfi H, Heffron GJ, Amador-Noguez D, Christofk HR, Wagner G, Rabinowitz JD, Asara JM, Cantley LC. Evidence for an alternative glycolytic pathway in rapidly proliferating cells. *Science* 2010; **329**: 1492-1499 [PMID: 20847263 DOI: 10.1126/science.1188015]
8 **Garber K**. Energy deregulation: licensing tumors to grow. *Science* 2006; **312**: 1158-1159 [PMID: 16728625 DOI: 10.1126/science.312.5777.1158]
9 **Macheda ML**, Rogers S, Best JD. Molecular and cellular regulation of glucose transporter (GLUT) proteins in cancer. *J Cell Physiol* 2005; **202**: 654-662 [PMID: 15389572 DOI: 10.1002/jcp.20166]
10 **Kunkel M**, Reichert TE, Benz P, Lehr HA, Jeong JH, Wieand S, Bartenstein P, Wagner W, Whiteside TL. Overexpression of Glut-1 and increased glucose metabolism in tumors are associated with a poor prognosis in patients with oral squamous cell carcinoma. *Cancer* 2003; **97**: 1015-1024 [PMID: 12569601 DOI: 10.1002/cncr.11159]
11 **Zhou S**, Wang S, Wu Q, Fan J, Wang Q. Expression of glucose transporter-1 and -3 in the head and neck carcinoma--the correlation of the expression with the biological behaviors. *ORL J Otorhinolaryngol Relat Spec* 2008; **70**: 189-194 [PMID: 18401196 DOI: 10.1159/000124293]
12 **Roh JL**, Cho KJ, Kwon GY, Ryu CH, Chang HW, Choi SH, Nam SY, Kim SY. The prognostic value of hypoxia markers in T2-staged oral tongue cancer. *Oral Oncol* 2009; **45**: 63-68 [PMID: 18620902 DOI: 10.1016/j.oraloncology.2008.03.017]
13 **De Schutter H**, Landuyt W, Verbeken E, Goethals L, Hermans R, Nuyts S. The prognostic value of the hypoxia markers CA IX and GLUT 1 and the cytokines VEGF and IL 6 in head and neck squamous cell carcinoma treated by radiotherapy +/- chemotherapy. *BMC Cancer* 2005; **5**: 42 [PMID: 15847702 DOI: 10.1186/1471-2407-5-42]
14 **Minn H**, Joensuu H, Ahonen A, Klemi P. Fluorodeoxyglucose imaging: a method to assess the proliferative activity of human cancer in vivo. Comparison with DNA flow cytometry in head and neck tumors. *Cancer* 1988; **61**: 1776-1781 [PMID: 3355975 DOI: 3.0.CO;]
15 **Haberkorn U**, Strauss LG, Reisser C, Haag D, Dimitrakopoulou A, Ziegler S, Oberdorfer F, Rudat V, van Kaick G. Glucose uptake, perfusion, and cell proliferation in head and neck tumors: relation of positron emission tomography to flow cytometry. *J Nucl Med* 1991; **32**: 1548-1555 [PMID: 1869977]
16 **Tomasi G**, Turkheimer F, Aboagye E. Importance of quantification for the analysis of PET data in oncology: review of current methods and trends for the future. *Mol Imaging Biol* 2012; **14**: 131-146 [PMID: 21842339 DOI: 10.1007/s11307-011-0514-2]
17 **Boellaard R**. Standards for PET image acquisition and quantitative data analysis. *J Nucl Med* 2009; **50** Suppl 1: 11S-20S [PMID: 19380405 DOI: 10.2967/jnumed.108.057182]
18 **Kinahan PE**, Fletcher JW. Positron emission tomography-computed tomography standardized uptake values in clinical practice and assessing response to therapy. *Semin Ultrasound CT MR* 2010; **31**: 496-505 [PMID: 21147377 DOI: 10.1053/j.sult.2010.10.001]
19 **Huang SC**. Anatomy of SUV. Standardized uptake value. *Nucl Med Biol* 2000; **27**: 643-646 [PMID: 11091106 DOI: 10.1016/S0969-8051(00)00155-4]
20 **Thie JA**. Understanding the standardized uptake value, its methods, and implications for usage. *J Nucl Med* 2004; **45**: 1431-1434 [PMID: 15347707]
21 **Lindholm P**, Minn H, Leskinen-Kallio S, Bergman J, Ruotsalainen U, Joensuu H. Influence of the blood glucose concentration on FDG uptake in cancer--a PET study. *J Nucl Med* 1993; **34**: 1-6 [PMID: 8418248]
22 **Jereczek-Fossa BA**, Jassem J, Orecchia R. Cervical lymph node metastases of squamous cell carcinoma from an unknown primary. *Cancer Treat Rev* 2004; **30**: 153-164 [PMID: 15023433 DOI: 10.1016/j.ctrv.2003.10.001]
23 **Lee DJ**, Rostock RA, Harris A, Kashima H, Johns M. Clinical evaluation of patients with metastatic squamous carcinoma of the neck with occult primary tumor. *South Med J* 1986; **79**: 979-983 [PMID: 3738594 DOI: 10.1097/00007611-198608000-00015]
24 **Rusthoven KE**, Koshy M, Paulino AC. The role of fluorodeoxyglucose positron emission tomography in cervical lymph node metastases from an unknown primary tumor. *Cancer* 2004; **101**: 2641-2649 [PMID: 15517576 DOI: 10.1002/cncr.20687]
25 **Rudmik L**, Lau HY, Matthews TW, Bosch JD, Kloiber R, Molnar CP, Dort JC. Clinical utility of PET/CT in the evaluation of head and neck squamous cell carcinoma with an unknown primary: a prospective clinical trial. *Head Neck* 2011; **33**: 935-940 [PMID: 21674668 DOI: 10.1002/hed.21566]
26 **Som PM**. Detection of metastasis in cervical lymph nodes: CT and MR criteria and differential diagnosis. *AJR Am J Roentgenol* 1992; **158**: 961-969 [PMID: 1566697 DOI: 10.2214/ajr.158.5.1566697]
27 **Adams S**, Baum RP, Stuckensen T, Bitter K, Hör G. Prospective comparison of 18F-FDG PET with conventional imaging modalities (CT, MRI, US) in lymph node staging of head and neck cancer. *Eur J Nucl Med* 1998; **25**: 1255-1260 [PMID: 9724374 DOI: 10.1007/s002590050293]
28 **Di Martino E**, Nowak B, Hassan HA, Hausmann R, Adam G, Buell U, Westhofen M. Diagnosis and staging of head and neck cancer: a comparison of modern imaging modalities (positron emission tomography, computed tomography, color-coded duplex sonography) with panendoscopic and histopathologic findings. *Arch Otolaryngol Head Neck Surg* 2000; **126**: 1457-1461 [PMID: 11115282 DOI: 10.1001/archotol.126.12.1457]
29 **Brouwer J**, Senft A, de Bree R, Comans EF, Golding RP, Castelijns JA, Hoekstra OS, Leemans CR. Screening for distant metastases in patients with head and neck cancer: is there a role for (18)FDG-PET? *Oral Oncol* 2006; **42**: 275-280

[PMID: 16266820 DOI: 10.1016/j.oraloncology.2005.07.009]
30 **Goerres GW**, Schmid DT, Grätz KW, von Schulthess GK, Eyrich GK. Impact of whole body positron emission tomography on initial staging and therapy in patients with squamous cell carcinoma of the oral cavity. *Oral Oncol* 2003; **39**: 547-551 [PMID: 12798396 DOI: 10.1016/S1368-8375(03)00016-2]
31 **Lonneux M**, Lawson G, Ide C, Bausart R, Remacle M, Pauwels S. Positron emission tomography with fluorodeoxyglucose for suspected head and neck tumor recurrence in the symptomatic patient. *Laryngoscope* 2000; **110**: 1493-1497 [PMID: 10983949 DOI: 10.1097/00005537-200009000-00016]
32 **Ng SH**, Chan SC, Liao CT, Chang JT, Ko SF, Wang HM, Chin SC, Lin CY, Huang SF, Yen TC. Distant metastases and synchronous second primary tumors in patients with newly diagnosed oropharyngeal and hypopharyngeal carcinomas: evaluation of (18)F-FDG PET and extended-field multidetector row CT. *Neuroradiology* 2008; **50**: 969-979 [PMID: 18600319 DOI: 10.1007/s00234-008-0426-2]
33 **Teknos TN**, Rosenthal EL, Lee D, Taylor R, Marn CS. Positron emission tomography in the evaluation of stage III and IV head and neck cancer. *Head Neck* 2001; **23**: 1056-1060 [PMID: 11774391 DOI: 10.1002/hed.10006]
34 **Schwartz DL**, Rajendran J, Yueh B, Coltrera M, Anzai Y, Krohn K, Eary J. Staging of head and neck squamous cell cancer with extended-field FDG-PET. *Arch Otolaryngol Head Neck Surg* 2003; **129**: 1173-1178 [PMID: 14623746 DOI: 10.1001/archotol.129.11.1173]
35 **Haerle SK**, Schmid DT, Ahmad N, Hany TF, Stoeckli SJ. The value of (18)F-FDG PET/CT for the detection of distant metastases in high-risk patients with head and neck squamous cell carcinoma. *Oral Oncol* 2011; **47**: 653-659 [PMID: 21658990 DOI: 10.1016/j.oraloncology.2011.05.011]
36 **Schmid DT**, Stoeckli SJ, Bandhauer F, Huguenin P, Schmid S, von Schulthess GK, Goerres GW. Impact of positron emission tomography on the initial staging and therapy in locoregional advanced squamous cell carcinoma of the head and neck. *Laryngoscope* 2003; **113**: 888-891 [PMID: 12792328 DOI: 10.1097/00005537-200305000-00021]
37 **Strobel K**, Haerle SK, Stoeckli SJ, Schrank M, Soyka JD, Veit-Haibach P, Hany TF. Head and neck squamous cell carcinoma (HNSCC)--detection of synchronous primaries with (18)F-FDG-PET/CT. *Eur J Nucl Med Mol Imaging* 2009; **36**: 919-927 [PMID: 19205699 DOI: 10.1007/s00259-009-1064-6]
38 **Kondo N**, Tsukuda M, Nishimura G. Diagnostic sensitivity of ^{18}fluorodeoxyglucose positron emission tomography for detecting synchronous multiple primary cancers in head and neck cancer patients. *Eur Arch Otorhinolaryngol* 2012; **269**: 1503-1507 [PMID: 21984059 DOI: 10.1007/s00405-011-1784-7]
39 **Adelstein DJ**, Li Y, Adams GL, Wagner H, Kish JA, Ensley JF, Schuller DE, Forastiere AA. An intergroup phase III comparison of standard radiation therapy and two schedules of concurrent chemoradiotherapy in patients with unresectable squamous cell head and neck cancer. *J Clin Oncol* 2003; **21**: 92-98 [PMID: 12506176 DOI: 10.1200/JCO.2003.01.008]
40 **Bernier J**, Domenge C, Ozsahin M, Matuszewska K, Lefèbvre JL, Greiner RH, Giralt J, Maingon P, Rolland F, Bolla M, Cognetti F, Bourhis J, Kirkpatrick A, van Glabbeke M. Postoperative irradiation with or without concomitant chemotherapy for locally advanced head and neck cancer. *N Engl J Med* 2004; **350**: 1945-1952 [PMID: 15128894 DOI: 10.1056/NEJMoa032641]
41 **Cooper JS**, Pajak TF, Forastiere AA, Jacobs J, Campbell BH, Saxman SB, Kish JA, Kim HE, Cmelak AJ, Rotman M, Machtay M, Ensley JF, Chao KS, Schultz CJ, Lee N, Fu KK. Postoperative concurrent radiotherapy and chemotherapy for high-risk squamous-cell carcinoma of the head and neck. *N Engl J Med* 2004; **350**: 1937-1944 [PMID: 15128893 DOI: 10.1056/NEJMoa032646]
42 **Grégoire V**, De Neve W, Eisbruch A, Lee N, Van den Weyngaert D, Van Gestel D. Intensity-modulated radiation therapy for head and neck carcinoma. *Oncologist* 2007; **12**: 555-564 [PMID: 17522243 DOI: 10.1634/theoncologist.12-5-555]
43 **Lee N**, Puri DR, Blanco AI, Chao KS. Intensity-modulated radiation therapy in head and neck cancers: an update. *Head Neck* 2007; **29**: 387-400 [PMID: 16358297 DOI: 10.1002/hed.20332]
44 **Chao KS**, Deasy JO, Markman J, Haynie J, Perez CA, Purdy JA, Low DA. A prospective study of salivary function sparing in patients with head-and-neck cancers receiving intensity-modulated or three-dimensional radiation therapy: initial results. *Int J Radiat Oncol Biol Phys* 2001; **49**: 907-916 [PMID: 11240231 DOI: 10.1016/S0360-3016(00)01441-3]
45 **Lin A**, Kim HM, Terrell JE, Dawson LA, Ship JA, Eisbruch A. Quality of life after parotid-sparing IMRT for head-and-neck cancer: a prospective longitudinal study. *Int J Radiat Oncol Biol Phys* 2003; **57**: 61-70 [PMID: 12909216 DOI: 10.1016/S0360-3016(03)00361-4]
46 **Yao M**, Karnell LH, Funk GF, Lu H, Dornfeld K, Buatti JM. Health-related quality-of-life outcomes following IMRT versus conventional radiotherapy for oropharyngeal squamous cell carcinoma. *Int J Radiat Oncol Biol Phys* 2007; **69**: 1354-1360 [PMID: 17689885 DOI: 10.1016/j.ijrobp.2007.05.003]
47 **Ciernik IF**, Dizendorf E, Baumert BG, Reiner B, Burger C, Davis JB, Lütolf UM, Steinert HC, Von Schulthess GK. Radiation treatment planning with an integrated positron emission and computer tomography (PET/CT): a feasibility study. *Int J Radiat Oncol Biol Phys* 2003; **57**: 853-863 [PMID: 14529793 DOI: 10.1016/S0360-3016(03)00346-8]
48 **Deantonio L**, Beldì D, Gambaro G, Loi G, Brambilla M, Inglese E, Krengli M. FDG-PET/CT imaging for staging and radiotherapy treatment planning of head and neck carcinoma. *Radiat Oncol* 2008; **3**: 29 [PMID: 18801181 DOI: 10.1186/1748-717X-3-29]
49 **Paulino AC**, Koshy M, Howell R, Schuster D, Davis LW. Comparison of CT- and FDG-PET-defined gross tumor volume in intensity-modulated radiotherapy for head-and-neck cancer. *Int J Radiat Oncol Biol Phys* 2005; **61**: 1385-1392 [PMID: 15817341 DOI: 10.1016/j.ijrobp.2004.08.037]
50 **El-Bassiouni M**, Ciernik IF, Davis JB, El-Attar I, Reiner B, Burger C, Goerres GW, Studer GM. [18FDG] PET-CT-based intensity-modulated radiotherapy treatment planning of head and neck cancer. *Int J Radiat Oncol Biol Phys* 2007; **69**: 286-293 [PMID: 17707283 DOI: 10.1016/j.ijrobp.2007.04.053]
51 **Guido A**, Fuccio L, Rombi B, Castellucci P, Cecconi A, Bunkheila F, Fuccio C, Spezi E, Angelini AL, Barbieri E. Combined 18F-FDG-PET/CT imaging in radiotherapy target delineation for head-and-neck cancer. *Int J Radiat Oncol Biol Phys* 2009; **73**: 759-763 [PMID: 18834671 DOI: 10.1016/j.ijrobp.2008.04.059]
52 **Wang D**, Schultz CJ, Jursinic PA, Bialkowski M, Zhu XR, Brown WD, Rand SD, Michel MA, Campbell BH, Wong S, Li XA, Wilson JF. Initial experience of FDG-PET/CT guided IMRT of head-and-neck carcinoma. *Int J Radiat Oncol Biol Phys* 2006; **65**: 143-151 [PMID: 16618577 DOI: 10.1016/j.ijrobp.2005.11.048]
53 **Shintani SA**, Foote RL, Lowe VJ, Brown PD, Garces YI, Kasperbauer JL. Utility of PET/CT imaging performed early after surgical resection in the adjuvant treatment planning for head and neck cancer. *Int J Radiat Oncol Biol Phys* 2008; **70**: 322-329 [PMID: 17889447 DOI: 10.1016/j.ijrobp.2007.06.038]
54 **Liao CT**, Fan KH, Lin CY, Wang HM, Huang SF, Chen IH, Kang CJ, Ng SH, Hsueh C, Lee LY, Lin CH, Yen TC. Impact of a second FDG PET scan before adjuvant therapy for the early detection of residual/relapsing tumours in high-risk patients with oral cavity cancer and pathological extracapsular spread. *Eur J Nucl Med Mol Imaging* 2012; **39**: 944-955 [PMID: 22434050 DOI: 10.1007/s00259-012-2103-2]
55 **Mees G**, Dierckx R, Vangestel C, Van de Wiele C. Molecular imaging of hypoxia with radiolabelled agents. *Eur J Nucl Med Mol Imaging* 2009; **36**: 1674-1686 [PMID: 19565239 DOI:

10.1007/s00259-009-1195-9]
56 **Pugachev A**, Ruan S, Carlin S, Larson SM, Campa J, Ling CC, Humm JL. Dependence of FDG uptake on tumor microenvironment. *Int J Radiat Oncol Biol Phys* 2005; **62**: 545-553 [PMID: 15890599 DOI: 10.1016/j.ijrobp.2005.02.009]
57 **Schwartz DL**, Ford EC, Rajendran J, Yueh B, Coltrera MD, Virgin J, Anzai Y, Haynor D, Lewellen B, Mattes D, Kinahan P, Meyer J, Phillips M, Leblanc M, Krohn K, Eary J, Laramore GE. FDG-PET/CT-guided intensity modulated head and neck radiotherapy: a pilot investigation. *Head Neck* 2005; **27**: 478-487 [PMID: 15772953 DOI: 10.1002/hed.20177]
58 **Madani I**, Duthoy W, Derie C, De Gersem W, Boterberg T, Saerens M, Jacobs F, Grégoire V, Lonneux M, Vakaet L, Vanderstraeten B, Bauters W, Bonte K, Thierens H, De Neve W. Positron emission tomography-guided, focal-dose escalation using intensity-modulated radiotherapy for head and neck cancer. *Int J Radiat Oncol Biol Phys* 2007; **68**: 126-135 [PMID: 17448871 DOI: 10.1016/j.ijrobp.2006.12.070]
59 **Duprez F**, De Neve W, De Gersem W, Coghe M, Madani I. Adaptive dose painting by numbers for head-and-neck cancer. *Int J Radiat Oncol Biol Phys* 2011; **80**: 1045-1055 [PMID: 20643512 DOI: 10.1016/j.ijrobp.2010.03.028]
60 **Hentschel M**, Appold S, Schreiber A, Abramyuk A, Abolmaali N, Kotzerke J, Baumann M, Zöphel K. Serial FDG-PET on patients with head and neck cancer: implications for radiation therapy. *Int J Radiat Biol* 2009; **85**: 796-804 [PMID: 19728194 DOI: 10.1080/09553000903039180]
61 **Andrade RS**, Heron DE, Degirmenci B, Filho PA, Branstetter BF, Seethala RR, Ferris RL, Avril N. Posttreatment assessment of response using FDG-PET/CT for patients treated with definitive radiation therapy for head and neck cancers. *Int J Radiat Oncol Biol Phys* 2006; **65**: 1315-1322 [PMID: 16750327 DOI: 10.1016/j.ijrobp.2006.03.015]
62 **Porceddu SV**, Jarmolowski E, Hicks RJ, Ware R, Weih L, Rischin D, Corry J, Peters LJ. Utility of positron emission tomography for the detection of disease in residual neck nodes after (chemo)radiotherapy in head and neck cancer. *Head Neck* 2005; **27**: 175-181 [PMID: 15627258 DOI: 10.1002/hed.20130]
63 **Yao M**, Smith RB, Graham MM, Hoffman HT, Tan H, Funk GF, Graham SM, Chang K, Dornfeld KJ, Menda Y, Buatti JM. The role of FDG PET in management of neck metastasis from head-and-neck cancer after definitive radiation treatment. *Int J Radiat Oncol Biol Phys* 2005; **63**: 991-999 [PMID: 16099601 DOI: 10.1016/j.ijrobp.2005.03.066]
64 **Porceddu SV**, Pryor DI, Burmeister E, Burmeister BH, Poulsen MG, Foote MC, Panizza B, Coman S, McFarlane D, Coman W. Results of a prospective study of positron emission tomography-directed management of residual nodal abnormalities in node-positive head and neck cancer after definitive radiotherapy with or without systemic therapy. *Head Neck* 2011; **33**: 1675-1682 [PMID: 22076976 DOI: 10.1002/hed.21655]
65 **Moeller BJ**, Rana V, Cannon BA, Williams MD, Sturgis EM, Ginsberg LE, Macapinlac HA, Lee JJ, Ang KK, Chao KS, Chronowski GM, Frank SJ, Morrison WH, Rosenthal DI, Weber RS, Garden AS, Lippman SM, Schwartz DL. Prospective risk-adjusted [18F]Fluorodeoxyglucose positron emission tomography and computed tomography assessment of radiation response in head and neck cancer. *J Clin Oncol* 2009; **27**: 2509-2515 [PMID: 19332725 DOI: 10.1200/JCO.2008.19.3300]
66 **Gupta T**, Master Z, Kannan S, Agarwal JP, Ghsoh-Laskar S, Rangarajan V, Murthy V, Budrukkar A. Diagnostic performance of post-treatment FDG PET or FDG PET/CT imaging in head and neck cancer: a systematic review and meta-analysis. *Eur J Nucl Med Mol Imaging* 2011; **38**: 2083-2095 [PMID: 21853309 DOI: 10.1007/s00259-011-1893-y]
67 **McDermott M**, Hughes M, Rath T, Johnson JT, Heron DE, Kubicek GJ, Kim SW, Ferris RL, Duvvuri U, Ohr JP, Branstetter BF. Negative predictive value of surveillance PET/CT in head and neck squamous cell cancer. *AJNR Am J Neuroradiol* 2013; **34**: 1632-1636 [PMID: 23639557 DOI: 10.3174/ajnr.A3494]
68 **Siddiqui F**, Faulhaber PF, Yao M, Le QT. The application of fdg-pet as prognostic indicators in head and neck squamous cell carcinoma. *PET Clin* 2012; **7**: 381
69 **Allal AS**, Slosman DO, Kebdani T, Allaoua M, Lehmann W, Dulguerov P. Prediction of outcome in head-and-neck cancer patients using the standardized uptake value of 2-[18F]fluoro-2-deoxy-D-glucose. *Int J Radiat Oncol Biol Phys* 2004; **59**: 1295-1300 [PMID: 15275712 DOI: 10.1016/j.ijrobp.2003.12.039]
70 **Vernon MR**, Maheshwari M, Schultz CJ, Michel MA, Wong SJ, Campbell BH, Massey BL, Wilson JF, Wang D. Clinical outcomes of patients receiving integrated PET/CT-guided radiotherapy for head and neck carcinoma. *Int J Radiat Oncol Biol Phys* 2008; **70**: 678-684 [PMID: 18262086 DOI: 10.1016/j.ijrobp.2007.10.044]
71 **Moeller BJ**, Rana V, Cannon BA, Williams MD, Sturgis EM, Ginsberg LE, Macapinlac HA, Lee JJ, Ang KK, Chao KS, Chronowski GM, Frank SJ, Morrison WH, Rosenthal DI, Weber RS, Garden AS, Lippman SM, Schwartz DL. Prospective imaging assessment of mortality risk after head-and-neck radiotherapy. *Int J Radiat Oncol Biol Phys* 2010; **78**: 667-674 [PMID: 20171802 DOI: 10.1016/j.ijrobp.2009.08.063]
72 **La TH**, Filion EJ, Turnbull BB, Chu JN, Lee P, Nguyen K, Maxim P, Quon A, Graves EE, Loo BW, Le QT. Metabolic tumor volume predicts for recurrence and death in head-and-neck cancer. *Int J Radiat Oncol Biol Phys* 2009; **74**: 1335-1341 [PMID: 19289263 DOI: 10.1016/j.ijrobp.2008.10.060]
73 **Tang C**, Murphy JD, Khong B, La TH, Kong C, Fischbein NJ, Colevas AD, Iagaru AH, Graves EE, Loo BW, Le QT. Validation that metabolic tumor volume predicts outcome in head-and-neck cancer. *Int J Radiat Oncol Biol Phys* 2012; **83**: 1514-1520 [PMID: 22270174]
74 **Schwartz D**, Harris J, Yao M, Trotti A, Garden A, Jones C, Harari PM, Foote R, Holland J, Ang K. Metabolic tumor volume as a predictive imaging biomarker in head and neck cancer: Pilot results from rtog 0522. *Int J Radiat Oncol Biol Phys* 2013; **87**: S192 [DOI: 10.1016/j.ijrobp.2013.06.496]
75 **Kikuchi M**, Shinohara S, Nakamoto Y, Usami Y, Fujiwara K, Adachi T, Hori SY, Tona Y, Yamazaki H, Imai Y, Naito Y. Sequential FDG-PET/CT after neoadjuvant chemotherapy is a predictor of histopathologic response in patients with head and neck squamous cell carcinoma. *Mol Imaging Biol* 2011; **13**: 368-377 [PMID: 20552285 DOI: 10.1007/s11307-010-0364-3]
76 **Hentschel M**, Appold S, Schreiber A, Abolmaali N, Abramyuk A, Dörr W, Kotzerke J, Baumann M, Zöphel K. Early FDG PET at 10 or 20 Gy under chemoradiotherapy is prognostic for locoregional control and overall survival in patients with head and neck cancer. *Eur J Nucl Med Mol Imaging* 2011; **38**: 1203-1211 [PMID: 21350962 DOI: 10.1007/s00259-011-1759-3]
77 **Yao M**, Lu M, Savvides PS, Rezaee R, Zender CA, Lavertu P, Buatti JM, Machtay M. Distant metastases in head-and-neck squamous cell carcinoma treated with intensity-modulated radiotherapy. *Int J Radiat Oncol Biol Phys* 2012; **83**: 684-689 [PMID: 22169673 DOI: 10.1016/j.ijrobp.2011.07.014]
78 **Hamberg LM**, Hunter GJ, Alpert NM, Choi NC, Babich JW, Fischman AJ. The dose uptake ratio as an index of glucose metabolism: useful parameter or oversimplification? *J Nucl Med* 1994; **35**: 1308-1312 [PMID: 8046485]
79 **Keyes JW**. SUV: standard uptake or silly useless value? *J Nucl Med* 1995; **36**: 1836-1839 [PMID: 7562051]
80 **Kurien G**, Hu J, Harris J, Seikaly H. Cost-effectiveness of positron emission tomography/computed tomography in the management of advanced head and neck cancer. *J Otolaryngol Head Neck Surg* 2011; **40**: 468-472 [PMID: 22420434]
81 **Sher DJ**, Tishler RB, Annino D, Punglia RS. Cost-effectiveness of CT and PET-CT for determining the need for

adjuvant neck dissection in locally advanced head and neck cancer. *Ann Oncol* 2010; **21**: 1072-1077 [PMID: 19833820 DOI: 10.1093/annonc/mdp405]

82 **Berker Y**, Franke J, Salomon A, Palmowski M, Donker HC, Temur Y, Mottaghy FM, Kuhl C, Izquierdo-Garcia D, Fayad ZA, Kiessling F, Schulz V. MRI-based attenuation correction for hybrid PET/MRI systems: a 4-class tissue segmentation technique using a combined ultrashort-echo-time/Dixon MRI sequence. *J Nucl Med* 2012; **53**: 796-804 [PMID: 22505568 DOI: 10.2967/jnumed.111.092577]

83 **Drzezga A**, Souvatzoglou M, Eiber M, Beer AJ, Fürst S, Martinez-Möller A, Nekolla SG, Ziegler S, Ganter C, Rummeny EJ, Schwaiger M. First clinical experience with integrated whole-body PET/MR: comparison to PET/CT in patients with oncologic diagnoses. *J Nucl Med* 2012; **53**: 845-855 [PMID: 22534830 DOI: 10.2967/jnumed.111.098608]

84 **Keereman V**, Fierens Y, Broux T, De Deene Y, Lonneux M, Vandenberghe S. MRI-based attenuation correction for PET/MRI using ultrashort echo time sequences. *J Nucl Med* 2010; **51**: 812-818 [PMID: 20439508 DOI: 10.2967/jnumed.109.065425]

85 **Torigian DA**, Zaidi H, Kwee TC, Saboury B, Udupa JK, Cho ZH, Alavi A. PET/MR imaging: technical aspects and potential clinical applications. *Radiology* 2013; **267**: 26-44 [PMID: 23525716 DOI: 10.1148/radiol.13121038]

86 **Wang TJC**, Menda Y, Cheng SK, Wu CC, Lee NY. New tracers pet in head and neck squamous cell carcinoma. *PET Clin* 2012; **7**: 431-441 [DOI: 10.1016/j.cpet.2012.06.009]

P- Reviewers: Ciorba A, Raz E **S- Editor**: Wen LL **L- Editor**: A **E- Editor**: Zhang DN

World Journal of Radiology

Submit a Manuscript: http://www.wjgnet.com/esps/
Help Desk: http://www.wjgnet.com/esps/helpdesk.aspx
DOI: 10.4329/wjr.v6.i6.252

World J Radiol 2014 June 28; 6(6): 252-260
ISSN 1949-8470 (online)
© 2014 Baishideng Publishing Group Inc. All rights reserved.

TOPIC HIGHLIGHT

WJR 6th Anniversary Special Issues (7): PET

Congenital hyperinsulinism: Role of fluorine-18L-3, 4 hydroxyphenylalanine positron emission tomography scanning

Jaya Sujatha Gopal-Kothandapani, Khalid Hussain

Jaya Sujatha Gopal-Kothandapani, Department of Paediatric Endocrinology, Royal Manchester Children's Hospital, Manchester M13 9WL, United Kingdom
Khalid Hussain, Department of Paediatric Endocrinology, Great Ormond Street Hospital for Children NHS Trust and the Institute of Child Health, University College London, London WC1N 1EH, United Kingdom
Khalid Hussain, Developmental Endocrinology Research Group, Molecular Genetics Unit, Institute of Child Health, University College London, London WC1N 1EH, United Kingdom
Author contributions: Gopal-Kothandapani JS drafted the article; and Hussain K reviewed it critically, revised and approved the final version
Correspondence to: Dr. Khalid Hussain, Reader in Paediatric Endocrinology, Developmental Endocrinology Research Group, Molecular Genetics Unit, Institute of Child Health, University College London, 30 Guilford Street, London WC1N 1EH, United Kingdom. khalid.hussain@ucl.ac.uk
Telephone: +44-20-79052128 Fax: +44-20-74046191
Received: February 11, 2014 Revised: March 19, 2014
Accepted: May 16, 2014
Published online: June 28, 2014

Abstract

Congenital hyperinsulinism (CHI) is a rare but complex heterogeneous disorder caused by unregulated secretion of insulin from the β-cells of the pancreas leading to severe hypoglycaemia and neuroglycopaenia. Swift diagnosis and institution of appropriate management is crucial to prevent or minimise adverse neurodevelopmental outcome in children with CHI. Histologically there are two major subtypes of CHI, diffuse and focal disease and the management approach will significantly differ depending on the type of the lesion. Patients with medically unresponsive diffuse disease require a near total pancreatectomy, which then leads on to the development of iatrogenic diabetes mellitus and pancreatic exocrine insufficiency. However patients with focal disease only require a limited pancreatectomy to remove only the focal lesion thus providing complete cure to the patient. Hence the preoperative differentiation of the histological subtypes of CHI becomes paramount in the management of CHI. Fluorine-18L-3, 4-hydroxyphenylalanine positron emission tomography (^{18}F-DOPA-PET) is now the gold standard for pre-operative differentiation of focal from diffuse disease and localisation of the focal lesion. The aim of this review article is to give a clinical overview of CHI, then review the role of dopamine in β-cell physiology and finally discuss the role of ^{18}F-DOPA-PET imaging in the management of CHI.

© 2014 Baishideng Publishing Group Inc. All rights reserved.

Key words: Congenital hyperinsulinism; Fluorine-18L-3, 4-hydroxyphenylalanine positron emission tomography; Focal congenital hyperinsulinism; Diffuse congenital hyperinsulinism; Ectopic congenital hyperinsulinism; Standardized uptake value

Core tip: This manuscript describes how the advent of fluorine-18L-3, 4-hydroxyphenylalanine positron emission tomography (^{18}F-DOPA-PET) scanning has revolutionised the management of patients with a very complex condition called congenital hyperinsulinism. 18F-DOPA-PET scanning allows the accurate pre-operative localisation of the focal lesion in these patients which can then be surgically removed allowing complete cure from the hypoglycaemia.

Gopal-Kothandapani JS, Hussain K. Congenital hyperinsulinism: Role of fluorine-18L-3, 4 hydroxyphenylalanine positron emission tomography scanning. *World J Radiol* 2014; 6(6): 252-260 Available from: URL: http://www.wjgnet.com/1949-8470/full/v6/i6/252.htm DOI: http://dx.doi.org/10.4329/wjr.v6.i6.252

INTRODUCTION

Congenital hyperinsulinism (CHI) is a heterogeneous condition due to the dysregulated and inappropriate secretion of insulin from the β-cells of the pancreas leading to severe hypoglycaemia in infants. The incidence of CHI is 1 in 50000 in the general population and 1 in 2500 in the consanguineous cohorts[1]. Based on the clinical presentation-CHI can be classified into two major subgroups, transient or persistent and based on histology into three forms such as focal (40%), diffuse (50%) or atypical (10%)[2]. Transient CHI is observed in children who are born small for gestational age, those with intrauterine growth restriction (IUGR), those subjected to birth asphyxia and those born to mothers with diabetes mellitus (pre or gestational diabetes) and can last up to a week[3]. However it can last longer up to a few months in some children with IUGR[4].

The insulin secreting β-cells of the pancreas consists of a potassium channel (K_{ATP} channel) which plays a crucial role in insulin secretion and glucose homeostasis[5]. The K_{ATP} channel proteins are encoded by two genes. These are "sulphonylurea receptor subunit" (SUR1 encoded by *ABCC8*) and the "inward rectifying potassium channel subunit" (Kir6.2 encoded by *KCNJ11*) genes[6]. Both these genes are localised to chromosome 11p15.1[7]. Nearly 90% of medically unresponsive persistent CHI is caused by loss of function (recessive inactivating) mutations in these two subunits of the K_{ATP} channel involved in regulating insulin secretion[8]. They are predominantly autosomal recessive (AR) and rarely autosomal dominant (AD) in inheritance.

Mutations in genes encoding enzymes involved in insulin secretion are rare causes of CHI. They are (1) glutamate dehydrogenase (GDH) encoded by *GLUD1* gene (AD); (2) glucokinase (GCK) encoded by *GCK* gene (AD); (3) L-3-hydroxyacyl-coenzyme A dehydrogenase (HADH) encoded by HADH gene (AR); (4) hepatocyte nuclear factor 4-alpha (HNF4-a) encoded by *HNF4A* gene(AD); (5) monocarboxylate transporter (MCT1) encoded by *SLC16A1* gene (AD); and (6) uncoupling protein 2 encoded by *UCP2* gene (AD)[9]. No genetic aetiology has been identified in about 70%-80% of patients who are responsive to medical therapy with diazoxide.

Of the three histological forms of CHI, the typical diffuse form is characterised by the abundant distribution of enlarged and hyperchromatic nuclei throughout the islets[2]. It is predominantly caused by recessive loss of function mutations in the K_{ATP} channel (*ABCC8* and *KCNJ11* genes) and when unresponsive to medical therapy requires a near total (≥ 95%) pancreatectomy[2] (Figure 1). The focal form is characterised by an isolated cluster of abnormal insulin producing cells with 'normal 'surrounding tissue within the pancreas (Figure 2). Histologically it involves focal adenomatous hyperplasia of the islet cells with ductuloinsular complexes and scattered giant β-cell nuclei surrounded by normal pancreatic parenchyma[2,10,11]. Focal CHI is always sporadic in inheritance and caused by the paternal heterozygous mutation

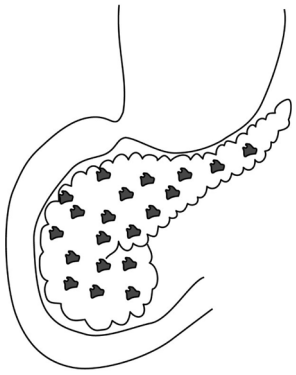

Diffuse:
Entire pancreas affected
Associated with mutations in ABCC8/ KCNJ11/GCK/GLUD1/HNF4A/ HADH and SLC16A1

Figure 1 Diffuse lesion where the entire pancreas is affected. It is associated with recessive and dominant mutations in the *ABCC8/KCNJ11/GCK/GLUD1/HNF4A/HADH* and *SLC16A1*.

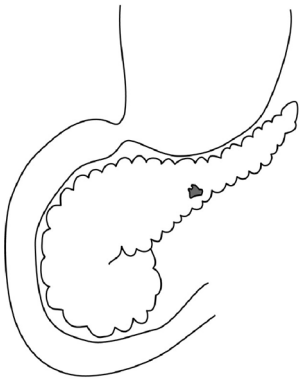

Focal:
Localised region of pancreas affected
Associated with a paternal mutation in ABCC8/KCNJ11 and paternal UPD encompassing 11p5.1 to 11p15.5 in the focal area

Figure 2 Focal lesion affecting only a single region of the pancreas. It is associated with a paternal mutation in the *ABCC8* or *KCNJ11* and paternal uniparental disomy encompassing 11p5.1 to 11p5.5 in the focal area.

in *ABCC8/KCNJ11* genes along with somatic loss of maternal allele in the focal hyperplastic tissue requiring a focal lesionectomy[12].

Nearly 10% of CHI is of atypical form, the molecular mechanism and histopathological differentiation of which is yet to be completely understood[13]. Children with persistent CHI often require high glucose concentrations (> 8mg/kg/min) to maintain euglycemia. The diagnosis of CHI is primarily made by biochemical investigations demonstrating detectable levels of insulin in relation to hypoglycaemia along with reduced/absent free fatty acids and ketone bodies[12]. Current medical management for CHI includes Diazoxide along with Chlorothiazide as the first line therapy and Octreotide as a second line drug[12].

Children who are not responding to medical management, and in whom the genetic testing is inconclusive or in favour of a focal lesion, should undergo 18F-DOPA-PET scan to ascertain the type of lesion whether it is fo-

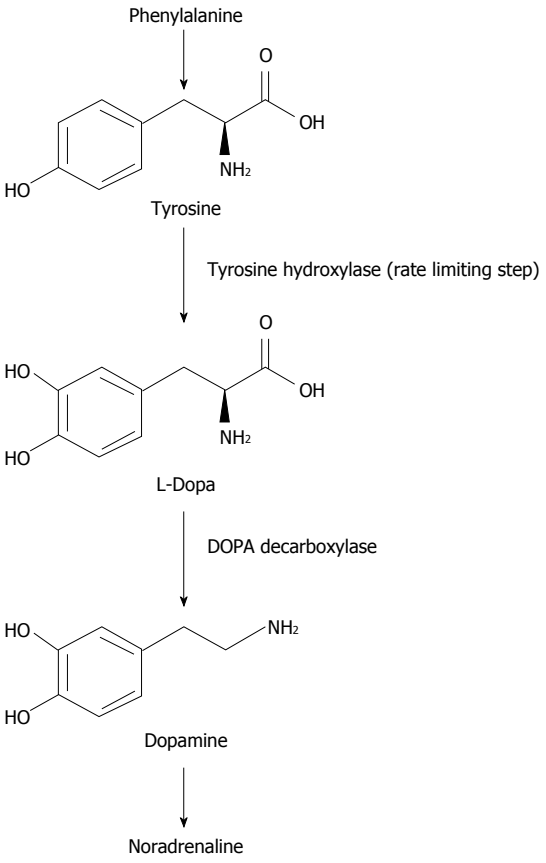

Figure 3 Dopamine biochemistry. Phenylalanine is converted into L-Tyrosine. L-Tyrosine is then converted into L-Dopa by Tyrosine Hydroxylase. L-Dopa is then converted into Dopamine by DOPA decarboxylase.

cal or diffuse and provide guidance towards surgery[1].

Pre-operative delineation of the subtype of the lesion becomes extremely crucial as the management approach and the treatment modalities differ significantly based on the type of the lesion. Focal CHI typically does not respond to medical management and a focal lesionectomy provides a definite cure for the condition by avoiding further hypoglycaemic episodes and its neurological complications. A focal lesionectomy also minimises the risk of iatrogenic diabetes mellitus and exocrine pancreatic insufficiency. Children with diffuse CHI warrant a sub total or a near total pancreatectomy to prevent brain damage from neuroglycopaenia, however the risk of developing diabetes mellitus and exocrine insufficiency in later life is quite high[14].

DOPAMINE METABOLISM

Dopamine is synthesised from a non-essential amino acid, tyrosine which is first converted to L-dopa by tyrosine hydroxylase. This is the rate limiting step in dopamine production. Then L-Dopa is decarboxylated to dopamine by DOPA decarboxylase. Dopamine is then oxidised to nor-adrenaline (Figure 3).

Dopamine plays different roles in various internal organs. In the brain, it acts as a neurotransmitter and plays a major role in neuropsychiatric and movement disorders such as Schizophrenia and Parkinson's disease[15]. It also acts as a local chemical messenger in other organs such as bloods vessels, kidney, gastrointestinal mucosa and including pancreas[16].

Dopamine exerts its effects by binding to and activating receptors on the surface of cells. In humans five subtypes of dopamine receptors have been identified, labelled D1 through D5[16]. All of them exert their effects *via* a complex second messenger system [*e.g.*, cyclic AMP]. Dopamine signalling is mediated by five cloned receptors, grouped into D1-like (D1 and D5 receptors) and D2-like (D2, D3 and D4 receptors) families. The presence of dopamine receptors from both families has been identified in human isolated islets[16]. D2 receptor expression was confirmed by immunodetection revealing localization on insulin secretory granules of human β-cells[16].

Studies carried out in mouse pancreatic islets have shown pancreatic islets as the site for Dopamine synthesis and storage outside the central nervous system and both Dopamine and L-Dopa exerts a negative feedback action on insulin secretion in correlation with the reduction in intracellular [Ca^{2+}] influx[17,18].

A study done recently has shown a negative feedback regulatory circuit for glucose-stimulated insulin secretion in purified human islets *in vitro*[19]. The release of dopamine and insulin together in response to the glucose load is demonstrated by the *in-vitro* infusion of dopamine into the insulin-containing secretory granules of human β-cells. Dopamine in turn exerts an antagonistic action on the D2 receptors that are also expressed on β-cells and thus inhibiting insulin secretion[19].

Neuroendocrine cells and pancreatic islets take up L-DOPA and convert it into Dopamine by the enzyme DOPA decarboxylase, which is expressed in β-cells of the pancreatic islets[20-23]. Thus decarboxylation of the L-DOPA to dopamine in the β-cells of the pancreatic islets allows localization of the lesion by means of PET scanning, using radioactive isomer ^{18}F-L-DOPA[24]. ^{18}F-DOPA is a radiotracer analogue of DOPA and this radioactive tracer is taken up, decarboxylated and stored in cytoplasmic secretory granules by both the endocrine and exocrine cells of the pancreas[23,25]. This mechanism acts as the principle behind the use of this non-invasive ^{18}F-DOPA-PET imaging technique as the diagnostic tool of choice in localising the focal lesion. Both focal and diffuse forms have high DOPA decarboxylase activity and in focal lesions there is excessive tracer uptake in the lesion when compared to the rest of the pancreas (Figure 4).

In diffuse CHI there is generalised increased tracer uptake with a relatively higher uptake in the head when compared to the rest of the pancreas[14,26,27]. ^{18}F-DOPA is excreted by kidneys hence normal bio-distribution is seen in kidneys, ureter and urinary bladder. An excessive uptake is also seen in gall bladder and biliary tract and a low uptake is seen in liver, heart and basal ganglia[26].

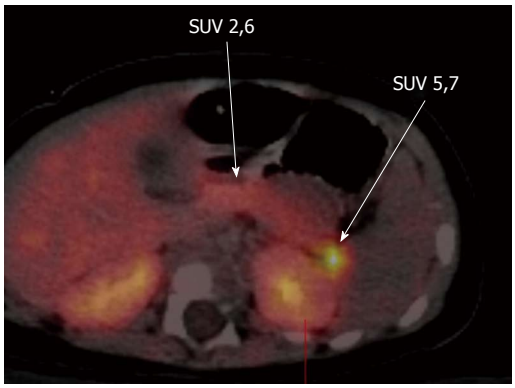

Figure 4 Fluorine-18L-3, 4-hydroxyphenylalanine positron emission tomography scan showing the focal lesion in the tail of the pancreas.

DIAGNOSTIC METHODS TO LOCALISE FOCAL LESION

Until recently the methods used to localise the focal lesion were (1) Hepatic portal venous sampling (PVS)[28,29]; (2) arterial calcium stimulation test[30,31]; and (3) tolbutamide response test[32]. PVS is invasive, time consuming, technically challenging and is associated with risk of severe hypoglycaemia and the accuracy is only about 70%[28,33]. Arterial calcium stimulation and tolbutamide response test are not found to be accurate in distinguishing between focal and diffuse CHI[30-32,34,35] Imaging modalities such as computed tomography (CT) and magnetic resonance imaging (MRI) has not been found very useful in localising the focal lesion[14].

^{18}F-DOPA-PET/CT was first reported for the localisation of the focal lesion by Riberio *et al*[13] in 2005 and Otonkoski *et al*[36] in 2006. Since then several studies have shown that ^{18}F-DOPA-PET/CT provides precise differentiation between focal and diffuse forms albeit exact localisation of the lesion may not be accurately attributed by the scan technique[13,21,37]. However, ^{18}F-DOPA-PET/CT is non-invasive, relatively simple to use and more efficient than the invasive procedures such as PVS, and arterial calcium stimulation tests in differentiating and localising the pancreatic lesions[38]. The sensitivity and specificity of ^{18}F-DOPA-PET/CT in detecting focal lesions measuring between 2 mm and 10 mm is approximately 90% and 100% respectively[39]. Thus the use of ^{18}F-DOPA-PET/CT has revolutionised the surgical outcome in these children with CHI.

USE OF ^{18}F-DOPA-PET/CT IN CHI

The use of ^{18}F-DOPA-PET/CT in distinguishing between focal and diffuse CHI was first reported by Riberio *et al*[13], where the authors subjected 15 neonates to ^{18}F-DOPA-PET scan. Abnormal focal uptake was observed in 5 children and diffuse uptake in the rest. Histopathology findings of all 5 patients with focal lesion and 4 patients with diffuse uptake who underwent surgery matched with their PET scan findings.

Otonkoski *et al*[36] used ^{18}F-DOPA-PET/CT in 14 patients (*ABCC8* mutation in 11/14 patients) and found focal uptake in 5 patients, diffuse uptake in the remaining 9 patients. ^{18}F-DOPA-PET/CT findings were confirmed by histology in all 5 patients with focal uptake and 4 out of 9 in patients with diffuse uptake. This group also measured the standardized uptake value (SUV) of ^{18}F-DOPA and found a SUV of > 50% higher uptake than the maximum SUV of the unaffected part of the pancreas in the focal group which corresponded with the histology findings. The remaining 9 patients with a diffuse uptake on the ^{18}F-DOPA-PET/CT scan had a SUV ratio of < 1.5. Histology findings confirmed diffuse disease in 4 patients and pancreatic venous sampling in 4 patients. The authors concluded by proposing ^{18}F-DOPA-PET/CT as the best modality of choice in locating a focal lesion[36].

Riberio *et al*[40] did a retrospective study in 2007 on forty nine children with CHI who had undergone ^{18}F-DOPA-PET/CT scanning. They identified abnormal focal pancreatic uptake of ^{18}F-DOPA in 15 children, where diffuse radio-tracer uptake was observed in the pancreatic area in the other 34 children. They also subjected 12 of the 49 children for pancreatic venous sampling (PVS) and 31 for MRI. In children who underwent both PET and PVS, the results were concordant in 11 out of 12. The authors concluded that PET scan with ^{18}F-DOPA is an accurate non-invasive technique allowing differential diagnosis between focal and diffuse forms of CHI[40].

Arbizu Lostao *et al*[41] reported their first patient from Spain in whom the diagnosis of focal CHI was made in a 13 month old child using combined genetic analysis [paternal heterozygous mutation (G111R) in the *ABCC8* gene] and ^{18}F-DOPA-PET/CT imaging (focal uptake in the body of the pancreas) was successfully treated by surgery. This case report reiterates the importance of performing combined investigations towards the successful management of CHI.

Barthlen *et al*[22] in 2008 reported the correlation of ^{18}F-DOPA-PET/CT scan findings with the intra-operative findings in 9 out of 10 children. A limited resection was found to be curative in 8 out of 9 children. They also reported their follow up data on these children with no evidence of diabetes or exocrine pancreatic insufficiency[22].

Cherubini *et al*[42] have reported that ^{18}F-DOPA-PET/CT imaging can distinguish between focal and diffuse lesions in majority of the cases and 100% accurate in locating the focal lesion. The authors also highlighted the potentiating effects of non-invasive imaging technique using ^{18}F-DOPA-PET/CT imaging combined with laparoscopic pancreatic surgery in the prompt localisation and excision of the focal lesion, preventing iatrogenic diabetes mellitus in later life[42].

Yorifuji *et al*[43] reported a boy with focal CHI whose disease activity was not consistent with the uptake of ^{18}F DOPA. A diagnosis of CHI was made on day 2 of his life when he presented with hypoglycaemic seizures. A paternal heterozygous mutation c.4186G 1T (p.D1396Y)

in the *ABCC8* was identified followed by an uptake in the body of pancreas in the ^{18}F-DOPA-PET/CT scan. A diagnosis of focal CHI was made and he was managed conservatively with frequent feeding regime. He achieved spontaneous remission at 1 year and 10 mo of age and a follow up ^{18}F-DOPA-PET/CT scan revealed no difference in uptake between the two scans despite achieving clinical remission. Further to this an arterial stimulation venous sampling test was done which showed a low basal and stimulated insulin release illustrating that ^{18}F-DOPA-PET/CT uptake may not always correlate with the insulin secreting capacity of the β-cells and the spontaneous remission of hypoglycaemia can be a functional process and not due to the apoptotic death of β abnormal cells[43].

Zani *et al*[44] evaluated the accuracy of ^{18}F-DOPA-PET/CT imaging technique in differentiating between focal and diffuse lesions and localisation of the focal lesion. The authors reviewed the results of ^{18}F-DOPA-PET/CT scan performed in 19 patients. Five of them had diffuse uptake and the same was confirmed by histology. The remaining 14 patients showed a focal uptake which was confirmed by histology however the localisation was not accurate in 5 children leading to incorrect surgical resection. The authors concluded that ^{18}F-DOPA-PET/CT scan can distinguish between focal and diffuse CHI and the exact localisation in only 2/3 of patients with focal lesions. The authors also suggested undertaking intraoperative histological confirmation of the focal lesion prior to complete excision[44].

Masue *et al*[45] reported their experience of the use of ^{18}F-DOPA-PET/CT in 17 Japanese children by assessing their results either by simple inspection or by calculating the pancreas percentage and compared those results with the genetic analysis and histology. Pancreas percentage is the expression of uptake of the head, body and tail of the pancreas as the total maximum SUV of the whole pancreas. They found the localisation and histology was consistent in all 17 children. However the overall results were consistent with the molecular diagnosis and histology in only 7/17 and 6/12 patients respectively. They also reported a substantial improvement in the accuracy of PET studies by using pancreatic percentage[45].

Ismail *et al*[12] reported the marked variation in the clinical, genetic, radiological and histopathological features of focal CHI in 3 of their patients. All 3 of them had paternal heterozygous mutation in *ABCC8* gene (c.3992-9G → A in the first 2 patients and c.4477G → A in third patient). Of the 2 patients, first patient was responded to Diazoxide but not the second patient. The focal lesions in these 2 patients were accurately localised using ^{18}F-DOPA-PET/CT imaging. Both of them underwent focal lesionectomy and were completely cured. Histology confirmed the presence of focal nodules with large nuclei along with the remaining normal pancreatic tissue in the first 2 patients. The authors proposed that unknown genetic or environmental factors may influence the phenotypic variation in response to treatment and some focal lesions can respond to medical management. The authors have also highlighted that a paternally inherited c.3992-9G → A mutation in the *ABCC8* gene is associated with a mild focal phenotype responding to medical management in some patients of Ashkenazi Jewish origin[12]. This finding is based on previous reports that nearly 90% of CHI in Ashkenazi Jewish population is associated with c.3992-9G → A mutation and p.F1388del in the *ABCC8* gene[46]. The third patient had undergone two ^{18}F-DOPA-PET/CT imaging, with an unusually large focal lesion involving the whole pancreas. The first scan showed the tracer uptake in the body and tail and the second scan performed post lesionectomy showed a tracer uptake in the head of the pancreas and the patient underwent 2 pancreatic surgeries. Macroscopically this patient had a normal looking pancreas but microscopically islet cell nodules with large nuclei were found along with some normal pancreatic tissue. Despite undergoing the second surgery this patient was reported to be dependent on continuous gastrostomy feeds to maintain euglycemia[12].

Giurgea *et al*[47] reported that the size of the focal lesion is determined by the timing when the somatic loss of maternal allele occurs during the gestational age[47]. The earlier it occurs the larger the size of the focal lesion can be, as found in the 3 patient in this report. Also it has been suggested that an unknown mechanism might play a role in different rate of tracer uptake in different regions of pancreas in large focal lesions[47].

Meintjes *et al*[26] recently evaluated and reported the accuracy of delineating the focal and diffuse CHI using ^{18}F fluoro-L-DOPA/CT and contrast enhanced CT. They performed 22 ^{18}F fluoro-L-DOPA/CT and contrast enhanced CT studies on 18 patients and assessed those results using visual assessment followed by quantitative comparison of SUVs measured by calculating the uptake on head, body and tail of the pancreas. They derived an SUV ratio using the formula-highest SUV (max)/next highest SUV (max). The authors also proposed a time activity curve which showed the focal pancreatic islet uptake relatively constant over time suggesting performing imaging at 20 min and 50 min after the radio tracer injection. The use of intravenous contrast agents during CT provides invaluable information for the surgeons in delineating the anatomical landmarks while performing surgery.

Of the 18 patients 13 showed diffuse with an SUV ratio of < 1.3 and five showed focal uptake with an SUV ratio of > 1.5 with an SUV (max) 50% higher than that of the unaffected area of the pancreas. Out of these five patients four of them had paternal *ABCC8* mutation. All five patients were cured after limited focal resection with three of them requiring second ^{18}F-L-DOPA/CT and contrast enhanced CT and surgery. Of the 13 patients who had diffuse disease, 9 of them were negative for *ABCC8/KCNJ11* mutations and 3 had positive paternal *ABCC8* mutation. Out of 13, 2 patients underwent surgery and 11 patients remain on high dose Diazoxide treatment one of them had 3 pancreatectomies without

cure. The authors concluded by highlighting the importance of per-operative ^{18}F-L-DOPA/CT and contrast enhanced CT studies in not only distinguishing between the focal and the diffuse disease but also the precise localisation of the anatomical landmarks[26].

Laje *et al*[48] did a retrospective review to determine the accuracy of ^{18}F-DOPA-PET/CT scan in diagnosing focal CH on 105 children in whom a pre-operative ^{18}F-DOPA-PET/CT scan was undertaken. Out of 105 patients, 53 patients had focal lesion and the remaining 52 patients had diffuse disease. Eight out of 53 patients with focal lesion were reported to have diffuse disease on their pre-operative ^{18}F-DOPA-PET/CT scan. The location of the eight missed lesions was head (3), body (2) and tail (3) which showed a homo/heterogeneous tracer uptake throughout the pancreas. Thus the sensitivity of ^{18}F-DOPA-PET/CT scan in diagnosing a focal lesion was 85% based on this study. Two out of 52 patients with diffuse disease were reported to have focal lesion on their pre-operative ^{18}F-DOPA-PET/CT scan with a specificity of 96%. The positive predictive value of the study was 96% with 45 out of 47 patients having a true focal lesion. The authors concluded that the sensitivity and specificity of the ^{18}F-DOPA-PET/CT scan varies based on the location of the lesion and the experience of the radiologists[48].

A meta-analysis was performed and published recently by Yang J and his colleagues reviewing the diagnostic role of ^{18}F-DOPA PET and ^{18}F-DOPA PET/CT imaging in CHI in 10 studies involving 181 children. The pooled sensitivity and the specificity in detecting focal CHI using ^{18}F DOPA PET and PET/CT was reported to be 88% (95%CI: 80%-94%) and 79% (95%CI: 69%-87%) respectively on a per-patient-based analysis in this systematic review. The area under the summary receiver operating characteristic curve (SROC) was estimated to be 0.92% suggesting that ^{18}F-DOPA PET and PET/CT imaging are accurate tools for distinguishing focal diagnosing CHI, although there is a minimal risk of both false positive and false negative results. The authors concluded that ^{18}F-DOPA PET is very helpful in differentiating between focal and diffuse lesions, and should be the first investigation of choice when the genetic test results are inconclusive and ^{18}F-DOPA PET/CT is very helpful in localising the lesion and thereby improving the treatment outcome in focal CHI[27].

Blomberg *et al*[38] conducted a systematic review and meta-analysis recently to quantify the diagnostic performance of pancreatic venous sampling (PVS), selective pancreatic arterial calcium stimulation with hepatic venous sampling (ASVS) and ^{18}F-DOPA-PET/CT in diagnosing and localising focal CH. They reported that ^{18}F-DOPA-PET/CT is superior in distinguishing focal from diffuse CH with a summary diagnostic odds ratio (DOR) of 73.2 when compared to PVS (summary DOR 23.5) and ASVS (summary DOR, 4.3). Also the pooled accuracy for localising a focal lesion by ^{18}F-DOPA-PET/CT is higher (0.82) when compared to PVS (0.76) and ASVS (0.64). Thus this review concluded that ^{18}F-DOPA-PET/CT is superior in diagnosing and localising focal CHI lesion in patients requiring surgery albeit the limitation of the review is the inclusion of small sample sizes and high probability of bias leading to the overestimation of diagnostic accuracy[38].

ECTOPIC PANCREAS AND THE ROLE OF ^{18}F-DOPA-PET/CT

The pancreas begins to develop from the distal end of the foregut endoderm during the fourth week when both the dorsal and ventral pancreatic buds grow into the mesogastrium[49]. Thus the pancreatic acinar and the islet cells are derived from the endodermal cells lining the upper and duodenal region of the foregut[50]. During the course of this development an ectopic pancreatic tissue may occur in the stomach, duodenum, jejunum, ileum and rarely in Meckel's diverticulum, appendix, biliary tract or lungs[49].

There have been reports of ectopic pancreatic tissue causing CHI in both adults and children. We reported a child with persistent and severe hyperinsulinaemic hypoglycaemia (HH) despite undergoing three pancreatectomies with a choledochoduodenostomy and a cholecystectomy. An ^{18}F-DOPA-PET/CT scan localised the ectopic lesion in the vicinity of the former head of pancreas. The same lesion was found to be localized near the duodenum, either in the duodenal wall or cavity on the magnetic resonance scan (MRI). He is subsequently managed medically[33].

Peranteau *et al*[51] in 2007 reported another patient with persistent hypoglycaemia despite undergoing a near-total pancreatectomy. A subsequent ^{18}F-DOPA-PET/CT scan demonstrated one focus in the remnant pancreatic head and 3 in the abdomen. The lesion in the pancreatic remnant was removed completing a total pancreatectomy and further abdominal exploration revealed 4 pancreatic ectopic rests in the jejunum. The lesions were surgically removed and the histopathology confirmed focal islet cell hyperplasia in all the lesions. This patient required insulin therapy for a short term post operatively.

In both of these patients ^{18}F-DOPA-PET/CT scan was performed post near total pancreatectomy with the persistence of hypoglycaemic symptoms. However a preoperative localisation of the focal lesions would have led to the removal of local and ectopic lesions and preservation of the rest of the pancreas. Thus the use of ^{18}F-DOPA-PET/CT scan in the management of CHI is justified in identification of both focal lesions within the pancreas and ectopic pancreatic tissue[51].

A standardised protocol for the use of ^{18}F-DOPA-PET/CT was derived in 2005 and advocated to achieve maximum acquisition with minimum radiation. This guideline was derived based on the survey conducted in 2005 reviewing the experience of all the PET centres. The result of the survey showed that ^{18}F-DOPA-PET/CT has 94% sensitivity and 100% specificity. Thus pre-

operative performance of ^{18}F-DOPA-PET/CT has been proposed as the most accurate way of localising the focus enabling limited resection and thereby preventing the risk of iatrogenic diabetes[14]. Studies recommended performing ^{18}F-DOPA/CT studies only in tertiary endocrine centre equipped with necessary expertise to perform and interpret the results[14].

CONCLUSION

We conclude that ^{18}F-DOPA-PET/CT is a safe, non-invasive and the most preferred investigation of choice (1) to distinguish between the focal and diffuse forms of CHI; and (2) to enable accurate localisation and enucleation of the focal lesion preventing the risk of developing iatrogenic diabetes mellitus and pancreatic insufficiency. However a multi-disciplinary team (MDT) approach is essential and has to be undertaken in a tertiary centre built-in with necessary expertise for the successful interpretation and management of CHI patients.

REFERENCES

1 **Arnoux JB**, Verkarre V, Saint-Martin C, Montravers F, Brassier A, Valayannopoulos V, Brunelle F, Fournet JC, Robert JJ, Aigrain Y, Bellanné-Chantelot C, de Lonlay P. Congenital hyperinsulinism: current trends in diagnosis and therapy. *Orphanet J Rare Dis* 2011; **6**: 63 [PMID: 21967988 DOI: 10.1186/1750-1172-6-63]

2 **Rahier J**, Guiot Y, Sempoux C. Persistent hyperinsulinaemic hypoglycaemia of infancy: a heterogeneous syndrome unrelated to nesidioblastosis. *Arch Dis Child Fetal Neonatal Ed* 2000; **82**: F108-F112 [PMID: 10685982]

3 **Yap F**, Högler W, Vora A, Halliday R, Ambler G. Severe transient hyperinsulinaemic hypoglycaemia: two neonates without predisposing factors and a review of the literature. *Eur J Pediatr* 2004; **163**: 38-41 [PMID: 14586649 DOI: 10.1007/s00431-003-1328-2]

4 **Fafoula O**, Alkhayyat H, Hussain K. Prolonged hyperinsulinaemic hypoglycaemia in newborns with intrauterine growth retardation. *Arch Dis Child Fetal Neonatal Ed* 2006; **91**: F467 [PMID: 17056857 DOI: 10.1136/adc.2006.095919]

5 **Ashcroft FM**, Harrison DE, Ashcroft SJ. Glucose induces closure of single potassium channels in isolated rat pancreatic beta-cells. *Nature* 1984; **312**: 446-448 [PMID: 6095103]

6 **Thomas PM**, Cote GJ, Wohllk N, Haddad B, Mathew PM, Rabl W, Aguilar-Bryan L, Gagel RF, Bryan J. Mutations in the sulfonylurea receptor gene in familial persistent hyperinsulinemic hypoglycemia of infancy. *Science* 1995; **268**: 426-429 [PMID: 7716548 DOI: 10.1126/science.7716548]

7 **de Lonlay P**, Fournet JC, Rahier J, Gross-Morand MS, Poggi-Travert F, Foussier V, Bonnefont JP, Brusset MC, Brunelle F, Robert JJ, Nihoul-Fékété C, Saudubray JM, Junien C. Somatic deletion of the imprinted 11p15 region in sporadic persistent hyperinsulinemic hypoglycemia of infancy is specific of focal adenomatous hyperplasia and endorses partial pancreatectomy. *J Clin Invest* 1997; **100**: 802-807 [PMID: 9259578]

8 **Flanagan SE**, Clauin S, Bellanné-Chantelot C, de Lonlay P, Harries LW, Gloyn AL, Ellard S. Update of mutations in the genes encoding the pancreatic beta-cell K(ATP) channel subunits Kir6.2 (KCNJ11) and sulfonylurea receptor 1 (ABCC8) in diabetes mellitus and hyperinsulinism. *Hum Mutat* 2009; **30**: 170-180 [PMID: 18767144 DOI: 10.1002/humu.20838]

9 **Kapoor RR**, Flanagan SE, James C, Shield J, Ellard S, Hussain K. Hyperinsulinaemic hypoglycaemia. *Arch Dis Child* 2009; **94**: 450-457 [PMID: 19193661 DOI: 10.1136/adc.2008.148171]

10 **Goossens A**, Gepts W, Saudubray JM, Bonnefont JP, Nihoul-Fekete PU, Klöppel G. Diffuse and focal nesidioblastosis. A clinicopathological study of 24 patients with persistent neonatal hyperinsulinemic hypoglycemia. *Am J Surg Pathol* 1989; **13**: 766-775 [PMID: 2669541]

11 **Klöppel G**, Reinecke-Lüthge A, Koschoreck F. Focal and Diffuse Beta Cell Changes in Persistent Hyperinsulinemic Hypoglycemia of Infancy. *Endocr Pathol* 1999; **10**: 299-304 [PMID: 12114766]

12 **Ismail D**, Kapoor RR, Smith VV, Ashworth M, Blankenstein O, Pierro A, Flanagan SE, Ellard S, Hussain K. The heterogeneity of focal forms of congenital hyperinsulinism. *J Clin Endocrinol Metab* 2012; **97**: E94-E99 [PMID: 22031516 DOI: 10.1210/jc.2011-1628]

13 **Ribeiro MJ**, De Lonlay P, Delzescaux T, Boddaert N, Jaubert F, Bourgeois S, Dollé F, Nihoul-Fékété C, Syrota A, Brunelle F. Characterization of hyperinsulinism in infancy assessed with PET and 18F-fluoro-L-DOPA. *J Nucl Med* 2005; **46**: 560-566 [PMID: 15809476]

14 **Mohnike K**, Blankenstein O, Christesen HT, De Lonlay J, Hussain K, Koopmans KP, Minn H, Mohnike W, Mutair A, Otonkoski T, Rahier J, Ribeiro M, Schoenle E, Fékété CN. Proposal for a standardized protocol for 18F-DOPA-PET (PET/CT) in congenital hyperinsulinism. *Horm Res* 2006; **66**: 40-42 [PMID: 16710094 DOI: 10.1159/000093471]

15 **Callier S**, Snapyan M, Le Crom S, Prou D, Vincent JD, Vernier P. Evolution and cell biology of dopamine receptors in vertebrates. *Biol Cell* 2003; **95**: 489-502 [PMID: 14597267 DOI: 10.1016/S0248-4900(03)00089-3]

16 **Rubí B**, Ljubicic S, Pournourmohammadi S, Carobbio S, Armanet M, Bartley C, Maechler P. Dopamine D2-like receptors are expressed in pancreatic beta cells and mediate inhibition of insulin secretion. *J Biol Chem* 2005; **280**: 36824-36832 [PMID: 16129680 DOI: 10.1074/jbc.M505560200]

17 **Ustione A**, Piston DW. Dopamine synthesis and D3 receptor activation in pancreatic β-cells regulates insulin secretion and intracellular [Ca(2+)] oscillations. *Mol Endocrinol* 2012; **26**: 1928-1940 [PMID: 22918877 DOI: 10.1210/me.2012-1226]

18 **Ericson LE**, Håkanson R, Lundquist I. Accumulation of dopamine in mouse pancreatic B-cells following injection of L-DOPA. Localization to secretory granules and inhibition of insulin secretion. *Diabetologia* 1977; **13**: 117-124 [PMID: 404204 DOI: 10.1007/BF00745138]

19 **Simpson N**, Maffei A, Freeby M, Burroughs S, Freyberg Z, Javitch J, Leibel RL, Harris PE. Dopamine-mediated autocrine inhibitory circuit regulating human insulin secretion in vitro. *Mol Endocrinol* 2012; **26**: 1757-1772 [PMID: 22915827 DOI: 10.1210/me.2012-1101]

20 **Lindström P**. Aromatic-L-amino-acid decarboxylase activity in mouse pancreatic islets. *Biochim Biophys Acta* 1986; **884**: 276-281 [PMID: 3533158]

21 **Hardy OT**, Hernandez-Pampaloni M, Saffer JR, Suchi M, Ruchelli E, Zhuang H, Ganguly A, Freifelder R, Adzick NS, Alavi A, Stanley CA. Diagnosis and localization of focal congenital hyperinsulinism by 18F-fluorodopa PET scan. *J Pediatr* 2007; **150**: 140-145 [PMID: 17236890]

22 **Barthlen W**, Blankenstein O, Mau H, Koch M, Höhne C, Mohnike W, Eberhard T, Fuechtner F, Lorenz-Depiereux B, Mohnike K. Evaluation of [18F]fluoro-L-DOPA positron emission tomography-computed tomography for surgery in focal congenital hyperinsulinism. *J Clin Endocrinol Metab* 2008; **93**: 869-875 [PMID: 18073294 DOI: 10.1210/jc.2007-2036]

23 **de Lonlay P**, Simon-Carre A, Ribeiro MJ, Boddaert N, Giurgea I, Laborde K, Bellanné-Chantelot C, Verkarre V, Polak M, Rahier J, Syrota A, Seidenwurm D, Nihoul-Fékété C, Robert JJ, Brunelle F, Jaubert F. Congenital hyperinsulinism: pancreatic [18F]fluoro-L-dihydroxyphenylalanine (DOPA) positron emission tomography and immunohistochemistry study of DOPA decarboxylase and insulin secretion. *J Clin Endocrinol*

Metab 2006; **91**: 933-940 [PMID: 16403819 DOI: 10.1210/jc.2005-1713]
24 **Jager PL**, Chirakal R, Marriott CJ, Brouwers AH, Koopmans KP, Gulenchyn KY. 6-L-18F-fluorodihydroxyphenylalanine PET in neuroendocrine tumors: basic aspects and emerging clinical applications. *J Nucl Med* 2008; **49**: 573-586 [PMID: 18344441 DOI: 10.2967/jnumed.107.045708]
25 **Koopmans KP**, Neels ON, Kema IP, Elsinga PH, Links TP, de Vries EG, Jager PL. Molecular imaging in neuroendocrine tumors: molecular uptake mechanisms and clinical results. *Crit Rev Oncol Hematol* 2009; **71**: 199-213 [PMID: 19362010 DOI: 10.1016/j.critrevonc.2009.02.009]
26 **Meintjes M**, Endozo R, Dickson J, Erlandsson K, Hussain K, Townsend C, Menezes L, Bomanji J. 18F-DOPA PET and enhanced CT imaging for congenital hyperinsulinism: initial UK experience from a technologist's perspective. *Nucl Med Commun* 2013; **34**: 601-608 [PMID: 23571817 DOI: 10.1097/MNM.0b013e32836069d0]
27 **Yang J**, Hao R, Zhu X. Diagnostic role of 18F-dihydroxyphenylalanine positron emission tomography in patients with congenital hyperinsulinism: a meta-analysis. *Nucl Med Commun* 2013; **34**: 347-353 [PMID: 23376859 DOI: 10.1097/MNM.0b013e32835e6ac6]
28 **Brunelle F**, Negre V, Barth MO, Fekete CN, Czernichow P, Saudubray JM, Kuntz F, Tach T, Lallemand D. Pancreatic venous samplings in infants and children with primary hyperinsulinism. *Pediatr Radiol* 1989; **19**: 100-103 [PMID: 2537942 DOI: 10.1007/BF02387895]
29 **Dubois J**, Brunelle F, Touati G, Sebag G, Nuttin C, Thach T, Nikoul-Fekete C, Rahier J, Saudubray JM. Hyperinsulinism in children: diagnostic value of pancreatic venous sampling correlated with clinical, pathological and surgical outcome in 25 cases. *Pediatr Radiol* 1995; **25**: 512-516 [PMID: 8545179]
30 **Chigot V**, De Lonlay P, Nassogne MC, Laborde K, Delagne V, Fournet JC, Nihoul-Fékété C, Saudubray JM, Brunelle F. Pancreatic arterial calcium stimulation in the diagnosis and localisation of persistent hyperinsulinemic hypoglycaemia of infancy. *Pediatr Radiol* 2001; **31**: 650-655 [PMID: 11512008 DOI: 10.1007/s0024710310650]
31 **Abernethy LJ**, Davidson DC, Lamont GL, Shepherd RM, Dunne MJ. Intra-arterial calcium stimulation test in the investigation of hyperinsulinaemic hypoglycaemia. *Arch Dis Child* 1998; **78**: 359-363 [PMID: 9623401]
32 **Stanley CA**, Thornton PS, Ganguly A, MacMullen C, Underwood P, Bhatia P, Steinkrauss L, Wanner L, Kaye R, Ruchelli E, Suchi M, Adzick NS. Preoperative evaluation of infants with focal or diffuse congenital hyperinsulinism by intravenous acute insulin response tests and selective pancreatic arterial calcium stimulation. *J Clin Endocrinol Metab* 2004; **89**: 288-296 [PMID: 14715863 DOI: 10.1210/jc.2003-030965]
33 **Hussain K**, Seppänen M, Näntö-Salonen K, Adzick NS, Stanley CA, Thornton P, Minn H. The diagnosis of ectopic focal hyperinsulinism of infancy with [18F]-dopa positron emission tomography. *J Clin Endocrinol Metab* 2006; **91**: 2839-2842 [PMID: 16684819 DOI: 10.1210/jc.2006-0455]
34 **Huopio H**, Jääskeläinen J, Komulainen J, Miettinen R, Kärkkäinen P, Laakso M, Tapanainen P, Voutilainen R, Otonkoski T. Acute insulin response tests for the differential diagnosis of congenital hyperinsulinism. *J Clin Endocrinol Metab* 2002; **87**: 4502-4507 [PMID: 12364426 DOI: 10.1210/jc.2002-020378]
35 **Giurgea I**, Laborde K, Touati G, Bellanné-Chantelot C, Nassogne MC, Sempoux C, Jaubert F, Khoa N, Chigot V, Rahier J, Brunelle F, Nihoul-Fékété C, Dunne MJ, Stanley C, Saudubray JM, Robert JJ, de Lonlay P. Acute insulin responses to calcium and tolbutamide do not differentiate focal from diffuse congenital hyperinsulinism. *J Clin Endocrinol Metab* 2004; **89**: 925-929 [PMID: 14764815 DOI: 10.1210/jc.2003-030941]
36 **Otonkoski T**, Näntö-Salonen K, Seppänen M, Veijola R, Huopio H, Hussain K, Tapanainen P, Eskola O, Parkkola R, Ekström K, Guiot Y, Rahier J, Laakso M, Rintala R, Nuutila P, Minn H. Noninvasive diagnosis of focal hyperinsulinism of infancy with [18F]-DOPA positron emission tomography. *Diabetes* 2006; **55**: 13-18 [PMID: 16380471]
37 **Mohnike K**, Blankenstein O, Minn H, Mohnike W, Fuchtner F, Otonkoski T. [18F]-DOPA positron emission tomography for preoperative localization in congenital hyperinsulinism. *Horm Res* 2008; **70**: 65-72 [PMID: 18547951 DOI: 10.1159/000137655]
38 **Blomberg BA**, Moghbel MC, Saboury B, Stanley CA, Alavi A. The value of radiologic interventions and (18)F-DOPA PET in diagnosing and localizing focal congenital hyperinsulinism: systematic review and meta-analysis. *Mol Imaging Biol* 2013; **15**: 97-105 [PMID: 22752652 DOI: 10.1007/s11307-012-0572-0]
39 **Beheshti M**, Pöcher S, Vali R, Waldenberger P, Broinger G, Nader M, Kohlfürst S, Pirich C, Dralle H, Langsteger W. The value of 18F-DOPA PET-CT in patients with medullary thyroid carcinoma: comparison with 18F-FDG PET-CT. *Eur Radiol* 2009; **19**: 1425-1434 [PMID: 19156423 DOI: 10.1007/s00330-008-1280-7]
40 **Ribeiro MJ**, Boddaert N, Bellanné-Chantelot C, Bourgeois S, Valayannopoulos V, Delzescaux T, Jaubert F, Nihoul-Fékété C, Brunelle F, De Lonlay P. The added value of [18F]fluoro-L-DOPA PET in the diagnosis of hyperinsulinism of infancy: a retrospective study involving 49 children. *Eur J Nucl Med Mol Imaging* 2007; **34**: 2120-2128 [PMID: 17661030 DOI: 10.1007/s00259-007-0498-y]
41 **Arbizu Lostao J**, Fernández-Marmiesse A, Garrastachu Zumarrán P, Martino Casado E, Azcona San Julián C, Carracedo A, Richter Echevarría JA. [18F-fluoro-L-DOPA PET-CT imaging combined with genetic analysis for optimal classification and treatment in a child with severe congenital hyperinsulinism]. *An Pediatr (Barc)* 2008; **68**: 481-485 [PMID: 18447993]
42 **Cherubini V**, Bagalini LS, Ianilli A, Marigliano M, Biagioni M, Carnielli V, Iasonni V, Berbellini A, Hussain K, Gabrielli O. Rapid genetic analysis, imaging with 18F-DOPA-PET/CT scan and laparoscopic surgery in congenital hyperinsulinism. *J Pediatr Endocrinol Metab* 2010; **23**: 171-177 [PMID: 20432820]
43 **Yorifuji T**, Hosokawa Y, Fujimaru R, Kawakita R, Doi H, Matsumoto T, Nishibori H, Masue M. Lasting 18F-DOPA PET uptake after clinical remission of the focal form of congenital hyperinsulinism. *Horm Res Paediatr* 2011; **76**: 286-290 [PMID: 21912073 DOI: 10.1159/000328056]
44 **Zani A**, Nah SA, Ron O, Totonelli G, Ismail D, Smith VV, Ashworth M, Blankenstein O, Mohnike W, De Coppi P, Eaton S, Hussain K, Pierro A. The predictive value of preoperative fluorine-18-L-3,4-dihydroxyphenylalanine positron emission tomography-computed tomography scans in children with congenital hyperinsulinism of infancy. *J Pediatr Surg* 2011; **46**: 204-208 [PMID: 21238668 DOI: 10.1016/j.jpedsurg.2010.09.093]
45 **Masue M**, Nishibori H, Fukuyama S, Yoshizawa A, Okamoto S, Doi R, Uemoto S, Tokumi T, Kasai T, Yorifuji T. Diagnostic accuracy of [18F]-fluoro-L-dihydroxyphenylalanine positron emission tomography scan for persistent congenital hyperinsulinism in Japan. *Clin Endocrinol (Oxf)* 2011; **75**: 342-346 [PMID: 21521340 DOI: 10.1111/j.1365-2265.2011.04072.x]
46 **Nestorowicz A**, Wilson BA, Schoor KP, Inoue H, Glaser B, Landau H, Stanley CA, Thornton PS, Clement JP, Bryan J, Aguilar-Bryan L, Permutt MA. Mutations in the sulonylurea receptor gene are associated with familial hyperinsulinism in Ashkenazi Jews. *Hum Mol Genet* 1996; **5**: 1813-1822 [PMID: 8923011 DOI: 6w0181]
47 **Giurgea I**, Sempoux C, Bellanné-Chantelot C, Ribeiro M, Hubert L, Boddaert N, Saudubray JM, Robert JJ, Brunelle F, Rahier J, Jaubert F, Nihoul-Fékété C, de Lonlay P. The Knudson's two-hit model and timing of somatic mutation may account for the phenotypic diversity of focal congenital

hyperinsulinism. *J Clin Endocrinol Metab* 2006; **91**: 4118-4123 [PMID: 16882742 DOI: 10.1210/jc.2006-0397]
48 **Laje P**, States LJ, Zhuang H, Becker SA, Palladino AA, Stanley CA, Adzick NS. Accuracy of PET/CT Scan in the diagnosis of the focal form of congenital hyperinsulinism. *J Pediatr Surg* 2013; **48**: 388-393 [PMID: 23414871 DOI: 10.1016/j.jpedsurg.2012.11.025]
49 **Cagirici U**, Ozbaran M, Veral A, Posacioglu H. Ectopic mediastinal pancreas. *Eur J Cardiothorac Surg* 2001; **19**: 514-515 [PMID: 11306324]
50 **Edlund H**. Developmental biology of the pancreas. *Diabetes* 2001; **50** Suppl 1: S5-S9 [PMID: 11272202]
51 **Peranteau WH**, Bathaii SM, Pawel B, Hardy O, Alavi A, Stanley CA, Adzick NS. Multiple ectopic lesions of focal islet adenomatosis identified by positron emission tomography scan in an infant with congenital hyperinsulinism. *J Pediatr Surg* 2007; **42**: 188-192 [PMID: 17208563 DOI: 10.1016/j.jpedsurg.2006.09.046]

P- Reviewers: Das UN, Shyng SL **S- Editor**: Wen LL
L- Editor: A **E- Editor**: Zhang DN

World Journal of Radiology

Submit a Manuscript: http://www.wjgnet.com/esps/
Help Desk: http://www.wjgnet.com/esps/helpdesk.aspx
DOI: 10.4329/wjr.v6.i6.261

World J Radiol 2014 June 28; 6(6): 261-273
ISSN 1949-8470 (online)
© 2014 Baishideng Publishing Group Inc. All rights reserved.

TOPIC HIGHLIGHT

WJR 6th Anniversary Special Issues (8): fMRI

Sustained attention in psychosis: Neuroimaging findings

Gianna Sepede, Maria Chiara Spano, Marco Lorusso, Domenico De Berardis, Rosa Maria Salerno, Massimo Di Giannantonio, Francesco Gambi

Gianna Sepede, Maria Chiara Spano, Marco Lorusso, Rosa Maria Salerno, Massimo Di Giannantonio, Francesco Gambi, Department of Neuroscience and Imaging, Institute for Advanced Biomedical Technologies, University "G. D'Annunzio" of Chieti, "G. d'Annunzio" University of Chieti, 66013 Chieti Scalo (CH), Italy
Domenico De Berardis, Department of Mental Health, National Health Trust, 64100 Teramo, Italy
Author contributions: Sepede G, Gambi F, Salerno RM and Di Giannantonio M designed the research; Sepede G, Spano MC, Lorusso M and De Berardis D performed the PubMed research, selected the papers included in the qualitative review and summarized the results; Sepede G, Gambi F, Salerno RM and Di Giannantonio M wrote the paper; Spano MC and Lorusso M edited the language and contributed equally to this work.
Correspondence to: Gianna Sepede, MD, PhD, Department of Neuroscience and Imaging, Institute for Advanced Biomedical Technologies, University "G. D'Annunzio" of Chieti, Via dei Vestini 33, 66013 Chieti Scalo (CH), Italy. gsepede@libero.it
Telephone: +39-871-3556901 Fax: +39-871-3556930
Received: December 23, 2013 Revised: February 7, 2014
Accepted: May 16, 2014
Published online: June 28, 2014

Abstract

To provide a systematic review of scientific literature on functional magnetic resonance imaging (fMRI) studies on sustained attention in psychosis. We searched PubMed to identify fMRI studies pertaining sustained attention in both affective and non-affective psychosis. Only studies conducted on adult patients using a sustained attention task during fMRI scanning were included in the final review. The search was conducted on September 10th, 2013. 15 fMRI studies met our inclusion criteria: 12 studies were focused on Schizophrenia and 3 on Bipolar Disorder Type I (BDI). Only half of the Schizophrenia studies and two of the BDI studies reported behavioral abnormalities, but all of them evidenced significant functional differences in brain regions related to the sustained attention system. Altered functioning of the insula was found in both Schizophrenia and BDI, and therefore proposed as a candidate trait marker for psychosis in general. On the other hand, other brain regions were differently impaired in affective and non-affective psychosis: alterations of cingulate cortex and thalamus seemed to be more common in Schizophrenia and amygdala dysfunctions in BDI. Neural correlates of sustained attention seem to be of great interest in the study of psychosis, highlighting differences and similarities between Schizophrenia and BDI.

© 2014 Baishideng Publishing Group Inc. All rights reserved.

Key words: Sustained attention; Affective psychosis; Non-affective psychosis; Schizophrenia; Bipolar disorder; Functional magnetic resonance imaging; Insula

Core tip: In the present paper, we systematically reviewed functional magnetic resonance imaging studies investigating sustained attention in affective and non-affective psychosis. We found that differences between cases (patients, unaffected relatives of psychotic probands) and controls in terms of functional activation of sustained attention system structures were detectable even when the groups performed comparably. In particular, the insular cortex seems to be a trait marker for psychosis in general, whereas other regions (thalamus, cingulate cortex, amygdala) seem to be differently impaired in affective and non-affective psychosis.

Sepede G, Spano MC, Lorusso M, De Berardis D, Salerno RM, Di Giannantonio M, Gambi F. Sustained attention in psychosis: Neuroimaging findings. *World J Radiol* 2014; 6(6): 261-273 Available from: URL: http://www.wjgnet.com/1949-8470/full/v6/i6/261.htm DOI: http://dx.doi.org/10.4329/wjr.v6.i6.261

INTRODUCTION

Sustained attention can be defined as the ability to main-

tain a high vigilance level for prolonged periods of time, allowing the subjects to respond in an appropriate way to infrequent and unpredictable stimuli[1].

Abnormalities in sustained attention have been reported in both schizophrenic[2-4] and Bipolar Disorder (BD) patients[5-8] and several studies suggested a correlation with a worse prognosis and a poorer quality of life[9-12]. Sustained attention deficits seem to be independent from medications[13,14] and illness states[15]. Studies comparing directly schizophrenic and BD patients found that the two groups were qualitatively similar in sustained attention deficits[16], even though schizophrenic patients were usually quantitatively more impaired[17-20]. A reduced attentional performance has also been higlighted in non-affected relatives of schizophrenic[21,22] and bipolar patients[23]: it has been therefore proposed as a candidate endophenotype for both affective[24-26] and non-affective psychosis[27-30]. Candidate endophenotypes must be associated with illness, state independent, heritable, and found in unaffected relatives of probands at a higher rate than in general population[31]. By contrast, some behavioral studies failed to find any significant performance deficit in schizophrenic patients[32], in bipolar patients[33] or in unaffected relatives of bipolar probands[34,35], so the role of sustained attention as a trait-market of psychosis is still controversial. The discordant results reported in scientific literature may be due to the differences in experimental paradigms and inclusion/exclusion criteria.

The most commonly used tasks to assess sustained attention are the "oddball paradigms", where subjects are required to identify rare and unpredictable target stimuli presented among a stream of frequent non-target stimuli[36,37] or among both frequent and rare non-target stimuli, usually called "standards" and "novels" respectively[38,39]. A particular kind of oddball paradigm is the Continuous Performance Test (CPT), initially developed by Beck *et al*[40] and nowadays considered a well validated instrument to measure sustained attention in both research and clinical settings[41]. There are numerous versions of CPT, differing from one another for the sensorial modalities (visual or auditory)[42,43] the perceptual complexity of the stimuli (CPT with degraded stimuli: DS-CPT)[44] and the response required: only on targets, on both targets and non-targets and only on non-targets (Conners' CPT Ⅱ)[45]. Other CPT versions increase the number of stimuli presented per minute to intensify the attentional load (*e.g.*, the Rapid Visual Information Processing task, RVIP)[46]. Some CPTs are designed to assess both sustained attention and working memory resources, *e.g.*, the CPT-AX (a character or number preceded by another character or number as a target)[47] or the CPI-IP (identical pairs of stimuli as a target)[48].Several scores are used to measure the behavioral performance in oddball paradigms: the rate of correct targets ("hits", "H") and incorrect targets ("omission errors"); the rate of correct non-target ("correct rejections") and incorrect non-target ("false alarms", "FA") "commission") and the mean reaction times (RT) to the stimuli. Subjects who respond accurately and rapidly to both target and non-target are considered good performers, whereas a high number of omissions indicate a reduced attention and a high number of commissions indicate augmented impulsivity. Using the signal detection theory[49] other measures of accuracy may be calculated, such as the sensitivity index (*d'*, *d-prime*), its nonparametric analog (*A'*, *A-prime*) and the response criterion (*B"*, beta, *ln b*). *d'* is the standardized difference between hit rate and false alarm rate [*d'* = z(Hits) - z (False alarms)] and it is considered a good measure of discriminability. *B"* instead represents an index of response bias, the subject's tendency to under respond or over respond [*B"* = (1-H) - FA (1-FA)/H(1-H)+FA (1-FA)].

Functional neuroimaging studies increase the possibility to detect subtle differences in brain functioning even in behaviorally intact subjects. In healthy individuals, sustained attention tasks usually elicit a widespread cortical and subcortical network, including dorsal and medial prefrontal cortex, parietal, temporal and occipital areas, cingulate gyrus, insula, cerebellum, and basal ganglia[50-53]. Different components of sustained attention have their anatomical and functional correlates in different brain regions: subcortical structures have been associated with arousal control, dorsal frontal and temporoparietal cortex with attention maintenance over time, and anterior ventromedial regions, such as anterior cingulate cortex (ACC) and anterior insula, with conflict monitoring, target detection and error signaling[54]. Moreover, ACC and insula are reported to play a crucial role in emotional regulation, linking emotion to cognition[55,56].

The aim of the present paper is to review fMRI correlates of sustained attention in affective and non-affective psychosis, discussing the literature findings and the role of sustained attention as a candidate endophenotype for psychotic disorders.

SEARCH

We searched PubMed to identify functional magnetic resonance (fMRI) studies investigating sustained attention in affective and non-affective psychosis. The following search words were used, both alone and in combination: sustained attention, fMRI, affective psychosis, non-affective psychosis, Schizophrenia, Bipolar Disorder. The search was conducted on September 10th, 2013 and yielded 42 records. Moreover, we manually checked the reference lists of the identified articles and we found 9 further potential studies, for a total number of 51 records. Inclusion criteria were the following: articles written in English, patients' age ⩾ 18 years, psychotic patients and/or subjects at augmented risk for psychosis, studies providing both behavioral and fMRI results during a sustained attention task. Structural MRI studies and fMRI studies reporting data acquired during paradigms other than sustained attention tasks or during resting state were excluded.

By reading titles and abstracts, we excluded 18 records. By reading the full texts of the 33 remaining arti-

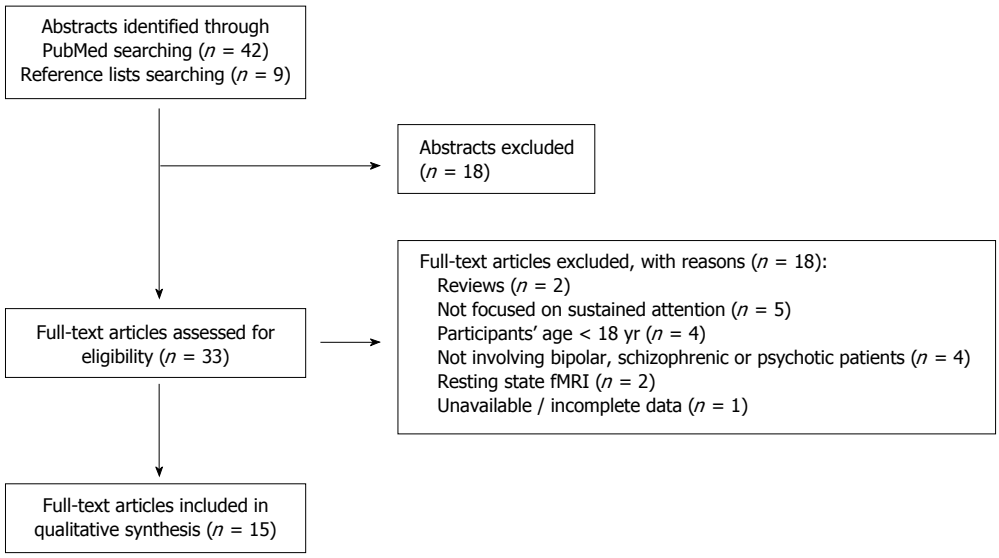

Figure 1 Flow chart of the systematic review. fMRI: Functional magnetic resonance imaging.

cles, we identified15 papers meeting our inclusion criteria and therefore included in the qualitative synthesis (Figure 1).

RESEARCH

A total number of 578 subjects was tested by the 15 studies included in the qualitative synthesis: 272 normal comparisons (NC), 173 schizophrenic patients (SCZ), 17 unaffected relatives of schizophrenics (REL-SCZ), 10 subjects at ultra high risk for Schizophrenia (UHR-SCZ), 84 Bipolar Disorder type I patients (BDI) and 22 unaffected relatives of BDI patients (REL-BDI). The majority of SCZ were male (68.8%), conversely to what observed in BDI, where males represented only 30.9% of the total.

Sustained attention in schizophrenia

A total number of 12 studies was selected[57-68]. The characteristic of the groups and the results of the studies are depicted in Table 1.

Right handedness was an inclusion criteria in 6 studies[57,59,60,63,66,68]. Nine studies enrolled only SCZ, one had both a SCZ group and an additional group of UHR-SCZ[61] and two had only REL-SCZ[66,68]. In the study by Morey *et al*[61], patients were divided into early SCZ (mean illness duration 1.7 years) and chronic SCZ (mean illness duration 15.3 years). In the study by Honey *et al*[60], patients were divided into SCZ with both negative and positive symptoms (*n* = 11) and SCZ with predominantly positive symptoms (*n* = 11). The SCZ (*n* = 173) enrolled in the studies were clinically stable and in the majority of cases were medicated (range: 87.5%-100%). Only 2 of the 10 UHR-SCZ received medications at the moment of the scanning, whereas all the REL-SCZ (*n* = 17) and the NC (*n* = 204) were drug naïve. In seven of the 10 studies including a SCZ group, the mean illness duration was also reported[58-63,65] and it ranged from 1.7 to 33 years. The UHR-SCZ group in the study by Morey *et al*[61] met at least one of the following criteria: (1) reporting brief intermittent psychotic states; (2) reporting attenuated positive symptom states; and (3) being first-degree relatives of schizophrenic/schizotypal probands plus reporting a significant recent loss of social/work functioning. The 11 REL-SCZ enrolled by Sepede *et al*[68] were all unaffected siblings of schizophrenic patients, whereas the 6 REL-SCZ enrolled by Filbey *et al*[66] were presumed obligate carriers of schizophrenia (POCs): unaffected subjects having a first-degree relative (sibling or parent) plus a child affected by schizophrenia. Ten of the 12 studies used visual stimuli, whereas the other two[62,65] used auditory stimuli. The tasks administered were: oddball tasks (*n* = 4), CPT-X (*n* = 1), DS-CPT-X (*n* = 2), CPT-IP (*n* = 2), RVIP (*n* = 1), and other attention tasks (*n* = 2), with a total duration of the experiment ranging from 6 to 49 min.

FMRI images were acquired using a 1.5 T scanner in seven studies, a 3 T scanner in 2 studies and a 4 T scanner in three studies. A block design was used to present the tasks in six studies, whereas an event-related design was used in other five studies. Only one study[67] used a block/event-related mixed design. A whole brain approach was used in eight studies to analyze the BOLD FMRI signal whereas three studies[60,61,67] used a region of interest (ROI) approach and/or a masked brain analysis, limiting the analysis to areas known to be involved in sustained attention processing and/or to areas showing significant between-group or within-condition differences. Only one study[64] used the ROI analysis after the whole brain analysis. In the study by Honey *et al*[60], connectivity analyses were also performed.

Behavioral results

In four of the ten studies involving SCZ (*n* = 57), no significant behavioral differences were found with respect to NC[57,58,63,64]. In the other six studies, SCZ (*n* = 116) performed worse than NC: a reduced accuracy was evi-

Table 1 Functional magnetic resonance imaging studies of sustained attention in Schizophrenia

Ref.	Participants	Task and behavioral results	fMRI methods and results
Volz *et al*[57], 1999	SCZ (n = 14), age 34.1 ± 12.3, males 78.6%, medicated 100% NC (n = 20), age 28.2 ± 5.7, males 60%	CPT-IP. Type of stimuli: letters TNS = 720, Target = 25%, SET = 600 ms, ISI = 1200 ms, TET = 30 min Required response: on targets. Behavioral measures: hit rate, mean RT, d', ln b Results: no between group differences	1.5 T, block design (4 blocks). baseline: finger tapping Whole brain analysis. Imaging package: SPM96 Results: NC > SCZ in the R mesial PFC, ACC and L TH
Eyler *et al*[58], 2004	SCZ (n = 8)/SCA (n = 1) age 58.9 ± 9.9, males 55.6%, illness duration: 33 yr, medicated 100% NC (n = 10), age 59.8 ± 5.7, 12 males 60%	CPT-X. Type of stimuli: letters. TNS = 72 Target = 33.3% ISI = 500 ms, TET = 6 min 3 s Required response: on targets Behavioral measures: mean RT, d' Results: no between group differences	1.5 T, block design. baseline: digit fixation 8 task blocks and 9 baseline blocks Whole brain analysis. Imaging package: AFNI Results: NC > SCZ in R IFG/insula (BA 47/45) SCZ > NC in R postcentral gyrus (BA 3) and L cerebellum
Salgado-Pineda *et al*[59], 2004	SCZ (n = 14), age 25.5 ± 4.1, males 50%, medicated 100%, illness duration: 1.9 yr NC (n = 14), age 25.1 ± 3.3, males 50%	CPT-IP. Type of stimuli: numbers. TNS = 900 Target = 15% ISI = 1100 ms, TET = 14min Required response: on targets Behavioral measures: omission errors, commission errors, mean RT, d', ln b Results: Between group differences -omissions, commission and d': NC > SCZ -mean RT: SCZ > NC	1.5 T, block design. baseline: digit response 2 task blocks and 2 baseline blocks. Whole brain analysis. Imaging package: SPM2 Results: NC > SCZ in R IFG (BA 44), R angular gyrus (BA 39), R STG (BA 37), R MTG (BA 21), R TH
Honey *et al*[60], 2005	N-SCZ: SCZ with both negative and positive symptoms: (n = 11), age 42.6 ± 9.2, males 90.9%, age of onset: 22.2 yr, medicated 100%	CPT-X with 2 levels of difficulty: undegraded and degraded stimuli (0% and 40% pixel inverted). Type of stimuli: digits TNS = 280 Target = 25% SET = 42 ms, ISI = 958 ms TET = 6 min	3T, block design, baseline: screen fixation 10 task blocks and 10 baseline blocks. Imaging package: SPM2 Masked brain analysis (ROIs involved in attention processing, differentiating the groups and showing a task related activity associated to attentional load). Connectivity analysis (seed ROIs: ACC and cerebellar vermis)
	P-SCZ: SCZ with predominant positive symptoms: (n = 11) age 41.1 ± 9.2, males 81.8%, age of onset: 24.7 yr, medicated 100%	Required response: on targets Behavioral measures: mean RT, d' Results: N-SCZ were less accurate than NC in target discrimination (d')	Results Task *vs* baseline: NC > (P-SCZ = N-SCZ) in R and L angular gyrus, MFG, L putamen (P-SCZ = N-SCZ) > NC in R and L SFG, R and L IPL, R SPL, R post central gyrus, L precentral gyrus, R and L TH, ACC, PCC, R MiFG, R IFG, cerebellum; P-SCZ > N-SCZ in R STG, R MiFG and L SPL
	NC (n = 12), age 33.3 ± 11.8, 12 males 83.3%		Connectivity with ACC: NC > (P-SCZ = N-SCZ) in R and L MSFG, R and L IFG; (P-SCZ = N-SCZ) > NC in R and L precentral gyrus, R postcentral gyrus, cerebellum; P-SCZ > N-SCZ in ACC; N-SCZ > P-SCZ in SMA Connectivity with cerebellum: NC > (P-SCZ = N-SCZ) in R and L MSFG, L MFG; (P-SCZ = N-SCZ) > NC in L MiFG; P-SCZ>N-SCZ in R and L IFG, ACC, L SPL, R precentral gyrus, L postcentral gyrus
Morey *et al*[61], 2005	UHR (n = 10), age 22.6 ± 4.4, male 50%, medicated 20%,	Visual oddball task Type of stimuli: circles ("targets"), squares (frequent non targets-"standards"), objects (rare non targets-"novels")	1.5T, 7 runs. Event-related design. Imaging package: SPM99 ROI analysis: ACC, MiFG, IFG, BG, and TH. Conditions: -Targets -Novels -Standards (baseline)
	Early SCZ (n = 15) age 24.1 ± 6.5, male 67%, age of onset 22.3 yr, illness duration 1.7 yr, medicated 86.7%	TNS = 1400 Target = 3% SET = 500 ms, ISI = 1500 ms, TET = 36 min 24 s Required response: on both targets and non-targets	Results Targets *vs* novels activations -in ACC, MiFG and IFC: NC > UHR, Early SCZ and Chronic SCZ -in IFG: (1) NC> Early SCZ and Chronic SCZ; (2) only NC and UHR showed R > L activations, whereas Early SCZ and Chronic SCZ showed a reduced laterality

	Chronic SCZ (n = 11) age 38.1 ± 7.7, male 82%, age of onset 22.9 yr, illness duration 15.3 yr, medicated 100% NC (n = 16) age 28.0 ± 11.6, male 59% Older NC (n = 10) age 34.0 ± 12.1, male 67%	Behavioral measures: hit rate, d', B'' Results: Between group differences: -Hit rate: NC > Early SCZ and chronic SCZ -d': NC > UHR, Early SCZ and Chronic SCZ	Target *vs* baseline activations: -in ACC, MiFG and IFC: NC > Early SCZ and Chronic SCZ -in BG and TH: NC > Early SCZ and Chronic SCZ (results confirmed comparing Chronic SCZ with Older NC)
Liddle *et al*[62], 2006	SCZ (n = 24)/SCA (n = 4) age 31.6 ± 10.1, males 67.9%, illness duration 7 yr, medicated 96.4%	Auditory oddball task Type of stimuli: 1500 Hz tones ("targets"), 1000 Hz tones (frequent non targets-"standards"), noises (rare non targets-"novels")	1.5 T, event related design, whole brain analysis Imaging package: SPM99. Conditions: -correct targets -correct novels -correct standards (baseline) -missed targets -standard false alarms
	NC (n = 28), age 28.2 ± 8.9, males 75 %	TNS = 488 Target = 10% SET = 200 ms, ISI = 2000 ms, TET = 16 min Required response: on targets Behavioral measures: RT, omissions, commissions Results: SCZ were significantly slower and less accurate than NC	Results Targets *vs* baseline activations: NC > SCZ: in L and R amygdala, R hippocampus, R and L STS, L and R insula, R and L orbitofrontal cortex (BA 47), ACC, PCC, L and R SPL, R and L IPL, L and R middle IFG, L and R superior MFG, L and R TH, L and R striatum, L and R cerebellum Results Targets *vs* novels activations: NC > SCZ in: L amygdala, L orbitofrontal cortex (BA 47), L anterior insula, rostral ACC and L striatum
Gur *et al*[63], 2007	SCZ (n = 22), age 30.5 ± 9.1, males 59.1%, age of onset 22.5 yr, illness duration 12.4 yr, medicated 95.5%	Visual oddball task. Stimuli: colored shapes Type of stimuli: red circles ("targets"), green circles (frequent non targets-"standards"), fractal images (rare non targets-"novels")	4T, event related design, whole brain analysis. Imaging package: FEAT/FMRIB. Conditions: -targets -novels -standards (baseline)
	NC (n = 28), age 31.6 ± 8.5, males 57.1 %	TNS = 200 Target = 15% SET = 1000 ms, ISI = 2000 ms, TET = 7 min Required response: on targets Behavioral measures: hit rate, RT Results: no between group differences	Results Targets *vs* baseline activations: NC > SCZ in R and L STG, L insula, R and L putamen, ACC, PCC, L SFG, L TH SCZ > NC in R insula, R MiFG, L IPL Novels *vs* baseline activations: NC > SCZ in L IOG and L IPL SCZ > NC in L MOG, L fusiform, L precuneus, L IFG, R angular gyrus, SOG, SPL, MiFG
Harrison *et al*[64], 2007	SCZ (n = 12), age 32.2 ± 8.0, males 100%, medicated 100%	Multi-Source Interference Task (MSIT). Type of stimuli: digits SET = 2000 ms, ISI = 500 ms TNS = 160, TET = 11 min Required response: on all stimuli Behavioral measures: correct responses, RT	3T, block design. Imaging package: SPM5 Conditions: -low difficulty Task ("baseline") -high difficulty Task ("Task") -fixation ("Rest") Whole brain analysis and ROI analysis of deactivation ("Rest"-"Task") in medial PCC/rostral ACC and PCC/Precuneus
	NC (n = 14), age 31.7 ± 8.0, males 100%	Results: no between group differences	Results SCZ > NC in deactivation of medial PCC/rostral ACC and PCC/Precuneus. In SCZ the magnitude of deactivation correlates with response speed and level of emotional awareness
Wolf *et al*[65], 2008	SCZ (n = 16)/SCA (n = 1) age 31.9 ± 7.1, males 53 %, illness duration 9.9 yr, medicated 94.1%	Auditory oddball task Type of stimuli: 2000 Hz tones ("targets"), 1000 Hz tones (frequent non targets-"standards"), sounds (rare non targets-"novels")	4T, event-related whole brain analysis. Imaging package: FEAT/FSL. Conditions: -targets -novels -standards (baseline)
	NC (n = 21), age 28.6 ± 7.1, males 52%	TNS = 200 Target = 15% SET = 150 ms, ISI = 1850 ms, TET = 6 min and 40 s Required response: on targets Behavioral measures: hit rate, RT Results: SCZ were significantly slower than NC	Results Targets *vs* baseline activations: SCZ > NC in: L precentral gyrus, ACC/SMA, L and R insula, L hippocampus, L and R STG/MTG, L superior MOG Novels *vs* baseline activations: SCZ > NC in: L IFG
Filbey *et al*[66], 2008	POC-SCZ (n = 6) age 53, males 33.3% medicated 0% (drug naïve)	Sustained attention task Type of stimuli: colored circles Required response: on targets Behavioral measures: RT	1.5T. Block design. Imaging package: FSL Whole brain analysis baseline condition: circles fixation

	NC (n = 8) age 41, males 62.5%	Results: no between group differences	Results NC > POC-SCZ in: R IPL (BA 7), R SPL (BA 7), R MTG (BA 21), R MOG (BA 18), R PCC (BA 31), R SFG (BA 10), R lingual gyrus (BA 18/19), R precentral gyrus (BA 9/43), R parahippocampal gyrus (BA 28), L cuneus (BA 18), L striatum; POC-SCZ > NC in: L STG (BA 21), L SFG (BA9) and R MTG (BA 19)
Carter *et al*[67], 2010	SCZ (n = 9), age 29.8 ± 12.0, males 100%	Visual selective attention task Type of stimuli: colored circles	4T. Block/event-related mixed design. 10 runs. Imaging package: SPM. Conditions: -target events (3 s before-13.5 s after the event) -transient activation (3 s before-7.5 s after the onset of task block) -sustained activation (15 s before-70.5 s after the onset of task block)
	NC (n = 12), age 25.5 ± 4.6, males 100%	TNS = 1960 Target = 5 % SET = 500 ms, ISI = 1000 ms TET = 49 min Required response: on both targets and non-targets Behavioral measures: correct targets, RT Results -correct target percentage: NC > SCZ -RT: SCZ > NC	Masked brain analysis and ROI analysis in ACC, IFG, MiFG, IPS, BG, caudate and TH Results -During transient activation NC > SCZ in: MiFG, IPS, caudate and TH -During target events NC > SCZ in TH In NC: positive correlation between accuracy and TH activation during sustained activation condition; In SCZ: negative correlation between RT and BG activation during target events
Sepede *et al*[68], 2010	REL-SCZ (n = 11), age 34.4 ± 8.8, males 45.5% medicated 0% (drug naïve), smokers 36.4% NC (n = 11), age 32.0 ± 5.2, males 45.5%, smokers 36.4%	CPT-X with 3 levels of difficulty: undegraded and degraded stimuli (0%, 25% and 40% pixel inverted). Type of stimuli: digits TNT = 210, Target = 16% SET = 200 ms, ISI = 2000 ms, TET = 42 min Required response: on targets and non-targets Behavioral measures: correct targets, correct non-targets, RT Results: no between group differences	1.5T, event-related design, 3 runs (0%, 25% and 40% degraded) Whole brain analysis. Imaging package: BrainVoyager QX 1.9 Task conditions: -correct responses on target -incorrect responses on target -correct responses on non-targets (baseline) Results Correct targets *vs* baseline: NC > REL-SCZ in R precentral gyrus (BA 6/9), R and L insula (BA 13), MFG/dorsal ACC (BA 9/32) REL-SCZ > NC in deactivating PCC/retrosplenial cortex (BA 23/31) Incorrect target *vs* baseline: REL-SCZ > NC in L insula/IFG (BA 13/47) and R TH

SCZ: Schizophrenic patients; NC: Normal comparisons; SCA: Schizoaffective patients; REL-SCZ: Unaffected first degree relatives of schizophrenic patients; POC-SCZ: Presumed Obligate carriers of schizophrenic patients; UHR: Ultra high risk subjects; SET: Stimulus exposure time; ISI: Interstimulus interval; TNS: Total number of stimuli; TNT: Total number of targets; TET: Total experiment time; RT: Response time; R: Right; L: Left; PFC: Prefrontal cortex; ACC: Anterior cingulate cortex; PCC: Posterior cingulate cortex; MFG: Medial frontal gyrus; MSFG: Medial superior frontal gyrus; IFG: Inferior frontal gyrus; SFG: Superior frontal gyrus; SMA: Supplementary motor area; IPL: Inferior parietal lobule; SPL: Superior parietal lobule; IPS: Intraparietal sulcus; MTG: Middle temporal gyrus; STG: Superior temporal gyrus; STS: Superior temporal sulcus; MOG: Middle occipital gyrus; IOG: Inferior occipital gyrus; TH: Thalamus; BG: Basal ganglia.

denced by Honey *et al*[60] and Morey *et al*[61], whereas Wolf *et al*[65] reported an increased mean reaction time and Salgado *et al*[59], Liddle *et al*[62] and Carter *et al*[67] reported both reduced accuracy and increased mean reaction times with respect to NC. In their 10 UHR subjects, Morey *et al*[61] reported a reduced accuracy. On the contrary, the 17 REL-SCZ enrolled by Filbey *et al*[66] and Sepede *et al*[68] performed similarly to controls.

FMRI results

Significant between-group differences in several brain regions were found in all the selected studies, even when the groups performed comparably. The most reported differences were observed in cingulate gyrus, thalamus (TH), inferior parietal lobule (IPL), inferior frontal gyrus (IFG) and insula. The anterior part of the cingulate cortex (ACC) significantly differentiated the groups in seven studies: SCZ showed a reduced activation with respect to NC in 4 SCZ groups[57,61-63], and the same pattern was observed in the UHR subjects enrolled by Morey *et al*[61] and in the REL-SCZ enrolled by Sepede *et al*[68] By contrast, two studies[60,65] reported an augmented activation in SCZ with respect to NC. Also the posterior part of the cingulate cortex (PCC) significantly differentiated the groups in six studies. Honey *et al*[60] reported an increased activation in the SCZ with respect to NC, whereas a decreased

activation was found by Gur *et al*[63] and Liddle *et al*[62] Interestingly, in three studies, the PCC was reported to be deactivated during attention task, with respect to the baseline/control task, and the amount of the deactivation was larger in SCZ[64] and REL-SCZ[66,68] with respect to NC. A significant hypoactivation of the IFG was found in five studies[58-62]. The medial regions of the prefrontal cortex, located dorso-rostrally with respect to the cingulate cortex, appeared to be hyperactivated in SCZ[57,60] or REL-SCZ[68].

The insular cortex significantly differentiated the groups in five studies. A reduced activation in SCZ was reported bilaterally by Liddle *et al*[62] and limited to the right emisphere by Eyler *et al*[58] By contrast, Gur *et al*[63] found a reduced activation in the R insula, counterbalanced by an augmented activation in the L insula, and Wolf *et al*[65] reported a bilateral augmented activation. In the event-related study by Sepede *et al*[68], REL-SCZ hyperactivated the bilateral insula during correct target responses and hyperactivated the L insula during wrong target responses. An altered functioning of the inferior parietal lobule (IPL) was detected in 4 studies, three showing a reduced activation in SCZ with respect to NC[60,62,66], one an increased activation[63]. Other parietal regions were also reported to differentiate the groups. In the angular gyrus Salgado *et al*[59] and Honey *et al*[60] reported a reduced activation, Gur *et al*[63] an increased activation; in the superior parietal lobule (SPL) Liddle *et al*[62] and Filbey *et al*[66] found a reduced activation, Honey *et al*[60] an increased activation in SCZ with respect to NC.

When considering the subcortical regions, SCZ significantly hyperactivated the TH in six studies[57,59,61,62,63,67], whereas Sepede *et al*[68] found an increased activation during wrong target responses in REL-SCZ. Other subcortical structures, such as the basal ganglia, appeared to be less activated in SCZ with respect to NC in 4 studies[60,61,63].

SUSTAINED ATTENTION IN BIPOLAR DISORDER

Three studies enrolled BDI patients[69-71] and one of these studies had also a group of unaffected, drug-naïve, BDI-REL[71]. The characteristic of the groups and the results of the studies are depicted in Table 2. Right handedness was an inclusion criteria in two studies[69,71]. The BDI (n = 84) enrolled in the three studies were euthymic (n = 34) or affected by a manic/mixed episode (n = 50). About 80% of the 74 patients in the studies by Fleck *et al*[70] and Sepede *et al*[71] were under medication at the moment of the fMRI scanning, whereas the 10 BDI in the study by Strakowsky *et al*[69] were drug free. All the NC (n = 68) and the BDI-REL (n = 22) were drug naïve. In two of the studies[69,71], the mean illness duration was also reported and it was 2.2 and 4.7 years respectively. The presence of psychotic features during the acute phases of the illness (95.8%) was reported only by Sepede *et al*[71] All the three selected studies used a visual CPT to assess sustained attention (CPT-IP: n = 2; DS-CPT-X: n = 1), with a total duration of the experiment ranging from 6 to 15 min.

FMRI images were acquired using a 1.5 T (n = 1), a 3 T (n = 1) or a 4 T (n = 1) scanner, presenting the tasks with an event-related design (n = 2) or a block design (n = 1). A whole brain approach was used in two studies to analyze the BOLD FMRI, whereas Fleck *et al*[70] performed a whole brain analysis followed by a ROI analysis.

Behavioral results

In their group of 10 euthymic and unmedicated BDI, Strakowski *et al*[69] did not find any behavioral deficit with respect to NC. On the contrary, both Fleck *et al*[70] and Sepede *et al*[71] reported a reduced target accuracy in their manic/mixed (n = 50) or euthymic (n = 24) BDI patients. An impaired performance was also found in the group of 22 unaffected and unmedicated BDI-REL enrolled by Sepede *et al*[71].

FMRI results

Significant between-group differences in several brain regions were found in all the three selected studies, even when the groups performed comparably. The regions more reported to differentiate the groups were: IFG, insula, amygdala and IPL.

The IFG/insula showed an altered pattern of activation in all the three selected studies: an augmented activation in BDI with respect to NC was found by Strakowski *et al*[69], whereas Fleck *et al*[70] reported a reduced activation. In the study by Sepede *et al*[71], BDI showed a reduced activation during correct target responses and an augmented activation during wrong target responses, with REL-BDI showing an intermediate pattern of functioning between BDI and NC. The amygdala was found to be more activated with respect to NC in two studies, involving euthymic[69] or manic[70] BDI. The IPL seemed to be hyperactivated in the euthymic BDI enrolled by Strakowski *et al*[69] and in the REL-BDI by Sepede *et al*[71].

DISCUSSION

In this paper we systematically reviewed fMRI studies on sustained attention in affective and non-affective psychosis.

We found several studies on Schizophrenia that met our inclusion criteria, whereas the publications on BDI were very few. This result is quite surprising, considering the large amount of behavioral data that reported sustained attention deficits in both acute and euthymic phases of BDI.

Summarizing the literature findings on affective and non-affective psychosis, we highlighted that patients and at-risk subjects significantly differed from healthy comparisons in the functioning of several brain regions belonging to the sustained attention system, even when they were behaviorally intact. There were regions that seemed more impaired in Schizophrenia, other more impaired in Bipolar Disorder and other that appeared altered in both

Table 2 Functional magnetic resonance imaging studies of sustained attention in bipolar disorder

Ref.	Participants	Task and behavioral results	FMRI methods and results
Strakowski *et al*[69], 2004	BDI (n = 10), age 25.5 ± 8.1, males 40%, euthymic, age of onset 23 yr, illness duration 2.2 yr, medicated 0% (drug free)	CPT-IP. Type of stimuli: digits TNS = 400 SET = 700 ms, ISI = 750, TET = 6 min Required response: on targets. Behavioral measures: d', percent correct, percent false positive	3T, block design, 5 task blocks and 5 baseline blocks Baseline: digits fixation Whole brain analysis. Imaging package: CHIPS
	NC (n = 10), age25.3 ± 7.3, males 40%	Results: no between-group differences	Results: BDI > NC in: R IFG/insula (BA 13/47), R and L ventral PFC (BA 10/47), parahippocampus/amygdala (BA 34), MOG/MTG (BA 18/19/39), R IPL (BA 40), R SPL (BA 7/40), L postcentral gyrus (BA 43), hypothalamus; NC > BDI in: L fusyform gyrus (BA 20) and L MFG (BA 11)
Fleck *et al*[70], 2012	BDI (n = 50), age 30 ± 10, males 30%, manic, medicated 80%	CPT-IP. Type of stimuli: digits TNS = 900, Target = 15%, SET = 750 ms, ISI = 1000 ms, TET = 15 min	4T, Event-related design, 3 runs (periods) Whole brain analysis. Imaging package: AFNI ROi based analysis: anterior-limbic network (IFG, BG, TH, amygdala, cerebellar vermis) + SFG Baseline: visual count down condition Task conditions: -hits, misses and false alarms -correct rejections on non-targets
	NC (n = 34), age 31 ± 9, males 41%	Required response: on targets Behavioral measures: A', B'', RT, correct rejection Results: patients performed worse in terms of correct rejections and showed a trend *vs* a reduced A'	Results: In period 1: NC > BD in cerebellum; BD > NC in TH; NC > BD in deactivation of L PCC and R angular gyrus In period 2: NC > BD in bilateral IFG and L TH In period 3: NC > BD in activation of R IFG Over time: BD activated and NC deactivated L striatum and bilateral amygdala Unmedicated BD > medicated BD in activation of R IFG and cerebellum
Sepede *et al*[71], 2012	BDI (n = 24), age 34.8 ± 8.0, males 41.7%, euthymic, age of onset 29.9, illness duration 4.7 yr, psychotic features during acute phases 95.8%, medicated 83.3%	CPT-X with 2 levels of difficulty: undegraded and degraded stimuli (0% and 40% pixel inverted) Type of stimuli: digits TNT = 80, Target = 20%, TNS = 408 ± 30 SET = 200 ms, ISI = 2000 ms, TET = 14 min	1.5T, event-related design, 2 runs (0%, and 40% degraded). Whole brain analysis. Imaging package: BrainVoyager QX 1.9.Task conditions: -correct responses on target -incorrect responses on target -correct responses on non-targets (baseline)
	REL-BDI (n = 22), age 31.5 ± 7.3, males 31.8% medicated 0% (drug naïve)	Required response: on targets and non-targets Behavioral measures: correct target, correct non-targets, incorrect target, incorrect non-target, mean RT	Results Correct target *vs* baseline: (NC = REL-BDI) > BDI in R insula (BA13) REL-BDI > (NC = BDI) in deactivating PCC/retrosplenial cortex (BA 23/29) During the 40% degraded run, correct target condition: REL-BDI > (NC = BDI) in R and L IPL (BA 40), L insula/IFG (BA 13/45)
	NC (n = 24), age 32.5 ± 6.2, males 33.3%	Results: both BDI and REL-BDI were less accurate than NC in target recognition (percent correct target)	Incorrect target *vs* baseline: (BDI = REL-BDI) > NC in middle PCC (BA 31) and R insula/IFG (BA 13/45) BDI > REL-BDI > NC in L insula (BA 13)

BDI: Bipolar disorder type I patients; REL-BDI: Unaffected relatives of bipolar disorder type I patients; NC: Normal comparisons; PFC: Prefrontal cortex; ACC: Anterior cingulate cortex; PCC: Posterior cingulate cortex; MFG: Medial frontal gyrus; SFG: Superior frontal gyrus; IFG: Inferior frontal gyrus; IPL: Inferior parietal lobule; SPL: Superior parietal lobule; MTG: Middle temporal gyrus; MOG: Middle occipital gyrus; TH: Thalamus; BG: Basal ganglia; R: Right; L: Left.

conditions.

In the studies on schizophrenic patients and subjects at augmented risk for schizophrenia, the most frequent dysfunctions were located in the cingulate gyrus and in the thalamus. The anterior part of the cingulate gyrus is a key region in sustained attention, cognitive control and error processing[72-74]. An altered function of ACC has been consistently reported in both schizophrenic patients and unaffected relatives[75,76] during attentional control[77] conflict/error monitoring[78-81], working memory[82-84] and semantic[85] tasks.

The posterior part of the cingulate gyrus is usu-

ally deactivated during active tasks with respect to rest conditions, and it is therefore considered a part of the Default Mode Network (DMN) of the brain[86]. It has a crucial role not only in internally focused tasks, but also in active regulation of the arousal state and in balancing between internally and externally oriented attention[87]. A lower volume of PCC/retrosplenial cortex has been associated to a poorer outcome in Schizophrenia[88], and an altered function of this region has been evidenced during semantic[89], self-evaluation[90,91] and fear-conditioning[92] tasks.

The thalamus is a subcortical structure whose integrity is needed to the correct functioning of cognitive processes. It is not a simple passive relay station, but a nodal link actively connecting top-down to bottom-up components of the attention/arousal system[1,93] and different cortical regions via cortico-thalamo-cortical pathways[94]. Both structural and functional MRI studies on Schizophrenia frequently reported significant abnormalities in schizophrenic patients, so a disruption of thalamocortical connections was suggested as one of the possible neural basis of cognitive and sensorial symptoms of Schizophrenia[95-98].

With regard to Bipolar Disorder, amygdala was found to be altered in two of the three reviewed. In humans, the amygdala plays a key role in detecting dangers and other emotionally salient stimuli in the environment, in order to make the subject ready to react in an appropriate way[99]. During emotional tasks, an altered functioning of the amygdala in BD has been extensively reported, especially in manic patients[100-103], but also during depressive[104] and euthymic states[105,106] of the illness. An important finding highlighted by the current review is that an augmented activation of the amygdala was observed also during attention tasks without any emotional components, this results suggesting that emotional limbic areas may interfere with cognition in BD[107].

In our systematic review we reported that an altered functioning of the insula during sustained attention task was frequently found in both Schizophrenia and Bipolar Disorder.

The insular cortex, due to its location at the interface of frontal, parietal and temporal lobes, is involved in cognitive, emotional and somato-sensorial processes[56,108], providing a hub that integrates salient stimuli with autonomic and sensorial data[109]. Many studies reported an insular dysfunction in Schizophrenia, Bipolar Disorder, and "at-risk subjects", during both tasks[110-115] and resting state[116-119], thus suggesting a key role of this region in vulnerability for psychosis, regardless of the affective or non-affective diagnostic distinction.

CONCLUSION

In the present paper, we systematically reviewed fMRI studies pertaining sustained attention in affective and non-affective psychosis.

We found that differences between cases (patients, unaffected relatives of psychotic probands) and controls in terms of functional activation in brain regions belonging to the sustained attention system were detectable even when the groups performed comparably. In particular, the insular cortex seems to be a trait marker for psychosis in general, whereas other regions seem to be differently impaired in affective and non-affective psychosis: alterations of the cingulate cortex and thalamus appear to be more common in Schizophrenia whereas amygdalar dysfunctions may be more frequently observed in Bipolar Disorder. Therefore, investigating neural correlates of sustained attention seem to be of great interest in the study of affective and non-affective psychosis as it may clarify differences and similarities between these two disabling psychiatric conditions.

Limits of the study

An important limitation of the present paper is that we included in the qualitative synthesis only those studies conducted on selected versions of CPTs that were focused on sustained attention, excluding papers with CPT versions designed to measure other cognitive functions, such as working memory or emotional processing. Moreover, it's possible that our search strategy did not succeed in finding all the available literature on the topic and that adding other search words (*i.e.*, Continuous performance Test, oddball task) or other data bases would have improved the results. Due to the small number of published studies on Bipolar Disorder, our results should be interpreted with caution and further research are needed to clarify the role of sustained attention in affective psychosis.

REFERENCES

1 **Sarter M**, Givens B, Bruno JP. The cognitive neuroscience of sustained attention: where top-down meets bottom-up. *Brain Res Brain Res Rev* 2001; **35**: 146-160 [PMID: 11336780 DOI: 10.1016/S0165-0173(01)00044-3]

2 **Suwa H**, Matsushima E, Ohta K, Mori K. Attention disorders in schizophrenia. *Psychiatry Clin Neurosci* 2004; **58**: 249-256 [PMID: 15149289 DOI: 10.1111/j.1440-1819.2004.01227.x]

3 **Hahn B**, Robinson BM, Kaiser ST, Matveeva TM, Harvey AN, Luck SJ, Gold JM. Kraepelin and Bleuler had it right: people with schizophrenia have deficits sustaining attention over time. *J Abnorm Psychol* 2012; **121**: 641-648 [PMID: 22686867 DOI: 10.1037/a0028492]

4 **Üçok A**, Direk N, Koyuncu A, Keskin-Ergen Y, Yüksel Ç, Güler J, Karadayı G, Akturan E, Devrim-Üçok M. Cognitive deficits in clinical and familial high risk groups for psychosis are common as in first episode schizophrenia. *Schizophr Res* 2013; **151**: 265-269 [PMID: 24262680 DOI: 10.1016/j.schres.2013.10.030]

5 **Harmer CJ**, Clark L, Grayson L, Goodwin GM. Sustained attention deficit in bipolar disorder is not a working memory impairment in disguise. *Neuropsychologia* 2002; **40**: 1586-1590 [PMID: 11985840 DOI: 10.1016/S0028-3932(02)00019-2]

6 **Bora E**, Yucel M, Pantelis C. Cognitive endophenotypes of bipolar disorder: a meta-analysis of neuropsychological deficits in euthymic patients and their first-degree relatives. *J Affect Disord* 2009; **113**: 1-20 [PMID: 18684514 DOI: 10.1016/j.jad.2008.06.009]

7 **Clark L**, Iversen SD, Goodwin GM. Sustained attention

deficit in bipolar disorder. *Br J Psychiatry* 2002; **180**: 313-319 [PMID: 11925353 DOI: 10.1192/bjp.180.4.313]
8 **Robinson LJ**, Thompson JM, Gallagher P, Gray JM, Young AH, Ferrier IN. Performance monitoring and executive control of attention in euthymic bipolar disorder: employing the CPT-AX paradigm. *Psychiatry Res* 2013; **210**: 457-464 [PMID: 23880481 DOI: 10.1016/j.psychres.2013.06.039]
9 **Hofer A**, Baumgartner S, Bodner T, Edlinger M, Hummer M, Kemmler G, Rettenbacher MA, Fleischhacker WW. Patient outcomes in schizophrenia II: the impact of cognition. *Eur Psychiatry* 2005; **20**: 395-402 [PMID: 16171654 DOI: 10.1016/j.eurpsy.2005.02.006]
10 **González-Blanch C**, Perez-Iglesias R, Pardo-García G, Rodríguez-Sánchez JM, Martínez-García O, Vázquez-Barquero JL, Crespo-Facorro B. Prognostic value of cognitive functioning for global functional recovery in first-episode schizophrenia. *Psychol Med* 2010; **40**: 935-944 [PMID: 19751542 DOI: 10.1017/S0033291709991267]
11 **Martino DJ**, Marengo E, Igoa A, Scápola M, Ais ED, Perinot L, Strejilevich SA. Neurocognitive and symptomatic predictors of functional outcome in bipolar disorders: a prospective 1 year follow-up study. *J Affect Disord* 2009; **116**: 37-42 [PMID: 19033081 DOI: 10.1016/j.jad.2008.10.023]
12 **Pattanayak RD**, Sagar R, Mehta M. Neuropsychological performance in euthymic Indian patients with bipolar disorder type I: correlation between quality of life and global functioning. *Psychiatry Clin Neurosci* 2012; **66**: 553-563 [PMID: 23252921 DOI: 10.1111/j.1440-1819.2012.02400.x]
13 **Liu SK**, Chen WJ, Chang CJ, Lin HN. Effects of atypical neuroleptics on sustained attention deficits in schizophrenia: a trial of risperidone versus haloperidol. *Neuropsychopharmacology* 2000; **22**: 311-319 [PMID: 10693159 DOI: 10.1016/S0893-133X(99)00137-2]
14 **Goswami U**, Sharma A, Varma A, Gulrajani C, Ferrier IN, Young AH, Gallagher P, Thompson JM, Moore PB. The neurocognitive performance of drug-free and medicated euthymic bipolar patients do not differ. *Acta Psychiatr Scand* 2009; **120**: 456-463 [PMID: 19416126 DOI: 10.1111/j.1600-0447.2009.01390.x]
15 **Martínez-Arán A**, Vieta E, Reinares M, Colom F, Torrent C, Sánchez-Moreno J, Benabarre A, Goikolea JM, Comes M, Salamero M. Cognitive function across manic or hypomanic, depressed, and euthymic states in bipolar disorder. *Am J Psychiatry* 2004; **161**: 262-270 [PMID: 14754775 DOI: 10.1176/appi.ajp.161.2.262]
16 **Sánchez-Morla EM**, Barabash A, Martínez-Vizcaíno V, Tabarés-Seisdedos R, Balanzá-Martínez V, Cabranes-Díaz JA, Baca-Baldomero E, Gómez JL. Comparative study of neurocognitive function in euthymic bipolar patients and stabilized schizophrenic patients. *Psychiatry Res* 2009; **169**: 220-228 [PMID: 19758705 DOI: 10.1016/j.psychres.2008.06.032]
17 **Liu SK**, Chiu CH, Chang CJ, Hwang TJ, Hwu HG, Chen WJ. Deficits in sustained attention in schizophrenia and affective disorders: stable versus state-dependent markers. *Am J Psychiatry* 2002; **159**: 975-982 [PMID: 12042186 DOI: 10.1176/appi.ajp.159.6.975]
18 **Dickerson F**, Boronow JJ, Stallings C, Origoni AE, Cole SK, Yolken RH. Cognitive functioning in schizophrenia and bipolar disorder: comparison of performance on the Repeatable Battery for the Assessment of Neuropsychological Status. *Psychiatry Res* 2004; **129**: 45-53 [PMID: 15572184 DOI: 10.1016/j.psychres.2004.07.002]
19 **Altshuler LL**, Ventura J, van Gorp WG, Green MF, Theberge DC, Mintz J. Neurocognitive function in clinically stable men with bipolar I disorder or schizophrenia and normal control subjects. *Biol Psychiatry* 2004; **56**: 560-569 [PMID: 15476685 DOI: 10.1016/j.biopsych.2004.08.002]
20 **Schretlen DJ**, Cascella NG, Meyer SM, Kingery LR, Testa SM, Munro CA, Pulver AE, Rivkin P, Rao VA, Diaz-Asper CM, Dickerson FB, Yolken RH, Pearlson GD. Neuropsychological functioning in bipolar disorder and schizophrenia. *Biol Psychiatry* 2007; **62**: 179-186 [PMID: 17161829 DOI: 10.1016/j.biopsych.2006.09.025]
21 **Birkett P**, Sigmundsson T, Sharma T, Toulopoulou T, Griffiths TD, Reveley A, Murray R. Reaction time and sustained attention in schizophrenia and its genetic predisposition. *Schizophr Res* 2007; **95**: 76-85 [PMID: 17630256 DOI: 10.1016/j.schres.2007.05.030]
22 **Hilti CC**, Hilti LM, Heinemann D, Robbins T, Seifritz E, Cattapan-Ludewig K. Impaired performance on the Rapid Visual Information Processing task (RVIP) could be an endophenotype of schizophrenia. *Psychiatry Res* 2010; **177**: 60-64 [PMID: 20110130 DOI: 10.1016/j.psychres.2009.12.012]
23 **Trivedi JK**, Goel D, Dhyani M, Sharma S, Singh AP, Sinha PK, Tandon R. Neurocognition in first-degree healthy relatives (siblings) of bipolar affective disorder patients. *Psychiatry Clin Neurosci* 2008; **62**: 190-196 [PMID: 18412842 DOI: 10.1111/j.1440-1819.2008.01754.x]
24 **Fridberg DJ**, Hetrick WP, Brenner CA, Shekhar A, Steffen AN, Malloy FW, O'Donnell BF. Relationships between auditory event-related potentials and mood state, medication, and comorbid psychiatric illness in patients with bipolar disorder. *Bipolar Disord* 2009; **11**: 857-866 [PMID: 19922554 DOI: 10.1111/j.1399-5618.2009.00758.x]
25 **Arts B**, Jabben N, Krabbendam L, van Os J. A 2-year naturalistic study on cognitive functioning in bipolar disorder. *Acta Psychiatr Scand* 2011; **123**: 190-205 [PMID: 20846251 DOI: 10.1111/j.1600-0447.2010.01601.x]
26 **Ancín I**, Santos JL, Teijeira C, Sánchez-Morla EM, Bescós MJ, Argudo I, Torrijos S, Vázquez-Alvarez B, De La Vega I, López-Ibor JJ, Barabash A, Cabranes-Díaz JA. Sustained attention as a potential endophenotype for bipolar disorder. *Acta Psychiatr Scand* 2010; **122**: 235-245 [PMID: 20105148 DOI: 10.1111/j.1600-0447.2009.01532.x]
27 **Chen WJ**, Faraone SV. Sustained attention deficits as markers of genetic susceptibility to schizophrenia. *Am J Med Genet* 2000; **97**: 52-57 [PMID: 10813804]
28 **Cornblatt BA**, Malhotra AK. Impaired attention as an endophenotype for molecular genetic studies of schizophrenia. *Am J Med Genet* 2001; **105**: 11-15 [PMID: 11424979]
29 **Giakoumaki SG**, Roussos P, Pallis EG, Bitsios P. Sustained attention and working memory deficits follow a familial pattern in schizophrenia. *Arch Clin Neuropsychol* 2011; **26**: 687-695 [PMID: 21813556 DOI: 10.1093/arclin/acr060]
30 **Gottesman II**, Gould TD. The endophenotype concept in psychiatry: etymology and strategic intentions. *Am J Psychiatry* 2003; **160**: 636-645 [PMID: 12668349 DOI: 10.1176/appi.ajp.160.4.636]
31 **Wang Q**, Chan R, Sun J, Yao J, Deng W, Sun X, Liu X, Sham PC, Ma X, Meng H, Murray RM, Collier DA, Li T. Reaction time of the Continuous Performance Test is an endophenotypic marker for schizophrenia: a study of first-episode neuroleptic-naive schizophrenia, their non-psychotic first-degree relatives and healthy population controls. *Schizophr Res* 2007; **89**: 293-298 [PMID: 17055704 DOI: 10.1016/j.schres.2006.08.030]
32 **Jones LA**, Cardno AG, Sanders RD, Owen MJ, Williams J. Sustained and selective attention as measures of genetic liability to schizophrenia. *Schizophr Res* 2001; **48**: 263-272 [PMID: 11295379 DOI: 10.1016/S0920-9964(00)00136-5]
33 **Addington J**, Addington D. Attentional vulnerability indicators in schizophrenia and bipolar disorder. *Schizophr Res* 1997; **23**: 197-204 [PMID: 9075297 DOI: 10.1016/S0920-9964(96)00105-3]
34 **Clark L**, Kempton MJ, Scarnà A, Grasby PM, Goodwin GM. Sustained attention-deficit confirmed in euthymic bipolar disorder but not in first-degree relatives of bipolar patients or euthymic unipolar depression. *Biol Psychiatry* 2005; **57**: 183-187 [PMID: 15652878 DOI: 10.1016/j.biopsych.2004.11.007]

35 **Walshe M**, Schulze KK, Stahl D, Hall MH, Chaddock C, Morris R, Marshall N, McDonald C, Murray RM, Bramon E, Kravariti E. Sustained attention in bipolar I disorder patients with familial psychosis and their first-degree relatives. *Psychiatry Res* 2012; **199**: 70-73 [PMID: 22513042 DOI: 10.1016/j.psychres.2012.03.018]

36 **Huettel SA**, McCarthy G. What is odd in the oddball task? Prefrontal cortex is activated by dynamic changes in response strategy. *Neuropsychologia* 2004; **42**: 379-386 [PMID: 14670576 DOI: 10.1016/j.neuropsychologia.2003.07.009]

37 **Kim H**. Involvement of the dorsal and ventral attention networks in oddball stimulus processing: a meta-analysis. *Hum Brain Mapp* 2014; **35**: 2265-2284 [PMID: 23900833 DOI: 10.1002/hbm.22326]

38 **Huang S**, Belliveau JW, Tengshe C, Ahveninen J. Brain networks of novelty-driven involuntary and cued voluntary auditory attention shifting. *PLoS One* 2012; **7**: e44062 [PMID: 22937153 DOI: 10.1371/journal.pone.0044062]

39 **Zaehle T**, Bauch EM, Hinrichs H, Schmitt FC, Voges J, Heinze HJ, Bunzeck N. Nucleus accumbens activity dissociates different forms of salience: evidence from human intracranial recordings. *J Neurosci* 2013; **33**: 8764-8771 [PMID: 23678119 DOI: 10.1523/JNEUROSCI.5276-12.2013]

40 **Beck LH**, Bransome ED, Mirsky AF, Rosvold HE, Sarason I. A continuous performance test of brain damage. *J Consult Psychol* 1956; **20**: 343-350 [PMID: 13367264 DOI: 10.1037/h0043220]

41 **Riccio CA**, Reynolds CR, Lowe P, Moore JJ. The continuous performance test: a window on the neural substrates for attention? *Arch Clin Neuropsychol* 2002; **17**: 235-272 [PMID: 14589726 DOI: 10.1016/S0887-6177(01)00111-1]

42 **Baker DB**, Taylor CJ, Leyva C. Continuous performance tests: a comparison of modalities. *J Clin Psychol* 1995; **51**: 548-551 [PMID: 7593677]

43 **Kasai K**, Nakagome K, Hiramatsu K, Fukuda M, Honda M, Iwanami A. Psychophysiological index during auditory selective attention correlates with visual continuous performance test sensitivity in normal adults. *Int J Psychophysiol* 2002; **45**: 211-225 [PMID: 12208528 DOI: 10.1016/S0167-8760(02)00013-2]

44 **Nuechterlein KH**, Parasuraman R, Jiang Q. Visual sustained attention: image degradation produces rapid sensitivity decrement over time. *Science* 1983; **220**: 327-329 [PMID: 6836276 DOI: 10.1126/science.6836276]

45 **Conners CK**, MHS Staff. Conners' Continuous Performance Test (CPT II) computer programs for Windows technical guide and software manual. North Tonawanda, NY: Multi-Health Systems: 2000

46 **Chen WJ**, Hsiao CK, Hsiao LL, Hwu HG. Performance of the Continuous Performance Test among community samples. *Schizophr Bull* 1998; **24**: 163-174 [PMID: 9502554 DOI: 10.1093/oxfordjournals.schbul.a033308]

47 **Cornblatt BA**, Lenzenweger MF, Erlenmeyer-Kimling L. The continuous performance test, identical pairs version: II. Contrasting attentional profiles in schizophrenic and depressed patients. *Psychiatry Res* 1989; **29**: 65-85 [PMID: 2772099 DOI: 10.1016/0165-1781(89)90188-1]

48 **Coull JT**, Frith CD, Frackowiak RS, Grasby PM. A fronto-parietal network for rapid visual information processing: a PET study of sustained attention and working memory. *Neuropsychologia* 1996; **34**: 1085-1095 [PMID: 8904746 DOI: 10.1016/0028-3932(96)00029-2]

49 **Green DM**, Swets JA. Signal detection theory and psychophysics. New York: Wiley: 1966

50 **Adler CM**, Sax KW, Holland SK, Schmithorst V, Rosenberg L, Strakowski SM. Changes in neuronal activation with increasing attention demand in healthy volunteers: an fMRI study. *Synapse* 2001; **42**: 266-272 [PMID: 11746725 DOI: 10.1002/syn.1112]

51 **Ogg RJ**, Zou P, Allen DN, Hutchins SB, Dutkiewicz RM, Mulhern RK. Neural correlates of a clinical continuous performance test. *Magn Reson Imaging* 2008; **26**: 504-512 [PMID: 18068933 DOI: 10.1016/j.mri.2007.09.004]

52 **Mantini D**, Corbetta M, Perrucci MG, Romani GL, Del Gratta C. Large-scale brain networks account for sustained and transient activity during target detection. *Neuroimage* 2009; **44**: 265-274 [PMID: 18793734 DOI: 10.1016/j.neuroimage.2008.08.019]

53 **Grahn JA**, Manly T. Common neural recruitment across diverse sustained attention tasks. *PLoS One* 2012; **7**: e49556 [PMID: 23185360 DOI: 10.1371/journal.pone.0049556]

54 **Lawrence NS**, Ross TJ, Hoffmann R, Garavan H, Stein EA. Multiple neuronal networks mediate sustained attention. *J Cogn Neurosci* 2003; **15**: 1028-1038 [PMID: 14614813 DOI: 10.1162/089892903770007416]

55 **Bush G**, Luu P, Posner MI. Cognitive and emotional influences in anterior cingulate cortex. *Trends Cogn Sci* 2000; **4**: 215-222 [PMID: 10827444 DOI: 10.1016/S1364-6613(00)01483-2]

56 **Kurth F**, Zilles K, Fox PT, Laird AR, Eickhoff SB. A link between the systems: functional differentiation and integration within the human insula revealed by meta-analysis. *Brain Struct Funct* 2010; **214**: 519-534 [PMID: 20512376 DOI: 10.1007/s00429-010-0255-z]

57 **Volz H**, Gaser C, Häger F, Rzanny R, Pönisch J, Mentzel H, Kaiser WA, Sauer H. Decreased frontal activation in schizophrenics during stimulation with the continuous performance test--a functional magnetic resonance imaging study. *Eur Psychiatry* 1999; **14**: 17-24 [PMID: 10572321 DOI: 10.1016/S0924-9338(99)80711-1]

58 **Eyler LT**, Olsen RK, Jeste DV, Brown GG. Abnormal brain response of chronic schizophrenia patients despite normal performance during a visual vigilance task. *Psychiatry Res* 2004; **130**: 245-257 [PMID: 15135158 DOI: 10.1016/j.pscychresns.2004.01.003]

59 **Salgado-Pineda P**, Junqué C, Vendrell P, Baeza I, Bargalló N, Falcón C, Bernardo M. Decreased cerebral activation during CPT performance: structural and functional deficits in schizophrenic patients. *Neuroimage* 2004; **21**: 840-847 [PMID: 15006650 DOI: 10.1016/j.neuroimage.2003.10.027]

60 **Honey GD**, Pomarol-Clotet E, Corlett PR, Honey RA, McKenna PJ, Bullmore ET, Fletcher PC. Functional dysconnectivity in schizophrenia associated with attentional modulation of motor function. *Brain* 2005; **128**: 2597-2611 [PMID: 16183659 DOI: 10.1093/brain/awh632]

61 **Morey RA**, Inan S, Mitchell TV, Perkins DO, Lieberman JA, Belger A. Imaging frontostriatal function in ultra-high-risk, early, and chronic schizophrenia during executive processing. *Arch Gen Psychiatry* 2005; **62**: 254-262 [PMID: 15753238 DOI: 10.1001/archpsyc.62.3.254]

62 **Liddle PF**, Laurens KR, Kiehl KA, Ngan ET. Abnormal function of the brain system supporting motivated attention in medicated patients with schizophrenia: an fMRI study. *Psychol Med* 2006; **36**: 1097-1108 [PMID: 16650349 DOI: 10.1017/S0033291706007677]

63 **Gur RE**, Turetsky BI, Loughead J, Snyder W, Kohler C, Elliott M, Pratiwadi R, Ragland JD, Bilker WB, Siegel SJ, Kanes SJ, Arnold SE, Gur RC. Visual attention circuitry in schizophrenia investigated with oddball event-related functional magnetic resonance imaging. *Am J Psychiatry* 2007; **164**: 442-449 [PMID: 17329469 DOI: 10.1176/appi.ajp.164.3.442]

64 **Harrison BJ**, Yücel M, Pujol J, Pantelis C. Task-induced deactivation of midline cortical regions in schizophrenia assessed with fMRI. *Schizophr Res* 2007; **91**: 82-86 [PMID: 17307337 DOI: 10.1016/j.schres.2006.12.027]

65 **Wolf DH**, Turetsky BI, Loughead J, Elliott MA, Pratiwadi R, Gur RE, Gur RC. Auditory Oddball fMRI in Schizophrenia: Association of Negative Symptoms with Regional Hypoactivation to Novel Distractors. *Brain Imaging Behav* 2008; **2**: 132-145 [PMID: 19756228 DOI: 10.1007/s11682-008-9022-7]

66 **Filbey FM**, Russell T, Morris RG, Murray RM, McDonald C.

Functional magnetic resonance imaging (fMRI) of attention processes in presumed obligate carriers of schizophrenia: preliminary findings. *Ann Gen Psychiatry* 2008; **7**: 18 [PMID: 18834530 DOI: 10.1186/1744-859X-7-18]
67 **Carter JD**, Bizzell J, Kim C, Bellion C, Carpenter KL, Dichter G, Belger A. Attention deficits in schizophrenia--preliminary evidence of dissociable transient and sustained deficits. *Schizophr Res* 2010; **122**: 104-112 [PMID: 20554160 DOI: 10.1016/j.schres.2010.03.019]
68 **Sepede G**, Ferretti A, Perrucci MG, Gambi F, Di Donato F, Nuccetelli F, Del Gratta C, Tartaro A, Salerno RM, Ferro FM, Romani GL. Altered brain response without behavioral attention deficits in healthy siblings of schizophrenic patients: an event-related fMRI study. *Neuroimage* 2010; **49**: 1080-1090 [PMID: 19646537 DOI: 10.1016/j.neuroimage.2009.07.053]
69 **Strakowski SM**, Adler CM, Holland SK, Mills N, DelBello MP. A preliminary FMRI study of sustained attention in euthymic, unmedicated bipolar disorder. *Neuropsychopharmacology* 2004; **29**: 1734-1740 [PMID: 15173843]
70 **Fleck DE**, Eliassen JC, Durling M, Lamy M, Adler CM, DelBello MP, Shear PK, Cerullo MA, Lee JH, Strakowski SM. Functional MRI of sustained attention in bipolar mania. *Mol Psychiatry* 2012; **17**: 325-336 [PMID: 20975662 DOI: 10.1038/mp.2010.108]
71 **Sepede G**, De Berardis D, Campanella D, Perrucci MG, Ferretti A, Serroni N, Moschetta FS, Del Gratta C, Salerno RM, Ferro FM, Di Giannantonio M, Onofrj M, Romani GL, Gambi F. Impaired sustained attention in euthymic bipolar disorder patients and non-affected relatives: an fMRI study. *Bipolar Disord* 2012; **14**: 764-779 [PMID: 23036083 DOI: 10.1111/BDI.12007]
72 **Badgaiyan RD**, Posner MI. Mapping the cingulate cortex in response selection and monitoring. *Neuroimage* 1998; **7**: 255-260 [PMID: 9597666 DOI: 10.1006/nimg.1998.0326]
73 **Hester R**, Fassbender C, Garavan H. Individual differences in error processing: a review and reanalysis of three event-related fMRI studies using the GO/NOGO task. *Cereb Cortex* 2004; **14**: 986-994 [PMID: 15115734 DOI: 10.1093/cercor/bhh059]
74 **Kerns JG**, Cohen JD, MacDonald AW, Cho RY, Stenger VA, Carter CS. Anterior cingulate conflict monitoring and adjustments in control. *Science* 2004; **303**: 1023-1026 [PMID: 14963333 DOI: 10.1126/science.1089910]
75 **Eisenberg DP**, Berman KF. Executive function, neural circuitry, and genetic mechanisms in schizophrenia. *Neuropsychopharmacology* 2010; **35**: 258-277 [PMID: 19693005 DOI: 10.1038/npp.2009.111]
76 **Rasetti R**, Weinberger DR. Intermediate phenotypes in psychiatric disorders. *Curr Opin Genet Dev* 2011; **21**: 340-348 [PMID: 21376566 DOI: 10.1016/j.gde.2011.02.003]
77 **Blasi G**, Taurisano P, Papazacharias A, Caforio G, Romano R, Lobianco L, Fazio L, Di Giorgio A, Latorre V, Sambataro F, Popolizio T, Nardini M, Mattay VS, Weinberger DR, Bertolino A. Nonlinear response of the anterior cingulate and prefrontal cortex in schizophrenia as a function of variable attentional control. *Cereb Cortex* 2010; **20**: 837-845 [PMID: 19633177 DOI: 10.1093/cercor/bhp146]
78 **Laurens KR**, Ngan ET, Bates AT, Kiehl KA, Liddle PF. Rostral anterior cingulate cortex dysfunction during error processing in schizophrenia. *Brain* 2003; **126**: 610-622 [PMID: 12566282 DOI: 10.1093/brain/awg056]
79 **Kerns JG**, Cohen JD, MacDonald AW, Johnson MK, Stenger VA, Aizenstein H, Carter CS. Decreased conflict- and error-related activity in the anterior cingulate cortex in subjects with schizophrenia. *Am J Psychiatry* 2005; **162**: 1833-1839 [PMID: 16199829 DOI: 10.1176/appi.ajp.162.10.1833]
80 **Polli FE**, Barton JJ, Thakkar KN, Greve DN, Goff DC, Rauch SL, Manoach DS. Reduced error-related activation in two anterior cingulate circuits is related to impaired performance in schizophrenia. *Brain* 2008; **131**: 971-986 [PMID: 18158315 DOI: 10.1093/brain/awm307]
81 **Sambataro F**, Mattay VS, Thurin K, Safrin M, Rasetti R, Blasi G, Callicott JH, Weinberger DR. Altered cerebral response during cognitive control: a potential indicator of genetic liability for schizophrenia. *Neuropsychopharmacology* 2013; **38**: 846-853 [PMID: 23299932 DOI: 10.1038/npp.2012.250]
82 **Barch DM**, Carter CS, Braver TS, Sabb FW, MacDonald A, Noll DC, Cohen JD. Selective deficits in prefrontal cortex function in medication-naive patients with schizophrenia. *Arch Gen Psychiatry* 2001; **58**: 280-288 [PMID: 11231835 DOI: 10.1001/archpsyc.58.3.280]
83 **Henseler I**, Falkai P, Gruber O. A systematic fMRI investigation of the brain systems subserving different working memory components in schizophrenia. *Eur J Neurosci* 2009; **30**: 693-702 [PMID: 19686473 DOI: 10.1111/j.1460-9568.2009.06850.x]
84 **Karch S**, Leicht G, Giegling I, Lutz J, Kunz J, Buselmeier M, Hey P, Spörl A, Jäger L, Meindl T, Pogarell O, Möller HJ, Hegerl U, Rujescu D, Mulert C. Inefficient neural activity in patients with schizophrenia and nonpsychotic relatives of schizophrenic patients: evidence from a working memory task. *J Psychiatr Res* 2009; **43**: 1185-1194 [PMID: 19426993 DOI: 10.1016/j.jpsychires.2009.04.004]
85 **Sass K**, Heim S, Sachs O, Straube B, Schneider F, Habel U, Kircher T. Neural correlates of semantic associations in patients with schizophrenia. *Eur Arch Psychiatry Clin Neurosci* 2014; **264**: 143-154 [PMID: 23880958]
86 **Buckner RL**, Andrews-Hanna JR, Schacter DL. The brain's default network: anatomy, function, and relevance to disease. *Ann N Y Acad Sci* 2008; **1124**: 1-38 [PMID: 18400922 DOI: 10.1196/annals.1440.011]
87 **Leech R**, Sharp DJ. The role of the posterior cingulate cortex in cognition and disease. *Brain* 2014; **137**: 12-32 [PMID: 23869106]
88 **Mitelman SA**, Shihabuddin L, Brickman AM, Hazlett EA, Buchsbaum MS. Volume of the cingulate and outcome in schizophrenia. *Schizophr Res* 2005; **72**: 91-108 [PMID: 15560955 DOI: 10.1016/j.schres.2004.02.011]
89 **Tendolkar I**, Weis S, Guddat O, Fernández G, Brockhaus-Dumke A, Specht K, Klosterkötter J, Reul J, Ruhrmann S. Evidence for a dysfunctional retrosplenial cortex in patients with schizophrenia: a functional magnetic resonance imaging study with a semantic-perceptual contrast. *Neurosci Lett* 2004; **369**: 4-8 [PMID: 15380297 DOI: 10.1016/j.neulet.2004.07.024]
90 **Bedford NJ**, Surguladze S, Giampietro V, Brammer MJ, David AS. Self-evaluation in schizophrenia: an fMRI study with implications for the understanding of insight. *BMC Psychiatry* 2012; **12**: 106 [PMID: 22876974 DOI: 10.1186/1471-244X-12-106]
91 **van der Meer L**, de Vos AE, Stiekema AP, Pijnenborg GH, van Tol MJ, Nolen WA, David AS, Aleman A. Insight in schizophrenia: involvement of self-reflection networks? *Schizophr Bull* 2013; **39**: 1288-1295 [PMID: 23104865 DOI: 10.1093/schbul/sbs122]
92 **Holt DJ**, Coombs G, Zeidan MA, Goff DC, Milad MR. Failure of neural responses to safety cues in schizophrenia. *Arch Gen Psychiatry* 2012; **69**: 893-903 [PMID: 22945619 DOI: 10.1001/archgenpsychiatry.2011.2310]
93 **Coull JT**. Neural correlates of attention and arousal: insights from electrophysiology, functional neuroimaging and psychopharmacology. *Prog Neurobiol* 1998; **55**: 343-361 [PMID: 9654384 DOI: 10.1016/S0301-0082(98)00011-2]
94 **Sherman SM**, Guillery RW. Exploring the role of the thalamus and its role in cortical function. Cambridge: MIT Press, 2006
95 **Sim K**, Cullen T, Ongur D, Heckers S. Testing models of thalamic dysfunction in schizophrenia using neuroimaging. *J Neural Transm* 2006; **113**: 907-928 [PMID: 16252070 DOI: 10.1007/s00702-005-0363-8]

96 **Cronenwett WJ**, Csernansky J. Thalamic pathology in schizophrenia. *Curr Top Behav Neurosci* 2010; **4**: 509-528 [PMID: 21312411 DOI: 10.1007/7854_2010_55]

97 **Byne W**, Hazlett EA, Buchsbaum MS, Kemether E. The thalamus and schizophrenia: current status of research. *Acta Neuropathol* 2009; **117**: 347-368 [PMID: 18604544 DOI: 10.1007/s00401-008-0404-0]

98 **Shepherd AM**, Laurens KR, Matheson SL, Carr VJ, Green MJ. Systematic meta-review and quality assessment of the structural brain alterations in schizophrenia. *Neurosci Biobehav Rev* 2012; **36**: 1342-1356 [PMID: 22244985 DOI: 10.1016/j.neubiorev.2011.12.015]

99 **LeDoux JE**. Emotion circuits in the brain. *Annu Rev Neurosci* 2000; **23**: 155-184 [PMID: 10845062 DOI: 10.1146/annurev.neuro.23.1.155]

100 **Altshuler L**, Bookheimer S, Proenza MA, Townsend J, Sabb F, Firestine A, Bartzokis G, Mintz J, Mazziotta J, Cohen MS. Increased amygdala activation during mania: a functional magnetic resonance imaging study. *Am J Psychiatry* 2005; **162**: 1211-1213 [PMID: 15930074 DOI: 10.1176/appi.ajp.162.6.1211]

101 **Foland LC**, Altshuler LL, Bookheimer SY, Eisenberger N, Townsend J, Thompson PM. Evidence for deficient modulation of amygdala response by prefrontal cortex in bipolar mania. *Psychiatry Res* 2008; **162**: 27-37 [PMID: 18063349 DOI: 10.1016/j.pscychresns.2007.04.007]

102 **Bermpohl F**, Dalanay U, Kahnt T, Sajonz B, Heimann H, Ricken R, Stoy M, Hägele C, Schlagenhauf F, Adli M, Wrase J, Ströhle A, Heinz A, Bauer M. A preliminary study of increased amygdala activation to positive affective stimuli in mania. *Bipolar Disord* 2009; **11**: 70-75 [PMID: 19133968 DOI: 10.1111/j.1399-5618.2008.00648.x]

103 **Strakowski SM**, Eliassen JC, Lamy M, Cerullo MA, Allendorfer JB, Madore M, Lee JH, Welge JA, DelBello MP, Fleck DE, Adler CM. Functional magnetic resonance imaging brain activation in bipolar mania: evidence for disruption of the ventrolateral prefrontal-amygdala emotional pathway. *Biol Psychiatry* 2011; **69**: 381-388 [PMID: 21051038 DOI: 10.1016/j.biopsych.2010.09.019]

104 **Malhi GS**, Lagopoulos J, Ward PB, Kumari V, Mitchell PB, Parker GB, Ivanovski B, Sachdev P. Cognitive generation of affect in bipolar depression: an fMRI study. *Eur J Neurosci* 2004; **19**: 741-754 [PMID: 14984424 DOI: 10.1111/j.0953-816X.2003.03159.x]

105 **Lagopoulos J**, Malhi GS. A functional magnetic resonance imaging study of emotional Stroop in euthymic bipolar disorder. *Neuroreport* 2007; **18**: 1583-1587 [PMID: 17885606 DOI: 10.1097/WNR.0b013e3282efa07a]

106 **Surguladze SA**, Marshall N, Schulze K, Hall MH, Walshe M, Bramon E, Phillips ML, Murray RM, McDonald C. Exaggerated neural response to emotional faces in patients with bipolar disorder and their first-degree relatives. *Neuroimage* 2010; **53**: 58-64 [PMID: 20595014 DOI: 10.1016/j.neuroimage.2010.05.069]

107 **Gruber O**, Tost H, Henseler I, Schmael C, Scherk H, Ende G, Ruf M, Falkai P, Rietschel M. Pathological amygdala activation during working memory performance: Evidence for a pathophysiological trait marker in bipolar affective disorder. *Hum Brain Mapp* 2010; **31**: 115-125 [PMID: 19603410 DOI: 10.1002/hbm.20849]

108 **Mutschler I**, Wieckhorst B, Kowalevski S, Derix J, Wentlandt J, Schulze-Bonhage A, Ball T. Functional organization of the human anterior insular cortex. *Neurosci Lett* 2009; **457**: 66-70 [PMID: 19429164 DOI: 10.1016/j.neulet.2009.03.101]

109 **Menon V**, Uddin LQ. Saliency, switching, attention and control: a network model of insula function. *Brain Struct Funct* 2010; **214**: 655-667 [PMID: 20512370 DOI: 10.1007/s00429-010-0262-0]

110 **Pujol N**, Penadés R, Rametti G, Catalán R, Vidal-Piñeiro D, Palacios E, Bargallo N, Bernardo M, Junqué C. Inferior frontal and insular cortical thinning is related to dysfunctional brain activation/deactivation during working memory task in schizophrenic patients. *Psychiatry Res* 2013; **214**: 94-101 [PMID: 23993992 DOI: 10.1016/j.pscychresns.2013.06.008]

111 **Vu MA**, Thermenos HW, Terry DP, Wolfe DJ, Voglmaier MM, Niznikiewicz MA, McCarley RW, Seidman LJ, Dickey CC. Working memory in schizotypal personality disorder: fMRI activation and deactivation differences. *Schizophr Res* 2013; **151**: 113-123 [PMID: 24161536 DOI: 10.1016/j.schres.2013.09.013]

112 **Linnman C**, Coombs G, Goff DC, Holt DJ. Lack of insula reactivity to aversive stimuli in schizophrenia. *Schizophr Res* 2013; **143**: 150-157 [PMID: 23201307 DOI: 10.1016/j.schres.2012.10.038]

113 **Hummer TA**, Hulvershorn LA, Karne HS, Gunn AD, Wang Y, Anand A. Emotional response inhibition in bipolar disorder: a functional magnetic resonance imaging study of trait- and state-related abnormalities. *Biol Psychiatry* 2013; **73**: 136-143 [PMID: 22871393 DOI: 10.1016/j.biopsych.2012.06.036]

114 **Cooper D**, Barker V, Radua J, Fusar-Poli P, Lawrie SM. Multimodal voxel-based meta-analysis of structural and functional magnetic resonance imaging studies in those at elevated genetic risk of developing schizophrenia. *Psychiatry Res* 2014; **221**: 69-77 [PMID: 24239093 DOI: 10.1016/j.pscychresns.2013.07.008]

115 **Palaniyappan L**, Simmonite M, White TP, Liddle EB, Liddle PF. Neural primacy of the salience processing system in schizophrenia. *Neuron* 2013; **79**: 814-828 [PMID: 23972602 DOI: 10.1016/j.neuron.2013.06.027]

116 **Moran LV**, Tagamets MA, Sampath H, O'Donnell A, Stein EA, Kochunov P, Hong LE. Disruption of anterior insula modulation of large-scale brain networks in schizophrenia. *Biol Psychiatry* 2013; **74**: 467-474 [PMID: 23623456 DOI: 10.1016/j.biopsych.2013.02.029]

117 **He Z**, Deng W, Li M, Chen Z, Jiang L, Wang Q, Huang C, Collier DA, Gong Q, Ma X, Zhang N, Li T. Aberrant intrinsic brain activity and cognitive deficit in first-episode treatment-naive patients with schizophrenia. *Psychol Med* 2013; **43**: 769-780 [PMID: 22883428 DOI: 10.1017/S0033291712001638]

118 **Vargas C**, López-Jaramillo C, Vieta E. A systematic literature review of resting state network--functional MRI in bipolar disorder. *J Affect Disord* 2013; **150**: 727-735 [PMID: 23830141 DOI: 10.1016/j.jad.2013.05.083]

119 **Whalley HC**, Sussmann JE, Romaniuk L, Stewart T, Papmeyer M, Sprooten E, Hackett S, Hall J, Lawrie SM, McIntosh AM. Prediction of depression in individuals at high familial risk of mood disorders using functional magnetic resonance imaging. *PLoS One* 2013; **8**: e57357 [PMID: 23483904 DOI: 10.1371/journal.pone.0057357]

P- Reviewers: Serafini G, J Aguilar E **S- Editor**: Wen LL
L- Editor: A **E- Editor**: Zhang DN

World Journal of Radiology

Submit a Manuscript: http://www.wjgnet.com/esps/
Help Desk: http://www.wjgnet.com/esps/helpdesk.aspx
DOI: 10.4329/wjr.v6.i6.274

World J Radiol 2014 June 28; 6(6): 274-283
ISSN 1949-8470 (online)
© 2014 Baishideng Publishing Group Inc. All rights reserved.

TOPIC HIGHLIGHT

WJR 6th Anniversary Special Issues (8): fMRI

Rotator cuff disorders: How to write a surgically relevant magnetic resonance imaging report?

Ahmed M Tawfik, Ahmad El-Morsy, Mohamed Aboelnour Badran

Ahmed M Tawfik, Ahmad El-Morsy, Diagnostic and Interventional Radiology Department, Faculty of Medicine, Mansoura University, Mansoura 35112, Egypt
Mohamed Aboelnour Badran, Orthopaedic Surgery Department, Faculty of Medicine, Mansoura University, Mansoura 35112, Egypt
Author contributions: Tawfik AM, El-Morsy A and Badran MA designed the article; Tawfik AM and El-Morsy A acquired the data; Tawfik AM, El-Morsy A and Badran MA wrote the draft; Tawfik AM, El-Morsy A and Badran MA approved the final version.
Correspondence to: Ahmed M Tawfik, MD, PhD, Lecturer of Radiology and Consultant Radiologist, Diagnostic and Interventional Radiology Department, Faculty of Medicine, Mansoura University, El-Gomhoreya Street, Mansoura 35112, Egypt. ahm_m_tawfik@hotmail.com
Telephone: +20-50-2262239 Fax: +20-50-2259147
Received: December 28, 2013 Revised: April 7, 2014
Accepted: May 14, 2014
Published online: June 28, 2014

Abstract

Evaluation of rotator cuff is a common indication for magnetic resonance imaging (MRI) scanning of the shoulder. Conventional MRI is the most commonly used technique, while magnetic resonance (MR) arthrography is reserved for certain cases. Rotator cuff disorders are thought to be caused by a combination of internal and external mechanisms. A well-structured MRI report should comment on the relevant anatomic structures including the acromial type and orientation, the presence of os acromiale, acromio-clavicular degenerative spurs and fluid in the subacromial subdeltoid bursa. In addition, specific injuries of the rotator cuff tendons and the condition of the long head of biceps should be accurately reported. The size and extent of tendon tears, tendon retraction and fatty degeneration or atrophy of the muscles are all essential components of a surgically relevant MRI report.

© 2014 Baishideng Publishing Group Inc. All rights reserved.

Key words: Magnetic resonance imaging; Rotator cuff tendons; Tendon tear; Review; Shoulder

Core tip: This review discusses the relevant anatomy of rotator cuff, mechanisms of rotator cuff injury, techniques of magnetic resonance imaging (MRI) used as well as all relevant MRI findings in an easy and ordered manner with illustrative figures and examples.

Tawfik AM, El-Morsy A, Badran MA. Rotator cuff disorders: How to write a surgically relevant magnetic resonance imaging report? *World J Radiol* 2014; 6(6): 274-283 Available from: URL: http://www.wjgnet.com/1949-8470/full/v6/i6/274.htm
DOI: http://dx.doi.org/10.4329/wjr.v6.i6.274

INTRODUCTION

Rotator cuff disorders are common in the middle and old age population. They are a major cause of chronic shoulder pain. In addition, rotator cuff disorders result in loss of strength and stability of the shoulder[1,2].

The balanced combination between accurate clinical examination, clear view of the patient's needs and disabilities and precise radiological diagnostic modalities is invaluable in the correct formulation of the treatment plan of the patient whether surgically or conservatively. Magnetic resonance imaging (MRI), which is considered by many authors the modality of choice for diagnosing rotator cuff disorders[3,4], has a very important role in achieving this balance.

In this article, we discuss the techniques of MRI of the shoulder; the relevant rotator cuff anatomy, mechanisms of injury, and the specific imaging findings of rotator cuff disorders that are important for formulating a well-structured and complete MRI report.

MRI TECHNIQUE

MR imaging of the shoulder for evaluation of rotator cuff disorders may be carried out either conventionally (non-arthrographic), or with direct contrast distension of the joint (MR arthrography). Magnetic resonance arthrography was reported to be the most accurate imaging technique for diagnosis of both partial and full-thickness rotator cuff tears[5,6], but is limited by invasiveness and necessity of fluoroscopic guidance for injection, and therefore not routinely used for rotator cuff disorders[7,8]. An alternative technique, indirect MR arthrography, is a non-invasive technique using intravenous rather than intra-articular contrast to provide the arthrographic effect[9,10]. Continuous advances in MRI field strength, gradients, and coil technology have allowed even more accuracy for conventional MRI than that reported in the early literature, and conventional MRI is still the most commonly used technique for diagnosis of rotator cuff tears[3,11,12].

MR imaging is typically performed in the supine position with the arm by the side of the patient, in the neutral position. Images must be obtained in axial, coronal oblique and sagittal oblique planes[13]. The sequences used may vary but typically include T1-, proton density- and T2-weighted sequences and it is recommended to have both fat-suppressed and non-fat-suppressed sequences. Additional imaging in the abduction external rotation (ABER) position of the shoulder was reported to improve sensitivity and increase diagnostic confidence for partial-thickness tears of the supraspinatus tendon[10,14]. However, this technique is not widely spread due to difficult positioning and prolonged scan time.

ROTATOR CUFF ANATOMY

The rotator cuff consists of four muscles; the supraspinatus, infraspinatus, subscapularis and teres minor muscles. The supraspinatus muscle originates from the supraspinous fossa of the scapula and passes on the superior aspect of the humeral head to be inserted in the greater tuberosity. The infraspinatus muscle originates from the infraspinous fossa and shares a common tendinous insertion with the supraspinatus tendon on the greater tuberosity; together with the tendon of teres minor muscle[15]. On the other hand, the subscapularis muscle originates from the subscapular fossa of the scapula and its wide tendon inserts in the lesser tuberosity, separated from the insertion of the other rotator muscles by the rotator interval.

The long head of biceps tendon is anatomically and functionally related to the rotator cuff. The tendon arises from the supraglenoid tubercle and its proximal segment (2-3 cm) is intra-articular. It exits the gleno-humeral joint and passes through the rotator interval between the subscapularis and supraspinatus tendons into the bicipital (intertubercular) groove of the proximal humerus[16].

MECHANISMS OF ROTATOR CUFF INJURY

The exact pathophysiology of rotator cuff injury, after exclusion of acute trauma, is still not fully understood. The current understanding is that rotator cuff degeneration is caused by a multifactorial pathogenesis, including both internal and external mechanisms[17,18].

Internal mechanisms

Those are mechanisms that originate from within the tendons in the form of degenerative processes, possibly age-related, that result in alterations in the tendon biology, morphology, vascularity and mechanical properties[18,19].

External mechanisms

External mechanisms include the well-known impingement syndromes, of which the subacromial impingement is the commonest. Subacromial impingement is defined as entrapment of the subacromial subdeltoid bursa and the supraspinatus tendon between the coraco-acromial arch and the greater tuberosity of the humerus. The main causes of this type of impingement include abnormal acromion configuration[20], osteoarthritis of the acromioclavicular (AC) joint and narrowed subacromial space[21].

Another type of impingement syndromes is subcoracoid impingement; defined as entrapment of the subscapularis tendon in the coracohumeral interval (the space between the coracoid process and the anterior humerus). It is usually caused by abnormal coracoid configuration that may be congenital, traumatic or iatrogenic[17,21].

Less common types of impingement include secondary external impingement due to glenohumeral instability in the absence of outlet stenosis of the rotator cuff tendons[22], as well as internal impingement (intra-articular) due to compression of the articular surface of the tendons between the humeral head and glenoid[23].

MRI FINDINGS

Acromion type

The acromion was classified according to its shape into three types (Figure 1). Type I has a flat under surface, type Ⅱ a concave under surface and type three a concave under surface with anterior hook. Some authors added a further type Ⅳ to the original classification describing a convex under surface[24,25]. The shape of acromion is best depicted on sagittal oblique MR images lateral to the AC joint plane. The most common type is type Ⅱ, while type Ⅲ is the one most commonly associated with rotator cuff tears where its anterior hook causes injury of the anterior fibres of the supraspinatus tendon[26].

Acromion orientation

Normally, the acromion has no slope either anteriorly,

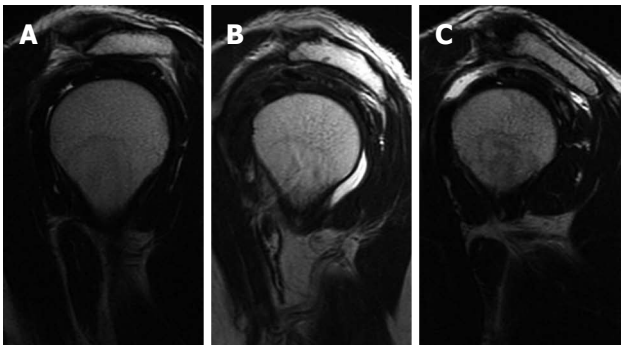

Figure 1 Acromion types. Sagittal oblique T2-weighted images of different patients showing type Ⅰ flat acromion (A), type Ⅱ concave under surface (B) and type Ⅲ concave under surface with anterior hook (C).

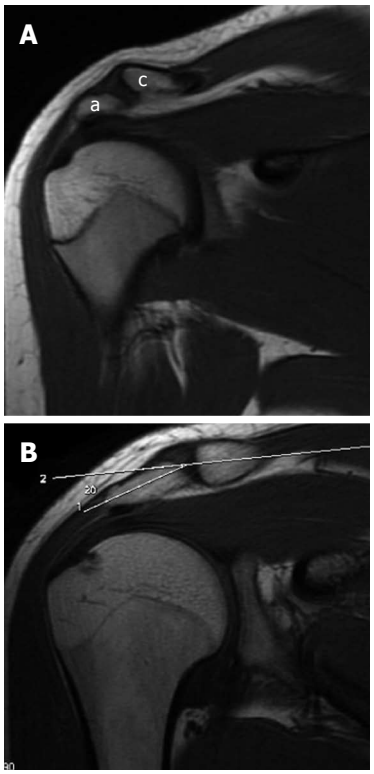

Figure 2 Acromion orientation. A: Coronal oblique T1-weighted image shows low lying acromion (a) in relation to the clavicle (c) at the Acromio-clavicular joint level; B: Coronal oblique T1-weighted image in another patient shows infero-lateral slope of the acromion. The angle between the acromion and the clavicle is tilted by 20 degrees.

laterally or inferiorly. A lateral or anterior down-sloping acromion and a low-lying acromion are thought to play a role in the development of subacromial impingement[21].

A low-lying acromion is diagnosed when the lower acromial surface is below the lower surface of the clavicle at the AC joint level on the anterior coronal oblique MR image (Figure 2A). On the same image showing the AC joint, an infero-lateral slope is detected by measuring the angle between the acromion axis and the clavicle (Figure 2B); an angle more than 10 degrees is abnormal[27]. An anterior slope is diagnosed on sagittal oblique images when the anterior part of the acromion is closer to the

Figure 3 Os acromiale. Axial T1-weighted image showing the os acromiale.

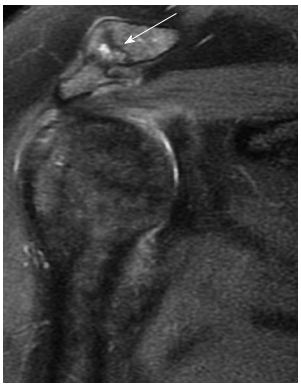

Figure 4 Acromio-clavicular joint osteoarthritis. Coronal oblique fat-sat proton-density-weighted image shows degenerative changes of the acromio-clavicular joint (arrow) in a patient with rotator cuff tear.

related part of the humeral convexity than its posterior part.

Os acromiale

The acromion is formed from multiple ossification centres with complete fusion between the ages of 22 and 25 years. If one of the ossification centres fails to fuse, an accessory ossicle is formed; the os acromiale[28]. The os acromiale is mobile and is thought to contribute to impingement, but the reported incidence in normal population is between 1% and 15%[28]. It is best assessed in the upper axial images (Figure 3) where a low signal space is detected between the high signal marrow of the distal acromion and the non-fused ossicle[25]. On coronal oblique images it can be suspected by the presence of the so called "double AC joint"; the normal AC joint appears on the anterior image and the pseudo-articulation of the os acromiale appears on the posterior one[27].

AC joint

Osteoarthritis of the AC joint (Figure 4) is a common finding in patients with rotator cuff disorders. However, its role in impingement remains unclear and could either be a risk factor for impingement or a result of rotator cuff injury and disturbed shoulder biomechanics. A large osteophyte arising from the inferior surface of

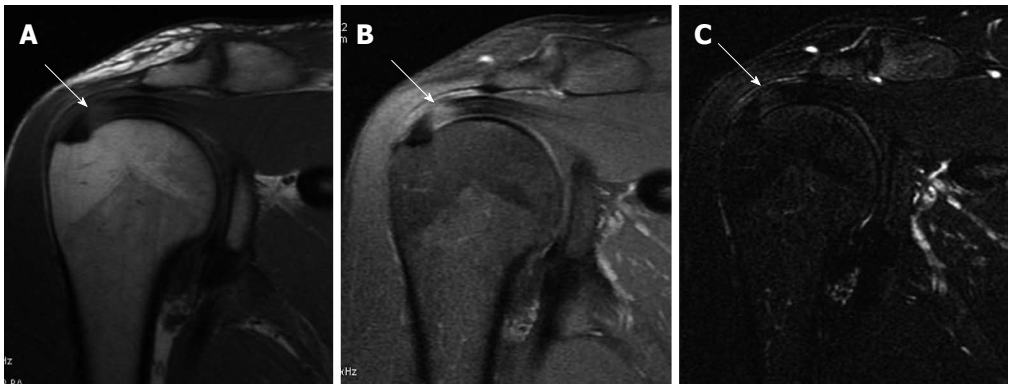

Figure 5 Supraspinatus tendinosis. A: Coronal oblique T1-weighted image. B: Coronal oblique fat-sat proton-density image. Images (A) and (B) show focal high signal intensity within the distal supraspinatus tendon (arrow); C: Coronal oblique fat-sat T2-weighted image shows focal high signal at the same site within supraspinatus tendon (arrow). Final diagnosis was tendinosis.

Figure 6 Partial interstitial supraspinatus tendon tear. Coronal oblique fat-sat proton-density-weighted image showing focal high signal within the supraspinatus tendon fibres (arrow). Also note the associated high signal intensity fluid in the subacromial subdeltoid bursa.

the joint is thought to be a cause of tendon tear[29]. MRI is more sensitive than radiography for detection of AC joint degenerative disease. MRI can differentiate joint enlargement due to capsular hypertrophy (intermediate signal intensity) form joint effusion (bright signal on T2-weighted images). Osteophytes appear in late stages of the disease[30].

Subacromial subdeltoid bursa

The subacromial subdeltoid bursa is a synovial lined structure between the acromion and deltoid muscle externally and the rotator cuff tendons internally. The subacromial and subdeltoid components are connected in 95% of individuals. Normally it is not connected with the joint space but communication occurs in association with full thickness supraspinatus tears[31,32].

The normal bursa usually does not exceed 2 mm in thickness and is usually located posteriorly. On coronal MRI, features suggesting abnormal amount of fluid include thickness of fluid signal more than 3 mm, fluid signal medial to the level of the AC joint, and fluid in the anterior part of the bursa[33].

Rotator cuff tendons and specific injuries

Tendinitis and tendinosis: Tendinitis and tendinosis typically appear as focal areas of increased signal intensity on proton density weighted images, that is less than that of fluid on T2-weighted images (Figure 5). Chronic forms are associated with thickening (tendinosis)[34].

Partial thickness tear: A partial thickness tear appears on fat-suppressed T2-weighted MR images as fluid signal intensity with thinning, or an incomplete gap, in the tendon[3]. The supraspinatus tendon is usually about 12 mm in average cranio-caudal thickness. Partial thickness tears are classified according to their depth into either grade Ⅰ, in which less than one fourth of the fibres is torn; grade Ⅱ, when more than one fourth and less than half of the tendon thickness is torn and grade Ⅲ, when more than half of the tendon thickness is torn[24,35].

According to the tear site, partial thickness tears of the supraspinatus tendon are classified into bursal; articular surface or intra-tendinous tears (Figure 6). Articular surface tears are more common[35].

Full thickness tear: A full-thickness tendon tear appears as a focal, well-defined area of increased signal intensity on both T1- and T2-weighted images (Figure 7), that traverses the whole thickness of the tendon from the bursal to the articular surface[7,36].

Full-thickness tendon tears are classified according to the tear dimensions as small (less than 1 cm), medium (between 1 and 3 cm), large (between 3 and 5 cm) or massive (exceeding 5 cm)[24]. The dimensions are measured on coronal and sagittal T2 fat-suppressed images[37].

The degree of retraction of the torn supraspinatus tendon is typically assessed on coronal oblique images. When the tendon stump is still close to the insertion site, it is classified as stage 1. A stump retracted to the level of the humeral head is classified as stage 2, while stage 3 denotes retraction of the stump to the level of the glenoid[38,39].

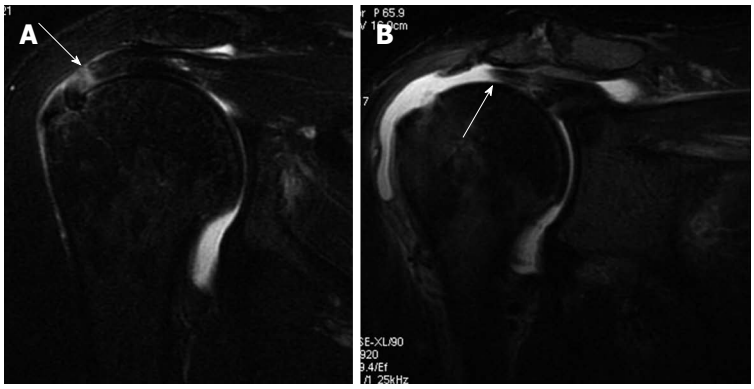

Figure 7 Full-thickness supraspinatus tendon tears in two different patients. A: Coronal oblique fat-sat T2-weighted image shows full-thickness supraspinatus tendon tear without significant tendinous retraction (arrow); B: Coronal oblique fat-sat T2-weighted image in another patient shows torn retracted supraspinatus tendon (arrow).

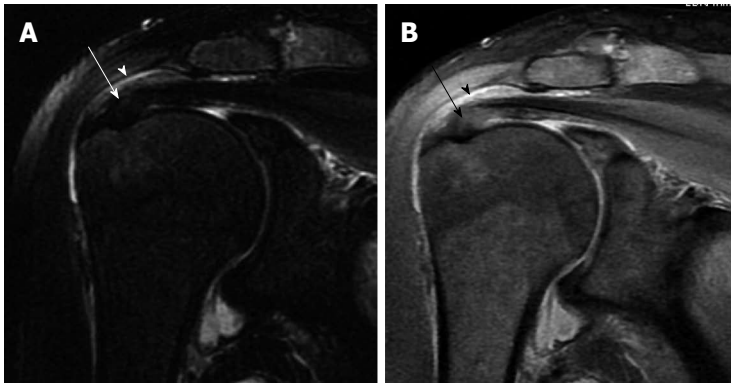

Figure 8 Subacromial impingement. A: Coronal oblique fat-sat T2-weighted image; B: Coronal oblique fat-sat proton-density-weighted image. Both images show findings associated with subacromial impingement in the form of osteoarthritis of the acromio-clavicular joint, distended subacromial subdeltoid bursa by fluid signal (arrowhead) and focal thickening of the distal supraspinatus tendon with partial irregularity of the bursal surface reported as partial tear (arrow).

Figure 9 Magic angle artifact. A: Coronal oblique T1-weighted image. B: Coronal oblique fat-sat proton-density image. Images (A) and (B) show focal high signal intensity within the distal supraspinatus tendon (arrow); C: Coronal oblique fat-sat T2-weighted image shows normal signal of the supraspinatus tendon (arrow). Final diagnosis was magic angle artifact with normal tendon.

Supraspinatus tendon: The most common site for rotator cuff tears is the supraspinatus tendon, especially at its distal part 1 to 2 cm from its insertion, the so called "critical zone", where the vascularity is low and the effect of subacromial space narrowing or subacromial impingement is maximized (Figure 8)[26].

The supraspinatus tendon is best evaluated on the coronal oblique images. A potential pitfall is the magic angle artefact (Figure 9); that may occur whenever parallel collagen fibres are oriented at 55 degrees relative to the magnetic field. This effect is common at the distal end of the supraspinatus tendon and appears as high signal mimicking tendinitis or partial tear on short time of echo (TE) MR sequences. However, the high signal intensity

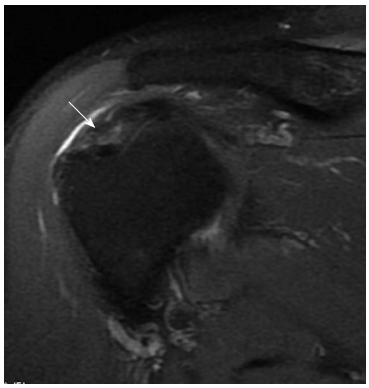

Figure 10 Infraspinatus tendinosis. Posterior coronal oblique fat-sat proton-density-weighted image showing focal thickening of the infraspinatus tendon fibres with abnormal high signal diagnosed as tendinosis (arrow). Also note fluid signal within the subacromial subdeltoid bursa.

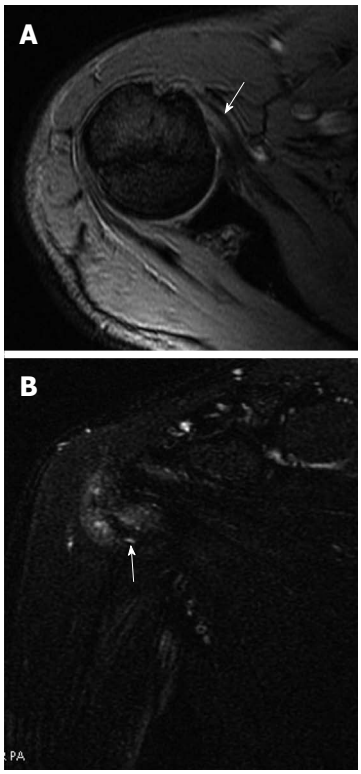

Figure 11 Subscapularis tendinosis. A: Axial gradient-recalled echo image showing focal high signal within the subscapularis tendon with fibres thickening (arrow); B: Anterior coronal oblique fat-sat T2-weighted image of the same patient showing high signal within the lower fibres of the subscapularis tendon (arrow).

disappears on using long TE sequences; for example T2 fat-suppressed sequence[25].

Infraspinatus tendon: The infraspinatus tendon is most commonly torn as an extension from supraspinatus tear (postero-superior cuff tear)[39]. The infraspinatus tendon is best evaluated on posterior coronal oblique fat-suppressed T2-weighted or STIR images (Figure 10). A second look may also be carried out on the upper axial images as well as on sagittal images[13].

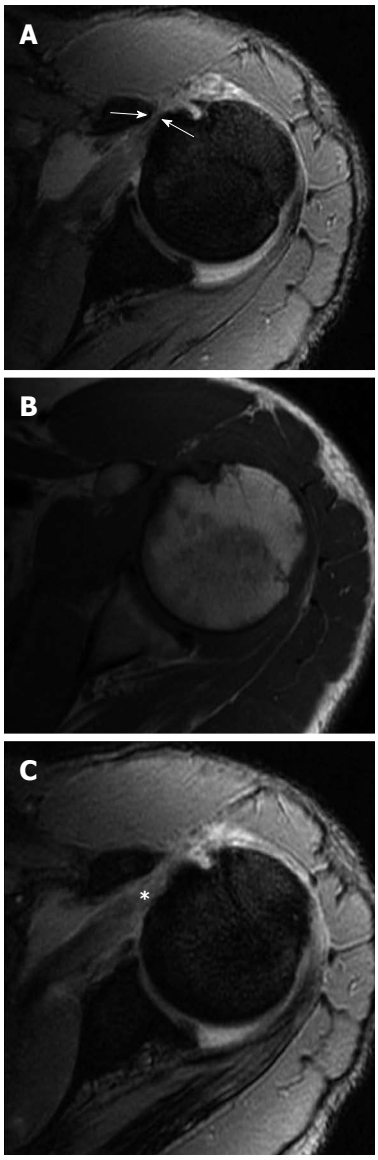

Figure 12 Sub-coracoid impingement. A and C: Axial gradient-recalled echo images; B: Axial T1-weighted image showing narrowed coraco-humeral distance (arrows in A) with tapered coracoid process, thickening and abnormal high signal of the subscapularis tendon (asterisk in C).

Subscapularis tendon: Subscapularis tendon tears may occur as a component of massive rotator cuff tears[40,41]. The tendinous part of the subscapularis tendon is the broadest tendon among the rotator cuff and therefore commonly affected by tears and tendinitis (Figure 11).

The subscapularis tendon may be affected in isolation in traumatic injury[41]. Subcoracoid impingement, which is a cause of subscapularis degenerative tears (Figure 12), is suspected when the distance between the coracoid process and the lesser tuberosity of the humerus is less than 6 mm on axial MR images[21,42]. Other reported associated MRI signs include subcortical bone marrow edema of the coracoid process and lesser tuberosity of the huemrus.

Teres minor tendon: The teres minor tendon is the least injured among rotator cuff tendons[43]. The teres minor

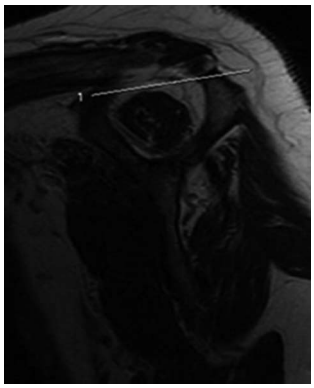

Figure 13 Supraspinatus muscle atrophy, tangent sign. Sagittal oblique T1-weighted image showing the upper border of supraspinatus muscle below the line extending between the scapular plate and spine.

tendon is best evaluated on posterior coronal oblique and axial MR images and to less extent on sagittal images.

Muscle atrophy and fatty degeneration

Atrophy of the supraspinatus muscle could be assessed by calculating the occupation ratio of the supraspinatus fossa. On the most lateral oblique sagittal image, atrophy of the supraspinatus muscle is diagnosed if the supraspinatus muscle occupies less than half the area of the fossa[44,45].

The tangent sign (Figure 13) describes an additional straight line drawn from the top of the coracoid process to the top of the spine of the scapula on the same oblique sagittal image as above. Atrophy is diagnosed when the superior border of the muscle lies below the tangent line[24,45,46].

Fatty degeneration of the supraspinatus muscles could be assessed on the T1-weighted oblique sagittal image in which the spine and body of the scapula appear. Fatty degeneration could be classified as either low (grade 0; no fat or grade 1; some fatty streaks) or moderate (grade 2; muscle > fat) or advanced (grade 3; muscle = fat and grade 4; muscle < fat)[47-49].

Long head biceps tendon

MR evaluation of the intra-articular segment of the long head biceps tendon (LHBT) is best carried out on both oblique sagittal and oblique coronal images, while the extra-articular segment is best evaluated on axial images. The LHBT tendon is covered with a synovial sheath connected with the joint space along its course within the bicipital grove[30,50]. Therefore, fluid signal around the tendon may be seen in cases of joint effusion, nevertheless in proportionate amount, and should not be mistaken for tenosynovitis. Tenosynovitis of the LHBT is diagnosed if fluid is detected around the tendon only or if the amount of fluid around the tendon is clearly out of proportion to that in the glenohumeral joint[51]. Tendinosis of the LHBT is suspected when focal thickening and high signal (but less than that of fluid) of the tendon

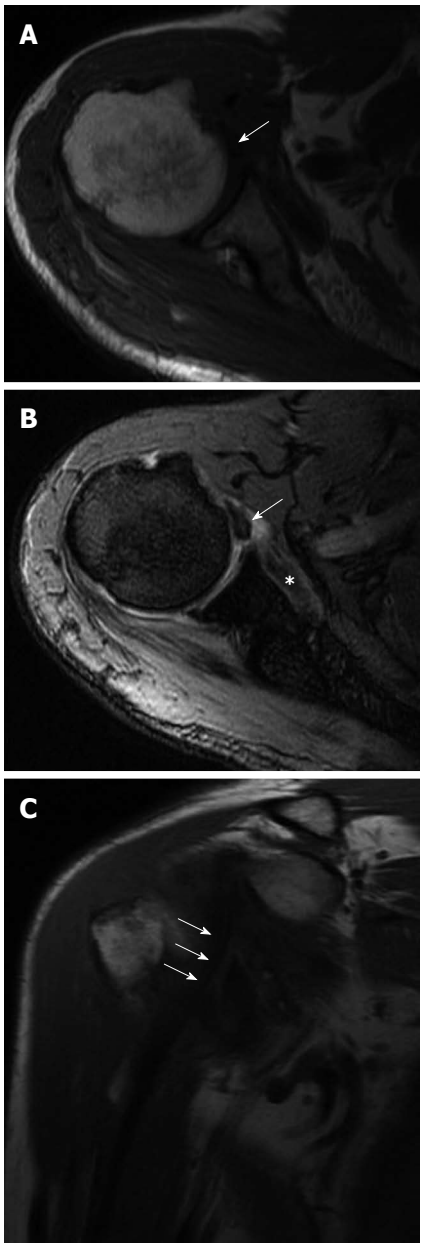

Figure 14 Subscapularis tendon avulsion with long head of biceps tendon dislocation. A: Axial T1-weighed image; B: Axial gradient-recalled echo image; C: Coronal oblique T1-weighted images showing avulsion of the subscapularis tendon (asterisk in B) with muscular atrophy and long head biceps tendon dislocation (arrows) with diffuse tendinous thickening and high signal.

or part of it is noted, usually associated with fluid signal within the synovial covering[52]. The most commonly affected part is the supra-humeral portion or the horizontal part and it may be a result of impingement. Tears of the LHBT vary from partial to complete tear to tendon avulsion. Tears appear as focal areas of high signal intensity, similar to that of fluid on T2-weighted images. Avulsion is diagnosed by noting the absence of the intra-articular segment of the tendon with no signs of dislocation. A dislocated LHBT (Figure 14) is often medially displaced, and is commonly associated with subscapularis tendon tear[50-52].

Figure 15 Calcific tendinopathy. Coronal oblique fat-sat proton-density-weighted image showings focal area of signal void (calcifications) within the distal supraspinatus tendon fibres (arrows). Diagnosis was confirmed by ultrasonography.

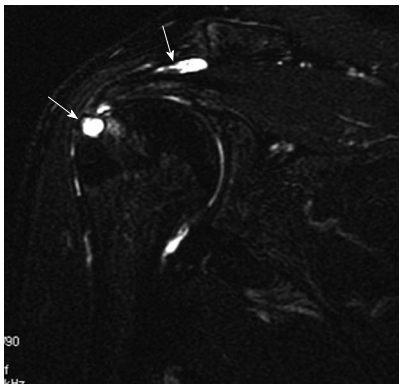

Figure 16 Bony degenerative changes. Coronal oblique fat-sat T2-weighted image showing focal fluid-like high signal within the distal supraspinatus tendon fibres reported as partial capsular surface tear with subcortical cystic erosion of the greater tuberosity at the rotor cuff insertion (thin arrow). Also note fluid signal within the subacromial subdeltoid bursa reported as bursitis (thick arrow).

Other findings

Bony changes: Erosions and degenerative changes of the lateral aspect of the greater tuberosity of the humerus (Figure 15) are common associated findings in rotator cuff disorders[30]. This finding is important for surgical planning as it significantly decreases the hold of anchors used during repair of torn rotator cuff tendons.

Calcific tendinopathy: Calcific tendinopathy most commonly affects the supraspinatus tendon, less commonly the infraspinatus and other tendons. On MRI, calcifications typically appear as focal areas of signal void on all spin echo sequences (Figure 16), and is usually difficult to detect within the natively low signal tendon[7,53]. The area of signal void increases on gradient-recalled echo sequence due to susceptibility effects[30].

CONCLUSION

Evaluation of rotator cuff disorders is one of the commonest indications for magnetic resonance (MR) imaging of the shoulder. Complete and accurate interpretation of MR images is essential to provide the treating clinician with adequate information for choosing the best therapy and avoiding unnecessary interventions. Radiologists should be familiar with the technique of MRI of the shoulder, the anatomy of the rotator cuff and the mechanisms of rotator cuff injury. A well-structured MRI report should include full comment on the rotator cuff tendons and all other relevant structures.

REFERENCES

1 **Meislin RJ**, Sperling JW, Stitik TP. Persistent shoulder pain: epidemiology, pathophysiology, and diagnosis. *Am J Orthop (Belle Mead NJ)* 2005; **34**: 5-9 [PMID: 16450690]

2 **Burbank KM**, Stevenson JH, Czarnecki GR, Dorfman J. Chronic shoulder pain: part I. Evaluation and diagnosis. *Am Fam Physician* 2008; **77**: 453-460 [PMID: 18326164]

3 **Magee T**, Williams D. 3.0-T MRI of the supraspinatus tendon. *AJR Am J Roentgenol* 2006; **187**: 881-886 [PMID: 16985129 DOI: 10.2214/AJR.05.1047]

4 **Tuite MJ**. Magnetic resonance imaging of rotator cuff disease and external impingement. *Magn Reson Imaging Clin N Am* 2012; **20**: 187-200, ix [PMID: 22469399 DOI: 10.1016/j.mric.2012.01.011]

5 **Waldt S**, Bruegel M, Mueller D, Holzapfel K, Imhoff AB, Rummeny EJ, Woertler K. Rotator cuff tears: assessment with MR arthrography in 275 patients with arthroscopic correlation. *Eur Radiol* 2007; **17**: 491-498 [PMID: 16969638 DOI: 10.1007/s00330-006-0370-7]

6 **de Jesus JO**, Parker L, Frangos AJ, Nazarian LN. Accuracy of MRI, MR arthrography, and ultrasound in the diagnosis of rotator cuff tears: a meta-analysis. *AJR Am J Roentgenol* 2009; **192**: 1701-1707 [PMID: 19457838 DOI: 10.2214/AJR.08.1241]

7 **Teh J**. Imaging of shoulder pathology. *Orthopaedics and Trauma* 2011; **25**: 19-29 [DOI: 10.1016/j.mporth.2010.03.008]

8 **Jana M**, Gamanagatti S. Magnetic resonance imaging in glenohumeral instability. *World J Radiol* 2011; **3**: 224-232 [PMID: 22007285 DOI: 10.4329/wjr.v3.i9.224]

9 **Yagci B**, Manisali M, Yilmaz E, Ozkan M, Ekin A, Ozaksoy D, Kovanlikaya I. Indirect MR arthrography of the shoulder in detection of rotator cuff ruptures. *Eur Radiol* 2001; **11**: 258-262 [PMID: 11218024 DOI: 10.1007/s003300000546]

10 **Herold T**, Bachthaler M, Hamer OW, Hente R, Feuerbach S, Fellner C, Strotzer M, Lenhart M, Paetzel C. Indirect MR arthrography of the shoulder: use of abduction and external rotation to detect full- and partial-thickness tears of the supraspinatus tendon. *Radiology* 2006; **240**: 152-160 [PMID: 16709790 DOI: 10.1148/radiol.2393050453]

11 **Dinnes J**, Loveman E, McIntyre L, Waugh N. The effectiveness of diagnostic tests for the assessment of shoulder pain due to soft tissue disorders: a systematic review. *Health Technol Assess* 2003; **7**: iii, 1-166 [PMID: 14567906]

12 **Foad A**, Wijdicks CA. The accuracy of magnetic resonance imaging and magnetic resonance arthrogram versus arthroscopy in the diagnosis of subscapularis tendon injury. *Arthroscopy* 2012; **28**: 636-641 [PMID: 22281195 DOI: 10.1016/j.arthro.2011]

13 **Farshad-Amacker NA**, Jain Palrecha S, Farshad M. The primer for sports medicine professionals on imaging: the shoulder. *Sports Health* 2013; **5**: 50-77 [PMID: 24381700 DOI: 10.1177/1941738112468265]

14 **Schreinemachers SA**, van der Hulst VP, Willems WJ, Bipat S, van der Woude HJ. Detection of partial-thickness supraspinatus tendon tears: is a single direct MR arthrography series in ABER position as accurate as conventional MR arthrography? *Skeletal Radiol* 2009; **38**: 967-975 [PMID: 19294377 DOI:

10.1007/s00256-009-0680-3]
15 **Mochizuki T**, Sugaya H, Uomizu M, Maeda K, Matsuki K, Sekiya I, Muneta T, Akita K. Humeral insertion of the supraspinatus and infraspinatus. New anatomical findings regarding the footprint of the rotator cuff. *J Bone Joint Surg Am* 2008; **90**: 962-969 [PMID: 18451386 DOI: 10.2106/JBJS.G.00427]
16 **Denard PJ**, Dai X, Hanypsiak BT, Burkhart SS. Anatomy of the biceps tendon: implications for restoring physiological length-tension relation during biceps tenodesis with interference screw fixation. *Arthroscopy* 2012; **28**: 1352-1358 [PMID: 22925883 DOI: 10.1016/j.arthro.2012.04.143]
17 **Seagger RM**, Wallace AL. Degenerative rotator cuff disease and impingement. *Orthopaedics and Trauma* 2011; **25**: 1-10 [DOI: 10.1016/j.mporth.2010.08.005]
18 **Seitz AL**, McClure PW, Finucane S, Boardman ND, Michener LA. Mechanisms of rotator cuff tendinopathy: intrinsic, extrinsic, or both? *Clin Biomech (Bristol, Avon)* 2011; **26**: 1-12 [PMID: 20846766 DOI: 10.1016/j.clinbiomech.2010.08.001]
19 **Via AG**, De Cupis M, Spoliti M, Oliva F. Clinical and biological aspects of rotator cuff tears. *Muscles Ligaments Tendons J* 2013; **3**: 70-79 [PMID: 23888289 DOI: 10.11138/mltj/2013.3.2.070]
20 **Balke M**, Schmidt C, Dedy N, Banerjee M, Bouillon B, Liem D. Correlation of acromial morphology with impingement syndrome and rotator cuff tears. *Acta Orthop* 2013; **84**: 178-183 [PMID: 23409811 DOI: 10.3109/17453674.2013.773413]
21 **Mulyadi E**, Harish S, O'Neill J, Rebello R. MRI of impingement syndromes of the shoulder. *Clin Radiol* 2009; **64**: 307-318 [PMID: 19185661 DOI: 10.1016/j.crad.2008.08.013]
22 **Cowderoy GA**, Lisle DA, O'Connell PT. Overuse and impingement syndromes of the shoulder in the athlete. *Magn Reson Imaging Clin N Am* 2009; **17**: 577-93, v [PMID: 19887291 DOI: 10.1016/j.mric.2009.06.003]
23 **Giaroli EL**, Major NM, Higgins LD. MRI of internal impingement of the shoulder. *AJR Am J Roentgenol* 2005; **185**: 925-929 [PMID: 16177410]
24 **Morag Y**, Jacobson JA, Miller B, De Maeseneer M, Girish G, Jamadar D. MR imaging of rotator cuff injury: what the clinician needs to know. *Radiographics* 2006; **26**: 1045-1065 [PMID: 16844931 DOI: 10.1148/rg.264055087]
25 **Fitzpatrick D**, Walz DM. Shoulder MR imaging normal variants and imaging artifacts. *Magn Reson Imaging Clin N Am* 2010; **18**: 615-632 [PMID: 21111969 DOI: 10.1016/j.mric.2010.07.006]
26 **Khan Y**, Nagy MT, Malal J, Waseem M. The painful shoulder: shoulder impingement syndrome. *Open Orthop J* 2013; **7**: 347-351 [PMID: 24082973 DOI: 10.2174/1874325001307010347]
27 **Stabler A**. Impingement and Rotator Cuff Disease. In: Davies AM, Hodler J, editors. Imaging of the Shoulder: Techniques and Applications. 1st ed. Berlin Heidelberg: Springer-Verlag, 2004: 121-159
28 **Boehm TD**, Rolf O, Martetschlaeger F, Kenn W, Gohlke F. Rotator cuff tears associated with os acromiale. *Acta Orthop* 2005; **76**: 241-244 [PMID: 16097551 DOI: 10.1080/00016470510030643]
29 **Roidis NT**, Motamed S, Vaishnav S, Ebramzadeh E, Karachalios TS, Itamura JM. The influence of the acromioclavicular joint degeneration on supraspinatus outlet impingement and the acromion shape. *J Orthop Surg (Hong Kong)* 2009; **17**: 331-334 [PMID: 20065375]
30 **Vahlensieck M**. MRI of the shoulder. *Eur Radiol* 2000; **10**: 242-249 [PMID: 10663753 DOI: 10.1007/s003300050040]
31 **van Holsbeeck M**, Strouse PJ. Sonography of the shoulder: evaluation of the subacromial-subdeltoid bursa. *AJR Am J Roentgenol* 1993; **160**: 561-564 [PMID: 8430553 DOI: 10.2214/ajr.160.3.8430553]
32 **Precerutti M**, Garioni E, Madonia L, Draghi F. US anatomy of the shoulder: Pictorial essay. *J Ultrasound* 2010; **13**: 179-187 [PMID: 23396832 DOI: 10.1016/j.jus.2010.10.005]
33 **White EA**, Schweitzer ME, Haims AH. Range of normal and abnormal subacromial/subdeltoid bursa fluid. *J Comput Assist Tomogr* 2006; **30**: 316-320 [PMID: 16628056 DOI: 10.1097/00004728-200603000-00030]
34 **Sein ML**, Walton J, Linklater J, Harris C, Dugal T, Appleyard R, Kirkbride B, Kuah D, Murrell GA. Reliability of MRI assessment of supraspinatus tendinopathy. *Br J Sports Med* 2007; **41**: e9 [PMID: 17289860 DOI: 10.1136/bjsm.2006.034421]
35 **Finnan RP**, Crosby LA. Partial-thickness rotator cuff tears. *J Shoulder Elbow Surg* 2010; **19**: 609-616 [PMID: 20171904 DOI: 10.1016/j.jse.2009.10.017]
36 **Reinus WR**, Shady KL, Mirowitz SA, Totty WG. MR diagnosis of rotator cuff tears of the shoulder: value of using T2-weighted fat-saturated images. *AJR Am J Roentgenol* 1995; **164**: 1451-1455 [PMID: 7754891 DOI: 10.2214/ajr.164.6.7754891]
37 **Dwyer T**, Razmjou H, Henry P, Gosselin-Fournier S, Holtby R. Association between pre-operative magnetic resonance imaging and reparability of large and massive rotator cuff tears. *Knee Surg Sports Traumatol Arthrosc* 2013; Epub ahead of print [PMID: 24170190 DOI: 10.1007/s00167-013-2745-z]
38 **Patte D**. Classification of rotator cuff lesions. *Clin Orthop Relat Res* 1990; (**254**): 81-86 [PMID: 2323151]
39 **Cooper A**, Ali A. Rotator cuff tears. *Surgery* 2013; **31**: 168-171 [DOI: 10.1016/j.mpsur.2013.01.017]
40 **Bergin D**, Parker L, Zoga A, Morrison W. Abnormalities on MRI of the subscapularis tendon in the presence of a full-thickness supraspinatus tendon tear. *AJR Am J Roentgenol* 2006; **186**: 454-459 [PMID: 16423952]
41 **Lyons RP**, Green A. Subscapularis tendon tears. *J Am Acad Orthop Surg* 2005; **13**: 353-363 [PMID: 16148361]
42 **Richards DP**, Burkhart SS, Campbell SE. Relation between narrowed coracohumeral distance and subscapularis tears. *Arthroscopy* 2005; **21**: 1223-1228 [PMID: 16226651 DOI: 10.1016/j.arthro.2005.06.015]
43 **Melis B**, DeFranco MJ, Lädermann A, Barthelemy R, Walch G. The teres minor muscle in rotator cuff tendon tears. *Skeletal Radiol* 2011; **40**: 1335-1344 [PMID: 21604212 DOI: 10.1007/s00256-011-1178-3]
44 **Thomazeau H**, Rolland Y, Lucas C, Duval JM, Langlais F. Atrophy of the supraspinatus belly. Assessment by MRI in 55 patients with rotator cuff pathology. *Acta Orthop Scand* 1996; **67**: 264-268 [PMID: 8686465 DOI: 10.3109/17453679608994685]
45 **Moosmayer S**, Tariq R, Stiris MG, Smith HJ. MRI of symptomatic and asymptomatic full-thickness rotator cuff tears. A comparison of findings in 100 subjects. *Acta Orthop* 2010; **81**: 361-366 [PMID: 20450423 DOI: 10.3109/17453674.2010.483993]
46 **Zanetti M**, Gerber C, Hodler J. Quantitative assessment of the muscles of the rotator cuff with magnetic resonance imaging. *Invest Radiol* 1998; **33**: 163-170 [PMID: 9525755 DOI: 10.1097/00004424-199803000-00006]
47 **Goutallier D**, Postel JM, Bernageau J, Lavau L, Voisin MC. Fatty muscle degeneration in cuff ruptures. Pre- and postoperative evaluation by CT scan. *Clin Orthop Relat Res* 1994; (**304**): 78-83 [PMID: 8020238]
48 **Fuchs B**, Weishaupt D, Zanetti M, Hodler J, Gerber C. Fatty degeneration of the muscles of the rotator cuff: assessment by computed tomography versus magnetic resonance imaging. *J Shoulder Elbow Surg* 1999; **8**: 599-605 [PMID: 10633896 DOI: 10.1016/S1058-2746(99)90097-6]
49 **Oh JH**, Kim SH, Choi JA, Kim Y, Oh CH. Reliability of the grading system for fatty degeneration of rotator cuff muscles. *Clin Orthop Relat Res* 2010; **468**: 1558-1564 [PMID: 19347412 DOI: 10.1007/s11999-009-0818-6]
50 **Nakata W**, Katou S, Fujita A, Nakata M, Lefor AT, Sugimoto H. Biceps pulley: normal anatomy and associated lesions at MR arthrography. *Radiographics* 2011; **31**: 791-810 [PMID: 21571657 DOI: 10.1148/rg.313105507]

51 **Beall DP**, Williamson EE, Ly JQ, Adkins MC, Emery RL, Jones TP, Rowland CM. Association of biceps tendon tears with rotator cuff abnormalities: degree of correlation with tears of the anterior and superior portions of the rotator cuff. *AJR Am J Roentgenol* 2003; **180**: 633-639 [PMID: 12591665 DOI: 10.2214/ajr.180.3.1800633]

52 **Vinson EN**, Wittstein J, Garrigues GE, Taylor DC. MRI of selected abnormalities at the anterior superior aspect of the shoulder: potential pitfalls and subtle diagnoses. *AJR Am J Roentgenol* 2012; **199**: 534-545 [PMID: 22915393 DOI: 10.2214/AJR.12.8789]

53 **Zubler C**, Mengiardi B, Schmid MR, Hodler J, Jost B, Pfirrmann CW. MR arthrography in calcific tendinitis of the shoulder: diagnostic performance and pitfalls. *Eur Radiol* 2007; **17**: 1603-1610 [PMID: 17036154 DOI: 10.1007/s00330-006-0428-6]

P- Reviewer: Iagulli ND **S- Editor**: Ji FF **L- Editor**: A
E- Editor: Zhang DN

World Journal of Radiology

Submit a Manuscript: http://www.wjgnet.com/esps/
Help Desk: http://www.wjgnet.com/esps/helpdesk.aspx
DOI: 10.4329/wjr.v6.i6.284

World J Radiol 2014 June 28; 6(6): 284-300
ISSN 1949-8470 (online)
© 2014 Baishideng Publishing Group Inc. All rights reserved.

REVIEW

A handy review of carpal tunnel syndrome: From anatomy to diagnosis and treatment

Mohammad Ghasemi-rad, Emad Nosair, Andrea Vegh, Afshin Mohammadi, Adam Akkad, Emal Lesha, Mohammad Hossein Mohammadi, Doaa Sayed, Ali Davarian, Tooraj Maleki-Miyandoab, Anwarul Hasan

Mohammad Ghasemi-rad, Andrea Vegh, Adam Akkad, Emal Lesha, Mohammad Hossein Mohammadi, Anwarul Hasan, Center for Biomedical Engineering, Department of Medicine, Brigham and Women's Hospital, Harvard Medical School, Cambridge, MA 02139, United States
Mohammad Ghasemi-rad, Adam Akkad, Anwarul Hasan, Harvard-MIT Division of Health Sciences and Technology, Massachusetts Institute of Technology, Cambridge, MA 02139, United States
Emad Nosair, Anatomical Sciences, Basic Medical Sciences Department, College of Medicine, Sharjah University, Sharjah 27272, The United Arab Emirates
Andrea Vegh, Department of Materials Science and Engineering, University of Toronto, Toronto, Ontario M5S1A4, Canada
Afshin Mohammadi, Tooraj Maleki-Miyandoab, Department of Radiology, Imam Khomainee Hospital, Urmia University of Medical Sciences, Urmia 5716763111, Iran
Emal Lesha, College of Science and Mathematics, University of Massachusetts Boston, Boston, MA 02138, United States
Mohammad Hossein Mohammadi, Department of Chemical Engineering, Sharif University of Technology, Tehran 1136511155, Iran
Doaa Sayed, Department of Clinical Dentistry, College of Dentistry, Ajman University of Science and Technology, Ajman 2441, The United Arab Emirates
Ali Davarian, Department of Biochemistry and Molecular Biophysics, Washington University School of Medicine, St. Louis, MO 63110, United States
Anwarul Hasan, Biomedical Engineering, and Department of Mechanical Engineering, American University of Beirut, Beirut 1107 2020, Lebanon
Author contributions: All authors contributed to this paper.
Correspondence to: Dr. Anwarul Hasan, Biomedical Engineering, Department of Mechanical Engineering, American University of Beirut, Beirut 1107 2020, Lebanon. mh211@aub.edu.lb
Telephone: +961-7-6597214 Fax: +961-1-744462
Received: December 18, 2013 Revised: March 28, 2014
Accepted: May 8, 2014
Published online: June 28, 2014

Abstract

Carpal tunnel syndrome (CTS) is the most commonly diagnosed disabling condition of the upper extremities. It is the most commonly known and prevalent type of peripheral entrapment neuropathy that accounts for about 90% of all entrapment neuropathies. This review aims to provide an outline of CTS by considering anatomy, pathophysiology, clinical manifestation, diagnostic modalities and management of this common condition, with an emphasis on the diagnostic imaging evaluation.

© 2014 Baishideng Publishing Group Inc. All rights reserved.

Key words: Carpal tunnel syndrome; Anatomy; Ultrasonography; Magnetic resonance imaging; Computed tomography; Ultrasonography; Diagnosis; Nerve conduction study; Treatment

Core tip: A review of the carpal tunnel syndrome (CTS) highlighting anatomy, diagnosis and eventual treatment. This paper synthesizes all the aspects necessary to properly and successfully treat CTS, unlike past reviews which have focused on simply just one or a few factors. This review contains all the necessary material to fully understand CTS.

Ghasemi-rad M, Nosair E, Vegh A, Mohammadi A, Akkad A, Lesha E, Mohammadi MH, Sayed D, Davarian A, Maleki-Miyandoab T, Hasan A. A handy review of carpal tunnel syndrome: From anatomy to diagnosis and treatment. *World J Radiol* 2014; 6(6): 284-300 Available from: URL: http://www.wjgnet.com/1949-8470/full/v6/i6/284.htm DOI: http://dx.doi.org/10.4329/wjr.v6.i6.284

INTRODUCTION

In the United States, about 2.7 million doctors' office visits/year are related to patients complaining about finger, hand or wrist symptoms[1]. The diagnosis of these symp-

toms can include various types of nerve entrapments, tendon disorders, overuse of muscles or nonspecific pain syndromes[1]. The most common type among them is carpal tunnel syndrome (CTS), which accounts for 90% of all entrapment neuropathies[2,3] and is one of the most commonly diagnosed disorders of the upper extremities[3,4]. It is expected that 1 in 5 patients who complain of symptoms of pain, numbness and a tingling sensation in the hands will be diagnosed with CTS based on clinical examination and electrophysiological testing[3]. CTS is estimated to occur in 3.8% of the general population[3,5], with an incidence rate of 276:100000 per year[6], and happens more frequently in women than in men, with a prevalence rate of 9.2% in women and 6% in men[3,7]. It is most often seen bilaterally at a peak age range of 40 to 60 years old; however, it has been seen in patients as young as twenty and as old as eighty-seven years old[3,8].

The carpal tunnel (CT) is found at the base of the palm. It is bounded partly by the eight carpal bones and partly by a tough fibrous roof called the transverse carpal ligament (TCL). The tunnel gives passage to: (1) eight digital flexor tendons (two for each of the medial four fingers); (2) flexor pollicis longus (FPL) tendon for the thumb; (3) their flexor synovial sheaths; and (4) the median nerve (MN)[1]. CT is therefore quite tightly packed and any condition that might increase the volume of the structures inside it can cause compression of the MN. This in turn might lead to ischemia of the nerve which presents as pain and paresthesia[1,8].

The American Academy of Orthopedic Surgeons (AAOS) defines CTS as "a symptomatic compression neuropathy of the median nerve at the level of the wrist"[3,9]. MN gives sensory branches to the lateral three fingers and the lateral half of the ring finger so that when it is compressed, symptoms of CTS are manifested in those fingers[3]. The palm of the hand, however, remains unaffected by CTS as it is supplied by the sensory cutaneous branch of median nerve (PCBMN). This branch arises about 6 cm proximally to the TCL, then passes superficially to the ligament so it is not affected by the pressure changes within the CT[3].

Furthermore, the most common diagnosis in patients with symptoms of pain and numbness is idiopathic CTS with a tingling sensation along the MN distribution in the hands[10]. Although this syndrome is widely recognized, its etiology remains largely unclear. Recent biomechanical, MRI and histological studies have strongly suggested the close relationship of the dysfunction of neuronal vasculature, synovial tissue and flexor tendons within the CT and the development of idiopathic CTS[11,12].

CT is the fibro-osseous pathway on the palmar aspect of the wrist which connects the anterior compartment of the distal forearm with the mid-palmar space of the hand. On its bottom, the CT is made up of the carpal bones articulating together to form a backward convex bony arch, resulting in formation on the dorsal side and concave on the palmar side, forming a tunnel-like groove called the *sulcus carpi*. This osseous groove is topped volar by the tough flexor retinaculum (FR), which arches over the carpus, thus converting the sulcus carpi into the CT.

FR can be differentiated into three continuous segments: (1) a proximal thin segment called the volar carpal ligament. It is the thickened deep antebrachial fascia of the forearm; (2) the middle tough segment is the TCL; and (3) the distal segment is formed from an aponeurosis which extends distally between the thenar and hypothenar muscles. Therefore, it is recommended to have a more extensive surgical release instead of only resection of the middle segment of the FR[13].

The width of the CT is about 20 mm at the level of the hook of hamate, which is narrower compared to its proximal (24 mm) or distal (25 mm) end[13,14] counterparts. Moreover, the narrowest sectional area of the tunnel is located 1 cm beyond the midline of the distal row of the carpal bones where its sectional area is about 1.6 cm^2[15].

In healthy individuals, the intra-CT pressure is about 3-5 mmHg when the wrist is in a neutral position[16,17]. MN blood flow was found to be impaired when the CT pressure approached or exceeded 20-30 mmHg. Common functional positions of the wrist, *e.g.*, flexion, extension or even using a computer mouse, might result in an increase of tunnel compression pressures to levels high enough to impair MN blood flow[18]. For example, placing the hand on a computer mouse increase the CT pressure to 16-21 mmHg, while using the mouse to point and click increased the CT pressure up to 28 to 33 mmHg[19]. Interestingly, CT pressure was shown to increase to 63 mmHg with 40 degrees of wrist extension and 0 degrees of metacarpophalangeal flexion[20].

The position of adjacent muscular structures is thought to play a significant role in these positional increases in CT pressure[20]. In a study of the MN in fresh human cadavers, a significant distal bulk of the flexor digitorum superficialis (FDS) muscle was found to enter the proximal aspect of the tunnel during wrist extension[21]. Similarly, the lumbrical muscles were shown to enter the distal aspect of the tunnel during metacarpophalangeal flexion. Computer modeling suggests that when the metacarpophalangeal joints are flexed to 90 degrees, the lumbrical muscles remain in the CT, even if the wrist is kept extended[22].

A thorough knowledge of the complex anatomy of the CT and its surrounding structures in addition to an emphasis on its clinical applications is essential for a better understanding of the pathophysiology of CTS, along with its symptoms and signs. Such knowledge will enable surgeons to take the most appropriate and safest approach during open or endoscopic carpal tunnel release (ECTR) surgeries by accurately identifying structures at or near the CT in order to avoid or reduce its surgical complications and ensure optimal patient outcome. It is also important to be aware of the likely possible anatomical variations that might be the cause of MN compression or may be anticipated and more readily recognized by hand surgeons. This review aims to provide an overview of CTS by considering anatomy, pathophysiology, clinical manifestation, diagnostic modalities and manage-

ment of this common condition, with an emphasis on its diagnostic imaging evaluation.

CLINICAL AND SURGICAL ANATOMY OF CT

Movements of the wrist joint have an effect on the shape and width of the CT. The width of the tunnel decreases considerably during the normal range of wrist motion and since the bony walls of the tunnel are not rigid, the carpal bones move relative to each other with every wrist movement. Both flexion and extension increase the CT pressure. The cross section of the proximal opening of the CT was found to be significantly decreased with a flexing wrist joint. This is likely due to the radial shifting of the TCL and the movement of the distal end of the capitates bone. In extreme extension, the lunate bone compresses the passage as it is pushed towards the interior of the tunnel[15].

TCL is the thick (2-4 mm) central segment of the FR. It is a strong fibrous band formed from interwoven bundles of fibrous connective tissues[13] and is short and broad (average width is 25 mm and length is 31 mm)[23,24]. It extends from the distal part of the radius to the distal segment of the base of the third metacarpal. The mean proximal limit of its central portion is 11 mm distal to the capitate-lunate joint and the mean distal limit of its distal portion is 10 mm distal to the carpometacarpal joint of the third metacarpal[13].

Regarding laminar configuration of the TCL, four basic laminae were identified: (1) strong distal transverse; (2) proximal transverse; (3) ulnar oblique; and (4) radial oblique. The most common pattern showed predominance of the distal transverse and the ulnar oblique laminae in every layer of the FCL. In half of the dissected hand samples, the distal transverse and ulnar oblique laminae dominated in the superficial layer, while the proximal transverse and the radial oblique laminae dominated in the deep layer. So, the strong distal transverse lamina is likely to be excised during the final step of ECTR because of its superficial localization. This could be a major cause for the frequent occurrence of incomplete release. Moreover, the almost universal superficial ulnar oblique lamina predisposes to scarring, which may cause radial shifting of the ulnar neurovascular bundle and may affect the PCBMN. It is concluded that the minor complications of ECTR depend partly on the variations in the laminar arrangement of the TCL[25]. In another study performed on eight dissected TCLs, the transverse fibers were the most prominent (> 60%), followed by the oblique fibers in the pisiform-trapezium direction (18%), the oblique fibers in the scaphoid-hamate direction (13%) and finally the longitudinal fibers (8%)[26].

Borders of the TCL

The TCL is attached medially to the pisiform bone and hook of the hamate, while laterally it splits into superficial and deep laminae. The superficial lamina is attached to the tubercle of the scaphoid and trapezium and the deep lamina is attached to the medial lip of the groove on the trapezium. Together with this groove, the two laminae form a tunnel, lined by a synovial sheath containing the tendon of flexor carpi radialis (FCR)[24].

Proximal border of the TCL

Proximally, the TCL is attached to the volar carpal ligament which extends from the radius to the ulna over the flexor tendons as they enter the wrist[24]. This border corresponds to the distal flexion wrist crease, which also crosses the proximal end of scaphoid and pisiform bones.

Distal border of the TCL

This border is attached to the central portion of the palmar aponeurosis (PA). As measured along the axis of the radial border of the ring finger, the average distance between this border and the superficial palmar arch ranges from 5.5-19 mm[27-31]. The mean distance from this distal border to the nearest aspect of the motor branch of MN is about 2.7-6.5 mm[23,32].

Immediately proximal to the distal end of the TCL and in line with the axis of ring finger, a palmar fat pad (fat drop sign) is visualized overlapping this border. It is a reliable anatomic landmark during CT release which must be retracted in order to visualize the distal end of the TCL[14]. Its proximal aspect lies at about 2 mm proximally to the distal edge of the TCL. The distance between the distal end of the TCL and the palmar fat pad decreases by flexing the fingers, but the distance between the TCL and the palmar arch or the PCBMN is not markedly affected. When dividing the TCL from proximal to distal, visualization of the proximal part of the fat pad is a useful indication that the distal edge of the TCL is within approximately 2 mm and indicates that distal dissection beyond this level is unnecessary in order to avoid injury of the superficial palmar arch or the PCBMN[32].

Surfaces of the TCL

Palmar (volar) surface: This surface gives partial origin to all the thenar and hypothenar muscles except the abductor digiti minimi muscle and it also receives partial insertion from the flexor carpi ulnaris (FCU) and palmaris longus (PL).

This surface is entirely hidden by the muscular attachments, which makes it appear much deeper than surgeons think. This might urge surgeons to make a longer incision for good exposure of the TCL and to complete its division[33]. The middle part of this surface is crossed by the PL tendon (if present), with a nerve on each of its sides; palmar cutaneous branch of ulnar nerve (medially) and PCBMN (laterally). The ulnar nerve and vessels cross the medial part of this surface through a special fascial tunnel called the Guyon tunnel[33].

The superficial branch of the radial artery arises from the radial artery just before the latter curves round the carpus. It passes through and occasionally over the the-

nar muscles, which it supplies. It sometimes anastomoses with the end of ulnar artery to complete the superficial palmar arch[24].

When present, it is a slender and flattened tendon, which passes superficially to the TCL and lies medially to the tendon of FCR. It is partially inserted into its central part of the TCL and extends distally to attach to the proximal part of PA. Frequently, it sends a tendinous slip to the thenar muscles. The MN lies deep to this tendon but when absent, the nerve becomes separated from the skin only by a thin subcutaneous fat and deep fascia[24].

PCBMN arises from the MN proximal to the TCL. It pierces the deep fascia and runs superficially to the TCL, just laterally to the PL tendon. It then divides into lateral branches supplying the thenar skin, communicating with the lateral cutaneous nerve of forearm. The medial branches supply the central palmar skin and communicate with the palmar cutaneous branch of ulnar nerve[24].

Injury to the PCBMN is the most common complication of CT surgery[34] and it has been suggested that the mini incision done between the superficial palmar arch and the most distal part of the PCBMN in the palmar region is the safe zone for CT surgery[34]. Decreased levels of discomfort in patients undergoing endoscopic and subcutaneous types of CT release may be in part due to the preservation of the crossing cutaneous nerves during these procedures[35].

Communicating sensory branches may be multiple and often arise in the proximal forearm and sometimes from the anterior interosseous branch. They pass medially between FDS and FDP and behind the ulnar artery to join the ulnar nerve. This communication is a factor in explaining anomalous muscular innervations in the hand[24]. In relation to an incision for CT release, PCBMB was found to cross the incision only in one specimen (of 25 fresh frozen cadaveric hands), while its terminal branches were identified at the margin of the incision in another two specimens[35].

It arises from the ulnar nerve near the middle of the forearm at about 4.9 cm proximally to the pisiform bone. It then runs distally just medially and parallel to the PL tendon. It enters the palm of hand superficially to the TCL. In 24 specimens, at least one, usually multiple, transverse palmar cutaneous branch was identified originating at about 3 mm distally to the pisiform within Guyon's canal. In another 10 specimens (of 25 hands), a nerve of Henle arose at about 14.0 cm proximally to the pisiform, travelling with the ulnar neurovascular bundle to the wrist flexion crease[35].

They pass superficially to the FR and enter the hand by passing through a groove between the pisiform (medially) and the hook of hamate (laterally and more distally). The ulnar artery is radial to the nerve and can be easily felt on the ulnar side of the front of the wrist. They usually pass just over the ulnar to the superior portion of the hook of the hamate. Over the FR, they are kept in place by a fascial extension from the volar carpal ligament, forming the ulnar canal (Guyon's canal). This extension is attached medially to the pisiform bone and blends laterally with the TCL[33]. They lie in the shelter of the lateral edge of the tendon of FCU[24]. Pisiform bone is palpated at the base of the hypothenar eminence and serves to mark the entry on its lateral side of the ulnar nerve and artery into the hand. The mean distance from the radial aspect of the pisiform to the radial border of Guyon's canal and the ulnar edge of the PL tendon is about 10.3 mm and 16.1 mm respectively[23]. As the ulnar nerve passes between the pisiform and hook of hamate, it terminates by dividing into superficial and deep branches.

With the wrist in neutral position, a looped ulnar artery runs from 2-7 mm medially[27] to 1-4 mm laterally to the hook of the hamate[36]. It then continues to form the superficial palmar arch. With the wrist in radial deviation, the looped ulnar artery migrates to the ulnar side of Guyon's canal (-2-2 mm radially to the hook of the hamate). During ulnar deviation of the wrist, the ulnar artery shifts more laterally beyond the hook of the hamate (2-7 mm). So, in order to minimize postoperative bleeding and avoid iatrogenic ulnar vascular and neural injury, it is recommended to: (1) transect the TCL over 4-5 mm apart from the lateral margin of the hook of the hamate without placing the edge of the scalpel toward the ulnar side; (2) not to transect the TCL in the ulnar deviation wrist position[27]; and (3) make the proximal portal just medial to the PL tendon in order to spare the ulnar neurovascular structures[36]. However, injury to the ulnar artery within Guyon's canal has not been a problem during ECTR surgery[14].

Variations: (1) An anomaly of the ulnar nerve with an aberrant branch was observed to cross the CT incision[37]; and (2) A small arterial branch (average diameter, 0.7 mm) arising from the ulnar artery ran transversely just over the TCL in 6 (of the 24 specimens). This branch was consistently located within 15 mm proximally to the TCL distal margin[27].

The deep surface of the TCL: With the carpal bones, this surface forms the CT which is traversed by nine flexor tendons of the fingers, their flexor synovial sheathes and the median nerve.

The median nerve is the softest and most volar structure in the CT. Its average cross-sectional area is 6.19 mm[38]. It lies directly beneath the TCL and is superficial to the nine digital flexor tendons (Figure 1). Proximally to the TCL, the MN lies just laterally to the tendons of FDS and between the tendons of FCR and PL (Figure 2). Its location extends an average of 11 mm radially to the hook of hamate[27]. Distally to the TCL, it enlarges and flattens and usually divides into five or six branches: (1) the recurrent motor branch; (2) three proper digital nerves (two to the thumb and one to the radial side of index finger); and (3) two common digital nerves (one to index/ middle and one to middle/ ring)[24]. Trapped or pinched nerves have a useful electrical property for the diagnosis in that the speed of its conduction slows at the

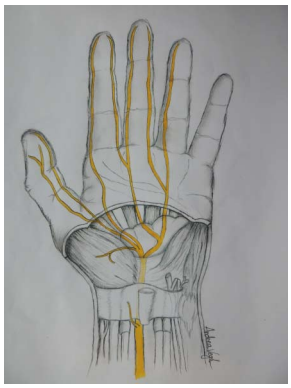

Figure 1 Sketch of the palm, showing specific details of the inner structures of the carpal tunnel (inside the wrist). The median nerve and its branches after the wrist are marked in yellow.

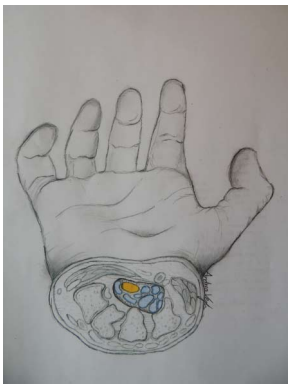

Figure 2 Sketch of the cross-section of the carpal tunnel on a hand. Median nerve is shown in yellow and the nine flexor tendons are marked in blue.

site of trouble due to demyelination.

Anomalies of the median nerve: Variations of the MN at the wrist were reported in about 11% of the examined specimens. Neural variations arising from the medial aspect of the MN were common and could be a cause of iatrogenic injury during endoscopic or open release[39].

In a study performed on 246 carpal tunnels at operation, four groups of variations were described: (1) variations in the course of MN were found in 12%; (2) accessory branches at the distal portion of the CT in 7%; (3) high divisions of the MN in 3%; and (4) accessory branches proximal to the carpal canal in 1.5%. These findings emphasize the importance of approaching the MN from the ulnar side when opening the CT[40].

High bifurcation of the MN

Persistent median artery: the median artery is a transitory vessel that represents the embryological axial artery of the forearm. It normally regresses in the second fetal month[41,42]. Its persistence in the human adult has been documented as two different types: as a large, long vessel which reaches the hand (palmar type); or as a small and short vessel which ends before reaching the wrist joint (antebrachial type)[43,44]. It occurred in about 3.4%-20% of a 646 population sample of hands[37,45]. It is more frequent in females than in males, occurring unilaterally more often than bilaterally and slightly more frequently on the right than on the left. Most frequently, it arises from the caudal angle between the ulnar artery and its common interosseous trunk (59%). Other origins may be from the ulnar artery or from the common interosseous trunk. It ends as the 1st, 2nd or 1st and 2nd common digital arteries (65%) or joins the superficial palmar arch (35%). It pierces the MN in the upper third of the forearm in 41% of cases with the palmar type[45]. The median artery in its palmar type passes under the FR, running in the CT together with the MN and flexor tendons. This relationship has been considered an etiological factor in CTS[46].

An aberrant sensory branch arising from the ulnar side of the MN and piercing the ulnar margin of the TCL was found in 3% of hands (of 110 in operations)[39].

Martin-Gruber anastomosis is a motor communicating nerve, which may cross over from the median to ulnar nerve in the forearm (motor not sensory connections). It occurs in two patterns: either from the MN in the proximal forearm to the ulnar nerve in the middle to distal third of the forearm; or from the anterior interosseous nerve to the ulnar nerve[47].

Other motor anastomoses between the MN and ulnar nerve include: (1) motor branch of the MN to superficial head of flexor pollicis brevis (FPB) and ulnar nerve to the deep head of the FPB; (2) anastomosis, of the MN and ulnar motor branches through first lumbrical or through innervation of the adductor pollicis muscle; (3) branch of the MN to third lumbrical joining neural branch to this muscle from deep branch of ulnar nerve; (4) the MN may also form anastomoses with branch of radial nerve close to abductor pollicis brevis which has the radial nerve innervating this muscle; and (5) first dorsal interosseous, adductor pollicis or even abductor digiti minimi may be innervated by the MN[47].

Motor branch (recurrent or thenar branch)

It is a short and thick branch commonly arising from the radial side of the MN. It may however, arise from the volar or the ulnar side of the MN[14]. It may be the first palmar branch or a terminal branch which arises level with the digital branches of MN. It runs laterally, just distal to the TCL, with a slight recurrent curve beneath the part of the PA covering the thenar muscles. It runs around the distal border of the TCL to lie superficially to the FPB, which it usually supplies, and continues either superficially to the muscle or through it. It gives a branch to the abductor pollicis brevis, which enters the medial edge of the muscle and then passes deep to it to supply the opponens pollicis, piercing its medial edge. Its terminal part occasionally gives a branch to the 1st dorsal interosseous, which may be its sole or partial innervation. It may arise in the CT and pierces the TCL, a point of surgical importance[24]. The position of the motor branch (in 30 hands) was extraligamentous in 46%-60%, subligamentous in 31%-34% and transligamentous in 6%-23% of

116 fresh frozen cadaveric hands[34,40]. So, the most common pattern of the motor branch is extraligamentous and recurrent. The mean distance between the distal edge of the TCL and this branch is about 2.7-6.5 mm[23,32].

The flexor tendons

The flexor tendons are the four tendons of the FDS, four tendons of the FDP and the tendon of the FPL. The superficialis tendons are all separate and the tendons for the middle and ring fingers lie superficially to those for the index and little fingers. The MN lies superficially to the tendons of FDS. The profundus tendons are still deeper to the FDS tendons. Only the slip to the index finger is separate; the other three are still fused and lie medially to the index slip[33]. The FPL tendon passes radially through a special canal between the two laminae of the TCL and the groove of trapezium. It is surrounded by a separate synovial sheath called the "radial bursa" which extends along the thumb as far as the insertion of the tendon at the base of the distal phalanx. Proximally, the radial bursa extends to a point 2.5 cm above the wrist joint/TC. It is sometimes connected to the base of the second metacarpal or may be absent[24].

MECHANICS OF FLEXOR TENDONS AND THE MN WITH FINGER AND WRIST MOVEMENTS

Along their course, the long flexor tendons pass through a flexor pulley system which includes the TCL, PA and the digital pulleys, where the lubricant effect of synovial fluid maintains low friction between these tendon and the pulleys. *In vivo* and during active flexion and extension of the wrist and fingers, measurements revealed that longitudinal tendon excursion is about 24-50 mm[48,49], while MN excursion was found to range from 11-28 mm during wrist and elbow movement[50,51].

It is highly suggested that non-inflammatory fibrosis and thickening of the synovium is a leading cause for MN compression[52]. These synovial changes also alter the gliding characteristic of the subsynovial connective tissue (SSCT), where it moves en bloc with the tendons and MN, which may play a role in the etiology of CTS[53,54]. About 90% of the synovial specimens resected from patients with idiopathic CTS did not exhibit inflammatory changes, but mostly edema or fibrosis[55,56]. Other findings of chronic synovial degeneration were reported as indicated by the increase in fibroblast density, collagen fiber size and vascular proliferation[57].

Additionally, the flexor tendons move upwards (volar displacement) from the floor of the CT during active finger movement[58-60]. This movement causes a force of compression/ reaction between the tendons and the TCL. Almost the same amount of force of the flexor tendon could be applied to the TCL during finger movement[61].

Because the SSCT and tendon are physically connected, a decrease in SSCT motion (due to fibrosis) relative to the tendon would increase the shear strain on the SSCT with tendon motion. Thus, this result suggests that the SSCT may be predisposed to maximum shear injury from activity done in 60 degrees of wrist flexion more than the motion in all other wrist positions[62]. During hand and finger motions, friction between the FDS tendon and the MN is thought to play a role in the development of cumulative trauma disorders[62]. Also, the ratio of MN excursion to tendon excursion was much lower in finger-only motions compared to wrist motions with or without finger motion[63]. High velocity tendon motion was reported to predispose to SSCT shear injury[64].

A step forward damage in the SSCT in the CT was observed to follow repeated stretch tests within the physiological range of tendon excursion[12,62]. Similarly, repetitive hand activities caused thickening of the synovial lining of the tendons that share the CT with the MN[20,65].

Furthermore, shear tension and injury of the SSCT in CTS patients is significantly higher than that in normal subjects[66] and the excursion of the MN is markedly reduced[50,51]. This finding may be consistent with the fact that fibrosis of the synovial tissue within the CT is often observed in CTS patients.

PALMAR APPONEUROSIS (STRUCTURE AND FUNCTION)

The deep fascia of the palm of hand (palmar fascia) is thin over the thenar and hypothenar eminences, but its central portion, the PA, is triangular in shape. It has great strength and thickness. Its apex is continuous proximally with the distal border of TCL and receives the expanded tendon of the PL. Its base divides below into four slips, one for each finger[33].

The PA covers the central compartment of the hand which contains the long flexor tendons and their synovial sheaths, the lumbricals, the superficial palmar arch and branches of the median and ulnar nerves with their digital nerves and vessels. Between the flexor tendons and the fascia covering the deep palmar muscles lies the medial central palmar (mid-palmar) space which is continuous with the space of at distal forearm in front of pronator quadratus (Space of Parona) via the CT[24].

The deeper part of each slip subdivides into two processes, which are inserted into the fibrous sheaths of the flexor tendons. At the points of division into the slips, numerous strong transverse fascicular fibers of the PA are positioned at the proximal margin of the flexor tendon sheath. They bind the separate processes together and are attached by vertical septa to the underlying transverse metacarpal ligament, thus forming a tunnel around the flexor tendon and a PA pulley for the flexor tendons in conjunction with the first and second annular pulleys of the digital flexor mechanism[67,68].

The PA pulley might be considered as important as the annular and cruciate flexor tendon pulleys. The PA decreases the tendency to bowstring around the metacar-

pophalangeal joint with a combination of proximal annular pulleys[69].

The PA forms a fibrotendinous complex that functions as the tendinous extension of the PL when present and as a strong stabilizing structure for the palmar skin of the hand. It has a deeper transverse portion that crosses the palm at the proximal end of the metacarpal bones.

Aponeurosis provides firm attachment to overlying skin, helps to form the ridges in the palm, which in turn help to increase friction so that we can grasp objects firmly, protects underlying structures and provides attachment to muscles. The transverse fascicular fibers of the PA at the proximal margin of the flexor tendon sheath appear to function as a pulley[67].

CLINICAL DIAGNOSIS OF CTS

The stages of CTS symptoms and signs can be categorized into three stages. In the first stage, the patient will awaken from sleep with a feeling of a numb or swollen hand, with no actual swelling visible. They may feel severe pain coming from their wrist emanating to their shoulder, with a tingling in their hand and fingers known as brachialgia paresthetica nocturna. Patients will note that shaking or flicking of their hand will stop the pain and that their hand may feel stiff in the morning. The second stage involves the symptoms being felt during the day. These may be felt especially when the patient performs repeated hand or wrist movements or if they remain in the same position for a long time. Patients may also notice clumsiness when using their hands to grip objects, resulting in the objects falling. The third and final stage occurs when there is hypotrophy or atrophy of the thenar eminence. When this stage is reached, sensory symptoms may no longer be felt at all[70].

When diagnosing a patient with CTS, it is important to create a case history relevant to the characteristic signs of CTS. The patient must be questioned about whether their symptoms occur mainly at night or during the day, whether certain positions or repeated movements provoke their symptoms, if they use any vibratory instruments for work, whether their symptoms are felt in the hand, wrist or shoulder (and where in the areas symptoms are felt), what patients may do to alleviate symptoms (shaking, flicking, *etc.*), or if the patient may have a predisposing factor[70]. Many factors may in fact be connected to CTS. They can include inflammatory arthritis, diabetes mellitus, pregnancy, hypothyroidism, Colles' fracture, acromegaly, amyloidosis, adiposity, myxedema, chronic polyarthritis or the use of corticosteroids and estrogens[1,70].

A proper physical examination of the patient's hand and wrist is an important first step towards the diagnosis of CTS as certain physical findings may suggest the presence of other conditions. Abrasions or ecchymosis on the wrist and hands may indicate that there has been injury to the tissue, which could also include injury to the median nerve. If bony abnormalities like the boutonniere deformity, the swan neck deformity or the ulnar deviation of the wrist are found, it could be concluded that the patient suffers from rheumatoid arthritis. If bossing on the carpal or distal phalanx is observed, osteoarthritis may be the cause. Other neuropathy syndromes or carpometacarpal arthritis may be suspected if thenar atrophy is seen as this condition usually happens only with severe and chronic CTS, which is not as common[71].

Since patient history and physical examination have only limited diagnostic value and do not reveal the specific areas of symptom occurrence, patients can additionally be asked to fill out a self-diagnosis questionnaire known as the Katz Hand Diagram. A Katz Hand Diagram allows the patient to specify where they are experiencing symptoms and to classify the symptoms as numbness, pain, tingling or hypoesthesia. The completed symptom diagram can then be classified into one of three patterns of CTS.

Classical pattern: symptoms experienced by at least two of either the first, second or third fingers. Symptoms may also involve the fourth and fifth fingers, as well as wrist pain and radiation of pain proximally to the wrist however should not involve the palm or dorsum of the hand is not allowed. Probable/possible pattern: includes the same symptoms as in the classical pattern, however the palmar symptoms should only be limited to the median side. Possible pattern: symptoms involving only one of the first, second or third finger. Unlikely pattern: no symptoms are present at all in the first, second or third finger[70].

A classical or probable diagram indicates the presence of CTS (sensitivity = 64%; specificity = 73%)[70-73]. An additional subjective test is referred to as the flick sign (sensitivity = 93%; specificity = 96%)[71,73] where the patient is simply asked whether or not they relieve the symptoms which awaken them at night with flicking or shaking of their hands. If the patient reports that this does happen to them, this may be indicative of CTS[74].

Additionally, traditional tests known as provocative tests can be easily conducted by the physician on the patient to determine the possibility of CTS. One such test is a wrist flexion test known as Phalen's test (sensitivity = 57%-91%; specificity = 33%-86%)[71,73,74] that involves the patient placing their elbows on a flat surface, maintaining their forearms vertically and allowing their wrists to fall into flexion for up to one minute.

The "reverse Phalen's test" (sensitivity = 57%; specificity = 78%)[74], also known as the wrist extension test or "Wormser's test"[75], is also possible and involves the patient actively extending their fingers and wrist for two minutes. Another well known test is Tinel's sign (sensitivity = 23%-60%; specificity = 64%-87%)[71,73,74], where the physician taps along the patient's median nerve near the carpal tunnel. Durkan's test (sensitivity = 64%; specificity = 83%)[74], or carpal compression, is a test where the physician presses on the proximal edge of the carpal ligament with their thumb, compressing the median nerve.

The hand elevation test (sensitivity = 75.5%; specificity = 98.5%)[76] is done by asking the patient to raise both of their arms, along with their elbows and shoulders, and holding the position for up to two minutes. The tourniquet test (sensitivity = 21%-59%; specificity = 36%-87%)[73,74], or Gillet test, is performed by having the physician raise a blood pressure cuff placed on the patient's arm to the level of their systolic blood pressure. For all of the above noted tests, if paresthesia develops or increases in the median nerve distribution within one minute or less, then the test is deemed to have a positive result and CTS in the patient may be suspected[1,74].

It is important to note that, although provocative tests and physical examination are simple and low cost methods to test for reproduction of the patient's symptoms and to determine if CTS should be suspected, provocative tests have scarce or no diagnostic value[1,70,71] and physical examination has inadequate predictive value if the likelihood of CTS is low[77]. There have been no trends identified between testing positive for various provocative tests and the severity of CTS[78] and therefore proper diagnostic conclusions based on these tests cannot be made.

Nerve conduction studies

Due to this lack of diagnostic value in the mentioned tests, if CTS is suspected in a patient, adjunctive electrodiagnostic tests can be performed for a better diagnosis as they quantify and stratify the severity of CTS[71]. These tests include nerve conduction studies and electromyography which may help with the future decision of treatment options and they have a sensitivity of 56% to 85% and a specificity of at least 94%[71]. Because of their high specificity and sensitivity percentages, nerve conduction studies are considered to be the gold standard for CTS diagnosis[3,72]. Nerve conduction studies provide insight on the median nerve's true physiological health on a quantitative basis by comparing the latency and the amplitude of the nerve across the carpal tunnel to another nerve segment not passing through the carpal tunnel (*e.g.*, the radial or ulnar nerve)[3]. This is done by transcutaneously stimulating the nerve to create an action potential through an electrical pulse and having the depolarization wave detected by a recording electrode, that has been placed proximally or distally, and defining the response time of the median nerve as the "sensory conduction velocity" (SCV)[3,70,79].

It is necessary to compare the response of the median nerve to another nerve not within the carpal tunnel due to the fact that there are different factors like gender, age, obesity, temperature, finger diameter or concurrent systemic disease that can influence the latency or amplitude of the median nerve[3,80,81]. Using these controls increases the accuracy and sensitivity of diagnosis, with a sensitivity of 80%-92% and a specificity of 80%-99%[3,79]. Additional data may also be obtained by studying the distal motor latency (DML) in the median and ulnar nerves in the same hand[3].

Diagnostic criteria for CTS in nerve conduction studies include the median nerve showing extended amounts of sensory and motor latencies as well as delayed or diminished sensory and motor conduction velocities[3]. Nerve conduction studies focus on defining whether there has been damage to the median nerve inside the carpal tunnel to quantify the severity of this nerve damage using a scale and to define the physiology of this injury as a conduction block, demyelination or axonal degeneration[3,9,70]. The electrophysiological classification of the severity of CTS has been defined by the American Association of Electrodiagnostic Medicine (AAEM) and is as follows: (1) Negative CTS: normal findings on all tests (including comparative and segmental studies); (2) Minimal CTS: abnormal findings only on comparative or segmental tests; (3) Mild CTS: SCV is slowed in the finger-wrist tract with normal DML; (4) Moderate CTS: SCV is slowed in the finger-wrist tract with increased DML; (5) Severe CTS: absence of sensory response is seen in the finger-wrist tract with increased DML; and (6) Extreme CTS: complete absence of a thenar motor response[3,70,82].

Nerve conduction studies can be paired with electromyography in order to tell the difference between muscle weakness that has been created by neurological disorders and primary muscle conditions[71]. Adjunctive tests are, however, best used for patients who present with untypical symptoms and examination or if they possess an intermediate probability of having CTS. Although nerve conduction studies are a more accurate way of diagnosing CTS, they cannot be used for every patient showing symptoms of CTS as this would be expensive and inefficient[3,72]. Although nerve conduction studies are the most sensitive and accurate way to diagnose CTS, false positives and false negatives are still possible and account for 16%-34% of "clinically defined CTS" going undiagnosed[3,83].

When diagnosing CTS, it is important to remember that many other conditions can produce similar symptoms to CTS[71]. A thorough physical examination along with an accurate patient history is an important first step for a correct diagnosis and the following list include some of the conditions that CTS must be differentiated from, along with the physical findings they are associated with: Wrist arthritis: seen in patients experiencing limited motion at the wrist or if there are radiological findings of arthritis; Carpometacarpal arthritis of thumb: characterized by joint line pain, pain experienced during motion or arthritis in radiological findings; Cervical radiculopathy (C6-C7)*:* symptoms can include neck pain and numbness in the thumb and index finger only; Flexor carpi radialis tenosynovitis: can be suspected if there is tenderness near the base of the thumb; Ulnar or cubital tunnel syndrome: signs can include first dorsal interosseous weakness or tingling in the fourth and fifth digit; Median nerve compression at elbow: if there is tenderness at the proximal forearm; Raynaud's phenomenon: if the patient has a history of symptoms related to cold exposure; Vibration

white finger: seen in patients who use vibrating hand tools at work; Volar radial ganglion: if a mass near the base of thumb is found above the wrist flexion crease; Brachial plexopathy (in particular of the upper trunk); Thoracic outlet syndrome and CNS disorders (multiple sclerosis, small cerebral infarction)[3,70,71].

Electrodiagnostic testing can be helpful with a differential diagnosis by being able to identify other hand dysesthesia conditions like cervical radiculopathy, polyneuropathy or median nerve entrapment syndromes[73,84]. Additionally, needle electromyography specifically may be helpful with disorders that are proximal to the median nerve as well as to rule out a radiculopathy[70].

Quantitative sensory testing is also used for sensory or motor tests to give quantitative results when diagnosing CTS. These tests include testing for touch threshold using Semmes-Weinstein Monofilaments (SWMF) (sensitivity = 59%-72%; specificity = 59%-62%)[73,74], also referred to as Weinstein Enhances Sensory Test (WEST), where a five piece SWMF/WEST set is used and the filaments are applied onto digit pulps. Positive results of this test are deemed as a threshold greater than 2.83 in digits D1-D3 (an abnormal result); usually D2 or D3 are also assessed and comparison with D5 can improve the specificity as it eliminates thresholds that are larger than 2.83 due to aged or calloused skin. Another quantitative test is the two-point discrimination test (sensitivity = 6%-32%; specificity = 64%-99%)[73,74] where the patient is asked to differentiate between the touch of prongs as they are applied until the skin blanches. Positive results (an abnormal finding) of this test are > 5 mm on pulps. Testing for the vibration threshold, measuring with either a tuning fork (sensitivity = 55%; specificity = 81%)[74] or vibrometer (sensitivity = 50%; specificity = 73%)[74], is also possible. These tests include applying a tuning fork (at 256 cps) tangentially to the fingertip pulp D1-D3 after hitting it to the affected side and comparative site or by applying a vibration stimulus to the digital pulp with a vibrometer and observing if the patient's feeling is different compared with the normal site (D5) or alternate site or, in the case of the vibrometer, if the thresholds are greater than norms for positive results. Current perception threshold (sensitivity = 80%; specificity = 61%)[74] is tested for by delivering different frequencies of current and touching the patient with the equipment delivering this current. This stimulates the sensory nerves and positive results can be identified by comparing the patient's thresholds and frequency ratios with established norms in a computer software analysis. Thenar weakness or thenar atrophy (sensitivity = 4%-28%; specificity = 82%-99%)[71,73] can also be tested for by visually inspecting the abductor pollicis brevis to look for loss of muscle bulk (positive result for thenar atrophy) or to use Oxford grading for the abductor pollicis brevis and observing a grade less than 5 (for thenar weakness). Thenar muscles are innervated by the median nerve, so the impairment of these muscles is indicative of the compromise of the motor fibers[74].

All in all, debate and disagreement still exist on the proper and accurate diagnosis of CTS. However, most experts can agree that the combination of nerve conduction studies (currently deemed the gold standard for diagnosis) and subjective symptoms allow for the most accurate way of diagnosing CTS[78].

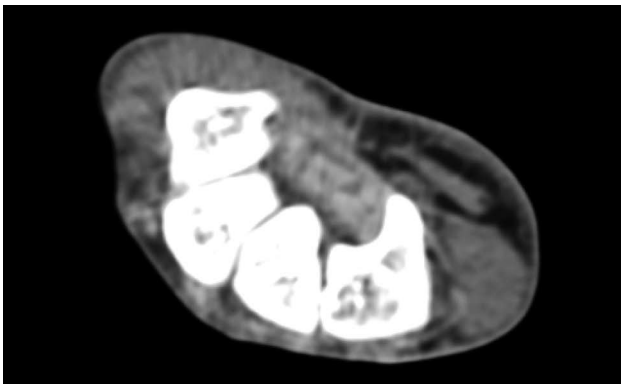

Figure 3 Axial computed tomography scan shows bony part of carpal tunnel at the level of outlet. Bony structures from left to right are HAMATE, CAPITATE, TRAPEZOID, TRAPEZIUM. FR (arrow) b and flexor tendons can be detected by computed tomography scan.

Computed tomography and conventional X-ray

Plain radiography has a limited role in diagnosing primary CTS as it cannot reveal the soft tissue part of the carpal tunnel. However, it might be useful in cases associated with bony stenosis, fracture and soft tissue calcification[85]. Therefore, it should not be indicated unless there is a history of trauma to the hand or limitation in the range of wrist movement. CT scanning might provide a better alternative than plain radiography to clearly visualize the bony part of the carpal tunnel (Figure 3).

It can easily reveal the unusual bony structures and the structure occupying the space within the carpal tunnel that are not discovered by external examination[86]. However, compression of the nerve cannot be clearly visualized unless it is due to the bony condition. In addition, several other reports have demonstrated the minor contribution of this approach in cases of primary CTS[87,88]. In summary, plain radiograph and CT scan play minor roles in CTS diagnosis and they are difficult to standardize due to their inherent limitations in evaluating soft tissue changes[85]. Therefore, CT scans and plain radiography should not be used as routine CTS diagnostic tools unless hard tissue related changes such as bone fracture, osseous carpal stenosis and calcifying of soft tissue are suspected[85].

Ultrasonography

Due to recent advances at increasing resolution of sonographic pictures, it is possible to acquire a high quality image of peripheral nerves and fascia. Ultrasonography (US) is also able to identify changes in the flexor retinaculum, perineural and intraneural vascularization of the median nerve in idiopathic carpal tunnel syndrome (Figures 4-7). It can also identify the causes for secondary CTS. A study

Figure 4 Axial ultrasound image shows flexor retinaculum bowing as an echogenic line (arrow) in carpal tunnel and cross sectional area of median nerve (stellate) in a patient with carpal tunnel syndrome.

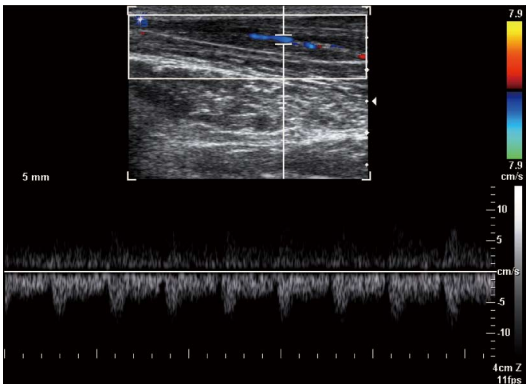

Figure 6 Spectral Doppler waveform of the median nerve shows low resistance hypervascularity of affected median nerve in a 40-year-old woman with severe carpal tunnel syndrome.

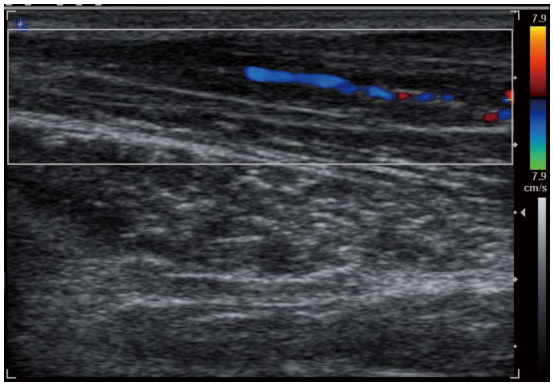

Figure 5 Longitudinal color Doppler sonogram in a 40-year-old woman with severe carpal tunnel syndrome shows intraneural hypervascularity in the median nerve.

Figure 7 Axial ultrasound image shows hypoechoic cable like neural fascicle (arrows) separated by substratum hyperechoic fat in a patient with secondary carpal tunnel syndrome due to lipofibromatous hamartoma of the median nerve.

by Nakamichi and Tachibana included 414 symptomatic wrists and 408 control wrists[89]. Both sonography and nerve conduction studies were performed and the results were compared. The cross-sectional area of the median nerve was measured at the distal edge of the flexor retinaculum, the hook of hamate and the pisiform. Clear differences between the symptomatic patients and control patients were observed at all three levels. Nakamichi and Tachibana proposed cut off values of the CSA for each level ranging from an average of 12 mm^2 to 13, 11 and 14 mm^2 at all three levels. Specificity was found to be greater than 95% with sensitivity ranging from 43%-57%[89].

Along the same lines, in a study carried out by El Miedany *et al*[90], sensitivity and specificity were determined by measuring the CSA at the carpal tunnel inlet. Sensitivity and specificity measurements were found to be much higher than those presented by Nakamichi and Tachibana[89]. The study included 96 symptomatic wrists and 156 control wrists, all of which were analyzed using both ultrasound and nerve conduction studies. Cut off for mild disease was 10 mm^2, moderate at 13 mm^2 and severe at 15 mm^2. Sensitivities and specifics for mild, moderate and severe disease were measured to be 98% and 100%, 98% and 97%, and 97% and 99%.

Theoretically, nerve enlargement results from a series of factors including inflammation, fibrosis, new axonal growth, endoneurial edema, demyelination, remyelination, *etc*. These indicators of increased CSA are all visible on US. Recent studies have shown that US is effective in confirming the diagnosis of CTS. One advantage that US has over NCS is that other lesions which display symptoms similar to CTS can be excluded from examination; these include tenosynovitis, mass lesions and anatomic defects. Moreover, US is low cost, readily available, noninvasive and total examination time is short. It can be recommended to use US as a replacement for clinical findings and first-line therapy in the diagnosis of CTS. However, in more complicated cases where diagnosis of CTS may require some confirmation, US would be a great tool as it is more sensitive and less invasive than nerve conduction studies.

It remains the case that there is not yet a reliable diagnostic standard for CTS. However, many of the studies in this review were able to rule out CTS if the CSA of the median nerve in the carpal tunnel inlet was below 10 mm^2. Flexor retinaculum bowing, flattening of the median nerve and decreased longitudinal excursion on

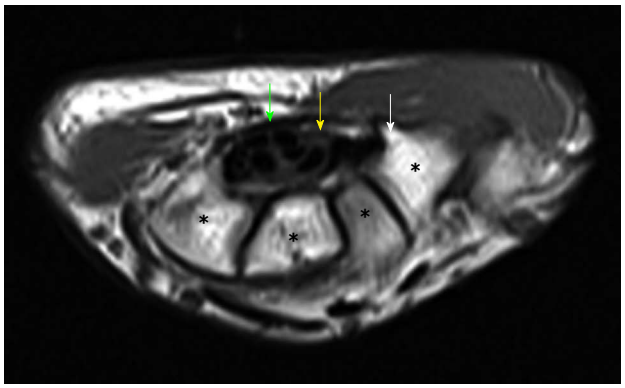

Figure 8 Axial T1W image of carpal tunnel at the level of tunnel outlet shows bony part of carpal tunnel as intermediate signal intensity composed from left to right hamate, capitates, trapezoid, trapezium. White arrow shows hook of hamate, yellow arrow shows median nerve, green arrow shows flexor retinaculum. Asterisks indicate carpal bones.

dynamic assessment are other measurements offered in addition to the CSA of the median nerve in the US assessment of CTS but are not as reliable. Limitations of US include axial and lateral resolution of the transducer that restrict the sonographic measurements as well as the challenge in differentiating the MN from the surrounding structures, especially in the distal CT. Ultrasonography can be implemented universally when a standardized protocol is used because the measurements are found to be reproducible.

Magnetic resonance imaging

Magnetic resonance (MR) imaging allows for good imaging of soft tissue. This makes MR imaging the optimal choice when studying CT in detail (Figure 8).

The drawbacks to MR imaging are that it is very costly, time consuming and not readily available. For these reasons, it is not advisable for MR imaging to be used in the diagnosis of CTS. The use of MR imaging is advisable in cases where the patient is resistant to therapy and/or for research. MR imaging does not add enough information of value to justify its use in the routine diagnosis of CTS in place of clinical and electrophysiological evaluation. Use of MR imaging can be justified in various circumstances, such as acute severe CTS following blunt trauma, arthritis, lack of evidence of nerve compression, surgical failure, long lasting CTS, detection of fibrous tissue and scars surrounding the MN and other anomalies of CT[91]. MRI can be used to determine the exact point of nerve entrapment, for diagnosis in the case of ambiguous symptoms and to identify space-occupying lesions[92].

MR imaging is useful for revealing the cause of nerve compression or elongation. Studies of MRI on CTS have shed tremendous light on the pathophysiology of idiopathic CTS. Typical indicators of idiopathic CTS are proximal enlargement of the cross-sectional area (CSA) of the median nerve of the carpal tunnel, greater signal intensity over the MN and palmar bowing of the TCL[93]. The degree to which these findings are evident depends on the stage of the disease as enlargement of the CSA and increased signal intensity become more pronounced as the disease progresses. On T2-weighted MRI scans, high-signal intensity over the median nerve can indicate any of the following: accumulation of the axonal transportation, myelin sheath degeneration or edema[94]. Enlargement of the structures within the carpal tunnel may be indicated by palmar bowing of the TCL. The severity of nerve compression can be determined accurately by sagittal images[95]. It must be noted that no parameter has been developed that is able to be used to define CTS clearly. However, MRI provides the greatest diagnostic sensitivity for idiopathic CTS[96]. MRI can be used to predict surgical outcomes in patients with CTS irrespective of NCSs. Moreover, patients prefer MRI to NCSs[96]. MRI studies have indicated that increased T2-signal intensity in the median nerve and bowing of the flexor retinaculum seem to be the most sensitive MR signs of CTS. Increases in CSA area, flattening of the MN and peritendon pathology are other potential indicators of CTS on MRI[97].

Previous reviews on MRI have pointed to the complications also encountered in this review. Original studies provide unsatisfactory descriptions of the reference diagnosis and only recruit asymptomatic referents[93]. Consensus criteria of CTS include symptoms, clinical findings and electrophysiological criteria[16,98]. The lack of consistency in diagnostic criteria provides for variations in patient spectra which takes a toll on the test accuracy[99]. A possible remedy for this in the future would be to include more detailed descriptions of the symptoms of the referents before the original studies.

Bak *et al*[100] studied twenty patients with CTS to determine if various MRI parameters correlated with nerve conduction test results. Results of the nerve conduction tests did not affect inclusion in the study. While no correlation was found, it should be noted that the patients did not show enlargement of the cross sectional area of the MN. The nerves seemed round rather than flat. Such a finding begs the question of diverse pathophysiological mechanisms behind CTS and how the diverse stages of chronicity of the disease affect the imaging outcome.

Unsatisfactory documentation of clinical characteristics has been shown to lead to overestimation of test accuracy. On the other hand, unsatisfactory documentation of reference diagnosis leads to underestimating test accuracy[99]. Additionally, insufficient blinding and a poor description of results may also lend to the overestimation of test accuracy.

Two studies that used referents with contralateral symptom-free hands did not find the cross sectional area of the median nerve to be enlarged[100,101], which is an observation made in other studies in which healthy volunteers were the referents. This finding can be attributed to other factors besides CTS. So long as there is a gold standard for the diagnosis of CTS, any other disease that causes similar symptoms may prove to hinder future studies.

TREATMENT OF CARPAL TUNNEL SYNDROME

Treatment of CTS can be classified as surgical and non-surgical. Surgical treatments include standard open carpal tunnel release, endoscopic carpal tunnel release, open carpal tunnel release combined with procedures and open carpal tunnel release using various incision techniques[102]. Non-surgical treatments, also referred to as conservative treatments, include a wider range of options such as splinting, cortical steroid injections, non-steroidal anti-inflammatory drugs, B6 vitamin, diuretics, ultrasound therapy, ergonomic positioning, manual therapy intervention, lidocaine patches and acupuncture[103-105]. Treatment decisions on carpal tunnel syndrome are based on the severity of the symptoms. Non-surgical treatments are recommended for patients with mild symptoms of CTS. Patients with moderate to severe symptoms are recommended for surgical evaluation.

Non-surgical treatment

Non-surgical treatment of CTS is recommended for patients that show mild to moderate symptoms of CTS. There is a variety of treatments that do not involve surgical procedures; however, splinting and steroids are most commonly used and supported by evidence[102]. The most common splinting method is the neutral splint, which involves the immobilization of the wrist in a neutral position. This neutralizes flexion and extension of the wrist, thus increasing carpal tunnel pressure[106](Gerritsen, 2001 #73). Neutral splinting is generally recommended for use for a period of 6 wk during night time, however studies have shown better improvement in the full time use of the splints[107]. Long term studies have shown considerable results of treatment success of night wrist splints at 3 mo of treatment[108] and after 12 mo of additional treatment after 6 wk treatment with night splints[109]. Other splinting methods include soft hand splints[106,110], volar wrist cock-up and modified ulnar gutter splints[111]. Soft hand splinting and neutral wrist splinting have been seen to show no significant differences within 3 mo of treatment[112]; however, soft hand splinting can be considered an alternative to neutral wrist splinting[113]. Treatment using steroids is done by local injection of corticosteroids directly into the patient's carpal tunnel. There is a risk associated with the injections and the possible decompression of the median nerve[114], thus different approaches have been used regarding the injection site of the steroid. Injection through the wrist crease has been done using a distal or proximal approach to the wrist crease, with the distal approach resulting in a more comfortable and alternative approach[115]. Other methods include intercarpal injections of steroids, shown to be a safe approach. Several studies have been conducted using an ulnar approach to the palmaris longus tendon[114,116] and have shown the treatment to be effective and risk free. Overall, treatments involving local steroid injections are effective in relieving symptoms associated with CTS for a short time, thus they are considered an effective short-term treatment[110,117,118]. Local anesthetic injections such as procaine hydrochloride have been shown to be effective additions to steroid injections; however, studies have shown that procaine hydrochloride injections are as effective as steroid injections in short term treatment of CTS[119,120].

A different approach to steroidal treatments is oral steroids such as prednisolone, proven effective for short-term treatment[121]. Studies involving several types of nonsteroidal anti-inflammatory drugs have concluded that NSAIDs have no effect in pain relief and treatment of CTS and their effect has been compared to that of a placebo[71,122]. However, other studies have shown effectiveness of NSAIDs drugs such as Naproxen in short term pain relief for CTS[123]. Several studies have concluded that pyridoxine and diuretics, such as trichlormethiazide, have no more effect than a placebo in the treatment of CTS[71,122]. Ergonomic positioning has been tested for possible effects on CTS and, despite the presence of pain relief after a period of 12 wk under treatment, the evidence was not enough to prove the effect of ergonomic positioning on CTS[124]. Heated lidocaine patches have also been identified as possible alternative short-term treatments for CTS, showing significant pain reduction following a two week study[105]. Acupuncture is another treatment approach for CTS. Studies have shown significant pain reduction in patients with CTS using proximal and distal acupoints, as well as improvement of overall subjective symptoms using sham acupoints[125,126]. Acupuncture has been shown to be as effective as night splints in the treatment of CTS[105]. Ultrasound therapy is another alternative conservative treatment that has been shown to have positive effects in short term treatments of CTS in patients showing mild to moderate symptoms[127,128]. Manual therapy intervention studies have concluded improved signs and symptoms for CTS[104]. It is important to note the role of sonography in assessing the possible effects on different types of treatments for CTS, including corticosteroid injection and splinting treatments[106].

Surgical treatment

Surgical treatment of CTS consists of the division of the transverse carpal ligament which reduces the pressure on the median nerve by increasing the space in the carpal tunnel[2]. Surgery is recommended for most patients with moderate to severe CTS. There are two different categories of methods used for surgical treatment of CTS: open release and endoscopic release. Open carpal tunnel release consists of the standard method of open release, as well as several modified methods. Modifications to the standard open carpal tunnel release (OCTR) include new incision techniques, such as the mini-open release, and addition of other procedures such as epineurotomy[102,129]. The standard open carpal tunnel release consists of a longitudinal incision at the base of the hand and in line with this incision, the incision of the subcutaneous tissue, the superficial palmar fascia and the muscle of the palmaris brevis[129]. The mini-open carpal tunnel release is a relatively new technique that consists of a longitudinal

incision that varies from 1.5-3.0 cm, placed in line with the radial border of the ring finger[129]. Different tools have been used for the mini-open carpal tunnel release, such as the Indiana Tome, the Knifelight, the Safeguard System and PSU retractor[129]. Epineurotomy has been used as an additional procedure to the OCTR, with the prospective of minimizing median nerve compression occurring after standard OCTR[72]. Endoscopic carpal tunnel release (ECTR) is another new technique that was developed by Okutsu and colleagues since 1986[131]. The two most commonly used methods of endoscopic carpal tunnel release are the single-portal and dual-portal technique; techniques that differ based on the number of ports used to access the carpal tunnel[130]. The single portal technique consists of the release of the transverse carpal ligament by using a single incision at the wrist. The double-portal technique consists of two incisions, one at the wrist and one at the palm of the hand. Several studies have tried to compare the efficiency and outcomes of the techniques involving carpal tunnel release procedures. Open carpal tunnel release and endoscopic carpal tunnel release have been shown to have no significant differences in outcomes within 12 wk of surgery[132] and within 1 and up to 5 years of surgery[129]. Mini-open carpal tunnel release and standard open carpal tunnel release have shown no significant differences within 4 mo of surgery[133] and within 6 mo of surgery[134]; however, mini-open carpal tunnel release has been shown to have better outcomes in earlier stages after surgery[134]. ECTR release is sometimes favored over OCTR as dividing the skin from below preserves the muscle and overlying skin, thus facilitating return to work; however, it has an increased risk of nerve or artery injury because of limitations in visualization[129]. ECTR has been shown to have better outcomes in muscle strength within 12 wk of surgery[132] and better outcomes compared to both standard open and mini-open release within 4 wk of surgery[133]. Additional epineurotomy procedures have been shown to have no significant difference in electrophysiological effects or nerve volume compared to the standard OCTR within 180 d after surgery[135].

CONCLUSION

This review has explored and emphasized one of the most common entrapment neuropathies. There are several imaging modalities for assessing this condition but after analyzing the various options, it seems as if ultrasound examination with high-frequency probes and improved power Doppler technology should be used as the primary imaging investigation in the initial evaluation of CTS as it is the most beneficial and accurate. ECTR has been shown to have better outcomes than both standard open and mini-open release.

REFERENCES

1 **Katz JN**, Simmons BP. Clinical practice. Carpal tunnel syndrome. *N Engl J Med* 2002; **346**: 1807-1812 [PMID: 12050342 DOI: 10.1056/NEJMcp013018]
2 **Aroori S**, Spence RA. Carpal tunnel syndrome. *Ulster Med J* 2008; **77**: 6-17 [PMID: 18269111]
3 **Ibrahim I**, Khan WS, Goddard N, Smitham P. Carpal tunnel syndrome: a review of the recent literature. *Open Orthop J* 2012; **6**: 69-76 [PMID: 22470412 DOI: 10.2174/1874325001206010069]
4 **Mashoof AA**, Levy HJ, Soifer TB, Miller-Soifer F, Bryk E, Vigorita V. Neural anatomy of the transverse carpal ligament. *Clin Orthop Relat Res* 2001; (**386**): 218-221 [PMID: 11347839]
5 **Uchiyama S**, Itsubo T, Nakamura K, Kato H, Yasutomi T, Momose T. Current concepts of carpal tunnel syndrome: pathophysiology, treatment, and evaluation. *J Orthop Sci* 2010; **15**: 1-13 [PMID: 20151245 DOI: 10.1007/s00776-009-1416-x]
6 **Mondelli M**, Giannini F, Giacchi M. Carpal tunnel syndrome incidence in a general population. *Neurology* 2002; **58**: 289-294 [PMID: 11805259]
7 **Rask MR**. Anterior interosseous nerve entrapment: (Kiloh-Nevin syndrome) report of seven cases. *Clin Orthop Relat Res* 1979; (**142**): 176-181 [PMID: 498633]
8 **Phalen GS**. The carpal-tunnel syndrome. Seventeen years' experience in diagnosis and treatment of six hundred fifty-four hands. *J Bone Joint Surg Am* 1966; **48**: 211-228 [PMID: 5934271]
9 **American Academy of Orthopedic Surgeons**. Clinical practice guidelines on diagnosis of carpal tunnel syndrome. 1st ed. Rosemont: American Academy of Orthopedic Surgeons, 2007: 5
10 **Boscheinen-Morrin J**, Conolly W. The Hand: Fundamentals of Therapy. 3rd ed. Oxford: Butterworth Heinemann, 2001: 249
11 **Sud V**, Tucci MA, Freeland AE, Smith WT, Grinspun K. Absorptive properties of synovium harvested from the carpal tunnel. *Microsurgery* 2002; **22**: 316-319 [PMID: 12404351 DOI: 10.1002/micr.10051]
12 **Vanhees M**, Morizaki Y, Thoreson AR, Larson D, Zhao C, An KN, Amadio PC. The effect of displacement on the mechanical properties of human cadaver subsynovial connective tissue. *J Orthop Res* 2012; **30**: 1732-1737 [PMID: 22573580 DOI: 10.1002/jor.22143]
13 **Cobb TK**, Dalley BK, Posteraro RH, Lewis RC. Anatomy of the flexor retinaculum. *J Hand Surg Am* 1993; **18**: 91-99 [PMID: 8423326 DOI: 10.1016/0363-5023(93)90251-W]
14 **Rotman MB**, Donovan JP. Practical anatomy of the carpal tunnel. *Hand Clin* 2002; **18**: 219-230 [PMID: 12371025]
15 **Schmidt H**, Lanz U. Surgical Anatomy of the Hand. 1 ed. New York: Thieme Stuttgart, 2003: 29
16 **Gelberman RH**, Hergenroeder PT, Hargens AR, Lundborg GN, Akeson WH. The carpal tunnel syndrome. A study of carpal canal pressures. *J Bone Joint Surg Am* 1981; **63**: 380-383 [PMID: 7204435]
17 **Rojviroj S**, Sirichativapee W, Kowsuwon W, Wongwiwattananon J, Tamnanthong N, Jeeravipoolvarn P. Pressures in the carpal tunnel. A comparison between patients with carpal tunnel syndrome and normal subjects. *J Bone Joint Surg Br* 1990; **72**: 516-518 [PMID: 2187880]
18 **Rydevik B**, Lundborg G, Bagge U. Effects of graded compression on intraneural blood blow. An in vivo study on rabbit tibial nerve. *J Hand Surg Am* 1981; **6**: 3-12 [PMID: 7204915]
19 **Keir PJ**, Bach JM, Rempel D. Effects of computer mouse design and task on carpal tunnel pressure. *Ergonomics* 1999; **42**: 1350-1360 [PMID: 10582504 DOI: 10.1080/001401399184992]
20 **Werner R**, Armstrong T. Carpal tunnel syndrome: ergonomic risk factors and intra carpal canal pressure, carpal tunnel syndrome. *Phys Med Rehabil Clin N Am* 1997; **8**: 555-569
21 **Byl C**, Puttlitz C, Byl N, Lotz J, Topp K. Strain in the median and ulnar nerves during upper-extremity positioning. *J Hand*

Surg Am 2002; **27**: 1032-1040 [PMID: 12457354 DOI: 10.1053/jhsu.2002.35886]
22 **Keir PJ**, Bach JM, Rempel DM. Effects of finger posture on carpal tunnel pressure during wrist motion. *J Hand Surg Am* 1998; **23**: 1004-1009 [PMID: 9848550 DOI: 10.1016/S0363-5023(98)80007-5]
23 **Vasiliadis HS**, Tokis AV, Andrikoula SI, Kordalis NV, Beris AE, Xenakis T, Georgoulis AD. Microsurgical dissection of the carpal tunnel with respect to neurovascular structures at risk during endoscopic carpal tunnel release. *Arthroscopy* 2006; **22**: 807-812 [PMID: 16904575 DOI: 10.1016/j.arthro.2006.03.021]
24 **Standring S**. Gray's Anatomy: The Anatomical Basis of Clinical Practice. 39 ed. New York: Elsevier/Churchill Livingstone, 2005: 913
25 **Isogai S**, Murakami G, Wada T, Akita K, Yamashita T, Ishii S. Laminar configuration of the transverse carpal ligament. *J Orthop Sci* 2002; **7**: 79-83 [PMID: 11819137 DOI: 10.1007/s007760200013]
26 **Prantil RK**, Xiu K, Kim KE, Gaitan DM, Sacks MS, Woo SL, Li ZM. Fiber orientation of the transverse carpal ligament. *Clin Anat* 2012; **25**: 478-482 [PMID: 22488997 DOI: 10.1002/ca.21257]
27 **Omokawa S**, Tanaka Y, Ryu J, Suzuki J, Kish VL. Anatomy of the ulnar artery as it relates to the transverse carpal ligament. *J Hand Surg Am* 2002; **27**: 101-104 [PMID: 11810622]
28 **Serra JM**, Benito JR, Monner J. Carpal tunnel release with short incision. *Plast Reconstr Surg* 1997; **99**: 129-135 [PMID: 8982196]
29 **Rotman MB**, Manske PR. Anatomic relationships of an endoscopic carpal tunnel device to surrounding structures. *J Hand Surg Am* 1993; **18**: 442-450 [PMID: 8515013 DOI: 10.1016/0363-5023(93)90089-L]
30 **Olave E**, Del Sol M, Gabriellp C, Mandiola E, Rodrigues CF. Biometric study of the relationships between palmar neurovascular structures, the flexor retinaculum and the distal wrist crease. *J Anat* 2001; **198**: 737-741 [PMID: 11465865]
31 **Sacks JM**, Kuo YR, Mclean K, Wollstein R, Lee WP. Anatomical relationships among the median nerve thenar branch, superficial palmar arch, and transverse carpal ligament. *Plast Reconstr Surg* 2007; **120**: 713-718 [PMID: 17700123 DOI: 10.1097/01.prs.0000270305.37677.e7]
32 **Madhav TJ**, To P, Stern PJ. The palmar fat pad is a reliable intraoperative landmark during carpal tunnel release. *J Hand Surg Am* 2009; **34**: 1204-1209 [PMID: 19540078 DOI: 10.1016/j.jhsa.2009.04.005]
33 **Decker GAG**, Du Plessis DJ. Lee McGregor's Synopsis of Surgical Anatomy. The Bath Press, Lower Bristol Road, Bath BA2 3 BL. 12 ed. Bristol: John Wright & Sons Ltd., 1986: 483
34 **Ozcanli H**, Coskun NK, Cengiz M, Oguz N, Sindel M. Definition of a safe-zone in open carpal tunnel surgery: a cadaver study. *Surg Radiol Anat* 2010; **32**: 203-206 [PMID: 19337677 DOI: 10.1007/s00276-009-0498-7]
35 **Martin CH**, Seiler JG, Lesesne JS. The cutaneous innervation of the palm: an anatomic study of the ulnar and median nerves. *J Hand Surg Am* 1996; **21**: 634-638 [PMID: 8842957 DOI: 10.1016/S0363-5023(96)80017-7]
36 **Hong JT**, Lee SW, Han SH, Son BC, Sung JH, Park CK, Park CK, Kang JK, Kim MC. Anatomy of neurovascular structures around the carpal tunnel during dynamic wrist motion for endoscopic carpal tunnel release. *Neurosurgery* 2006; **58**: ONS127-ONS33; discussion ONS127-ONS33; [PMID: 16543870 DOI: 10.1227/01.NEU.0000193883.02372.3E]
37 **Lindley SG**, Kleinert JM. Prevalence of anatomic variations encountered in elective carpal tunnel release. *J Hand Surg Am* 2003; **28**: 849-855 [PMID: 14507518]
38 **Mohammadi A**, Ghasemi-Rad M, Mladkova-Suchy N, Ansari S. Correlation between the severity of carpal tunnel syndrome and color Doppler sonography findings. *AJR Am J Roentgenol* 2012; **198**: W181-W184 [PMID: 22268209 DOI: 10.2214/AJR.11.7012]
39 **Beris AE**, Lykissas MG, Kontogeorgakos VA, Vekris MD, Korompilias AV. Anatomic variations of the median nerve in carpal tunnel release. *Clin Anat* 2008; **21**: 514-518 [PMID: 18567020 DOI: 10.1002/ca.20650]
40 **Lanz U**. Anatomical variations of the median nerve in the carpal tunnel. *J Hand Surg Am* 1977; **2**: 44-53 [PMID: 839054]
41 **De Vriese B**. Recherches sur l'e!volution des vaisseaux sanguins des membres chez l' homme. *Archives de Biologie* 1902; **18**: 665-730
42 **Müller E.** Beitrage zur Morphologie des Gefassystems. I. Die Armarterien des Menschen. *Anatomische Hefte* 1903; **22:** 377-575
43 **Salmon M**, Dor J. Les Arte res des Muscles des Membres et du Tronc. Paris: Masson, 1933: 53-55
44 **Huelin JG**, Barreiro FJ, Barcia EC. [Radio-anatomic study of the median artery]. *Acta Anat (Basel)* 1979; **105**: 250-255 [PMID: 539363]
45 **Rodríguez-Niedenführ M**, Sañudo JR, Vázquez T, Nearn L, Logan B, Parkin I. Median artery revisited. *J Anat* 1999; **195** (Pt 1): 57-63 [PMID: 10473293]
46 **Chalmers J**. Unusual causes of peripheral nerve compression. *Hand* 1978; **10**: 168-175 [PMID: 710998]
47 **Wheeless RC**. Textbook of Orthopaedics. Duke University Medical Center's Division of Orthopedic Surgery. Available from: URL: http://www.wheelessonline.com/ortho/anatomy_of_carpal_tunnel
48 **Wehbé MA**, Hunter JM. Flexor tendon gliding in the hand. Part I. In vivo excursions. *J Hand Surg Am* 1985; **10**: 570-574 [PMID: 4020072]
49 **Korstanje JW**, Schreuders TR, van der Sijde J, Hovius SE, Bosch JG, Selles RW. Ultrasonographic assessment of long finger tendon excursion in zone v during passive and active tendon gliding exercises. *J Hand Surg Am* 2010; **35**: 559-565 [PMID: 20223603 DOI: 10.1016/j.jhsa.2010.01.010]
50 **Hough AD**, Moore AP, Jones MP. Reduced longitudinal excursion of the median nerve in carpal tunnel syndrome. *Arch Phys Med Rehabil* 2007; **88**: 569-576 [PMID: 17466724 DOI: 10.1016/j.apmr.2007.02.015]
51 **Tüzüner S**, Inceoğlu S, Bilen FE. Median nerve excursion in response to wrist movement after endoscopic and open carpal tunnel release. *J Hand Surg Am* 2008; **33**: 1063-1068 [PMID: 18762098 DOI: 10.1016/j.jhsa.2008.03.007]
52 **Sternbach G**. The carpal tunnel syndrome. *J Emerg Med* 1999; **17**: 519-523 [PMID: 10338251]
53 **Ettema AM**, Zhao C, Amadio PC, O'Byrne MM, An KN. Gliding characteristics of flexor tendon and tenosynovium in carpal tunnel syndrome: a pilot study. *Clin Anat* 2007; **20**: 292-299 [PMID: 16944527 DOI: 10.1002/ca.20379]
54 **Netscher D**, Lee M, Thornby J, Polsen C. The effect of division of the transverse carpal ligament on flexor tendon excursion. *J Hand Surg Am* 1997; **22**: 1016-1024 [PMID: 9471069 DOI: 10.1016/S0363-5023(97)80041-X]
55 **Nakamichi K**, Tachibana S. Histology of the transverse carpal ligament and flexor tenosynovium in idiopathic carpal tunnel syndrome. *J Hand Surg Am* 1998; **23**: 1015-1024 [PMID: 9848552]
56 **Fuchs PC**, Nathan PA, Myers LD. Synovial histology in carpal tunnel syndrome. *J Hand Surg Am* 1991; **16**: 753-758 [PMID: 1880380]
57 **Jinrok O**, Zhao C, Amadio PC, An KN, Zobitz ME, Wold LE. Vascular pathologic changes in the flexor tenosynovium (subsynovial connective tissue) in idiopathic carpal tunnel syndrome. *J Orthop Res* 2004; **22**: 1310-1315 [PMID: 15475214 DOI: 10.1016/j.orthres.2004.03.005]
58 **Kiritsis PG**, Kline SC. Biomechanical changes after carpal tunnel release: a cadaveric model for comparing open, endoscopic, and step-cut lengthening techniques. *J Hand Surg Am* 1995; **20**: 173-180 [PMID: 7775747 DOI: 10.1016/S0363-5023(05)80003-6]

59 **Brown RK**, Peimer CA. Changes in digital flexor tendon mechanics after endoscopic and open carpal tunnel releases in cadaver wrists. *J Hand Surg Am* 2000; **25**: 112-119 [PMID: 10642480 DOI: 10.1053/jhsu.2000.jhsu025a0112]

60 **Richman JA**, Gelberman RH, Rydevik BL, Hajek PC, Braun RM, Gylys-Morin VM, Berthoty D. Carpal tunnel syndrome: morphologic changes after release of the transverse carpal ligament. *J Hand Surg Am* 1989; **14**: 852-857 [PMID: 2794405]

61 **Uchiyama S**, Amadio PC, Berglund LJ, An KN. Analysis of the gliding pattern of the canine flexor digitorum profundus tendon through the A2 pulley. *J Biomech* 2008; **41**: 1281-1288 [PMID: 18328488 DOI: 10.1016/j.jbiomech.2008.01.011]

62 **Yoshii Y**, Zhao C, Zhao KD, Zobitz ME, An KN, Amadio PC. The effect of wrist position on the relative motion of tendon, nerve, and subsynovial connective tissue within the carpal tunnel in a human cadaver model. *J Orthop Res* 2008; **26**: 1153-1158 [PMID: 18383182 DOI: 10.1002/jor.20640]

63 **Lopes MM**, Lawson W, Scott T, Keir PJ. Tendon and nerve excursion in the carpal tunnel in healthy and CTD wrists. *Clin Biomech (Bristol, Avon)* 2011; **26**: 930-936 [PMID: 21550703 DOI: 10.1016/j.clinbiomech.2011.03.014]

64 **Yoshii Y**, Zhao C, Henderson J, Zhao KD, An KN, Amadio PC. Velocity-dependent changes in the relative motion of the subsynovial connective tissue in the human carpal tunnel. *J Orthop Res* 2011; **29**: 62-66 [PMID: 20607819 DOI: 10.1002/jor.21181]

65 **Armstrong TJ**, Castelli WA, Evans FG, Diaz-Perez R. Some histological changes in carpal tunnel contents and their biomechanical implications. *J Occup Med* 1984; **26**: 197-201 [PMID: 6716187]

66 **Osamura N**, Zhao C, Zobitz ME, An KN, Amadio PC. Evaluation of the material properties of the subsynovial connective tissue in carpal tunnel syndrome. *Clin Biomech (Bristol, Avon)* 2007; **22**: 999-1003 [PMID: 17822815 DOI: 10.1016/j.clinbiomech.2007.07.009]

67 **Manske PR**, Lesker PA. Palmar aponeurosis pulley. *J Hand Surg Am* 1983; **8**: 259-263 [PMID: 6875224]

68 **Doyle JR**. Anatomy and function of the palmar aponeurosis pulley. *J Hand Surg Am* 1990; **15**: 78-82 [PMID: 2299172]

69 **Phillips C**, Mass D. Mechanical analysis of the palmar aponeurosis pulley in human cadavers. *J Hand Surg Am* 1996; **21**: 240-244 [PMID: 8683053 DOI: 10.1016/S0363-5023(96)80107-9]

70 **Alfonso C**, Jann S, Massa R, Torreggiani A. Diagnosis, treatment and follow-up of the carpal tunnel syndrome: a review. *Neurol Sci* 2010; **31**: 243-252 [PMID: 20145967 DOI: 10.1007/s10072-009-0213-9]

71 **LeBlanc KE**, Cestia W. Carpal tunnel syndrome. *Am Fam Physician* 2011; **83**: 952-958 [PMID: 21524035]

72 **Katz JN**, Stirrat CR, Larson MG, Fossel AH, Eaton HM, Liang MH. A self-administered hand symptom diagram for the diagnosis and epidemiologic study of carpal tunnel syndrome. *J Rheumatol* 1990; **17**: 1495-1498 [PMID: 2273490]

73 **D'Arcy CA**, McGee S. The rational clinical examination. Does this patient have carpal tunnel syndrome? *JAMA* 2000; **283**: 3110-3117 [PMID: 10865306]

74 **MacDermid JC**, Wessel J. Clinical diagnosis of carpal tunnel syndrome: a systematic review. *J Hand Ther* 2004; **17**: 309-319 [PMID: 15162113 DOI: 10.1197/j.jht.2004.02.015]

75 **Wormser P**. [Hallucinations and suppressor zones]. *Monatsschr Psychiatr Neurol* 1950; **119**: 340-346 [PMID: 15423368]

76 **Ahn DS**. Hand elevation: a new test for carpal tunnel syndrome. *Ann Plast Surg* 2001; **46**: 120-124 [PMID: 11216604]

77 **Katz JN**, Larson MG, Sabra A, Krarup C, Stirrat CR, Sethi R, Eaton HM, Fossel AH, Liang MH. The carpal tunnel syndrome: diagnostic utility of the history and physical examination findings. *Ann Intern Med* 1990; **112**: 321-327 [PMID: 2306060]

78 **Priganc VW**, Henry SM. The relationship among five common carpal tunnel syndrome tests and the severity of carpal tunnel syndrome. *J Hand Ther* 2003; **16**: 225-236 [PMID: 12943125]

79 **Werner RA**, Andary M. Carpal tunnel syndrome: pathophysiology and clinical neurophysiology. *Clin Neurophysiol* 2002; **113**: 1373-1381 [PMID: 12169318]

80 **Sunderland S**. The nerve lesion in the carpal tunnel syndrome. *J Neurol Neurosurg Psychiatry* 1976; **39**: 615-626 [PMID: 993794]

81 **Salerno DF**, Franzblau A, Werner RA, Bromberg MB, Armstrong TJ, Albers JW. Median and ulnar nerve conduction studies among workers: normative values. *Muscle Nerve* 1998; **21**: 999-1005 [PMID: 9655117]

82 **Padua L**, Lo Monaco M, Padua R, Gregori B, Tonali P. Neurophysiological classification of carpal tunnel syndrome: assessment of 600 symptomatic hands. *Ital J Neurol Sci* 1997; **18**: 145-150 [PMID: 9241561]

83 **Witt JC**, Hentz JG, Stevens JC. Carpal tunnel syndrome with normal nerve conduction studies. *Muscle Nerve* 2004; **29**: 515-522 [PMID: 15052616 DOI: 10.1002/mus.20019]

84 **Spinner RJ**, Bachman JW, Amadio PC. The many faces of carpal tunnel syndrome. *Mayo Clin Proc* 1989; **64**: 829-836 [PMID: 2671521]

85 **Buchberger W**. Radiologic imaging of the carpal tunnel. *Eur J Radiol* 1997; **25**: 112-117 [PMID: 9283839]

86 **Bleecker ML**, Agnew J. New techniques for the diagnosis of carpal tunnel syndrome. *Scand J Work Environ Health* 1987; **13**: 385-388 [PMID: 3324318]

87 **Merhar GL**, Clark RA, Schneider HJ, Stern PJ. High-resolution computed tomography of the wrist in patients with carpal tunnel syndrome. *Skeletal Radiol* 1986; **15**: 549-552 [PMID: 3775421]

88 **Schmitt R**, Lucas D, Buhmann S, Lanz U, Schindler G. [Computed tomographic findings in carpal tunnel syndrome]. *Rofo* 1988; **149**: 280-285 [PMID: 2843958 DOI: 10.1055/s-2008-1048342]

89 **Nakamichi K**, Tachibana S. The use of ultrasonography in detection of synovitis in carpal tunnel syndrome. *J Hand Surg Br* 1993; **18**: 176-179 [PMID: 8501366]

90 **El Miedany YM**, Aty SA, Ashour S. Ultrasonography versus nerve conduction study in patients with carpal tunnel syndrome: substantive or complementary tests? *Rheumatology (Oxford)* 2004; **43**: 887-895 [PMID: 15100417]

91 **Britz GW**, Haynor DR, Kuntz C, Goodkin R, Gitter A, Kliot M. Carpal tunnel syndrome: correlation of magnetic resonance imaging, clinical, electrodiagnostic, and intraoperative findings. *Neurosurgery* 1995; **37**: 1097-1103 [PMID: 8584150]

92 **Khalil C**, Hancart C, Le Thuc V, Chantelot C, Chechin D, Cotten A. Diffusion tensor imaging and tractography of the median nerve in carpal tunnel syndrome: preliminary results. *Eur Radiol* 2008; **18**: 2283-2291 [PMID: 18418602 DOI: 10.1007/s00330-008-0971-4]

93 **Mesgarzadeh M**, Schneck CD, Bonakdarpour A, Mitra A, Conaway D. Carpal tunnel: MR imaging. Part II. Carpal tunnel syndrome. *Radiology* 1989; **171**: 749-754 [PMID: 2541464 DOI: 10.1148/radiology.171.3.2541464]

94 **Does MD**, Snyder RE. Multiexponential T2 relaxation in degenerating peripheral nerve. *Magn Reson Med* 1996; **35**: 207-213 [PMID: 8622585]

95 **Cudlip SA**, Howe FA, Clifton A, Schwartz MS, Bell BA. Magnetic resonance neurography studies of the median nerve before and after carpal tunnel decompression. *J Neurosurg* 2002; **96**: 1046-1051 [PMID: 12066905 DOI: 10.3171/jns.2002.96.6.1046]

96 **Jarvik JG**, Yuen E, Haynor DR, Bradley CM, Fulton-Kehoe D, Smith-Weller T, Wu R, Kliot M, Kraft G, Wang L, Erlich V, Heagerty PJ, Franklin GM. MR nerve imaging in a prospective cohort of patients with suspected carpal tunnel syndrome. *Neurology* 2002; **58**: 1597-1602 [PMID: 12058085]

97 **Pasternack II**, Malmivaara A, Tervahartiala P, Forsberg H,

Vehmas T. Magnetic resonance imaging findings in respect to carpal tunnel syndrome. *Scand J Work Environ Health* 2003; **29**: 189-196 [PMID: 12828388]
98 **Stevens JC**. AAEM minimonograph #26: the electrodiagnosis of carpal tunnel syndrome. American Association of Electrodiagnostic Medicine. *Muscle Nerve* 1997; **20**: 1477-1486 [PMID: 9390659]
99 **Lijmer JG**, Mol BW, Heisterkamp S, Bonsel GJ, Prins MH, van der Meulen JH, Bossuyt PM. Empirical evidence of design-related bias in studies of diagnostic tests. *JAMA* 1999; **282**: 1061-1066 [PMID: 10493205]
100 **Bak L**, Bak S, Gaster P, Mathiesen F, Ellemann K, Bertheussen K, Zeeberg I. MR imaging of the wrist in carpal tunnel syndrome. *Acta Radiol* 1997; **38**: 1050-1052 [PMID: 9394668]
101 **Soccetti A**, Raffaelli P, Giovagnoni A, Ercolani P, Mercante O, Pelliccioni G. MR imaging in the diagnosis of carpal tunnel syndrome. *Ital J Orthop Traumatol* 1992; **18**: 123-127 [PMID: 1399527]
102 **Shi Q**, MacDermid JC. Is surgical intervention more effective than non-surgical treatment for carpal tunnel syndrome? A systematic review. *J Orthop Surg Res* 2011; **6**: 17 [PMID: 21477381 DOI: 10.1186/1749-799X-6-17]
103 **Kumnerddee W**, Kaewtong A. Efficacy of acupuncture versus night splinting for carpal tunnel syndrome: a randomized clinical trial. *J Med Assoc Thai* 2010; **93**: 1463-1469 [PMID: 21344811]
104 **Maddali Bongi S**, Signorini M, Bassetti M, Del Rosso A, Orlandi M, De Scisciolo G. A manual therapy intervention improves symptoms in patients with carpal tunnel syndrome: a pilot study. *Rheumatol Int* 2013; **33**: 1233-1241 [PMID: 23064542 DOI: 10.1007/s00296-012-2507-0]
105 **Nalamachu S**, Nalamasu R, Jenkins J, Marriott T. An Open-Label Pilot Study Evaluating the Effectiveness of the Heated Lidocaine/Tetracaine Patch for the Treatment of Pain Associated with Carpal Tunnel Syndrome. *Pain Pract* 2013; Epub ahead of print [PMID: 23906384 DOI: 10.1111/papr.12105]
106 **Gerritsen AA**, Scholten RJ, Assendelft WJ, Kuiper H, de Vet HC, Bouter LM. Splinting or surgery for carpal tunnel syndrome? Design of a randomized controlled trial [ISRCTN18853827]. *BMC Neurol* 2001; **1**: 8 [PMID: 11801195]
107 **Walker WC**, Metzler M, Cifu DX, Swartz Z. Neutral wrist splinting in carpal tunnel syndrome: a comparison of night-only versus full-time wear instructions. *Arch Phys Med Rehabil* 2000; **81**: 424-429 [PMID: 10768530 DOI: 10.1053/mr.2000.3856]
108 **Povlsen B**, Bashir M, Wong F. Long-term result and patient reported outcome of wrist splint treatment for Carpal Tunnel Syndrome. *J Plast Surg Hand Surg* 2014; **48**: 175-178 [PMID: 24032598 DOI: 10.3109/2000656X.2013.837392]
109 **Gerritsen AA**, Korthals-de Bos IB, Laboyrie PM, de Vet HC, Scholten RJ, Bouter LM. Splinting for carpal tunnel syndrome: prognostic indicators of success. *J Neurol Neurosurg Psychiatry* 2003; **74**: 1342-1344 [PMID: 12933954]
110 **Ono S**, Clapham PJ, Chung KC. Optimal management of carpal tunnel syndrome. *Int J Gen Med* 2010; **3**: 255-261 [PMID: 20830201]
111 **Daniel ES**, Paul S. A comparison study of the volar wrist cock-up splint and ulnar gutter splint in carpal tunnel syndrome. *Occup Ther Health Care* 2000; **12**: 79-93 [PMID: 23931649 DOI: 10.1080/J003v12n04_06]
112 **De Angelis MV**, Pierfelice F, Di Giovanni P, Staniscia T, Uncini A. Efficacy of a soft hand brace and a wrist splint for carpal tunnel syndrome: a randomized controlled study. *Acta Neurol Scand* 2009; **119**: 68-74 [PMID: 18638040 DOI: 10.1111/j.1600-0404.2008.01072.x]
113 **Manente G**, Melchionda D, Staniscia T, D'Archivio C, Mazzone V, Macarini L. Changes in the carpal tunnel while wearing the Manu® soft hand brace: a sonographic study. *J Hand Surg Eur Vol* 2013; **38**: 57-60 [PMID: 22640934 DOI: 10.1177/1753193412446112]
114 **Jenkins PJ**, Duckworth AD, Watts AC, McEachan JE. Corticosteroid injection for carpal tunnel syndrome: a 5-year survivorship analysis. *Hand (N Y)* 2012; **7**: 151-156 [PMID: 23730233 DOI: 10.1007/s11552-012-9390-8]
115 **Kamanli A**, Bezgincan M, Kaya A. Comparison of local steroid injection into carpal tunnel via proximal and distal approach in patients with carpal tunnel syndrome. *Bratisl Lek Listy* 2011; **112**: 337-341 [PMID: 21692409]
116 **Smith J**, Wisniewski SJ, Finnoff JT, Payne JM. Sonographically guided carpal tunnel injections: the ulnar approach. *J Ultrasound Med* 2008; **27**: 1485-1490 [PMID: 18809959]
117 **Martin BI**, Levenson LM, Hollingworth W, Kliot M, Heagerty PJ, Turner JA, Jarvik JG. Randomized clinical trial of surgery versus conservative therapy for carpal tunnel syndrome [ISRCTN84286481]. *BMC Musculoskelet Disord* 2005; **6**: 2 [PMID: 15656907 DOI: 10.1186/1471-2474-6-2]
118 **Carlson H**, Colbert A, Frydl J, Arnall E, Elliot M, Carlson N. Current options for nonsurgical management of carpal tunnel syndrome. *Int J Clin Rheumtol* 2010; **5**: 129-142 [PMID: 20490348 DOI: 10.2217/IJR.09.63]
119 **Karadaş O**, Omaç OK, Tok F, Ozgül A, Odabaşi Z. Effects of steroid with repetitive procaine HCl injection in the management of carpal tunnel syndrome: an ultrasonographic study. *J Neurol Sci* 2012; **316**: 76-78 [PMID: 22336701 DOI: 10.1016/j.jns.2012.01.023]
120 **Karadaş Ö**, Tok F, Akarsu S, Tekin L, Balaban B. Triamcinolone acetonide vs procaine hydrochloride injection in the management of carpal tunnel syndrome: randomized placebo-controlled study. *J Rehabil Med* 2012; **44**: 601-604 [PMID: 22674243 DOI: 10.2340/16501977-0990]
121 **Chang MH**, Ger LP, Hsieh PF, Huang SY. A randomised clinical trial of oral steroids in the treatment of carpal tunnel syndrome: a long term follow up. *J Neurol Neurosurg Psychiatry* 2002; **73**: 710-714 [PMID: 12438475]
122 **Chang MH**, Chiang HT, Lee SS, Ger LP, Lo YK. Oral drug of choice in carpal tunnel syndrome. *Neurology* 1998; **51**: 390-393 [PMID: 9710008]
123 **Nalamachu S**, Crockett RS, Gammaitoni AR, Gould EM. A comparison of the lidocaine patch 5% vs naproxen 500 mg twice daily for the relief of pain associated with carpal tunnel syndrome: a 6-week, randomized, parallel-group study. *MedGenMed* 2006; **8**: 33 [PMID: 17406167]
124 **Buchan S**, Amirfeyz R. Cochrane corner: ergonomic positioning or equipment for treating carpal tunnel syndrome. *J Hand Surg Eur Vol* 2013; **38**: 580-581 [PMID: 23704309 DOI: 10.1177/1753193413478507]
125 **Maeda Y**, Kettner N, Lee J, Kim J, Cina S, Malatesta C, Gerber J, McManus C, Im J, Libby A, Mezzacappa P, Morse LR, Park K, Audette J, Napadow V. Acupuncture-evoked response in somatosensory and prefrontal cortices predicts immediate pain reduction in carpal tunnel syndrome. *Evid Based Complement Alternat Med* 2013; **2013**: 795906 [PMID: 23843881 DOI: 10.1155/2013/795906]
126 **Khosrawi S**, Moghtaderi A, Haghighat S. Acupuncture in treatment of carpal tunnel syndrome: A randomized controlled trial study. *J Res Med Sci* 2012; **17**: 1-7 [PMID: 23248650]
127 **Piravej K**, Boonhong J. Effect of ultrasound thermotherapy in mild to moderate carpal tunnel syndrome. *J Med Assoc Thai* 2004; **87** Suppl 2: S100-S106 [PMID: 16083171]
128 **Ebenbichler GR**, Resch KL, Nicolakis P, Wiesinger GF, Uhl F, Ghanem AH, Fialka V. Ultrasound treatment for treating the carpal tunnel syndrome: randomised "sham" controlled trial. *BMJ* 1998; **316**: 731-735 [PMID: 9529407]
129 **Mintalucci DJ**, Leinberry CF. Open versus endoscopic carpal tunnel release. *Orthop Clin North Am* 2012; **43**: 431-437 [PMID: 23026458]
130 **Wongsiri S**, Suwanno P, Tangtrakulwanich B, Yuenyongviwat V, Wongsiri E. A new tool for mini-open carpal tunnel release

- the PSU retractor. *BMC Musculoskelet Disord* 2008; **9**: 126 [PMID: 18808664 DOI: 10.1186/1471-2474-9-126]
131 **Okutsu I**, Ninomiya S, Takatori Y, Ugawa Y. Endoscopic management of carpal tunnel syndrome. *Arthroscopy* 1989; **5**: 11-18 [PMID: 2706046]
132 **Ejiri S**, Kikuchi S, Maruya M, Sekiguchi Y, Kawakami R, Konno S. Short-term results of endoscopic (Okutsu method) versus palmar incision open carpal tunnel release: a prospective randomized controlled trial. *Fukushima J Med Sci* 2012; **58**: 49-59 [PMID: 22790892]
133 **Aslani HR**, Alizadeh K, Eajazi A, Karimi A, Karimi MH, Zaferani Z, Hosseini Khameneh SM. Comparison of carpal tunnel release with three different techniques. *Clin Neurol Neurosurg* 2012; **114**: 965-968 [PMID: 22421246 DOI: 10.1016/j.clineuro.2012.02.017]
134 **Yücetaş SC**, Yildirim A. Comparative results of standard open and mini open, KnifeLight instrument-assisted carpal tunnel release. *J Neurol Surg A Cent Eur Neurosurg* 2013; **74**: 393-399 [PMID: 23929411 DOI: 10.1055/s-0033-1342932]
135 **Crnković T**, Bilić R, Trkulja V, Cesarik M, Gotovac N, Kolundžić R. The effect of epineurotomy on the median nerve volume after the carpal tunnel release: a prospective randomised double-blind controlled trial. *Int Orthop* 2012; **36**: 1885-1892 [PMID: 22588692 DOI: 10.1007/s00264-012-1565-y]

P- Reviewers: Cerimagic D, Karadas O **S- Editor**: Song XX
L- Editor: Roemmele A **E- Editor**: Zhang DN

World Journal of Radiology

Submit a Manuscript: http://www.wjgnet.com/esps/
Help Desk: http://www.wjgnet.com/esps/helpdesk.aspx
DOI: 10.4329/wjr.v6.i6.301

World J Radiol 2014 June 28; 6(6): 301-312
ISSN 1949-8470 (online)
© 2014 Baishideng Publishing Group Inc. All rights reserved.

REVIEW

Neuroimaging in Huntington's disease

Flavia Niccolini, Marios Politis

Flavia Niccolini, Marios Politis, Neurodegeneration Imaging Group, Department of Clinical Neuroscience, King's College London, London SE5 8AF, United Kingdom
Flavia Niccolini, Marios Politis, Division of Brain Sciences, Department of Medicine, Hammersmith Hospital, Imperial College London, London W12 0NN, United Kingdom
Author contributions: Niccolini F collected the materials for the literature review and wrote the first draft of the manuscript; Politis M reviewed and edited this article.
Correspondence to: Marios Politis, MD, MSc, PhD, Senior Clinical Lecturer, Head of the Neurodegeneration Imaging Group, Department of Clinical Neuroscience, King's College London, 16 De Crespigny Park, London SE5 8AF, United Kingdom. marios.politis@kcl.ac.uk
Telephone: +44-207-8485682 Fax: +44-207-8480988
Received: December 11, 2013 Revised: February 28, 2014
Accepted: May 8, 2014
Published online: June 28, 2014

Abstract

Huntington's disease (HD) is a progressive and fatal neurodegenerative disorder caused by an expanded trinucleotide CAG sequence in huntingtin gene (HTT) on chromosome 4. HD manifests with chorea, cognitive and psychiatric symptoms. Although advances in genetics allow identification of individuals carrying the *HD* gene, much is still unknown about the mechanisms underlying the development of overt clinical symptoms and the transitional period between premanifestation and manifestation of the disease. HD has no cure and patients rely only in symptomatic treatment. There is an urgent need to identify biomarkers that are able to monitor disease progression and assess the development and efficacy of novel disease modifying drugs. Over the past years, neuroimaging techniques such as magnetic resonance imaging (MRI) and positron emission tomography (PET) have provided important advances in our understanding of HD. MRI provides information about structural and functional organization of the brain, while PET can detect molecular changes in the brain. MRI and PET are able to detect changes in the brains of *HD* gene carriers years ahead of the manifestation of the disease and have also proved to be powerful in assessing disease progression. However, no single technique has been validated as an optimal biomarker. An integrative multimodal imaging approach, which combines different MRI and PET techniques, could be recommended for monitoring potential neuroprotective and preventive therapies in HD. In this article we review the current neuroimaging literature in HD.

© 2014 Baishideng Publishing Group Inc. All rights reserved.

Key words: Huntington's disease; Premanifest Huntington's disease gene carriers; Functional magnetic resonance imaging; Magnetic resonance imaging; Positron emission tomography

Core tip: Huntington's disease (HD) is a hereditary and fatal neurodegenerative disorder. Although advances in genetics allow identification of individuals carrying the *HD* gene, much is still unknown about the mechanisms underlying the development of overt clinical symptoms and the transitional period between premanifestation and manifestation of the disease. Neuroimaging techniques such as magnetic resonance imaging and positron emission tomography may be a suitable biomarker for monitoring disease progression in HD and for assessing the efficacy of future disease modifying therapies. In this article, we provide an overview of the findings from neuroimaging techniques in HD.

Niccolini F, Politis M. Neuroimaging in Huntington's disease. *World J Radiol* 2014; 6(6): 301-312 Available from: URL: http://www.wjgnet.com/1949-8470/full/v6/i6/301.htm DOI: http://dx.doi.org/10.4329/wjr.v6.i6.301

INTRODUCTION

Huntington's disease (HD) is an inherited neurodegenerative disorder characterised by chorea, cognitive dysfunction and psychiatric symptoms caused by an expanded

trinucleotide CAG sequence in huntingtin gene (HTT), which is on chromosome 4[1]. HD prevalence varies by ethnic origin and different genetic profiles, in Caucasian populations of North America and Western Europe is 5.70 per 100000 whereas in Asian population is lower (0.40 per 100000)[2]. Although juvenile onset and late onset of HD are not uncommon, the disease usually appears at mid-40s, and there is an inverse correlation between age of onset and the size of the CAG repeat expansion[3]. However, subclinical changes and pathological processes are thought to precede the initiation of symptoms by several years[4,5].

HD pathology is characterised by the formation of intranuclear inclusions of mutated huntingtin in the brain. These aggregates have been shown to interact and impair the function of a number of transcription factors leading to the loss of GABAergic medium spiny neurons (MSNs) in the striatum but also in cortical areas[6,7]. Currently there is no proven biomarker for HD, no effective treatment, and the disease will eventually lead to death, typically 15-20 years following symptomatic onset[8]. Much is still unknown about the mechanisms that underlie the clinical symptoms and the rate of progression from pre-clinical signs to development of overt symptoms.

Neuroimaging techniques such as magnetic resonance imaging (MRI) and functional MRI (fMRI) have played a critical role in characterizing structural and functional changes in the brain during the asymptomatic and symptomatic stage of the disease. PET imaging, by measuring the distribution of a radionuclide (radioligand) that is introduced into the body on a biologically active molecule, is a powerful technique for investigating *in vivo* abnormalities in brain metabolism and receptor distributions[9]. This analytical imaging method has the potential to give both structural and kinetic information and in comparison with other imaging techniques, provides high sensitivity, and high spatial and temporal resolution[10]. PET with the application of different radioligands has been used to measure metabolic changes in the brain of HD several years before disease onset (Table 1). In this article, we provide an overview of the findings from neuroimaging techniques in HD.

LITERATURE RESEARCH

PubMed was searched for papers that were published before December 2013. The following key words were used in the search: "Huntington's disease", "positron emission tomography", "magnetic resonance imaging", "functional magnetic imaging". Additional papers were identified from citations in the articles found in PubMed. Only articles published in English were considered. A total number of 37 MRI and 49 PET studies were reviewed.

MRI

Structural MRI studies

The most consistent change in the HD brain is a significant progressive volumetric loss of the striatum[4,11-20]. A reduction of 50%-54% in mean putamen volume and 28%-29% in mean caudate volume has been reported in patients with mild to moderate HD[11,12]. Striatal atrophy has been also documented in early HD patients with Total Functional Capacity (TFC) scores between I-Ⅱ[14,15] and in premanifest *HD* gene carriers who were even 15-20 years before predicted disease onset[4,13,16-20]. The amount of volume loss in the striatum correlates with the age of onset, the disease duration and the CAG repeat length[14,15,21]. While motor impairment correlates with increased putamen atrophy, Mini-Mental Status Examination scores (MMSE) and cognitive assessments are inversely correlated with the amount of caudate volume loss[11,12].

Cortical volume loss has been also reported in HD patients[17-20,22,23]. Cortical thinning occurs early during the course of the disease and seems to be topographically selective proceeding from posterior to anterior cortical regions as the disease progresses[22,23]. Individual variability in regional cortical thinning may also have a role in explaining phenotypic variability. For example, HD patients with more prominent bradykinesia showed significant cortical volume loss in frontal regions including the pre-motor and supplementary motor areas compared to HD patients with chorea[23]. Additionally, regional cortical atrophy correlates with clinical measures such as TFC, Unified HD rating scale (UHDRS) and cognitive tests enhancing the role of this measurement as potential biomarker for assessing neuroprotective therapies[23]. Widespread white matter (WM) atrophy has been identified in HD patients and has been associated with longer CAG length and decline in cognitive and motor performance[24]. Changes in WM volume are detectable up to 12-15 years before the predicted onset and correlate with cognitive functions underlining the role of structural connectivity degeneration in the pathogenesis of HD[25]. Diffusion tensor imaging (DTI) studies have also reported WM tract abnormalities in premanifest *HD* gene carriers and alterations in diffusion indices were correlated with cognitive performance[26-28]. Dumas and coworkers[28] have found abnormal WM connections of the sensori-motor cortex, which correlated with the 5-year probability for symptomatic conversion.

TRACK-HD is a multicentre longitudinal study, which focused in identifying sensitive and reliable biomarkers in premanifest *HD* gene carriers and early HD patients[17-20]. Four groups were enrolled in TRACK-HD: 120 premanifest *HD* gene carriers which were subdivided in pre-HD A and pre-HD B according to the proximity to predicted disease onset (pre-HD A > 10.8 years; pre-HD B < 10.8 years), and 123 early HD patients subdivided in two groups according to the TFC scores (HD stage Ⅰ, HD stage Ⅱ). At 12 months follow-up significantly increased total brain volume atrophy rates were reported in both premanifest *HD* gene carriers and early HD patients. Caudate and putamen volume was reported reduced by 1.4% to 4.5% compared with baseline in premanifest and early HD group. Atrophy of WM was also increased in all groups[18]. Over 24 mo, greater increases

Table 1 Key positron emission tomography imaging studies in Huntington's disease

Ref.	Subjects	PET radiopharmaceutical	Main findings
Dopaminergic system			
Ginovart *et al*[56], 1997	5 HD patients 5 HCs	^{11}C-b-CIT ^{11}C-SCH23390 ^{11}C-raclopride	50% decrease in striatal dopamine transporter (DAT) binding. 40% decrease in striatal D1 and D2 receptors binding. D1 and D2 binding in the striatum was significantly associated with the duration of symptoms Reduced D1 receptors binding in the temporal cortex
Bohnen *et al*[57], 2000	19 HD patients 64 HCs	^{11}C-DTBZ	Reduced nigrostriatal density of VMAT2 (caudate: 33%, putamen: 56%-75%)
Sedvall *et al*[58], 1994	5 HD patients 1 premanifest *HD* gene carrier 5 HCs	^{11}C-SCH 23390	75% reduction in striatal D1 receptor density in HD patients D1 binding in the premanifest *HD* gene carrier was in the lower range of the HCs
Turjanski *et al*[55], 1995	10 HD patients 9 HCs for ^{11}C-raclopride and 6 HCs for ^{11}C-SCH 23390	^{11}C-SCH 23390 ^{11}C-raclopride	Parallel reduction of striatal D1 and D2 receptor binding (31%-39%) with greater loss of mean striatal D1 and D2 binding in the akinetic-rigid patients than those choreic patients without rigidity
Lawrence *et al*[60], 1998	17 premanifest *HD* gene carriers	^{11}C-SCH 23390 ^{11}C-raclopride	Correlation between striatal D1 and D2 receptors binding and cognitive performance
Pavese *et al*[61], 2003	12 HD patients HCs from previous studies	^{11}C-raclopride	4.8% annual reduction in striatal D2 receptor binding D2 reduction receptor density in extrastriatal regions including amygdala, temporal and frontal cortex
Andrews *et al*[64], 1999	9 premanifest *HD* gene carriers 4 HD patients 7 HCs 3 subjects at risk for HD	^{11}C-SCH 23390 ^{11}C-raclopride	Mean annual loss of D1 and D2 binding of 2% and 4% respectively in the group of asymptomatic *HD* gene carriers Mean annual loss of D1 binding of 5% and D2 binding of 3% in symptomatic HD patients UHDRS motor scores and TFC correlated with PET measures of striatal dopamine receptor in both groups Premanifest *HD* gene carriers with active progression had an increased mean annual loss of D1 and D2 receptor binding (5% and 6.5% respectively)
Pavese *et al*[62], 2010	16 HD patients 11 premanifest *HD* gene carriers HCs from previous studies	^{11}C-raclopride	62.5% of symptomatic HD patients and 54.5% of premanifest carriers showed cortical reductions in D2 binding HD patients with decreased cortical D2 binding had worse scores on neuropsychological tests assessing attention and executive functions than subjects without cortical dopamine dysfunction
Antonini *et al*[66], 1998	10 premanifest gene carriers 8 HD patients	^{11}C-raclopride	Correlation between CAG repeat length and the estimated percentage loss of striatal D2 binding after age correction in premanifest *HD* gene carriers and HD patients Rate of disease progression is faster during the earlier asymptomatic stages of the disease
Brain activation and metabolism			
Antonini *et al*[65], 1996	10 premanifest *HD* gene carriers 8 HD patients HCs from previous studies	^{18}F-FDG ^{11}C-raclopride	Annual loss of 2.3% in striatal glucose metabolism and 6.3% annual decline in D2 receptor binding
Kuwert *et al*[75], 1990	23 HD patients 21 HCs	^{18}F-FDG	Decreases of caudate and regional cortical metabolism correlated with cognitive decline
Ciarmiello *et al*[79], 2006	24 premanifest *HD* gene carriers 47 HD patients 30 HCs	^{18}F-FDG	Significant decrease in glucose uptake in the cortex (frontal and temporal lobes) and striatum in both premanifest *HD* gene carriers and HD patients Striatal and cortical hypometabolism in premanfest *HD* gene carriers precedes neuronal loss
Ciarmiello *et al*[80], 2012	43 premanifest *HD* gene carriers	^{18}F-FDG	Premanifest *HD* gene carriers who phenoconverted after five years from the PET scan had a mean glucose uptake in the caudate significantly lower than the those who remained symptom-free after five years
Weeks *et al*[83], 1997	7 HD patients 7 HCs	$H_2{}^{15}O$	Impaired activation of the striatum and its frontal motor projection areas during motor tasks such as paced joystick movements
Tang *et al*[87], 2013	12 premanifest *HD* gene carriers 12 HCs	^{18}F-FDG ^{11}C-raclopride	Network analysis showed a significant spatial covariance pattern characterized by progressive changes in striato-thalamic and cortical metabolic activity network activity increased linearly over 7 yr and was not influenced by intercurrent phenoconversion
Neuroinflammation and activated microglia			
Pavese *et al*[99], 2006	11 HD patients 10 HCs	^{11}C-PK11195 ^{11}C-raclopride	Significant microglial activation in the striatum and cortical regions of HD patients Striatal ^{11}C-PK11195 binding correlates with loss of striatal dopamine D2 binding

Tai *et al*[100], 2007	11 premanifest *HD* gene carriers 10 HCs	^{11}C-PK11195 ^{11}C-raclopride	Striatal ^{11}C-PK11195 binding correlated with UHDRS scores Increased striatal and cortical microglial activation in premanifest *HD* gene carriers Higher striatal ^{11}C-PK11195 binding correlated with lower striatal D2 binding
Politis *et al*[101], 2011	8 premanifest *HD* gene carriers 8 HCs (^{11}C-raclopride) 8 HCs (^{11}C-PK11195)	^{11}C-PK11195 ^{11}C-raclopride	Increased levels of activated microglia in areas of the striatum associated with cognition and other areas related to cognitive function Levels of microglial activation correlated with clinical scales of disease severity and motor dysfunction and with a higher probability of HD onset over the next 5 yr
Cannabinoid system			
Van Laere *et al*[111], 2010	20 HD patients 14 HCs	^{18}FMK-9470	Decrease of CB1 availability throughout the gray matter of the cerebrum, cerebellum, and brain stem in HD patients.

PET: Positron emission tomography; HD: Huntington's disease.

in caudate and putamen atrophy were observed in all four subgroups. Higher rates of whole brain and grey matter (GM) loss were reported in pre-HD B, HD-I and HD-Ⅱ; whereas in the pre-HD A GM atrophy was confined to the striatum. Interestingly, WM atrophy around the striatum and within the corpus callosum and posterior WM tract was observed even in the earliest premanifest stage[19]. At 36 mo, early HD patients showed further significant increases in whole brain, caudate, putamen and GM atrophy and these measures were strongly associated to TFC decline. Although in pre-HD A group increased rates of whole brain, striatal and WM atrophy were observed, these were not accompanied by progressive worsening of motor and cognitive performance. On the contrary, pre-HD B showed higher rates of brain structural loss compared to pre-HD A group and these were associated with significant decline in several motor and cognitive tests. Furthermore, striatal and GM volume measures were sensitive predictors of subsequent clinical diagnosis of HD in the pre-HD B group[20]. Taken together, these findings suggest that MRI measures are able to track pathology in premanifest and manifest *HD* gene carriers and could be useful for the designing of future clinical trials.

Functional MRI studies

There is growing evidence that the severity of clinical manifestations in HD does not depend only on neuronal loss but also on neuronal dysfunction and circuitry reorganization, and these processes may occur at an early stage of the disease, possibly prior to neurodegeneration. Functional neuroimaging approaches such as functional MRI (fMRI) provide a dynamic images of the brain aiding to elucidate neural activity by measuring haemodynamic response (blood flow) of neural activation. Data from manifest HD patients have shown reduced task-activation in several subcortical and cortical regions as well as increased activation in different cortical areas, which were interpreted as a compensatory mechanism for task performances[29-34]. Interestingly, in premanifest *HD* gene carriers further from disease onset increased activation in several brain regions was observed, whereas premanifest *HD* gene carriers closer to disease onset showed reduced activation in the striatum[35-38]. Using fMRI and a group independent component analysis, Unschuld and colleagues[39] investigated networks of functional connectivity while performing a Stroop colour-naming task in both healthy controls and premanifest *HD* gene carriers and correlated with depressive symptoms. Stroop related activity of the ventromedial prefrontal cortex was more significantly correlated with depressive symptoms in premanifest *HD* gene carriers than healthy controls. This correlation was stronger in the premanifest HD subgroup with CAG repeat length greater than 42[39]. Using a Tower of London fMRI task, the same group found significantly reduced functional coupling between the medial prefrontal cortex area and the left premotor cortex in a group of premanifest HD gene carriers and early manifest HD subjects[40]. These findings suggest that impaired brain network connectivity reflects cognitive and mood dysfunction in HD subject even at the earlier stage of the disease. Recently, studies have been focused in investigating functional brain connectivity patterns at rest with fMRI (resting state fMRI). This approach has the potential to give insight into functional changes without the interference of cognitive ability to perform a given task[41,42]. Resting state fMRI data have shown intrinsic reductions in functional connectivity in both premanifest and manifest *HD* gene carriers[43-45]. In premanifest HD gene carriers reduced blood-oxygen-level-dependent (BOLD) synchrony was observed between the caudate and premotor cortex[46]. Using a method that measures changes in synchrony in BOLD signal amplitude and across space, Poudel and coworkers[44] have found several abnormal networks in both premanifest and manifest HD subjects. For example, they have reported a decreased resting state synchronization in the sensori-motor network of premanifest *HD* gene carriers, and interestingly, the level of synchrony was associated with motor performance as measured by speeded self-paced tapping[44]. Overall these findings show abnormal functional network connectivity in both premanifest and manifest HD, suggesting that resting state fMRI may be useful in measuring early neuronal dysfunction and for monitoring progression of the disease.

Neurovascular alterations have been also found in premanifest *HD* gene carriers. Cortical arteriolar cerebral blood volume (CBV_a) was significantly elevated in pre-

manifest *HD* gene carriers compared to normal controls and correlated with genetic measures such as the CAG-age product score and the estimated years to onset[47]. Metabolic brain changes may also occur in premanifest *HD* gene carriers and they may precede structural brain changes[48]. N-acetylaspartate (NAA) and glutamate levels were decreased in the posterior cingulate cortex of 12 premanifest *HD* gene carriers and they correlated with cognitive decline as measured with the Montreal Cognitive Assessment[47]. Neurovascular alterations and metabolic brain changes occurs before substantial brain atrophy suggesting that they may be used as potential biomarker for clinical and therapeutic future studies.

PET

Dopaminergic system

Altered dopamine signalling may play a key role in the pathogenesis of HD[49,50]. In particular, striatal MSNs expressing dopamine receptors are primarily affected in HD, whereas presynaptic dopaminergic nerve terminals are relatively spared[51]. PET studies in premanifest and manifest *HD* gene carriers have shown severe involvement of the postsynaptic dopaminergic system, whereas the dopaminergic nerve terminals seem to be less affected[52-55]. An ^{18}F-fluorodopa case-study did not demonstrate diminished striatal dopamine synthesis capacity suggesting an intact nigrostriatal pathway[52]. However, Ginovart and coworker[56], using PET with ^{11}C-b-CIT, have found a 50% decrease in striatal dopamine transporter (DAT) binding. In line with this finding, nigrostriatal density of the type-2 vesicular monoamine transporter (VMAT2) was found reduced in HD patients[57]. It still remains unclear whether degeneration of nigrostriatal dopaminergic neurons or presynaptic terminal dysfunction takes place in HD.

Investigations of postsynaptic dopaminergic systems, specifically the role of D1 and D2 receptors, which are highly expressed in MSNs, have shown reduced receptor densities and activity in the striatum of HD patients even at the early stage of the disease. The radioligand ^{11}C-SCH23390 is a selective antagonist of D1 receptors while ^{11}C-raclopride is a selective reversible antagonist of D2 receptors. Striatal D1-dopamine receptor density was found reduced by 75% in five HD patients with mild to moderate disease compared to a group of healthy controls[58]. Additionally, one premanifest *HD* gene carrier showed D1 binding in the lower range of the control subjects[58]. Turjanski and colleagues[55] have studied 10 non-neuroleptic treated patients with HD with either the choreic or the akinetic-rigid predominant phenotypes of the disease. They found severe parallel reduction of striatal D1 and D2 receptor binding with greater loss of mean striatal D1 and D2 binding in the akinetic-rigid patients than those choreic patients without rigidity[55]. However, there were no significant correlations between D1 and D2 striatal receptor binding and the duration of symptoms. Mean ^{11}C-SCH23390 and ^{11}C-raclopride binding was found to be reduced by 40% in the striatum of five patients with HD[56]. The degree of the decrease in D1 and D2 binding in the striatum was significantly associated with the duration of symptoms indicating that these two receptors may be reliable quantitative markers for monitoring disease progression[56]. Moreover, a reduction in D1 receptor binding was found also in the temporal cortex suggesting that dopaminergic abnormalities occur in cortical areas and may play a role in the development of cognitive dysfunction observed in HD[56]. Specifically, striatal D1 and D2 receptor density showed strong relationships with performance in several tasks assessing executive function, visuospatial ability, episodic memory, verbal fluency, perceptual speed and reasoning in a group of five HD patients[59]. Thus, cortico-striatal and/or thalamo-cortical circuity may be associated with cognitive impairment in HD[59]. A correlation between striatal D1 and D2 receptors binding, but mainly D2, and cognitive performance was found also in 17 premanifest *HD* gene carriers, in whom both striatal dopamine receptor levels and cognitive performance were lower in the subjects closer to the predicted disease onset[60]. Using ^{11}C-raclopride PET and statistical parametric mapping, Pavese and coworkers[61] have found a reduction in D2 receptor density in cortical regions of symptomatic HD patients, which were also evident in frontal and/or temporal regions in 55% of premanifest *HD* gene carriers[62], suggesting that changes in cortical D2 receptor availability might be an early event in HD pathophysiology. Van Oostrom and colleagues[63] have also reported a reduction in striatal D2 receptor availability in 50% of premanifest *HD* gene carriers and these reductions correlated with increases in cumulative disease load as measured by disease burden (CAG index).

Clinically manifested HD patients have been shown to have constant loss of D2 receptor availability at around 5% per year in striatal and extrastriatal regions including frontal and temporal cortex, though no correlation between changes in UHDRS motor scores and reductions in striatal binding were observed[61]. Longitudinal ^{11}C-raclopride PET studies in premanifest *HD* gene carriers have reported rates of decline from 4%[64] up to 6.3%[65]. Andrews and coworkers[64] investigated striatal dopamine D1 and D2 receptor binding over a follow-up period of 40 mo in nine premanifest *HD* gene carriers and four symptomatic HD patients. They reported a mean annual loss of D1 and D2 binding of 2% and 4% respectively in the group of premanifest *HD* gene carriers and a mean annual loss of D1 binding of 5% and D2 binding of 3% in symptomatic HD patients[64]. Additionally, UHDRS motor scores and TFC correlated with PET measures of striatal dopamine receptor in both groups. Interestingly, premanifest *HD* gene carriers who demonstrated active progression had an increased mean annual loss of D1 and D2 receptor binding (5% and 6.5% respectively). Thus, the authors conclude that PET measures of striatal D1 and D2 dopamine binding may be used to identify asymptomatic *HD* gene carriers who are actively

progressive[64]. A reduction in the striatal dopamine D2 binding, in particular in the putamen, correlates weakly with the increasing probability of symptomatic conversion within 5 years, as calculated by an age and CAG repeat based model[51]. Although, putaminal D2 binding correlated with predicted time to disease onset, the rate of change of D2 receptor changes were not increased around the onset of HD symptoms[51]. A cross-sectional study by Antonini and colleagues[66] indicated that striatal degeneration in HD patients might proceed in a non-linear fashion. They found a correlation between CAG repeat length and the estimated percentage loss of striatal D2 binding after age correction in premanifest *HD* gene carriers and symptomatic HD patients. While CAG repeat length influenced the rate of disease progression, the slopes of the correlation for asymptomatic mutation carriers and patients were significantly different, implying that the rate of disease progression is faster during the earlier asymptomatic stages of the disease[66]. These data suggest that striatal D2 measures are more sensitive in premanifest HD than later in the disease.

While the loss of striatal dopamine D2 receptors is well known, few studies have addressed the extrastriatal D2 receptor distribution in patients with HD. Statistical parametric mapping of ^{11}C-raclopride binding in patients with HD suggest a loss of cortical dopamine D2 receptors in symptomatic HD patients[61,62]. A significant reduction in postsynaptic dopamine D2 receptor binding was also found in the hypothalamus of nine premanifest HD patients and in 10 asymptomatic *HD* gene carriers[67]. These findings suggest that hypothalamic dysfunction occurs early during the course of the disease and may be responsible for the development of commonly reported nonmotor symptoms in HD including progressive weight loss, alterations in sexual behaviour and disturbances in the wake-sleep cycle[67].

Using PET with ^{11}C-FLB457, a radioligand with high affinity for dopamine D2 receptor, Esmaeilzadeh and coworkers[68] have investigated density of dopamine D2 receptors in extrastriatal brain regions in patients with mild to moderate HD. They found that unlike from striatum, D2 receptors seem to be relatively spared in the brain extrastriatal regions in HD patients suggesting that D2 receptor binding in brain regions outside the striatum may not be a reliable biomarker in HD[68].

Moreover, PET with D1 and D2 receptor radioligands has been used to assess the efficacy of restorative therapy. In 1998, a multicentre open label pilot study was designed to evaluate the safety and efficacy of bilateral fetal striatal transplantation in HD[69]. Five HD patients were transplanted and followed up clinically and with PET over a 3-10 year postoperative period[70,71]. No significant differences were found over time between patients, grafted and non-grafted on the UHDRS and striatal D1 and D2 binding suggesting that there was no obvious surviving striatal graft tissue[70,71].

Brain activation and metabolism

Measurements of cerebral blood flow and glucose metabolism could serve as an index of neuronal integrity and functional state of the synapse[72,73]. Striatal glucose hypometabolism and regional reductions in cortical glucose have been identified in HD patients and have been found to correlate with motor and cognitive symptoms[65,74,75]. Specifically, decreases of caudate and regional cortical metabolism correlated with cognitive decline[75,76], whereas striatal hypometabolism was associated with motor deficits and reduced TFC[77]. Striatal and cortical hypometabolism has been also found in premanifest *HD* gene carriers to precede neuronal loss[78-80]. A recent ^{18}F-FDG PET study has shown that premanifest *HD* gene carriers who became symptomatic after five years from the PET scan had a mean glucose uptake in the caudate significantly lower than those who did not convert, and this difference was independent of mutation size[80]. These findings suggest that reduced glucose levels may be contribute to the time of HD onset. In a combined ^{18}F-FDG and ^{11}C-raclopride longitudinal study, premanifest *HD* gene carriers showed an annual loss of 2.3% in striatal glucose metabolism and 6.3% annual decline in D2 receptor binding[65]. These findings suggest that glucose metabolism is a less sensitive marker of disease progression compared to ^{11}C-raclopride[65]. On the other hand, decreased cortical metabolism in the early stage of HD is indicative of rapid progression[81]. Indeed, cortical metabolism in the frontotemporal and parietal cortices was significantly lower in early HD subjects with faster progression of the disease as measured with the UHDRS and Independence Scale[81].

PET with $H_2{}^{15}O$ has been used to investigate changes of motor-associated cortical activation in HD[82,83]. During motor tasks such as paced joystick movements or sequential finger-to thumb opposition, HD patients showed impaired activation of the striatum and its frontal motor projection areas[82,83] along with enhanced activity of the parietal areas[82] and insular areas[83]. These findings suggest that the loss of MSNs in the striatum leads to impairment of the basal ganglia-thalamo-cortical motor output and may induce a compensatory recruitment of additional accessory motor pathways[82,83]. Moreover, different patterns of brain activation have been showed in HD patients during word generation task[84]. HD patients showed decreased cerebral blood flows in the anterior cingulate and the inferior frontal gyri, which are important in lexical selection and a compensatory activation of the left supramarginal gyrus and the right inferior frontal gyrus, suggesting that compensatory language strategies are present in HD[84].

^{18}F-FDG PET imaging and network approaches have been used to identify spatial covariance patterns in premanifest HD[85-87]. A cross-sectional analysis of metabolic changes from premanifest *HD* gene carriers and healthy controls, has reported a reproducible disease related pattern, characterized by relative bilateral increases in thalamic, occipital, and cerebellar glucose metabolism associated with bilateral decreases in striatal metabolism, which discriminated between the HD and healthy control groups[86]. However, this pattern in *HD* gene carriers

did not show consistent changes over time, thus limiting its utility as a network biomarker of preclinical disease progression[86]. Recently, Tang and coworkers[87] demonstrated the feasibility of network-based approach by using longitudinal metabolic imaging data from premanifest HD carriers to identify and a distinct spatial covariance pattern associated with disease progression. Changes in pattern expression over a seven years period were used to quantify the rate of progression in the preclinical period[87]. They found a significant spatial covariance pattern characterized by progressive changes in striato-thalamic and cortical metabolic activity which increased linearly over 7 years and was not influenced by symptomatic conversion[87]. Additionally, premanifest *HD* gene carriers which showed further increases in metabolic network activity at baseline (> 2 SD above the normal mean) had a greater risk of symptomatic conversion in the following 5-year period[87]. These findings suggest that metabolic network measurements may provide a sensitive tool for evaluating disease progression prior to clinical diagnosis.

Measures of glucose brain metabolism have been used to assess the restoration of striato-cortical function in five HD patients who underwent bilateral striatal transplantation[88,89]. In 2-year follow-up of these five patients, Gaura and colleagues[89] reported that the three patients, who showed clinical improvement or stabilization, had increased in striatal/cortical glucose metabolic rate, which is suggestive of restoration of function of striatal-cortical connections. Conversely, findings from NEST-UK multicentre study failed to show significant change in ^{18}F-FDG uptake over 2 years of follow-up[70]. Thus, the ability of bilateral striatal transplantation to restore striato-cortical pathways remains to be elucidated.

Neuroinflammation and activated microglia

Recent evidence suggests that microglial activation plays a role in the pathogenesis of HD[90,91]. Microglia constitute about 10% of the total brain cell population, and represent the main immunocompetent phagocytic cells in the central nervous system[92]. Although microglial activation is unlikely to initiate neuronal death, it could contribute to the neurodegenerative processes[93,94]. Indeed, upon exposure to neuronal insults such the presence of abnormal huntingtin protein aggregations, microglia become activated and release pro-inflammatory cytokines (*e.g.*, TNF-α and IL-1β). These cytokines in turn cause further activation of microglia, resulting in a self-propagating inflammatory cascade, which may lead to neuronal death. Microglial activation upregulates the expression of the 18 kDa translocator protein (TSPO) which is involved in the release of proinflammatory cytokines during inflammation and is present at very low levels in the normal healthy CNS[95,96]. The upregulation of TSPO expression can be detected *in vivo* with PET and selective radioligands such as ^{11}C-PK11195[97,98]. Using PET with ^{11}C-PK11195, Pavese and coworkers[99] have found significant microglial activation in the striatum and cortical regions of symptomatic HD patients, and reported that striatal PK binding correlates with loss of striatal dopamine D2 binding as measured with ^{11}C-raclopride PET. Additionally, striatal ^{11}C-PK11195 binding correlated with clinical severity as measured with the UHDRS[99]. In premanifest *HD* gene carriers ^{11}C-PK11195 binding was found to be also increased in striatum and cortical regions compared to a group of normal controls, and higher striatal ^{11}C-PK11195 binding correlated with lower striatal D2 binding[100]. These findings suggest that early and widespread microglial activation occurs in premanifest *HD* gene carriers and it is associated with subclinical striatal neuronal loss of dopamine D2 receptor binding, indicating a potential role of activated microglia in HD pathogenesis.

A more recent multimodal imaging study using MRI, ^{11}C-PK11195 and ^{11}C-raclopride PET, has showed increased levels of activated microglia in several brain areas across *HD* gene carriers who were either premanifest or manifested patients[101]. Of particular interest, high levels of activated microglia were observed in the associative part of the striatum, which is involved in cognitive function. High levels of microglial activation in the associative striatum and in the brain regions related to cognitive function correlated with a higher probability of symptomatic HD onset over the next 5 years in the group of premanifest *HD* gene carriers[101]. These findings highlighted the role of immune response in the pathophysiology and clinical expression of HD.

Cannabinoid system

Dysregulation of the endocannabinoid system may play a critical role in the pathogenesis of HD. The type 1 cannabinoid receptors (CB1R) are expressed in the basal ganglia, mainly in the GABA-ergic striatal MSNs expressing D1 and D2 receptors and are a key modulator of synaptic transmission in the brain[102-104]. Evidences from animal models of HD and postmortem tissue of HD brain have shown that decreased levels of CB1R and CB1 messenger RNA[105-107]. Recently, in vivo imaging of CB1R has become feasible using PET with ^{18}FMK-9470[108] and ^{11}C-MePPEP[109,110]. Using PET with ^{18}FMK-9470, Van Laere and coworkers[111] have investigated the levels of CB1R in the brain of 20 symptomatic HD patients. They found decreased CB1R availability throughout the grey matter of the cerebrum, cerebellum, and brain stem in HD patients. Further studies of CB1R system in premanifest *HD* gene carriers are expected in order to further understand the role of this system in the pathophysiology of HD.

CONCLUSION

Currently, there are no therapies able to slow down progression in HD and symptomatic treatments such as acetylcholinesterase inhibitors have provided limited evidence of their efficacy in HD[112]. Identification of reliable biomarkers of HD progression will be important for the development and evaluation of disease-modifying treatments. Neuroimaging techniques may be a suitable biomarker for monitoring disease progression in HD

and for assessing the efficacy of future disease modifying therapies. Although MRI techniques have shown to be useful for monitoring disease progression, PET imaging is able to detect changes and specific targets early in pre-manifest HD stages. However, at this stage an integrative multimodal imaging approach, which combines different MRI and PET techniques, could be recommended.

REFERENCES

1 A novel gene containing a trinucleotide repeat that is expanded and unstable on Huntington's disease chromosomes. The Huntington's Disease Collaborative Research Group. *Cell* 1993; **72**: 971-983 [PMID: 8458085 DOI: 10.1016/0092-8674(93)90585-E]

2 **Pringsheim T**, Wiltshire K, Day L, Dykeman J, Steeves T, Jette N. The incidence and prevalence of Huntington's disease: a systematic review and meta-analysis. *Mov Disord* 2012; **27**: 1083-1091 [PMID: 22692795 DOI: 10.1002/mds.25075]

3 **Djoussé L**, Knowlton B, Hayden M, Almqvist EW, Brinkman R, Ross C, Margolis R, Rosenblatt A, Durr A, Dode C, Morrison PJ, Novelletto A, Frontali M, Trent RJ, McCusker E, Gómez-Tortosa E, Mayo D, Jones R, Zanko A, Nance M, Abramson R, Suchowersky O, Paulsen J, Harrison M, Yang Q, Cupples LA, Gusella JF, MacDonald ME, Myers RH. Interaction of normal and expanded CAG repeat sizes influences age at onset of Huntington disease. *Am J Med Genet A* 2003; **119A**: 279-282 [PMID: 12784292 DOI: 10.1002/ajmg.a.20190]

4 **Paulsen JS**, Langbehn DR, Stout JC, Aylward E, Ross CA, Nance M, Guttman M, Johnson S, MacDonald M, Beglinger LJ, Duff K, Kayson E, Biglan K, Shoulson I, Oakes D, Hayden M. Detection of Huntington's disease decades before diagnosis: the Predict-HD study. *J Neurol Neurosurg Psychiatry* 2008; **79**: 874-880 [PMID: 18096682 DOI: 10.1136/jnnp.2007.128728]

5 **Duff K**, Paulsen J, Mills J, Beglinger LJ, Moser DJ, Smith MM, Langbehn D, Stout J, Queller S, Harrington DL. Mild cognitive impairment in prediagnosed Huntington disease. *Neurology* 2010; **75**: 500-507 [PMID: 20610833 DOI: 10.1212/WNL.0b013e3181eccfa2]

6 **Davies SW**, Turmaine M, Cozens BA, DiFiglia M, Sharp AH, Ross CA, Scherzinger E, Wanker EE, Mangiarini L, Bates GP. Formation of neuronal intranuclear inclusions underlies the neurological dysfunction in mice transgenic for the HD mutation. *Cell* 1997; **90**: 537-548 [PMID: 9267033 DOI: 10.1016/S0092-8674(00)80513-9]

7 **Li SH**, Cheng AL, Zhou H, Lam S, Rao M, Li H, Li XJ. Interaction of Huntington disease protein with transcriptional activator Sp1. *Mol Cell Biol* 2002; **22**: 1277-1287 [PMID: 11839795 DOI: 10.1128/MCB.22.5.1277-1287.2002]

8 **Browne SE**, Beal MF. Oxidative damage in Huntington's disease pathogenesis. *Antioxid Redox Signal* 2006; **8**: 2061-2073 [PMID: 17034350 DOI: 10.1089/ars.2006.8.2061]

9 **Politis M**, Piccini P. Positron emission tomography imaging in neurological disorders. *J Neurol* 2012; **259**: 1769-1780 [PMID: 22297461 DOI: 10.1007/s00415-012-6428-3]

10 **Phelps ME**. Positron emission tomography provides molecular imaging of biological processes. *Proc Natl Acad Sci USA* 2000; **97**: 9226-9233 [PMID: 10922074 DOI: 10.1073/pnas.97.16.9226]

11 **Harris GJ**, Pearlson GD, Peyser CE, Aylward EH, Roberts J, Barta PE, Chase GA, Folstein SE. Putamen volume reduction on magnetic resonance imaging exceeds caudate changes in mild Huntington's disease. *Ann Neurol* 1992; **31**: 69-75 [PMID: 1531910 DOI: 10.1002/ana.410310113]

12 **Harris GJ**, Aylward EH, Peyser CE, Pearlson GD, Brandt J, Roberts-Twillie JV, Barta PE, Folstein SE. Single photon emission computed tomographic blood flow and magnetic resonance volume imaging of basal ganglia in Huntington's disease. *Arch Neurol* 1996; **53**: 316-324 [PMID: 8929153 DOI: 10.1001/archneur.1996.00550040044013]

13 **Aylward EH**, Codori AM, Barta PE, Pearlson GD, Harris GJ, Brandt J. Basal ganglia volume and proximity to onset in presymptomatic Huntington disease. *Arch Neurol* 1996; **53**: 1293-1296 [PMID: 8970459 DOI: 10.1001/archneur.1996.00550120105023]

14 **Rosas HD**, Goodman J, Chen YI, Jenkins BG, Kennedy DN, Makris N, Patti M, Seidman LJ, Beal MF, Koroshetz WJ. Striatal volume loss in HD as measured by MRI and the influence of CAG repeat. *Neurology* 2001; **57**: 1025-1028 [PMID: 11571328 DOI: 10.1212/WNL.57.6.1025]

15 **Rosas HD**, Koroshetz WJ, Chen YI, Skeuse C, Vangel M, Cudkowicz ME, Caplan K, Marek K, Seidman LJ, Makris N, Jenkins BG, Goldstein JM. Evidence for more widespread cerebral pathology in early HD: an MRI-based morphometric analysis. *Neurology* 2003; **60**: 1615-1620 [PMID: 12771251 DOI: 10.1212/01.WNL.0000065888.88988.6E]

16 **Paulsen JS**, Hayden M, Stout JC, Langbehn DR, Aylward E, Ross CA, Guttman M, Nance M, Kieburtz K, Oakes D, Shoulson I, Kayson E, Johnson S, Penziner E. Preparing for preventive clinical trials: the Predict-HD study. *Arch Neurol* 2006; **63**: 883-890 [PMID: 16769871 DOI: 10.1001/archneur.63.6.883]

17 **Tabrizi SJ**, Langbehn DR, Leavitt BR, Roos RA, Durr A, Craufurd D, Kennard C, Hicks SL, Fox NC, Scahill RI, Borowsky B, Tobin AJ, Rosas HD, Johnson H, Reilmann R, Landwehrmeyer B, Stout JC. Biological and clinical manifestations of Huntington's disease in the longitudinal TRACK-HD study: cross-sectional analysis of baseline data. *Lancet Neurol* 2009; **8**: 791-801 [PMID: 19646924 DOI: 10.1016/S1474-4422(09)70170-X]

18 **Tabrizi SJ**, Scahill RI, Durr A, Roos RA, Leavitt BR, Jones R, Landwehrmeyer GB, Fox NC, Johnson H, Hicks SL, Kennard C, Craufurd D, Frost C, Langbehn DR, Reilmann R, Stout JC. Biological and clinical changes in premanifest and early stage Huntington's disease in the TRACK-HD study: the 12-month longitudinal analysis. *Lancet Neurol* 2011; **10**: 31-42 [PMID: 21130037 DOI: 10.1016/S1474-4422(10)70276-3]

19 **Tabrizi SJ**, Reilmann R, Roos RA, Durr A, Leavitt B, Owen G, Jones R, Johnson H, Craufurd D, Hicks SL, Kennard C, Landwehrmeyer B, Stout JC, Borowsky B, Scahill RI, Frost C, Langbehn DR. Potential endpoints for clinical trials in premanifest and early Huntington's disease in the TRACK-HD study: analysis of 24 month observational data. *Lancet Neurol* 2012; **11**: 42-53 [PMID: 22137354 DOI: 10.1016/S1474-4422(11)70263-0]

20 **Tabrizi SJ**, Scahill RI, Owen G, Durr A, Leavitt BR, Roos RA, Borowsky B, Landwehrmeyer B, Frost C, Johnson H, Craufurd D, Reilmann R, Stout JC, Langbehn DR. Predictors of phenotypic progression and disease onset in premanifest and early-stage Huntington's disease in the TRACK-HD study: analysis of 36-month observational data. *Lancet Neurol* 2013; **12**: 637-649 [PMID: 23664844]

21 **Aylward EH**, Li Q, Stine OC, Ranen N, Sherr M, Barta PE, Bylsma FW, Pearlson GD, Ross CA. Longitudinal change in basal ganglia volume in patients with Huntington's disease. *Neurology* 1997; **48**: 394-399 [PMID: 9040728 DOI: 10.1212/WNL.48.2.394]

22 **Rosas HD**, Liu AK, Hersch S, Glessner M, Ferrante RJ, Salat DH, van der Kouwe A, Jenkins BG, Dale AM, Fischl B. Regional and progressive thinning of the cortical ribbon in Huntington's disease. *Neurology* 2002; **58**: 695-701 [PMID: 11889230 DOI: 10.1212/WNL.58.5.695]

23 **Rosas HD**, Salat DH, Lee SY, Zaleta AK, Pappu V, Fischl B, Greve D, Hevelone N, Hersch SM. Cerebral cortex and the clinical expression of Huntington's disease: complexity and heterogeneity. *Brain* 2008; **131**: 1057-1068 [PMID: 18337273 DOI: 10.1093/brain/awn025]

24 **Hobbs NZ**, Henley SM, Ridgway GR, Wild EJ, Barker RA,

Scahill RI, Barnes J, Fox NC, Tabrizi SJ. The progression of regional atrophy in premanifest and early Huntington's disease: a longitudinal voxel-based morphometry study. *J Neurol Neurosurg Psychiatry* 2010; **81**: 756-763 [PMID: 19955112 DOI: 10.1136/jnnp.2009.190702]

25 **Paulsen JS**, Nopoulos PC, Aylward E, Ross CA, Johnson H, Magnotta VA, Juhl A, Pierson RK, Mills J, Langbehn D, Nance M. Striatal and white matter predictors of estimated diagnosis for Huntington disease. *Brain Res Bull* 2010; **82**: 201-207 [PMID: 20385209 DOI: 10.1016/j.brainresbull.2010.04.003]

26 **Reading SA**, Yassa MA, Bakker A, Dziorny AC, Gourley LM, Yallapragada V, Rosenblatt A, Margolis RL, Aylward EH, Brandt J, Mori S, van Zijl P, Bassett SS, Ross CA. Regional white matter change in pre-symptomatic Huntington's disease: a diffusion tensor imaging study. *Psychiatry Res* 2005; **140**: 55-62 [PMID: 16199141 DOI: 10.1016/j.pscychresns.2005.05.011]

27 **Rosas HD**, Tuch DS, Hevelone ND, Zaleta AK, Vangel M, Hersch SM, Salat DH. Diffusion tensor imaging in presymptomatic and early Huntington's disease: Selective white matter pathology and its relationship to clinical measures. *Mov Disord* 2006; **21**: 1317-1325 [PMID: 16755582 DOI: 10.1002/mds.20979]

28 **Dumas EM**, van den Bogaard SJ, Ruber ME, Reilman RR, Stout JC, Craufurd D, Hicks SL, Kennard C, Tabrizi SJ, van Buchem MA, van der Grond J, Roos RA. Early changes in white matter pathways of the sensorimotor cortex in premanifest Huntington's disease. *Hum Brain Mapp* 2012; **33**: 203-212 [PMID: 21264990 DOI: 10.1002/hbm.21205]

29 **Dierks T**, Linden DE, Hertel A, Günther T, Lanfermann H, Niesen A, Frölich L, Zanella FE, Hör G, Goebel R, Maurer K. Multimodal imaging of residual function and compensatory resource allocation in cortical atrophy: a case study of parietal lobe function in a patient with Huntington's disease. *Psychiatry Res* 1998; **84**: 27-35 [PMID: 9870415 DOI: 10.1016/S0925-4927(98)00040-7]

30 **Clark VP**, Lai S, Deckel AW. Altered functional MRI responses in Huntington's disease. *Neuroreport* 2002; **13**: 703-706 [PMID: 11973474 DOI: 10.1097/00001756-200204160-00033]

31 **Kim JS**, Reading SA, Brashers-Krug T, Calhoun VD, Ross CA, Pearlson GD. Functional MRI study of a serial reaction time task in Huntington's disease. *Psychiatry Res* 2004; **131**: 23-30 [PMID: 15246452 DOI: 10.1016/j.pscychresns.2004.03.002]

32 **Georgiou-Karistianis N**, Sritharan A, Farrow M, Cunnington R, Stout J, Bradshaw J, Churchyard A, Brawn TL, Chua P, Chiu E, Thiruvady D, Egan G. Increased cortical recruitment in Huntington's disease using a Simon task. *Neuropsychologia* 2007; **45**: 1791-1800 [PMID: 17321554 DOI: 10.1016/j.neuropsychologia.2006.12.023]

33 **Georgiou-Karistianis N**, Stout JC, Domínguez D JF, Carron SP, Ando A, Churchyard A, Chua P, Bohanna I, Dymowski AR, Poudel G, Egan GF. Functional magnetic resonance imaging of working memory in Huntington's disease: cross-sectional data from the IMAGE-HD study. *Hum Brain Mapp* 2014; **35**: 1847-1864 [PMID: 23913754 DOI: 10.1002/hbm.22296]

34 **Thiruvady DR**, Georgiou-Karistianis N, Egan GF, Ray S, Sritharan A, Farrow M, Churchyard A, Chua P, Bradshaw JL, Brawn TL, Cunnington R. Functional connectivity of the prefrontal cortex in Huntington's disease. *J Neurol Neurosurg Psychiatry* 2007; **78**: 127-133 [PMID: 17028117 DOI: 10.1136/jnnp.2006.098368]

35 **Paulsen JS**, Zimbelman JL, Hinton SC, Langbehn DR, Leveroni CL, Benjamin ML, Reynolds NC, Rao SM. fMRI biomarker of early neuronal dysfunction in presymptomatic Huntington's Disease. *AJNR Am J Neuroradiol* 2004; **25**: 1715-1721 [PMID: 15569736]

36 **Reading SA**, Dziorny AC, Peroutka LA, Schreiber M, Gourley LM, Yallapragada V, Rosenblatt A, Margolis RL, Pekar JJ, Pearlson GD, Aylward E, Brandt J, Bassett SS, Ross CA. Functional brain changes in presymptomatic Huntington's disease. *Ann Neurol* 2004; **55**: 879-883 [PMID: 15174024 DOI: 10.1002/ana.20121]

37 **Wolf RC**, Vasic N, Schönfeldt-Lecuona C, Landwehrmeyer GB, Ecker D. Dorsolateral prefrontal cortex dysfunction in presymptomatic Huntington's disease: evidence from event-related fMRI. *Brain* 2007; **130**: 2845-2857 [PMID: 17855375 DOI: 10.1093/brain/awm210]

38 **Wolf RC**, Sambataro F, Vasic N, Schönfeldt-Lecuona C, Ecker D, Landwehrmeyer B. Aberrant connectivity of lateral prefrontal networks in presymptomatic Huntington's disease. *Exp Neurol* 2008; **213**: 137-144 [PMID: 18588876 DOI: 10.1016/j.expneurol.2008.05.017]

39 **Unschuld PG**, Joel SE, Pekar JJ, Reading SA, Oishi K, McEntee J, Shanahan M, Bakker A, Margolis RL, Bassett SS, Rosenblatt A, Mori S, van Zijl PC, Ross CA, Redgrave GW. Depressive symptoms in prodromal Huntington's Disease correlate with Stroop-interference related functional connectivity in the ventromedial prefrontal cortex. *Psychiatry Res* 2012; **203**: 166-174 [PMID: 22974690 DOI: 10.1016/j.pscychresns.2012.01.002]

40 **Unschuld PG**, Liu X, Shanahan M, Margolis RL, Bassett SS, Brandt J, Schretlen DJ, Redgrave GW, Hua J, Hock C, Reading SA, van Zijl PC, Pekar JJ, Ross CA. Prefrontal executive function associated coupling relates to Huntington's disease stage. *Cortex* 2013; **49**: 2661-2673 [PMID: 23906595 DOI: 10.1016/j.cortex.2013.05.015]

41 **Fox MD**, Raichle ME. Spontaneous fluctuations in brain activity observed with functional magnetic resonance imaging. *Nat Rev Neurosci* 2007; **8**: 700-711 [PMID: 17704812 DOI: 10.1038/nrn2201]

42 **Greicius M**. Resting-state functional connectivity in neuropsychiatric disorders. *Curr Opin Neurol* 2008; **21**: 424-430 [PMID: 18607202 DOI: 10.1097/WCO.0b013e328306f2c5]

43 **Dumas EM**, van den Bogaard SJ, Hart EP, Soeter RP, van Buchem MA, van der Grond J, Rombouts SA, Roos RA. Reduced functional brain connectivity prior to and after disease onset in Huntington's disease. *Neuroimage Clin* 2013; **2**: 377-384 [PMID: 24179791 DOI: 10.1016/j.nicl.2013.03.001]

44 **Poudel GR**, Egan GF, Churchyard A, Chua P, Stout JC, Georgiou-Karistianis N. Abnormal synchrony of resting state networks in premanifest and symptomatic Huntington disease: the IMAGE-HD study. *J Psychiatry Neurosci* 2014; **39**: 87-96 [PMID: 24083458 DOI: 10.1503/jpn.120226]

45 **Werner CJ**, Dogan I, Saß C, Mirzazade S, Schiefer J, Shah NJ, Schulz JB, Reetz K. Altered resting-state connectivity in Huntington's disease. *Hum Brain Mapp* 2014; **35**: 2582-2593 [PMID: 23982979 DOI: 10.1002/hbm.22351]

46 **Unschuld PG**, Joel SE, Liu X, Shanahan M, Margolis RL, Biglan KM, Bassett SS, Schretlen DJ, Redgrave GW, van Zijl PC, Pekar JJ, Ross CA. Impaired cortico-striatal functional connectivity in prodromal Huntington's Disease. *Neurosci Lett* 2012; **514**: 204-209 [PMID: 22425717 DOI: 10.1016/j.neulet.2012.02.095]

47 **Hua J**, Unschuld PG, Margolis RL, van Zijl PC, Ross CA. Elevated arteriolar cerebral blood volume in prodromal Huntington's disease. *Mov Disord* 2014; **29**: 396-401 [PMID: 23847161 DOI: 10.1002/mds.25591]

48 **Unschuld PG**, Edden RA, Carass A, Liu X, Shanahan M, Wang X, Oishi K, Brandt J, Bassett SS, Redgrave GW, Margolis RL, van Zijl PC, Barker PB, Ross CA. Brain metabolite alterations and cognitive dysfunction in early Huntington's disease. *Mov Disord* 2012; **27**: 895-902 [PMID: 22649062 DOI: 10.1002/mds.25010]

49 **Tang TS**, Chen X, Liu J, Bezprozvanny I. Dopaminergic signaling and striatal neurodegeneration in Huntington's disease. *J Neurosci* 2007; **27**: 7899-7910 [PMID: 17652581 DOI:

10.1523/JNEUROSCI.1396-07.2007]
50 **van Oostrom JC**, Dekker M, Willemsen AT, de Jong BM, Roos RA, Leenders KL. Changes in striatal dopamine D2 receptor binding in pre-clinical Huntington's disease. *Eur J Neurol* 2009; **16**: 226-231 [PMID: 19138335 DOI: 10.1111/j.1468-1331.2008.02390.x]
51 **Reiner A**, Albin RL, Anderson KD, D'Amato CJ, Penney JB, Young AB. Differential loss of striatal projection neurons in Huntington disease. *Proc Natl Acad Sci USA* 1988; **85**: 5733-5737 [PMID: 2456581 DOI: 10.1073/pnas.85.15.5733]
52 **Leenders KL**, Frackowiak RS, Quinn N, Marsden CD. Brain energy metabolism and dopaminergic function in Huntington's disease measured in vivo using positron emission tomography. *Mov Disord* 1986; **1**: 69-77 [PMID: 2973559 DOI: 10.1002/mds.870010110]
53 **Hägglund J**, Aquilonius SM, Eckernäs SA, Hartvig P, Lundquist H, Gullberg P, Långström B. Dopamine receptor properties in Parkinson's disease and Huntington's chorea evaluated by positron emission tomography using 11C-N-methyl-spiperone. *Acta Neurol Scand* 1987; **75**: 87-94 [PMID: 2953165 DOI: 10.1111/j.1600-0404.1987.tb07900.x]
54 **Brandt J**, Folstein SE, Wong DF, Links J, Dannals RF, McDonnell-Sill A, Starkstein S, Anders P, Strauss ME, Tune LE. D2 receptors in Huntington's disease: positron emission tomography findings and clinical correlates. *J Neuropsychiatry Clin Neurosci* 1990; **2**: 20-27 [PMID: 1983772]
55 **Turjanski N**, Weeks R, Dolan R, Harding AE, Brooks DJ. Striatal D1 and D2 receptor binding in patients with Huntington's disease and other choreas. A PET study. *Brain* 1995; **118** (Pt 3): 689-696 [PMID: 7600086 DOI: 10.1093/brain/118.3.689]
56 **Ginovart N**, Lundin A, Farde L, Halldin C, Bäckman L, Swahn CG, Pauli S, Sedvall G. PET study of the pre- and post-synaptic dopaminergic markers for the neurodegenerative process in Huntington's disease. *Brain* 1997; **120** (Pt 3): 503-514 [PMID: 9126061 DOI: 10.1093/brain/120.3.503]
57 **Bohnen NI**, Koeppe RA, Meyer P, Ficaro E, Wernette K, Kilbourn MR, Kuhl DE, Frey KA, Albin RL. Decreased striatal monoaminergic terminals in Huntington disease. *Neurology* 2000; **54**: 1753-1759 [PMID: 10802780 DOI: 10.1212/WNL.54.9.1753]
58 **Sedvall G**, Karlsson P, Lundin A, Anvret M, Suhara T, Halldin C, Farde L. Dopamine D1 receptor number--a sensitive PET marker for early brain degeneration in Huntington' s disease. *Eur Arch Psychiatry Clin Neurosci* 1994; **243**: 249-255 [PMID: 8172940 DOI: 10.1007/BF02191583]
59 **Bäckman L**, Robins-Wahlin TB, Lundin A, Ginovart N, Farde L. Cognitive deficits in Huntington's disease are predicted by dopaminergic PET markers and brain volumes. *Brain* 1997; **120** (Pt 12): 2207-2217 [PMID: 9448576 DOI: 10.1093/brain/120.12.2207]
60 **Lawrence AD**, Weeks RA, Brooks DJ, Andrews TC, Watkins LH, Harding AE, Robbins TW, Sahakian BJ. The relationship between striatal dopamine receptor binding and cognitive performance in Huntington's disease. *Brain* 1998; **121** (Pt 7): 1343-1355 [PMID: 9679785 DOI: 10.1093/brain/121.7.1343]
61 **Pavese N**, Andrews TC, Brooks DJ, Ho AK, Rosser AE, Barker RA, Robbins TW, Sahakian BJ, Dunnett SB, Piccini P. Progressive striatal and cortical dopamine receptor dysfunction in Huntington's disease: a PET study. *Brain* 2003; **126**: 1127-1135 [PMID: 12690052 DOI: 10.1093/brain/awg119]
62 **Pavese N**, Politis M, Tai YF, Barker RA, Tabrizi SJ, Mason SL, Brooks DJ, Piccini P. Cortical dopamine dysfunction in symptomatic and premanifest Huntington's disease gene carriers. *Neurobiol Dis* 2010; **37**: 356-361 [PMID: 19853661 DOI: 10.1016/j.nbd.2009.10.015]
63 **van Oostrom JC**, Maguire RP, Verschuuren-Bemelmans CC, Veenma-van der Duin L, Pruim J, Roos RA, Leenders KL. Striatal dopamine D2 receptors, metabolism, and volume in preclinical Huntington disease. *Neurology* 2005; **65**: 941-943 [PMID: 16186542 DOI: 10.1212/01.wnl.0000176071.08694.cc]
64 **Andrews TC**, Weeks RA, Turjanski N, Gunn RN, Watkins LH, Sahakian B, Hodges JR, Rosser AE, Wood NW, Brooks DJ. Huntington's disease progression. PET and clinical observations. *Brain* 1999; **122** (Pt 12): 2353-2363 [PMID: 10581228 DOI: 10.1093/brain/122.12.2353]
65 **Antonini A**, Leenders KL, Spiegel R, Meier D, Vontobel P, Weigell-Weber M, Sanchez-Pernaute R, de Yébenez JG, Boesiger P, Weindl A, Maguire RP. Striatal glucose metabolism and dopamine D2 receptor binding in asymptomatic gene carriers and patients with Huntington's disease. *Brain* 1996; **119** (Pt 6): 2085-2095 [PMID: 9010012 DOI: 10.1093/brain/119.6.2085]
66 **Antonini A**, Leenders KL, Eidelberg D. [11C]raclopride-PET studies of the Huntington's disease rate of progression: relevance of the trinucleotide repeat length. *Ann Neurol* 1998; **43**: 253-255 [PMID: 9485067 DOI: 10.1002/ana.410430216]
67 **Politis M**, Pavese N, Tai YF, Tabrizi SJ, Barker RA, Piccini P. Hypothalamic involvement in Huntington's disease: an in vivo PET study. *Brain* 2008; **131**: 2860-2869 [PMID: 18829696 DOI: 10.1093/brain/awn244]
68 **Esmaeilzadeh M**, Farde L, Karlsson P, Varrone A, Halldin C, Waters S, Tedroff J. Extrastriatal dopamine D(2) receptor binding in Huntington's disease. *Hum Brain Mapp* 2011; **32**: 1626-1636 [PMID: 20886576 DOI: 10.1002/hbm.21134]
69 **Rosser AE**, Barker RA, Harrower T, Watts C, Farrington M, Ho AK, Burnstein RM, Menon DK, Gillard JH, Pickard J, Dunnett SB. Unilateral transplantation of human primary fetal tissue in four patients with Huntington's disease: NEST-UK safety report ISRCTN no 36485475. *J Neurol Neurosurg Psychiatry* 2002; **73**: 678-685 [PMID: 12438470 DOI: 10.1136/jnnp.73.6.678]
70 **Furtado S**, Sossi V, Hauser RA, Samii A, Schulzer M, Murphy CB, Freeman TB, Stoessl AJ. Positron emission tomography after fetal transplantation in Huntington's disease. *Ann Neurol* 2005; **58**: 331-337 [PMID: 16049929 DOI: 10.1002/ana.20564]
71 **Barker RA**, Mason SL, Harrower TP, Swain RA, Ho AK, Sahakian BJ, Mathur R, Elneil S, Thornton S, Hurrelbrink C, Armstrong RJ, Tyers P, Smith E, Carpenter A, Piccini P, Tai YF, Brooks DJ, Pavese N, Watts C, Pickard JD, Rosser AE, Dunnett SB. The long-term safety and efficacy of bilateral transplantation of human fetal striatal tissue in patients with mild to moderate Huntington's disease. *J Neurol Neurosurg Psychiatry* 2013; **84**: 657-665 [PMID: 23345280 DOI: 10.1136/jnnp-2012-302441]
72 **Sokoloff L**. Localization of functional activity in the central nervous system by measurement of glucose utilization with radioactive deoxyglucose. *J Cereb Blood Flow Metab* 1981; **1**: 7-36 [PMID: 7035471 DOI: 10.1038/jcbfm.1981.4]
73 **Sokoloff L**. Energetics of functional activation in neural tissues. *Neurochem Res* 1999; **24**: 321-329 [PMID: 9972882 DOI: 10.1023/A:1022534709672]
74 **Mazziotta JC**, Phelps ME, Pahl JJ, Huang SC, Baxter LR, Riege WH, Hoffman JM, Kuhl DE, Lanto AB, Wapenski JA. Reduced cerebral glucose metabolism in asymptomatic subjects at risk for Huntington's disease. *N Engl J Med* 1987; **316**: 357-362 [PMID: 2949152 DOI: 10.1056/NEJM198702123160701]
75 **Kuwert T**, Lange HW, Langen KJ, Herzog H, Aulich A, Feinendegen LE. Cortical and subcortical glucose consumption measured by PET in patients with Huntington's disease. *Brain* 1990; **113** (Pt 5): 1405-1423 [PMID: 2147116 DOI: 10.1093/brain/113.5.1405]
76 **Berent S**, Giordani B, Lehtinen S, Markel D, Penney JB, Buchtel HA, Starosta-Rubinstein S, Hichwa R, Young AB. Positron emission tomographic scan investigations of Huntington's disease: cerebral metabolic correlates of cognitive function. *Ann Neurol* 1988; **23**: 541-546 [PMID: 2970247 DOI: 10.1002/ana.410230603]

77 **Young AB**, Penney JB, Starosta-Rubinstein S, Markel DS, Berent S, Giordani B, Ehrenkaufer R, Jewett D, Hichwa R. PET scan investigations of Huntington's disease: cerebral metabolic correlates of neurological features and functional decline. *Ann Neurol* 1986; **20**: 296-303 [PMID: 2945510 DOI: 10.1002/ana.410200305]

78 **Hayden MR**, Martin WR, Stoessl AJ, Clark C, Hollenberg S, Adam MJ, Ammann W, Harrop R, Rogers J, Ruth T. Positron emission tomography in the early diagnosis of Huntington's disease. *Neurology* 1986; **36**: 888-894 [PMID: 2940474 DOI: 10.1212/WNL.36.7.888]

79 **Ciarmiello A**, Cannella M, Lastoria S, Simonelli M, Frati L, Rubinsztein DC, Squitieri F. Brain white-matter volume loss and glucose hypometabolism precede the clinical symptoms of Huntington's disease. *J Nucl Med* 2006; **47**: 215-222 [PMID: 16455626]

80 **Ciarmiello A**, Giovacchini G, Orobello S, Bruselli L, Elifani F, Squitieri F. 18F-FDG PET uptake in the pre-Huntington disease caudate affects the time-to-onset independently of CAG expansion size. *Eur J Nucl Med Mol Imaging* 2012; **39**: 1030-1036 [PMID: 22526956 DOI: 10.1007/s00259-012-2114-z]

81 **Shin H**, Kim MH, Lee SJ, Lee KH, Kim MJ, Kim JS, Cho JW. Decreased Metabolism in the Cerebral Cortex in Early-Stage Huntington's Disease: A Possible Biomarker of Disease Progression? *J Clin Neurol* 2013; **9**: 21-25 [PMID: 23346156 DOI: 10.3988/jcn.2013.9.1.21]

82 **Bartenstein P**, Weindl A, Spiegel S, Boecker H, Wenzel R, Ceballos-Baumann AO, Minoshima S, Conrad B. Central motor processing in Huntington's disease. A PET study. *Brain* 1997; **120** (Pt 9): 1553-1567 [PMID: 9313639 DOI: 10.1093/brain/120.9.1553]

83 **Weeks RA**, Ceballos-Baumann A, Piccini P, Boecker H, Harding AE, Brooks DJ. Cortical control of movement in Huntington's disease. A PET activation study. *Brain* 1997; **120** (Pt 9): 1569-1578 [PMID: 9313640 DOI: 10.1093/brain/120.9.1569]

84 **Lepron E**, Péran P, Cardebat D, Démonet JF. A PET study of word generation in Huntington's disease: effects of lexical competition and verb/noun category. *Brain Lang* 2009; **110**: 49-60 [PMID: 19615733 DOI: 10.1016/j.bandl.2009.05.004]

85 **Feigin A**, Leenders KL, Moeller JR, Missimer J, Kuenig G, Spetsieris P, Antonini A, Eidelberg D. Metabolic network abnormalities in early Huntington's disease: an [(18)F]FDG PET study. *J Nucl Med* 2001; **42**: 1591-1595 [PMID: 11696626]

86 **Feigin A**, Tang C, Ma Y, Mattis P, Zgaljardic D, Guttman M, Paulsen JS, Dhawan V, Eidelberg D. Thalamic metabolism and symptom onset in preclinical Huntington's disease. *Brain* 2007; **130**: 2858-2867 [PMID: 17893097 DOI: 10.1093/brain/awm217]

87 **Tang CC**, Feigin A, Ma Y, Habeck C, Paulsen JS, Leenders KL, Teune LK, van Oostrom JC, Guttman M, Dhawan V, Eidelberg D. Metabolic network as a progression biomarker of premanifest Huntington's disease. *J Clin Invest* 2013; **123**: 4076-4088 [PMID: 23985564 DOI: 10.1172/JCI69411]

88 **Bachoud-Lévi AC**, Rémy P, Nguyen JP, Brugières P, Lefaucheur JP, Bourdet C, Baudic S, Gaura V, Maison P, Haddad B, Boissé MF, Grandmougin T, Jény R, Bartolomeo P, Dalla Barba G, Degos JD, Lisovoski F, Ergis AM, Pailhous E, Cesaro P, Hantraye P, Peschanski M. Motor and cognitive improvements in patients with Huntington's disease after neural transplantation. *Lancet* 2000; **356**: 1975-1979 [PMID: 11130527 DOI: 10.1016/S0140-6736(00)03310-9]

89 **Gaura V**, Bachoud-Lévi AC, Ribeiro MJ, Nguyen JP, Frouin V, Baudic S, Brugières P, Mangin JF, Boissé MF, Palfi S, Cesaro P, Samson Y, Hantraye P, Peschanski M, Remy P. Striatal neural grafting improves cortical metabolism in Huntington's disease patients. *Brain* 2004; **127**: 65-72 [PMID: 14607797 DOI: 10.1093/brain/awh003]

90 **Messmer K**, Reynolds GP. Increased peripheral benzodiazepine binding sites in the brain of patients with Huntington's disease. *Neurosci Lett* 1998; **241**: 53-56 [PMID: 9502214 DOI: 10.1016/S0304-3940(97)00967-1]

91 **Sapp E**, Kegel KB, Aronin N, Hashikawa T, Uchiyama Y, Tohyama K, Bhide PG, Vonsattel JP, DiFiglia M. Early and progressive accumulation of reactive microglia in the Huntington disease brain. *J Neuropathol Exp Neurol* 2001; **60**: 161-172 [PMID: 11273004]

92 **Kreutzberg GW**. Microglia: a sensor for pathological events in the CNS. *Trends Neurosci* 1996; **19**: 312-318 [PMID: 8843599 DOI: 10.1016/0166-2236(96)10049-7]

93 **Melton LM**, Keith AB, Davis S, Oakley AE, Edwardson JA, Morris CM. Chronic glial activation, neurodegeneration, and APP immunoreactive deposits following acute administration of double-stranded RNA. *Glia* 2003; **44**: 1-12 [PMID: 12951652 DOI: 10.1002/glia.10276]

94 **Nakanishi H**. Microglial functions and proteases. *Mol Neurobiol* 2003; **27**: 163-176 [PMID: 12777686]

95 **Banati RB**. Visualising microglial activation in vivo. *Glia* 2002; **40**: 206-217 [PMID: 12379908 DOI: 10.1002/glia.10144]

96 **Wilms H**, Claasen J, Röhl C, Sievers J, Deuschl G, Lucius R. Involvement of benzodiazepine receptors in neuroinflammatory and neurodegenerative diseases: evidence from activated microglial cells in vitro. *Neurobiol Dis* 2003; **14**: 417-424 [PMID: 14678758 DOI: 10.1016/j.nbd.2003.07.002]

97 **Banati RB**, Goerres GW, Myers R, Gunn RN, Turkheimer FE, Kreutzberg GW, Brooks DJ, Jones T, Duncan JS. [11C](R)-PK11195 positron emission tomography imaging of activated microglia in vivo in Rasmussen's encephalitis. *Neurology* 1999; **53**: 2199-2203 [PMID: 10599809 DOI: 10.1212/WNL.53.9.2199]

98 **Banati RB**, Newcombe J, Gunn RN, Cagnin A, Turkheimer F, Heppner F, Price G, Wegner F, Giovannoni G, Miller DH, Perkin GD, Smith T, Hewson AK, Bydder G, Kreutzberg GW, Jones T, Cuzner ML, Myers R. The peripheral benzodiazepine binding site in the brain in multiple sclerosis: quantitative in vivo imaging of microglia as a measure of disease activity. *Brain* 2000; **123** (Pt 11): 2321-2337 [PMID: 11050032 DOI: 10.1093/brain/123.11.2321]

99 **Pavese N**, Gerhard A, Tai YF, Ho AK, Turkheimer F, Barker RA, Brooks DJ, Piccini P. Microglial activation correlates with severity in Huntington disease: a clinical and PET study. *Neurology* 2006; **66**: 1638-1643 [PMID: 16769933 DOI: 10.1212/01.wnl.0000222734.56412.17]

100 **Tai YF**, Pavese N, Gerhard A, Tabrizi SJ, Barker RA, Brooks DJ, Piccini P. Microglial activation in presymptomatic Huntington's disease gene carriers. *Brain* 2007; **130**: 1759-1766 [PMID: 17400599 DOI: 10.1093/brain/awm044]

101 **Politis M**, Pavese N, Tai YF, Kiferle L, Mason SL, Brooks DJ, Tabrizi SJ, Barker RA, Piccini P. Microglial activation in regions related to cognitive function predicts disease onset in Huntington's disease: a multimodal imaging study. *Hum Brain Mapp* 2011; **32**: 258-270 [PMID: 21229614 DOI: 10.1002/hbm.21008]

102 **Herkenham M**, Lynn AB, de Costa BR, Richfield EK. Neuronal localization of cannabinoid receptors in the basal ganglia of the rat. *Brain Res* 1991; **547**: 267-274 [PMID: 1909204 DOI: 10.1016/0006-8993(91)90970-7]

103 **Mailleux P**, Vanderhaeghen JJ. Localization of cannabinoid receptor in the human developing and adult basal ganglia. Higher levels in the striatonigral neurons. *Neurosci Lett* 1992; **148**: 173-176 [PMID: 1300492 DOI: 10.1016/0304-3940(92)90832-R]

104 **Glass M**, Brotchie JM, Maneuf YP. Modulation of neurotransmission by cannabinoids in the basal ganglia. *Eur J Neurosci* 1997; **9**: 199-203 [PMID: 9058040 DOI: 10.1111/j.1460-9568.1997.tb01390.x]

105 **Glass M**, Dragunow M, Faull RL. The pattern of neurodegeneration in Huntington's disease: a comparative study of cannabinoid, dopamine, adenosine and GABA(A) receptor alterations in the human basal ganglia in Huntington's dis-

ease. *Neuroscience* 2000; **97**: 505-519 [PMID: 10828533 DOI: 10.1016/S0306-4522(00)00008-7]
106 **Casteels C**, Martinez E, Bormans G, Camon L, de Vera N, Baekelandt V, Planas AM, Van Laere K. Type 1 cannabinoid receptor mapping with [18F]MK-9470 PET in the rat brain after quinolinic acid lesion: a comparison to dopamine receptors and glucose metabolism. *Eur J Nucl Med Mol Imaging* 2010; **37**: 2354-2363 [PMID: 20680268 DOI: 10.1007/s00259-010-1574-2]
107 **Casteels C**, Vandeputte C, Rangarajan JR, Dresselaers T, Riess O, Bormans G, Maes F, Himmelreich U, Nguyen H, Van Laere K. Metabolic and type 1 cannabinoid receptor imaging of a transgenic rat model in the early phase of Huntington disease. *Exp Neurol* 2011; **229**: 440-449 [PMID: 21459091 DOI: 10.1016/j.expneurol.2011.03.014]
108 **Burns HD**, Van Laere K, Sanabria-Bohórquez S, Hamill TG, Bormans G, Eng WS, Gibson R, Ryan C, Connolly B, Patel S, Krause S, Vanko A, Van Hecken A, Dupont P, De Lepeleire I, Rothenberg P, Stoch SA, Cote J, Hagmann WK, Jewell JP, Lin LS, Liu P, Goulet MT, Gottesdiener K, Wagner JA, de Hoon J, Mortelmans L, Fong TM, Hargreaves RJ. [18F]MK-9470, a positron emission tomography (PET) tracer for in vivo human PET brain imaging of the cannabinoid-1 receptor. *Proc Natl Acad Sci USA* 2007; **104**: 9800-9805 [PMID: 17535893 DOI: 10.1073/pnas.0703472104]
109 **Yasuno F**, Brown AK, Zoghbi SS, Krushinski JH, Chernet E, Tauscher J, Schaus JM, Phebus LA, Chesterfield AK, Felder CC, Gladding RL, Hong J, Halldin C, Pike VW, Innis RB. The PET radioligand [11C]MePPEP binds reversibly and with high specific signal to cannabinoid CB1 receptors in nonhuman primate brain. *Neuropsychopharmacology* 2008; **33**: 259-269 [PMID: 17392732 DOI: 10.1038/sj.npp.1301402]
110 **Terry GE**, Liow JS, Zoghbi SS, Hirvonen J, Farris AG, Lerner A, Tauscher JT, Schaus JM, Phebus L, Felder CC, Morse CL, Hong JS, Pike VW, Halldin C, Innis RB. Quantitation of cannabinoid CB1 receptors in healthy human brain using positron emission tomography and an inverse agonist radioligand. *Neuroimage* 2009; **48**: 362-370 [PMID: 19573609 DOI: 10.1016/j.neuroimage.2009.06.059]
111 **Van Laere K**, Casteels C, Dhollander I, Goffin K, Grachev I, Bormans G, Vandenberghe W. Widespread decrease of type 1 cannabinoid receptor availability in Huntington disease in vivo. *J Nucl Med* 2010; **51**: 1413-1417 [PMID: 20720046 DOI: 10.2967/jnumed.110.077156]
112 **Vattakatuchery JJ**, Kurien R. Acetylcholinesterase inhibitors in cognitive impairment in Huntington's disease: A brief review. *World J Psychiatry* 2013; **3**: 62-64 [PMID: 24255877 DOI: 10.5498/wjp.v3.i3.62]

P- Reviewers: Arsalidou M, Jeong Y, Orlacchio A, Walter M
S- Editor: Ma YJ **L- Editor**: A **E- Editor**: Zhang DN

World Journal of Radiology

Submit a Manuscript: http://www.wjgnet.com/esps/
Help Desk: http://www.wjgnet.com/esps/helpdesk.aspx
DOI: 10.4329/wjr.v6.i6.313

World J Radiol 2014 June 28; 6(6): 313-328
ISSN 1949-8470 (online)
© 2014 Baishideng Publishing Group Inc. All rights reserved.

REVIEW

Imaging of the small bowel: Crohn's disease in paediatric patients

Emanuele Casciani, Chiara De Vincentiis, Elisabetta Polettini, Gabriele Masselli, Giovanni Di Nardo, Fortunata Civitelli, Salvatore Cucchiara, Gian Franco Gualdi

Emanuele Casciani, Elisabetta Polettini, Gabriele Masselli, Gian Franco Gualdi, Department of Emergency Radiology, "La Sapienza" University-Hospital Umberto I, 00166 Rome, Italy
Chiara De Vincentiis, Department of Radiology, "La Sapienza" University-Sant'Andrea's Hospital, 00189 Rome, Italy
Giovanni Di Nardo, Fortunata Civitelli, Salvatore Cucchiara, Department of Pediatrics, Gastroenterology and Liver Unit, "La Sapienza" University-Hospital Umberto I, 00166 Rome, Italy
Author contributions: Casciani E designed the study and wrote the manuscript; De Vincentiis C helped to write the manuscript; Polettini E, Masselli G, Di Nardo G, Civitelli F, Cucchiara S and Gualdi GF provided the collection of part of the material; all the authors were also involved in editing the manuscript.
Correspondence to: Dr. Emanuele Casciani, Department of Emergency Radiology, "La Sapienza" University-Hospital Umberto I, Viale del Policlinico 155, 00161 Roma, Italy. emanuelecasciani@gmail.com
Telephone: +39-06-49979465 Fax: +39-06-6630218
Received: November 27, 2013 Revised: April 14, 2014
Accepted: May 16, 2014
Published online: June 28, 2014

© 2014 Baishideng Publishing Group Inc. All rights reserved.

Key words: Barium studies; Ultrasonography; Computed tomography; Magnetic resonance; Positron emission tomography-computed tomography

Core tip: Nowadays there is a great awareness of the risks associated with the use of ionizing radiation, particularly in children. This article evaluates all the imaging methods now available for the study of Crohn's disease in pediatric patients emphasizing the magnetic resonance imaging.

Casciani E, De Vincentiis C, Polettini E, Masselli G, Di Nardo G, Civitelli F, Cucchiara S, Gualdi GF. Imaging of the small bowel: Crohn's disease in paediatric patients. *World J Radiol* 2014; 6(6): 313-328 Available from: URL: http://www.wjgnet.com/1949-8470/full/v6/i6/313.htm DOI: http://dx.doi.org/10.4329/wjr.v6.i6.313

Abstract

In more than 20% of all patients, the Crohn's disease presents before the age of 18 years. The diagnosis and management of Crohn's disease in children has changed dramatically over the last decade, mainly due to increased awareness, availability of newer diagnostic modalities such as magnetic resonance imaging (MRI) and newer, more powerful treatments such as biologics. Imaging of the small bowel is needed for diagnosis, management, follow-up and also evaluation of the disease in terms of location, extent, activity and complications. We review all the methods (barium examinations, ultrasonography, computed tomography, MR, and computed tomography- positron emission tomography) commonly used for imaging the small bowel in paediatric patients with Crohn's disease analyzing the advantages and disadvantages of each modality, with particular emphasis on MR imaging.

INTRODUCTION

Crohn's disease (CD) begins in childhood, below 20 years of age, in 20% of cases and may involve characteristically any part of the gastrointestinal (GI) tract. The Paris classification has recently revised the Montreal classification, that had several weakness points relating children's classification[1]. Important modifications developed regarding CD include classifying age at diagnosis as A1a (0 to < 10 years), A1b (10 to < 17 years), A2 (17 to 40 years), and A3 (> 40 years), distinguishing disease above the distal ileum as L4a (proximal to ligament of Treitz) and L4b (ligament of Treitz to above distal ileum), allowing both stricturing and penetrating disease to be classified in the same patient (B2B3), and denoting, at any time, the presence of growth failure in the patient as G1 versus G0 (never growth failure)[2].

Although the exact frequency of the small bowel (SB)

CD is unknown, most gastroenterologists believe that its prevalence has been underestimated and that it may have an increased incidence among children and young adolescents[2]. A recent study performed in pediatric patients with magnetic resonance (MR) enterography[3], according to previous studies[4], confirmed that the involvement of the terminal ileum is common to more than three times compared to that of the jejunum and the rest of the ileum. Moreover, the involvement of the jejunum alone is uncommon and it is more difficult to investigate because of its tendency to stay non distended[3].

The clinical importance of the SB CD phenotype is the impact that a diffuse SB disease is expected to have on a child's growth and development. Moreover, patients with SB CD are more likely to experience complications, including intestinal obstruction and less commonly fistulization[4,5].

Thus, objective evaluation of the SB is essential in differentiating CD from other enteropathies and in directing the management of the patients with inflammatory bowel disease (IBD)[6,7]. The morphological evaluation of the SB, useful in the diagnosis and management of CD, has long been made only with conventional radiology. In the last decade there has been a progressive improvement of cross-sectional imaging [ultrasonography (US), computed tomography (CT), and magnetic resonance (MR)] that has significantly changed the way to diagnose and treat the patients[8,9]. Indeed, their accuracy in detecting mucosal alterations and transmural and perienteric inflammations, has led to a new disease staging, a detection of asymptomatic disease and a better assessment of response to therapy[10]. For these reasons modern cross-sectional imaging have replaced the traditional fluoroscopy-based for visualization of the SB. In the "Porto criteria" small-bowel follow-through (SBFT) was the recommended imaging modality in children[11]. However, concerns about the proven increased risk of high radiation exposure in pediatric patients mandates the use of alternative techniques when possible[12-14]. In the European Crohn's and Colitis Organization (ECCO) guidelines[14] it is stated that MR and CT enterography or enteroclysis are the imaging modalities with the highest diagnostic accuracy. Moreover in the pediatric section of the ECCO guidelines[15,16] dynamic contrast-enhanced MRI is considered the best imaging to show most of the CD's lesions without exposure to ionizing radiation. In the same way the Appropriateness Criteria of the American College of Radiology[17] point out that, in the pediatric patients, MR enterography may have sensitivity and specificity similar to CT enterography and avoids radiation risks. Ultimately the same accuracy, the choice of examination depends on several variables, such as institutional preferences and resources (US, CT, or MR scan), age and compliance of the patient, the eventually acute presentation, and finally radiologist expertise.

In this article we discuss all the methods commonly used for imaging the small bowel in paediatric patients with Crohn's disease analyzing the advantages and disadvantages of each modality, with particular emphasis on MR imaging.

BARIUM STUDIES

Traditionally in children with suspected CD has been studied with barium studies, enteroclysis (SBE) or SB follow-through (SBFT), considered to be the gold standard examination for the SB[18,19]. SBE was considered the best exam for SB disease, however children poorly tolerate the required insertion of a naso-jejunal tube. SBFT has long been considered as the most common, non-invasive, inexpensive and easily accessible radiological method[14], but, currently, it has only a secondary role in small bowel imaging. US and MR enterography are methods of choice for imaging SB diseases in pediatric populations.

Early mucosal changes, such as aphthous ulceration, can be detected by SBFT. This technique can also assess bowel motility that help to differentiate strictures from mural thickening and allows a functional evaluation of the pathological segment studying the SB transit time[14-16].

Although SBE and SBFT can effectively depict the presence of mucosal abnormalities effectively, including fissures, cobblestone mucosa, pseudo-polyps, and skip lesions, they are imprecise for the diagnosis of transmural and extramural disease[14,20,21], except in the overt forms (Figure 1).

A retrospective analysis of 164 children revealed a diagnostic sensitivity of only 45% for SB radiography compared with ileo-colonoscopy[22]. Moreover, SBFT is not accurate for the detection of active CD in the SB[20-23]. In fact, it can directly examine the mucosa demonstrating early active mucosal disease such as aphthous and linear ulcers, but it does not allow to evaluate the small bowel wall and the mesentery, except with indirect signs. Moreover, superimposed bowel loops or non-palpable bowel loops deep in the pelvis can hide active disease or its complications[20].

Concerns regarding the risks of radiation exposure in the pediatric population has increased with the spread use of these imaging studies. Children especially are at risk because they are inherently more radiosensitive and because they have more remaining years of life during which a radiation-induced cancer could develop[24].

A major disadvantage of barium studies, especially in children, is the radiation exposure, particularly if fluoroscopy time is not kept to a minimum[13]. Gaca *et al*[13] studied a total of 176 children with CD who underwent averaging 1.2 SBFTs. On average SBFT took 5.1 min with 3.3 abdominal radiographs. The effective doses (mSv) for a 5-min fluoroscopy were 0.15 for the central abdomen, 0.35 for the right lower quadrant, and 0.56 for the pelvis, yielding an average effective dose for SBFT (5-min fluoroscopy, 3.3 abdominal radiographs) of 1.8-2.2 mSv. Although 5 min of fluoroscopy time for an SBFT might seem excessive, this was calculated based on the average of 30 examinations performed by five experienced pediatric radiologists[13]. In the young population of CD

Figure 1 Barium studies in patients with Crohn's disease. Double-contrast barium enema examination (A and B) demonstrate longitudinal (arrows) and perpendicular (arrowheads) ulcerations in the terminal ileum. Small-bowel follow-through (C) demonstrates an abscess cavity (white arrow) with fistulae connecting the cavity to the adjacent small bowel (black arrows).

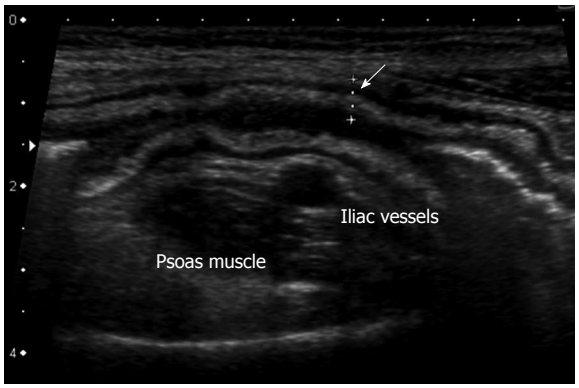

Figure 2 Thickening of the bowel wall, 5 mm, (arrow) with wall layers preserved. The hyperechoic band corresponds to thickened submucosa.

patients, the ionizing radiation required for SBE limits the use of this technique for the follow-up of the disease. Moreover, SBFT and SBE examinations can often result in incomplete studies. In fact they cause more patient discomfort compared with CT[25] and MRI[26], barium contrast can be poorly tolerated by children especially in severe and advanced disease and abdominal pain can limit compression preventing the adequate visualization of overlapping loops.

ULTRASONOGRAPHY

US has the distinct advantage of being widely available, inexpensive, non-invasive, radiation-free and relatively easy to perform[7,27]. Over the past few years, improvements in US equipment such as high-frequency transducers (7-12 MHz), combined with oral and intravenous (CE-US) contrast agents[28,29], have overcome some of the obstacles in bowel US that existed in the past, thus raising a great enthusiasm for its use in IBD children.

US can be considered a valuable tool in the preliminary diagnostic process of paediatric patients with suspected IBD, prior to further invasive tests[30,31].

Inflamed bowel can show both mural and extramural pathological changes. Bowel wall thickness is the most important US sign of IBD (Figure 2), with different thickness values used as a threshold for a positive diagnosis in the various reports (from 1.5 mm to 3 mm in the terminal ileum and < 2 mm in the colon)[27,32-35].

The other US signs are altered echogenicity, loss of

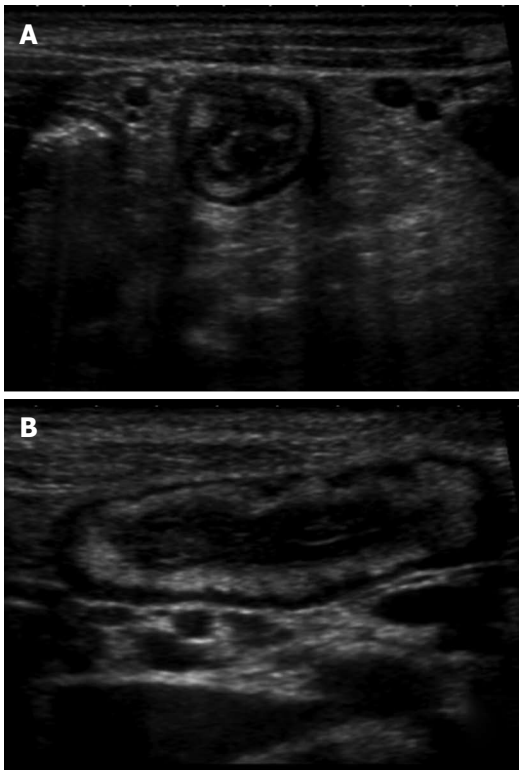

Figure 3 Transversal (A) and longitudinal (B) section of a thickened ileal loop due to Crohn's disease. The "target" sign, corresponding to remarkable bowel wall thickness, is visible as a strong echogenic centre surrounded by a hypoechoic border (A). The adjacent mesentery is thickened and hyperechoic, due to the transmural nature of inflammation in Crohn's disease (A and B).

the normally visible stratification (Figure 3), increased Colour-Doppler signal denoting hyperaemia (Figure 4) and relative decrease or lack in peristalsis signifying some degree of stiffness[31]. Extra-mural findings include changes involving the surrounding mesentery, that appears thickened and hyperechoic and generally shows enlarged mesenteric lymph-nodes (Figure 4)[30,36].

Bowel US and ileocolonoscopy with histology have demonstrated an overall sensitivity of 74 and 88% and a specificity of 78 and 93%, respectively, in the detection of SB CD lesions[35,37]. The sensitivity of US in the detection of SB lesions is greater for those of the terminal ileum (approximately 90%-95%) than for those of the proximal SB (75%)[38]. US is useful for the follow-up

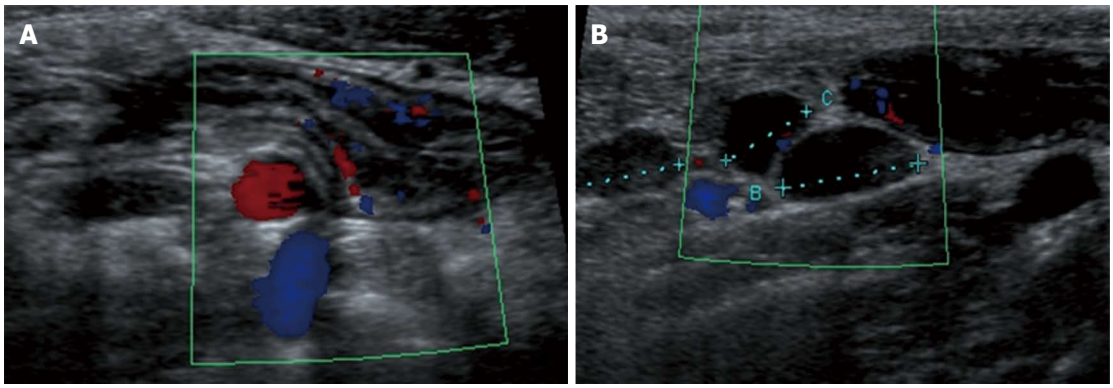

Figure 4 Longitudinal view of the terminal ileum in a 13-year-old boy with active Crohn's disease. The bowel wall is thickened and shows increase in Color Doppler signals denoting inflammatory hyperemia (A). Note in (B) the fibrofatty proliferation of the surrounding mesentery which appears hyperechoic and the enlarged mesenteric lymph-nodes.

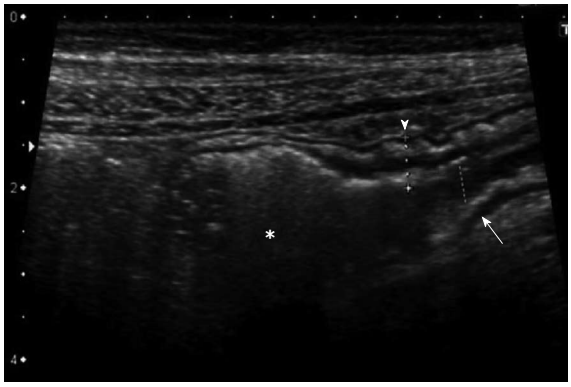

Figure 5 Longitudinal section of a distal ileal loop showing stiffness, mural thickening (arrowhead), lumen narrowing (arrow) and mild dilatation of the pre-stenotic segment (asterisk), suggesting a fibrotic nature of the stenosis.

of patients with CD[39,40]. and in early identifying intra-abdominal complications, such as abscesses, fistulae and strictures[41-44]. The reported sensitivity of US in detecting CD strictures approximately is 74%-80%[41]. US can also aid differentiate between fibrotic and inflammatory strictures. An increased Colour-Doppler signal in the stenosis is suggestive of activity, while poor vascularity of the bowel wall, an adjacent loops' retraction and a pre-stenotic bowel segment distension are suggestive of fibrotic stenosis (Figure 5)[31].

Some challenges about US still remain: US strongly relies on the operator's experience and skill more than other imaging modalities, and it requires an high resolution equipment. Moreover, even in expert hands, US may result in false positive findings[34]: thickening of the intestinal wall is not specific for CD, also being present in infectious, neoplastic and other inflammatory conditions. US may also provide false negative results[38,42], for example in obese patients or when CD is characterized by only superficial lesions, like isolated aphthous ulcers and mucosal erosions, or in presence of intestinal gas that make hardly visible the bowel wall, particularly the proximal ones.

Small Intestine Contrast US (SICUS). Some studies in adults have demonstrated that the so called SICUS, enables to overcome limits of standard US. Dissociation of intestinal overlapping loops and visualization of the entire SB, from the Treitz angle to the ileo-cecal valve, are obtained by distending the SB with an oral anechoic non-absorbable contrast solution (iso-osmolar polyethylene glycol)[36]. Briefly, US examination in performed after the ingestion of the oral contrast solution, that fill in the loops, and the administration of the intravenous (*iv*) contrast. Unfortunately the procedure is time consuming, requiring in some cases more than 2 hours. Pallotta *et al*[28] studied 148 patients, 57 with a known diagnosis of CD, showing SICUS to be more sensitive and specific (94% and 98%, respectively) than conventional US (57% and 100% respectively) in assessing SB lesions. The use of an oral contrast agent can significantly improve US sensitivity, approximately of 90% (Figure 6) and of over 75% for a single and multiple SB stenosis, respectively[42].

SICUS can make a dynamic evaluation of the affected segment differentiating between inflammatory and fibrotic stenosis. In fact, it can assess lumen stenosis and dilatation of the prestenotic segment, mural thickness with bowel wall stratification pattern and peristalsis of the affected segment differentiating between. SICUS is a very promising technique in children with CD, but its use in pediatric patients has still to be investigated.

CROSS SECTIONAL IMAGING

Good distension of SB loops during the CT and MRI examination is crucial for the correct evaluation of bowel wall abnormalities since collapsed SB loops are difficult to evaluate for bowel wall thickening or hyper-enhancement. Distension of the SB can be achieved by fluid administration after naso-jejunal intubation (CT/MR enteroclysis)[45,46] or per Os (CT/MR enterography)[47,48]. Although better distension of the loops is obtained with the MR/CT enteroclysis, there are various studies that show comparable accuracy between the two techniques[20,45,47,48]. The placement of the nasojejunal tube, necessary for the enteroclysis, is invasive, requires the use of ionizing

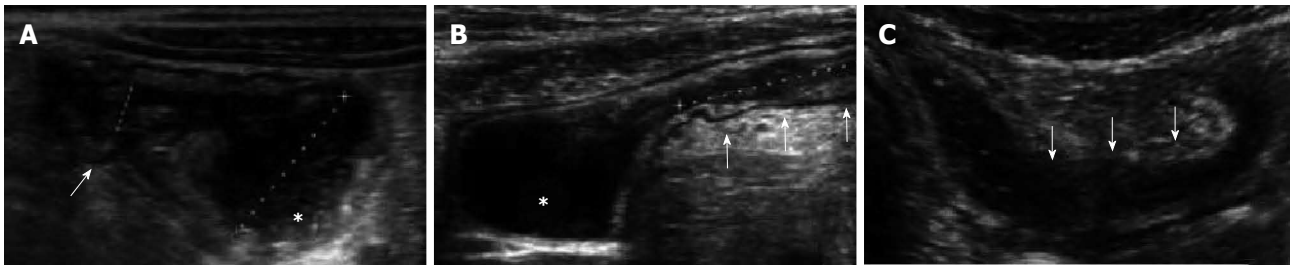

Figure 6 The oral anechoic contrast solution, (polyethylene glycol), allows a better definition of lumen narrowing (arrow) and pre-stenotic dilatation (asterisk) as well as a more accurate measurement of the length of the stenosis. Small intestine contrast ultrasonography also provides a dynamic assessment of the stenotic bowel loop: poor distensibility and presence of pre-stenotic dilatation suggest fibrosis, whereas normal distensibility and preserved peristalsis are features of inflammatory stenosis.

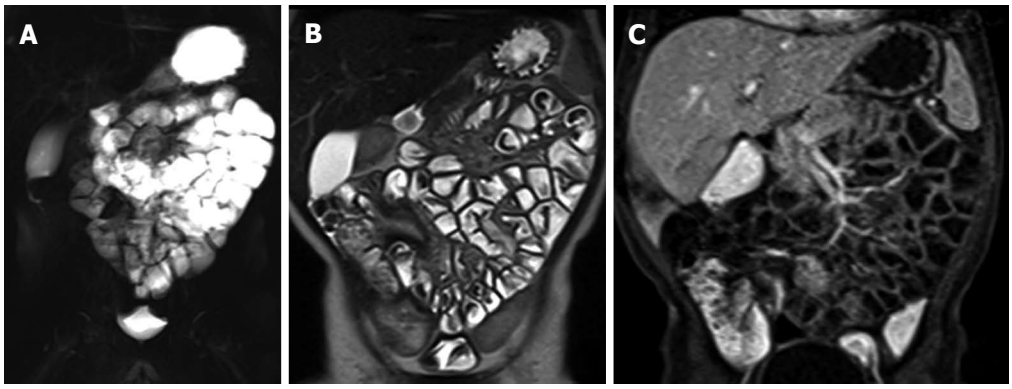

Figure 7 Magnetic resonance enteroclysis under anesthesia in one-year old male with Crohn's disease at colonoscopy. Coronal thick-slab HASTE image (A) shows good opacification of proximal and distal small bowel. The coronal T2-weighted (T2-w) image (B) and coronal fat-suppressed (FS) three-dimensional (3D) T1-weighted (T1-w) breath-hold gradient-echo (GE) image (C) are performed in free breathing.

radiations, which also entails the need for coordination between MR/CT suites and fluoroscopy units, and it can be very anxiety provoking resulting in poor patient tolerance. Moreover, the increased time and costs compared to enterography, make CT/MR enterography the preferred imaging method, respect to CT/MR enteroclysis, in pediatric patients.

An important limitation of CT/MR enterography is the need to drink an important amount of fluid in a short time, particularly uncomfortable in young patients. The assessment of mucosal abnormalities requires a correct distension of the loops obtained only with a proper timing of the study both in scanning or fluid ingestion. The collapsed bowel loops may mimic wall thickening and hyper-enhancement, leading to false-positive results.

The younger patients and the parents have to be motivated and aware of the importance of performing an adequate SB distension, which is fundamental for obtaining an optimal MR examination. The presence of a parent in the MR room is reassuring for younger children.

Most children diagnosed with IBD are of school age or adolescence. In a study from uniform data collected from a cohort of pediatric patients with IBD (1370 children), the mean age at diagnosis was 10.3 years with 47.7% diagnosed at 6 to 12 years of age and 36.9% at 13 to 17 years of age[49]. In our experience, children of this age are generally able to undergo the exam without sedation.

In the event a child refuses to drink the contrast agent, we will offer placement of a temporary nasogastric tube for contrast agent delivery. The enteric tube will be removed right after all of the contrast material is given and before the MR examination begins.

Patients under the age of 6 years, who require anesthesia do not undergo MR enterography and are usually imaged by using high-resolution bowel US or MR enteroclysis under anesthesia. The positioning of the tube takes place after the anesthesia. Children between 6 mo and 6 years of age are usually sedated with the intravenous injection of midazolam (Versed; Hoffman-La Roche, Basel, Switzerland) (0.05 mg per kilogram of body weight) or pentobarbital (Nembutal; Ovation Pharmaceuticals, Deerfield, Ill) (5 mg per kilogram of body weight). The sequences are performed in free breathing, making them as short as possible (Figure 7).

Computed Tomography

The relatively high radiation exposure is a limitation to the use of multi-detector CT (MDCT) enterography in children, and, in fact, most data regarding this method come from studies in adults[50]. The only recent pediatric IBD population's study[51] concluded that MDCT can be used as an alternative to barium studies for the evaluation

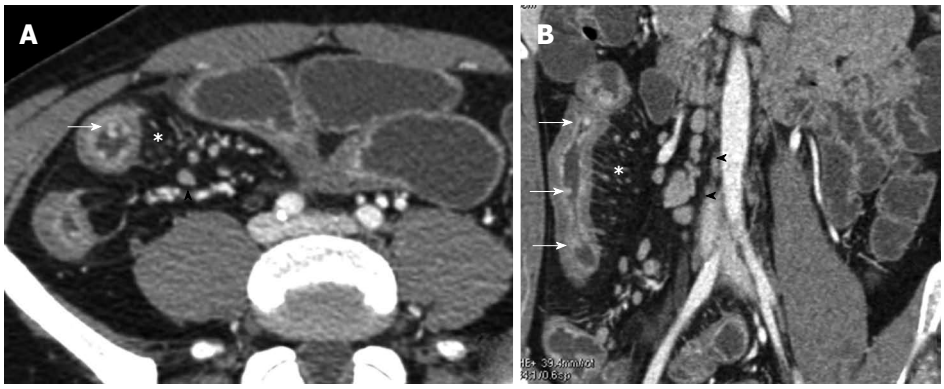

Figure 8 Transverse (A) and coronal (B) computed tomography show bowel wall thickening and mucosal hyper-enhancement with pseudo polyps (white arrows) as well as mesenteric lymph nodes, that are irregular in size and shape (black arrowhead) and increased mesenteric vascularity (asterisk). These features may be detected in case of acute exacerbation on a background of longstanding disease.

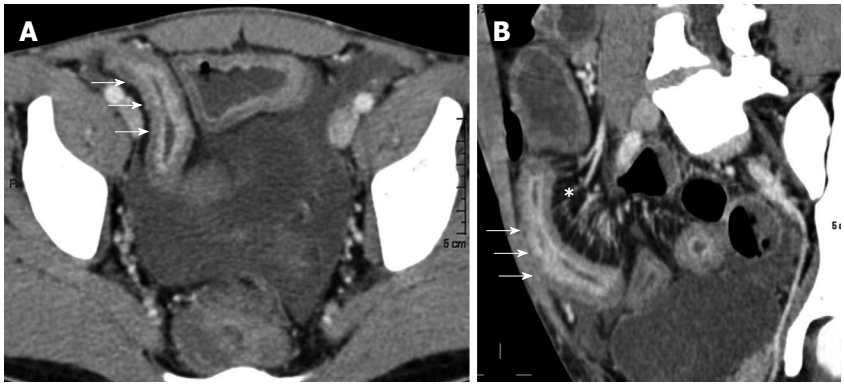

Figure 9 Transverse (A) and MRP sagittal (B) computed tomography show stratified enhancement of terminal ileum (arrows), and hyperemic mesentery with the "comb sign" (asterisk).

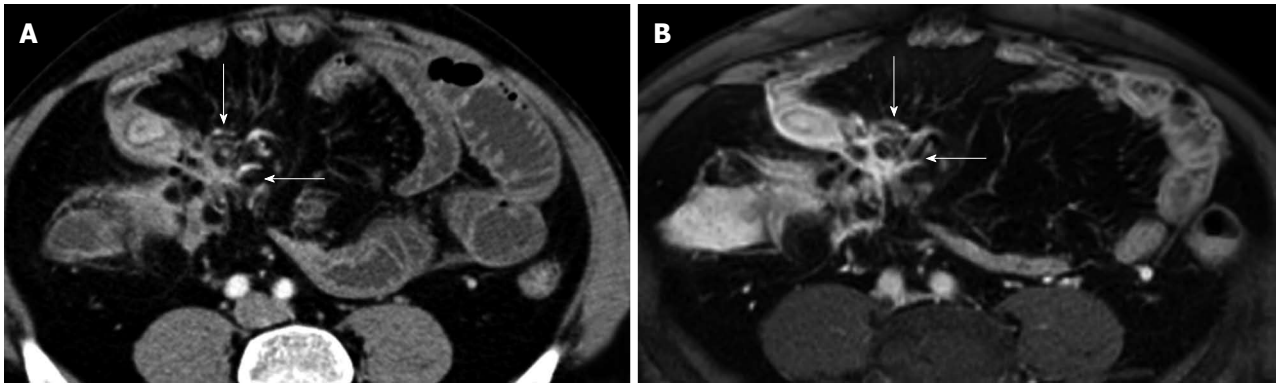

Figure 10 Transverse computed tomography (A) and post contrast T1-fat sat magnetic resonance imaging (B) images show a complex network between closely adherent small bowel loops appearing as a stellate configuration (arrows) due to entero-enteric fistulas.

of the SB and that most of the children prefer CT rather than barium studies. Several studies on adult population showed that is an excellent non-invasive tool for diagnosing CD, and for the follow-up of the disease during therapy[19,20,52-54]. CT enterography can establish disease extension and activity on the basis of wall thickness and increased *iv* contrast enhancement. In recent studies bowel wall thickness is considered pathological when exceeds 3 mm[55,56] (Figure 8). A sign of active disease is an increased bowel wall enhancement after administration of *iv* contrast medium[57,58]. The post-contrast wall pattern depends on the different enhancement of the mucosa and/or serosa and the submucosa, usually hypodense for the presence of edema, and can be seen as mural stratification or target sign (Figure 9), with two or three different layers of density respectively. In chronic CD, the affected segments may present a non-enhancement pattern after contrast medium, with the loss of mural stratifica-

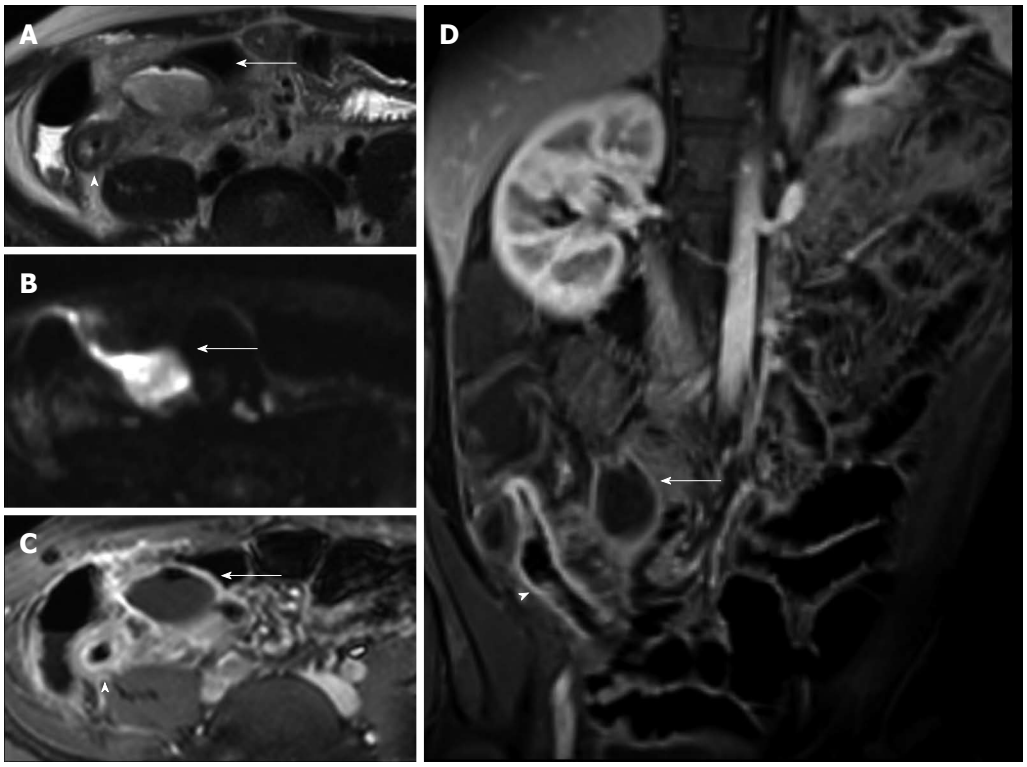

Figure 11 Eighteen-years-old female with active Crohn's disease and abscess. Transverse T2-w (A), DWI (B), transverse (C) and coronal (D) post-contrast FS-T1-w image (C) show inflamed segments of the terminal ileum (arrowhead) with pericecal fluid-collection around ticked and hype-vascular walls (arrow), according to abscess. A small air bubble in the antideclive portion of the fluid collection is visible in the transverse T2-w (A) and transverse post-contrast FS-T1-w image (C).

tion, suggestive of fibrosis. Another typical extramural lesion in CD is the comb sign due to an increased vascularity of the mesentery seen in the images as tortuous dilated vessels associated with a wide spacing of the vasa recta (Figure 8).

The most reliable criterion to define a stricture is a localized, persistent narrowing, whose functional effects may be judged from pre-stenotic dilatation[59]. CT, together with MRI, is the most accurate technique to detect the presence of extraluminal complications, such as abscesses, fistulae (Figure 10) and inflammatory conglomerates in CD[20,46,53,54,60-62].

CT has a high accuracy in the imaging of CD but it is limited by the use of ionizing radiations especially in children particularly in these type of chronic diseases that require a close follow up[13,63].

The radiation dose can be significantly reduce by the use of last generation MDCT scan with specific pediatric protocols[64,65] which include the introduction of noise to simulate low-dose exams[66].

Still, in pediatric patients MR must be preferred to MDCT, since it does not use ionizing radiation to which children are more vulnerable than adults for their longer life expectancy. Moreover, despite new formulations and improved safety, iodinated contrast media for CT are not without risk and the risks must be balanced against the possible benefits. However, in the hospitals without MR scan, or where it is difficult to schedule an emergent MRI, or in emergency situations, such as high-grade SB occlusion, MDCT remains the best technique in pediatric patients, too. In fact CT has greater availability and it is less time-consuming than MR (20-30 min for MR, respect to 10 s for MDCT).

Magnetic Resonance

The main advantages of MRI are, in addition to the lack of ionizing radiations, a superior soft tissue contrast with a better assessment of trans and extramural disease, its noninvasiveness and the multiplanar capability. Additionally, some MRI sequences (diffusion, perfusion, motility) can provide functional and quantitative information of the bowel wall (diffusion, perfusion, motility) that CT cannot obtain. Especially, diffusion-weighted sequence does not significantly increase the time of the examination and may provide helpful clues for the identification of areas of active inflammation and of abscesses (Figure 11) without *iv* contrast agent. Moreover, the use of cine MRI in patients suffering from CD proves the association of motility changes of the SB wall and extraluminal alterations, which can help in the differential diagnosis between fibrotic and inflammatory stenosis[67].

In relation to imaging features, CD may present as active inflammation (without strictures or fistulas), penetrating lesions, or fibrostenotic disease[68]. Patients may present characteristics of more than one disease subtypes.

Active disease. Various MR imaging findings have been proposed as correlating with CD activity. Increased wall thickening and mural contrast enhancement (CE) on MRI were found to be sensitive and specific for active CD in pediatric population[69]. Laghi *et al*[69] found a strong

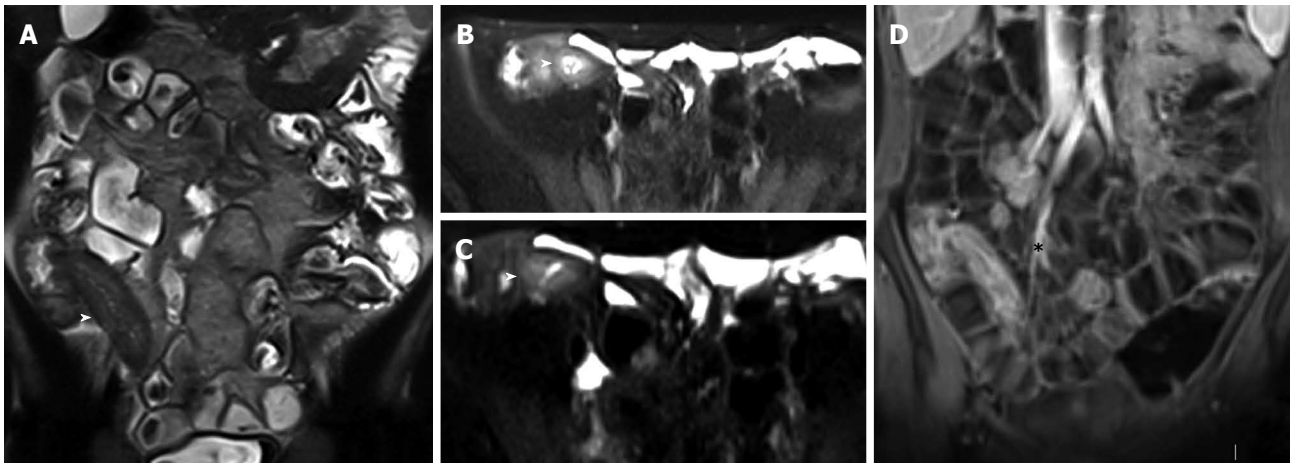

Figure 12 Thirteen years old male with active Crohn's disease. Coronal T2-weighted image (A), and transverse fat saturation T2-weighted images (B and C), show mural thickness and increased mural signal (arrowhead in B, C, and D) in the terminal ileum due to edema. Coronal post-contrast T1-weighted fat-suppressed image (D) at the same level shows mural stratification (asterisk).

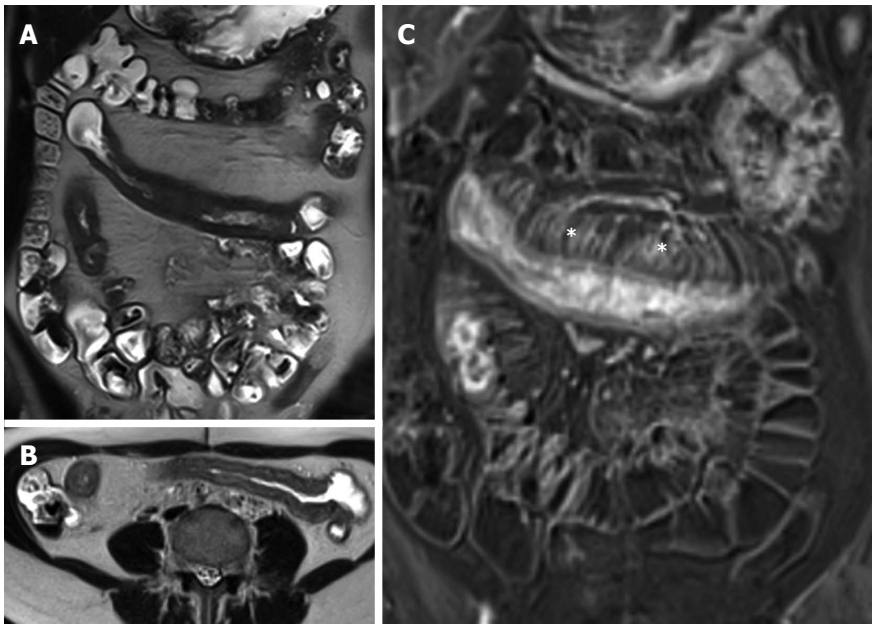

Figure 13 Thirteen years old female with active Crohn's disease. Coronal (A), transverse (B) T2-weighted images show thickened, inflamed segments of ileum and fat proliferating in the mesentery. The thin layer of high signal on T2 in b represents edema. The mass of the fat will displace adjacent small bowel. Coronal post-contrast T1-weighted fat-suppressed image (C) shows increased vascularity (asterisks), named "comb sign", adjacent to a hyper-enhancing thickened segment of ileum.

correlation between a semi-quantitative score (reflecting bowel-wall CE and thickening) and Pediatric Crohn's Disease Activity Index (PCDAI) in CD patients. In a recent study on pediatric population, Alexopoulou *et al*[70] showed that the MR percentage of CE (%CE) of the bowel wall do not correlate with PCDAI values. Other studies have reported similar results in the past[71,72], while a correlation with C-reactive protein (CRP) was already demonstrated in pediatric[70] and adult[71] population. In children, clinical evaluation of disease activity may be even more subjective due to incomplete cooperation, and this explains the observed lack of correlation between PCDAI and %CE values, while in contrast, %CE values were correlated with CRP, which is a more objective marker of inflammation[70].

The wall thickening, its high mural signal intensity on T2-weighted fat-saturated (FS-T2-w) images, and the presence of mural stratification on post-contrast T1-weighted fat-saturated (FS-T1-w) images reflect histologic features of acute SB inflammation in CD[69,71,72] (Figure 12). A purely quantitative approach would be desirable for MRI evaluation of active disease. However, in patients with CD, measurements of the bowel wall MR signal intensity are subjected to wide limits of both inter- and intra-reader agreement, which may substantially limit their utility when applied to the development of quantitative measures of inflammatory activity in the affected bowel segments[73,74].

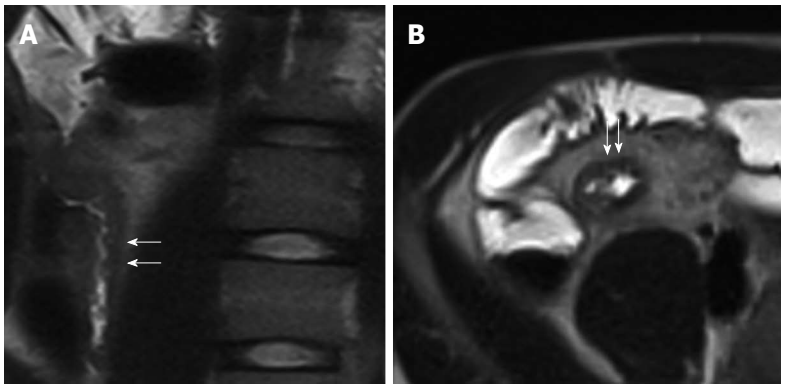

Figure 14 Coronal (A), transverse (B) T2-weighted images show thickened, inflamed segments of the terminal ileum with deep ulcers seen as high-contrast protrusions within bowel wall (arrows).

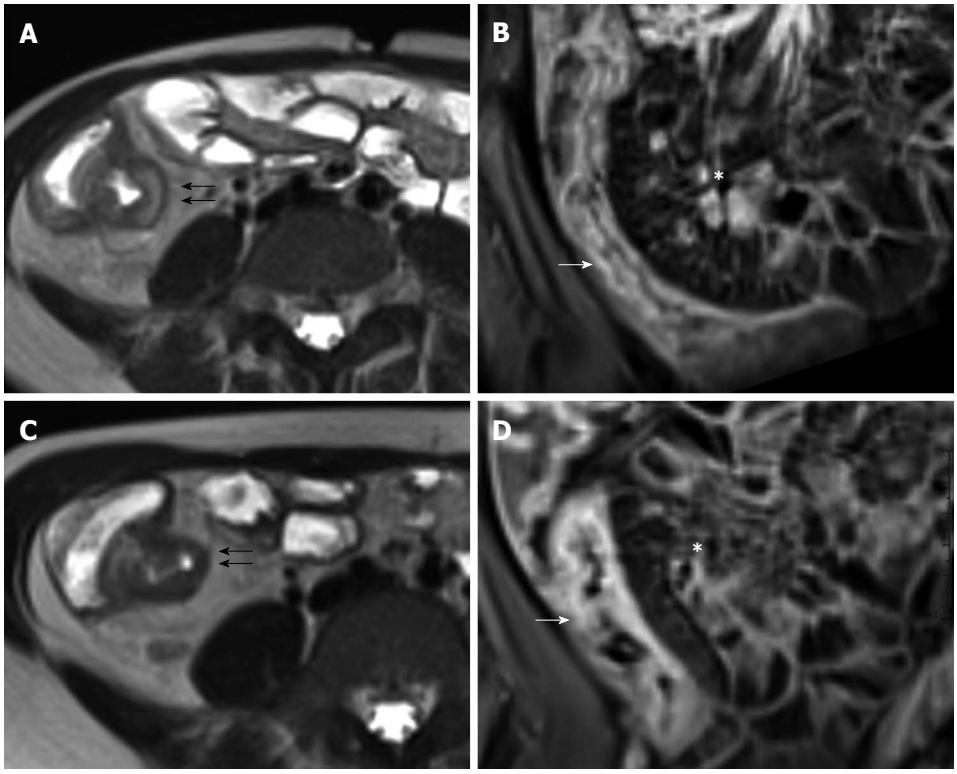

Figure 15 Twelve years old female with active disease and follow-up. Transverse T2-weighted image (A) shows mural thickening (arrows) and increased mural signal (arrow) in the terminal ileum and coronal T1-weighted image (B) shows mural stratification (arrow), increased mesenteric vascularity adjacent to the inflamed bowel loop (the comb sign), and enlargement and hyper-enhancement of lymph-nodes (asterisk). In the same patient and at the same level, six months later after therapy, transverse T2-weighted image (C) shows the loss of increased mural signal (arrow) and coronal T1-weighted image (D) shows homogeneous enhancement without mural stratification (arrow), reduction of increased mesenteric vascularity adjacent to the inflamed bowel loop, and disappearance of lymp-nodes (asterisk).

Acute inflammation can also present with the comb sign (Figure 13), due to an increased vascularity of the mesentery, ulcers (Figure 14) and enlarged and high enhancing lymph-nodes[74-77].

A proper luminal distension is essential to assess ulcers on MRI, especially if superficial[74]. In a systematic review of seven studies[52], MRI showed an accuracy of 91%, 62% and 62% in correctly staging a frank, mild and in remission disease, respectively. MRI more often overstaged than understaged disease activity in CD, but in most of these patients radiological staging and disease staging by the reference standard differed one grade. However, this review has the limit of including old studies without considering the new state-of-the-art techniques.

Actually radiologist use different protocols and features for grading CD, as recently showed by Ziech *et al*[78]. The authors show that the most frequently used MR protocols include T2-w (79%) and CE FS-T1-w (83%) sequences and that the features most frequently seen as important for grading are the presence of bowel wall thickening (79% of radiologists), abscesses (75%) and CE (75%) and stratification (46%) at T1-w images.

Currently, the most important applications of MR care the confirmation of the disease and the follow-up of patients with an already established diagnosis of CD, both by monitoring the response to medical treatment by assessing disease activity (Figure 15) and by early identify-

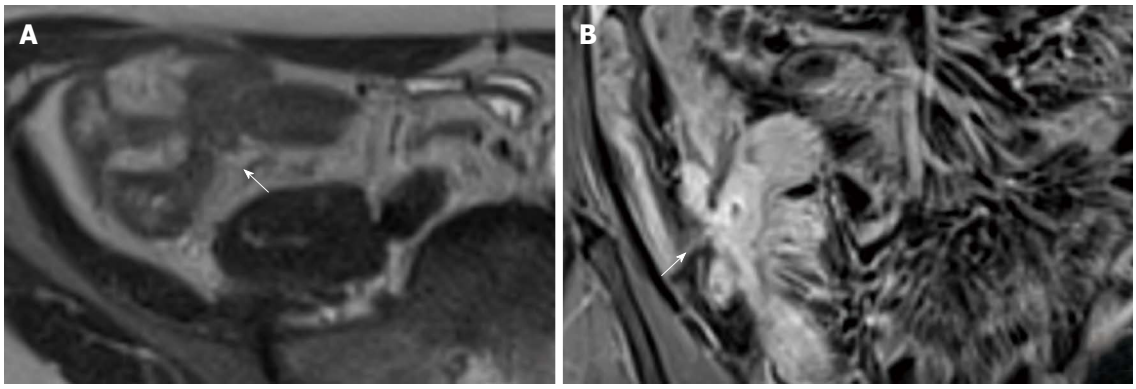

Figure 16 Transverse T2-w image (A) and coronal post-contrast FS-T1-w image (B) show cluster of bowel loops (arrow) interconnected by fistulas and adhesions.

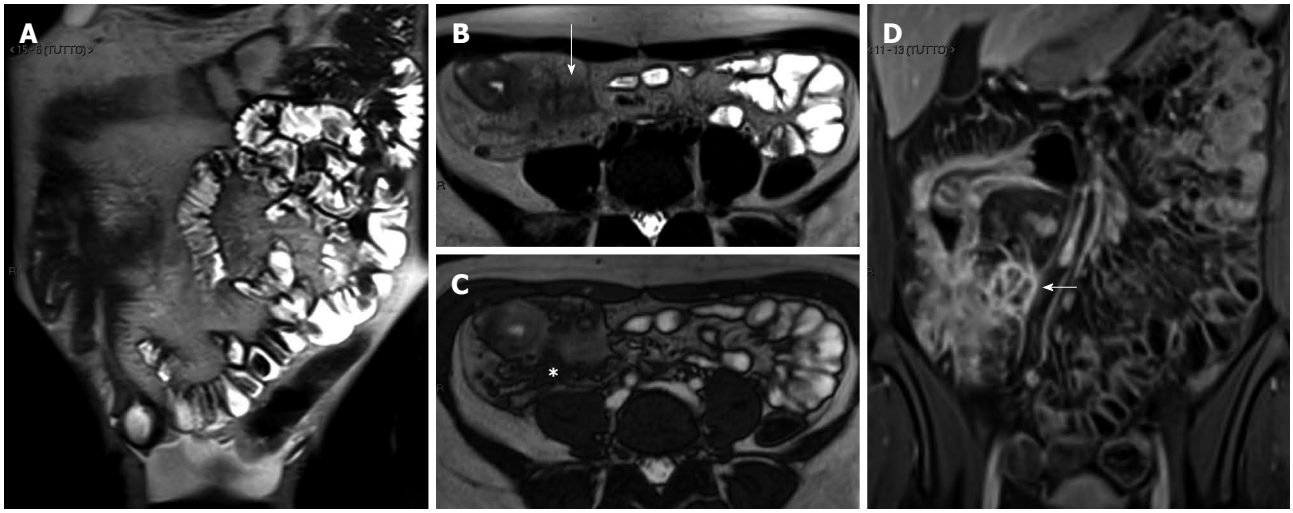

Figure 17 Coronal (A) and transverse (B and C) CE FS-T1-w 3D gradient-echo image show a small abscess close to the terminal ileum (arrows). Mural stratification and "comb sign" of the right colon flessure (black arrow), cecum (curved arrow), and appendix (white arrow) and homogeneous avid enhance of the terminal ileum (arrowhead). Enlargement and hyper-enhancement lymp-nodes (asterisk) are also visible.

ing of abscesses, fistulae and strictures.

Penetrating disease

Transmural inflammation can result from ulcers that deeply penetrate the bowel wall forming serpiginous tracts and fistulas.

MR enterography is accurate in identifying extraluminal complications of CD. In young adults MR enterography showed a diagnostic value similar to MDCT enterography at least for acute complications of CD, such as fistulas and abscesses[79]. The abscesses can be treated by percutaneous interventions. Whereas penetrating disease may benefit from antibiotics or biologic therapies, while the use of steroids is usually avoided. Because of the exquisite sensitivity to detect fluid as well as its superior soft tissue contrast, MR easily depicts entero-entero (Figure 16), entero-vesicular, entero-cutaneous, perianal fistulaes and abscesses (Figure 17). MR imaging may also detect small volumes of gas within an abscess (Figure 11). MR enterography can assess fistulizations, sinus tracts, and abscesses, especially with the use of post-contrast FS-T1-w images (Figure 10) because of their avidly enhancing walls[80]. Entero-enteric fistulas often form a complex network between closely adherent SB loops that may appear as a stellate configuration on CE MR images.

Fibrostenosing disease

Over the time, chronic inflammation of the bowel wall may evolve in mural fibrosis that can lead to intestinal occlusion if it causes strictures. The identification of fibrotic stenosis is fundamental for they are not responsive to medical therapy and need surgical resection. In general MR enterography has a good accuracy in assessing SB strictures that are considered significant if the dilatation of the upstream bowel exceeds 3 cm[77] (Figure 18). When there is mural fibrosis with permanent strictures, the thickened bowel wall of the pathological segment does not show a hyperintensity on T2-w images or a stratified post-contrast pattern on T1-w images typical of acute inflammation[74]. These items may be useful to distinguish between transient strictures supported by acute inflammation or fibrostenosing disease (Figure 19).

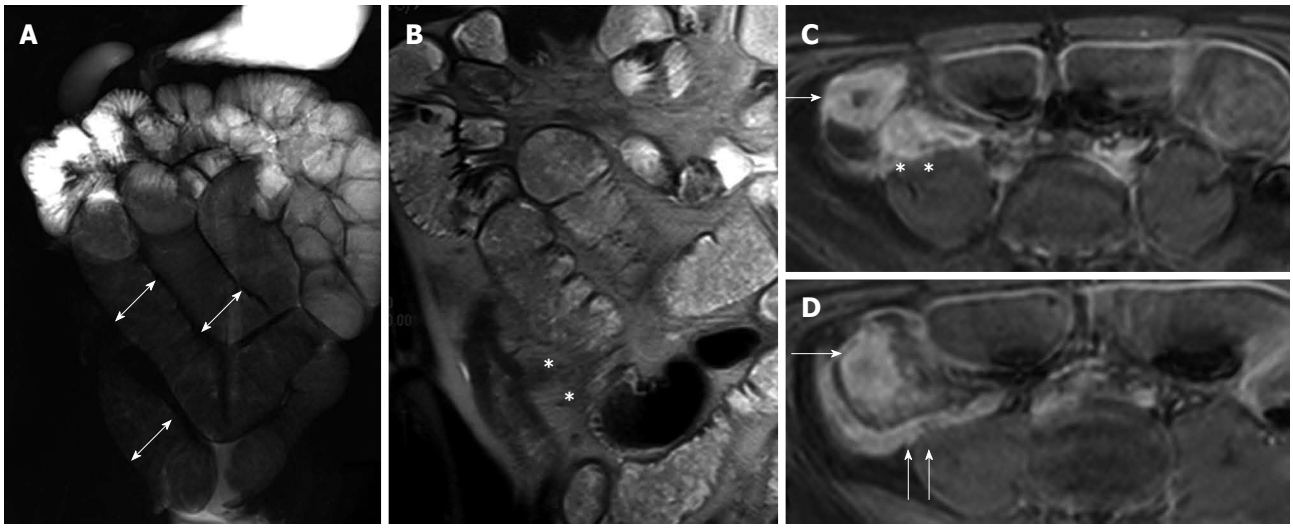

Figure 18 Fifteen years old male with small bowel obstruction caused by fibrotic stricture. Thick-slab T2-w sequence (A) shows bowel dilatation greater than 3 cm (double arrows), according to functionally significant stricture. Coronal T2-w sequence (B) shows mural thickening of the terminal ileum without increased wall signal (asterisks). Transverse (C and D) CE FS-T1-w 3D GE show a homogeneous avidly enhancing of the cecum (arrow in C and D), terminal ileum (asterisks in C) and appendix (arrows in D). These findings can be finding in the small bowel obstruction due to fibrotic stricture.

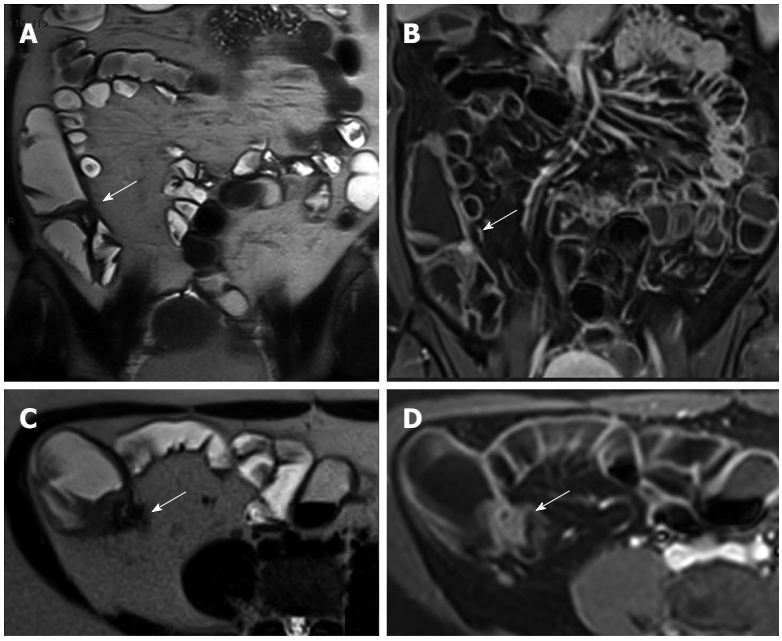

Figure 19 Eighteen-years-old female with long standing Crohn's disease. Coronal (A), transverse (B) T2-w images and coronal (C), transverse (D) post-contrast FS-T1-w images show thickening and hyper-enhancement of the ileocecal valve causing stricture.

Cine MRI sequences, allowing the evaluation of bowel motility, can further help this differential diagnosis. Inflammation along the mesenteric border often result in pseudosacculations along the antimesenteric border and can be thought of as the MR equivalent of the mesenteric border linear ulcer seen at SBFT examination (Figure 20). In general, the affected segments are characterized by increased rigidity, loss of distensibility and diminished peristalsis.

Suspected CD: In young patients with suspected CD, MR enterography is a valid method to diagnose or exclude the disease. Particularly, it can be used as the first radiological modality in pediatric patients in which the results of endoscopy examinations are normal but a high suspicion of CD is still present[81]. However, there is much debate about the best modality to use to examine the SB, because wireless endoscopic examinations, like radiological studies, have their advantages, such as the non-invasiveness and the high diagnostic accuracy in evaluating the small intestine, especially in patients who cannot undergo MR, whose bowel loops are not optimally distended or who are uncooperative, and disadvantages, such as capsule retention due to ileal strictures and

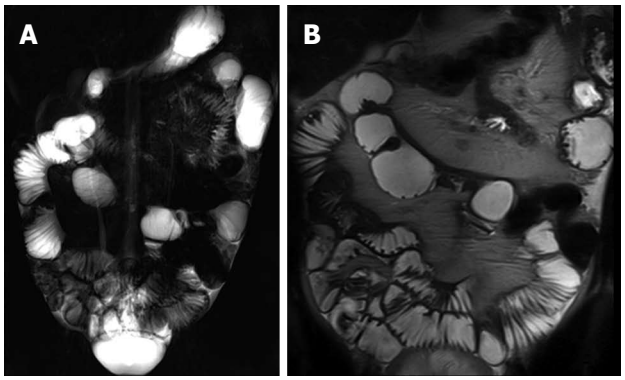

Figure 20 Coronal thick-slab HASTE (A) and coronal T2-weighted (B) images show pseudosacculations produced by asymmetric thickening of the ileal mesenteric border.

delayed capsule transit due to inflammatory lesions[82,83]. If a bowel obstruction is suspected, MR enterography is preferred to capsule endoscopy for the risk of capsule retention[84]. Moreover, MR enterography can help the diagnosis of terminal ileitis in symptomatic patients when endoscopy is unsuccessful.

Additional MRI findings: Extra-intestinal lesions are detected with MRI in 24%-58% of patients[84-86]. Herfarth *et al*[86] performed MR enteroclysis in 710 patients with a suspicion or a diagnosis of IBD finding extra-intestinal lesions in 57% of patients of which the 12% of great clinical importance. The colonic features of CD at MR enterography can reliably be diagnosed only in severe inflammation (Figure 21).

The detection of colonic mild disease can be very difficult even if the colon is well distended with the help of a rectal enema (MR colonography); moreover the main weaknesses of MR colonography is the impossibility of obtaining tissue sampling. However, Rimola *et al*[87] demonstrated good correlations between the presence and the severity of CD lesions depicted with endoscopy and MR Colonography.

MR is an effective imaging technique for the evaluation of patients with perianal CD. During MR enterography, it is possible to perform specific pelvic sequences, such as FS-T2-w, to evaluate perianal CD, increasing only few minutes of exam time (Figure 22).

MR has an accuracy of 76%-100% compared to examination under anesthesia for fistulae and may provide additional information[88]. This technique is an important tool because it can accurately reveal the location and extent of disease, including a clinically undetected fistula or abscess, and it can guide surgery[89].

3T MRI: There has been little experience of the use of 3 Tesla (T) MR imaging in children with CD, but it seems to have the advantage of increasing the signal-to-noise ratio (SNR) of approximately 1.7-1.8 times compared to 1.5T MR. This increases the spatial and/or temporal resolution, improving the detection of early, superficial or subtle abnormalities. However, the 3T advantages are potentially offset by other issues such as greater chemical shift, susceptibility artifact, B1 inhomogeneity and specific absorption rate[90,91].

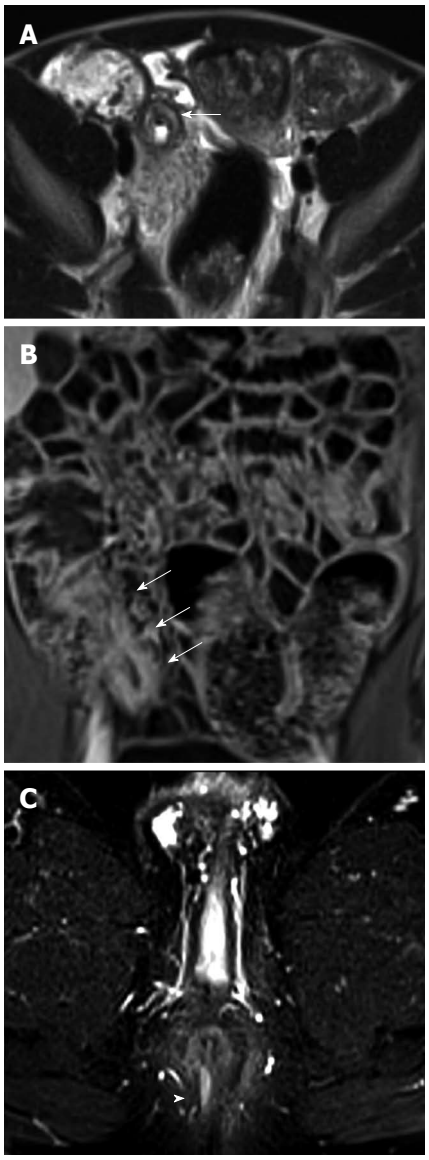

Figure 21 Colonic distention is optimized with a rectal enema. Coronal T2-w (A) and post-contrast FS-T1-w (B) images show bowel wall thickening, and mural stratification of terminal ileum (arrow) and sigma (arrows) walls.

PET-CT ENTEROGRAPHY

Combining the morphologic patterns obtained by CT enterography with the ^{18}F-FDG metabolic activity obtained by PET, PET-CT enterography as a single test may provide accurately fused morphologic, physiologic, and metabolic imaging, useful in the diagnosis, evaluation of activity, follow-up, and objective assessment of CD[92]. Groshar *et al*[93] showed a statistically significant difference in mean SUV max among the different mural patterns revealed on CT enterography: intramural edema (active inflammation), intramural soft tissue attenuation (inflammatory infiltrate), and intramural fat (chronic inflamma-

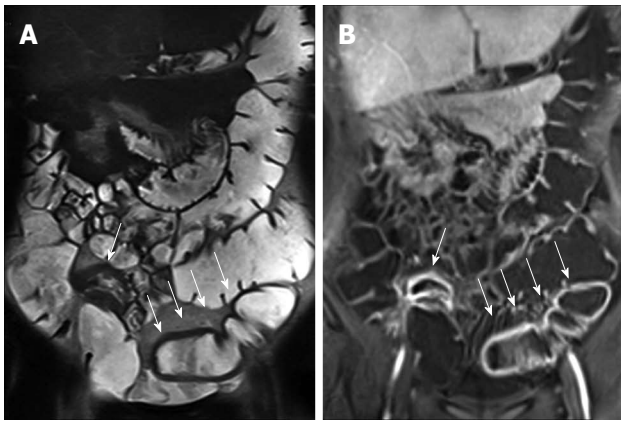

Figure 22 Twelve years old male with terminal ileum Crohn's disease and perianal fistula. Transverse T2-w (A) and post-contrast FS-T1-w (B) shows terminal ileum submucosa edema (black arrow) and mural stratification (arrows), respectively. Transverse FS-T2-w (C) image shows perianal fistula (arrowhead) in the same patient.

tion). Therefore, PET-CT data could help to distinguish between acute inflammation and fibrotic strictures. However, physiologic uptake of FDG by the intestine can lead to false positive results[94,95]. Moreover, the effective dose from PET-CT is actually too high for pediatric patients[92].

CONCLUSION

The diagnosis and management of CD in children has changed dramatically over the last decade, mainly due to the increased awareness of the risk of the ionizing radiations, the availability of improved diagnostic modalities, and newer, more powerful treatments such as biologics. Techniques without ionizing radiation (US and MRI) are the preferred modalities for the evaluation of the SB in pediatric patients. The goals of the proximal future studies will be the development of a MR validated score system capable of measuring intestinal damage and inflammatory disease activity in children with CD. In future, a potential new imaging technique could be the PET-MR, which combines the morphological MR images with the functional PET information. Several radiopharmaceuticals are now available for imaging CD, but new tracers could change the future of the diagnostic imaging.

REFERENCES

1 **Levine A**, Griffiths A, Markowitz J, Wilson DC, Turner D, Russell RK, Fell J, Ruemmele FM, Walters T, Sherlock M, Dubinsky M, Hyams JS. Pediatric modification of the Montreal classification for inflammatory bowel disease: the Paris classification. *Inflamm Bowel Dis* 2011; **17**: 1314-1321 [PMID: 21560194 DOI: 10.1002/ibd.21493]

2 **Cuffari C**, Dubinsky M, Darbari A, Sena L, Baldassano R. Crohn's jejunoileitis: the pediatrician's perspective on diagnosis and management. *Inflamm Bowel Dis* 2005; **11**: 696-704 [PMID: 15973125]

3 **Torkzad MR**, Ullberg U, Nyström N, Blomqvist L, Hellström P, Fagerberg UL. Manifestations of small bowel disease in pediatric Crohn's disease on magnetic resonance enterography. *Inflamm Bowel Dis* 2012; **18**: 520-528 [PMID: 21538711 DOI: 10.1002/ibd.21725]

4 **Shikhare G**, Kugathasan S. Inflammatory bowel disease in children: current trends. *J Gastroenterol* 2010; **45**: 673-682 [PMID: 20414789 DOI: 10.1007/s00535-010-0241-5]

5 **Chouraki V**, Savoye G, Dauchet L, Vernier-Massouille G, Dupas JL, Merle V, Laberenne JE, Salomez JL, Lerebours E, Turck D, Cortot A, Gower-Rousseau C, Colombel JF. The changing pattern of Crohn's disease incidence in northern France: a continuing increase in the 10- to 19-year-old age bracket (1988-2007). *Aliment Pharmacol Ther* 2011; **33**: 1133-1142 [PMID: 21488915 DOI: 10.1111/j.1365-2036.2011.04628.x]

6 **Cuffari C**, Darbari A. Inflammatory bowel disease in the pediatric and adolescent patient. *Gastroenterol Clin North Am* 2002; **31**: 275-291 [PMID: 12122738]

7 **Stuart S**, Conner T, Ahmed A, Steward M, Maclachlan J, Wylie P, Beal I. The smaller bowel: imaging the small bowel in paediatric Crohn's disease. *Postgrad Med J* 2011; **87**: 288-297 [PMID: 21242573 DOI: 10.1136/pgmj.2010.106641]

8 **Mackalski BA**, Bernstein CN. New diagnostic imaging tools for inflammatory bowel disease. *Gut* 2006; **55**: 733-741 [PMID: 16609136]

9 **Fletcher JG**, Fidler JL, Bruining DH, Huprich JE. New concepts in intestinal imaging for inflammatory bowel diseases. *Gastroenterology* 2011; **140**: 1795-1806 [PMID: 21530746 DOI: 10.1053/j.gastro.2011.02.013]

10 **Pariente B**, Cosnes J, Danese S, Sandborn WJ, Lewin M, Fletcher JG, Chowers Y, D'Haens G, Feagan BG, Hibi T, Hommes DW, Irvine EJ, Kamm MA, Loftus EV, Louis E, Michetti P, Munkholm P, Oresland T, Panés J, Peyrin-Biroulet L, Reinisch W, Sands BE, Schoelmerich J, Schreiber S, Tilg H, Travis S, van Assche G, Vecchi M, Mary JY, Colombel JF, Lémann M. Development of the Crohn's disease digestive damage score, the Lémann score. *Inflamm Bowel Dis* 2011; **17**: 1415-1422 [PMID: 21560202 DOI: 10.1002/ibd.21506]

11 **IBD Working Group of the European Society for Paediatric Gastroenterology, Hepatology and Nutrition**. Inflammatory bowel disease in children and adolescents: recommendations for diagnosis--the Porto criteria. *J Pediatr Gastroenterol Nutr* 2005; **41**: 1-7 [PMID: 15990620]

12 **Desmond AN**, O'Regan K, Curran C, McWilliams S, Fitzgerald T, Maher MM, Shanahan F. Crohn's disease: factors associated with exposure to high levels of diagnostic radiation. *Gut* 2008; **57**: 1524-1529 [PMID: 18443021 DOI: 10.1136/gut.2008.151415]

13 **Gaca AM**, Jaffe TA, Delaney S, Yoshizumi T, Toncheva G, Nguyen G, Frush DP. Radiation doses from small-bowel follow-through and abdomen/pelvis MDCT in pediatric Crohn disease. *Pediatr Radiol* 2008; **38**: 285-291 [PMID: 18183380 DOI: 10.1007/s00247-007-0702-z]

14 **Panes J**, Bouhnik Y, Reinisch W, Stoker J, Taylor SA, Baumgart DC, Danese S, Halligan S, Marincek B, Matos C, Peyrin-Biroulet L, Rimola J, Rogler G, van Assche G, Ardizzone S, Ba-Ssalamah A, Bali MA, Bellini D, Biancone L, Castiglione F, Ehehalt R, Grassi R, Kucharzik T, Maccioni F, Maconi G, Magro F, Martín-Comín J, Morana G, Pendsé D, Sebastian S, Signore A, Tolan D, Tielbeek JA, Weishaupt D, Wiarda B, Laghi A. Imaging techniques for assessment of inflammatory bowel disease: joint ECCO and ESGAR evidence-based consensus guidelines. *J Crohns Colitis* 2013; **7**: 556-585 [PMID: 23583097 DOI: 10.1016]

15 **Van Assche G**, Dignass A, Panes J, Beaugerie L, Karagiannis J, Allez M, Ochsenkühn T, Orchard T, Rogler G, Louis E, Kupcinskas L, Mantzaris G, Travis S, Stange E. The second European evidence-based Consensus on the diagnosis and management of Crohn's disease: Definitions and diagnosis. *J Crohns Colitis* 2010; **4**: 7-27 [PMID: 21122488 DOI: 10.1016/j.crohns.2009.12.003]

16 **Van Assche G**, Dignass A, Reinisch W, van der Woude CJ, Sturm A, De Vos M, Guslandi M, Oldenburg B, Dotan I, Marteau P, Ardizzone A, Baumgart DC, D'Haens G, Gionch-

etti P, Portela F, Vucelic B, Söderholm J, Escher J, Koletzko S, Kolho KL, Lukas M, Mottet C, Tilg H, Vermeire S, Carbonnel F, Cole A, Novacek G, Reinshagen M, Tsianos E, Herrlinger K, Oldenburg B, Bouhnik Y, Kiesslich R, Stange E, Travis S, Lindsay J. The second European evidence-based Consensus on the diagnosis and management of Crohn's disease: Special situations. *J Crohns Colitis* 2010; **4**: 63-101 [PMID: 21122490 DOI: 10.1016/j.crohns.2009.09.009]

17 **Huprich JE**, Rosen MP, Fidler JL, Gay SB, Grant TH, Greene FL, Lalani T, Miller FH, Rockey DC, Sudakoff GS, Gunderman R, Coley BD. ACR Appropriateness Criteria on Crohn's disease. *J Am Coll Radiol* 2010; **7**: 94-102 [PMID: 20142082 DOI: 10.1016/j.jacr.2009.10.009]

18 **Kurugoglu S**, Korman U, Adaletli I, Selcuk D. Enteroclysis in older children and teenagers. *Pediatr Radiol* 2007; **37**: 457-466 [PMID: 17377787]

19 **Brown S**, Applegate KE, Sandrasegaran K, Jennings SG, Garrett J, Skantharajah A, Maglinte DT. Fluoroscopic and CT enteroclysis in children: initial experience, technical feasibility, and utility. *Pediatr Radiol* 2008; **38**: 497-510 [PMID: 18256816 DOI: 10.1007/s00247-008-0754-8]

20 **Wold PB**, Fletcher JG, Johnson CD, Sandborn WJ. Assessment of small bowel Crohn disease: noninvasive peroral CT enterography compared with other imaging methods and endoscopy--feasibility study. *Radiology* 2003; **229**: 275-281 [PMID: 12944602]

21 **Hara AK**, Leighton JA, Heigh RI, Sharma VK, Silva AC, De Petris G, Hentz JG, Fleischer DE. Crohn disease of the small bowel: preliminary comparison among CT enterography, capsule endoscopy, small-bowel follow-through, and ileoscopy. *Radiology* 2006; **238**: 128-134 [PMID: 16373764]

22 **Batres LA**, Maller ES, Ruchelli E, Mahboubi S, Baldassano RN. Terminal ileum intubation in pediatric colonoscopy and diagnostic value of conventional small bowel contrast radiography in pediatric inflammatory bowel disease. *J Pediatr Gastroenterol Nutr* 2002; **35**: 320-323 [PMID: 12352520]

23 **Triester SL**, Leighton JA, Leontiadis GI, Gurudu SR, Fleischer DE, Hara AK, Heigh RI, Shiff AD, Sharma VK. A meta-analysis of the yield of capsule endoscopy compared to other diagnostic modalities in patients with non-stricturing small bowel Crohn's disease. *Am J Gastroenterol* 2006; **101**: 954-964 [PMID: 16696781]

24 **Krille L**, Zeeb H, Jahnen A, Mildenberger P, Seidenbusch M, Schneider K, Weisser G, Hammer G, Scholz P, Blettner M. Computed tomographies and cancer risk in children: a literature overview of CT practices, risk estimations and an epidemiologic cohort study proposal. *Radiat Environ Biophys* 2012; **51**: 103-111 [PMID: 22310909 DOI: 10.1007/s00411-012-0405-1]

25 **Hara AK**, Leighton JA, Sharma VK, Fleischer DE. Small bowel: preliminary comparison of capsule endoscopy with barium study and CT. *Radiology* 2004; **230**: 260-265 [PMID: 14617764]

26 **Albert JG**, Martiny F, Krummenerl A, Stock K, Lesske J, Göbel CM, Lotterer E, Nietsch HH, Behrmann C, Fleig WE. Diagnosis of small bowel Crohn's disease: a prospective comparison of capsule endoscopy with magnetic resonance imaging and fluoroscopic enteroclysis. *Gut* 2005; **54**: 1721-1727 [PMID: 16020490]

27 **Alison M**, Kheniche A, Azoulay R, Roche S, Sebag G, Belarbi N. Ultrasonography of Crohn disease in children. *Pediatr Radiol* 2007; **37**: 1071-1082 [PMID: 17899062]

28 **Pallotta N**, Tomei E, Viscido A, Calabrese E, Marcheggiano A, Caprilli R, Corazziari E. Small intestine contrast ultrasonography: an alternative to radiology in the assessment of small bowel disease. *Inflamm Bowel Dis* 2005; **11**: 146-153 [PMID: 15677908]

29 **Migaleddu V**, Quaia E, Scanu D, Carla S, Bertolotto M, Campisi G, Sirigu D, Virgilio G. Inflammatory activity in Crohn's disease: CE-US. *Abdom Imaging* 2011; **36**: 142-148 [PMID: 20464392 DOI: 10.1007/s00261-010-9622-8]

30 **Maconi G**, Radice E, Greco S, Bianchi Porro G. Bowel ultrasound in Crohn's disease. *Best Pract Res Clin Gastroenterol* 2006; **20**: 93-112 [PMID: 16473803]

31 **Fraquelli M**, Colli A, Casazza G, Paggi S, Colucci A, Massironi S, Duca P, Conte D. Role of US in detection of Crohn disease: meta-analysis. *Radiology* 2005; **236**: 95-101 [PMID: 15987966]

32 **Darge K**, Anupindi S, Keener H, Rompel O. Ultrasound of the bowel in children: how we do it. *Pediatr Radiol* 2010; **40**: 528-536 [PMID: 20225117 DOI: 10.1007/s00247-010-1550-9]

33 **Haber HP**, Busch A, Ziebach R, Stern M. Bowel wall thickness measured by ultrasound as a marker of Crohn's disease activity in children. *Lancet* 2000; **355**: 1239-1240 [PMID: 10770308]

34 **Haber HP**, Stern M. Intestinal ultrasonography in children and young adults: bowel wall thickness is age dependent. *J Ultrasound Med* 2000; **19**: 315-321 [PMID: 10811404]

35 **Faure C**, Belarbi N, Mougenot JF, Besnard M, Hugot JP, Cézard JP, Hassan M, Navarro J. Ultrasonographic assessment of inflammatory bowel disease in children: comparison with ileocolonoscopy. *J Pediatr* 1997; **130**: 147-151 [PMID: 9003865]

36 **Maconi G**, Di Sabatino A, Ardizzone S, Greco S, Colombo E, Russo A, Cassinotti A, Casini V, Corazza GR, Bianchi Porro G. Prevalence and clinical significance of sonographic detection of enlarged regional lymph nodes in Crohn's disease. *Scand J Gastroenterol* 2005; **40**: 1328-1333 [PMID: 16243717]

37 **Bremner AR**, Griffiths M, Argent JD, Fairhurst JJ, Beattie RM. Sonographic evaluation of inflammatory bowel disease: a prospective, blinded, comparative study. *Pediatr Radiol* 2006; **36**: 947-953 [PMID: 16845511]

38 **Parente F**, Maconi G, Bollani S, Anderloni A, Sampietro G, Cristaldi M, Franceschelli N, Bianco R, Taschieri AM, Bianchi Porro G. Bowel ultrasound in assessment of Crohn's disease and detection of related small bowel strictures: a prospective comparative study versus x ray and intraoperative findings. *Gut* 2002; **50**: 490-495 [PMID: 11889068]

39 **Scholbach T**, Herrero I, Scholbach J. Dynamic color Doppler sonography of intestinal wall in patients with Crohn disease compared with healthy subjects. *J Pediatr Gastroenterol Nutr* 2004; **39**: 524-528 [PMID: 15572893]

40 **Drews BH**, Barth TF, Hänle MM, Akinli AS, Mason RA, Muche R, Thiel R, Pauls S, Klaus J, von Boyen G, Kratzer W. Comparison of sonographically measured bowel wall vascularity, histology, and disease activity in Crohn's disease. *Eur Radiol* 2009; **19**: 1379-1386 [PMID: 19184036 DOI: 10.1007/s00330-008-1290-5]

41 **Maconi G**, Bollani S, Bianchi Porro G. Ultrasonographic detection of intestinal complications in Crohn's disease. *Dig Dis Sci* 1996; **41**: 1643-1648 [PMID: 8769293]

42 **Parente F**, Greco S, Molteni M, Anderloni A, Sampietro GM, Danelli PG, Bianco R, Gallus S, Bianchi Porro G. Oral contrast enhanced bowel ultrasonography in the assessment of small intestine Crohn's disease. A prospective comparison with conventional ultrasound, x ray studies, and ileocolonoscopy. *Gut* 2004; **53**: 1652-1657 [PMID: 15479688]

43 **Castiglione F**, de Sio I, Cozzolino A, Rispo A, Manguso F, Del Vecchio Blanco G, Di Girolamo E, Castellano L, Ciacci C, Mazzacca G. Bowel wall thickness at abdominal ultrasound and the one-year-risk of surgery in patients with Crohn's disease. *Am J Gastroenterol* 2004; **99**: 1977-1983 [PMID: 15447760]

44 **Pallotta N**, Baccini F, Corazziari E. Contrast ultrasonography of the normal small bowel. *Ultrasound Med Biol* 1999; **25**: 1335-1340 [PMID: 10626620]

45 **Schreyer AG**, Geissler A, Albrich H, Schölmerich J, Feuerbach S, Rogler G, Völk M, Herfarth H. Abdominal MRI after enteroclysis or with oral contrast in patients with suspected or proven Crohn's disease. *Clin Gastroenterol Hepatol* 2004; **2**:

491-497 [PMID: 15181618]
46 **Masselli G**, Casciani E, Polettini E, Lanciotti S, Bertini L, Gualdi G. Assessment of Crohn's disease in the small bowel: Prospective comparison of magnetic resonance enteroclysis with conventional enteroclysis. *Eur Radiol* 2006; **16**: 2817-2827 [PMID: 16799782]
47 **Negaard A**, Paulsen V, Sandvik L, Berstad AE, Borthne A, Try K, Lygren I, Storaas T, Klow NE. A prospective randomized comparison between two MRI studies of the small bowel in Crohn's disease, the oral contrast method and MR enteroclysis. *Eur Radiol* 2007; **17**: 2294-2301 [PMID: 17483955]
48 **Masselli G**, Casciani E, Polettini E, Gualdi G. Comparison of MR enteroclysis with MR enterography and conventional enteroclysis in patients with Crohn's disease. *Eur Radiol* 2008; **18**: 438-447 [PMID: 17899102]
49 **Heyman MB**, Kirschner BS, Gold BD, Ferry G, Baldassano R, Cohen SA, Winter HS, Fain P, King C, Smith T, El-Serag HB. Children with early-onset inflammatory bowel disease (IBD): analysis of a pediatric IBD consortium registry. *J Pediatr* 2005; **146**: 35-40 [PMID: 15644819]
50 **Dillman JR**, Adler J, Zimmermann EM, Strouse PJ. CT enterography of pediatric Crohn disease. *Pediatr Radiol* 2010; **40**: 97-105 [PMID: 19936733 DOI: 10.1007/s00247-009-1465-5]
51 **Jamieson DH**, Shipman PJ, Israel DM, Jacobson K. Comparison of multidetector CT and barium studies of the small bowel: inflammatory bowel disease in children. *AJR Am J Roentgenol* 2003; **180**: 1211-1216 [PMID: 12704025]
52 **Horsthuis K**, Bipat S, Bennink RJ, Stoker J. Inflammatory bowel disease diagnosed with US, MR, scintigraphy, and CT: meta-analysis of prospective studies. *Radiology* 2008; **247**: 64-79 [PMID: 18372465 DOI: 10.1148/radiol.2471070611]
53 **Siddiki HA**, Fidler JL, Fletcher JG, Burton SS, Huprich JE, Hough DM, Johnson CD, Bruining DH, Loftus EV, Sandborn WJ, Pardi DS, Mandrekar JN. Prospective comparison of state-of-the-art MR enterography and CT enterography in small-bowel Crohn's disease. *AJR Am J Roentgenol* 2009; **193**: 113-121 [PMID: 19542402 DOI: 10.2214/AJR.08.2027]
54 **Lee SS**, Kim AY, Yang SK, Chung JW, Kim SY, Park SH, Ha HK. Crohn disease of the small bowel: comparison of CT enterography, MR enterography, and small-bowel follow-through as diagnostic techniques. *Radiology* 2009; **251**: 751-761 [PMID: 19276325 DOI: 10.1148/radiol.2513081184]
55 **Paulsen SR**, Huprich JE, Fletcher JG, Booya F, Young BM, Fidler JL, Johnson CD, Barlow JM, Earnest F. CT enterography as a diagnostic tool in evaluating small bowel disorders: review of clinical experience with over 700 cases. *Radiographics* 2006; **26**: 641-657; discussion 657-662 [PMID: 16702444]
56 **Macari M**, Megibow AJ, Balthazar EJ. A pattern approach to the abnormal small bowel: observations at MDCT and CT enterography. *AJR Am J Roentgenol* 2007; **188**: 1344-1355 [PMID: 17449781]
57 **Booya F**, Fletcher JG, Huprich JE, Barlow JM, Johnson CD, Fidler JL, Solem CA, Sandborn WJ, Loftus EV, Harmsen WS. Active Crohn disease: CT findings and interobserver agreement for enteric phase CT enterography. *Radiology* 2006; **241**: 787-795 [PMID: 17032911]
58 **Bodily KD**, Fletcher JG, Solem CA, Johnson CD, Fidler JL, Barlow JM, Bruesewitz MR, McCollough CH, Sandborn WJ, Loftus EV, Harmsen WS, Crownhart BS. Crohn Disease: mural attenuation and thickness at contrast-enhanced CT Enterography--correlation with endoscopic and histologic findings of inflammation. *Radiology* 2006; **238**: 505-516 [PMID: 16436815]
59 **Silverberg MS**, Satsangi J, Ahmad T, Arnott ID, Bernstein CN, Brant SR, Caprilli R, Colombel JF, Gasche C, Geboes K, Jewell DP, Karban A, Loftus EV, Peña AS, Riddell RH, Sachar DB, Schreiber S, Steinhart AH, Targan SR, Vermeire S, Warren BF. Toward an integrated clinical, molecular and serological classification of inflammatory bowel disease: report of a Working Party of the 2005 Montreal World Congress of Gastroenterology. *Can J Gastroenterol* 2005; **19** Suppl A: 5A-36A [PMID: 16151544]
60 **Schmidt S**, Lepori D, Meuwly JY, Duvoisin B, Meuli R, Michetti P, Felley C, Schnyder P, van Melle G, Denys A. Prospective comparison of MR enteroclysis with multidetector spiral-CT enteroclysis: interobserver agreement and sensitivity by means of "sign-by-sign" correlation. *Eur Radiol* 2003; **13**: 1303-1311 [PMID: 12764646]
61 **Gourtsoyiannis NC**, Grammatikakis J, Papamastorakis G, Koutroumbakis J, Prassopoulos P, Rousomoustakaki M, Papanikolaou N. Imaging of small intestinal Crohn's disease: comparison between MR enteroclysis and conventional enteroclysis. *Eur Radiol* 2006; **16**: 1915-1925 [PMID: 16673093]
62 **Spalinger J**, Patriquin H, Miron MC, Marx G, Herzog D, Dubois J, Dubinsky M, Seidman EG. Doppler US in patients with crohn disease: vessel density in the diseased bowel reflects disease activity. *Radiology* 2000; **217**: 787-791 [PMID: 11110944]
63 **Jaffe TA**, Gaca AM, Delaney S, Yoshizumi TT, Toncheva G, Nguyen G, Frush DP. Radiation doses from small-bowel follow-through and abdominopelvic MDCT in Crohn's disease. *AJR Am J Roentgenol* 2007; **189**: 1015-1022 [PMID: 17954634]
64 **Silva AC**, Lawder HJ, Hara A, Kujak J, Pavlicek W. Innovations in CT dose reduction strategy: application of the adaptive statistical iterative reconstruction algorithm. *AJR Am J Roentgenol* 2010; **194**: 191-199 [PMID: 20028923 DOI: 10.2214/AJR.09.2953]
65 **Allen BC**, Baker ME, Einstein DM, Remer EM, Herts BR, Achkar JP, Davros WJ, Novak E, Obuchowski NA. Effect of altering automatic exposure control settings and quality reference mAs on radiation dose, image quality, and diagnostic efficacy in MDCT enterography of active inflammatory Crohn's disease. *AJR Am J Roentgenol* 2010; **195**: 89-100 [PMID: 20566801 DOI: 10.2214/AJR.09.3611]
66 **Kambadakone AR**, Prakash P, Hahn PF, Sahani DV. Low-dose CT examinations in Crohn's disease: Impact on image quality, diagnostic performance, and radiation dose. *AJR Am J Roentgenol* 2010; **195**: 78-88 [PMID: 20566800 DOI: 10.2214/AJR.09.3420]
67 **Froehlich JM**, Waldherr C, Stoupis C, Erturk SM, Patak MA. MR motility imaging in Crohn's disease improves lesion detection compared with standard MR imaging. *Eur Radiol* 2010; **20**: 1945-1951 [PMID: 20379822 DOI: 10.1007/s00330-010-1759-x]
68 **Leyendecker JR**, Bloomfeld RS, DiSantis DJ, Waters GS, Mott R, Bechtold RE. MR enterography in the management of patients with Crohn disease. *Radiographics* 2009; **29**: 1827-1846 [PMID: 19959524 DOI: 10.1148/rg.296095510]
69 **Laghi A**, Borrelli O, Paolantonio P, Dito L, Buena de Mesquita M, Falconieri P, Passariello R, Cucchiara S. Contrast enhanced magnetic resonance imaging of the terminal ileum in children with Crohn's disease. *Gut* 2003; **52**: 393-397 [PMID: 12584222]
70 **Alexopoulou E**, Roma E, Loggitsi D, Economopoulos N, Papakonstantinou O, Panagiotou I, Pahoula I, Kelekis NL. Magnetic resonance imaging of the small bowel in children with idiopathic inflammatory bowel disease: evaluation of disease activity. *Pediatr Radiol* 2009; **39**: 791-797 [PMID: 19452148 DOI: 10.1007/s00247-009-1272-z]
71 **Schunk K**, Kern A, Oberholzer K, Kalden P, Mayer I, Orth T, Wanitschke R. Hydro-MRI in Crohn's disease: appraisal of disease activity. *Invest Radiol* 2000; **35**: 431-437 [PMID: 10901105]
72 **Durno CA**, Sherman P, Williams T, Shuckett B, Dupuis A, Griffiths AM. Magnetic resonance imaging to distinguish the type and severity of pediatric inflammatory bowel diseases. *J Pediatr Gastroenterol Nutr* 2000; **30**: 170-174 [PMID: 10697136]
73 **Koh DM**, Miao Y, Chinn RJ, Amin Z, Zeegen R, Westaby D, Healy JC. MR imaging evaluation of the activity of Crohn's disease. *AJR Am J Roentgenol* 2001; **177**: 1325-1332 [PMID:

11717076]
74 **Sharman A**, Zealley IA, Greenhalgh R, Bassett P, Taylor SA. MRI of small bowel Crohn's disease: determining the reproducibility of bowel wall gadolinium enhancement measurements. *Eur Radiol* 2009; **19**: 1960-1967 [PMID: 19308416 DOI: 10.1007/s00330-009-1371-0]
75 **Punwani S**, Rodriguez-Justo M, Bainbridge A, Greenhalgh R, De Vita E, Bloom S, Cohen R, Windsor A, Obichere A, Hansmann A, Novelli M, Halligan S, Taylor SA. Mural inflammation in Crohn disease: location-matched histologic validation of MR imaging features. *Radiology* 2009; **252**: 712-720 [PMID: 19635832 DOI: 10.1148/radiol.2523082167]
76 **Malagò R**, Manfredi R, Benini L, D'Alpaos G, Mucelli RP. Assessment of Crohn's disease activity in the small bowel with MR-enteroclysis: clinico-radiological correlations. *Abdom Imaging* 2008; **33**: 669-675 [PMID: 18228087 DOI: 10.1007/s00261-008-9368-8]
77 **Tolan DJ**, Greenhalgh R, Zealley IA, Halligan S, Taylor SA. MR enterographic manifestations of small bowel Crohn disease. *Radiographics* 2010; **30**: 367-384 [PMID: 20228323 DOI: 10.1148/rg.302095028]
78 **Ziech ML**, Bossuyt PM, Laghi A, Lauenstein TC, Taylor SA, Stoker J. Grading luminal Crohn's disease: which MRI features are considered as important? *Eur J Radiol* 2012; **81**: e467-e472 [PMID: 21684703 DOI: 10.1016/j.ejrad.2011.05.033]
79 **Schmidt S**, Guibal A, Meuwly JY, Michetti P, Felley C, Meuli R, Schnyder P, Denys A. Acute complications of Crohn's disease: comparison of multidetector-row computed tomographic enterography with magnetic resonance enterography. *Digestion* 2010; **82**: 229-238 [PMID: 20588038 DOI: 10.1159/000288521]
80 **Schmidt S**, Chevallier P, Bessoud B, Meuwly JY, Felley C, Meuli R, Schnyder P, Denys A. Diagnostic performance of MRI for detection of intestinal fistulas in patients with complicated inflammatory bowel conditions. *Eur Radiol* 2007; **17**: 2957-2963 [PMID: 17492288]
81 **Gee MS**, Nimkin K, Hsu M, Israel EJ, Biller JA, Katz AJ, Mino-Kenudson M, Harisinghani MG. Prospective evaluation of MR enterography as the primary imaging modality for pediatric Crohn disease assessment. *AJR Am J Roentgenol* 2011; **197**: 224-231 [PMID: 21701034 DOI: 10.2214/AJR.10.5970]
82 **Tillack C**, Seiderer J, Brand S, Göke B, Reiser MF, Schaefer C, Diepolder H, Ochsenkühn T, Herrmann KA. Correlation of magnetic resonance enteroclysis (MRE) and wireless capsule endoscopy (CE) in the diagnosis of small bowel lesions in Crohn's disease. *Inflamm Bowel Dis* 2008; **14**: 1219-1228 [PMID: 18484672 DOI: 10.1002/ibd.20466]
83 **Casciani E**, Masselli G, Di Nardo G, Polettini E, Bertini L, Oliva S, Floriani I, Cucchiara S, Gualdi G. MR enterography versus capsule endoscopy in paediatric patients with suspected Crohn's disease. *Eur Radiol* 2011; **21**: 823-831 [PMID: 20922391 DOI: 10.1007/s00330-010-1976-3]
84 **Cheifetz AS**, Kornbluth AA, Legnani P, Schmelkin I, Brown A, Lichtiger S, Lewis BS. The risk of retention of the capsule endoscope in patients with known or suspected Crohn's disease. *Am J Gastroenterol* 2006; **101**: 2218-2222 [PMID: 16848804]
85 **Jensen MD**, Nathan T, Kjeldsen J, Rafaelsen SR. Incidental findings at MRI-enterography in patients with suspected or known Crohn's disease. *World J Gastroenterol* 2010; **16**: 76-82 [PMID: 20039452]
86 **Herfarth HH**, Grunert M, Klebl F, Strauch U, Feuerbach S, Schölmerich J, Rogler G, Schreyer AG. Frequency and nature of incidental extra-enteric lesions found on magnetic resonance enterography (MR-E) in patients with inflammatory bowel diseases (IBD). *PLoS One* 2009; **4**: e4863 [PMID: 19337373 DOI: 10.1371/journal.pone.0004863]
87 **Rimola J**, Rodriguez S, García-Bosch O, Ordás I, Ayala E, Aceituno M, Pellisé M, Ayuso C, Ricart E, Donoso L, Panés J. Magnetic resonance for assessment of disease activity and severity in ileocolonic Crohn's disease. *Gut* 2009; **58**: 1113-1120 [PMID: 19136510 DOI: 10.1136/gut.2008.167957]
88 **Haggett PJ**, Moore NR, Shearman JD, Travis SP, Jewell DP, Mortensen NJ. Pelvic and perineal complications of Crohn's disease: assessment using magnetic resonance imaging. *Gut* 1995; **36**: 407-410 [PMID: 7698701]
89 **Beets-Tan RG**, Beets GL, van der Hoop AG, Kessels AG, Vliegen RF, Baeten CG, van Engelshoven JM. Preoperative MR imaging of anal fistulas: Does it really help the surgeon? *Radiology* 2001; **218**: 75-84 [PMID: 11152782]
90 **Dagia C**, Ditchfield M, Kean M, Catto-Smith T. Imaging for Crohn disease: use of 3-T MRI in a paediatric setting. *J Med Imaging Radiat Oncol* 2008; **52**: 480-488 [PMID: 19032394 DOI: 10.1111/j.1440-1673.2008.01993.x]
91 **Dagia C**, Ditchfield M, Kean M, Catto-Smith A. Feasibility of 3-T MRI for the evaluation of Crohn disease in children. *Pediatr Radiol* 2010; **40**: 1615-1624 [PMID: 20689946 DOI: 10.1007/s00247-010-1781-9]
92 **Shyn PB**, Mortele KJ, Britz-Cunningham SH, Friedman S, Odze RD, Burakoff R, Goldberg JE, Erturk M, Silverman SG. Low-dose 18F-FDG PET/CT enterography: improving on CT enterography assessment of patients with Crohn disease. *J Nucl Med* 2010; **51**: 1841-1848 [PMID: 21078803 DOI: 10.2967/jnumed.110.080796]
93 **Groshar D**, Bernstine H, Stern D, Sosna J, Eligalashvili M, Gurbuz EG, Niv Y, Fraser G. PET/CT enterography in Crohn disease: correlation of disease activity on CT enterography with 18F-FDG uptake. *J Nucl Med* 2010; **51**: 1009-1014 [PMID: 20554741 DOI: 10.2967/jnumed.109.073130]
94 **Spier BJ**, Perlman SB, Jaskowiak CJ, Reichelderfer M. PET/CT in the evaluation of inflammatory bowel disease: studies in patients before and after treatment. *Mol Imaging Biol* 2010; **12**: 85-88 [PMID: 19430844 DOI: 10.1007/s11307-009-0232-1]
95 **Lemberg DA**, Issenman RM, Cawdron R, Green T, Mernagh J, Skehan SJ, Nahmias C, Jacobson K. Positron emission tomography in the investigation of pediatric inflammatory bowel disease. *Inflamm Bowel Dis* 2005; **11**: 733-738 [PMID: 16043988]

P- Reviewers: Keita AV, Maccioni F, Mayol J **S- Editor**: Wen LL
L- Editor: A **E- Editor**: Zhang DN

World Journal of Radiology

Submit a Manuscript: http://www.wjgnet.com/esps/
Help Desk: http://www.wjgnet.com/esps/helpdesk.aspx
DOI: 10.4329/wjr.v6.i6.329

World J Radiol 2014 June 28; 6(6): 329-343
ISSN 1949-8470 (online)
© 2014 Baishideng Publishing Group Inc. All rights reserved.

REVIEW

Comparative review of vertebroplasty and kyphoplasty

Fernando Ruiz Santiago, Alicia Santiago Chinchilla, Luis Guzmán Álvarez, Antonio Luis Pérez Abela, Maria del Mar Castellano García, Miguel Pajares López

Fernando Ruiz Santiago, Luis Guzmán Álvarez, Maria del Mar Castellano García, Radiology Department, Hospital of Traumatology, 18014 Granada, Spain
Alicia Santiago Chinchilla, Radiology Department, Ciudad Sanitaria Virgen de las Nieves, 18014 Granada, Spain
Antonio Luis Pérez Abela, Traumatology Department, Hospital of Traumatology, 18014 Granada, Spain
Miguel Pajares López, Traumatology Department, Hospital Clínico San Cecilio, 18012 Granada, Spain
Author contributions: Ruiz Santiago F, Santiago Chinchilla A and Guzmán Álvarez L contributed to study concepts; Ruiz Santiago F, Santiago Chinchilla A, Guzmán Álvarez L and Pérez Abela AL contributed to study design; all authors contributed to data acquisition, manuscript preparation and manuscript review.
Correspondence to: Fernando Ruiz Santiago, Philosophical Doctor, Chairman of Musculoskeletal Radiology, Radiology Department, Hospital of Traumatology, Carretera de Jaen SN, 18014 Granada, Spain. ferusan12@gmail.com
Telephone: +34-627-633829
Received: December 23, 2013 Revised: February 18, 2014
Accepted: May 8, 2014
Published online: June 28, 2014

Key words: Vertebroplasty; Kyphoplasty; Osteoporosis; Vertebral fracture; spine metastasis

Core tip: This extended review of current literature on vertebral augmentation is supported by our wide experience in the treatment of vertebral fractures. The most innovative topics are the possibility of treating multilevel vertebral fractures in the same session and the failure of vertebral augmentation due to mechanical disruption of the cement. This is intended to present a thorough review to physicians interested in osteoporosis and vertebral fractures.

Ruiz Santiago F, Santiago Chinchilla A, Guzmán Álvarez L, Pérez Abela AL, Castellano García MM, Pajares López M. Comparative review of vertebroplasty and kyphoplasty. *World J Radiol* 2014; 6(6): 329-343 Available from: URL: http://www.wjgnet.com/1949-8470/full/v6/i6/329.htm DOI: http://dx.doi.org/10.4329/wjr.v6.i6.329

Abstract

The aim of this review is to compare the effectiveness of percutaneous vertebroplasty and kyphoplasty to treat pain and improve functional outcome from vertebral fractures secondary to osteoporosis and tumor conditions. In 2009, two open randomized controlled trials published in the New England Journal of Medicine questioned the value of vertebroplasty in treating vertebral compression fractures. Nevertheless, the practice of physicians treating these conditions has barely changed. The objective of this review is to try to clarify the most important issues, based on our own experience and the reported evidence about both techniques, and to guide towards the most appropriate choice of treatment of vertebral fractures, although many questions still remain unanswered.

© 2014 Baishideng Publishing Group Inc. All rights reserved.

INTRODUCTION

The treatment of pain related to vertebral body fractures by vertebroplasty or kyphoplasty has become a widespread practice. The main reported advantages of Kyphoplasty *vs* vertebroplasty are restoration of vertebral body height and a lower rate of cement extravasation. Although both techniques would appear effective in achieving pain relief, the impact on functional outcome is not sufficiently proved.

The choice of vertebroplasty or kyphoplasty and the selection of patients for one or other procedure remain unresolved questions. These issues are complicated by the considerable competition between the procedures and the conflicting claims made for each[1]. The degree of pain relief and functional improvement obtained must play an important role in the choice between these techniques. Previous studies reported good outcomes that remained stable during long follow-up periods for both vertebro-

plasty and kyphoplasty[2,3]. However, comparative studies are scarce. At present, different devices claiming advantages over more traditional methods are being developed.

Due to the existing controversies regarding the treatment of vertebral fractures, the objective of this review is to analyze the evidence of current literature supported by our own experience.

EPIDEMIOLOGY AND TYPES OF VERTEBRAL FRACTURES

Vertebral fractures can be secondary to high or low energy trauma. With population ageing most of the fractures (85%) are due to low energy trauma. These are more frequent in women and its prevalence increase with age in both sexes. High energy fractures are more frequent in men and are not related with older age. The incidence of clinically diagnosed vertebral fractures was assessed in a population-based study in Rochester, Minnesota, 1985-1989. The overall age- and sex-adjusted incidence rate was 117 per 100000 person-years (95%CI: 105 to 130). The age-adjusted rate in women (145 per 100000 person-years) was almost twice that in men (73 per 100000 person-years). Of all fractures, 47 (14%) followed severe trauma, 282 (83%) followed moderate or no trauma, and 12 (3%) were pathologic[4].

Vertebral compression fractures (VCF) are the most common fracture in osteoporotic patients, followed by hip, wrist or ankle fractures. These are known as low energy fractures or insufficiency fractures because the main cause is the fragility of bone that make it prone to injury with minimal or not trauma. After suffering the first vertebral fracture, the risk of developing new vertebral fractures increases 5-10 times[5].

Pathologic vertebral fractures are secondary to osseous involvement by a localized debilitating condition, mainly tumors. Most are due to malignancies such as metastases, myeloma and primary bone tumors, although benign tumors like haemangioma can also lead to a vertebral fracture. The spine is the musculoskeletal target most affected by metastases, mainly secondary to breast, lung, prostate, kidney and thyroid tumors[6]. Nevertheless, even in oncologic patients, a third of the vertebral fractures are due to coexisting osteoporosis[7]. Imaging techniques and biopsy help to differentiate the underlying cause.

Vertebral fractures happen in 50%-70% of patients with multiple myeloma. It may lead to spinal cord compression until 15% of the patients. On imaging its appearance may be misleading, simulating an osteoporotic vertebral compression fracture[8].

IMAGING OF VERTEBRAL FRACTURES

Conventional Radiographs are usually the first technique used to study patients with suspected vertebral fracture. While its ability to diagnose high energy posttraumatic fractures is high, its findings may be misleading diagnosing pathologic or insufficiency fractures.

When a high energy fracture is detected radiographically, many authors suggest the addition of computed tomography (CT) to the study, as it allows for better definition of fracture anatomy. When the clinical presentation suggests a fracture and conventional radiography is not diagnostic, a multi-slice CT or magnetic resonance imaging (MRI) help to clear out traumatisms of spine. A prospective study found a CT sensitivity of 99% in detecting fractures compared to 87% with plain-film radiography[9].

Osteoporotic vertebral fractures deformity usually is presented in two ways, wedge and biconcave (fish vertebra or diabolo-shaped vertebra) types, while pathological fractures often demonstrate predominately osteolytic changes. The presence of air collections within a vertebral body is considered a sign of vertebral cleft that may be due to fracture instability and/or necrosis (Kummel' s disease) and is more frequently associated to benign osteoporotic fractures[10]. Nevertheless cases associated to metastasis and myeloma has been described[11] (Figure 1).

A 15% vertebral body height loss constitutes a vertebral compression fracture. The leading cause of vertebral compression fractures is osteoporosis. Morphologic changes that allow for the diagnosis of an osteoporotic fracture may require time for their development. Therefore, the absence of a fracture on plain-film radiography in an osteoporotic patient does not rule it out, and when symptoms persist, a MRI should be performed. MRI can detect fractures without vertebral deformities and can better discriminate between benign and malignant fractures[12]. Additionally, MRI provides valuable information on factors such as the degree of edema, vertebral deformities, and invasion of the spinal canal, all of which are useful data for planning medical, percutaneous (kyphoplasty, vertebroplasty) or surgical treatment[13].

Plain-film radiography is somewhat insensitive when it comes to the visualization of the bone destruction or marrow replacement, requiring, depending on the size of the lesion, between 30%-50% of bone density loss before the lesions become visible[14]. The detection of blastic lesions may also be delayed with conventional radiography. One study reported that in the case of breast cancer, plain film detection of blastic lesion may be delayed by 3-6 mo[15].

Based on vertebral morphology and bone marrow signal, MRI can differentiate between osteoporotic and pathologic fractures with high confidence. Pathologic fractures may show complete substitution of normal bone marrow or, when incomplete, tend to show and nodular or patchy pattern. Morphologic signs are a convex vertebral border, due to expansion by growing tumor, and the presence of asymmetric paravertebral mass. Acute osteoporotic vertebral fractures tend to show a band-like pattern of subchondral edema and, quite often, the lineal pattern of the vertebral fracture can be depicted inside the edema[13]. A retropulsed bone fragment and the presence of intra vertebral cleft are characteristic

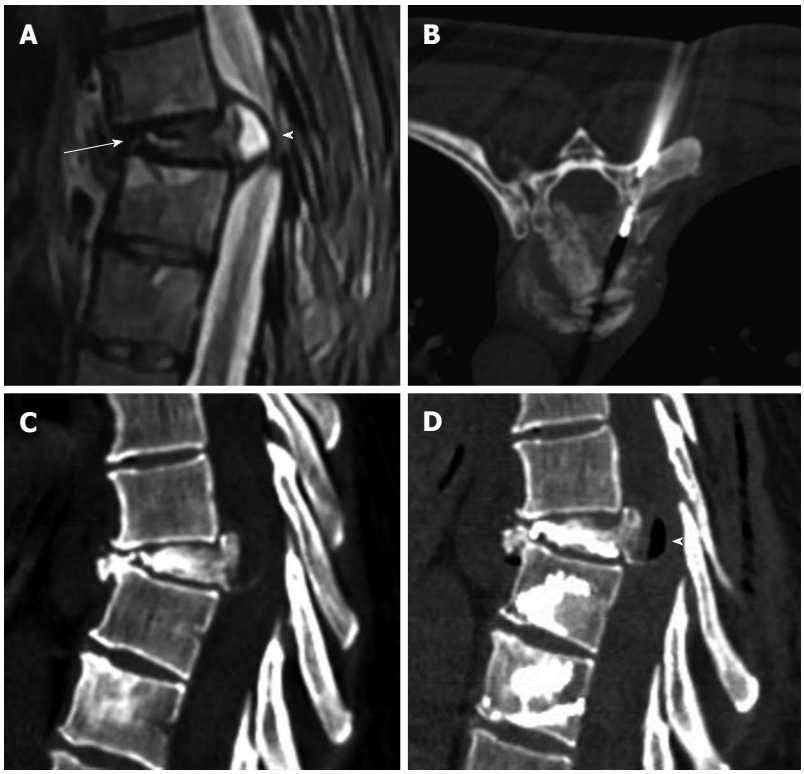

Figure 1 Sagittal T2 weighted (A) image shows metastatic compression fracture with intravertebral cleft (arrow) and epidural cyst (arrowhead), computed tomography guided biopsy (B), Sagittal computed tomography before (C) and after (D) vertebroplasty showing air filling of the cyst (arrowhead).

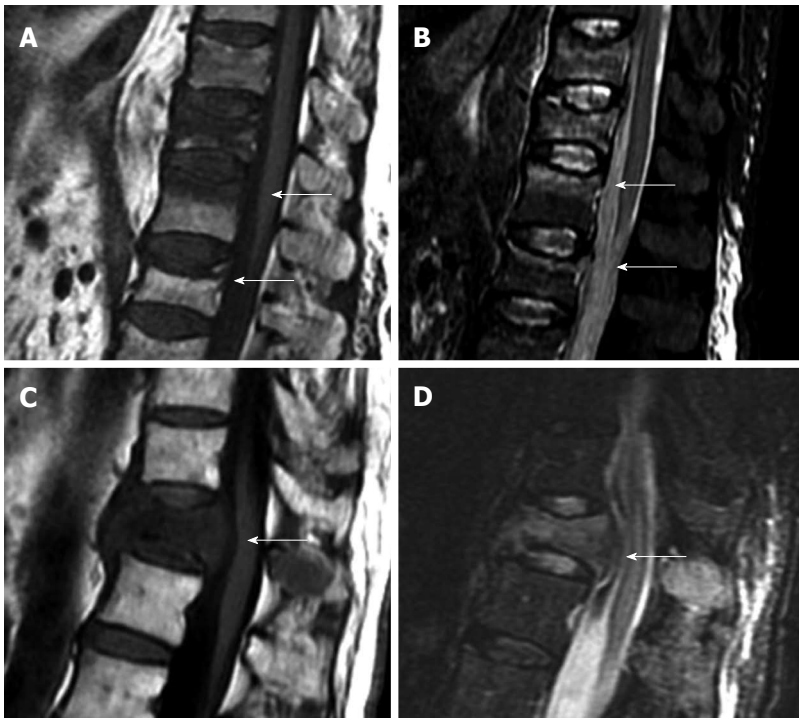

Figure 2 Sagittal T1 weighted (A) and STIR (B) images of osteoporotic fractures with typical band-like subchondral edema (arrows), sagittal T1 weighted (C) and STIR images (D) of a pathologic fracture, due to vertebral metastases, with typical convex border (arrows).

of benign compression fractures[11]. Chronic vertebral compression fractures are characterized by morphologic changes with recovery of normal signal of the bone marrow (Figure 2).

MEDICAL TREATMENT OF VERTEBRAL FRACTURES

Non-operative treatment of traumatic vertebral compression fractures is usually appropriate for patients with normal neurological status without suspected radiological instability, with an anterior vertebral body height > 50% of the posterior height and a Kyphotic angulation < 25°; or incomplete injury of the posterior column of the vertebral body[16,17]. Although in some cases early closed reduction and casting can be performed, bracing alone and physiotherapy in younger patients (< 65 years) is usually the best treatment option. A short period of bed rest (less

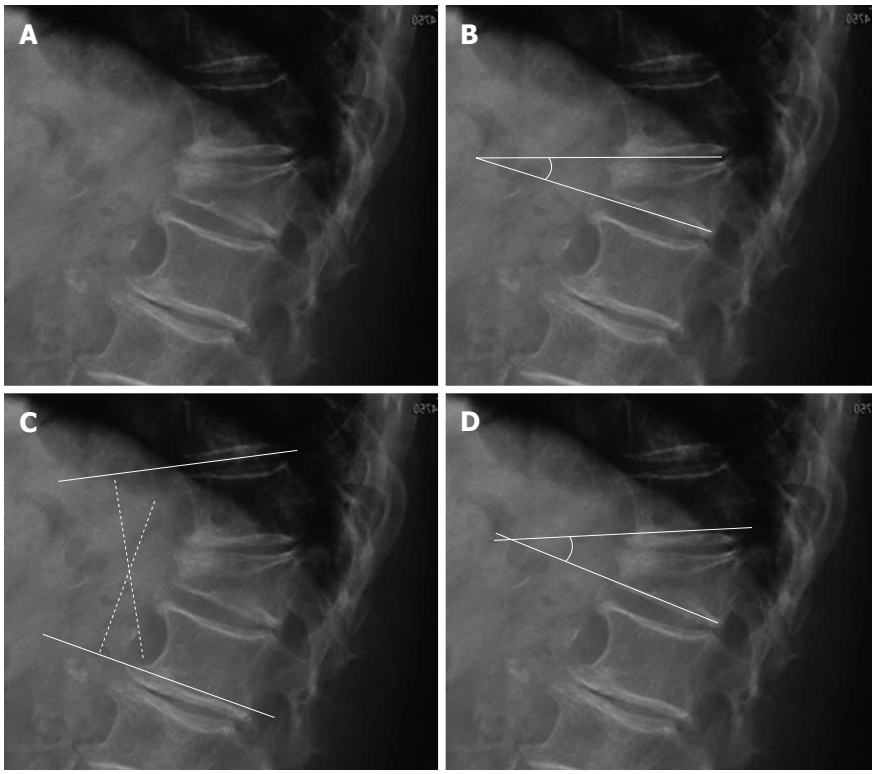

Figure 3 Segmental kyphotic deformity. A: Wedge fracture of T12; B: Local vertebral kyphosis angle; C: Regional kyphosis; D: Segmental kyphosis (SK). One vertebra, one disc=one segment. Sagittal index (SI): SI = SK-X (X = +5 in the thoracic spine, X = -10 in the lumbar spine, X = 0 in T12-L1).

than 1 wk) avoids complications caused by immobilization. In older patients, percutaneous vertebral augmentation may promote early mobilization and reduce analgesic intake[17].

Traditional treatment for osteoporotic fractures has been medical, including lifestyle changes (diet, smoking and exercise), pain management with rest, analgesic and anti-inflammatory drugs and external brace. Medical treatment for osteoporosis includes calcium supplements, vitamin D, hormone replacement and bisphosphonates. These treatments have strong effects on pain, but minimal effect on vertebral stability, vertebral height restoration or reduction of kyphotic deformity. Side effects of chronic medication and rest are increased demineralization of bone and greater risk of developing new fractures. Surgery is left for fractures with vertebral instability or neurological compression.

Traditional treatment for painful vertebral metastases is based on rest, braces, analgesic drugs, radiotherapy and chemotherapy. External beam radiation therapy is the current gold standard treatment for cancer patients with localized bone pain. Nevertheless, 20%-30% of patients do not experience pain relief with this approach. Radiation treatment can also result in additional early bone loss due to inflammation, and limited weight-bearing should be recommended during radiation to prevent pathological fractures. Radiotherapy control of pain is achieved in approximately 70%-80% of the cases, but its maximum effects usually takes place 1 mo after the beginning of treatment and osseous reinforcement up to 2 to 4 mo after, increasing the risk of vertebral collapse with its biomechanical consequences[18].

PERCUTANEOUS AND SURGICAL TREATMENT OF VERTEBRAL FRACTURES

Criteria for surgical indication of high-energy fractures are variable[19]. In our center, surgery is mainly indicated when the body fracture is associated to injury of the posterior column or in cases with neurologic deficit (deterioration of the initial neurologic status constitutes an emergency. It can also be indicated in cases without neurological deficit when there are other radiological signs of instability: central canal narrowing > 50%, vertebral height loss > 50%, fracture-dislocation, local vertebral kyphosis > 25º-30º, regional traumatic angle of kyphosis > 20% and sagittal index (SI) > 15º.

Local vertebral kyphosis angle is measured between the tangent to the upper endplate and the lower endplate of the injured vertebra. Regional kyphosis is the angle defined by the tangent to the upper endplate of the vertebra overlying the fracture and the tangent to the lower endplate of the vertebra underlying the injured vertebra. The SI is defined as segmental kyphotic deformity minus baseline sagittal contour in the segment with the fractured vertebral body. The segmental kyphotic deformity is the angle between the inferior endplate of the injured vertebra and the inferior endplate of the overlying vertebra. The baseline sagittal contour in each vertebral segment arbitrarily amounts to +5° for the thoracic region, 0° T12-L1 and -10° for the lumbar spine segments (Figure 3). The normal index is 0[20].

Accepted methods for surgical decompression and stabilization include anterior or posterior approaches and

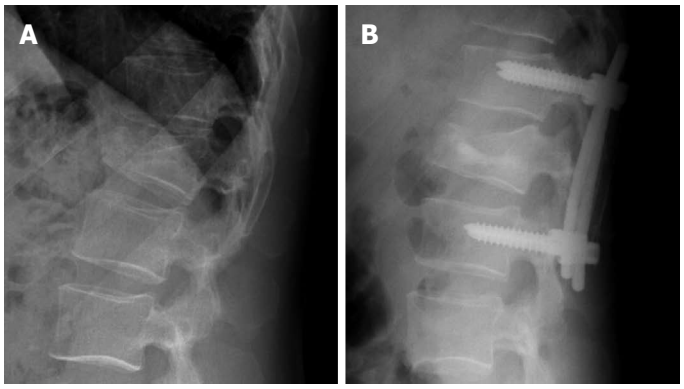

Figure 4 Forty-five years old man with acute Wedge impaction fracture of L1 (A) treated by posterior instrumentation and vertebral body kyphoplasty using biological cement (B).

a combination of both procedures. Instrumented fusion is better than laminectomy alone because it does not restore neurological function and it's associated with significant complications, such as persistent spinal instability and progressive kyphosis, mechanical pain and worsening of neurological injury[19].

Sometimes, instrumentation is complemented with VT or KP. Transpedicular vertebral augmentation for the direct restoration of burst fractures in combination with posterior instrumentation may avoid the surgical anterior reconstruction. The aim is to reinforce the anterior column and prevent anterior vertebral body height loss[21] (Figure 4).

The role of vertebroplasty and kyphoplasty in the treatment of high energy vertebral fractures is not still well defined, although good results with regard pain relief and quality of life have been reported using both procedures[22,23]. In young patients it has been suggested the use of biological cement, instead of PPMA, due to its capacity of integrating with bone[24]. Nevertheless, it has been reported that low resistance against flexural, tractive, and shear forces compared to PMMA, may lead to a higher risk of cement failure and subsequent loss of correction, mainly when fracture of the posterior wall of the vertebra is present[25]. The aim of treating percutaneously these fractures is to recovery vertebral height and to obtain early relieving of pain in order to reducing recovery time in young active population.

The principal surgical options for treatment of osteoporotic VCFs are decompression and fusion. The success of surgical instrumentation is compromised by poor bone quality[26]. As a result, interest in new and quick methods for pain relief and early functional restoration has increased. Percutaneous treatment of osteoporotic fractures is mainly indicated after failure of medical treatment, when the patient has a disabling pain or when there are severe side effects due to analgesic medication. In order to minimize these effects in patients with VCFs and reduce prolonged hospital resource utilization, VP and KP have been increasingly used with the expectation of a more rapid pain relief and earlier mobilization than that achieved with medical pain management[27]. Recently a randomized non-blinded trial appeared, strongly indicating that vertebroplasty is dramatically superior to conservative therapy[28].

Surgery in vertebral metastases is left for lesions affecting a unique vertebra or for treating neurological deficit secondary to compression or instability. Inconveniences of surgery are long recovery times and high morbidity and mortality[29].

Although external beam radiation therapy is the current gold standard treatment for cancer patients with localized bone pain we have to take into consideration that the life expectancy of most patients with bone metastases is limited, and that around 12-20 wk are usually required before maximum benefits are obtained from post-radiation therapy. In these cases vertebral augmentation techniques in isolation or combined with thermal ablation provide the earliest possible pain relief[30].

HISTORICAL NOTES

Deramon and Galibert performed the first vertebroplasty in France in 1984. It was performed in a patient with an aggressive haemangioma at the C2 level with resolution of pain. The results were so gratifying that cement injections were soon used in more patients with symptomatic hemangiomas and fractures due to tumors. The application of vertebroplasty in osteoporotic VCF was first published in 1989[31]. The hopeful analgesic effect led to the widespread use of augmentation for treating osteoporotic VCF[32]. Over the last years, osteoporotic fractures have become the main indication for vertebroplasty[33].

Kyphoplasty is the most widely used modification of vertebroplasty and was developed specifically for use in the osteoporotic vertebra. The basic idea behind this procedure was to raise the end plate of fractured vertebral body with an orthopedic balloon to achieve a more favorable angle of kyphosis before the cement augmentation. Therefore, a cavity is first created within the vertebral body before injecting the cement. The first kyphoplasty was performed by the orthopedic specialist Mark Reiley in California in 1998 with good results[34].

TECHNICAL ISSUES

Vertebroplasty involves the injection of polymethilmetacrhilathe (PMMA) cement into an injured vertebral body *via* a needle that is placed percutaneously either using a transpedicular or extrapedicular approach. The

Figure 5 Sagittal STIR image (A) in a patient with multiple thoracolumbar compression fractures, eight vertebrae were treated in the same procedure (B and C).

injection has to be forced to surpass the local pressure of the trabecular bone of treated vertebra increasing the risk of leakage through the cracks of the fractured vertebra. It may be performed under general anesthesia, although more commonly the patient is given a local anesthetic at the injection site and conscious sedation[35].

Kyphoplasty, a modification of vertebroplasty, involves the percutaneous insertion of an inflatable high-pressure bone tamp into the fractured vertebral body with the aim of elevate the end-plates by creating a cavity inside the vertebral body that filled with cement help to restore and stabilize the vertebral height. The cavity allows low pressure injection of more viscous cement, lowering the risk of extravasation[33].

PMMA is the most frequent cement used in these procedures. It is the result of the polymerization of methyl methacrylate monomers to PMMA polymers. It is cheap, easy to manipulate, allows combination with radiopaque materials and gives the appropriate stiffness and strength to the vertebral body. However, it does not have osteoinductive or osteoconductive properties and, therefore, it will not integrate itself to host bone over time. Its stiffness may promote mechanical overload to adjacent vertebral bodies[25].

New biological materials have been introduced as alternatives to PMMA, such as calcium phosphate and hydroxyapatite. These are not exothermic, allowing the deposition of new bone that, eventually, could replace the cement. These cements would in time become incorporated into the patient's bone, therefore functioning in a more physiological and biomechanically compatible fashion. This requires the presence of trabecular bone and the haversian canal system, thus cavity creation with a balloon will probably never be a part of the future of biological cements and prophylactic vertebroplasty[33]. Nevertheless, biological cements are expensive; their manipulation is not easy due to their high viscosity that makes difficult the interstitial diffusion inside the vertebral body[36]. These materials have been recommended in high-energy fractures of young patients[37], although other authors find a high rate of mechanical failure with these materials, due to its lower resistance to shear, flexion and distraction forces[25].

The number of vertebrae augmentable per session also remains unclear, although extensive augmentation to more than three vertebral levels per session has been shown as feasible[38]. However, it may lead to an increase of the amount of bone marrow floating to the pulmonary capillary system, increasing the risk of pulmonary fat embolism. Also, with PMMA there is some risk of incomplete polymerization, leading to increased residual toxic monomers that may result in adverse systemic effects, such as hypotension, bradycardia, asystole and bronchospasm. If the amount of cement injected in each vertebral body due to these reasons is reduced, it might result in incomplete stabilization of some vertebral body fractures leading to residual instability and pain. Notwithstanding, we have treated some cases of multilevel fractures in one single operative session with quite good results[35] (Figure 5). We recommend carefully planning the positioning of the needles and the amount of cement to be injected; taking into account the anatomical characteristics of each vertebral fracture, such as location of the fracture lines, integrity of vertebral walls and the presence of vertebral clefts.

CLINICAL SUCCESS OF VERTEBROPLASTY AND KYPHOPLASTY

Analgesic effect effects of these techniques can rely in many factors, such as ablation of C-nociceptive fibers by the thermal effect of the cement, mechanical stabilization of the fracture, height restoration of the vertebral body. The thermal effect also leads to tumor necrosis in patients with metastases[39].

Mechanical stabilization of the vertebral body relies on basal bone density, volume and localization of the injected cement. The filling of 14% to 30% of the volume is able to recover vertebral stiffness, although partial recovery of the stiffness, below the pre-fracture state, would be enough to obtain clinical healing[40].

Cadaveric studies have shown greater recovery of vertebral height with kyphoplasty (5.1 mm) than with vertebroplasty (2.3 mm)[41]. Yet, clinical studies are contradictory. While some authors found greater height restoration with kyphoplasty[42], others didn't find differences between both techniques[43]. In comparison with cadaver studies, the disk and paravertebral soft tissues may hinder augmentation with more aggressive techniques in living patients.

Vertebroplasty can mainly restore vertebral height when there is fragment instability with intravertebral clefts, indicating non-union of the fracture fragments. The cleft may be filled with greater amount of cement, mainly when there is integrity of the walls of the vertebral body, without extravasations leading loss of intravertebral pressure[41,44] (Figure 6).

Relationship between vertebral height restoration and

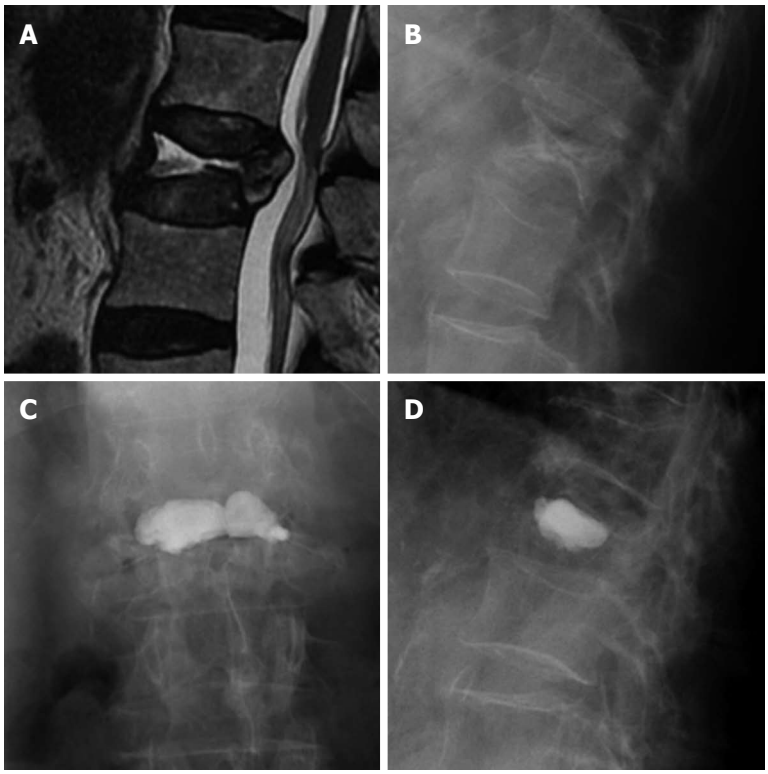

Figure 6 Sagittal T2 weighted image (A) and lateral X-ray film (B) of a vertebral fracture with intravertebral cleft, AP (C) and lateral (D) view after vertebroplasty.

clinical evolution is not well established. Some studies found no better pain resolution with height restoration and don't consider this factor mandatory in order to achieve pain control[45].

Another issue to consider is the stability over time of the height restoration. A follow up of height loss after performing these techniques shows the loss to be greater in kyphoplasty, due to less homogeneous distribution of cement, than in vertebroplasty, where the cement intermingles with host bone. Therefore, height recovery differences tend to vanish with time[46].

Short-term pain relief has been demonstrated in osteoporotic and tumor fractures treated with vertebroplaty and kyphoplasty[47,48]. Long-term outcomes have not been so well established, although some reports state that the beneficial effects of vertebroplasty remain after a follow-up period of several years[49,50].

Compared with medical treatments, pain relief after VP seems on the whole significantly superior. The follow-up point at which the difference becomes insignificant varies between studies at 3 mo[51], 6 mo[52] or 1 year[53]. Regarding Kyphoplasty, two prospective controlled studies evaluated and compared the efficacy and safety of this technique *vs* medical management and found better long-term pain relief and superior functional outcome with kyphoplasty, up to 3 years[54,55].

CLINICAL EVIDENCE OF AUGMENTATION EFFECTIVENESS

Two recent randomized works[56,57] stated that there is not better results between vertebroplasty and a sham treatment that only inject local anesthetic in the fractured area. Nevertheless, bias in both studies may invalidate their conclusions[58]. First of all, the small sample size avoid that a better evolution in the vertebroplastic group reaches statistical significance. Second at all, the percentage of control patients that chose to pass to the vertebroplasty group was high enough to invalidate the randomization of the studies. With regard selection of the patients, those with high pain scores were not included. These patients tend to show better results after vertebroplasty[59]. Another important factor was the inclusion of a high percentage of non-acute fractures; therefore, it is unclear if the origin of the back pain was the osteoporotic VCF or other common reasons for back pain in the elderly, such as arthritis of facet joint or disc pain. By nature of the patient population studied, "sham" facet injections may have led to decreased facet pain. Local anesthetic infiltration of the posterior longitudinal ligament is an established treatment for osteoarthritis back pain. Perhaps a sham procedure in which a dry needle was inserted might have been a more appropriate control. Other differences with previous studies are lower amount of injected PMMA, non-confirmation by imaging of vertebral fractures previous to procedure in patients with known fractures of less than 1 year and a lack of standardization of the medical treatment. The interpretation of the data is even more difficult due to the absence of a medical treatment group[60].

It has been stated that a percentage of patients with pain following VCF do not have pain arising from the fracture itself, but due to instability or overload on the facet joints produced by adjacent vertebral body deformity[61]. Since both causes of pain, VCF and osteoarthritis, may concur at the same time, we often combine

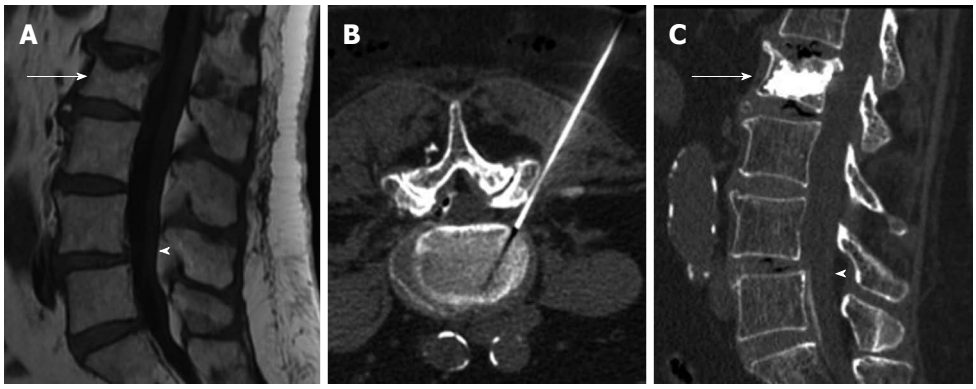

Figure 7 Sagittal T1 weighted image (A) showing vertebral compression fracture of L2 (arrow) and degenerative spondylolisthesis of L4 (arrowhead), computed tomography guided transforaminal epidural injection (B), Sagittal computed tomography after vertebroplasty (arrow) and epidural injection (arrowhead) (C).

vertebroplasty and spinal injection in the same session, mainly in older patients, relying on edema detected at the facet joints or on degenerative vertebral endplates changes, at the same or at a different level of the fractured vertebrae (Figure 7). This is supported by previous studies that found overall facet joint signal-change scores significantly higher at vertebral body levels affected by an acute/subacute compression fracture than in control levels with either normal bodies or chronic compression fractures[62]. This practice does not add too much time to vertebroplasty procedures, avoiding multiple scheduling of patients.

It is highly recommended to perform a spine MRI close before any of these percutaneous procedures[63]. The presence of a pattern of bone marrow edema is associated with a good clinical short term success relieving pain[54]. Nevertheless, improvement has been also demonstrated in patients with vertebral fractures without bone marrow edema[64].

Grades of recommendation of these techniques are based on the clinical evidence of published papers as follow[65]: Good evidence [level I studies with consistent findings; *e.g.*, high quality randomized controlled trials (RCT)], Fair evidence (level Ⅱ or Ⅲ studies with consistent findings; *e.g.*, low quality RCT, case/control and cohorts studies), Poor quality evidence (level Ⅳ or Ⅴ studies with consistent findings; *e.g.*, case series and expert opinions), or Insufficient evidence (inconsistent findings or lack of investigation for or against recommending intervention).

Meta-Analysis of published papers show fair to good evidence that in patients with osteoporotic VCF outcomes on physical disability, general health and pain relief are better with VP and KP than with medical management within the first 3 to 6 mo after intervention. Nevertheless, there is fair evidence that by the first or second year after intervention, VP provides a similar degree of pain control and physical function as that attained with optimal medical management. There is insufficient evidence whether KP results in greater pain relief one and 2 years after intervention[27].

Although not assessed in comparative studies, the reported degree of acute pain improvement in tumor-associated vertebral compression fractures is far better than that typically reported with radiation and medical management. Nevertheless, studies yield poor-quality evidence[27].

COMPLICATION OF TREATMENT OF VERTEBRAL FRACTURES

The aggregate rates of complications of vertebroplasty and kyphoplasty are small; ranging from 2%, when treating osteoporotic compression fractures, to 10% in cases related to malignant tumors[46].

The main risk of these percutaneous procedures is the extravasation of PMMA. Investigations on cement leakage in vertebroplasty report a rate of 11%-76%. In investigations on kyphoplasty, cement leakage data ranges from 4.8% to 39%. Cement leakage is reported at a higher rate if CT scans are used[45]. There are many routes by which cement may leak from a vertebra: paravertebral leakage, venous leakage or leakage into the spinal canal and intervertebral foramen (Figure 8). Injury of the surrounding soft tissues is mainly due to the high temperature of polymerization of PMMA. The most sensitive structures are neural tissues, spinal cord and nerve roots. Fortunately, most of the extravasations are to the disk or paravertebral tissues, hence asymptomatic. Transient radicular symptoms have been described in up to 3%-4% of the patients[66] and only isolated cases of paraplegia after these procedures have been reported, most of them due to failure of technical issues[48].

The monomers that don't contribute to the polymerization have systemic cardio-pulmonary effects. Pulmonary embolism can be due not only to the cement but also to the fat from the bone marrow extruded into the venous system by the high pressure injected cement or by inflating the balloons[67].

The relationship between percutaneous vertebral augmentation and the development of new fractures it is not well stated. Previous studies have found a greater rate of

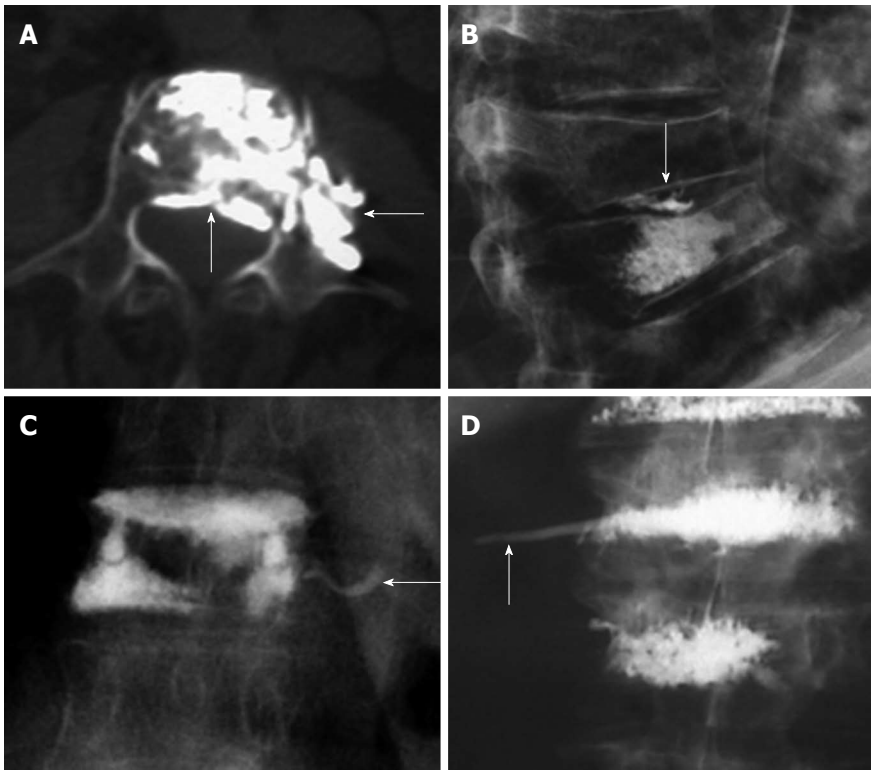

Figure 8 Axial computed tomography shows extravasations to epidural space and paravertebral area (arrows) (A), leakage to the intervertebral disc (arrow) (B), venous leakage (arrow) (C), tail of cement in the path of the needle (arrow) (D).

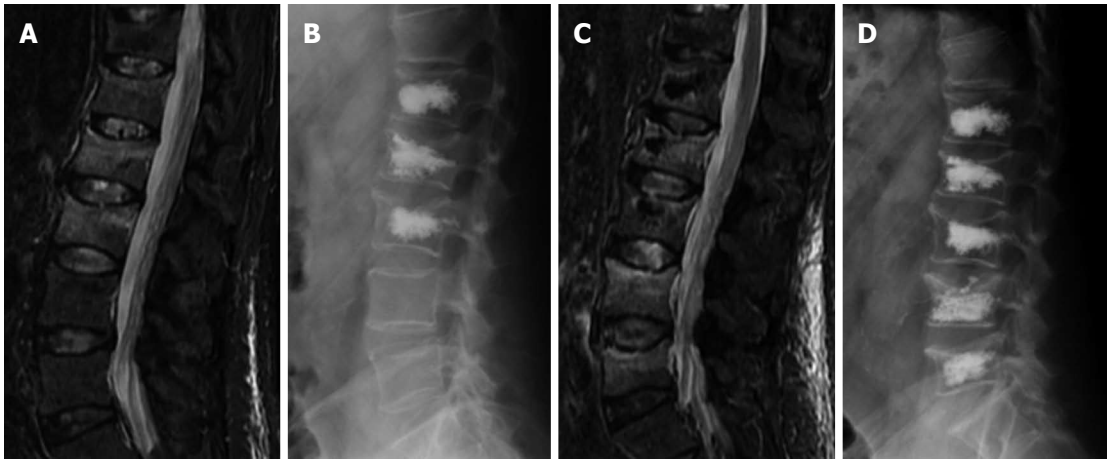

Figure 9 Sagittal STIR magnetic resonance image (A) shows fractures with edema of L1 to L3. Kyphoplasty was performed in these vertebrae (B), 3 wk later back pain returned and magnetic resonance imaging showed development of new fractures in L4 and L5 (C), vertebroplasty was performed at these levels (D).

new fractures in these patients than in the osteoporotic population, but the same as in those osteoporotic patients that have already developed a fracture[68]. Another article found fewer incidences of new fractures in patients treated with kyphoplasty than in patients managed with medical therapy. This was attributed to improvement of mechanical conditions due to vertebral height restoration and kyphotic correction[36]. The higher incidence of fractures in the early postoperative period could potentially be explained by increased patient activity and higher stress secondary to a diminished level of pain (Figure 9).

The possibility of treating adjacent vertebrae to the fractured vertebra is not supported by evidence studies[69], but we think that it is highly recommended treating a non-fractured vertebra when both, the upper and lower adjacent vertebrae, have been cemented.

Another complication is incomplete stabilization or residual instability of treated vertebral bodies. Due to the lack of data in spine literature regarding this issue as a cause of procedural failure, there are no figures. Relapse of vertebral instability may be due to mechanical failure of the cement, mainly when biological substitutes are used in fractures with loss of integrity of the posterior vertebral wall[25]. Incomplete filling of vertebral fracture lines may be followed by persistent instability with residual edema. When a vertebral cleft or cyst exists, kyphoplasty might be more prone to cause instability than vertebroplasty because the cement ball does not intermingle

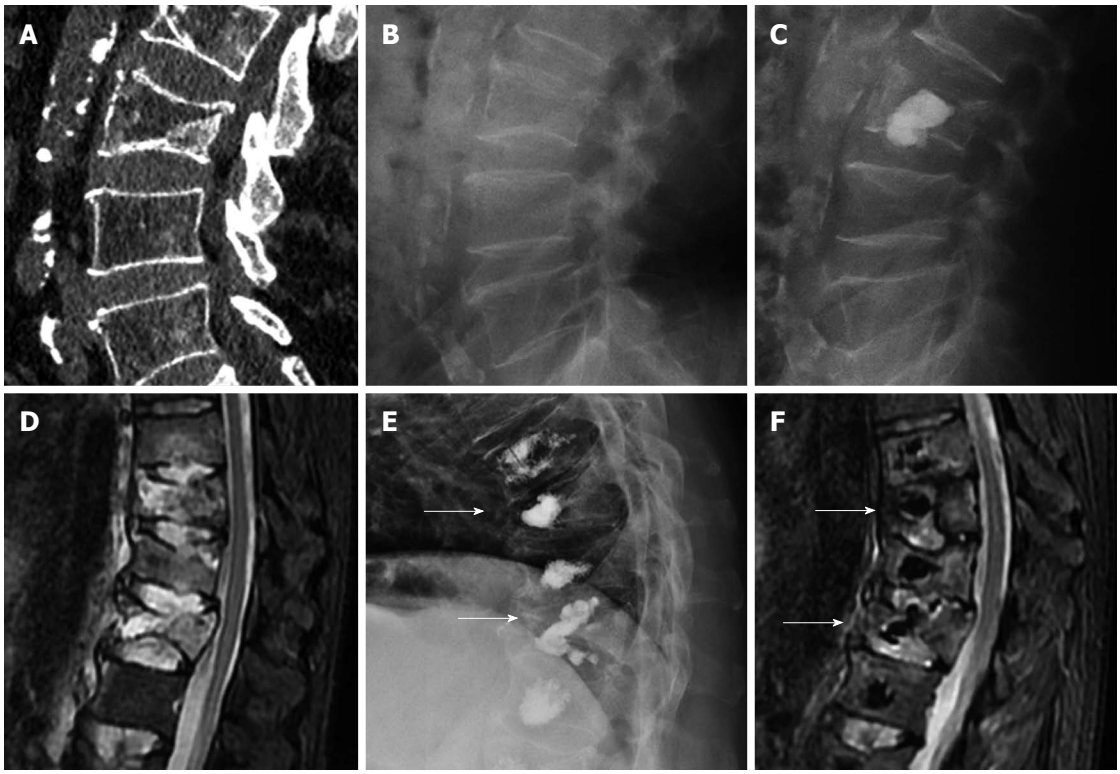

Figure 10 Sagittal computed tomography (A) a lateral radiography (B) showing fracture of L3 with intravertebral cyst (arrow), after Kyphoplasty (C) the ball of cement is not incorporated to the instable vertebral fracture, sagittal STIR image showing multiple thoracolumbar fractures with edema (D), treated with vertebroplasty, the cement do not stabilized the fracture of T10 and T12 (arrows) with persistent edema 6 mo after the procedure (E, F).

with vertebral trabeculae (Figure 10).

WHAT TREATMENT DO I CHOOSE?

Percutaneous vertebral augmentation has been shown to be more effective than prolonged non-operative medical treatment in patients with painful VCFs when adequate analgesia and improved functional status has not been achieved by nonoperative therapy[70]. The choice of vertebroplasty or kyphoplasty and the selection of patients for one or other procedure remain unresolved questions. These issues are complicated by the considerable competition between the procedures and the conflicting claims made for each[1]. Choice may well be influenced by degree of pain relief, functional improvement and anatomic and technical factors; including operator's experience or preference. Previous studies reported good outcomes that remained stable during long follow-up periods for both vertebroplasty[71,72] and kyphoplasty[73,74]. However, comparative studies are scarce and acknowledge the need of more high quality randomized controlled trials[75]. A recent meta-analysis found significant differences regarding anatomical restoration by kyphoplasty versus vertebroplasty, such as a mean long term kyphotic correction of 2.64°, mean anterior vertebral height recovery of 3.67 mm and lower risk of cement extravasation (risk ratio of 0.7)[76]. Nevertheless, these anatomic differences were not clinically relevant because most of the studies comparing both techniques found no differences in clinical outcome in osteoporotic patients[77-79]. Although a systematic review found greater quality of life and disability improvement in kyphoplasty over vertebroplasty, the need to define confounding variables was pointed out, because the selection of patients may depend on different indications for KP or VP in non-randomized studies, thus leading to misleading conclusions[80]. An example could be a recent prospective study, included in this systematic review, that found better results in kyphoplasty patients but that was clearly biased because two of the oldest patients were arbitrarily reallocated in the vertebroplasty group[81].

Based on these data, we recommend vertebroplasty as the primary treatment for osteoporotic VCF that do not respond to medical treatment. Kyphoplasty, which is a much more costly procedure, should only be used as an alternative approach in selected patients, such as those with a recent fracture affecting one or two vertebrae.

FUTURE DEVELOPMENTS

A variety of modifications of these techniques with variable success is being used. The commercial success of Kyphoplasty led to the development of several similar devices, but none have shown any benefit over vertebroplasty in an independent head-to-head trial[33].

Now that the Kyphon device is off patent, there are legions of copycat devices available from most manufacturers. A modified procedure employs reusable hinged-tip curet to manually create a cavity in fractured vertebral

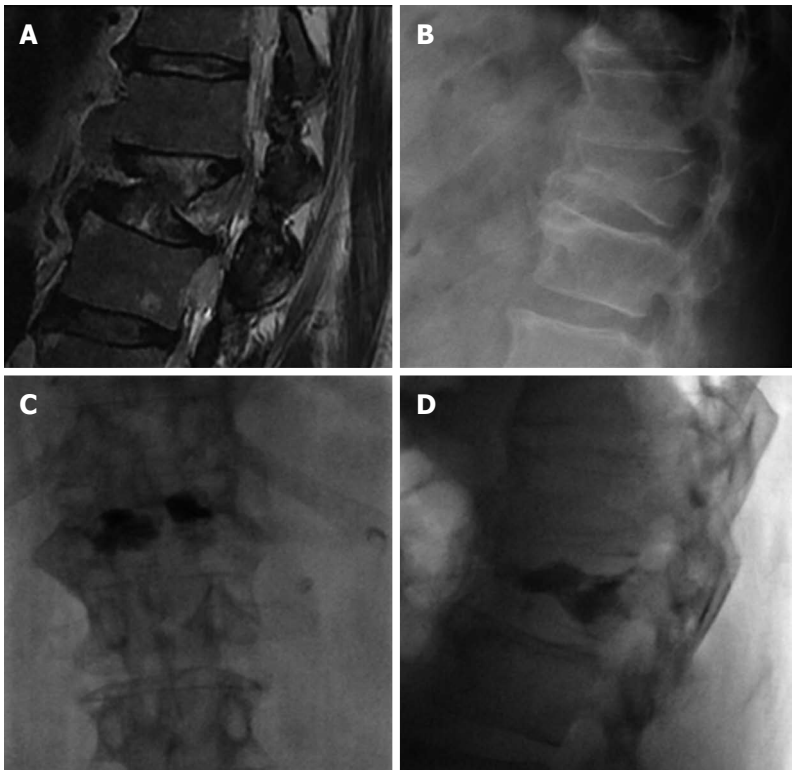

Figure 11 Sagittal T2 magnetic resonance weighted image (A) and lateral X-ray film (B) showing a severe collapse of L1, AP (C) and lateral (D) view after vesselplasty.

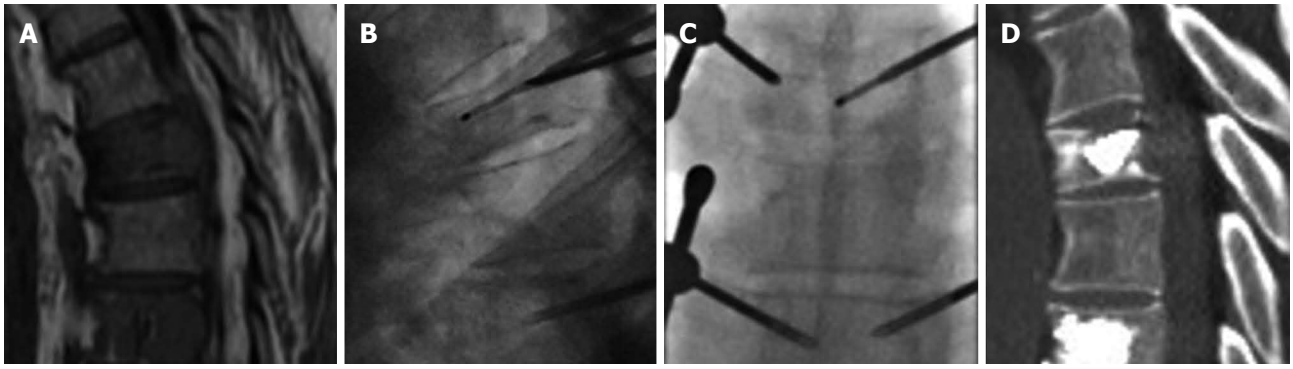

Figure 12 Sagittal magnetic resonance imaging T1 weighted image of a patient with vertebral metastases (A), radiofrequency thermal ablation was performed before cementation (B, C), post procedure computed tomography (D).

bodies under fluoroscopy guidance, allowing low resistance injection of more viscous cement[82]. We have often used a similar curet to create space for the balloon when the hardness of the vertebral body prevented the balloon from creating a cavity of the appropriate size.

Vesselplasty has been introduced as a new alternative to vertebroplasty and kyphoplasty. It has been devised to obtain control of the volume of injected cement and restoration of the vertebral body height. It was first performed in 2004 by Darwono. Instead of using a balloon to create a cavity, vesselplasty uses a polyethylene terephthalate balloon container (vessel) that serves as both, a vertebral body expander and a bone cement container. Introduced into the collapsed vertebral body, it is expanded by the injection of PMMA. Due to the porous structure of the vessel, a small amount of bone cement interdigitates with the trabecular bone around the vessel increasing its stability[83]. We are now introducing this technique in our hospital and we have found it very useful in cases of severe vertebral collapse, where the vessel acts as a prosthetic material that minimally restores the crushed vertebral body (Figure 11).

Another issue is the combination of percutaneous cementoplasty using polymethyl methacrylate with other techniques, such as radiofrequency thermal ablation (RFTA). It is sometimes indicated to reinforce bone structures and stabilize bones with high risk of pathologic fractures resulting from metastatic disease, and it is especially indicated for weight bearing bones. The combined use of RF ablation and cementoplasty appears to be useful in order to achieve tumor necrosis and stabilize the fractured vertebrae. The coagulation necrosis produced by RFTA may promote the homogenous distribution of the bone cement within the ablated lesion. The

clinical use of this combined therapy has been reported in several studies, but experience with this approach in vertebral fractures is still limited. Bone cement heats up to 80 ℃, which may help to strengthen the anticancer effects of RFTA[84] (Figure 12). Radiofrequency assistance and heating the needle tip constantly can also be used to increase cement viscosity, lowering the extravasation.

CONCLUSION

This extended review try to update the knowledge about vertebral augmentation based in current literature and our own experience. However, operator's experience or preference is also important clues in deciding appropriate treatment of vertebral fracture. Nevertheless, we hope this review will be helpful to clinician dealing with spinal diseases.

REFERENCES

1 **Mathis JM**. Percutaneous vertebroplasty or kyphoplasty: which one do I choose? *Skeletal Radiol* 2006; **35**: 629-631 [PMID: 16703391 DOI: 10.1007/s00256-006-0145-x]
2 **Boonen S**, Van Meirhaeghe J, Bastian L, Cummings SR, Ranstam J, Tillman JB, Eastell R, Talmadge K, Wardlaw D. Balloon kyphoplasty for the treatment of acute vertebral compression fractures: 2-year results from a randomized trial. *J Bone Miner Res* 2011; **26**: 1627-1637 [PMID: 21337428 DOI: 10.1002/jbmr.364]
3 **Farrokhi MR**, Alibai E, Maghami Z. Randomized controlled trial of percutaneous vertebroplasty versus optimal medical management for the relief of pain and disability in acute osteoporotic vertebral compression fractures. *J Neurosurg Spine* 2011; **14**: 561-569 [PMID: 21375382 DOI: 10.3171/2010.12.SPINE10286]
4 **Cooper C**, Atkinson EJ, O'Fallon WM, Melton LJ. Incidence of clinically diagnosed vertebral fractures: a population-based study in Rochester, Minnesota, 1985-1989. *J Bone Miner Res* 1992; **7**: 221-227 [PMID: 1570766 DOI: 10.1002/jbmr.5650070214]
5 **Lindsay R**, Silverman SL, Cooper C, Hanley DA, Barton I, Broy SB, Licata A, Benhamou L, Geusens P, Flowers K, Stracke H, Seeman E. Risk of new vertebral fracture in the year following a fracture. *JAMA* 2001; **285**: 320-323 [PMID: 11176842 DOI: 10.1001/jama.285.3.320]
6 **Galasko CS**. Skeletal metastases. *Clin Orthop Relat Res* 1986; (**210**): 18-30 [PMID: 3757360]
7 **Tan SB**, Kozak JA, Mawad ME. The limitations of magnetic resonance imaging in the diagnosis of pathologic vertebral fractures. *Spine (Phila Pa 1976)* 1991; **16**: 919-923 [PMID: 1948377 DOI: 10.1097/00007632-199108000-00009]
8 **Baur A**, Stabler A, Huber A, Reiser M. Diffusion-weighted magnetic resonance imaging of spinal bone marrow. *Semin Musculoskelet Radiol* 2001; **5**: 35-42 [PMID: 11371334 DOI: 10.1055/s-2001-12921]
9 **Hauser CJ**, Visvikis G, Hinrichs C, Eber CD, Cho K, Lavery RF, Livingston DH. Prospective validation of computed tomographic screening of the thoracolumbar spine in trauma. *J Trauma* 2003; **55**: 228-34; discussion 234-5 [PMID: 12913630 DOI: 10.1097/01.TA.0000076622.19246.CF]
10 **Freedman BA**, Heller JG. Kummel disease: a not-so-rare complication of osteoporotic vertebral compression fractures. *J Am Board Fam Med* 2009; **22**: 75-78 [PMID: 19124637 DOI: 10.3122/jabfm.2009.01.080100]
11 **Baur A**, Stäbler A, Arbogast S, Duerr HR, Bartl R, Reiser M. Acute osteoporotic and neoplastic vertebral compression fractures: fluid sign at MR imaging. *Radiology* 2002; **225**: 730-735 [PMID: 12461253 DOI: 10.1148/radiol.2253011413]
12 **McKiernan FE**. The broadening spectrum of osteoporotic vertebral fracture. *Skeletal Radiol* 2009; **38**: 303-308 [PMID: 19183993 DOI: 10.1007/s00256-008-0632-3]
13 **Cuénod CA**, Laredo JD, Chevret S, Hamze B, Naouri JF, Chapaux X, Bondeville JM, Tubiana JM. Acute vertebral collapse due to osteoporosis or malignancy: appearance on unenhanced and gadolinium-enhanced MR images. *Radiology* 1996; **199**: 541-549 [PMID: 8668809]
14 **Kamholtz R**, Sze G. Current imaging in spinal metastatic disease. *Semin Oncol* 1991; **18**: 158-169 [PMID: 2014400]
15 **Kunkler IH**, Merrick MV, Rodger A. Bone scintigraphy in breast cancer: a nine-year follow-up. *Clin Radiol* 1985; **36**: 279-282 [PMID: 4064511 DOI: 10.1016/S0009-9260(85)80060-X]
16 **Tezer M**, Erturer RE, Ozturk C, Ozturk I, Kuzgun U. Conservative treatment of fractures of the thoracolumbar spine. *Int Orthop* 2005; **29**: 78-82 [PMID: 15714305 DOI: 10.1007/s00264-004-0619-1]
17 **Weninger P**, Schultz A, Hertz H. Conservative management of thoracolumbar and lumbar spine compression and burst fractures: functional and radiographic outcomes in 136 cases treated by closed reduction and casting. *Arch Orthop Trauma Surg* 2009; **129**: 207-219 [PMID: 19009303 DOI: 10.1007/s00402-008-0780-x]
18 **Gerszten PC**, Mendel E, Yamada Y. Radiotherapy and radiosurgery for metastatic spine disease: what are the options, indications, and outcomes? *Spine (Phila Pa 1976)* 2009; **34**: S78-S92 [PMID: 19829280 DOI: 10.1097/BRS.0b013e3181b8b6f5]
19 **Alpantaki K**, Bano A, Pasku D, Mavrogenis AF, Papagelopoulos PJ, Sapkas GS, Korres DS, Katonis P. Thoracolumbar burst fractures: a systematic review of management. *Orthopedics* 2010; **33**: 422-429 [PMID: 20806752 DOI: 10.3928/01477447-20100429-24]
20 **Farcy JP**, Weidenbaum M, Glassman SD. Sagittal index in management of thoracolumbar burst fractures. *Spine (Phila Pa 1976)* 1990; **15**: 958-965 [PMID: 2259988 DOI: 10.1097/00007632-199009000-00022]
21 **Verlaan JJ**, Dhert WJ, Verbout AJ, Oner FC. Balloon vertebroplasty in combination with pedicle screw instrumentation: a novel technique to treat thoracic and lumbar burst fractures. *Spine (Phila Pa 1976)* 2005; **30**: E73-E79 [PMID: 15682000 DOI: 10.1097/01.brs.0000152162.64015.fb]
22 **Schmelzer-Schmied N**, Cartens C, Meeder PJ, Dafonseca K. Comparison of kyphoplasty with use of a calcium phosphate cement and non-operative therapy in patients with traumatic non-osteoporotic vertebral fractures. *Eur Spine J* 2009; **18**: 624-629 [PMID: 19165509 DOI: 10.1007/s00586-008-0880-x]
23 **Knavel EM**, Thielen KR, Kallmes DF. Vertebroplasty for the treatment of traumatic nonosteoporotic compression fractures. *AJNR Am J Neuroradiol* 2009; **30**: 323-327 [PMID: 19039045 DOI: 10.3174/ajnr.A1356]
24 **Korovessis P**, Hadjipavlou A, Repantis T. Minimal invasive short posterior instrumentation plus balloon kyphoplasty with calcium phosphate for burst and severe compression lumbar fractures. *Spine (Phila Pa 1976)* 2008; **33**: 658-667 [PMID: 18344860 DOI: 10.1097/BRS.0b013e318166e0bb]
25 **Blattert TR**, Jestaedt L, Weckbach A. Suitability of a calcium phosphate cement in osteoporotic vertebral body fracture augmentation: a controlled, randomized, clinical trial of balloon kyphoplasty comparing calcium phosphate versus polymethylmethacrylate. *Spine (Phila Pa 1976)* 2009; **34**: 108-114 [PMID: 19139662 DOI: 10.1097/BRS.0b013e31818f8bc1]
26 **Lieberman IH**, Dudeney S, Reinhardt MK, Bell G. Initial outcome and efficacy of "kyphoplasty" in the treatment of painful osteoporotic vertebral compression fractures. *Spine (Phila Pa 1976)* 2001; **26**: 1631-1638 [PMID: 11464159 DOI: 10.1097/00007632-200107150-00026]

27 **McGirt MJ**, Parker SL, Wolinsky JP, Witham TF, Bydon A, Gokaslan ZL. Vertebroplasty and kyphoplasty for the treatment of vertebral compression fractures: an evidenced-based review of the literature. *Spine J* 2009; **9**: 501-508 [PMID: 19251485 DOI: 10.1016/j.spinee.2009.01.003]

28 **Klazen CA**, Lohle PN, de Vries J, Jansen FH, Tielbeek AV, Blonk MC, Venmans A, van Rooij WJ, Schoemaker MC, Juttmann JR, Lo TH, Verhaar HJ, van der Graaf Y, van Everdingen KJ, Muller AF, Elgersma OE, Halkema DR, Fransen H, Janssens X, Buskens E, Mali WP. Vertebroplasty versus conservative treatment in acute osteoporotic vertebral compression fractures (Vertos II): an open-label randomised trial. *Lancet* 2010; **376**: 1085-1092 [PMID: 20701962 DOI: 10.1016/S0140-6736(10)60954-3]

29 **Jacofsky DJ**, Papagelopoulos PJ, Sim FH. Advances and challenges in the surgical treatment of metastatic bone disease. *Clin Orthop Relat Res* 2003; (415 Suppl): S14-S18 [PMID: 14600588 DOI: 10.1097/01.blo0000093046.96273.07]

30 **Callstrom MR**, Charboneau JW, Goetz MP, Rubin J, Atwell TD, Farrell MA, Welch TJ, Maus TP. Image-guided ablation of painful metastatic bone tumors: a new and effective approach to a difficult problem. *Skeletal Radiol* 2006; **35**: 1-15 [PMID: 16205922 DOI: 10.1007/s00256-005-0003-2]

31 **Lapras C**, Mottolese C, Deruty R, Lapras C, Remond J, Duquesnel J. [Percutaneous injection of methyl-metacrylate in osteoporosis and severe vertebral osteolysis (Galibert's technic)]. *Ann Chir* 1989; **43**: 371-376 [PMID: 2757346]

32 **Gangi A**, Kastler BA, Dietemann JL. Percutaneous vertebroplasty guided by a combination of CT and fluoroscopy. *AJNR Am J Neuroradiol* 1994; **15**: 83-86 [PMID: 8141070]

33 **Hargunani R**, Le Corroller T, Khashoggi K, Murphy KJ, Munk PL. Percutaneous vertebral augmentation: the status of vertebroplasty and current controversies. *Semin Musculoskelet Radiol* 2011; **15**: 117-124 [PMID: 21500131 DOI: 10.1055/s-0031-1275594]

34 **Garfin SR**, Yuan HA, Reiley MA. New technologies in spine: kyphoplasty and vertebroplasty for the treatment of painful osteoporotic compression fractures. *Spine (Phila Pa 1976)* 2001; **26**: 1511-1515 [PMID: 11462078 DOI: 10.1097/00007632-200107150-00002]

35 **Ruiz Santiago F**, Pérez Abela AL, Almagro Ratia MM. [The end of vertebroplasties]. *Radiologia* 2012; **54**: 532-538 [PMID: 22578911 DOI: 10.1016/j.rx.2012.02.002]

36 **Grafe IA**, Baier M, Nöldge G, Weiss C, Da Fonseca K, Hillmeier J, Libicher M, Rudofsky G, Metzner C, Nawroth P, Meeder PJ, Kasperk C. Calcium-phosphate and polymethylmethacrylate cement in long-term outcome after kyphoplasty of painful osteoporotic vertebral fractures. *Spine (Phila Pa 1976)* 2008; **33**: 1284-1290 [PMID: 18469705 DOI: 10.1097/BRS.0b013e3181714a84]

37 **Nakano M**, Hirano N, Ishihara H, Kawaguchi Y, Watanabe H, Matsuura K. Calcium phosphate cement-based vertebroplasty compared with conservative treatment for osteoporotic compression fractures: a matched case-control study. *J Neurosurg Spine* 2006; **4**: 110-117 [PMID: 16506477 DOI: 10.3171/spi.2006.4.2.110]

38 **Mailli L**, Filippiadis DK, Brountzos EN, Alexopoulou E, Kelekis N, Kelekis A. Clinical outcome and safety of multilevel vertebroplasty: clinical experience and results. *Cardiovasc Intervent Radiol* 2013; **36**: 183-191 [PMID: 22735889 DOI: 10.1007/s00270-012-0379-z]

39 **Srikumaran U**, Wong W, Belkoff SM, McCarthy EF. Histopathologic analysis of human vertebral bodies after vertebral augmentation with polymethylmethacrylate with use of an inflatable bone tamp. A case report. *J Bone Joint Surg Am* 2005; **87**: 1838-1843 [PMID: 16085628 DOI: 10.2106/JBJS.D.02848]

40 **Molloy S**, Mathis JM, Belkoff SM. The effect of vertebral body percentage fill on mechanical behavior during percutaneous vertebroplasty. *Spine (Phila Pa 1976)* 2003; **28**: 1549-1554 [PMID: 12865843 DOI: 10.1097/01.BRS.0000076831.38265.8D]

41 **Hiwatashi A**, Yoshiura T, Yamashita K, Kamano H, Dashjamts T, Honda H. Morphologic change in vertebral body after percutaneous vertebroplasty: follow-up with MDCT. *AJR Am J Roentgenol* 2010; **195**: W207-W212 [PMID: 20729417 DOI: 10.2214/AJR.10.4195]

42 **Grohs JG**, Matzner M, Trieb K, Krepler P. Minimal invasive stabilization of osteoporotic vertebral fractures: a prospective nonrandomized comparison of vertebroplasty and balloon kyphoplasty. *J Spinal Disord Tech* 2005; **18**: 238-242 [PMID: 15905767]

43 **Hiwatashi A**, Westesson PL, Yoshiura T, Noguchi T, Togao O, Yamashita K, Kamano H, Honda H. Kyphoplasty and vertebroplasty produce the same degree of height restoration. *AJNR Am J Neuroradiol* 2009; **30**: 669-673 [PMID: 19131409 DOI: 10.3174/ajnr.A1442]

44 **Carlier RY**, Gordji H, Mompoint DM, Vernhet N, Feydy A, Vallée C. Osteoporotic vertebral collapse: percutaneous vertebroplasty and local kyphosis correction. *Radiology* 2004; **233**: 891-898 [PMID: 15486209 DOI: 10.1148/radiol.2333030400]

45 **Feltes C**, Fountas KN, Machinis T, Nikolakakos LG, Dimopoulos V, Davydov R, Kassam M, Johnston KW, Robinson JS. Immediate and early postoperative pain relief after kyphoplasty without significant restoration of vertebral body height in acute osteoporotic vertebral fractures. *Neurosurg Focus* 2005; **18**: e5 [PMID: 15771395 DOI: 10.3171/foc.2005.18.3.6]

46 **McCall T**, Cole C, Dailey A. Vertebroplasty and kyphoplasty: a comparative review of efficacy and adverse events. *Curr Rev Musculoskelet Med* 2008; **1**: 17-23 [PMID: 19468894 DOI: 10.1007/s12178-007-9013-0]

47 **Chi JH**, Gokaslan ZL. Vertebroplasty and kyphoplasty for spinal metastases. *Curr Opin Support Palliat Care* 2008; **2**: 9-13 [PMID: 18685387 DOI: 10.1097/SPC.0b013e3282f5d907]

48 **Garfin SR**, Buckley RA, Ledlie J. Balloon kyphoplasty for symptomatic vertebral body compression fractures results in rapid, significant, and sustained improvements in back pain, function, and quality of life for elderly patients. *Spine (Phila Pa 1976)* 2006; **31**: 2213-2220 [PMID: 16946656 DOI: 10.1097/01.brs.0000232803.71640.ba]

49 **Grados F**, Depriester C, Cayrolle G, Hardy N, Deramond H, Fardellone P. Long-term observations of vertebral osteoporotic fractures treated by percutaneous vertebroplasty. *Rheumatology (Oxford)* 2000; **39**: 1410-1414 [PMID: 11136886 DOI: 10.1093/rheumatology/39.12.1410]

50 **Pérez-Higueras A**, Alvarez L, Rossi RE, Quiñones D, Al-Assir I. Percutaneous vertebroplasty: long-term clinical and radiological outcome. *Neuroradiology* 2002; **44**: 950-954 [PMID: 12428134 DOI: 10.1007/s00234-002-0856-1]

51 **Rousing R**, Hansen KL, Andersen MO, Jespersen SM, Thomsen K, Lauritsen JM. Twelve-months follow-up in forty-nine patients with acute/semiacute osteoporotic vertebral fractures treated conservatively or with percutaneous vertebroplasty: a clinical randomized study. *Spine (Phila Pa 1976)* 2010; **35**: 478-482 [PMID: 20190623 DOI: 10.1097/BRS.0b013e3181b71bd1]

52 **Alvarez L**, Alcaraz M, Pérez-Higueras A, Granizo JJ, de Miguel I, Rossi RE, Quiñones D. Percutaneous vertebroplasty: functional improvement in patients with osteoporotic compression fractures. *Spine (Phila Pa 1976)* 2006; **31**: 1113-1118 [PMID: 16648745 DOI: 10.1097/01.brs.0000216487.97965.38]

53 **Nakano M**, Hirano N, Ishihara H, Kawaguchi Y, Matsuura K. Calcium phosphate cement leakage after percutaneous vertebroplasty for osteoporotic vertebral fractures: risk factor analysis for cement leakage. *J Neurosurg Spine* 2005; **2**: 27-33 [PMID: 15658123 DOI: 10.3171/spi.2005.2.1.0027]

54 **Wardlaw D**, Cummings SR, Van Meirhaeghe J, Bastian

L, Tillman JB, Ranstam J, Eastell R, Shabe P, Talmadge K, Boonen S. Efficacy and safety of balloon kyphoplasty compared with non-surgical care for vertebral compression fracture (FREE): a randomised controlled trial. *Lancet* 2009; **373**: 1016-1024 [PMID: 19246088 DOI: 10.1016/S0140-6736(09)60010-6]

55 **Kasperk C**, Grafe IA, Schmitt S, Nöldge G, Weiss C, Da Fonseca K, Hillmeier J, Libicher M, Sommer U, Rudofsky G, Meeder PJ, Nawroth P. Three-year outcomes after kyphoplasty in patients with osteoporosis with painful vertebral fractures. *J Vasc Interv Radiol* 2010; **21**: 701-709 [PMID: 20304677 DOI: 10.1016/j.jvir.2010.01.003]

56 **Buchbinder R**, Osborne RH, Ebeling PR, Wark JD, Mitchell P, Wriedt C, Graves S, Staples MP, Murphy B. A randomized trial of vertebroplasty for painful osteoporotic vertebral fractures. *N Engl J Med* 2009; **361**: 557-568 [PMID: 19657121 DOI: 10.1056/NEJMoa0900429]

57 **Kallmes DF**, Comstock BA, Heagerty PJ, Turner JA, Wilson DJ, Diamond TH, Edwards R, Gray LA, Stout L, Owen S, Hollingworth W, Ghdoke B, Annesley-Williams DJ, Ralston SH, Jarvik JG. A randomized trial of vertebroplasty for osteoporotic spinal fractures. *N Engl J Med* 2009; **361**: 569-579 [PMID: 19657122 DOI: 10.1056/NEJMoa0900563]

58 **Baerlocher MO**, Munk PL, Liu DM, Tomlinson G, Badii M, Kee ST, Loh CT, Hardy BW, Murphy KJ. Clinical utility of vertebroplasty: need for better evidence. *Radiology* 2010; **255**: 669-674 [PMID: 20501705 DOI: 10.1148/radiol.10092107]

59 **Ryu KS**, Park CK. The prognostic factors influencing on the therapeutic effect of percutaneous vertebroplasty in treating osteoporotic vertebral compression fractures. *J Korean Neurosurg Soc* 2009; **45**: 16-23 [PMID: 19242566 DOI: 10.3340/jkns.2009.45.1.16]

60 **Orr RD**. Vertebroplasty, cognitive dissonance, and evidence-based medicine: what do we do when the 'evidence' says we are wrong? *Cleve Clin J Med* 2010; **77**: 8-11 [PMID: 20048024 DOI: 10.3949/ccjm.77a.09146]

61 **Wilson DJ**, Owen S, Corkill RA. Facet joint injections as a means of reducing the need for vertebroplasty in insufficiency fractures of the spine. *Eur Radiol* 2011; **21**: 1772-1778 [PMID: 21487701 DOI: 10.1007/s00330-011-2115-5]

62 **Lehman VT**, Wood CP, Hunt CH, Carter RE, Allred JB, Diehn FE, Morris JM, Wald JT, Thielen KR. Facet joint signal change on MRI at levels of acute/subacute lumbar compression fractures. *AJNR Am J Neuroradiol* 2013; **34**: 1468-1473 [PMID: 23449650 DOI: 10.3174/ajnr.A3449]

63 **Benz BK**, Gemery JM, McIntyre JJ, Eskey CJ. Value of immediate preprocedure magnetic resonance imaging in patients scheduled to undergo vertebroplasty or kyphoplasty. *Spine (Phila Pa 1976)* 2009; **34**: 609-612 [PMID: 19282740 DOI: 10.1097/BRS.0b013e31819740bb]

64 **Brown DB**, Glaiberman CB, Gilula LA, Shimony JS. Correlation between preprocedural MRI findings and clinical outcomes in the treatment of chronic symptomatic vertebral compression fractures with percutaneous vertebroplasty. *AJR Am J Roentgenol* 2005; **184**: 1951-1955 [PMID: 15908560 DOI: 10.2214/ajr.184.6.01841951]

65 **Watters WC**, Baisden J, Gilbert TJ, Kreiner S, Resnick DK, Bono CM, Ghiselli G, Heggeness MH, Mazanec DJ, O'Neill C, Reitman CA, Shaffer WO, Summers JT, Toton JF. Degenerative lumbar spinal stenosis: an evidence-based clinical guideline for the diagnosis and treatment of degenerative lumbar spinal stenosis. *Spine J* 2008; **8**: 305-310 [PMID: 18082461 DOI: 10.1016/j.spinee.2007.10.033]

66 **Chiras J**, Barragán-Campos HM, Cormier E, Jean B, Rose M, LeJean L. [Vertebroplasty: state of the art]. *J Radiol* 2007; **88**: 1255-1260 [PMID: 17878871 DOI: 10.1016/S0221-0363(07)91335-9]

67 **Choe DH**, Marom EM, Ahrar K, Truong MT, Madewell JE. Pulmonary embolism of polymethyl methacrylate during percutaneous vertebroplasty and kyphoplasty. *AJR Am J Roentgenol* 2004; **183**: 1097-1102 [PMID: 15385313 DOI: 10.2214/ajr.183.4.1831097]

68 **Hulme PA**, Krebs J, Ferguson SJ, Berlemann U. Vertebroplasty and kyphoplasty: a systematic review of 69 clinical studies. *Spine (Phila Pa 1976)* 2006; **31**: 1983-2001 [PMID: 16924218 DOI: 10.1097/01.brs.0000229254.89952.6b]

69 **Becker S**, Garoscio M, Meissner J, Tuschel A, Ogon M. Is there an indication for prophylactic balloon kyphoplasty? A pilot study. *Clin Orthop Relat Res* 2007; **458**: 83-89 [PMID: 17310933]

70 **Barr JD**, Jensen ME, Hirsch JA, McGraw JK, Barr RM, Brook AL, Meyers PM, Munk PL, Murphy KJ, O'Toole JE, Rasmussen PA, Ryken TC, Sanelli PC, Schwartzberg MS, Seidenwurm D, Tutton SM, Zoarski GH, Kuo MD, Rose SC, Cardella JF. Position statement on percutaneous vertebral augmentation: a consensus statement developed by the Society of Interventional Radiology (SIR), American Association of Neurological Surgeons (AANS) and the Congress of Neurological Surgeons (CNS), American College of Radiology (ACR), American Society of Neuroradiology (ASNR), American Society of Spine Radiology (ASSR), Canadian Interventional Radiology Association (CIRA), and the Society of NeuroInterventional Surgery (SNIS). *J Vasc Interv Radiol* 2014; **25**: 171-81 [PMID: 24325929 DOI: 10.1016/j.jvir.2013.10.001]

71 **Legroux-Gérot I**, Lormeau C, Boutry N, Cotten A, Duquesnoy B, Cortet B. Long-term follow-up of vertebral osteoporotic fractures treated by percutaneous vertebroplasty. *Clin Rheumatol* 2004; **23**: 310-317 [PMID: 15293091 DOI: 10.1007/s10067-004-0914-7]

72 **Masala S**, Mastrangeli R, Petrella MC, Massari F, Ursone A, Simonetti G. Percutaneous vertebroplasty in 1,253 levels: results and long-term effectiveness in a single centre. *Eur Radiol* 2009; **19**: 165-171 [PMID: 18704433 DOI: 10.1007/s00330-008-1133-4]

73 **Berlemann U**, Franz T, Orler R, Heini PF. Kyphoplasty for treatment of osteoporotic vertebral fractures: a prospective non-randomized study. *Eur Spine J* 2004; **13**: 496-501 [PMID: 15083353 DOI: 10.1007/s00586-004-0691-7]

74 **Khanna AJ**, Reinhardt MK, Togawa D, Lieberman IH. Functional outcomes of kyphoplasty for the treatment of osteoporotic and osteolytic vertebral compression fractures. *Osteoporos Int* 2006; **17**: 817-826 [PMID: 16518574 DOI: 10.1007/s00198-006-0068-3]

75 **Ma XL**, Xing D, Ma JX, Xu WG, Wang J, Chen Y. Balloon kyphoplasty versus percutaneous vertebroplasty in treating osteoporotic vertebral compression fracture: grading the evidence through a systematic review and meta-analysis. *Eur Spine J* 2012; **21**: 1844-1859 [PMID: 22832872 DOI: 10.1007/s00586-012-2441-6]

76 **Xing D**, Ma JX, Ma XL, Wang J, Xu WG, Chen Y, Song DH. A meta-analysis of balloon kyphoplasty compared to percutaneous vertebroplasty for treating osteoporotic vertebral compression fractures. *J Clin Neurosci* 2013; **20**: 795-803 [PMID: 23428914 DOI: 10.1016/j.jocn.2012.05.038]

77 **Eck JC**, Nachtigall D, Humphreys SC, Hodges SD. Comparison of vertebroplasty and balloon kyphoplasty for treatment of vertebral compression fractures: a meta-analysis of the literature. *Spine J* 2008; **8**: 488-497 [PMID: 17588820 DOI: 10.1016/j.spinee.2007.04.004]

78 **Liu JT**, Liao WJ, Tan WC, Lee JK, Liu CH, Chen YH, Lin TB. Balloon kyphoplasty versus vertebroplasty for treatment of osteoporotic vertebral compression fracture: a prospective, comparative, and randomized clinical study. *Osteoporos Int* 2010; **21**: 359-364 [PMID: 19513578 DOI: 10.1007/s00198-009-0952-8]

79 **Santiago FR**, Abela AP, Alvarez LG, Osuna RM, García Mdel M. Pain and functional outcome after vertebroplasty and kyphoplasty. A comparative study. *Eur J Radiol* 2010; **75**: e108-e113 [PMID: 20138724 DOI: 10.1016/j.ejrad.2010.01.010]

80 **Papanastassiou ID**, Phillips FM, Van Meirhaeghe J, Beren-

son JR, Andersson GB, Chung G, Small BJ, Aghayev K, Vrionis FD. Comparing effects of kyphoplasty, vertebroplasty, and non-surgical management in a systematic review of randomized and non-randomized controlled studies. *Eur Spine J* 2012; **21**: 1826-1843 [PMID: 22543412 DOI: 10.1007/s00586-012-2314-z]

81 **Kumar K**, Nguyen R, Bishop S. A comparative analysis of the results of vertebroplasty and kyphoplasty in osteoporotic vertebral compression fractures. *Neurosurgery* 2010; **67**: ons171-ons88; discussion ons188 [PMID: 20679931 DOI: 10.1227/01.NEU.0000380936.00143.11]

82 **Vallejo R**, Benyamin R, Floyd B, Casto JM, Joseph NJ, Mekhail N. Percutaneous cement injection into a created cavity for the treatment of vertebral body fracture: preliminary results of a new vertebroplasty technique. *Clin J Pain* 2006; **22**: 182-189 [PMID: 16428953 DOI: 10.1097/01.ajp.0000169675.41815.49]

83 **Flors L**, Lonjedo E, Leiva-Salinas C, Martí-Bonmatí L, Martínez-Rodrigo JJ, López-Pérez E, Figueres G, Raoli I. Vesselplasty: a new technical approach to treat symptomatic vertebral compression fractures. *AJR Am J Roentgenol* 2009; **193**: 218-226 [PMID: 19542417 DOI: 10.2214/AJR.08.1503]

84 **Georgy BA**, Wong W. Plasma-mediated radiofrequency ablation assisted percutaneous cement injection for treating advanced malignant vertebral compression fractures. *AJNR Am J Neuroradiol* 2007; **28**: 700-705 [PMID: 17416824]

P- Reviewers: Sebestyén A, Tajali SB, Teli MGA
S- Editor: Song XX **L- Editor**: A **E- Editor**: Zhang DN

World Journal of Radiology

Submit a Manuscript: http://www.wjgnet.com/esps/
Help Desk: http://www.wjgnet.com/esps/helpdesk.aspx
DOI: 10.4329/wjr.v6.i6.344

World J Radiol 2014 June 28; 6(6): 344-354
ISSN 1949-8470 (online)
© 2014 Baishideng Publishing Group Inc. All rights reserved.

REVIEW

Diffusion-weighted magnetic resonance imaging in management of bladder cancer, particularly with multimodal bladder-sparing strategy

Soichiro Yoshida, Fumitaka Koga, Shuichiro Kobayashi, Hiroshi Tanaka, Shiro Satoh, Yasuhisa Fujii, Kazunori Kihara

Soichiro Yoshida, Fumitaka Koga, Shuichiro Kobayashi, Yasuhisa Fujii, Kazunori Kihara, Department of Urology, Tokyo Medical and Dental University Graduate School, Tokyo 113-8677, Japan
Fumitaka Koga, Department of Urology, Tokyo Metropolitan Cancer and Infectious Diseases Center Komagome Hospital, Tokyo 113-0021, Japan
Hiroshi Tanaka, Shiro Satoh, Department of Radiology, Ochanomizu Surugadai Clinic, Tokyo 101-0062, Japan
Author contributions: Yoshida S, Kobayashi S, Tanaka H, Satoh S, Fujii Y and Kihara K contributed to conception; Yoshida S and Koga F wrote the paper.
Correspondence to: Fumitaka Koga, MD, PhD, Department of Urology, Tokyo Metropolitan Cancer and Infectious diseases Center Komagome Hospital, 3-18-22 Honkomagome, Bunkyo-ku, Tokyo 113-8677, Japan. f-koga@cick.jp
Telephone: +81-3-38232101 Fax: +81-3-38241552
Received: December 29, 2013 Revised: April 10, 2014
Accepted: May 14, 2014
Published online: June 28, 2014

Abstract

Bladder-sparing strategy for muscle-invasive bladder cancer (MIBC) is increasingly demanded instead of radical cystectomy plus urinary diversion. Multimodal therapeutic approaches consisting of transurethral resection, chemotherapy, radiotherapy and/or partial cystectomy improve patients' quality of life by preserving their native bladder and sexual function without compromising oncological outcomes. Because a favorable response to chemoradiotherapy (CRT) is a prerequisite for successful bladder preservation, predicting and monitoring therapeutic response is an essential part of this approach. Diffusion-weighted magnetic resonance imaging (DW-MRI) is a functional imaging technique increasingly applied to various types of cancers. Contrast in this imaging technique derives from differences in the motion of water molecules among tissues and this information is useful in assessing the biological behavior of cancers. Promising results in predicting and monitoring the response to CRT have been reported in several types of cancers. Recently, growing evidence has emerged showing that DW-MRI can serve as an imaging biomarker in the management of bladder cancer. The qualitative analysis of DW-MRI can be applied to detecting cancerous lesion and monitoring the response to CRT. Furthermore, the potential role of quantitative analysis by evaluating apparent diffusion coefficient values has been shown in characterizing bladder cancer for biological aggressiveness and sensitivity to CRT. DW-MRI is a potentially useful tool for the management of bladder cancer, particularly in multimodal bladder-sparing approaches for MIBC.

© 2014 Baishideng Publishing Group Inc. All rights reserved.

Key words: Diffusion magnetic resonance imaging; Bladder cancer; Urothelial carcinoma; Chemotherapy; Radiotherapy

Core tip: Diffusion-weighted magnetic resonance imaging (DW-MRI) is a functional imaging increasingly applied in the management of bladder cancer. This imaging offers unique information reflecting physiological character of the tissues by quantifying the diffusion of water molecules. DW-MRI provides accurate information for the diagnosis of bladder cancer in a noninvasive manner. Furthermore, growing evidence has emerged showing that DW-MRI can serve as an imaging biomarker of bladder cancer for assessing biologic aggressiveness and therapeutic sensitivity and for monitoring the therapeutic response. This review focuses on the potential role of DW-MRI in multimodal organ-preservation strategies for bladder cancer.

Yoshida S, Koga F, Kobayashi S, Tanaka H, Satoh S, Fujii Y, Kihara K. Diffusion-weighted magnetic resonance imaging in management of bladder cancer, particularly with multimodal bladder-sparing strategy. *World J Radiol* 2014; 6(6): 344-354 Available from: URL: http://www.wjgnet.com/1949-8470/full/v6/i6/344.htm DOI: http://dx.doi.org/10.4329/wjr.v6.i6.344

INTRODUCTION

Bladder cancer is the second most common genitourinary cancer in the United States and some 55600 new cases and 15100 deaths from bladder cancer are estimated to have occurred in 2012[1]. At the initial diagnosis, a third of all cases are diagnosed as muscle-invasive bladder cancer (MIBC)[2], and radical cystectomy has long been the treatment of choice for the treatment of localized MIBC. However, concern for patients' quality of life has strengthened the trend toward bladder-sparing approaches with various treatment modalities[3]. In this treatment approach, meticulous evaluation of the bladder cancer is essential. Diffusion-weighted magnetic resonance imaging (DW-MRI) is a functional imaging technique increasingly applied to various types of cancer. Recently, growing evidence has emerged showing that DW-MRI can serve as an imaging technique that is useful for characterizing the pathophysiology of cancer. The biological behavior assessed with this imaging technique will play an important role in multimodal organ-preserving strategies for MIBC. Thus, this review focuses on the potential role of DW-MRI in multimodal organ-preservation strategies for MIBC.

Trimodality bladder-sparing strategy for MIBC

Favorable oncological and functional outcomes using bladder-sparing trimodality therapy combined with transurethral resection of bladder tumor (TURBT), chemotherapy and radiotherapy have been reported by several groups including Harvard University, the University of Paris and the University of Erlangen in Germany[4-6]. In most trimodality bladder-sparing approaches, patients who achieve complete response (CR) after the trimodal treatment are selectively subjected to consolidative therapies for bladder preservation, whereas those who do not achieve CR are advised to undergo early radical cystectomy. The 5-year survival rates after trimodality bladder-preserving trials were reported to be 50%-60%, which is comparable to those of radical cystectomy series[7, 8].

In the trimodality bladder preservation strategies, clinically tumor-free status after TURBT followed by chemoradiotherapy (CRT), as well as lower T stage and completeness of the TURBT, are important prognostic factors[6,9-11]. However, even the patients who clinically achieved CR after TURBT followed by CRT still may develop local tumor recurrence and lymph node metastases. Zietman *et al*[12] reported that two-thirds of non-MIBC (NMIBC) recurrences developed in the original MIBC sites. Tunio *et al*[13] also showed that 21% of the MIBC patients who achieved CR after trimodality therapy developed MIBC recurrence, and 69% of the recurrences arose from the original MIBC site. This problem could be due, in part, to subclinical viable bladder cancer cells remaining in the original MIBC site, which were missed by conventional imaging studies and biopsy-based evaluation[14].

Limitations of conventional radiological evaluations in bladder-sparing strategy for MIBC

Contrast-enhanced CT and conventional MRI are the standard techniques that have been used for the radiological evaluation of urinary system tumors. While CT is generally used to screen for metastasis, MRI plays a pivotal role in the staging of bladder cancer because of its superior soft tissue delineation, especially in the context of muscle-invasion. The diagnostic accuracy of MRI in differentiating MIBC from NMIBC is reported to be 75%-92%[15,16]. However, these anatomical imaging techniques are not ideal for tissue characterization and assessing tumor aggressiveness. Furthermore, these anatomical imaging techniques often overestimate the extent of tumor after TURBT and CRT due to the post-treatment changes. In multimodal organ-preserving strategies, generally, prior to CRT, TURBT is performed for debulking of the tumor. Both TURBT and CRT can induce local fibrotic and inflammatory changes, both of which manifest as bladder wall thickening[17]. Additionally, after the combined therapy, bladder cancer may regress and present as a flat lesion. Therefore, anatomical assessment of therapeutic response based on the response evaluation criteria in solid tumors on T2WI is not appropriate for discriminating small remnants of cancerous tissue from these secondary changes. Dobson *et al*[18] showed the utility of dynamic contrast-enhanced (DCE) MRI for discriminating cancerous tissue from radiation-induced fibrosis in thickened bladder walls. However, inflammatory changes secondary to treatments may persist for many years[19]. These false-positive results on DCE are often problematic, and they lower its specificity for detecting residual bladder cancer[19]. Thus, the utility of T2WI and DCE is still limited in monitoring the therapeutic response after TURBT and CRT[20].

DIFFUSION-WEIGHTED MRI IN CANCER

Biophysical basis and clinical application

The DW-MRI technique was initially devised by Stejskal and Tanner in 1965. Since 1985, DW-MRI has been mainly used for neuroimaging, especially for diagnosis of acute cerebral infarction and intracranial tumors[21]. With the recent advent of echo planar imaging, high gradient amplitudes, multichannel coils, and parallel imaging, DW-MRI of the abdomen and pelvis has become possible, and a growing number of studies have demonstrated the usefulness of this imaging technique in the diagnosis of malignant tumors of the abdomen[22,23]. Because the signal of DW-MRI is derived from the inherent tissue contrast,

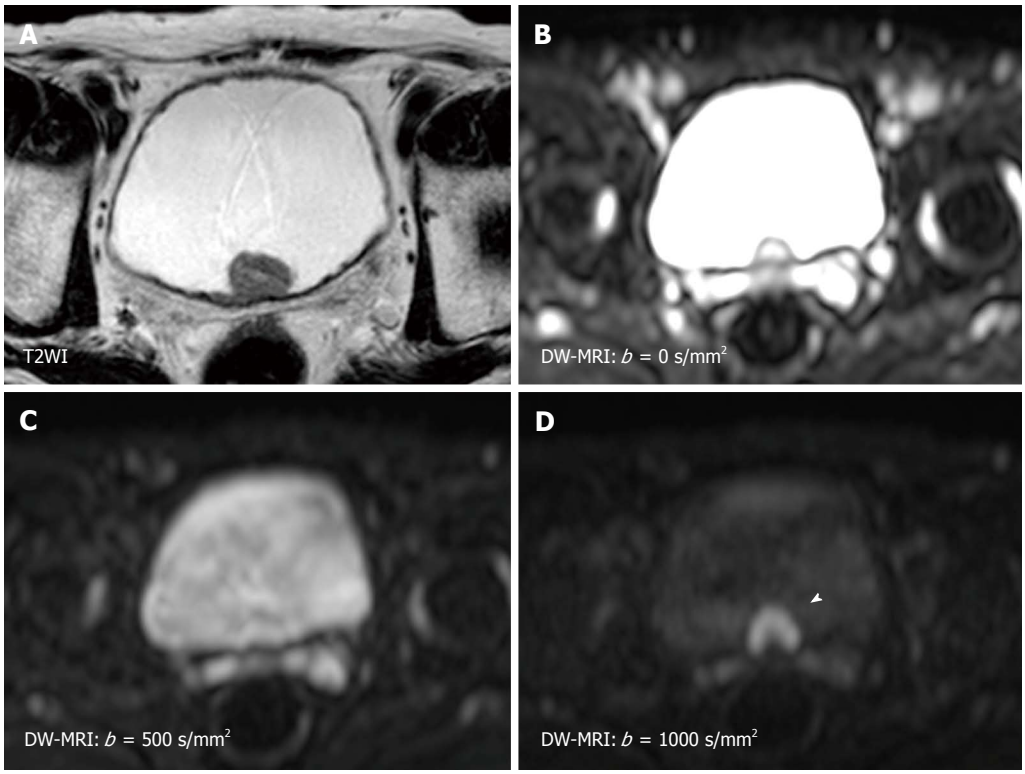

Figure 1 Magnetic resonance images of a 79-year-old man with non-muscle invasive bladder cancer (urothelial cancer, stage pTa, grade 2 > 3). A: T2WI shows a hypointense tumor at the trigone; B: The signal intensity of diffusion-weighted magnetic resonance imaging depends on both water diffusion and the T2 relaxation time; C: Due to the very long T2 relaxation time of urine, the signal of the urine in the bladder remains high on the diffusion-weighted magnetic resonance imaging with a *b*-value of 500 s/mm^2. This is known as the "T2 shine-through effect"; D: Using a *b*-value of 1000 s/mm^2 decreases the signal of the urine, as well as those of the seminal vesicles, while the bladder cancer (arrow head) shows little signal attenuation with the increased *b*-value.

this imaging technique requires no contrast agent and is applicable to patients with allergies to contrast agents or those with renal insufficiency. Furthermore, the addition of DW-MRI to a routine MRI examination requires only a few additional minutes and can be adopted for most current clinical MRI scanners.

DW-MRI is a functional imaging technique, the contrast of which results from quantifying the microscopic mobility of water molecules in tissue[22,23]. In biological tissues, the diffusion of water molecule is inversely correlated to the tissue cellularity and the integrity of cell membranes. In the area of tumor tissues, which have a high cellular density with intact cell membranes, water molecule diffusion is restricted, while the diffusion of water molecule is less restricted in areas of low cellular density. Areas where the diffusion is restricted generally show high signal intensity on DW-MRI, and malignant lesions typically show high signal intensity because of their higher cellularity, tissue disorganization, and decreased extracellular space, all of which restrict water diffusion. In recent years, an increasing number of studies have shown the usefulness of visual assessment of DW-MRI for detecting malignant tumors, and DW-MRI has quickly become a useful adjunct for assessing various types of tumors including bladder cancer[24-27].

Quantifying the degree of diffusion

The sensitivity of the diffusion is varied by changing the "*b*-value" which is proportional to the gradient amplitude, the duration of the applied gradient, and the time interval between the paired gradients[22,23]. Small *b*-values attenuate the signals of water molecules with a large degree of motion or a great diffusion distance. By using higher *b*-values, the perfusion in the intra-vascular space is restricted and slow-moving water molecules or small diffusion distances can be distinguished (Figure 1). Therefore, DW-MRI should be performed using three or more *b*-values including $b = 0$ s/mm^2, $b \geqslant 100$ s/mm^2, and $b \geqslant 500$ s/mm^2. Comparing the images obtained at different *b*-values is useful for characterizing the lesion. The apparent diffusion coefficient (ADC) value is assessed for quantitative evaluation of DW-MRI by evaluating the signal attenuation of tissue on DW-MRI with increasing *b*-values. Generally, the software automatically calculates the ADC values, and the calculated ADC values for each pixel of the image are displayed as a parametric map. By drawing regions of interests (ROI) on this ADC map, the ADC value of the delineated region can be easily obtained. However, because of their poor anatomical details, DW-MRI and ADC maps should be evaluated in combination with T1WI and T2WI, and the correlation with anatomical images is important to accurately set the ROI for the target lesion. Quantitative evaluation of DW-MRI by assessing the ADC value is potentially useful for tissue characterization based on the differences in water diffusion. The correlation of tumor ADC values with their

biological aggressiveness has been reported for various types of malignancies[28-30]. However, the reproducibility of the ADC value is an intrinsic limitation in ADC measurement because the ADC value depends on the MRI system and imaging protocol used. To standardize the ADC assessment, some trials using ADC ratio, calculated with respect to surrounding normal tissues, have been performed recently.

Predicting treatment sensitivity

The important clinical implication of DW-MRI in multimodal organ preservation strategies for MIBC is the ability to predict therapeutic response prior to treatment. In a number of prospective studies in various types of cancers including brain tumors and cervical and rectal cancers[31-35], the potential of DW-MRI to predict the sensitivity to radiotherapy has been shown. The tumors with higher ADC values are less likely to respond to the treatment. The hypothesized mechanism underlying this relationship is the presence of necrosis reflected in a higher ADC value, which predicts a poor outcome related to hypoxia-mediated radioresistance. Meanwhile, soon after the initiation of chemotherapy and/or radiotherapy, immediate cell death can be observed after the commencement of the treatment, which is reflected as an early increase in the ADC value. In cervical cancer and rectal cancer, this early increase in ADC value is observed in patients who show good response to CRT, and can be a potential early biomarker for treatment outcomes[35-38]. Following this early ADC increase, edema and fibrosis cause a subsequent ADC decrease[35-37].

Monitoring treatment response

Importantly, the DW-MRI can be an imaging biomarker in monitoring treatment effect. In response to successful treatment, cell necrosis and loss of cell membrane integrity are induced, leading to increased water diffusion. Furthermore, tumor apoptosis induced by treatment results in cell shrinkage. These changes are reflected by increases in ADC value[22]. Clinical studies in many types of malignancies, including liver cancer, cerebral gliomas, and soft-tissue sarcoma, have demonstrated the correlation between therapeutic effect and changes in water diffusion in tumors[39-41].

CLINICAL APPLICATION OF DW-MRI IN BLADDER CANCER

Detecting bladder cancer

Since the first report by Matsuki *et al*[26] showing the utility of DW-MRI for detecting bladder cancer, a number of studies have shown the usefulness of DW-MRI for the diagnosis of bladder cancer[24-27]. On DW-MRI with a high *b*-value, bladder cancers generally show a hyperintense signal, while the signals of the surrounding tissues, including urine, are much less intense[26,42] (Figure 1). This good signal contrast is obtained between bladder cancer and the surrounding tissue. The sensitivity, specificity and accuracy for detecting bladder cancer were reported to be 90%-98%, 92%-93% and 91%-97%, respectively[24,25,27]. In several studies, quantitative analysis consistently showed restricted diffusion and lower ADC values in bladder cancer compared with the surrounding structures[26,42].

Detecting lymph node metastasis

MIBC has the potential to metastasize to lymph nodes and distant organs, and detecting metastatic lesion is another problem in managing MIBC. At the time of surgery, 25% of the patients who undergo radical cystectomy have a lymph node metastasis. Lymph node staging has been generally performed by CT or conventional MRI based on size criteria and morphological appearance, and the accuracy for staging nodal disease ranges from 73% to 90%[43]. On DW-MRI, benign lymph nodes show high signal intensity due to their highly cellular structures composed of lymphoid elements (Figure 2). The utility of DW-MRI has been shown in lymph node staging in various cancers[44-48]. Papalia *et al*[49] showed that malignant lymph nodes have a significantly lower ADC value than benign lymph nodes with sensitivity of 76.4% and specificity of 89.4% in a study that included 36 patients with bladder cancer undergoing radical cystectomy. However, there is a substantial overlap in ADC values between malignant and benign lymph nodes, and discriminating malignant nodes from benign nodes on DW-MRI is still challenging[50]. Recently, Thoeny *et al*[51] reported an excellent diagnostic accuracy of 90% in detecting pelvic lymph nodal involvement by the combined use of ultrasmall super paramagnetic iron oxide (USPIO) and DW-MRI. This agent is taken up by macrophages resulting signal loss in normal lymph nodes, while the signal of metastatic lymph nodes is not influenced[51-55]. Further studies are needed to confirm this encouraging result.

Detecting bone metastasis

DW-MRI for evaluating primary bladder cancer occasionally shows abnormal signals of pelvic bones or femur heads. Bone metastasis typically shows clear high signal intensity on DW-MRI[56,57]. However, as well as benign bone tumors, hematopoietic bone marrow also appears as a hyperintense lesion on DW-MRI because of rich hematopoietic cells[58,59]. These false-positive findings in detecting metastasis should be kept in mind for staging bladder cancer[60]. Furthermore, identifying microscopic metastases or developing metastases remains a challenge, and a third of MIBC patients have undetected metastases at the initial diagnosis[61].

Characterizing histopathological features

Because the contrast of DW-MRI is based on difference in the degree of water diffusion between tissues, the spatial resolution of DW-MRI is generally low. However, using the clear contrast between bladder cancer and the surrounding tissues, the utility of DW-MRI for staging of

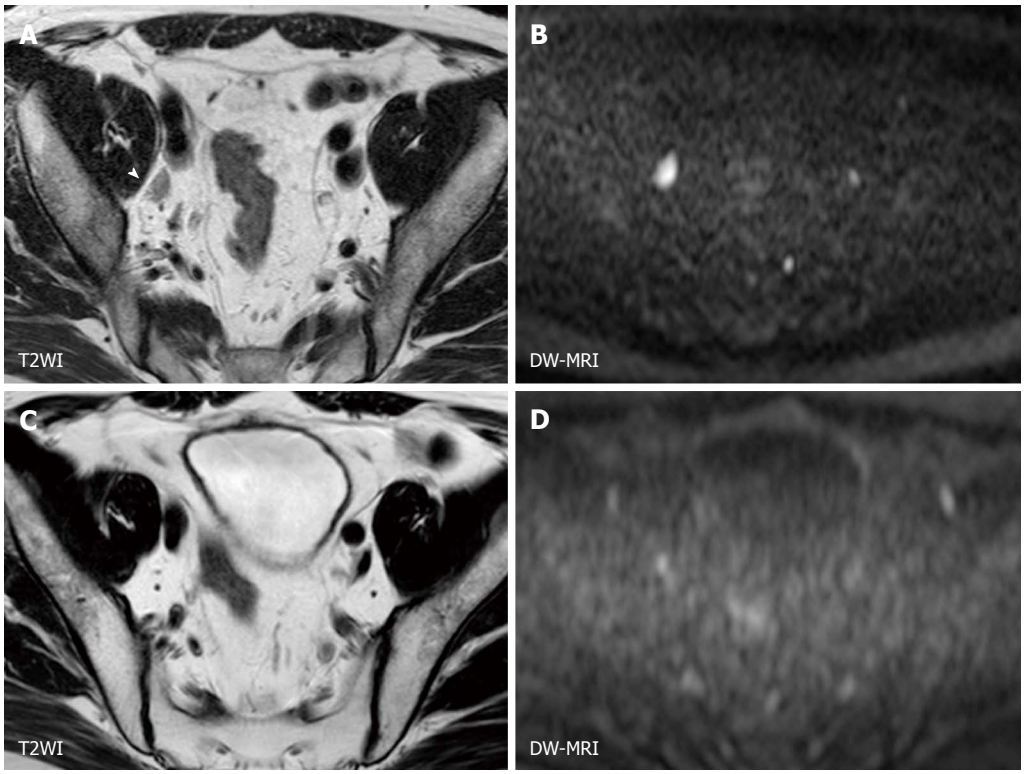

Figure 2 Magnetic resonance images of a 45-year-old man with muscle-invasive bladder cancer (urothelial cancer, stage cT3N1) before and after chemoradiotherapy. A: Before CRT, an enlarged right external iliac lymph node (arrow head) is visible on T2WI; B: The lymph node on the corresponding DW-MRI shows a hyperintense signal; C and D: After CRT, size reduction on T2WI (C) and signal attenuation on DW-MRI (D) in lymph node is evident, consistent with the expected treatment response. CRT: Chemoradiotherapy; DW-MRI: Diffusion-weighted magnetic resonance imaging.

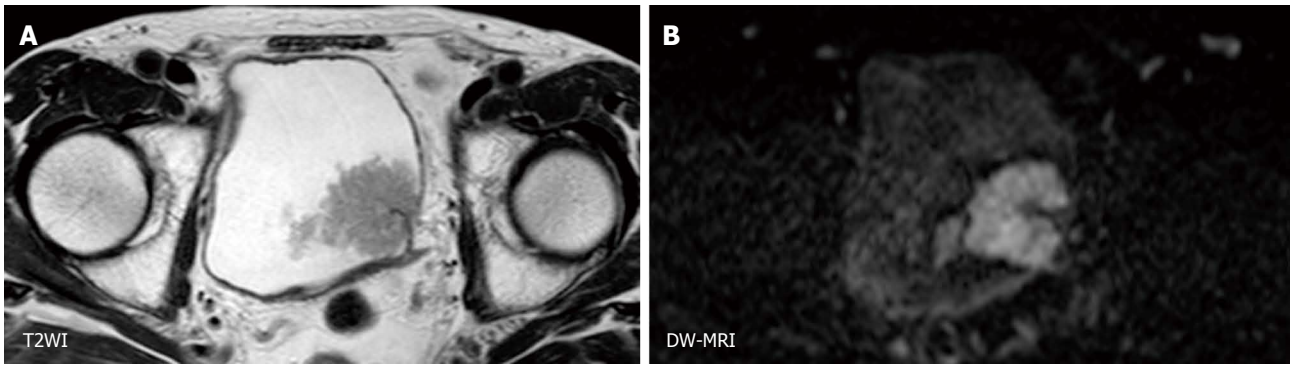

Figure 3 Magnetic resonance images of a 63-year-old man with non-muscle-invasive bladder cancer (urothelial cancer, stage pT1, grade 2 > 3). A: T2WI shows a large papillary tumor on the left bladder wall; B: DW-MRI displays a C-shaped high-signal tumor with a low-signal-intensity stalk connecting to the bladder wall. This C-shaped high signal is known as an "inchworm sign", which is a criterion for T staging in non-muscle-invasive bladder cancer (stage cT1 or less). DW-MRI: Diffusion-weighted magnetic resonance imaging.

bladder cancer based on the signal shape and contrast has been shown (Figure 3). On DW-MRI, bladder cancers generally show a hyperintense signal in distinct contrast to the hypointense signal of the submucosal layer and the intermediate signal of the intact bladder wall. On the basis of these findings, El-Assmy *et al*[62] reported the ability to discriminate MIBC from NMIBC with an accuracy of 63.6% in a study that included 106 patients. Takeuchi *et al*[63] reported that bladder cancer staging accuracy improved from 67 to 88% when DW-MRI was added to T2WI.

Furthermore, the utility of DW-MRI in characterizing bladder cancer has been consistently shown in multiple studies using quantitative analysis (Figures 4 and 5). Takeuchi *et al*[63] reported that the ADC value of grade 3 tumors was significantly lower than that of grade 1 and 2 tumors in a prospective study that included 40 patients. Avcu *et al*[64] also reported similar results showing an inverse correlation between the ADC value and the histological grade. The existence of a substantial overlap between the histological grades or stages poses a limit to qualitative analysis and the clinical application

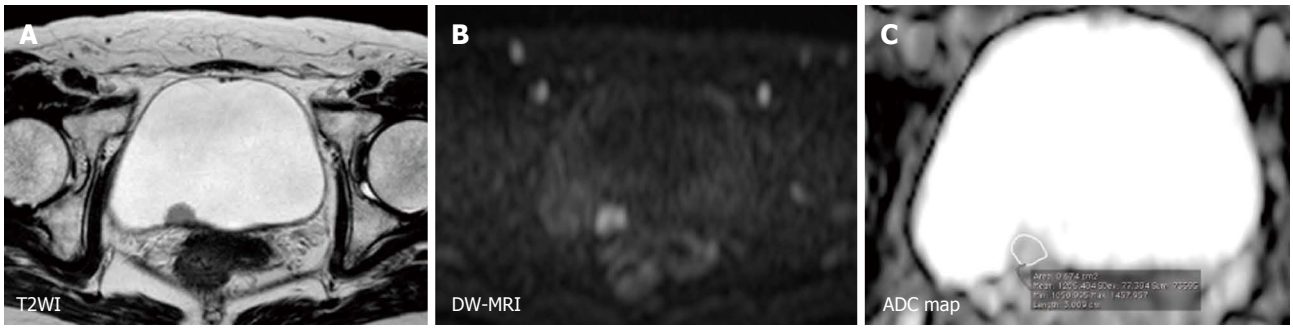

Figure 4 Magnetic resonance images of a 52-year-old woman with non-muscle-invasive bladder cancer (urothelial cancer, pTa, grade 2). A: T2WI shows a hypointense tumor at the posterior wall; B: DW-MRI displays the tumor as a high-signal mass; C: The corresponding ADC map demonstrates a lesser degree of restricted diffusion. The mean ADC value with the ROI positioned not extending over the tumor is 1.21 x 10^{-3} s/mm^2. DW-MRI: Diffusion-weighted magnetic resonance imaging; ADC: Apparent diffusion coefficient.

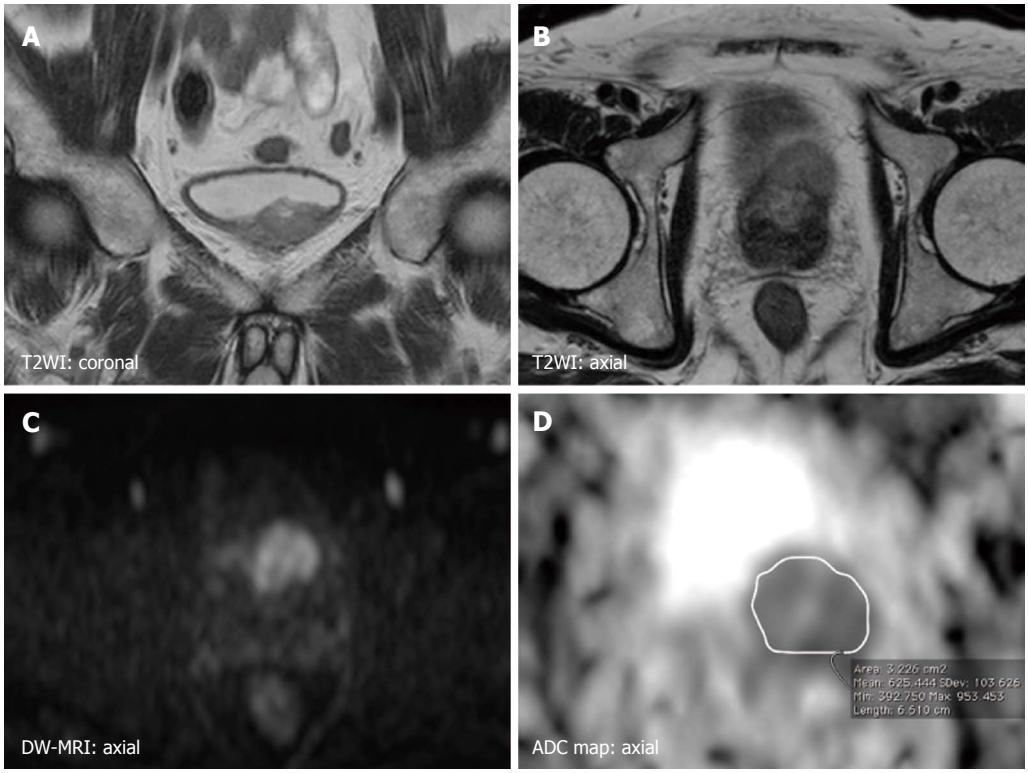

Figure 5 Magnetic resonance images of a 75-year-old man with muscle-invasive bladder cancer (urothelial cancer, stage cT4, grade 3). A and B: T2WI shows a large hypointense tumor at the bladder neck, invading the prostate; C: DW-MRI displays the tumor as a high-signal mass; D: The corresponding ADC map demonstrates restricted diffusion. The mean ADC value of the tumor is 0.63 x 10^{-3} mm^2/s. DW-MRI: Diffusion-weighted magnetic resonance imaging; ADC: Apparent diffusion coefficient.

of this technique. However, these studies indicated that advanced and aggressive bladder cancers tend to have a low ADC values. Actually, Kobayashi *et al*[27] found that clinically aggressive tumors, including MIBC and high-grade T1 tumors, had a significantly lower ADC value than the other less aggressive tumors. A threshold ADC value differentiated these two entities with 87% accuracy in a series of 121 patients. The underlying mechanisms whereby the ADC value reflects these tumor characters are thought to be the tumor cell morphological characters such as dense cellularity and large cellular size[22,23]. Recent studies have shown an inverse correlation between ADC value and the Ki-67 labeling index, a marker of cell proliferation, in bladder cancer[65-67]. These data suggest the potential of ADC value to serve as a quantitative biomarker characterizing the biological features of bladder cancer.

Predicting metastatic potential

The potential role of ADC values in predicting the metastatic potential of localized high-grade bladder cancers was shown in a small study that included 17 patients. This study showed that invasive high-grade bladder cancers with metastasis had lower ADC values than those without metastasis[68]. ADC value can be a supplemental parameter for predicting the presence of metastasis, which

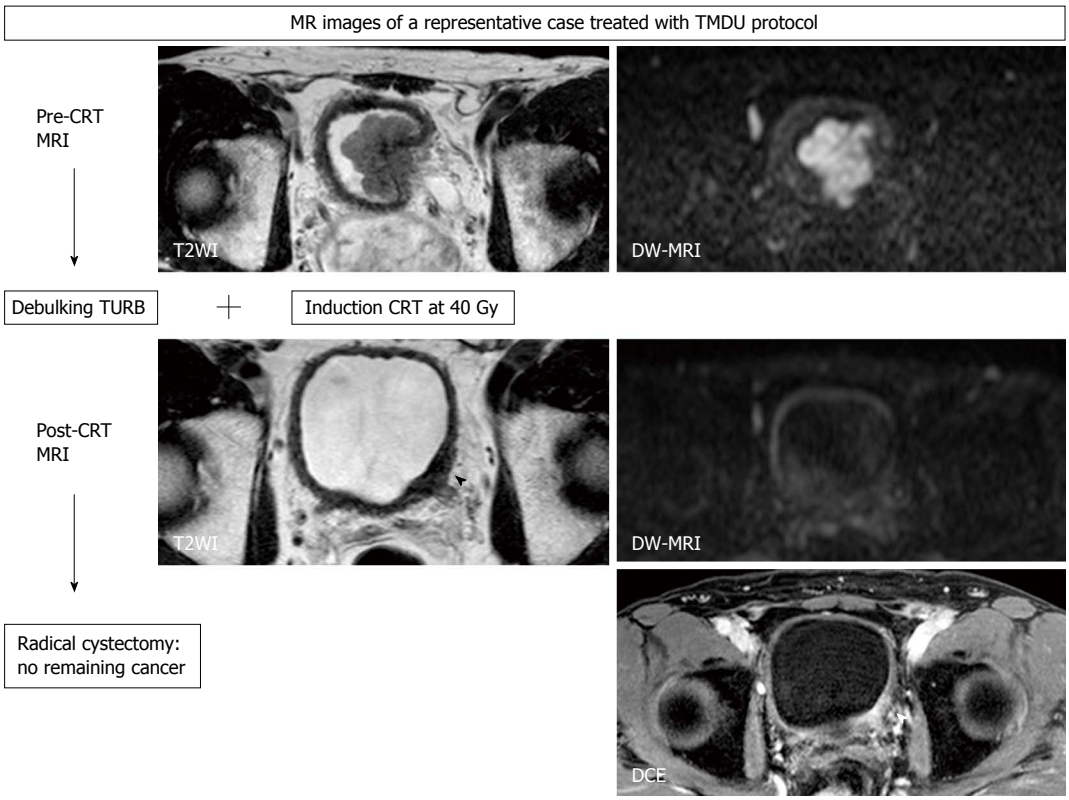

Figure 6 Magnetic resonance images of a 61-year-old man with muscle-invasive bladder cancer (urothelial cancer, stage cT3, grade 3) treated with the Tokyo Medical and Dental University protocol consisting of transurethral resection of bladder tumor and induction chemoradiotherapy (CRT) followed by radical or partial cystectomy. T2WI shows a large hypointense tumor at the bladder neck, invading the prostate. At the diagnosis, DW-MRI with a *b*-value of 1000 s/mm^2 displays a hyperintense lobulated mass. After TURBT and CRT, this lesion shows wall thickening (arrow head) on T2WI and enhancement on DCE, while the abnormal signal on DW-MRI is diminished to normal signal intensity. Histopathologic examination of the cystectomized sample reveals no remaining bladder cancer, revealing the findings of post-CRT T2WI and DCE to be false-positive findings reflecting post-treatment changes in bladder tissues. TURBT: Transurethral resection of bladder tumor; CRT: Chemoradiotherapy; DW-MRI: Diffusion-weighted magnetic resonance imaging; DCE: Dynamic contrast-enhanced.

has a great impact on treatment decisions.

POTENTIAL ROLES OF DW-MRI IN MULTIMODALITY BLADDER-SPARING STRATEGIES

Novel bladder-sparing approach incorporating consolidative partial cystectomy with pelvic lymph node dissection

We started a pilot study of a selective bladder-sparing protocol incorporating consolidative partial cystectomy with pelvic lymph node dissection after induction low-dose chemoradiotherapy (LCRT) in 1997 at Tokyo Medical and Dental University (TMDU)[10,11,14,69-71]. Consolidative partial cystectomy with pelvic lymph node dissection is intended to eradicate possible remaining subclinical residual tumor tissue in the original MIBC sites and micrometastases in the pelvic lymph nodes. Candidates for bladder preservation are selected based on the extent, location, and post-LCRT status of the tumor. More than one-third of MIBC patients without any metastasis meet our criteria for partial cystectomy. Partial cystectomy with pelvic lymph node dissection was performed in 70 patients following LCRT. A functional native bladder was preserved in 91% of patients, and none has developed MIBC or lymph node recurrence[10,14].

Predicting sensitivity to CRT

In the majority of CRT-based bladder-sparing protocols for localized MIBC, patients who achieve a clinical CR are subjected to consolidative treatment with CRT for bladder preservation. In these protocols, treatment effect cannot be histologically evaluated. In the above-mentioned bladder-sparing protocol incorporating partial cystectomy, histopathological therapeutic effects of LCRT can be assessed, which is one of advantages of the TMDU protocol. By comparing DW-MRIs taken before and after LCRT with this therapeutic effect, the utility of DW-MRI for predicting treatment sensitivity and in monitoring therapeutic response can be evaluated[20,67].

We found a significant inverse correlation between LCRT sensitivity and ADC value of the tumor[67]. LCRT-sensitive MIBCs had significantly lower ADC values than LCRT-resistant MIBCs. With a defined cut-off ADC value, the sensitivity, specificity and accuracy in predicting LCRT sensitivity were 92%, 90%, and 91%, respectively. These findings are consistent with previous reports on other tumors including brain, cervix and rectum[31-35]. However, the presence of necrosis is not common in

MIBC, which is understood to be the background of the correlation between lower ADC values and favorable CRT response. One possible explanation of this correlation found in MIBC is that the relationship between the proliferative activity and the ADC value of MIBC; highly proliferating MIBCs show low ADC values[65,67]. Because favorable CRT response in highly proliferating MIBC has been reported[72,73], a low ADC value would be predictive of a better CRT sensitivity of MIBC.

Monitoring response to CRT

We also showed the utility of DW-MRI in monitoring the therapeutic response of MIBC treated with LCRT, as has been reported for other cancers. The sensitivity/specificity/accuracy of T2WI, DCE, and DW-MRI in predicting pathologic CR were 43%/45%/44%, 57%/18%/33%, and 57%/92%/80%, respectively[20]. DW-MRI improved the accuracy for detecting the remaining cancer after LCRT, primarily due to its increased specificity (Figure 6). However, the low sensitivity in detecting small lesions is a notable limitation, which makes it difficult to detect microscopic residual cancers, as is the case with the other imaging techniques. Further studies are necessary to evaluate the potential of DW-MRI as an imaging technique in the context of bladder-sparing approaches. Multiple approaches, including DW-MRI and biopsies to monitor the therapeutic response, may improve the accuracy of these techniques. However, the limits discussed here in detecting remaining cancers justify partial cystectomies to eliminate the possibly of remaining microscopic tumors in the original invasive cancer site, even in the patients who achieve clinical CR after CRT.

CONCLUSION

Recent studies have shown that the DW-MRI is a unique imaging technique that provides qualitative and quantitative information on biological features of bladder cancer, and is potentially useful as an imaging technique in the management of bladder cancer, particularly in multimodal bladder-sparing strategies for MIBC. Further large prospective studies are needed to clarify the practical roles of DW-MRI in the management of bladder cancer.

REFERENCES

1 **Siegel R**, Naishadham D, Jemal A. Cancer statistics, 2012. *CA Cancer J Clin* 2012; **62**: 10-29 [PMID: 22237781 DOI: 10.3322/caac.20138]

2 **Tsukamoto T**, Kitamura H, Takahashi A, Masumori N. Treatment of invasive bladder cancer: lessons from the past and perspective for the future. *Jpn J Clin Oncol* 2004; **34**: 295-306 [PMID: 15333680 DOI: 10.1093/jjco/hyh048]

3 **Gilbert SM**, Wood DP, Dunn RL, Weizer AZ, Lee CT, Montie JE, Wei JT. Measuring health-related quality of life outcomes in bladder cancer patients using the Bladder Cancer Index (BCI). *Cancer* 2007; **109**: 1756-1762 [PMID: 17366596 DOI: 10.1002/cncr.22556]

4 **Housset M**, Maulard C, Chretien Y, Dufour B, Delanian S, Huart J, Colardelle F, Brunel P, Baillet F. Combined radiation and chemotherapy for invasive transitional-cell carcinoma of the bladder: a prospective study. *J Clin Oncol* 1993; **11**: 2150-2157 [PMID: 8229129]

5 **Kachnic LA**, Kaufman DS, Heney NM, Althausen AF, Griffin PP, Zietman AL, Shipley WU. Bladder preservation by combined modality therapy for invasive bladder cancer. *J Clin Oncol* 1997; **15**: 1022-1029 [PMID: 9060542]

6 **Rödel C**, Grabenbauer GG, Kühn R, Papadopoulos T, Dunst J, Meyer M, Schrott KM, Sauer R. Combined-modality treatment and selective organ preservation in invasive bladder cancer: long-term results. *J Clin Oncol* 2002; **20**: 3061-3071 [PMID: 12118019 DOI: 10.1200/JCO.2002.11.027]

7 **Eisenberg MS**, Dorin RP, Bartsch G, Cai J, Miranda G, Skinner EC. Early complications of cystectomy after high dose pelvic radiation. *J Urol* 2010; **184**: 2264-2269 [PMID: 20952024 DOI: 10.1016/j.juro.2010.08.007]

8 **Stein JP**, Lieskovsky G, Cote R, Groshen S, Feng AC, Boyd S, Skinner E, Bochner B, Thangathurai D, Mikhail M, Raghavan D, Skinner DG. Radical cystectomy in the treatment of invasive bladder cancer: long-term results in 1,054 patients. *J Clin Oncol* 2001; **19**: 666-675 [PMID: 11157016]

9 **Perdonà S**, Autorino R, Damiano R, De Sio M, Morrica B, Gallo L, Silvestro G, Farella A, De Placido S, Di Lorenzo G. Bladder-sparing, combined-modality approach for muscle-invasive bladder cancer: a multi-institutional, long-term experience. *Cancer* 2008; **112**: 75-83 [PMID: 18008364 DOI: 10.1002/cncr.23137]

10 **Koga F**, Kihara K, Yoshida S, Yokoyama M, Saito K, Masuda H, Fujii Y, Kawakami S. Selective bladder-sparing protocol consisting of induction low-dose chemoradiotherapy plus partial cystectomy with pelvic lymph node dissection against muscle-invasive bladder cancer: oncological outcomes of the initial 46 patients. *BJU Int* 2012; **109**: 860-866 [PMID: 21854531 DOI: 10.1111/j.1464-410X.2011.10425.x]

11 **Koga F**, Yoshida S, Kawakami S, Kageyama Y, Yokoyama M, Saito K, Fujii Y, Kobayashi T, Kihara K. Low-dose chemoradiotherapy followed by partial or radical cystectomy against muscle-invasive bladder cancer: an intent-to-treat survival analysis. *Urology* 2008; **72**: 384-388 [PMID: 18455771 DOI: 10.1016/j.urology.2008.03.017]

12 **Zietman AL**, Grocela J, Zehr E, Kaufman DS, Young RH, Althausen AF, Heney NM, Shipley WU. Selective bladder conservation using transurethral resection, chemotherapy, and radiation: management and consequences of Ta, T1, and Tis recurrence within the retained bladder. *Urology* 2001; **58**: 380-385 [PMID: 11549485 DOI: 10.1016/S0090-4295(01)01219-5]

13 **Tunio MA**, Hashmi A, Qayyum A, Mohsin R, Zaeem A. Whole-pelvis or bladder-only chemoradiation for lymph node-negative invasive bladder cancer: single-institution experience. *Int J Radiat Oncol Biol Phys* 2012; **82**: e457-e462 [PMID: 21945107 DOI: 10.1016/j.ijrobp.2011.05.051]

14 **Koga F**, Kihara K. Selective bladder preservation with curative intent for muscle-invasive bladder cancer: a contemporary review. *Int J Urol* 2012; **19**: 388-401 [PMID: 22409269 DOI: 10.1111/j.1442-2042.2012.02974.x]

15 **Tekes A**, Kamel I, Imam K, Szarf G, Schoenberg M, Nasir K, Thompson R, Bluemke D. Dynamic MRI of bladder cancer: evaluation of staging accuracy. *AJR Am J Roentgenol* 2005; **184**: 121-127 [PMID: 15615961 DOI: 10.2214/ajr.184.1.01840121]

16 **Hayashi N**, Tochigi H, Shiraishi T, Takeda K, Kawamura J. A new staging criterion for bladder carcinoma using gadolinium-enhanced magnetic resonance imaging with an endorectal surface coil: a comparison with ultrasonography. *BJU Int* 2000; **85**: 32-36 [PMID: 10619941 DOI: 10.1046/j.1464-410x.2000.00358.x]

17 **Raza SA**, Jhaveri KS. MR imaging of urinary bladder carcinoma and beyond. *Radiol Clin North Am* 2012; **50**: 1085-1110 [PMID: 23122040 DOI: 10.1016/j.rcl.2012.08.011]

18 **Dobson MJ**, Carrington BM, Collins CD, Ryder WD, Read G,

Hutchinson CE, Hawnaur JM. The assessment of irradiated bladder carcinoma using dynamic contrast-enhanced MR imaging. *Clin Radiol* 2001; **56**: 94-98 [PMID: 11222064 DOI: 10.1053/crad.2000.0560]
19 **Johnson RJ**, Carrington BM, Jenkins JP, Barnard RJ, Read G, Isherwood I. Accuracy in staging carcinoma of the bladder by magnetic resonance imaging. *Clin Radiol* 1990; **41**: 258-263 [PMID: 2340697 DOI: 10.1016/S0009-9260(05)81661-7]
20 **Yoshida S**, Koga F, Kawakami S, Ishii C, Tanaka H, Numao N, Sakai Y, Saito K, Masuda H, Fujii Y, Kihara K. Initial experience of diffusion-weighted magnetic resonance imaging to assess therapeutic response to induction chemoradiotherapy against muscle-invasive bladder cancer. *Urology* 2010; **75**: 387-391 [PMID: 19914691 DOI: 10.1016/j.urology.2009.06.111]
21 **Le Bihan D**, Breton E, Lallemand D, Grenier P, Cabanis E, Laval-Jeantet M. MR imaging of intravoxel incoherent motions: application to diffusion and perfusion in neurologic disorders. *Radiology* 1986; **161**: 401-407 [PMID: 3763909 DOI: 10.1148/radiology.161.2.3763909]
22 **Koh DM**, Collins DJ. Diffusion-weighted MRI in the body: applications and challenges in oncology. *AJR Am J Roentgenol* 2007; **188**: 1622-1635 [PMID: 17515386 DOI: 10.2214/AJR.06.1403]
23 **Padhani AR**, Liu G, Koh DM, Chenevert TL, Thoeny HC, Takahara T, Dzik-Jurasz A, Ross BD, Van Cauteren M, Collins D, Hammoud DA, Rustin GJ, Taouli B, Choyke PL. Diffusion-weighted magnetic resonance imaging as a cancer biomarker: consensus and recommendations. *Neoplasia* 2009; **11**: 102-125 [PMID: 19186405]
24 **Abou-El-Ghar ME**, El-Assmy A, Refaie HF, El-Diasty T. Bladder cancer: diagnosis with diffusion-weighted MR imaging in patients with gross hematuria. *Radiology* 2009; **251**: 415-421 [PMID: 19304915 DOI: 10.1148/radiol.2503080723]
25 **Ceylan K**, Taken K, Gecit I, Pirincci N, Gunes M, Tanik S, Karaman I. Comparison of cystoscopy with diffusion-weighted magnetic resonance images used in the diagnosis and follow-up of patients with bladder tumors. *Asian Pac J Cancer Prev* 2010; **11**: 1001-1004 [PMID: 21133614]
26 **Matsuki M**, Inada Y, Tatsugami F, Tanikake M, Narabayashi I, Katsuoka Y. Diffusion-weighted MR imaging for urinary bladder carcinoma: initial results. *Eur Radiol* 2007; **17**: 201-204 [PMID: 16865369 DOI: 10.1007/s00330-006-0281-7]
27 **Kobayashi S**, Koga F, Yoshida S, Masuda H, Ishii C, Tanaka H, Komai Y, Yokoyama M, Saito K, Fujii Y, Kawakami S, Kihara K. Diagnostic performance of diffusion-weighted magnetic resonance imaging in bladder cancer: potential utility of apparent diffusion coefficient values as a biomarker to predict clinical aggressiveness. *Eur Radiol* 2011; **21**: 2178-2186 [PMID: 21688007 DOI: 10.1007/s00330-011-2174-7]
28 **Costantini M**, Belli P, Rinaldi P, Bufi E, Giardina G, Franceschini G, Petrone G, Bonomo L. Diffusion-weighted imaging in breast cancer: relationship between apparent diffusion coefficient and tumour aggressiveness. *Clin Radiol* 2010; **65**: 1005-1012 [PMID: 21070905 DOI: 10.1016/j.crad.2010.07.008]
29 **Yoshida S**, Masuda H, Ishii C, Tanaka H, Fujii Y, Kawakami S, Kihara K. Usefulness of diffusion-weighted MRI in diagnosis of upper urinary tract cancer. *AJR Am J Roentgenol* 2011; **196**: 110-116 [PMID: 21178054 DOI: 10.2214/AJR.10.4632]
30 **Kitajima K**, Takahashi S, Ueno Y, Miyake H, Fujisawa M, Kawakami F, Sugimura K. Do apparent diffusion coefficient (ADC) values obtained using high b-values with a 3-T MRI correlate better than a transrectal ultrasound (TRUS)-guided biopsy with true Gleason scores obtained from radical prostatectomy specimens for patients with prostate cancer? *Eur J Radiol* 2013; **82**: 1219-1226 [PMID: 23518144 DOI: 10.1016/j.ejrad.2013.02.021]
31 **DeVries AF**, Kremser C, Hein PA, Griebel J, Krezcy A, Ofner D, Pfeiffer KP, Lukas P, Judmaier W. Tumor microcirculation and diffusion predict therapy outcome for primary rectal carcinoma. *Int J Radiat Oncol Biol Phys* 2003; **56**: 958-965 [PMID: 12829130 DOI: 10.1016/S0360-3016(03)00208-6]
32 **Liu Y**, Bai R, Sun H, Liu H, Zhao X, Li Y. Diffusion-weighted imaging in predicting and monitoring the response of uterine cervical cancer to combined chemoradiation. *Clin Radiol* 2009; **64**: 1067-1074 [PMID: 19822239 DOI: 10.1016/j.crad.2009.07.010]
33 **Mardor Y**, Roth Y, Ochershvilli A, Spiegelmann R, Tichler T, Daniels D, Maier SE, Nissim O, Ram Z, Baram J, Orenstein A, Pfeffer R. Pretreatment prediction of brain tumors' response to radiation therapy using high b-value diffusion-weighted MRI. *Neoplasia* 2004; **6**: 136-142 [PMID: 15140402 DOI: 10.1593/neo.03349]
34 **Dzik-Jurasz A**, Domenig C, George M, Wolber J, Padhani A, Brown G, Doran S. Diffusion MRI for prediction of response of rectal cancer to chemoradiation. *Lancet* 2002; **360**: 307-308 [PMID: 12147376 DOI: 10.1016/S0140-6736(02)09520-X]
35 **Sun YS**, Zhang XP, Tang L, Ji JF, Gu J, Cai Y, Zhang XY. Locally advanced rectal carcinoma treated with preoperative chemotherapy and radiation therapy: preliminary analysis of diffusion-weighted MR imaging for early detection of tumor histopathologic downstaging. *Radiology* 2010; **254**: 170-178 [PMID: 20019139 DOI: 10.1148/radiol.2541082230]
36 **Hein PA**, Kremser C, Judmaier W, Griebel J, Pfeiffer KP, Kreczy A, Hug EB, Lukas P, DeVries AF. Diffusion-weighted magnetic resonance imaging for monitoring diffusion changes in rectal carcinoma during combined, preoperative chemoradiation: preliminary results of a prospective study. *Eur J Radiol* 2003; **45**: 214-222 [PMID: 12595106 DOI: 10.1016/S0720-048X(02)00231-0]
37 **Kremser C**, Judmaier W, Hein P, Griebel J, Lukas P, de Vries A. Preliminary results on the influence of chemoradiation on apparent diffusion coefficients of primary rectal carcinoma measured by magnetic resonance imaging. *Strahlenther Onkol* 2003; **179**: 641-649 [PMID: 14628131 DOI: 10.1007/s00066-003-1045-9]
38 **Harry VN**, Semple SI, Gilbert FJ, Parkin DE. Diffusion-weighted magnetic resonance imaging in the early detection of response to chemoradiation in cervical cancer. *Gynecol Oncol* 2008; **111**: 213-220 [PMID: 18774597 DOI: 10.1016/j.ygyno.2008.07.048]
39 **Chen CY**, Li CW, Kuo YT, Jaw TS, Wu DK, Jao JC, Hsu JS, Liu GC. Early response of hepatocellular carcinoma to transcatheter arterial chemoembolization: choline levels and MR diffusion constants--initial experience. *Radiology* 2006; **239**: 448-456 [PMID: 16569781 DOI: 10.1148/radiol.2392042202]
40 **Chenevert TL**, McKeever PE, Ross BD. Monitoring early response of experimental brain tumors to therapy using diffusion magnetic resonance imaging. *Clin Cancer Res* 1997; **3**: 1457-1466 [PMID: 9815831]
41 **Einarsdóttir H**, Karlsson M, Wejde J, Bauer HC. Diffusion-weighted MRI of soft tissue tumours. *Eur Radiol* 2004; **14**: 959-963 [PMID: 14767604 DOI: 10.1007/s00330-004-2237-0]
42 **El-Assmy A**, Abou-El-Ghar ME, Refaie HF, El-Diasty T. Diffusion-weighted MR imaging in diagnosis of superficial and invasive urinary bladder carcinoma: a preliminary prospective study. *ScientificWorldJournal* 2008; **8**: 364-370 [PMID: 18454244 DOI: 10.1100/tsw.2008.55]
43 **Barentsz JO**, Jager GJ, van Vierzen PB, Witjes JA, Strijk SP, Peters H, Karssemeijer N, Ruijs SH. Staging urinary bladder cancer after transurethral biopsy: value of fast dynamic contrast-enhanced MR imaging. *Radiology* 1996; **201**: 185-193 [PMID: 8816542 DOI: 10.1148/radiology.201.1.8816542]
44 **Beer AJ**, Eiber M, Souvatzoglou M, Holzapfel K, Ganter C, Weirich G, Maurer T, Kübler H, Wester HJ, Gaa J, Krause BJ. Restricted water diffusibility as measured by diffusion-weighted MR imaging and choline uptake in (11)C-choline PET/CT are correlated in pelvic lymph nodes in patients with prostate cancer. *Mol Imaging Biol* 2011; **13**: 352-361 [PMID: 20490932 DOI: 10.1007/s11307-010-0337-6]

45 **Budiharto T**, Joniau S, Lerut E, Van den Bergh L, Mottaghy F, Deroose CM, Oyen R, Ameye F, Bogaerts K, Haustermans K, Van Poppel H. Prospective evaluation of 11C-choline positron emission tomography/computed tomography and diffusion-weighted magnetic resonance imaging for the nodal staging of prostate cancer with a high risk of lymph node metastases. *Eur Urol* 2011; **60**: 125-130 [PMID: 21292388 DOI: 10.1016/j.eururo.2011.01.015]

46 **Eiber M**, Beer AJ, Holzapfel K, Tauber R, Ganter C, Weirich G, Krause BJ, Rummeny EJ, Gaa J. Preliminary results for characterization of pelvic lymph nodes in patients with prostate cancer by diffusion-weighted MR-imaging. *Invest Radiol* 2010; **45**: 15-23 [PMID: 19996762 DOI: 10.1097/RLI.0b013e3181bbdc2f]

47 **Nakamatsu S**, Matsusue E, Miyoshi H, Kakite S, Kaminou T, Ogawa T. Correlation of apparent diffusion coefficients measured by diffusion-weighted MR imaging and standardized uptake values from FDG PET/CT in metastatic neck lymph nodes of head and neck squamous cell carcinomas. *Clin Imaging* 2012; **36**: 90-97 [PMID: 22370129 DOI: 10.1016/j.clinimag.2011.05.002]

48 **Rechichi G**, Galimberti S, Oriani M, Perego P, Valsecchi MG, Sironi S. ADC maps in the prediction of pelvic lymph nodal metastatic regions in endometrial cancer. *Eur Radiol* 2013; **23**: 65-74 [PMID: 22821394 DOI: 10.1007/s00330-012-2575-2]

49 **Papalia R**, Simone G, Grasso R, Augelli R, Faiella E, Guaglianone S, Cazzato R, Del Vescovo R, Ferriero M, Zobel B, Gallucci M. Diffusion-weighted magnetic resonance imaging in patients selected for radical cystectomy: detection rate of pelvic lymph node metastases. *BJU Int* 2012; **109**: 1031-1036 [PMID: 21883835 DOI: 10.1111/j.1464-410X.2011.10446.x]

50 **Mir N**, Sohaib SA, Collins D, Koh DM. Fusion of high b-value diffusion-weighted and T2-weighted MR images improves identification of lymph nodes in the pelvis. *J Med Imaging Radiat Oncol* 2010; **54**: 358-364 [PMID: 20718916 DOI: 10.1111/j.1754-9485.2010.02182.x]

51 **Thoeny HC**, Triantafyllou M, Birkhaeuser FD, Froehlich JM, Tshering DW, Binser T, Fleischmann A, Vermathen P, Studer UE. Combined ultrasmall superparamagnetic particles of iron oxide-enhanced and diffusion-weighted magnetic resonance imaging reliably detect pelvic lymph node metastases in normal-sized nodes of bladder and prostate cancer patients. *Eur Urol* 2009; **55**: 761-769 [PMID: 19144456 DOI: 10.1016/j.eururo.2008.12.034]

52 **Birkhäuser FD**, Studer UE, Froehlich JM, Triantafyllou M, Bains LJ, Petralia G, Vermathen P, Fleischmann A, Thoeny HC. Combined ultrasmall superparamagnetic particles of iron oxide-enhanced and diffusion-weighted magnetic resonance imaging facilitates detection of metastases in normal-sized pelvic lymph nodes of patients with bladder and prostate cancer. *Eur Urol* 2013; **64**: 953-960 [PMID: 23916692 DOI: 10.1016/j.eururo.2013.07.032]

53 **Fortuin AS**, Meijer H, Thompson LC, Witjes JA, Barentsz JO. Ferumoxtran-10 ultrasmall superparamagnetic iron oxide-enhanced diffusion-weighted imaging magnetic resonance imaging for detection of metastases in normal-sized lymph nodes in patients with bladder and prostate cancer: do we enter the era after extended pelvic lymph node dissection? *Eur Urol* 2013; **64**: 961-93; discussion 963 [PMID: 23972400 DOI: 10.1016/j.eururo.2013.08.017]

54 **Froehlich JM**, Triantafyllou M, Fleischmann A, Vermathen P, Thalmann GN, Thoeny HC. Does quantification of USPIO uptake-related signal loss allow differentiation of benign and malignant normal-sized pelvic lymph nodes? *Contrast Media Mol Imaging* 2012; **7**: 346-355 [PMID: 22539405 DOI: 10.1002/cmmi.503]

55 **Triantafyllou M**, Studer UE, Birkhäuser FD, Fleischmann A, Bains LJ, Petralia G, Christe A, Froehlich JM, Thoeny HC. Ultrasmall superparamagnetic particles of iron oxide allow for the detection of metastases in normal sized pelvic lymph nodes of patients with bladder and/or prostate cancer. *Eur J Cancer* 2013; **49**: 616-624 [PMID: 23084842 DOI: 10.1016/j.ejca.2012.09.034]

56 **Lecouvet FE**, El Mouedden J, Collette L, Coche E, Danse E, Jamar F, Machiels JP, Vande Berg B, Omoumi P, Tombal B. Can whole-body magnetic resonance imaging with diffusion-weighted imaging replace Tc 99m bone scanning and computed tomography for single-step detection of metastases in patients with high-risk prostate cancer? *Eur Urol* 2012; **62**: 68-75 [PMID: 22366187 DOI: 10.1016/j.eururo.2012.02.020]

57 **Mosavi F**, Johansson S, Sandberg DT, Turesson I, Sörensen J, Ahlström H. Whole-body diffusion-weighted MRI compared with (18)F-NaF PET/CT for detection of bone metastases in patients with high-risk prostate carcinoma. *AJR Am J Roentgenol* 2012; **199**: 1114-1120 [PMID: 23096187 DOI: 10.2214/ajr.11.8351]

58 **Ording Müller LS**, Avenarius D, Olsen OE. High signal in bone marrow at diffusion-weighted imaging with body background suppression (DWIBS) in healthy children. *Pediatr Radiol* 2011; **41**: 221-226 [PMID: 20652234 DOI: 10.1007/s00247-010-1774-8]

59 **Steiner RM**, Mitchell DG, Rao VM, Schweitzer ME. Magnetic resonance imaging of diffuse bone marrow disease. *Radiol Clin North Am* 1993; **31**: 383-409 [PMID: 8446756]

60 **Takeuchi M**, Suzuki T, Sasaki S, Ito M, Hamamoto S, Kawai N, Kohri K, Hara M, Shibamoto Y. Clinicopathologic significance of high signal intensity on diffusion-weighted MR imaging in the ureter, urethra, prostate and bone of patients with bladder cancer. *Acad Radiol* 2012; **19**: 827-833 [PMID: 22341371 DOI: 10.1016/j.acra.2012.01.013]

61 **Prout GR**, Griffin PP, Shipley WU. Bladder carcinoma as a systemic disease. *Cancer* 1979; **43**: 2532-2539 [PMID: 455239]

62 **El-Assmy A**, Abou-El-Ghar ME, Mosbah A, El-Nahas AR, Refaie HF, Hekal IA, El-Diasty T, Ibrahiem el H. Bladder tumour staging: comparison of diffusion- and T2-weighted MR imaging. *Eur Radiol* 2009; **19**: 1575-1581 [PMID: 19247665 DOI: 10.1007/s00330-009-1340-7]

63 **Takeuchi M**, Sasaki S, Ito M, Okada S, Takahashi S, Kawai T, Suzuki K, Oshima H, Hara M, Shibamoto Y. Urinary bladder cancer: diffusion-weighted MR imaging--accuracy for diagnosing T stage and estimating histologic grade. *Radiology* 2009; **251**: 112-121 [PMID: 19332849 DOI: 10.1148/radiol.2511080873]

64 **Avcu S**, Koseoglu MN, Ceylan K, Bulut MD, Unal O. The value of diffusion-weighted MRI in the diagnosis of malignant and benign urinary bladder lesions. *Br J Radiol* 2011; **84**: 875-882 [PMID: 21224296 DOI: 10.1259/bjr/30591350]

65 **Kobayashi S**, Koga F, Kajino K, Yoshita S, Ishii C, Tanaka H, Saito K, Masuda H, Fujii Y, Yamada T, Kihara K. Apparent diffusion coefficient value reflects invasive and proliferative potential of bladder cancer. *J Magn Reson Imaging* 2014; **39**: 172-178 [PMID: 23589321 DOI: 10.1002/jmri.24148]

66 **Yoshida S**, Kobayashi S, Koga F, Ishioka J, Ishii C, Tanaka H, Nakanishi Y, Matsuoka Y, Numao N, Saito K, Masuda H, Fujii Y, Kihara K. Apparent diffusion coefficient as a prognostic biomarker of upper urinary tract cancer: a preliminary report. *Eur Radiol* 2013; **23**: 2206-2214 [PMID: 23494496 DOI: 10.1007/s00330-013-2805-2]

67 **Yoshida S**, Koga F, Kobayashi S, Ishii C, Tanaka H, Tanaka H, Komai Y, Saito K, Masuda H, Fujii Y, Kawakami S, Kihara K. Role of diffusion-weighted magnetic resonance imaging in predicting sensitivity to chemoradiotherapy in muscle-invasive bladder cancer. *Int J Radiat Oncol Biol Phys* 2012; **83**: e21-e27 [PMID: 22414281 DOI: 10.1016/j.ijrobp.2011.11.065]

68 **Rosenkrantz AB**, Mussi TC, Spieler B, Melamed J, Taneja SS, Huang WC. High-grade bladder cancer: association of the apparent diffusion coefficient with metastatic disease: preliminary results. *J Magn Reson Imaging* 2012; **35**: 1478-1483 [PMID: 22282396 DOI: 10.1002/jmri.23590]

69 **Yoshida S**, Saito K, Koga F, Yokoyama M, Kageyama Y,

Masuda H, Kobayashi T, Kawakami S, Kihara K. C-reactive protein level predicts prognosis in patients with muscle-invasive bladder cancer treated with chemoradiotherapy. *BJU Int* 2008; **101**: 978-981 [PMID: 18190628 DOI: 10.1111/j.1464-410X.2007.07408.x]

70 **Kageyama Y**, Okada Y, Arai G, Hyochi N, Suzuki M, Masuda H, Hayashi T, Kawakami S, Okuno T, Ishizaka K, Kihara K. Preoperative concurrent chemoradiotherapy against muscle-invasive bladder cancer: results of partial cystectomy in elderly or high-risk patients. *Jpn J Clin Oncol* 2000; **30**: 553-556 [PMID: 11210165]

71 **Kageyama Y**, Yokoyama M, Sakai Y, Saito K, Koga F, Yano M, Arai G, Hyochi N, Masuda H, Fujii Y, Kawakami S, Kobayashi T, Kihara K. Favorable outcome of preoperative low dose chemoradiotherapy against muscle-invasive bladder cancer. *Am J Clin Oncol* 2003; **26**: 504-507 [PMID: 14528080 DOI: 10.1097/01.coc.0000037665.11701.22]

72 **Matsumoto H**, Wada T, Fukunaga K, Yoshihiro S, Matsuyama H, Naito K. Bax to Bcl-2 ratio and Ki-67 index are useful predictors of neoadjuvant chemoradiation therapy in bladder cancer. *Jpn J Clin Oncol* 2004; **34**: 124-130 [PMID: 15078907]

73 **Rödel C**, Grabenbauer GG, Rödel F, Birkenhake S, Kühn R, Martus P, Zörcher T, Fürsich D, Papadopoulos T, Dunst J, Schrott KM, Sauer R. Apoptosis, p53, bcl-2, and Ki-67 in invasive bladder carcinoma: possible predictors for response to radiochemotherapy and successful bladder preservation. *Int J Radiat Oncol Biol Phys* 2000; **46**: 1213-1221 [PMID: 10725634]

P- Reviewers: Msaouel P, Plataniotis G **S- Editor**: Ji FF
L- Editor: A **E- Editor**: Zhang DN

World Journal of Radiology

Submit a Manuscript: http://www.wjgnet.com/esps/
Help Desk: http://www.wjgnet.com/esps/helpdesk.aspx
DOI: 10.4329/wjr.v6.i6.355

World J Radiol 2014 June 28; 6(6): 355-365
ISSN 1949-8470 (online)
© 2014 Baishideng Publishing Group Inc. All rights reserved.

REVIEW

Multi-detector computed tomography in the diagnosis and management of acute aortic syndromes

James Thomas Patrick Decourcy Hallinan, Gopinathan Anil

James Thomas Patrick Decourcy Hallinan, Gopinathan Anil, Department of Diagnostic Imaging, National University Health System, Singapore 119074, Singapore
Author contributions: Hallinan JTPD and Anil G contributed equally to this work.
Correspondence to: Gopinathan Anil, MD, FRCR, FAMS, Department of Diagnostic Imaging, National University Hospital, 5 Lower Kent Ridge Road, Singapore 119074, Singapore. ivyanil10@gmail.com
Telephone: +65-97-296614 Fax: +65-67-797101
Received: January 14, 2014 Revised: February 26, 2014
Accepted: April 17, 2014
Published online: June 28, 2014

Abstract

Acute aortic syndrome (AAS) is a spectrum of conditions, which may ultimately progress to potentially life-threatening aortic rupture. This syndrome encompasses aortic dissection (AD), intramural haematoma, penetrating atherosclerotic ulcer and unstable thoracic aortic aneurysms. Multi-detector CT (MDCT) is crucial for the diagnosis of AAS, especially in the emergency setting due to its speed, accuracy and ready availability. This review attends to the value of appropriate imaging protocols in obtaining good quality images that can permit a confident diagnosis of AAS. AD is the most commonly encountered AAS and also the one with maximum potential to cause catastrophic outcome if not diagnosed and managed promptly. Hence, this review briefly addresses certain relevant clinical perspectives on this condition. Differentiating the false from the true lumen in AD is often essential; a spectrum of CT findings, *e.g.*, "beak sign", aortic "cobwebs" that allows such differentiation have been described with explicit illustrations. The value of non enhanced CT scans, especially useful in the diagnosis of an intramural hematoma has also been illustrated. Overlap in the clinical and imaging features of the various conditions presenting as AAS is not unusual. However, on most instances MDCT enables the right diagnosis. On select occasions MRI or trans-esophageal echocardiography may be required as a problem solving tool.

© 2014 Baishideng Publishing Group Inc. All rights reserved.

Key words: Acute aortic syndrome; Computed tomography scan; Aortic dissection; Intramural haematoma; Penetrating aortic ulcer; Aortic aneurysm

Core tip: Acute aortic syndrome (AAS) is a spectrum of conditions, which may ultimately progress to potentially life-threatening aortic rupture. This syndrome encompasses aortic dissection (AD), intramural haematoma, penetrating atherosclerotic ulcer and unstable thoracic aortic aneurysms. Multidetector computed tomography (MDCT) is crucial in the diagnosis of AAS in the emergency setting due to its speed, accuracy and ready availability. This review will focus on the use of MDCT in AAS including the imaging protocols, spectrum of radiological findings, implications for planning and follow-up of endovascular and surgical treatment, and potential diagnostic pitfalls.

Hallinan JTPD, Anil G. Multi-detector computed tomography in the diagnosis and management of acute aortic syndromes. *World J Radiol* 2014; 6(6): 355-365 Available from: URL: http://www.wjgnet.com/1949-8470/full/v6/i6/355.htm DOI: http://dx.doi.org/10.4329/wjr.v6.i6.355

INTRODUCTION

Acute aortic syndrome (AAS) is a term used to describe a constellation of emergency aortic conditions requiring prompt diagnosis and treatment. These inter-related conditions include aortic dissection (AD), intramural haematoma (IMH) and penetrating atherosclerotic ulcer (PAU)[1]. In addition, unstable thoracic aortic aneurysm

at high risk for rupture may also be considered an AAS. This syndrome has an estimated incidence of (2-3.5)/100000 per year[2]. The most common risk factors are hypertension and genetic conditions of the connective tissue such as Marfan's syndrome. The clinical presentations of the various entities of AAS are essentially indistinguishable from each other with severe chest or abdominal pain being the most common symptom. Clinical suspicion of AAS should herald prompt diagnostic imaging as mortality from AAS increases by approximately 1%-2% per hour[3]. MDCT typically with electrocardiographic gating (ECG-gated MDCT) is the technique of choice for diagnosis of AAS due to the rapid acquisition times and ready availability in the emergency department[4]. Other diagnostic imaging modalities include conventional and transoesophageal echocardiography and magnetic resonance imaging (MRI), that are usually reserved for problem solving or if there is contraindication to the use of iodinated contrast[1,2,5]. This review will focus on MDCT in the diagnosis of AAS. MDCT protocols will be discussed along with the discriminating and overlapping radiological diagnostic features of AAS.

MDCT PROTOCOL FOR AAS

MDCT angiography with electrocardiographic (ECG) gating enables the evaluation of AAS with reduced pulsation artefacts (Figure 1) in the ascending aorta compared to non-gated MDCT angiography[6]. The ECG-gating can either be performed prospectively (scanning performed at a specified segment of the cardiac cycle), or retrospectively (scanning performed throughout the cardiac cycle but data gathered in a specified segment of the cardiac cycle is selected retrospectively for generating images). A retrospective acquisition allows increased scope for correction of artefacts from dysrhythmias or motion, but comes at the cost of increased radiation exposure[1,6]. ECG-gating with motion-free images allows for improved assessment of the ascending aorta, aortic annulus, sinuses of Valsalva and coronary arteries[6,7]. There is also improved depiction of the site of primary intimal tear, extent of the intimomedial flap and involvement of the aortic branches. Studies have also shown a reduction in radiation dose of as much as 45%-50% using ECG-gated high pitch CT compared to non-ECG-synchronised standard-pitch CT[8,9]. Although ECG-gating is preferred, its absence rarely precludes the diagnosis of clinically significant acute aortic conditions if an experienced reader is interpreting the non-gated CT aortogram.

The details of the scan protocol vary according to the scanner system being used. As an illustration we have described here the protocol of ECG-gated CT angiography on a 64-section helical CT system (Somatom Sensation, Siemens, Erlangen, Germany) performed in our department. Z-axis coverage is determined on a planning topogram from the root of the neck to the common femoral artery bifurcation. A 100 mL bolus injection of intravenous contrast (Iohexol 300 mg/mL, Nycomed) is injected at a rate of 3-4 mL a second. Bolus tracking is used to trigger scanning when the attenuation of the descending aorta reaches 150 HU. Retrospective gating is typically used with images reconstructed at 78% of the R-R interval. The section thickness is 0.6 mm with 3 mm reconstructions in the axial, coronal and sagittal oblique planes sent to the PACS for reporting. Additional post processing is performed by the reporting radiologist when clinically indicated for three-dimensional reconstructions to obtain volume rendered images, maximum intensity projections and shaded surface display. Delayed phase images are useful in selected cases of suspected aortic rupture or in cases of dissection to determine the opacification of both the lumina. Although a contrast enhanced CT angiogram is the standard of care, a non-enhanced CT that precedes the angiogram is useful in AAS to evaluate for IMH, which can progress to frank dissection. NECT can also be useful to assess for secondary signs of aortic rupture such as hyperdense, haemorrhagic pericardial, pleural or mediastinal fluid collections. In patients with known allergy to iodinated contrast medium or at high risk of contrast induced nephropathy, the preliminary information obtained through a non-enhanced CT scan may sometimes suffice to make the further clinical decision.

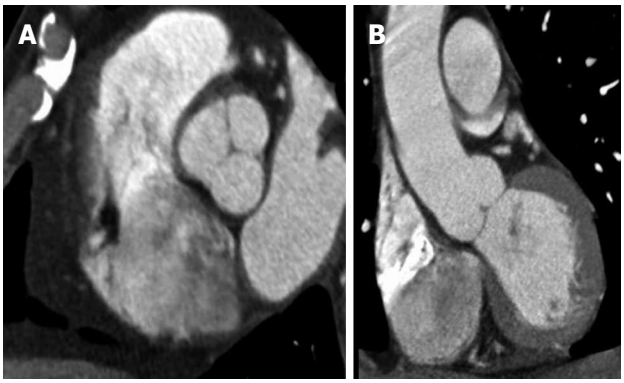

Figure 1 Cardiac-gated computed tomography aortogram in a 55-year-old with chest pain and suspected acute aortic syndrome. A: Axial oblique; B: Coronal reconstructions. No dissection or aneurysm was detected. Retrospective reconstruction at 78% of the cardiac cycle allowed for accurate evaluation of the aortic root and valve cusps in both axial oblique and coronal reconstructions with no pulsation artefacts.

AD

The most common pathology in AAS is AD that begins as a tear or ulcer in the aortic intima allowing blood to penetrate and disrupt the aortic media[2]. Haemorrhage may also occur *de novo* within the media due to rupture of the vasa vasorum leading to dissection. Irrespective of the initiating cause AD involves separation of the aortic layers and formation of a false lumen[10]. The false lumen is separated from the true lumen by an intimomedial flap (Figures 2-7). The dissection may then propagate in an antegrade and/or less likely retrograde fashion with a po-

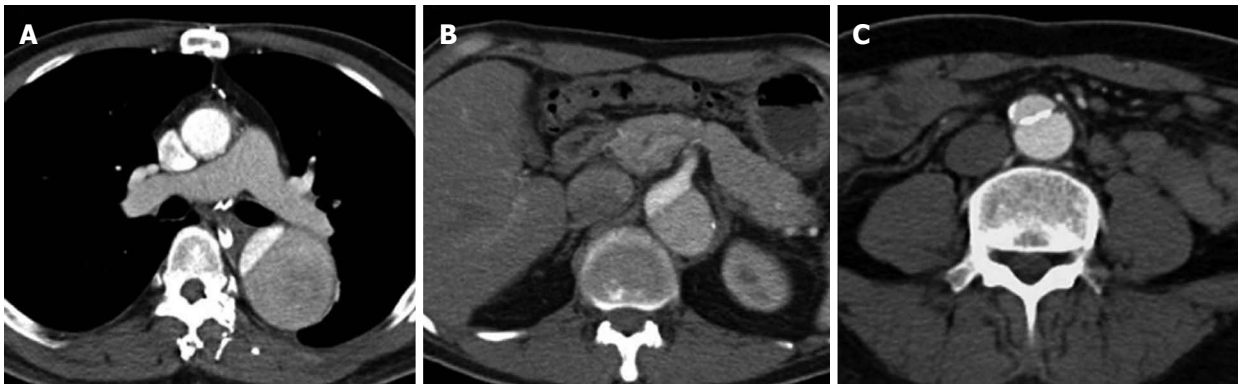

Figure 2 A 47-year-old gentleman with Stanford type B aortic dissection. The dissection flap is flat in all the computed tomography angiographic images. The ascending aorta is not involved and the true lumen is smaller in calibre and shows early and more intense enhancement than the false lumen at the level of the right pulmonary artery (A). The small calibre true lumen gives rise to the coeliac axis (B) and is outlined by atherosclerotic calcifications (C).

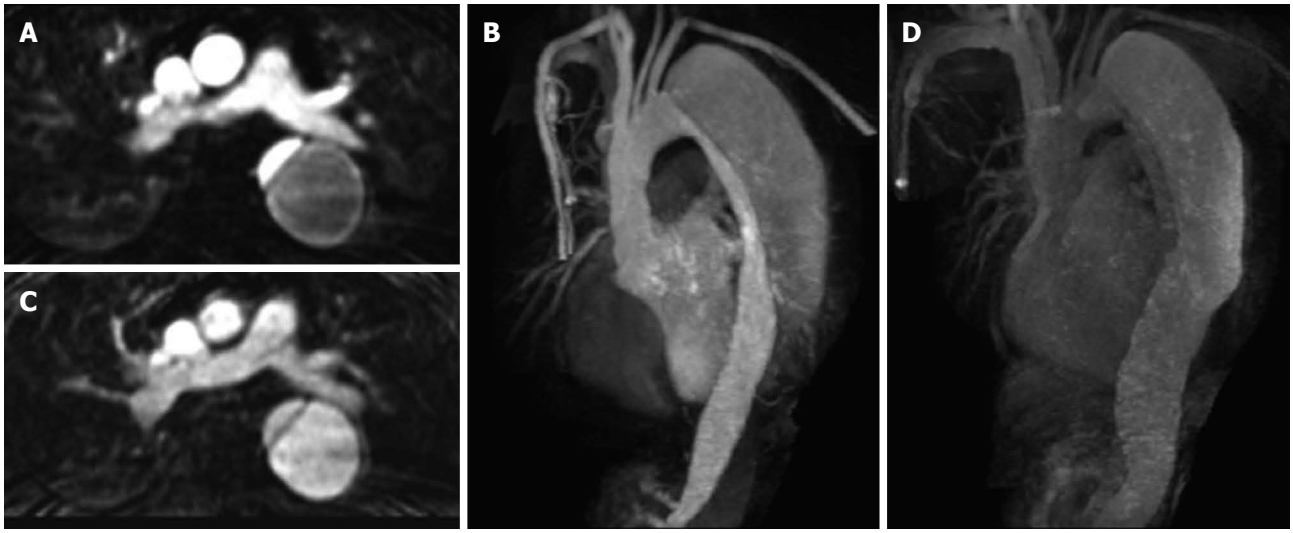

Figure 3 Axial contrast enhanced magnetic resonance aortogram of the same patient as in Figure 2 with type B aortic dissection. In the arterial phase image (A: Axial; B: Coronal 3D reconstruction; 30 s post injection) the true lumen is of small calibre and shows early intense contrast enhancement compared to the larger false lumen. In the second delayed phase (70 s post injection) the enhancement between the lumens becomes more similar (C: Axial; D: Coronal 3D reconstruction).

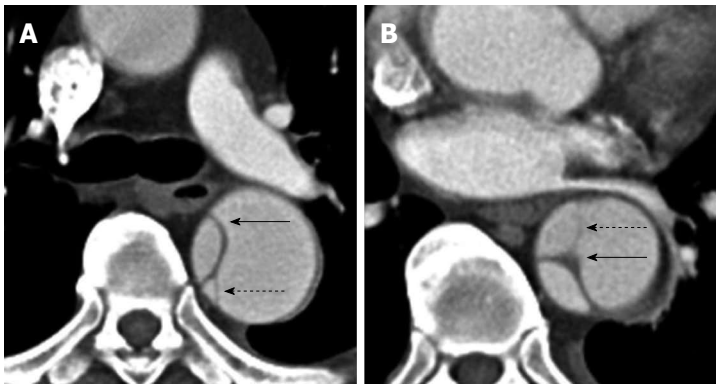

Figure 4 A 35-year-old gentleman with Marfan's syndrome and a type B aortic dissection. Axial images (A and B) from a computed tomography aortogram reveals an intimomedial flap (arrows) with strands of incompletely sheared aortic media or "cobwebs" seen in the descending thoracic aorta (dashed arrows).

tential to fenestrate back into the aortic lumen or rupture out through the adventitia with life threatening consequences[11]. Dissection can extend into aortic branches and when it involves major visceral arteries, it can lead to catastrophic consequences such as a cerebrovascular event, bowel ischemia, acute renal failure, limb gangrene *etc*.

Risk factors for dissection include hypertension, smoking, trauma (typically road traffic accidents), vas-

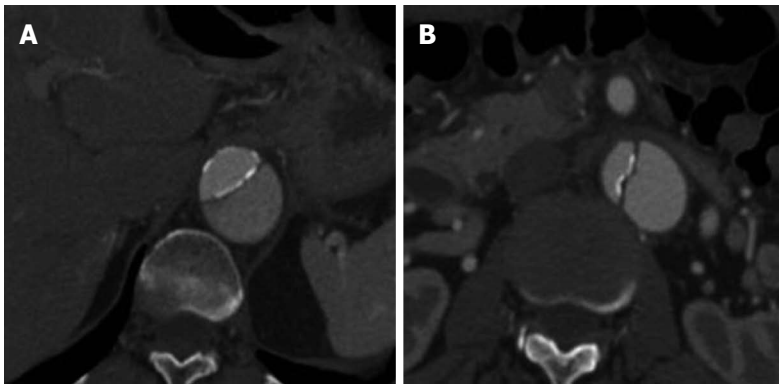

Figure 5 A 59-year-old lady with a type B aortic dissection. Axial images from a computed tomography aortogram show atherosclerotic calcifications outlining the true lumen at the lower thoracic aorta (A). The true lumen is of smaller calibre and shows early and more intense enhancement than the false lumen at this level. More inferiorly at the level of the left renal vein (B), eccentric intimomedial flap calcification (note the calcification along the true luminal aspect of the flap) is exquisitely demonstrated.

Figure 6 A 45-year-old with a type B aortic dissection. An axial image from a computed tomography aortogram at the upper abdominal aorta shows the "beak" sign (arrow): note the acute angle between the dissection flap and the outer wall of the larger calibre false lumen. The "beak" or space formed by the acute angle is filled with high-attenuation contrast-enhanced blood in this case but it may stay unopacified when filled with clots.

cular inflammation (*e.g.*, Takayasu's arteritis) or infection (*e.g.*, syphilis) and genetic connective tissue disorders (*e.g.*, Marfan's and Ehlers-Danlos syndromes). Propagation of the blood within the media to form a dissection requires pre-existing medial degeneration or cystic medial necrosis, which leads to a weakened aortic wall and represents the end point of many of the risk factors listed above[2,10].

Two anatomical classification systems exist for AD: De Bakey and Stanford. The Stanford classification is most commonly used as it has a direct bearing on the subsequent therapy. Stanford type A dissections involve the ascending aorta (proximal to the origin of the brachiocephalic artery origin) with or without aortic arch or descending aorta (distal to the left subclavian artery origin) involvement[2]. Type A dissections are typically treated as a surgical emergency. Mortality is estimated at 20% in the first 24 h without immediate surgical management and approximately 40% in the first week[12,13]. Complications of type A dissection include aortic regurgitation, aortic rupture, tamponade and compromise of the arch branches or coronary arteries leading to myocardial infarction. Type B constitutes all those dissections that do not involve the ascending aorta. It more often involves the descending aorta and is typically treated medically with anti-hypertensive medications. Without adequate management, uncomplicated type B dissections have an estimated 10% mortality at 1 mo in comparison to 50% for type A dissections[2,12]. Type B dissections can be complicated by branch disruption and end organ malperfusion, progression to type A dissection and rupture. The role of endovascular repair is well established in Stanford type B lesions while in select situations it may be performed even in type A lesions[14]. The aim of endovascular intervention is to occlude the intimal tear allowing for false lumen thrombosis and regression, typically by placing an aortic endograft. End-organ ischaemia and malperfusion may also be improved by placement of branch stents and the use of aortic fenestrations to relieve compression of the true by a distended false lumen[1,14,15].

MDCT angiography has a sensitivity and specificity of close to 100% for diagnosis of acute AD[16,17]. Cardiac synchronisation should be performed to limit pulsation artefacts in the ascending aorta, which on non-gated MDCT are often the cause of false-positive findings of a thoracic dissection. In AD, the role of MDCT angiography can be summarized as to identify[1,14,18]: (1) Sites of primary entry and re-entry; (2) Intimomedial flap, false and true lumen morphology along with the presence of calcifications and thrombus; (3) Extent of the dissection and involvement of the ascending and descending aorta; (4) Evidence of rupture; (5) Involvement of the aortic valve, coronary and aortic arch branches; (6) Abdominal aortic branch patency and evidence of end-organ malperfusion; and (7) Morphology and diameter of the aorta along with the patency, size and tortuosity of the iliac and femoral arteries (useful for endovascular treatment planning).

The intimomedial flap forms a double-barrelled aorta and separates the true from the false lumen[4]. This is seen in approximately 70% of cases on MDCT angiography and with three dimensional reconstructs the complex,

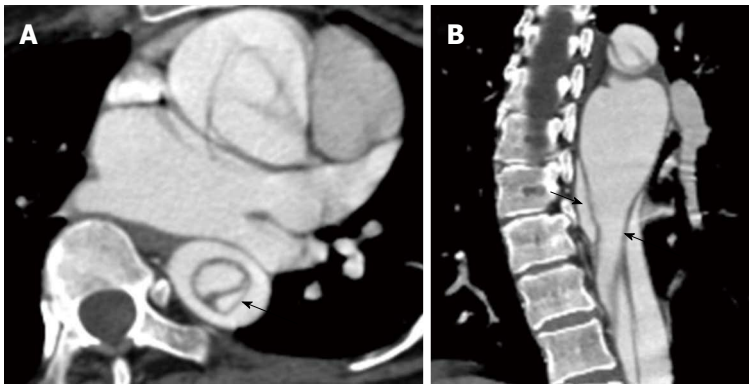

Figure 7 A 37-year-old gentleman with Marfan's syndrome and a type A aortic dissection. The axial image at the level of the left atrium shows an intimointimal intussusception type dissection in the descending thoracic aorta with the true lumen surrounded by the false lumen (A and B; intimomedial flap highlighted by the arrows).

often spiralling nature of the dissection can be seen in better detail[19]. Other appearances include a circumferential intimomedial flap due to complete dissection of the intima. The true lumen takes on a cylindrical or filiform shape and this may result in an intimointimal intussusception producing a "windsock" appearance (Figure 7). Differentiation between the false and true lumen is useful for endovascular treatment planning as an endograft should be placed within the true lumen[1,15].

The true lumen can usually be identified by tracing back or forth from an uninvolved portion of the aorta; this may be difficult if the aortic root is involved proximally or the dissection extends into the iliac vessels distally[1,20]. In these cases the most useful imaging signs include a false lumen that is larger in calibre than the true lumen and the "beak"sign[20]. In most cases of acute dissections the false lumen is larger in calibre than the true lumen. This is likely due to sustained systolic pressure in the false lumen exceeding that of the true lumen leading to compression. The "beak" sign (Figure 6) is only seen in the false lumen and is often present in most patients with dissection. It is usually noted both in acute and chronic dissection and is defined as the presence of an acute angle between the dissection flap and the outer wall of the false lumen; the space formed by the acute angle could be filled with high-attenuation material (contrast-enhanced blood) or low-attenuation material (hematoma)[21,22]. Other less common and less reliable signs for differentiation between the true and false lumen have been documented in the literature. The false lumen may contain thrombus and fine ribbons of low attenuation ("cobwebs"), which likely represent strands of incompletely sheared aortic media (Figure 4)[22]. Differential contrast enhancement between the true and false lumen is not unusual with the true lumen often showing early opacification with contrast in the arterial phase, while the false lumen starts opacifying later in the portovenous and delayed phase (Figure 3)[23]. The surface of the dissection flap that is calcified generally involves the intimal surface of the true lumen; this is described as eccentric flap calcification. The side of the flap subtending the false lumen will have soft tissue attenuation (Figure 5). In acute dissections the lumen with outer wall calcification tends to be the true lumen. Along with eccentric flap calcification this is due to the presence of atherosclerotic calcified plaque in the aortic intima of the true lumen (Figures 2 and 5). A less useful sign is the curvature of the intimomedial dissection flap. Researchers have found equal incidence of curvature of the flap towards or away from the false lumen. However, in chronic dissections the dissection flap is more likely to be flat. This is likely due to interval healing and development of fibrosis and thickening leading to reduced flap mobility[19,24].

A thrombosed dissection and an aneurysm with mural thrombus may have a similar appearance. The following features will aid the differentiation: (1) Mural thrombus would not have a spiralling pattern like a dissection; (2) Mural thrombus tends to have an irregular surface rather than the smooth surface of the dissection flap; and (3) in an aneurysm with mural thrombus, the calcium will be along the outer wall while in the thrombosed false lumen it would be along the flap. A thrombosed dissection can be indistinguishable from intramural hematoma; however the differentiation is of only academic interest since management stays the same in both conditions.

AORTIC IMH

Aortic IMH is considered a variant of dissection and is characterised by bleeding of the vasa vasorum in the aortic media without intimal tear (Figure 8). It accounted for 5.7% of AAS in the International Registry of Acute Aortic Dissection (IRAD)[12,25]. The vasa vasorum may spontaneously rupture or haemorrhage may occur due to an intimal defect/PAU[1]. IMH may progress to aneurysmal dilatation and rupture (20%-45%), provoke a secondary intimal tear that can progress to dissection (28%-47%), or may regress (10%)[26]. The most common site of IMH is in the descending aorta (approximately 2/3rds) and risk factors are similar to those for dissection with hypertension being the most prevalent one[2,25]. The clinical presentation of IMH is also similar to aortic dissection;

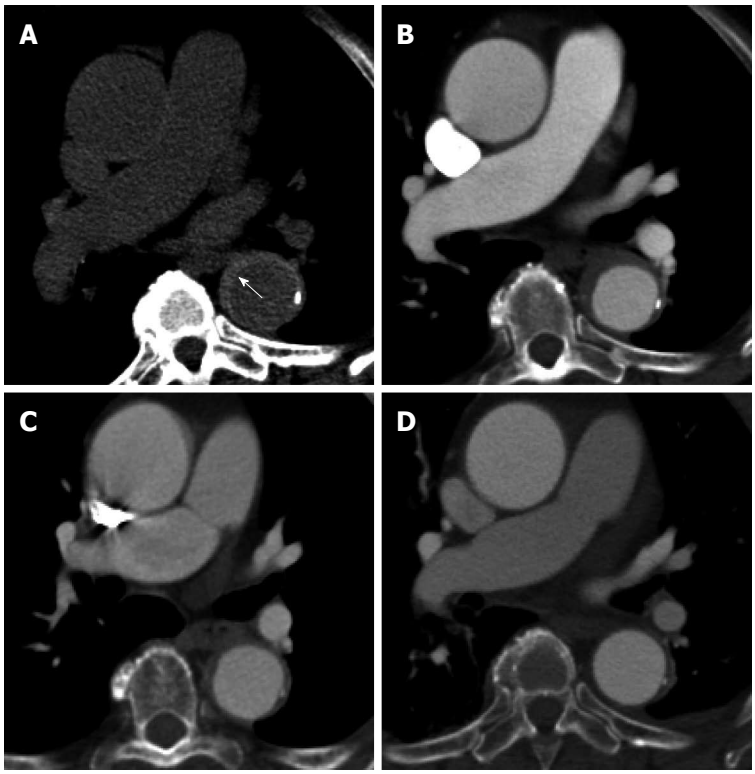

Figure 8 A 61-year-old lady with severe chest pain, breathlessness and a prior history of atrial flutter. Computed tomography aortogram in the emergency department shows hyperdense, eccentric wall thickening of the aortic wall consistent with an intramural haematoma (A, white arrow). A concurrent contrast enhanced axial image at the same level shows no leakage of contrast into this thickened aortic wall (B). The intramural haematoma shows partial resolution at 1 mo (C) and complete resolution at 6 mo (D).

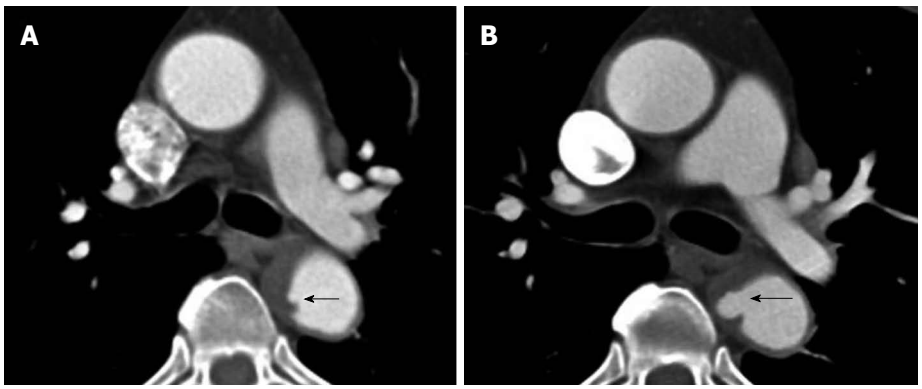

Figure 9 Computed tomography aortogram in a 75-year-old man shows an intramural hematoma (note the eccentric wall thickening in the descending aorta) with intimal surface defect (A: arrow). At one year follow up it has progressed into a frank penetrating ulcer (B: arrow).

chest pain is the usual symptom in ascending aortic IMH while back pain accompanies descending aortic IMH[27]. IMH is classified along the lines of dissection into Stanford type A and B categories[1]. Stanford type A IMH is typically treated surgically, with 30 d mortality of 14% *vs* 36% for those treated medically[28]. In contrast, type B IMH is initially treated medically with antihypertensive medications with a 30-d mortality of 8%[27]. However, close CT follow-up is recommended in these patients as aneurysmal dilatation or progression to frank dissection of the aorta will require emergency open surgical or endovascular repair[1,27].

On MDCT, IMH is seen as a hyperdense, crescent shaped region within the aortic wall on non-enhanced CT[1,4,29]. No enhancement is seen and by definition no intimomedial flap or tear should be visualized[30]. Unlike a dissection that spirals down, IMH tends to have constant circumferential relationship with the aortic lumen. With the higher resolution of modern imaging technologies, small projections or ulcerations can sometimes be seen communicating between the aortic lumen and the IMH[4,31]. Studies based on non-cardiac gated CT showed a sensitivity of greater than 96% for the detection of IMH using both unenhanced and contrast enhanced CT[1,32].

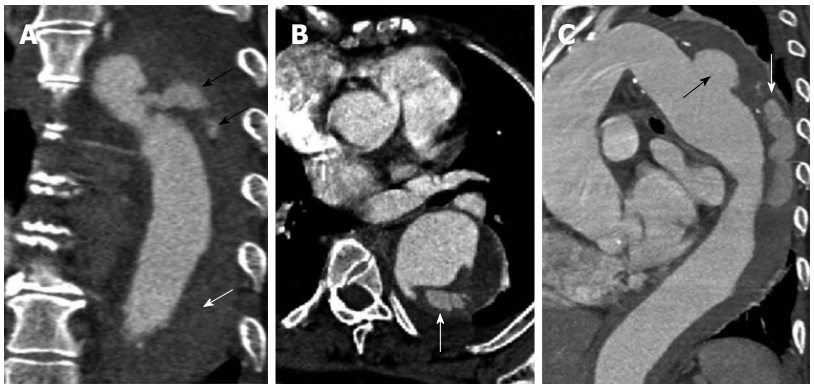

Figure 10 A 62-year-old with acute chest pain. A computed tomography aortogram (A-coronal) shows a penetrating atherosclerotic ulcer at the proximal descending aorta with contrast seen within the aortic media (black arrows) and non-opacifying hyperdensity throughout the rest of the descending thoracic aortic wall compatible with intramural haematoma (white arrow). The axial image (B) shows the contrast extending within the aortic wall and splitting the same. The sagittal oblique reconstruction (C) gives a better demonstration of the penetrating atherosclerotic ulcer at the distal aortic arch (black arrow) with intramural hematoma and progressing into an aortic dissection (white arrow).

PAU

This entity is a manifestation of advanced, severe atherosclerotic disease that leads to disruption of the aortic intima with extension of blood into the aortic media (Figure 9)[1,2,4]. This is in contrast to the underlying pathological process in AD, which usually results from disease of the media without any underlying atherosclerotic intimal plaque[33,34]. Disruption of the media by the deep ulceration may lead to vasa vasorum haemorrhage and IMH producing acute chest or back pain with risk of progression to aortic dissection[25,35]. PAU can also penetrate beyond the aortic media leading to focal outpouching of the adventitia, producing a pseudoaneurysm with risk of frank rupture[4,29]. Saccular aortic aneurysms may represent the end point of such PAU[36].

PAU most commonly occurs in the descending thoracic aorta (90%) and is associated with type B IMH in the majority of cases. It is seen as a focal contrast-filled outpouching into the aortic wall on MDCT (Figure 10)[37,38]. Other MDCT features include overhanging edges with a focal bulge of the external aortic contour. It can be differentiated from a benign atherosclerotic ulcer as the latter would not have contrast extending into the aortic media and would not be associated with an IMH[39]. Given the relationship with IMH the use of unenhanced images can improve visualisation of crescentic high attenuation haemorrhage in the aortic wall along with displacement of intimal calcifications[1,22].

The natural history and management of patients with PAU remains controversial. PAU tends to have a worse prognosis than dissection with increased incidence of rupture even if the ulcer is limited to the descending thoracic or abdominal aorta[25]. Most patients are symptomatic although in approximately a quarter of cases PAU may present incidentally[1,40]. The condition typically occurs in elderly patients with multiple co-morbidities and risk factors for atherosclerosis[41]. These factors, especially underlying coronary and peripheral arterial atherosclerosis, may preclude open surgical repair in this group of patients[42]. Open surgical repair, typically with a synthetic graft is performed in patients with ascending aortic PAU (these are rare) and in patients with haemodynamic instability and high risk of rupture, *e.g.*, rapid enlargement of the lesion[1,18]. Endovascular graft placement in patients with symptomatic PAU is an alternative with potentially lower morbidity and mortality[43-45]. Sometimes, conservative management with antihypertensive therapy may be adequate or may be the best option in PAU especially in asymptomatic patients with involvement of the descending aorta and in those who are poor candidates for any form of invasive treatment. The medically treated patients need at least an annual follow-up to assess for disease progression, which has a strong likelihood in initially symptomatic patients[19,44,46,47].

UNSTABLE THORACIC AORTIC ANEURYSM

Thoracic aortic aneurysms are relatively uncommon and defined as the permanent dilatation of the aorta to more than 150% of its usual diameter or greater than 5 cm. True aneurysms tend to be fusiform and involve all three layers of the aortic wall[48]. False or pseudoaneurysms are typically saccular and often limited by the adventitia alone (Figure 11). The most common cause for both types is atherosclerosis (approximately 70%), although false saccular aneurysms often arise following surgery, trauma or due to an infective/inflammatory aetiology[1,19,49].

Thoracic aortic aneurysms are often clinically asymptomatic but they are considered unstable when showing rapid increase in size or evidence of contained or impending rupture on MDCT. Unstable thoracic aortic aneurysms may be considered an AAS, especially when symptomatic as they are clinically indistinguishable from dissection, IMH or PAU[4]. The risk of rupture is related to the diameter of the aneurysm sac, with a significantly higher risk for those in the ascending aorta measuring greater than 6 cm, and 7.2 cm in the descending aorta[50].

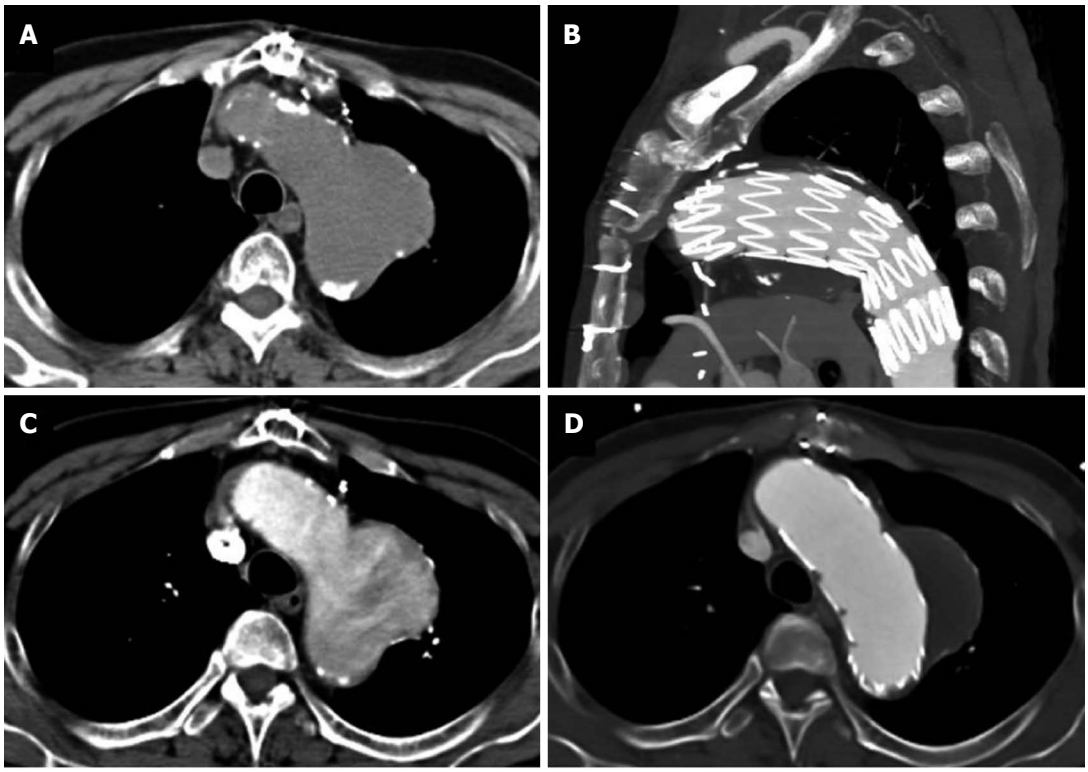

Figure 11 A 68-year-old with chest pain and long standing hypertension. A saccular aneurysm is seen arising from the lateral aortic arch just distal to the origin of the left subclavian artery on this computed tomography aortogram. Atherosclerotic calcifications are seen at the periphery of the aneurysm (A) and there is heterogeneous contrast opacification secondary to turbulent flow on the arterial phase (B). No evidence of rupture is apparent. The aneurysm was excluded using an aortic stent graft as seen in the sagittal plane (C). The excluded sac has completely thrombosed with no endoleak as seen on an axial image (D).

On serial CT scans an annual increase in diameter of the thoracic aortic aneurysm of at least 1 cm is also considered a sign of increased likelihood of rupture[19,51]. Other morphological MDCT signs of impending rupture should also be taken into account for therapeutic decision making. These include associated IMH with a high attenuating crescent in the aortic wall, discontinuity of circumferential intimal atherosclerotic calcifications within a fusiform aneurysm, a "draped" aortic appearance conforming to the anterolateral contour of an adjacent vertebral body, eccentric or nipple like contour to the aorta, and poor visualisation of the posterior aortic wall[1,19,52,53]. Frank rupture of a thoracic aortic aneurysm on MDCT is suggested by peri aneurysmal fat stranding, mediastinal haematoma, haemothorax most commonly on the left, hemopericardium or pericardial effusion and evidence of haemodynamic compromise, *e.g.*, collapsed IVC[1,19].

Therapy should be considered for all symptomatic aneurysms regardless of size due to the high risk of rupture. Otherwise surgical or endovascular therapy should be considered for ascending thoracic aortic aneurysms measuring greater than 5.5 cm, and those in the descending thoracic aorta measuring greater than 6 cm. Similar to dissection open surgical or hybrid surgical and endovascular techniques are the mainstay of ascending thoracic aortic aneurysm therapy[13]. Smaller aneurysms, typically less than 5.5 cm in diameter can be followed up with serial CT or MRI on an annual basis. However those with underlying genetic connective tissue predispositions to aneurysm formation such as Marfan's syndrome should be considered for therapy at smaller diameters. Overall decision on when to intervene should be tailored to the individual clinical scenario and involve an experienced multidisciplinary team[1,19,54,55].

OTHER IMAGING MODALITIES AND TECHNIQUES

This article has focused on the use of MDCT in the diagnosis and management of AASs while other imaging modalities including conventional angiography, transoesophageal or transthoracic echocardiography and MRI have a complimentary/alternative role in dealing with this clinical problem. MDCT also has some disadvantages including radiation exposure and potential risk of contrast induced nephropathy, which can be overcome by using alternative methods. Conventional angiography is historically the gold standard for evaluation of AASs. However it is invasive, unable to assess for IMH, and can lead to false negative exclusion of dissection. Transthoracic echocardiography can be used in the initial evaluation of suspected AASs in the emergency department. The technique can sometimes visualise the proximal extent of an aortic dissection but can provide vital secondary evidence of aortic root/valve dysfunction and pericardial effusions or tamponade. Invasive transoesophageal echocardiography can then be considered for further detailed

evaluation, and is especially valuable in unstable patients as it can be performed at the bedside. In experienced hands the technique has high sensitivity and specificity for ascending aortic dissection. It has the ability to detect the entry and re-entry site of dissection and can evaluate for the direction of flow within the false lumen. Additional evaluation of the aortic valvular and left ventricular function is useful to exclude proximal extension of the dissection into the aortic root and left coronary artery respectively. Transoesophageal echocardiography is of limited use at the proximal aortic arch since artefacts from air in the adjacent right main bronchus interferes with echocardiographic imaging. Other limitations of the technique include inability to visualise surrounding structures in the mediastinum, and inadequate assessment of anatomical detail required for planning endovascular or hybrid therapy[1-3].

MRI is a useful modality in the assessment of AASs but has limited scope in the emergency setting due to the longer acquisition times and potentially limited availability[1,2]. In stable patients it has a role in confirming IMH, when CT is indeterminate. It can provide high resolution multiphasic images of the aorta without the use of ionising radiation[56]. Real time examination of the aortic root and valve function can also be performed with MRI. This modality is likely to play an increasing role in the follow-up of patients with AASs allowing for a comprehensive assessment. MRI is also the modality of choice for patients with contraindications to CT and iodinated contrast[57].

CONCLUSION

MDCT is the modality of choice for the evaluation of suspected AAS in the emergency setting. High sensitivity, rapid acquisitions and easy access to the technique are its major advantages over transoesophageal echocardiography and MRI. There is a wide base of expertise available in interpreting MDCT with limited interpersonal variability in the inference. Most radiologists and vascular surgeons are comfortable and confident of using this modality in diagnosing and treating AAS. Detailed assessment of the morphology of the aorta using MDCT allows for the classification of the interlinked AASs and helps in determining the treatment. It permits assessment of life-threatening complications associated with acute aortic conditions. It is also useful in identifying some of the other conditions such as acute pulmonary embolism and pneumothorax that can mimic AAS.

REFERENCES

1 **Chiu KW**, Lakshminarayan R, Ettles DF. Acute aortic syndrome: CT findings. *Clin Radiol* 2013; **68**: 741-748 [PMID: 23582433 DOI: 10.1016/j.crad.2013.03.001]

2 **Nienaber CA**, Powell JT. Management of acute aortic syndromes. *Eur Heart J* 2012; **33**: 26-35b [PMID: 21810861 DOI: 10.1093/eurheartj/ehr186]

3 **Jánosi RA**, Erbel R, Konorza TF. Recent advances in the diagnosis of acute aortic syndromes. *Expert Opin Med Diagn* 2012; **6**: 529-540 [PMID: 23480835 DOI: 10.1517/17530059.2012.704362]

4 **Ueda T**, Chin A, Petrovitch I, Fleischmann D. A pictorial review of acute aortic syndrome: discriminating and overlapping features as revealed by ECG-gated multidetector-row CT angiography. *Insights Imaging* 2012; **3**: 561-571 [PMID: 23129238 DOI: 10.1007/s13244-012-0195-7]

5 **Akin I**, Kische S, Ince H, Nienaber C. Penetrating aortic ulcer, intramural hematoma, acute aortic syndrome: when to do what. *J Cardiovasc Surg (Torino)* 2012; **53**: 83-90 [PMID: 22433727]

6 **Fleischmann D**, Mitchell RS, Miller DC. Acute aortic syndromes: new insights from electrocardiographically gated computed tomography. *Semin Thorac Cardiovasc Surg* 2008; **20**: 340-347 [PMID: 19251175 DOI: 10.1053/j.semtcvs.2008.11.011]

7 **Chin AS**, Fleischmann D. State-of-the-art computed tomography angiography of acute aortic syndrome. *Semin Ultrasound CT MR* 2012; **33**: 222-234 [PMID: 22624967 DOI: 10.1053/j.sult.2012.01.003]

8 **Apfaltrer P**, Hanna EL, Schoepf UJ, Spears JR, Schoenberg SO, Fink C, Vliegenthart R. Radiation dose and image quality at high-pitch CT angiography of the aorta: intraindividual and interindividual comparisons with conventional CT angiography. *AJR Am J Roentgenol* 2012; **199**: 1402-1409 [PMID: 23169737 DOI: 10.2214/AJR.12.8652]

9 **Bolen MA**, Popovic ZB, Tandon N, Flamm SD, Schoenhagen P, Halliburton SS. Image quality, contrast enhancement, and radiation dose of ECG-triggered high-pitch CT versus non-ECG-triggered standard-pitch CT of the thoracoabdominal aorta. *AJR Am J Roentgenol* 2012; **198**: 931-938 [PMID: 22451563 DOI: 10.2214/AJR.11.6921]

10 **Mészáros I**, Mórocz J, Szlávi J, Schmidt J, Tornóci L, Nagy L, Szép L. Epidemiology and clinicopathology of aortic dissection. *Chest* 2000; **117**: 1271-1278 [PMID: 10807810]

11 **Golledge J**, Eagle KA. Acute aortic dissection. *Lancet* 2008; **372**: 55-66 [PMID: 18603160 DOI: 10.1016/S0140-6736(08)60994-0]

12 **Hagan PG**, Nienaber CA, Isselbacher EM, Bruckman D, Karavite DJ, Russman PL, Evangelista A, Fattori R, Suzuki T, Oh JK, Moore AG, Malouf JF, Pape LA, Gaca C, Sechtem U, Lenferink S, Deutsch HJ, Diedrichs H, Marcos y Robles J, Llovet A, Gilon D, Das SK, Armstrong WF, Deeb GM, Eagle KA. The International Registry of Acute Aortic Dissection (IRAD): new insights into an old disease. *JAMA* 2000; **283**: 897-903 [PMID: 10685714]

13 **Loebe M**, Ren D, Rodriguez L, La Francesca S, Bismuth J, Lumsden A. Acute and chronic thoracic aortic disease: surgical considerations. *HSR Proc Intensive Care Cardiovasc Anesth* 2012; **4**: 243-250 [PMID: 23439669]

14 **Fanelli F**, Dake MD. Standard of practice for the endovascular treatment of thoracic aortic aneurysms and type B dissections. *Cardiovasc Intervent Radiol* 2009; **32**: 849-860 [PMID: 19688371 DOI: 10.1007/s00270-009-9668-6.Epub]

15 **Patel PJ**, Grande W, Hieb RA. Endovascular management of acute aortic syndromes. *Semin Intervent Radiol* 2011; **28**: 10-23 [PMID: 22379272 DOI: 10.1055/s-0031-1273936]

16 **Manghat NE**, Morgan-Hughes GJ, Roobottom CA. Multidetector row computed tomography: imaging in acute aortic syndrome. *Clin Radiol* 2005; **60**: 1256-1267 [PMID: 16291307 DOI: 10.1016/j.crad.2005.06.011]

17 **Shiga T**, Wajima Z, Apfel CC, Inoue T, Ohe Y. Diagnostic accuracy of transesophageal echocardiography, helical computed tomography, and magnetic resonance imaging for suspected thoracic aortic dissection: systematic review and meta-analysis. *Arch Intern Med* 2006; **166**: 1350-1356 [PMID: 16831999 DOI: 10.1001/archinte.166.13.1350]

18 **Berger FH**, van Lienden KP, Smithuis R, Nicolaou S, van Delden OM. Acute aortic syndrome and blunt traumatic aortic injury: pictorial review of MDCT imaging. *Eur J*

Radiol 2010; **74**: 24-39 [PMID: 19665857 DOI: 10.1016/j.ejrad.2009.06.023.Epub]
19 **Smith AD**, Schoenhagen P. CT imaging for acute aortic syndrome. *Cleve Clin J Med* 2008; **75**: 7-9, 12, 15-7 passim [PMID: 18236724 DOI: 10.3949/ccjm.75.1.7]
20 **Batra P**, Bigoni B, Manning J, Aberle DR, Brown K, Hart E, Goldin J. Pitfalls in the diagnosis of thoracic aortic dissection at CT angiography. *Radiographics* 2000; **20**: 309-320 [PMID: 10715333 DOI: 10.1148/radiographics.20.2.g00mc04309]
21 **McMahon MA**, Squirrell CA. Multidetector CT of Aortic Dissection: A Pictorial Review. *Radiographics* 2010; **30**: 445-460 [PMID: 20228328 DOI: 10.1148/rg.302095104]
22 **Williams DM**, Joshi A, Dake MD, Deeb GM, Miller DC, Abrams GD. Aortic cobwebs: an anatomic marker identifying the false lumen in aortic dissection--imaging and pathologic correlation. *Radiology* 1994; **190**: 167-174 [PMID: 8259399]
23 **Castañer E**, Andreu M, Gallardo X, Mata JM, Cabezuelo MA, Pallardó Y. CT in nontraumatic acute thoracic aortic disease: typical and atypical features and complications. *Radiographics* 2003; **23** Spec No: S93-110 [PMID: 14557505 DOI: 10.1148/rg.23si035507]
24 **LePage MA**, Quint LE, Sonnad SS, Deeb GM, Williams DM. Aortic dissection: CT features that distinguish true lumen from false lumen. *AJR Am J Roentgenol* 2001; **177**: 207-211 [PMID: 11418429 DOI: 10.2214/ajr.177.1.1770207]
25 **Evangelista A**, Mukherjee D, Mehta RH, O'Gara PT, Fattori R, Cooper JV, Smith DE, Oh JK, Hutchison S, Sechtem U, Isselbacher EM, Nienaber CA, Pape LA, Eagle KA. Acute intramural hematoma of the aorta: a mystery in evolution. *Circulation* 2005; **111**: 1063-1070 [PMID: 15710757 DOI: 10.1161/01.CIR.0000156444.26393.80]
26 **Ganaha F**, Miller DC, Sugimoto K, Do YS, Minamiguchi H, Saito H, Mitchell RS, Dake MD. Prognosis of aortic intramural hematoma with and without penetrating atherosclerotic ulcer: a clinical and radiological analysis. *Circulation* 2002; **106**: 342-348 [PMID: 12119251 DOI: 10.1161/01.CIR.0000022164.26075.5A]
27 **von Kodolitsch Y**, Csösz SK, Koschyk DH, Schalwat I, Loose R, Karck M, Dieckmann C, Fattori R, Haverich A, Berger J, Meinertz T, Nienaber CA. Intramural hematoma of the aorta: predictors of progression to dissection and rupture. *Circulation* 2003; **107**: 1158-1163 [PMID: 12615795 DOI: 10.1161/01.CIR.0000052628.77047.EA]
28 **Attia R**, Young C, Fallouh HB, Scarci M. In patients with acute aortic intramural haematoma is open surgical repair superior to conservative management? *Interact Cardiovasc Thorac Surg* 2009; **9**: 868-871 [PMID: 19651636 DOI: 10.1510/icvts.2009.211854]
29 **Nienaber CA**, Richartz BM, Rehders T, Ince H, Petzsch M. Aortic intramural haematoma: natural history and predictive factors for complications. *Heart* 2004; **90**: 372-374 [PMID: 15020504 DOI: 10.1136/hrt.2003.027615]
30 **Litmanovich D**, Bankier AA, Cantin L, Raptopoulos V, Boiselle PM. CT and MRI in diseases of the aorta. *AJR Am J Roentgenol* 2009; **193**: 928-940 [PMID: 19770313 DOI: 10.2214/AJR.08.2166]
31 **Sueyoshi E**, Matsuoka Y, Imada T, Okimoto T, Sakamoto I, Hayashi K. New development of an ulcerlike projection in aortic intramural hematoma: CT evaluation. *Radiology* 2002; **224**: 536-541 [PMID: 12147853 DOI: 10.1148/radiol.2242011009]
32 **O'Gara PT**, DeSanctis RW. Acute aortic dissection and its variants. Toward a common diagnostic and therapeutic approach. *Circulation* 1995; **92**: 1376-1378 [PMID: 7664413 DOI: 10.1161/01.CIR.92.6.1376]
33 **Stanson AW**, Kazmier FJ, Hollier LH, Edwards WD, Pairolero PC, Sheedy PF, Joyce JW, Johnson MC. Penetrating atherosclerotic ulcers of the thoracic aorta: natural history and clinicopathologic correlations. *Ann Vasc Surg* 1986; **1**: 15-23 [PMID: 3504683 DOI: 10.1016/S0890-5096(06)60697-3]
34 **Timperley J**, Banning AP. Prognosis of aortic intramural hematoma with and without penetrating atherosclerotic ulcer: a clinical and radiological analysis. *Circulation* 2003; **107**: e63 [PMID: 12628960 DOI: 10.1161/01.CIR.0000057816.67442.15]
35 **Braverman AC**. Penetrating atherosclerotic ulcers of the aorta. *Curr Opin Cardiol* 1994; **9**: 591-597 [PMID: 7987039 DOI: 10.1097/00001573-199409000-00014]
36 **Quint LE**, Williams DM, Francis IR, Monaghan HM, Sonnad SS, Patel S, Deeb GM. Ulcerlike lesions of the aorta: imaging features and natural history. *Radiology* 2001; **218**: 719-723 [PMID: 11230645 DOI: 10.1148/radiology.218.3.r01mr24719]
37 **Coady MA**, Rizzo JA, Elefteriades JA. Pathologic variants of thoracic aortic dissections. Penetrating atherosclerotic ulcers and intramural hematomas. *Cardiol Clin* 1999; **17**: 637-657 [PMID: 10589337 DOI: 10.1016/S0733-8651(05)70106-5]
38 **Davies RR**, Goldstein LJ, Coady MA, Tittle SL, Rizzo JA, Kopf GS, Elefteriades JA. Yearly rupture or dissection rates for thoracic aortic aneurysms: simple prediction based on size. *Ann Thorac Surg* 2002; **73**: 17-27; discussion 27-8 [PMID: 11834007 DOI: 10.1016/S0003-4975(01)03236-2]
39 **Birchard KR**. Acute aortic syndrome and acute traumatic aortic injury. *Semin Roentgenol* 2009; **44**: 16-28 [PMID: 19064069 DOI: 10.1053/j.ro.2008.10.002]
40 **Cho KR**, Stanson AW, Potter DD, Cherry KJ, Schaff HV, Sundt TM. Penetrating atherosclerotic ulcer of the descending thoracic aorta and arch. *J Thorac Cardiovasc Surg* 2004; **127**: 1393-139; discussion 1393-139; [PMID: 15115998]
41 **Harris JA**, Bis KG, Glover JL, Bendick PJ, Shetty A, Brown OW. Penetrating atherosclerotic ulcers of the aorta. *J Vasc Surg* 1994; **19**: 90-8; discussion 98-9 [PMID: 8301743 DOI: 10.1016/S0741-5214(94)70124-5]
42 **Svensson LG**, Labib SB, Eisenhauer AC, Butterly JR. Intimal tear without hematoma: an important variant of aortic dissection that can elude current imaging techniques. *Circulation* 1999; **99**: 1331-1336 [PMID: 10077517]
43 **Brinster DR**. Endovascular repair of the descending thoracic aorta for penetrating atherosclerotic ulcer disease. *J Card Surg* 2009; **24**: 203-208 [PMID: 19178611 DOI: 10.1111/j.1540-8191.2008.00660.x.]
44 **Eggebrecht H**, Plicht B, Kahlert P, Erbel R. Intramural hematoma and penetrating ulcers: indications to endovascular treatment. *Eur J Vasc Endovasc Surg* 2009; **38**: 659-665 [PMID: 19800821 DOI: 10.1016/j.ejvs.2009.09.001]
45 **Patatas K**, Shrivastava V, Ettles DF. Penetrating atherosclerotic ulcer of the aorta: a continuing debate. *Clin Radiol* 2013; **68**: 753-759 [PMID: 23541075 DOI: 10.1016/j.crad.2012.11.014.Epub]
46 **Nathan DP**, Boonn W, Lai E, Wang GJ, Desai N, Woo EY, Fairman RM, Jackson BM. Presentation, complications, and natural history of penetrating atherosclerotic ulcer disease. *J Vasc Surg* 2012; **55**: 10-15 [PMID: 22047830 DOI: 10.1016/j.jvs.2011.08.005.Epub]
47 **Botta L**, Buttazzi K, Russo V, Parlapiano M, Gostoli V, Di Bartolomeo R, Fattori R. Endovascular repair for penetrating atherosclerotic ulcers of the descending thoracic aorta: early and mid-term results. *Ann Thorac Surg* 2008; **85**: 987-992 [PMID: 18291184 DOI: 10.1016/j.athoracsur.2007.10.079]
48 **Debakey ME**, Henly WS, Cooley DA, Morris GC, Crawford ES, Beall AC. Surgical management of dissecting aneurysms of the aorta. *J Thorac Cardiovasc Surg* 1965; **49**: 130-149 [PMID: 14261867]
49 **Agarwal PP**, Chughtai A, Matzinger FR, Kazerooni EA. Multidetector CT of thoracic aortic aneurysms. *Radiographics* 2009; **29**: 537-552 [PMID: 19325064 DOI: 10.1148/rg.292075080]
50 **Booher AM**, Eagle KA. Diagnosis and management issues in thoracic aortic aneurysm. *Am Heart J* 2011; **162**: 38-46.e1 [PMID: 21742088 DOI: 10.1016/j.ahj.2011.04.010]
51 **Coady MA**, Rizzo JA, Elefteriades JA. Developing surgical

intervention criteria for thoracic aortic aneurysms. *Cardiol Clin* 1999; **17**: 827-839 [PMID: 10589349 DOI: 10.1016/S0733-8651(05)70118-1]

52 **Bhalla S**, West OC. CT of nontraumatic thoracic aortic emergencies. *Semin Ultrasound CT MR* 2005; **26**: 281-304 [PMID: 16274000 DOI: 10.1053/j.sult.2005.07.002]

53 **Posniak HV**, Olson MC, Demos TC, Benjoya RA, Marsan RE. CT of thoracic aortic aneurysms. *Radiographics* 1990; **10**: 839-855 [PMID: 2217974 DOI: 10.1148/radiographics.10.5.2217974]

54 **Svensson LG**, Khitin L. Aortic cross-sectional area/height ratio timing of aortic surgery in asymptomatic patients with Marfan syndrome. *J Thorac Cardiovasc Surg* 2002; **123**: 360-361 [PMID: 11828302 DOI: 10.1067/mtc.2002.118497]

55 **Hiratzka LF**, Bakris GL, Beckman JA, Bersin RM, Carr VF, Casey DE, Eagle KA, Hermann LK, Isselbacher EM, Kazerooni EA, Kouchoukos NT, Lytle BW, Milewicz DM, Reich DL, Sen S, Shinn JA, Svensson LG, Williams DM. 2010 ACCF/AHA/AATS/ACR/ASA/SCA/SCAI/SIR/STS/SVM guidelines for the diagnosis and management of patients with Thoracic Aortic Disease: a report of the American College of Cardiology Foundation/American Heart Association Task Force on Practice Guidelines, American Association for Thoracic Surgery, American College of Radiology, American Stroke Association, Society of Cardiovascular Anesthesiologists, Society for Cardiovascular Angiography and Interventions, Society of Interventional Radiology, Society of Thoracic Surgeons, and Society for Vascular Medicine. *Circulation* 2010; **121**: e266-e369 [PMID: 20233780 DOI: 10.1161/CIR.0b013e3181d4739e]

56 **Evangelista A**, Carro A, Moral S, Teixido-Tura G, Rodríguez-Palomares JF, Cuéllar H, García-Dorado D. Imaging modalities for the early diagnosis of acute aortic syndrome. *Nat Rev Cardiol* 2013; **10**: 477-486 [PMID: 23797792 DOI: 10.1038/nrcardio.2013.92.Epub]

57 **Hunold P**, Bischoff P, Barkhausen J, Vogt FM. Acute chest pain: the role of MR imaging and MR angiography. *Eur J Radiol* 2012; **81**: 3680-3690 [PMID: 21543179 DOI: 10.1016/j.ejrad.2011.04.032.Epub]

P- Reviewers: Kato M, Kirali K Paraskevas KI **S- Editor**: Ji FF
L- Editor: A **E- Editor**: Zhang DN

World Journal of Radiology

Submit a Manuscript: http://www.wjgnet.com/esps/
Help Desk: http://www.wjgnet.com/esps/helpdesk.aspx
DOI: 10.4329/wjr.v6.i6.366

World J Radiol 2014 June 28; 6(6): 366-373
ISSN 1949-8470 (online)
© 2014 Baishideng Publishing Group Inc. All rights reserved.

MINIREVIEWS

Use of stereotactic radiosurgery in the treatment of gynecologic malignancies: A review

Beverly Long, Ramez N Eskander, Krishnansu S Tewari

Beverly Long, Department of Obstetrics and Gynecology, University of California, Irvine Medical Center, Orange, CA 92868, United States
Ramez N Eskander, Krishnansu S Tewari, Division of Gynecologic Oncology, Department of Obstetrics and Gynecology, University of California, Irvine Medical Center, Orange, CA 92868, United States
Author contributions: Long B and Eskander RN performed the literature review and wrote the manuscript; Tewari KS provided expert opinion and final review and final edits.
Correspondence to: Ramez N Eskander, MD, Division of Gynecologic Oncology, Department of Obstetrics and Gynecology, University of California, Irvine Medical Center, 101 The City Drive, Building 56, Room 260, Orange, CA 92868, United States. eskander@uci.edu
Telephone: +1-714-4566026 Fax: +1-714-4567754
Received: December 29, 2013 Revised: April 1, 2014
Accepted: April 17, 2014
Published online: June 28, 2014

Abstract

Recent retrospective studies have reported the use of stereotactic radiosurgery (SRS) in the treatment of gynecologic cancers. SRS uses real-time imaging and high dose radiation beams attached to precise robotic arms to target malignant lesions while sparing normal tissue. The purpose of this review is to examine the indications for SRS in gynecologic oncology, review the current literature regarding the use of SRS in gynecologic cancers, and identify future directions for research in this area. Literature on stereotactic radiosurgery was reviewed using the PubMed search engine. Articles written in English from 1993-2013 were reviewed, and 20 case series and clinical trials were included. The safety and efficacy SRS has been demonstrated in all gynecologic disease sites including cervical, endometrial, vulvar, vaginal, and ovarian cancers. Indications for its use include non-central pelvic recurrences in previously irradiated patients, complex or non-resectable disease recurrence, and solitary brain metastases. Toxicities are usually mild, though grade 3-4 toxicities have been reported. SRS is a promising second line treatment modality for patients with primary or recurrent disease who cannot undergo standard surgical or radiation therapy. Further research is required to determine optimal dosing and fractionation schedules, delineate appropriate patient populations, and assess longterm morbidity and survival.

© 2014 Baishideng Publishing Group Inc. All rights reserved.

Key words: Stereotactic radiosurgery; Stereotactic body radiotherapy; Gynecologic oncology

Core tip: Stereotactic radiosurgery is a novel treatment modality in gynecologic oncology. Its use has been reported for inoperable primary tumors, recurrent tumors in or near irradiated fields, and isolated pelvic nodal metastases. Associated toxicities are usually mild. Though further research is needed to establish the role of SRS in gynecologic oncology, it represents an important second line therapy in appropriately selected patients.

Long B, Eskander RN, Tewari KS. Use of stereotactic radiosurgery in the treatment of gynecologic malignancies: A review. *World J Radiol* 2014; 6(6): 366-373 Available from: URL: http://www.wjgnet.com/1949-8470/full/v6/i6/366.htm DOI: http://dx.doi.org/10.4329/wjr.v6.i6.366

INTRODUCTION

Stereotactic radiosurgery (SRS) is an emerging technology in the treatment of gynecologic cancers. It targets malignant lesions using real-time imaging in combination with high dose radiation beams attached to precise robotic arms. First used in the treatment of intracranial lesions, technological advancements in radiation and

image-guidance have allowed for its use in a variety of extracranial locations. Because SRS can focus on targets with sub-millimeter accuracy, it has been used for inoperable primary tumors near radiosensitive tissues, recurrent tumors in or near irradiated fields, and isolated pelvic nodal metastases. Its precise beams spare normal tissues and result in decreased toxicity when compared to conventional radiotherapy.

SRS is of particular interest in women with gynecologic malignancies, since many of these patients will recur in or near previously irradiated tissues, inoperable anatomic regions, or sites inaccessible to traditional radiation therapy[1]. Recent retrospective studies have reported on the safety and efficacy of SRS in the treatment of gynecologic cancers. The purpose of this review is to examine the indications for SRS in gynecologic oncology, review the current literature regarding the use of SRS in gynecologic cancers, and identify future directions for research in this area.

STEREOTACTIC RADIOSURGERY

Stereotactic radiosurgery combines the complex dose distributions of intensity modulated radiation therapy (IMRT), the accuracy, reproducibility, and high doses of radiosurgery, and the fractionation of external beam radiation therapy to build a technique capable of treating complex abdominal-pelvic tumors. In this method, linear accelerators generate multiple X-ray beams, which can precisely target malignant tissues using advanced treatment planning, real-time imaging, and/or fiducial marker localization. The precision of these X-ray beams allows delivery of high doses to the tumor while sparing normal tissues. Doses are usually divided into 1-5 fractions given over 1-2 wk. Body immobilizers may be used to maintain spatial relationships during treatment sessions. Real-time image guidance ensures accurate tumor location, as abdominal and pelvic structures can exhibit substantial inter- and intra-fraction movement.

SRS has been utilized for lung, liver, pancreatic, renal, prostate, spinal, and pelvic tumors. It was first described for use in liver and lung lesions in the 1980s and has been used for gynecologic cancers since 2006. Twelve, small retrospective case series and one phase II clinical trial have described single institution experiences with SRS in the treatment of uterine, cervical, vaginal, vulvar, and ovarian cancers (Table 1). These series include a combined 291 patients who have undergone SRS for distant, local, lateral pelvic, or isolated pelvic node recurrences or as a substitute for brachytherapy in primary disease. One study specifically reported hematologic toxicities associated with SRS. Populations in these studies were heterogeneous, and varying doses and fractionation schedules have been described. Differences in reporting these results make it difficult to calculate a composite rate of survival, loco-regional control, or disease response.

The largest population was described by Kunos *et al*[1], in a phase II clinical trial evaluating the safety and efficacy of SRS in 50 patients with recurrent cervical, endometrial, ovarian, and vulvar cancer. SRS was used to deliver 24 Gy in 3 fractions to a clinical target volume (CTV) that included the gross tumor volume (GTV) as well as surrounding fluorodeoxyglucose (FDG)-avid areas. The positron emission tomography (PET) images were overlaid and co-registered with computed tomography (CT) scans in order to accurately target the entire tumor site. One patient had a complete response, and the overall response rate (defined as complete response, partial response, or stable disease without progression) was 96%. Sixty-two percent of patients showed clinical benefit at 6 mo. Most toxicity was mild, though one patient did experience grade 4 hyperbilirubinemia and another developed an enterovaginal fistula. The study authors concluded that SRS was safe and efficacious for patients with recurrent gynecologic malignancies[1]. All other data are derived from case series, and no controlled trials have been published. While studies mostly describe patients with endometrial or cervical primaries, SRS has been utilized for all gynecologic disease sites.

CERVICAL CANCER

Since radiation therapy is commonly used in cervical cancer, SRS is an attractive option for inoperable patients with primary or recurrent disease. Overall, 76 cases describing the use of SRS in cervical cancer have been published in 9 series. Four papers describe its use in the primary setting (usually as a substitute for brachytherapy), while others report its use for loco-regional, para-aortic node, or pelvic side-wall recurrences. All series included only patients who were unsuitable or unwilling to undergo other treatment modalities such as brachytherapy or surgical resection.

The largest series of patients treated with SRS for primary disease was published by Hsieh *et al*[2] in 2013. They described 9 patients with locally advanced cervical cancer who were treated with SRS (*via* helical tomotherapy) as a replacement for brachytherapy boost after the standard dose of EBRT and concurrent cisplatin. These patients were unable to undergo the recommended brachytherapy due to anatomic factors or medical comorbidities. Though three-year actuarial loco-regional control was 77.8%, three-year disease free survival was only 28.6%. Distant metastases were the most common pattern of failure, suggesting efficacy of SRS in controlling central pelvic disease[2]. Mollà *et al*[3] reported similar results when treating primary disease. Their population included seven cervical cancer patients who underwent EBRT with SRS boost due to high-risk disease after initial surgical management. Only one patient recurred within the 12-month follow up period; however, actuarial values were not calculated. Toxicities were low in both series, consisting mostly of grade 1 or 2 sexual and GI symptoms. However, one patient did have grade 3 diarrhea, and another had grade 3 thrombocytopenia. One patient with stage 4A disease developed a rectovaginal fistula. Four patients

Table 1 Summary of case series of stereotactic radiosurgery

Ref.	*n*	Cancer types	Disease setting	Dose	Response/ control rate	Survival	Grade 3/4 toxicities	Patterns of failure
Molla *et al*[3]	16	Cervical (7) Uterine (9)	Primary (stage 1-3) and recurrence	EBRT 45 GyT SRS 14-20 Gy/2-5 fractions +/- para-aortic boost (2 pts)	15 pts NED at 12.6 mo (1 recurrence)	Not reported	Rectal bleeding (1)	Not reported
Deodato *et al*[13]	11	Ovarian (4) Cervical (4) Uterine (3)	Recurrence	SRS 20-30 Gy/4-6 fractions	83.3% overall response rate 63% recurrence at 19 mo	Not reported	None	Systemic/distant progression (*n* = 4) Local progression (*n* = 1) Local and systemic progression (*n* = 1)
Guckenburger *et al*[7]	19	Cervical (12) Uterine (7)	Recurrence	EBRT 50 Gy SRS 15 Gy/3 fractions +/- vaginal BT (3 pts)	3 yr local control rate 81%	Median OS 25 mo, PFS 16 mo	Intestino-vaginal fistula (2) Small bowel ileus (1)	Systemic progression (*n* = 7) Local tumor progression (*n* = 1) Comorbid illness (*n* = 1) Unknown (*n* = 1)
Choi *et al*[10]	30	Cervical (28) Uterine (2)	Recurrence	EBRT 27-45 Gy SRS 13-45 Gy/1-3 fractions	4 yr local control rate 67.4%	Median PFS 32 mo	Various (5)	Locoregional failure (13.8%) Distant mets (10.3%) Local and distant failure (6.9%)
Dewas *et al*[9]	16	Cervical (4) Uterine (1) Rectal (4) Anal (6) Bladder (1)	Recurrence	EBRT 36-66 Gy (3 pts) SRS 36 Gy/6 fractions	1 yr local control rate 51.4%	Median OS 11.5 mo (DFS 8.3 mo)	None	Not reported
Haas *et al*[6]	6	Cervical (6)	Primary (stage 3B-4)	EBRT 45 Gy SRS 19.5-20 Gy/ 3-5 fractions +/- 50.4-61.2 Gy IMRT boost (5 pts)	100% local control at 14 mo	100% at 14 mo	None	Not reported
Hsieh *et al*[2]	9	Cervical (9)	Primary (stage 3B-4A)	EBRT 50.4 Gy SRS 15-27 Gy/ 5-9 fractions	3 yr local control rate 77.8%	Median OS 13 mo	Diarrhea (1) Thrombocytopenia (1) Rectal bleeding (3) Rectovaginal fistula (1)	Distant metastases (44%)
Hsieh *et al*[2]	31	Uterine (31)	Primary (stage 1B-3C)	IMRT or SRS *via* HT 45-50.4 Gy/25-28 fractions ICBT 4.5-5 Gy x 2-6 fractions	Not reported	Median OS 21 mo	None	Distant metastases
Kubicek *et al*[19]	11	Cervical 7) Uterine (2) Vaginal (2)	Primary (stage 2-3C) and recurrence	EBRT or IMRT 45-50.4 Gy SRS 5-27.5 Gy/1-5 fractions	Not reported	73% overall survival at follow-up	Rectal bleeding (1)	Not reported
Kunos *et al*[20]	3	Vulvar (3)	Recurrence	SRS 24 Gy/3 fractions	Not reported	1-3 mo PFS	None	Out of field recurrence
Kunos *et al*[15]	5	Endometrial (1) 0varian (3) Cervical (1)	Recurrence	SRS 5-8 Gy x 3-5 fractions	Not reported	Not reported	Fatigue (1)	Distant metastases
Kunos *et al*[1] Phase Ⅱ trial	50	Cervix (9) Endometrial (14) Ovarian (25) Vulvar (2)	Recurrence	SRS 24 Gy/3 fractions	6 mo clinical benefit 68%	Median OS 20.2 mo	Hyperbilirubinemia (1) Enterovaginal fistula (1)	Out of field recurrence (62%)

EBRT: External beam radiation therapy; SRS: Stereotactic radiosurgery; NED: No evidence of disease; BT: Brachytherapy; OS: Overall survival: HT: Helical tomotherapy; IMRT: Intensity modulated radiation therapy; PFS: Progression free survival.

had rectal bleeding following treatment[3]. Two other papers by Hsieh *et al*[4,5] report similar findings in this patient population, and Haas *et al*[6] described 100% disease free survival at 14 mo in a series of six patients treated with SRS boost for primary disease.

These rates of local control exceed that of brachytherapy in many studies; however, the small sample sizes, short duration of follow-up, and lack of a brachytherapy control group make it impossible to compare the two treatments. Still, the authors of these papers suggest that SRS could be considered as an alternative to brachytherapy boost, especially in patients unsuited for brachytherapy.

SRS has been more frequently described for recur-

Figure 1 CyberKnife (left) and GammaKnife (right). The CyberKnife device employs a mobile frame to radiate tumors in complex locations. The GammaKnife provides head immobilization for more accurate radiation delivery.

rent disease. Guckenberger *et al*[7] describe its use in 12 patients with local recurrences of cervical cancer. Six patients in this study (which included patients with endometrial and cervical cancer) had undergone previous radiation, though most had received only vaginal brachytherapy. The majority of patients had been surgically treated for their primary disease. Those who had not had previous EBRT underwent standard external radiation at a dose of 45 Gy followed by a SRS boost using 14-20 Gy in 3 fractions. Patients previously treated with external beam radiation underwent only SRS. Loco-regional control was again excellent, with 81% loco-regional control at 3 years. Overall 3-year survival was 34%, and systemic disease progression remained the most common pattern of failure[7]. This survival rate is similar to that of patients who undergo brachytherapy boost after EBRT for recurrent disease.

Interestingly, while pelvic sidewall recurrences carry a poor prognosis in patients treated with brachytherapy boost, location was not found to be a prognostic factor for patients treated with SRS[8]. Dewas *et al*[9] included four cervical cancer patients in their series describing SRS for lateral pelvic recurrences of cervical, uterine, anal, rectal, and bladder cancers. In this study, previously irradiated patients were treated with CyberKnife SRS (36 Gy in 6 fractions) for lateral pelvic masses (Figure 1). While disease free survival remained relatively low (8.3 mo), the authors argued that this treatment delayed local progression, as these recurrences would usually progress much more rapidly, improving quality of life. No grade 3 or higher toxicities were noted, and self-reported pain scores were improved after treatment. However, results should be interpreted with caution, as none of these patients exhibited unequivocal response. Favorable response was reported based on decreased uptake of contrast material on follow up PET studies[9]. Further research is needed to determine whether SRS is superior to alternate radiation modalities in patients with lateral pelvic recurrences.

Another clinical challenge in recurrent cervical cancer occurs in patients with isolated, unresectable, para-aortic nodal recurrence. Though this type of recurrence is rare, it is associated with a poor prognosis and high post-treatment morbidity due to the radiosensitivity of surrounding organs, particularly the small bowel. Because of the precision of its radiation beams, SRS could be an excellent treatment modality for this type of recurrence. Choi *et al*[10] described their experience in 28 patients with cervical cancer recurrence confined to para-aortic nodes. These patients received EBRT followed by SRS boost with 33-45 Gy in 3 daily fractions. Twenty-five patients received cisplatin before, during, or immediately after their radiation courses. Four year overall survival was 50.1%, and 96.5% of patients had at least partial response. Median time to disease progression was 32 mo. Though this population is small, SRS appears to be associated with improved overall survival, fewer toxicities, and shorter treatment times when compared for EBRT for nodal para-aortic recurrence[11,12].

In combination, these reports indicate that SRS may be a promising therapeutic modality for primary and recurrent cervical cancer, especially in patients who have undergone previous radiation and/or are not candidates for surgical resection. Further studies are needed to clarify patient populations most likely to benefit from SRS. The role of concurrent chemotherapy with SRS is also an important area of research, as distant metastases are the most common sites of failure.

ENDOMETRIAL CANCER

SRS has been similarly studied in endometrial cancer. Seventy cases of SRS use for primary or recurrent endometrial cancer have been described in nine unique series. However, dosing regimens are not uniform, and study populations are heterogeneous. SRS has been used as a substitute for both EBRT and brachytherapy boost after

surgical therapy for high-risk disease, as well as in the treatment of recurrent endometrial cancer. It has also been used as a substitute for IMRT, due to it's improved accuracy and ability to target higher doses of radiation to precise areas of tissue.

The largest series of SRS in the primary setting was published by Hsieh *et al*[2]. They reported 31 cases of FIGO stage I B to ⅢC uterine cancer, in which either SRS or IMRT was used as a substitute for EBRT after surgical staging for primary disease. IMRT or SRS was followed by vaginal brachytherapy in all patients. Two patients received concurrent cisplatin. This study is unique in that it is the only study that has compared SRS to another treatment modality. However, the study was not powered to detect statistical differences between the groups. While the study found no differences in overall survival or toxicity in SRS when compared to IMRT, SRS did provide significantly better critical organ sparing for the rectum, bladder, femoral heads, and intestines when compared to IMRT using dose-volume histograms. One cervical stump failure occurred in each group, and no grade 3 or 4 toxicities were noted[2].

SRS has also been studied as a substitute for brachytherapy in patients with primary endometrial cancer. Mollà *et al*[3] included nine patients with FIGO stage Ⅰ-Ⅲ uterine cancer in their series describing SRS boost after primary or post-operative EBRT. As described above, patients received 45 Gy EBRT or IMRT followed by 14-20 Gy SRS, usually following surgical treatment for either endometrial or cervical cancer. While most subjects had primary disease, two patients were enrolled due to local relapse. Patients underwent therapy at varying doses and fractionations. At 12-month median follow up, no recurrences were reported for the endometrial cancer group. Mostly grade 1 or 2 toxicities were noted, though one of the patients with recurrent endometrial cancer experienced persistent (grade 3) rectal bleeding 18 mo after re-irradiation at the vaginal vault[3].

SRS is more commonly used in the setting of recurrent endometrial cancer, especially in previously irradiated patients. Both Guckenberger *et al*[7] and Deodato *et al*[13] have published separate series describing the use of SRS for distant or local recurrences of endometrial and cervical cancers. Favorable rates of local control were demonstrated, though statistics for cervical vs. uterine cancers were not separately reported. Both series were small, including only seven and three endometrial cancer patients, respectively[7,13]. Two patients with isolated para-aortic nodal recurrences of endometrial cancer were also included in the above-mentioned study by Choi *et al*[10] with results as described above. While it is likely that results from cervical cancer patients could be extrapolated to those with endometrial cancers, it is difficult to draw conclusions with these small patient populations. Study authors have suggested that SRS could benefit patients with pelvic or para-aortic node recurrences who are not candidates for exenteration or salvage radiotherapy; however, further studies are needed to confirm these results and delineate optimal SRS dosing and fractionation.

OVARIAN CANCER

While the use of radiation therapy is much more common in endometrial and cervical cancers, SRS has also been used in the treatment of recurrent or non-operative ovarian cancers. Higginson *et al*[14] describe the use of SRS for patients with isolated lung metastasis, para-aortic nodes, or vaginal cuff recurrences after primary surgery and adjuvant therapy.

Kunos *et al*[15] included three cases of ovarian cancer in a 2009 report of their single-institution experience with SRS. These cases involved patients with multiple local and distant recurrences treated with multiple courses of chemotherapy, prior radiation, and/or surgeries. One patient with FIGO stage ⅢC papillary serous cancer received primary surgery followed by two differing chemotherapy courses, as well as a repeat operation with intra-operative radiation before opting for SRS in the place of pelvic exenteration for a third relapse of her cancer. Stable disease remained after radiotherapy and the patient was without evidence of progression for 9 mo, treated with concurrent bevacizumab and cyclophosphamide. Another patient was free of disease at 10 mo after SRS was used to treat a persistent vaginal lesion following primary debulking, several chemotherapy courses, and external pelvic radiation. A third patient who underwent SRS after multiple surgeries, one dose of intra-operative radiation, and 3 mo of single-agent chemotherapy had stable disease at six month follow up with no more than grade 2 acute toxicities[15].

Deodato *et al*[13] described four other cases of SRS use in ovarian cancer. Three patients were without evidence of disease at 37, 31, and 19 mo after undergoing SRS to presacral lymph nodes, hepatic lesions, and supraclavicular nodes, respectively. One patient was alive with disease at 18 mo after SRS dosing to anterior mediastinal and left internal mammary nodes[13]. Further studies are needed to define the appropriate patient population for SRS use in ovarian cancer. Currently, SRS is only used as a palliative measure for patients with localized, recurrent disease.

TOXICITIES

Most toxicities associated with SRS are mild and self-limiting. They include grade 1-2 fatigue, diarrhea, dysuria, nausea, and sexual side effects. However, rare grade 3 toxicities have been reported in almost every series. Rectal bleeding was reported in 4 patients in two different series of patients receiving EBRT followed by SRS boost. One of these events occurred in a patient with a history of prior radiation; however, the other patients with rectal bleeding had not undergone previous radiation therapy. Four patients in three series reported enterovaginal fistulas; all of these occurred in the recurrent setting[1,2,7].

The largest study of toxicities associated with SRS was published by Kunos *et al*[16] in 2012. This retrospec-

tive series analyzed hematologic toxicity in 61 women treated with SRS for stage 4 gynecologic malignancies. Ninety-three percent of these patients had received chemotherapy prior to SRS. Twenty-five percent had grade 2 fatigue, but the incidence of grade 3 fatigue was only 3%. All symptoms resolved by 30 d post-radiation. No neutropenia was reported; however, 5% of women had grade 1 anemia (Hb < 10.0 g/dL), and there were single incidences of grade 1, 2, and 3 thrombocytopenia. Further studies are required to better estimate the rates of non-hematologic toxicities, though it is difficult to isolate SRS as the cause of morbidity, since many patients receive surgery, chemotherapy, and other methods of radiation prior to receiving SRS[16].

SRS IN GYNECOLOGIC CANCER

For now, the indications for SRS in gynecologic oncology remain undefined. Our review found three clinical scenarios for which SRS could provide benefit. These include non-central pelvic recurrences in previously irradiated patients, complex or unresectable disease recurrence, and solitary brain metastases (Table 2). This is an especially promising area of research, as few treatment options are available for these patients.

RECURRENT CERVICAL CANCER

Patients with locally advanced primary cervical cancer are usually treated with curative chemoradiation. Others may undergo primary surgery but require adjuvant chemoradiation due to high-risk pathologic features, positive margins, positive parametria or positive pelvic lymph nodes. In this population, utilization of traditional radiotherapy in a previously radiated field is associated with prohibitive toxicity, and thus, SRS may represent a suitable alternative. While central pelvic recurrences can be treated with surgical exenteration, many patients have non-central recurrences or comorbid conditions that make them unsuitable for aggressive surgical resection with significant quality of life implications. Currently, the majority of these patients are treated with systemic chemotherapy using cisplatin, paclitaxel, and bevacizumab (following presentation of GOG 240)[17] or are enrolled in clinical trials. Cyberknife SRS represents another therapeutic alternative and has decreased morbidity compared to exenteration. Series by Guckenberger, Dewas, and Deodata report mostly grade 1-2 toxicity, even in previously irradiated patients[7,9,13]. In one series, two out of the three patients with grade 3-4 toxicities had received prior radiation; however, most previously irradiated patients did not suffer significant morbidity[7].

COMPLEX OLIGOMETASTASES

Although the location of gynecologic cancer recurrence is unpredictable, patients with cervical and endometrial cancer commonly recur in the pelvis. A proportion, however, will have distant disease recurrence in complex locations involving the abdominal retro-peritoneum. Clinical options in this setting are limited, as access for adequate surgical resection is difficult to achieve. Treatment using chemotherapeutics or biologic agents is encouraged, and a combined approach utilizing systemic chemotherapy in conjunction with SRS is promising. Research regarding the above is limited, and given the unmet clinical need, warrants further investigation. There are well-defined selection criteria for utilization of SRS in the treatment of oligometastases for other primary disease sites such as lung, prostate and liver, and this data can may be extrapolated to gynecologic cancer patients.

Table 2 Indications for SRS in recurrent and metastatic gynecologic malignancy

Recurrent cervical cancer	Recurrence in a previously radiated fields Recurrence in patients who are not candidates for pelvic exenteration
Complex oligometastases	Unresectable oligometastases Oligometastases in abdominal retroperitoneum
Central nervous system and brain metastases	Intracranial lesions not accessible to Gamma Knife

CENTRAL NERVOUS SYSTEM AND BRAIN METASTASES

Central nervous system (CNS) and brain metastases are rare in gynecologic malignancies. Between 0.4%-1.2% of cervical cancers involve intracranial metastases, and percentages are similar for other pelvic disease sites. These lesions are usually treated with whole brain radiation or Gamma Knife stereotactic radiosurgery (Figure 1). A series by Menedez *et al*[18] included 14 patients with brain metastases from primary endometrial, ovarian, or cervical cancer. Patients received 16-20 Gy and experienced median survival of 5-13 mo. While the CyberKnife system is not well studied in gynecologic malignancies, its use is described for brain metastases in primary lung, breast, colon, and other cancers. CyberKnife eliminates the need for target fixation and allows for expanded treatment freedom for large or complex lesions.

The preference for Gamma Knife in the treatment of brain and spinal cord metastasis stems from the theoretical improvement in accuracy, 0.5 mm or less, over Cyber Knife (1 mm or less), although these measurements have been disputed (Figure 1). Additionally, the smaller size of the Gamma Knife collimators reduce the potential injury to neighboring normal brain tissue, improving long term morbidity. The Gamma Knife also improves precision using a rigid immobilization device to prevent head movement during treatment. Conversely, utilization of CyberKnife SRS, allows for improved therapeutic versatility given the dynamic nature of the robotic arms, compensating for target organ motion, and allowing access to portions of the CNS that are difficult to treat using

Gamma Knife therapy.

FUTURE RESEARCH

While SRS is a promising treatment modality for inoperable or recurrent gynecologic cancers, many aspects of treatment remain uncertain. The available series describing SRS use heterogeneous dosing and fractionation schedules, and the optimal regimen has not been delineated. Controlled trials comparing SRS to brachytherapy or IMRT are also needed. Studies of SRS use for adjuvant therapy in high risk disease could further define the role of SRS in gynecologic malignancies. Today, SRS remains a second line treatment, reserved for patients with primary disease who are unsuitable for standard surgical or radiation therapy or for recurrent disease in a previously irradiated field.

Because most patients in the above-mentioned series suffered disease recurrence or progression outside the treatment area, many researchers have proposed concurrent chemotherapy with SRS to prevent progression of occult disease. Twenty five patients reported in the literature have received concurrent cisplatin during SRS, and four patients have received other chemotherapy regimens within 4 mo of SRS[1,2,3,7,10]. However, this patient population is too small for any comparisons to be made regarding the benefits of concurrent chemotherapy. A phase I clinical trial of palliative SRS with gemcitabine and carboplatin is currently enrolling patients with recurrent or persistent cervical, endometrial, ovarian, vulvar, and vaginal cancers (NCT01652794).

CONCLUSION

SRS is an emerging area of radiation oncology, which has been successfully used in high risk gynecologic malignancies. Because of its unique ability to precisely target malignant lesions while sparing surrounding normal tissues, SRS can safely radiate tumors that may be difficult or impossible to treat with surgery or conventional radiotherapy. SRS has been described for all gynecologic malignancies and appears to have an excellent safety profile. Further research is necessary to determine optimal dosing and fractionation schedules, delineate appropriate patient populations, and evaluate long term survival and morbidity.

REFERENCES

1 **Kunos CA**, Brindle J, Waggoner S, Zanotti K, Resnick K, Fusco N, Adams R, Debernardo R. Phase II Clinical Trial of Robotic Stereotactic Body Radiosurgery for Metastatic Gynecologic Malignancies. *Front Oncol* 2012; **2**: 181 [PMID: 23227452 DOI: 10.3389/fonc.2012.00181]

2 **Hsieh CH**, Shueng PW, Hsiao SM, Wei MC, Wu WY, Sun HD, Tien HJ, Wang LY, Hsieh YP. Helical tomotherapy provides efficacy similar to that of intensity-modulated radiation therapy with dosimetric benefits for endometrial carcinoma. *Onco Targets Ther* 2012; **5**: 245-253 [PMID: 23055750 DOI: 10.2147/OTT.S35958]

3 **Mollà M**, Escude L, Nouet P, Popowski Y, Hidalgo A, Rouzaud M, Linero D, Miralbell R. Fractionated stereotactic radiotherapy boost for gynecologic tumors: an alternative to brachytherapy? *Int J Radiat Oncol Biol Phys* 2005; **62**: 118-124 [PMID: 15850911 DOI: 10.1016/j.ijrobp.2004.09.028]

4 **Hsieh CH**, Wei MC, Hsu YP, Chong NS, Chen YJ, Hsiao SM, Hsieh YP, Wang LY, Shueng PW. Should helical tomotherapy replace brachytherapy for cervical cancer? Case report. *BMC Cancer* 2010; **10**: 637 [PMID: 21092235 DOI: 10.1186/1471-2407-10-637.]

5 **Hsieh CH**, Wei MC, Lee HY, Hsiao SM, Chen CA, Wang LY, Hsieh YP, Tsai TH, Chen YJ, Shueng PW. Whole pelvic helical tomotherapy for locally advanced cervical cancer: technical implementation of IMRT with helical tomotherapy. *Radiat Oncol* 2009; **4**: 62 [PMID: 20003321 DOI: 10.1186/1748-717X-4-62]

6 **Haas JA**, Witten MR, Clancey O, Episcopia K, Accordino D, Chalas E. CyberKnife Boost for Patients with Cervical Cancer Unable to Undergo Brachytherapy. *Front Oncol* 2012; **2**: 25 [PMID: 22655266 DOI: 10.3389/fonc.2012.00025]

7 **Guckenberger M**, Bachmann J, Wulf J, Mueller G, Krieger T, Baier K, Richter A, Wilbert J, Flentje M. Stereotactic body radiotherapy for local boost irradiation in unfavourable locally recurrent gynaecological cancer. *Radiother Oncol* 2010; **94**: 53-59 [PMID: 20079550 DOI: 10.1016/j.radonc.2009.12.004]

8 **Jain P**, Hunter RD, Livsey JE, Coyle C, Swindell R, Davidson SE. Salvaging locoregional recurrence with radiotherapy after surgery in early cervical cancer. *Clin Oncol (R Coll Radiol)* 2007; **19**: 763-768 [PMID: 17931845 DOI: 10.1016/j.clon.2007.08.015]

9 **Dewas S**, Bibault JE, Mirabel X, Nickers P, Castelain B, Lacornerie T, Jarraya H, Lartigau E. Robotic image-guided reirradiation of lateral pelvic recurrences: preliminary results. *Radiat Oncol* 2011; **6**: 77 [PMID: 21699690 DOI: 10.1186/1748-717X-66-77]

10 **Choi CW**, Cho CK, Yoo SY, Kim MS, Yang KM, Yoo HJ, Seo YS, Kang JK, Lee DH, Lee KH, Lee ED, Rhu SY, Choi SC, Kim MH, Kim BJ. Image-guided stereotactic body radiation therapy in patients with isolated para-aortic lymph node metastases from uterine cervical and corpus cancer. *Int J Radiat Oncol Biol Phys* 2009; **74**: 147-153 [PMID: 18990511 DOI: 10.1016/j.ijrobp.2008.07.020]

11 **Grigsby PW**, Vest ML, Perez CA. Recurrent carcinoma of the cervix exclusively in the paraaortic nodes following radiation therapy. *Int J Radiat Oncol Biol Phys* 1994; **28**: 451-455 [PMID: 8276660 DOI: 10.1016/0360-3016(94)90070-1]

12 **Hong JH**, Tsai CS, Lai CH, Chang TC, Wang CC, Chou HH, Lee SP, Hsueh S. Recurrent squamous cell carcinoma of cervix after definitive radiotherapy. *Int J Radiat Oncol Biol Phys* 2004; **60**: 249-257 [PMID: 15337563 DOI: 10.1016/j.ijrobp.2004.02.044]

13 **Deodato F**, Macchia G, Grimaldi L, Ferrandina G, Lorusso D, Salutari V, Cilla S, Valentini V, Cellini N, Piermattei A, Scambia G, Morganti AG. Stereotactic radiotherapy in recurrent gynecological cancer: a case series. *Oncol Rep* 2009; **22**: 415-419 [PMID: 19578785 DOI: 10.3892/or_00000453]

14 **Higginson DS**, Morris DE, Jones EL, Clarke-Pearson D, Varia MA. Stereotactic body radiotherapy (SBRT): Technological innovation and application in gynecologic oncology. *Gynecol Oncol* 2011; **120**: 404-412 [PMID: 21194733 DOI: 10.1016/j.ygyno.2010.11.042]

15 **Kunos C**, Chen W, DeBernardo R, Waggoner S, Brindle J, Zhang Y, Williams J, Einstein D. Stereotactic body radiosurgery for pelvic relapse of gynecologic malignancies. *Technol Cancer Res Treat* 2009; **8**: 393-400 [PMID: 19754216]

16 **Kunos CA**, Debernardo R, Radivoyevitch T, Fabien J, Dobbins DC, Zhang Y, Brindle J. Hematological toxicity after robotic stereotactic body radiosurgery for treatment of metastatic gynecologic malignancies. *Int J Radiat Oncol Biol Phys* 2012; **84**: e35-e41 [PMID: 22543208 DOI: 10.1016j.ijrobp.2012.02.027]

17 **Tewari KS**, Sill MW, Long HJ, Penson RT, Huang H, Ramondetta LM, Landrum LM, Oaknin A, Reid TJ, Leitao MM, Michael HE, Monk BJ. Improved survival with bevacizumab in advanced cervical cancer. *N Engl J Med* 2014; **370**: 734-743 [PMID: 24552320 DOI: 10.1056/NEJMoa1309748]

18 **Menendez JY**, Bauer DF, Shannon CN, Fiveash J, Markert JM. Stereotactic radiosurgical treatment of brain metastasis of primary tumors that rarely metastasize to the central nervous system. *J Neurooncol* 2012; **109**: 513-519 [PMID: 22870850 DOI: 10.1007/s11060-012-0916-2]

19 **Kubicek GJ**, Xue J, Xu Q, Asbell SO, Hughes L, Kramer N, Youssef A, Chen Y, Aikens J, Saul H, Pahlajani N, LaCouture T. Stereotactic body radiotherapy as an alternative to brachytherapy in gynecologic cancer. *Biomed Res Int* 2013; **2013**: 898953 [PMID: 24000329 DOI: 10.1155/2013/898953]

20 **Kunos C**, von Gruenigen V, Waggoner S, Brindle J, Zhang Y, Myers B, Funkhouser G, Wessels B, Einstein D. Cyberknife radiosurgery for squamous cell carcinoma of vulva after prior pelvic radiation therapy. *Technol Cancer Res Treat* 2008; **7**: 375-380 [PMID: 18783287]

P- Reviewers: Baglaj MS, Sharma DN, Tsili AC
S- Editor: Wen LL **L- Editor**: A **E- Editor**: Zhang DN

World Journal of Radiology

Submit a Manuscript: http://www.wjgnet.com/esps/
Help Desk: http://www.wjgnet.com/esps/helpdesk.aspx
DOI: 10.4329/wjr.v6.i6.374

World J Radiol 2014 June 28; 6(6): 374-380
ISSN 1949-8470 (online)
© 2014 Baishideng Publishing Group Inc. All rights reserved.

CLINICAL TRIALS STUDY

Feasibility study of computed *vs* measured high b-value (1400 s/mm²) diffusion-weighted MR images of the prostate

Leonardo K Bittencourt, Ulrike I Attenberger, Daniel Lima, Ralph Strecker, Andre de Oliveira, Stefan O Schoenberg, Emerson L Gasparetto, Daniel Hausmann

Leonardo K Bittencourt, Daniel Lima, Emerson L Gasparetto, CDPI Ressonância Magnética, Avenida das Américas, 4666 Barra da Tijuca, RJ 22631-000, Brazil
Ulrike I Attenberger, Stefan O Schoenberg, Daniel Hausmann, Institute of Clinical Radiology and Nuclear Medicine, University of Heidelberg, University Hospital Mannheim, Theodor-Kutzer-Ufer 1-3, 68167 Mannheim, Germany
Ralph Strecker, Siemens Healthcare Brazil, Avenida Mutinga, 3800 Jardim Santo Elias, SP 05110-902, Brazil
Andre de Oliveira, Siemens AG Healthcare Sector, Henkestrasse 127, D-91052 Erlangen, Germany
Author contributions: Bittencourt LK and Hausmann D contributed equally to this work; Bittencourt LK, Hausmann D, Strecker R, de Oliveira A, Gasparetto EL designed the research; Hausmann D, Bittencourt LK and Strecker R performed the research; Hausmann D, Strecker R and de Oliveira A analyzed the data; Hausmann D, Bittencourt LK, Lima D, Schoenberg S, Attenberger UI and Strecker R wrote the paper.
Correspondence to: Dr. Daniel Hausmann, MD, Institute of Clinical Radiology and Nuclear Medicine, University of Heidelberg, University Hospital Mannheim, Theodor-Kutzer-Ufer 1-3, 68167 Mannheim,
Germany. daniel.hausmann@medma.uni-heidelberg.de
Telephone: +49-621-3832276 Fax: +49-621-3833817
Received: January 24, 2014 Revised: March 23, 2014
Accepted: April 17, 2014
Published online: June 28, 2014

Abstract

AIM: To evaluate the impact of computed b = 1400 s/mm² (C-b1400) *vs* measured b = 1400 s/mm² (M-b1400) diffusion-weighted images (DWI) on lesion detection rate, image quality and quality of lesion demarcation using a modern 3T-MR system based on a small-field-of-view sequence (sFOV).

METHODS: Thirty patients (PSA: 9.5 ± 8.7 ng/mL; 68 ± 12 years) referred for magnetic resonance imaging (MRI) of the prostate were enrolled in this study. All measurements were performed on a 3T MR system. For DWI, a single-shot EPI diffusion sequence (b = 0, 100, 400, 800 s/mm²) was utilized. C-b1400 was calculated voxelwise from the ADC and diffusion images. Additionally, M-b1400 was acquired for evaluation and comparison. Lesion detection rate and maximum lesion diameters were obtained and compared. Image quality and quality of lesion demarcation were rated according to a 5-point Likert-type scale. Ratios of lesion-to-bladder as well as prostate-to-bladder signal intensity (SI) were calculated to estimate the signal-to-noise-ratio (SNR).

RESULTS: Twenty-four lesions were detected on M-b1400 images and compared to C-b1400 images. C-b1400 detected three additional cancer suspicious lesions. Overall image quality was rated significantly better and SI ratios were significantly higher on C-b1400 (2.3 ± 0.8 *vs* 3.1 ± 1.0, $P < 0.001$; 5.6 ± 1.8 *vs* 2.8 ± 0.9, $P < 0.001$). Comparison of lesion size showed no significant differences between C- and M-b1400 ($P = 0.22$).

CONCLUSION: Combination of a high b-value extrapolation and sFOV may contribute to increase diagnostic accuracy of DWI without an increase of acquisition time, which may be useful to guide targeted prostate biopsies and to improve quality of multiparametric MRI (mMRI) especially under economical aspects in a private practice setting.

© 2014 Baishideng Publishing Group Inc. All rights reserved.

Key words: Prostate cancer; Magnetic resonance imaging; Diffusion-weighted imaging; Ultra-high b-values; Extrapolated b-values

Core tip: Prostate cancer is the most common malignant tumor entity in males. Combination of a high b-value extrapolation and small-field-of-view sequence readout may contribute to increase diagnostic accuracy

of diffusion-weighted images without an increase of acquisition time, which may be useful to guide targeted prostate biopsies and to improve quality of multiparametric magnetic resonance imaging especially under economical aspects in a private practice setting.

Bittencourt LK, Attenberger UI, Lima D, Strecker R, de Oliveira A, Schoenberg SO, Gasparetto EL, Hausmann D. Feasibility study of computed *vs* measured high b-value (1400 s/mm²) diffusion-weighted MR images of the prostate. *World J Radiol* 2014; 6(6): 374-380 Available from: URL: http://www.wjgnet.com/1949-8470/full/v6/i6/374.htm DOI: http://dx.doi.org/10.4329/wjr.v6.i6.374

INTRODUCTION

Prostate cancer (PCa) is currently the most commonly diagnosed non-skin cancer and the second leading cause of cancer related death in the United States[1]. Recent technical improvements such as the beneficiary SNR gains of higher field strength made MRI a valuable diagnostic measure that allows to detect prostate cancer with a high diagnostic accuracy even at earlier disease stages[2]. Multi-parametric MR (mMRI) imaging is the mainstay of prostate cancer imaging[3-6], most commonly consisting of T2-weighted imaging (T2w), diffusion-weighted-imaging (DWI), dynamic contrast-enhanced imaging (DCE) and proton MR spectroscopy imaging (MRSI)[7-10]. Among those, DWI is probably the most promising technique, especially for detection of peripheral zone (pz) tumors and estimation of Pca aggressiveness[11-13], but also for monitoring therapy[14]. Recent studies indicate that the measurement of high b-values (2000 s/mm^2) increases the lesion detection rate[15], even though the ability to discriminate malignant from benign tissue in the pz is limited due to a significant overlap of ADC-values[16]. In clinical routine, the standard protocol commonly involves b-values from 0 to 800 s/mm^2. The use of higher b-values is currently limited by the two following factors: reduction of SNR at b-values > 1000 s/mm^2 due to T2 signal decay as a consequence of a prolonged TE[17] and cost effectiveness considerations due to a prolonged acquisition time, especially in a private practice setting. Due to these shortcomings, techniques that allow for the calculation of a high b-value DWI based on routinely measured lower b-values[18] seem to be appealing. In this context, recent studies indicate that computed DWI (cDWI) is feasible with good SNR and without additional scan time, which may improve disease detection[18].

On the one hand high field strength imaging at 3 Tesla (T) with higher intrinsic SNR is superior to 1.5 T for the detection of prostate cancer[19], on the other hand susceptibility artifacts related to the proximity of the pz to the air-filled rectum are more relevant. Recently, small FOV (sFOV) imaging strategies for DWI based on[20] the use of 2d radiofrequency (RF) excitation pulses for the excitation of a small volume spanning of the prostate region only were developed to overcome these shortcomings of 3T MRI[21] and allow for a reduction of artifacts and a smooth fusion with morphologic T2w images. For this study a b1400 sequence was extrapolated from a sFOV and low (< 1000 s/mm^2) b-value protocol to combine the advantages of reduced distortion artifacts and higher SNR of computed images. The purpose of this study is to compare lesion detection rate, image quality and quality of lesion demarcation of a computed (C-b1400) and a measured b = 1400 s/mm^2 (M-b1400) sequence based on a sFOV image set utilizing a modern 3T MR-system.

MATERIALS AND METHODS

Study population

Thirty consecutive patients (median PSA: 9.5 ± 8.7 ng/mL; mean age: 68 ± 12 years) who underwent functional prostate MR at our institution were enrolled in this study.

Among the indications for the study, 21 patients were referred due to elevated PSA levels, 4 for PCa staging, 4 for surveillance of post-treatment recurrence and one for suspected prostatitis.

MR Imaging

All measurements were performed on a 3 T clinical whole-body MR scanner (Verio, Siemens Healthcare, Erlangen, Germany) and state-of-the-art mMRI parameters were applied[19]. One hundred mL endorectal gel was administered prior to the examination, in order to reduce artifacts due to heterogeneous rectal content. For DWI, a single-shot EPI diffusion sequence with the following parameters was utilized: TE/TR= 63/4200 ms, 8 averages, FOV 300 mm × 93 mm, matrix 192 × 60, slice thickness 3.6 mm, no gap, SPAIR fat saturation, b-values = 0, 100, 400, 800 s/mm². An outer volume suppression by two sharp defined coronal saturation bands was applied which allowed to reduce the acquisition to a small rectangular FOV with an inplane resolution of 1.5 mm × 1.5 mm to gain SNR and to reduce distortion artifcats. The conventional full excitation was used in the sequence, followed by a short EPI readout covering only the sFOV in anterior-posterior direction. Total scan time for this sequence was 5 min 49 s. The ADC was calculated from diffusion images with all the measured b-values. C-b1400 was calculated voxelwise from the ADC and diffusion images according to:

$S(b_{1400}) = S0 * \exp(- ADC*b_{1400})$ with the pixel intensity SO in b = 0 s/mm².

A b-value of 1400 s/mm² was chosen to keep sequence parameters similar. Additionally, the M-b1400 sequence (b = 1400 s/mm², TE/TR = 73/4400 ms, all other parameters identical, duration: 1min45s) was acquired immediately after the original DWI sequence for evaluation and comparison (Figure 1).

Image analysis

Data sets of every patient were analyzed by two radiologists (DH, 3 years of experience in prostate imaging) and (LKB, 6 years of experience in prostate imaging) in con-

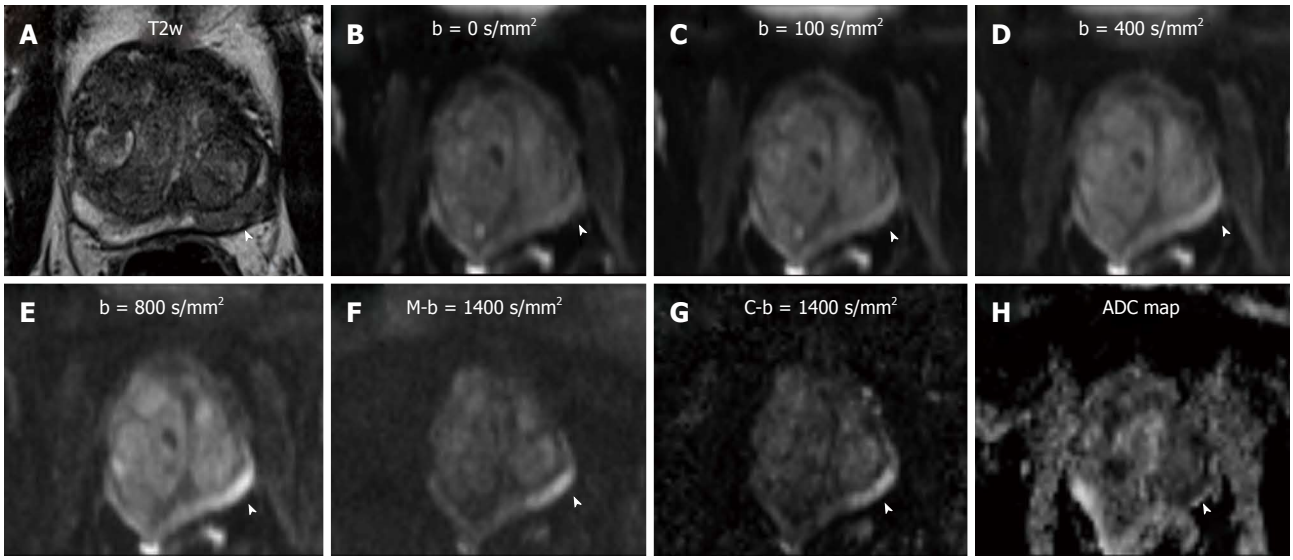

Figure 1 Axial T2-weighted image of an 88 years old patient with a PSA level of 8.2 ng/mL and negative findings upon digital rectal examination. T2w shows a focal hypointense lesion in the posterolateral left midgland pz (arrowhead in A). Measured b-values of 0, 100, 400 and 800 s/mm² (arrowheads in B, C, D and E, respectively) do not depict the suspected lesion with sufficient contrast to background prostate. M-b1400 shows good lesion-to-prostate contrast (arrowhead in F). C-b1400 depicts the lesion with the same lesion-to-prostate contrast and a slightly improved demarcation (arrowhead in G). The ADC value of the suspicious lesion was as low as 648 × 10^{-3} mm/s² [ADC map (H)].

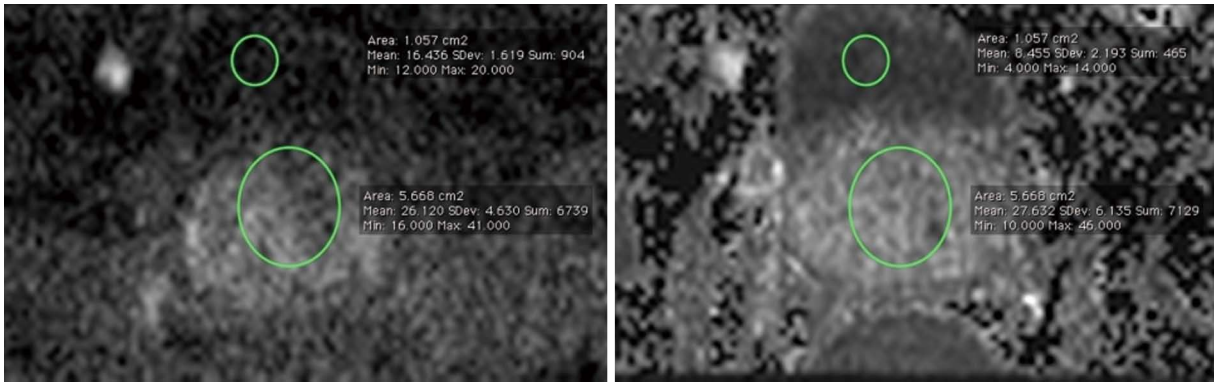

Figure 2 M-b1400 (left) and C-b1400 (right) images of a 63 years old patient with elevated PSA levels, at corresponding axial slice position. Region-of-interests were placed in the prostate and in the bladder content to obtain signal intensity-ratios to estimate signal-to-noise-ratio. Calculated b-value images show higher SI-ratios and more anatomical image details (*i.e.*, bladder contour).

sensus, For the measurement of prostate signal intensity, a region-of-interest (ROI) was placed overlying the visualized portion of the prostate at the level of the bladder. Another ROI which was placed in the bladder content served as reference. The size and the localization of these ROIs were chosen identical on both the C-b1400 and M-b1400, to allow for an adequate comparison (Figure 2).

Lesion detection rate (cancer suspicious lesions) as well as lesion diameters were obtained and compared. Image quality, quality of lesion demarcation and diagnostic confidence of the observers were rated according to a 5-point Likert-type scale from "1" ("excellent") to "5" ("poor"). Lesion-to-bladder and prostate-to-bladder signal-intensity (SI) ratios were obtained and compared to estimate signal-to-noise-ratio (SNR).

Statistical analysis

SPSS (Version 20; IBM SPSS Statistics, United States) was used for statistical analysis. Measured values did not show Gaussian distribution so Wilcoxon-tests were performed for comparison of C-b1400 and M-b1400.

RESULTS

Patients and lesions

In 30 consecutive patients, a total of 27 lesions were evaluated. Lesions were rated as prostate cancer (n = 15), nodules of benign prostate hyperplasia (BPH) (n = 8) and cancer recurrence (n = 4). Two patients presented with locally recurrent cancer after prostatectomy.

Image quality, lesion detection rate, lesion demarcation and diagnostic confidence

Image quality was rated significantly better in C-b1400 (mean = 2.3 ± 0.8) compared to M-b1400 (mean = 3.1 ± 1.0; P < 0.001). Moreover, the computed images sub-

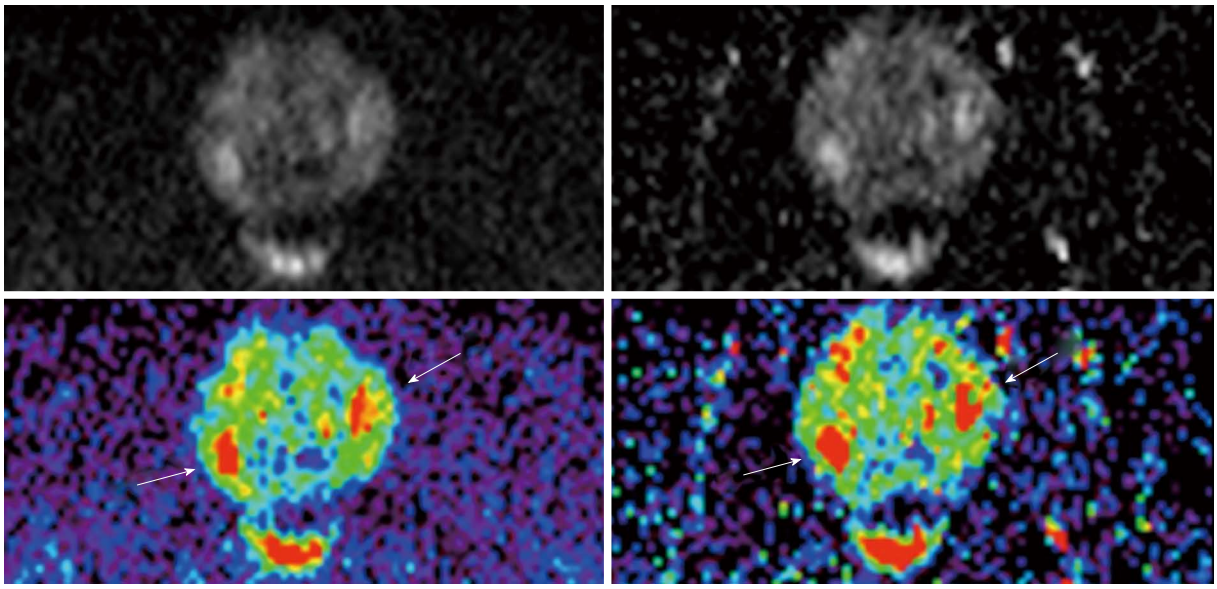

Figure 3 M-b1400 (left column) and C-b1400 (right column) images of the same patient. Demarcation of two oval hyperintense suspicious lesions is very good on both images (arrows).

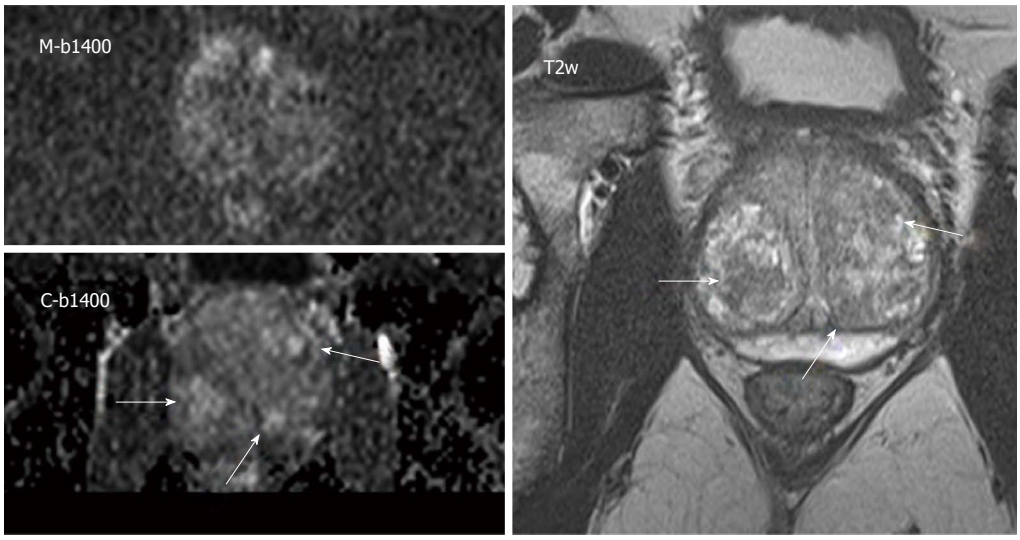

Figure 4 Images of a 68 years old patient with elevated PSA levels and signs of benign prostate hyperplasia. M-b1400 (upper image on the left) was acquired with reduced image quality due to distortion artifacts. The C-b1400 (below) in corresponding slice position and identical window level shows an improved image quality with demarcation of several lesions that were rated as benign benign prostate hyperplasia-nodules taking into account T2w (right image) and dynamic contrast-enhanced imaging.

jectively showed more anatomical detail. We did not find significant differences regarding the quality of lesion demarcation with a trend to better results of C-b1400 (mean = 2.6 ± 1.0 *vs* 2.8 ± 0.9, respectively; $P = 0.29$) (Figures 3 and 4).

C-b1400 detected 3 additional cancer suspicious lesions compared to M-b1400 images, which were confirmed by ADC maps, T2w and DCE evaluation. Overall diagnostic confidence was rated slightly better on C-b1400, even though results were not significantly different (2.2 ± 0.9 *vs* 2.1 ± 0.8, $P = 0.48$, respectively) (Table 1).

SI-ratios and lesion size

Significantly higher SI-ratio of prostate-to-bladder and lesion-to-bladder were obtained for C-b1400 compared to M-b1400 ($P < 0.001$ and $P < 0.001$, respectively).

Comparison of lesion size showed no significant differences between calculated and measured images ($P < 0.22$) (Table 2). All statistical data are given as means and standard deviations.

DISCUSSION

The study compared lesion detection rate, image quality and quality of lesion demarcation of a C-b1400 derived from a standard DWI protocol with M-b1400 images. A significantly better image quality of the C-b1400 was observed. Moreover, C-b1400 revealed more additional sus-

Table 1 Comparison of C-b1400 and M-b1400 images; image qualitiy, quality of lesion demarcation and level of confidence were rated according to a 5-point Likert-type scale

b = 1400 s/mm^2	Image quality (n = 30)	Lesion demarcation (n = 24)	Diagnostic confidence (n = 30)
M-b1400	3.1 ± 1.0	2.8 ± 0.9	2.2 ± 0.9
C-b1400	2.3 ± 0.8	2.6 ± 1.0	2.1 ± 0.8
P-value	< 0.001	0.29	0.48

Table 2 Objective parameters: Prostate-to-bladder and lesion-to-bladder signal intensity ratios were obtained to estimate signal-to-noise-ratio and contrast-to-noise ratio

b = 1400 s/mm^2	SI prostate/bladder (n = 28)	SI lesion/bladder (n = 24)	Lesion diameter (mm) (n = 24)
M-b1400	1.9 ± 0.5	2.8 ± 0.9	16.9 ± 10.0
C-b1400	3.7 ± 1.0	5.6 ± 1.8	17.7 ± 10.0
P-value	< 0.001	< 0.001	0.22

Lesion diameters are presented in units of mm. SI: Signal intensity.

picious lesions that were confirmed by comparison with ADC maps and T2w. C-b1400 exhibited higher prostate-to-bladder and lesion-to-bladder SI ratios than M-b1400, which could indicate better SNR.

Multiple studies have tried to determine an optimal b-value to visualize prostate cancer using DWI at 3 T. A study by Metens *et al*[22] assessed examinations of forty-one patients with biopsy proven prostate cancer who underwent 3 T DWI performed with 5 b-values (1000, 1500, 2000 and 2500 s/mm^2) using a 16-channel coil. Best lesion visibility, the central gland-to-lesion (CG-L) and the peripheral zone-to-lesion (PZ-L) contrast-to-noise ratio (CNR) were compared between different b-value images. In a subset of 29 patients a high resolution b = 1500 s/mm^2 DWI sequence was additionally assessed. The b = 1500 s/mm^2 and b = 2000 s/mm^2 images provided the best lesion visibility. The highest CG-L and PZ-L CNR were obtained with b = 1500 s/mm^2 ($P < 0.01$).

Another recent study assessed the diagnostic accuracy of 3T DWI for detection of prostate cancer by using different b-values. Seventy-three patients underwent MRI at 3 T. Three MRI sets were reviewed by two radiologists: MRI and DWI (b = 500 s/mm^2) (protocol A), MRI and DWI (b = 1000 s/mm^2) (protocol B), and MRI and DWI (b = 2000 s/mm^2) (protocol C). Areas under the receiver operating characteristic curve (AUCs) were calculated. The mean of the AUCs in protocol C was larger than those in protocol A and in protocol B ($P < 0.05$). The authors concluded that a b-value = 2000 s/mm^2 at 3 T can improve the diagnostic accuracy for detection of prostate cancer[15]. On the other hand, a study to determine whether the ADC obtained from a high b-value (2000 s/mm^2) is superior to that obtained from a standard b-value (1000 s/mm^2) in a monoexponential model to discriminate malignant from benign pz tissue found little diagnostic advantage of the high b-value due to significant ADC overlap[16].

Blackledge *et al*[18] described a method to extrapolate high-b-value images from DWI performed at lower b-values which allowed for an improved lesion conspicuity. Computation of DWI resulted in a higher SNR compared with measured DWI, especially at b-values > 840 s/mm^2. Moreover, in oncologic patients, a computed b-value of 2000 s/mm^2 showed good image quality and high background suppression. Evaluation of images with a computed b-value of 2000 s/mm^2 resulted in higher overall diagnostic sensitivity (96.0%) and specificity (96.6%), compared with a measured b-value of 900 s/mm^2 (sensitivity, 89.4%; specificity, 87.5%; $P < 0.01$).

In concordance with this study, our results suggest that computed b1400-images can be obtained with a better image quality due to lesser artifacts and more anatomical detail than measured b1400-images, probably as a benefit of the high SNR of the original lower b-value image sets. Nevertheless, there was no significant difference of the overall diagnostic confidence between the two image sets with a trend to better results for C-b1400 indicating a similar diagnostic performance of both, even though objectively three additional cancer suspicious lesions could be detected on C-b1400. Moreover, the comparison of the diameters of the largest lesions on measured and computed b1400 images did not reveal a significant difference between the techniques (Table 2).

Our study had a number of limitations. First of all, due to the private practice setting, there was no histopathologic confirmation of the assigned lesions. Then again, the study predominantly focused on image quality, lesion detection rate and lesion conspicuity. With regards to the reported ADC overlap of lesions, we believe that the primary value of the presented technique is to detect and draw attention to any lesion. The dignity of these lesions should be evaluated taking into account the clinical context of the patients and additional sequences such as T2w, DCE and MRSI. Moreover, we applied a mono-exponential model for the computation of C-b1400 images. Several recent publications report that there is a significant deviation from a pure Gaussian probabilistic model when applying high b-values ⩾ 1000 s/mm^2. It was confirmed that the deviation quantified by kurtosis has a greater sensitivity than ADC or the diffusion constant D for the differentiation between PCa and benign lesions of the pz (93.3% *vs* 78.5% and 83.5%)[23]. A more recently published study shows that kurtosis has the best performance in differentiating PCa from benign prostate, using different sets of b-values[24]. In both studies, high b-values up to 2000-2300 s/mm^2 were applied for acquisition which results in a relevant deviation from a pure Gaussian probabilistic model. On the other hand, the impact of kurtosis in ADC calculation using lower b-values up to 800 is small and can be neglected, which falls in the range of the b-values acquired in the present study[25]. Furthermore, in this preliminary feasibility study, patients were included consecutively, and the indications and clinical contexts for the examinations were not homogeneous. In addition, a major concern of b-values above 1000 s/mm^2 in DWI aquisition is their intrinsically lower SNR

and the consecutive compromise of the calculation of the ADC. In clinical practice, stronger diffusion encodings are usually achieved by the prolongation of the motion probing gradients, which leads to a longer TE and an increased T2 decay of the signal. As a result, the highest chosen b-value ultimately determines the TE of the whole diffusion scan and may thus affect the SNR of the whole image set. It is therefore appealing to avoid signal loss by maintaing a shorter TE for conventional diffusion acqusition protocol, while associating the computation of high b-value image sets (*i.e.*, above b = 1200 s/mm^2), in order to benefit from the better SNR of the calculated ADC. In this study, only the readout was reduced to a sFOV, whereas more sophisticated techniques combine a sFOV readout with a sFOV excitation pulse[20]. Finally, a direct measurement of SNR was not feasible due to the sFOV which did not allow for inclusion of surrounding air for precise calculations. Nevertheless, the prostate-to-bladder and lesion-to-bladder SI ratios were calculated as a potential surrogate for the actual SNR.

In conclusion, computed high b-value images derived from a sFOV DWI protocol is clinically feasible and may increase accuracy in comparison to measured b = 1400 s/mm^2 images, without an increase of examination time, which is especially important regarding further application in clinical routine in a time and cost-efficient manner. Additionally, this approach allows for the calculation of virtually any given b-value from the originally measured DWI sequence, which can be further fine-tuned for different clinical settings and applications.

Combination of a high b-value extrapolation and sFOV readout may contribute to increase diagnostic accuracy of DWI without an increase of acquisition time, which may be useful to guide targeted prostate biopsies and to improve quality of mMRI especially under economical aspects in a private practice setting. However, further studies are needed to proof the preliminary results of this study in larger cohorts of clinical patients.

COMMENTS

COMMENTS

Prostate cancer is the most common malignant tumor entity in males. Differentiation between benign and malignant prostatic disease is hindered by a similar appearance on morphologic images. Multiparametric magnetic resonance imaging (mMRI), mostly consisting of high-resolution T2-weighted sequences, Dynamic Contrast Enhanced Imaging (DCE) and Diffusion-Weighted Imaging (DWI) has extensively improved sensitivity and specificity of the examination. It has been demonstrated that high b-values of DWI contribute to improve lesion detection rate which helps to guide targeted prostate biopsies. These high b-values can either be measured directly or extrapolated based on a standard low b-value DWI sequence.

Research frontiers

The use of higher b-values is currently limited by the two following factors: reduction of SNR at b-values > 1000 s/mm^2 due to T2 signal decay as a consequence of a prolonged TE and cost effectiveness considerations due to a prolonged acquisition time, especially in a private practice setting. Due to these shortcomings, techniques that allow for the calculation of a high b-value DWI based on routinely measured lower b-values seem to be appealing. On the one hand high field strength imaging at 3 Tesla with higher intrinsic SNR is superior to 1.5 T for the detection of prostate cancer, on the other hand susceptibility artifacts related to the proximity of the peripheral zone to the air-filled rectum are more relevant. Recently, small FOV (sFOV) imaging strategies for DWI based on the use of 2d radiofrequency excitation pulses for the excitation of a small volume spanning of the prostate region only were developed to overcome these shortcomings of 3T MRI and allow for a reduction of artifacts and a smooth fusion with morphologic T2w images

Innovations and breakthroughs

For this study a b1400 sequence was extrapolated from a sFOV and low (< 1000 s/mm^2) b-value protocol to combine the advantages of reduced distortion artifacts and higher SNR of computed images. The purpose of this study is to compare lesion detection rate, image quality and quality of lesion demarcation of a computed (C-b1400) and a measured b = 1400 s/mm^2 (M-b1400) sequence based on a sFOV image set utilizing a modern 3T MR-system.

Applications

The study results suggest that extrapolated high b-value images may contribute to increase lesions detection rate in a cost- and time efficient manner, which may help to guide targeted prostate biopsies.

Terminology

Prostate cancer: Early prostate cancer usually causes no symptoms. Sometimes, however, prostate cancer does cause symptoms, often similar to those of diseases such as benign prostatic hyperplasia; Diffusion-weighted Imaging (DWI): DWI measures the movement of protons in between cells and is related to cell density. Low b-value images are rather T2-weighted and are sensitive to "T2-shine-through"-effects whereas high b-values are more useful to evaluate the properties of tissue diffusability.

Peer review

The authors compared the utility of computed *vs* measured high b-value DWI for the assessment of prostate lesions. It is well written.

REFERENCES

1 **Brawley OW**. Prostate cancer epidemiology in the United States. *World J Urol* 2012; **30**: 195-200 [PMID: 22476558 DOI: 10.1007/s00345-012-0824-2]

2 **Klimberg I**, Locke DR, Madore RA, Smith WW. Early prostate cancer: is there a need for new treatment options? *Urol Oncol* 2003; **21**: 105-116 [PMID: 12856638 DOI: 10.1016/S1078-1439(02)00211-9]

3 **Weidner AM**, Michaely HJ, Lemke A, Breitinger L, Wenz F, Marx A, Schoenberg SO, Dinter DJ. Value of multiparametric prostate MRI of the peripheral zone. *Z Med Phys* 2011; **21**: 198-205 [PMID: 21247742 DOI: 10.1016/j.zemedi.2010.12.004]

4 **Turkbey B**, Pinto PA, Mani H, Bernardo M, Pang Y, McKinney YL, Khurana K, Ravizzini GC, Albert PS, Merino MJ, Choyke PL. Prostate cancer: value of multiparametric MR imaging at 3 T for detection--histopathologic correlation. *Radiology* 2010; **255**: 89-99 [PMID: 20308447 DOI: 10.1148/radiol.09090475]

5 **Caldas ME**, Miranda LC, Bittencourt LK. Magnetic resonance imaging in staging of locoregional prostate cancer: comparison of results with analysis post-surgical histopathology. *Rev Col Bras Cir* 2010; **37**: 447-449 [PMID: 21340261]

6 **Hoeks CM**, Barentsz JO, Hambrock T, Yakar D, Somford DM, Heijmink SW, Scheenen TW, Vos PC, Huisman H, van Oort IM, Witjes JA, Heerschap A, Fütterer JJ. Prostate cancer: multiparametric MR imaging for detection, localization, and staging. *Radiology* 2011; **261**: 46-66 [PMID: 21931141 DOI: 10.1148/radiol.11091822]

7 **Scheenen TW**, Fütterer J, Weiland E, van Hecke P, Lemort M, Zechmann C, Schlemmer HP, Broome D, Villeirs G, Lu J, Barentsz J, Roell S, Heerschap A. Discriminating cancer from noncancer tissue in the prostate by 3-dimensional proton magnetic resonance spectroscopic imaging: a prospective multicenter validation study. *Invest Radiol* 2011; **46**: 25-33 [PMID: 21188832 DOI: 10.1097/RLI.0b013e3181f54081]

8 **Scherr MK**, Seitz M, Müller-Lisse UG, Ingrisch M, Reiser MF, Müller-Lisse UL. MR-perfusion (MRP) and diffusion-weighted imaging (DWI) in prostate cancer: quantitative and model-based gadobenate dimeglumine MRP parameters in detection of prostate cancer. *Eur J Radiol* 2010; **76**: 359-366

[PMID: 20471189 DOI: 10.1016/j.ejrad.2010.04.023]
9 **Schlemmer HP**. [Multiparametric MRI of the prostate: method for early detection of prostate cancer?]. *Rofo* 2010; **182**: 1067-1075 [PMID: 20972932 DOI: 10.1055/s-0029-1245786]
10 **Fütterer JJ**, Heijmink SW, Scheenen TW, Veltman J, Huisman HJ, Vos P, Hulsbergen-Van de Kaa CA, Witjes JA, Krabbe PF, Heerschap A, Barentsz JO. Prostate cancer localization with dynamic contrast-enhanced MR imaging and proton MR spectroscopic imaging. *Radiology* 2006; **241**: 449-458 [PMID: 16966484 DOI: 10.1148/radiol.2412051866]
11 **Bittencourt LK**, Barentsz JO, de Miranda LC, Gasparetto EL. Prostate MRI: diffusion-weighted imaging at 1.5T correlates better with prostatectomy Gleason Grades than TRUS-guided biopsies in peripheral zone tumours. *Eur Radiol* 2012; **22**: 468-475 [PMID: 21913058 DOI: 10.1007/s00330-011-2269-1]
12 **Oto A**, Yang C, Kayhan A, Tretiakova M, Antic T, Schmid-Tannwald C, Eggener S, Karczmar GS, Stadler WM. Diffusion-weighted and dynamic contrast-enhanced MRI of prostate cancer: correlation of quantitative MR parameters with Gleason score and tumor angiogenesis. *AJR Am J Roentgenol* 2011; **197**: 1382-1390 [PMID: 22109293 DOI: 10.2214/AJR.11.6861]
13 **Somford DM**, Hambrock T, Hulsbergen-van de Kaa CA, Fütterer JJ, van Oort IM, van Basten JP, Karthaus HF, Witjes JA, Barentsz JO. Initial experience with identifying high-grade prostate cancer using diffusion-weighted MR imaging (DWI) in patients with a Gleason score ≤ 3 + 3 = 6 upon schematic TRUS-guided biopsy: a radical prostatectomy correlated series. *Invest Radiol* 2012; **47**: 153-158 [PMID: 22293513]
14 **Park SY**, Kim CK, Park BK, Park W, Park HC, Han DH, Kim B. Early changes in apparent diffusion coefficient from diffusion-weighted MR imaging during radiotherapy for prostate cancer. *Int J Radiat Oncol Biol Phys* 2012; **83**: 749-755 [PMID: 22154286]
15 **Ohgiya Y**, Suyama J, Seino N, Hashizume T, Kawahara M, Sai S, Saiki M, Munechika J, Hirose M, Gokan T. Diagnostic accuracy of ultra-high-b-value 3.0-T diffusion-weighted MR imaging for detection of prostate cancer. *Clin Imaging* 2012; **36**: 526-531 [PMID: 22920357 DOI: 10.1016/j.clinimag.2011.11.016]
16 **Kitajima K**, Kaji Y, Kuroda K, Sugimura K. High b-value diffusion-weighted imaging in normal and malignant peripheral zone tissue of the prostate: effect of signal-to-noise ratio. *Magn Reson Med Sci* 2008; **7**: 93-99 [PMID: 18603841 DOI: 10.2463/mrms.7.93]
17 **Dietrich O**, Biffar A, Baur-Melnyk A, Reiser MF. Technical aspects of MR diffusion imaging of the body. *Eur J Radiol* 2010; **76**: 314-322 [PMID: 20299172 DOI: 10.1016/j.ejrad.2010.02.018]
18 **Blackledge MD**, Leach MO, Collins DJ, Koh DM. Computed diffusion-weighted MR imaging may improve tumor detection. *Radiology* 2011; **261**: 573-581 [PMID: 21852566 DOI: 10.1148/radiol.11101919]
19 **Barentsz JO**, Richenberg J, Clements R, Choyke P, Verma S, Villeirs G, Rouviere O, Logager V, Fütterer JJ. ESUR prostate MR guidelines 2012. *Eur Radiol* 2012; **22**: 746-757 [PMID: 22322308]
20 **Reischauer C**, Wilm BJ, Froehlich JM, Gutzeit A, Prikler L, Gablinger R, Boesiger P, Wentz KU. High-resolution diffusion tensor imaging of prostate cancer using a reduced FOV technique. *Eur J Radiol* 2011; **80**: e34-e41 [PMID: 20638208 DOI: 10.1016/j.ejrad.2010.06.038]
21 **Finsterbusch J**. Improving the performance of diffusion-weighted inner field-of-view echo-planar imaging based on 2D-selective radiofrequency excitations by tilting the excitation plane. *J Magn Reson Imaging* 2012; **35**: 984-992 [PMID: 22170770]
22 **Metens T**, Miranda D, Absil J, Matos C. What is the optimal b value in diffusion-weighted MR imaging to depict prostate cancer at 3T? *Eur Radiol* 2012; **22**: 703-709 [PMID: 21971824 DOI: 10.1007/s00330-011-2298-9]
23 **Rosenkrantz AB**, Sigmund EE, Johnson G, Babb JS, Mussi TC, Melamed J, Taneja SS, Lee VS, Jensen JH. Prostate cancer: feasibility and preliminary experience of a diffusional kurtosis model for detection and assessment of aggressiveness of peripheral zone cancer. *Radiology* 2012; **264**: 126-135 [PMID: 22550312 DOI: 10.1148/radiol.12112290]
24 **Mazzoni LN**, Lucarini S, Chiti S, Busoni S, Gori C, Menchi I. Diffusion-weighted signal models in healthy and cancerous peripheral prostate tissues: comparison of outcomes obtained at different b-values. *J Magn Reson Imaging* 2014; **39**: 512-518 [PMID: 23723087]
25 **Quentin M**, Blondin D, Klasen J, Lanzman RS, Miese FR, Arsov C, Albers P, Antoch G, Wittsack HJ. Comparison of different mathematical models of diffusion-weighted prostate MR imaging. *Magn Reson Imaging* 2012; **30**: 1468-1474 [PMID: 22819178]

P- Reviewers: Desai DJ, Msaouel P **S- Editor**: Wen LL
L- Editor: A **E- Editor**: Zhang DN

World Journal of Radiology

Submit a Manuscript: http://www.wjgnet.com/esps/
Help Desk: http://www.wjgnet.com/esps/helpdesk.aspx
DOI: 10.4329/wjr.v6.i6.381

World J Radiol 2014 June 28; 6(6): 381-387
ISSN 1949-8470 (online)
© 2014 Baishideng Publishing Group Inc. All rights reserved.

PROSPECTIVE STUDY

Coronary artery calcium score on low-dose computed tomography for lung cancer screening

Teresa Arcadi, Erica Maffei, Nicola Sverzellati, Cesare Mantini, Andrea I Guaricci, Carlo Tedeschi, Chiara Martini, Ludovico La Grutta, Filippo Cademartiri

Teresa Arcadi, Department of Radiology, SDN Foundation, IRCCS, 80131 Naples, Italy
Erica Maffei, Filippo Cademartiri, Cardio-Vascular Imaging Unit, Department of Radiology, Giovanni XXIII Clinic, Monastier di Treviso, 31050 Treviso, Italy
Erica Maffei, Filippo Cademartiri, Department of Radiology, Erasmus Medical Center University, Rotterdam, 3015 CE Rotterdam, The Netherlands
Nicola Sverzellati, Department of Radiology, Azienda Ospedaliero-Universitaria, 43100 Parma, Italy
Cesare Mantini, Department of Radiology, Università di Chieti, 66100 Chieti, Italy
Andrea I Guaricci, Department of Cardiology, Università di Foggia, 71121 Foggia, Italy
Carlo Tedeschi, Department of Cardiology, San Gennaro Hospital, Naples, 80136 Napoli, Italy
Ludovico La Grutta, Department of Radiology, University of Palermo, Italy
Author contributions: Maffei E, Sverzellati N and Cademartiri F conceived and designed the study; Arcadi T, Mantini C, Guaricci AI, Tedeschi C, Martini C and La Grutta L acquired and analysed data; Arcadi T and Maffei E drafted the manuscript; Sverzellati N, Mantini C, Guaricci AI, Tedeschi C, Martini C, La Grutta L and Cademartiri F revised the manuscript critically for important intellectual content; Arcadi T, Maffei E, Sverzellati N, Mantini C, Guaricci AI, Tedeschi C, Martini C, La Grutta L and Cademartiri F provided final approval for the version to be published.
Correspondence to: Dr. Filippo Cademartiri, MD, PhD, FESC, FSCCT, Professor, Cardio-Vascular Imaging Unit, Department of Radiology, Giovanni XXIII Clinic, Via Giovanni XXIII 7, Monastier di Treviso, 31050 Treviso, Italy. filippocademartiri@gmail.com
Telephone: +39-422-896710 Fax: +39-422-896507
Received: December 10, 2013 Revised: February 9, 2014
Accepted: May 8, 2014
Published online: June 28, 2014

Abstract

AIM: To evaluate the feasibility of coronary artery calcium score (CACS) on low-dose non-gated chest CT (ngCCT).

METHODS: Sixty consecutive individuals (30 males; 73 ± 7 years) scheduled for risk stratification by means of unenhanced ECG-triggered cardiac computed tomography (gCCT) underwent additional unenhanced ngCCT. All CT scans were performed on a 64-slice CT scanner (Somatom Sensation 64 Cardiac, Siemens, Germany). CACS was calculated using conventional methods/scores (Volume, Mass, Agatston) as previously described in literature. The CACS value obtained were compared. The Mayo Clinic classification was used to stratify cardiovascular risk based on Agatston CACS. Differences and correlations between the two methods were compared. A *P*-value < 0.05 was considered significant.

RESULTS: Mean CACS values were significantly higher for gCCT as compared to ngCCT (Volume: 418 ± 747 *vs* 332 ± 597; Mass: 89 ± 151 *vs* 78 ± 141; Agatston: 481 ± 854 *vs* 428 ± 776; $P < 0.05$). The correlation between the two values was always very high (Volume: $r = 0.95$; Mass: $r = 0.97$; Agatston: $r = 0.98$). Of the 6 patients with 0 Agatston score on gCCT, 2 (33%) showed an Agatston score > 0 in the ngCCT. Of the 3 patients with 1-10 Agatston score on gCCT, 1 (33%) showed an Agatston score of 0 in the ngCCT. Overall, 23 (38%) patients were reclassified in a different cardiovascular risk category, mostly (18/23; 78%) shifting to a lower risk in the ngCCT. The estimated radiation dose was significantly higher for gCCT (DLP 115.8 ± 50.7 *vs* 83.8 ± 16.3; Effective dose 1.6 ± 0.7 mSv *vs* 1.2 ± 0.2 mSv; $P < 0.01$).

CONCLUSION: CACS assessment is feasible on ngCCT; the variability of CACS values and the associated re-stratification of patients in cardiovascular risk groups should be taken into account.

© 2014 Baishideng Publishing Group Inc. All rights reserved.

Key words: Coronary artery calcium score; Lung cancer

screening; High-resolution computed tomography; Unenhanced chest computed tomography; Cardiovascular risk stratification

Core tip: Low dose chest computed tomography (CT)/high-resolution CT (HRCT) is entering the clinical practice for the screening of individuals at high risk of lung cancer. This study provides evidence that a surrogate stratification of cardiovascular risk can be performed on low-dose chest CT performed in the settings of lung cancer screening. This finding has some relevant consequences since lung cancer and atherosclerosis share some similarities concerning risk factors (smoking), patients' population (age decade and gender prevalence).

Arcadi T, Maffei E, Sverzellati N, Mantini C, Guaricci AI, Tedeschi C, Martini C, La Grutta L, Cademartiri F. Coronary artery calcium score on low-dose computed tomography for lung cancer screening. *World J Radiol* 2014; 6(6): 381-387 Available from: URL: http://www.wjgnet.com/1949-8470/full/v6/i6/381.htm DOI: http://dx.doi.org/10.4329/wjr.v6.i6.381

INTRODUCTION

Coronary artery calcium score (CACS) has been regarded as an independent predictor for cardiovascular risk stratification[1,2]. CACS has been performed in asymptomatic individuals for at least two decades using Electron-Beam Computed Tomography (EBCT) and more recently using Multi-Slice Computed Tomography (MSCT), however it has not entered guidelines for cardiovascular risk stratification until recently. In several countries it is applied as a part of primary prevention mostly based on self-referral.

With the introduction of MSCT the potential for anatomical screening has become a clinical reality[3,4]. Besides Coronary Artery Disease (*i.e.*, CACS), also colon cancer (*i.e.*, Virtual Colonoscopy) and lung cancer (*i.e.*, low-dose chest CT) have been proposed as topics for screening[5]. While CACS has already showed a potential for screening asymptomatic individuals, colon cancer screening and lung cancer screening are undergoing large multicenter studies to test whether CT is viable tool for this purpose[6-8].

A very basic observation relies on the fact that in the context of lung cancer screening, the data collected (*i.e.*, low-dose chest CT) are somehow similar to the ones collected for CACS assessment. The main difference relies on the fact that low-dose chest CT is not performed with ECG synchronization protocols (*i.e.*, retrospective ECG gating or prospective ECG triggering), however the increasing speed of MSCT equipment may reduce the discrepancy between the two protocols. The hypothesis is that in principle it is possible to assess CACS on low-dose chest CT (ngCCT: non-gated low-dose chest CT). Therefore, we wanted to test the differences between the CACS values obtained with ngCCT and conventional ECG-gated CT protocol (gCCT: gated Cardiac CT) in the same population of asymptomatic individuals. The aim of the study was compare the CACS values obtained with gCCT (as the reference standard) to ngCCT, and to verify the feasibility and variability of cardiovascular risk stratification using the two protocols.

A novelty of our paper is the comparison of gCCT CACS values with ngCCT ones obtained analyzing dataset reconstructed with 5 mm slice thickness and 5.0mm increment unlike other previously published studies based on dataset with 3 mm, 2.5mm, 1.5 mm or 1mm slice thickness[3,4,9,10]. The feasibility of cardiovascular risk stratification using non gated CACS values obtained with the same standard dataset routinely reconstructed (5mm slice thickness) would allow a wide and fast use in daily clinical practice. The description of the degree of cardiovascular risk reclassification using ngCCT *vs* gCCT values is another innovative aspect of our study.

MATERIALS AND METHODS

Patients

During a period of 6 mo we prospectively enrolled 60 consecutive asymptomatic individuals (30 males; 72 ± 10 years) who were referred for the assessment of CACS (Table 1). The individuals were excluded based on conventional contra-indications to Radiation Exposure (*i.e.*, potential or actual pregnancy, age < 50 years). All patients underwent two CT scans: the first (gCCT) for CACS purposes and the second for lung parenchyma (ngCCT) assessment, using conventional parameters.

We collected demographics (age, gender, height, weight), heart rate during the scans, and radiation dose for both scans in all patients.

Informed consent was obtained from all patients and the local Medical Ethical Committee approved the study.

CT scan

All individuals underwent two un-enhanced CT scans (Table 2). For gCCT, scanning was performed by using 64-slice CT system (Sensation 64 Cardiac, Siemens Medical Solutions, Forchheim, Germany) and spiral retrospective ECG gating technique. All CT scans of the heart (from the carina to the apex of the heart) were acquired during one inspiratory breath-hold without the use of the contrast medium and without the additional administration of chronotropic drugs. Scan parameters were: detector collimation: 32 mm × 0.6 mm, Z-axis focal spot alternation resulting in simultaneous acquisition of 64 slices; gantry rotation time: 330 ms; effective temporal resolution 165 ms; table feed per rotation: 3.84 mm; pitch 0.2; tube voltage 120 kV; tube power 150 mAs; direction in which data acquisition proceeded: cranio-caudal.

Image were reconstructed with the following parameters: slice thickness 3 mm, slice increment 1.5 mm, field of view (FOV) 150-180 mm, convolution kernel filtering for CACS (b35f). Temporal windows were set at -350ms prior to the next R wave.

For ngCCT, scanning was performed by using 64-slice

Table 1 Demographics *n* (%)

Clinical characteristics	Population (*n* = 60)
Age (yr, mean ± SD)	73.4 ± 7.1
Male gender	30 (50)
BMI (kg/m², mean ± SD)	25.9 ± 4.5
BSA (m², mean ± SD)	1.8 ± 0.2
Mean heart rate (bpm, mean ± SD)	73.0 ± 15.7
Additional negative chronotropic drugs	None

Baseline characteristics of study population. BMI: Body mass index; BSA: Body surface area.

Table 2 scan and reconstruction parameters

Parameters	gCCT	ngCCT
Scan parameters		
Technique	Spiral	Spiral
kV	120	120
mAs	150	30
Gantry rotation time (ms)	330	330
Individual detector width (mm)	1.2	0.6
Number of detectors	20 × 2	32 × 2
ECG gating	Yes	No
Prospective ECG modulation of tube current	Yes	No
Table feed/s (mm)	14.4	86.4
Pitch	0.2	1.5
Scan range	Carina-Apex	Chest
DLP (mGy; mean ± SD)	116 ± 51	84 ± 16[a]
Effective dose (mSv; factor = 0.014; mean ± SD)	2.0 ± 0.9	1.2 ± 0.5[a]
Effective dose (mSv; factor = 0.014; median, IQR)	1.61; 1.15-2.0	1.13; 1.05-1.20[a]
Reconstruction parameters		
Effective slice width (mm)	3.0	5.0
Reconstruction increment (mm)	1.5	5.0
FOV (mm)	140-160	250-300
Kernel filtering	B35f[1]	B30f (medium-smooth)

The Table shows the scan parameters for gCCT and ngCCT. gCCT *vs* ngCCT, [a]$P < 0.05$; [1]Dedicated filter for calcium scoring. gCCT: ECG gated cardiac computed tomography; ngCCT: Non-gated chest computed tomography; FOV: Field of view; ECG: Electrocardiogram; DLP: Dose length product.

CT system (Sensation 64 Cardiac, Siemens Medical Solutions, Forchheim, Germany) and spiral non ECG gated technique. All CT scans of the whole lung were acquired during one deep inspiratory breath-hold without the use of IV contrast medium. Neither electrocardiographic triggering, nor any dose-modulation system were used. The scanner was regularly calibrated to allow reliable measurements and comparison between examinations. Standard low dose chest CT parameters were: detector collimation 0.6 mm, slices per rotation 32 × 2, gantry rotation time 330 ms, pitch 1.5, tube voltage 120 kV, tube power 30 mAs.

Image were reconstructed with the following parameters: slice thickness 5 mm, slice increment 5mm, field of view (FOV) 250-300 mm, convolution kernel filtering medium-smooth (b30f).

CT data analysis

The images of the study population were transferred to a dedicated CT workstation (MMWP, Siemens Medical Solutions, Forchheim, Germany) and analyzed by one operator with more than five years of experience in cardiac imaging, who was blinded to participants' data and scan protocol. CACS assessment was performed using a dedicated software (CaScore, Siemens, Forchheim, Germany). For the purpose of intra- and inter-observer variability assessment the main observer re-red all scans and a second operator with three years of experience in cardiac imaging red the entire CT dataset. There was a time of 2 months between the two additional readings (one of the main operator for intra-observer variability and one for the additional reader for the inter-observer variability).

Statistical analysis

Continuous variables are expressed as mean ± SD and/or median, where appropriate. Differences between groups were compared using the Student's *t* and Wilcoxon tests, as appropriate. Correlation was assessed using the Pearson's *r* test while the bias was assessed using the Bland-Altman method. Intra- and inter-observer variability were assessed for all CACS measurements and compared using the Bland-Altman method.

Radiation dose (Dose Length Product: DLP) was estimated using the CTDIvol multiplied for the scan length. For the estimation of the effective dose a factor of 0.014 was applied[11].

Statistical analysis was performed with SPSS (version 12.0, SPSS Inc., Chicago, IL, United States) and MedCalc (version 9.3.0.0., MedCalc Software, Mariakerke, Belgium) software. Significance was set at $P < 0.05$.

RESULTS

The scans were successful in all patients. Mean heart rate during the scans was 73 ± 16 bpm.

CACS assessment

The time required to perform CACS was 3 ± 1 min.

Mean CACS values were significantly higher for gCCT as compared to ngCCT (Volume: 418 ± 747 *vs* 332 ± 597; Mass: 89 ± 151 *vs* 78 ± 141; Agatston: 481 ± 854 *vs* 428 ± 776; $P < 0.05$). The mean difference (Delta) between gCCT and ngCCT was 86 ± 267 for Volume, 11 ± 36 for Mass and 53 ± 188 for Agatston score, showing a sharp tendency for global underestimation of CACS in ngCCT (Table 3, Figures 1-3).

The correlation between values was always high (r = Volume: 0.95; Mass: 0.97; Agatston: 0.98) between the two scans. The correlation between heart rate and the difference between the two scans was very low (r = -0.09), suggesting that the variability was not related to heart rate. Instead there was a moderate correlation (r = 0.50) between the differences (delta) between the two scans and the Agatston score in gCCT, suggesting that the higher the CACS value, the higher the variability.

Intra- and Inter-observer variability was very limited

Table 3 coronary artery calcium score values

Parameters (mean ± SD)	gCCT	ngCCT	Delta (absolute)	Delta	*P*	*r*	R^2
Volume	418.1 ± 746.5	332.0 ± 596.9	-86.1 ± 263.8	-21%	< 0.05	0.947	0.896
Mass	88.9 ± 151.2	77.9 ± 140.5	-11.1 ± 35.5	-12%	< 0.05	0.973	0.946
Agatston	480.8 ± 853.7	427.7 ± 776.3	-53.1 ± 188.4	-11%	< 0.05	0.978	0.956

The Table shows the mean values of CACS Volume, Mass, and Agatston score for the study population. On average gCCT shows CACS values significantly higher with a high correlation to ngCCT. The percentage underestimation (delta) of ngCCT of Agatston score is -11%. CACS: Coronary artery calcium score; gCCT: ECG gated cardiac computed tomography; ngCCT: Non-gated chest computed tomography.

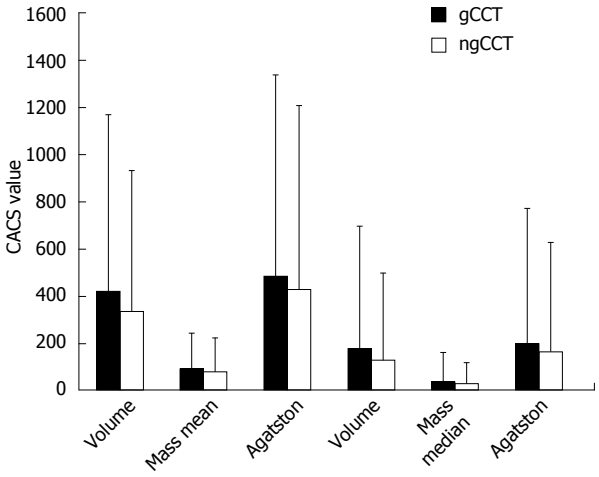

Figure 1 Coronary artery calcium score values. The Figure shows the mean and median values of Volume, Mass, and Agatston Score for gCCT and ngCCT in the total population. There is a sharp tendency to underestimate of ngCCT for all types of CACS score. gCCT: ECG gated cardiac computed tomography; ngCCT: Non-gated chest computed tomography; CACS: Coronary artery calcium score.

for both gCCT and ngCCT ($P > 0.05$). Intra-observer variability of Agatston score showed a bias of -0.148 for ngCCT and 0.057 for gCCT. Inter-observer of Agatston score showed a bias of -0.259 for ngCCT and 0.178 for gCCT.

Reclassification

With the tendency of ngCCT to underestimate CACS values we observed a relevant degree of reclassification (Table 4, Figure 4).

Overall, 23 (38%) patients were reclassified in a different cardiovascular risk category, mostly (18/23; 78%) shifting to a lower risk in the ngCCT; in 5/23 (22%) cases the CACS score shifted to a higher cardiovascular risk category.

Of the 6 patients with 0 Agatston score on gCCT, 2 (33%) showed an Agatston score > 0 in the ngCCT. Of the 3 patients with 1-10 Agatston score on gCCT, 1 (33%) showed an Agatston score of 0 in the ngCCT.

Two patients showed very different values of CACS between the two scans; they correspond both the very high values of Agatston score (> 1000); therefore, the difference is not relevant for stratification of risk. The main reason for such a difference (beside the lack of cardiac synchronization in ngCCT) was related to higher heart rates (> 80 bpm).

Radiation dose

The estimated radiation dose was significantly higher for gCCT (DLP 115.8 ± 50.7 *vs* 83.8 ± 16.3; Effective dose 1.6 ± 0.7 mSv *vs* 1.2 ± 0.2 mSv; $P < 0.01$).

DISCUSSION

A number of randomized lung cancer screening trials are currently undergoing with the aim of reducing mortality related to this life-threatening condition[12]. Although atherosclerotic vascular disease accounts for more death and disability than all types of cancer, the importance of detecting subclinical atherosclerosis and targeting prevention of future cardiovascular events is only now starting to be highlighted in the lung cancer screening setting[3,4,13-15]. Preliminary experiences shows a very high correlation between CACS assessed on low dose HRCT and cardiovascular events[4].

These findings are also suggesting that cardiovascular mortality as predicted by CACS is higher as compared to lung cancer mortality in a population of high risk smokers[4]. This finding can be expected from epidemiological data on all-cause mortality[8], however for the first time we have a tool that can stratify risk for both diseases. This is the first study that addressed the issue of CACS assessment in lung cancer screening context in a prospective cross-over fashion.

Our study is focused on showing the correlation between CACS obtained in conventional gCCT scans and in low-dose CT (ngCCT). The correlation we found is very high with a tendency of ngCCT to underestimate total calcium burden. The cardiovascular reclassification occurring in individuals undergoing HRCT, following the Mayo Clinic classification is important (about 38% of the individuals). Nevertheless, the predictive value on mortality has been shown to remain preserved[3,4].

The most important findings of our study are related to the classification of individuals with none or very low CACS values. In general one third of the individuals with CACS 0 (which means no evidence of CAD) are reclassified in higher category, while one third of the individuals with very low CACS (CACS 1-10) are reclassified as CACS 0. This is particularly important for the negative predictive value of CACS concerning obstructive CAD and cardiovascular events.

The technique applied to ngCCT in this study is the standard one (dataset reconstructed with 5 mm slice thickness and 5 mm slice increment) and does not re-

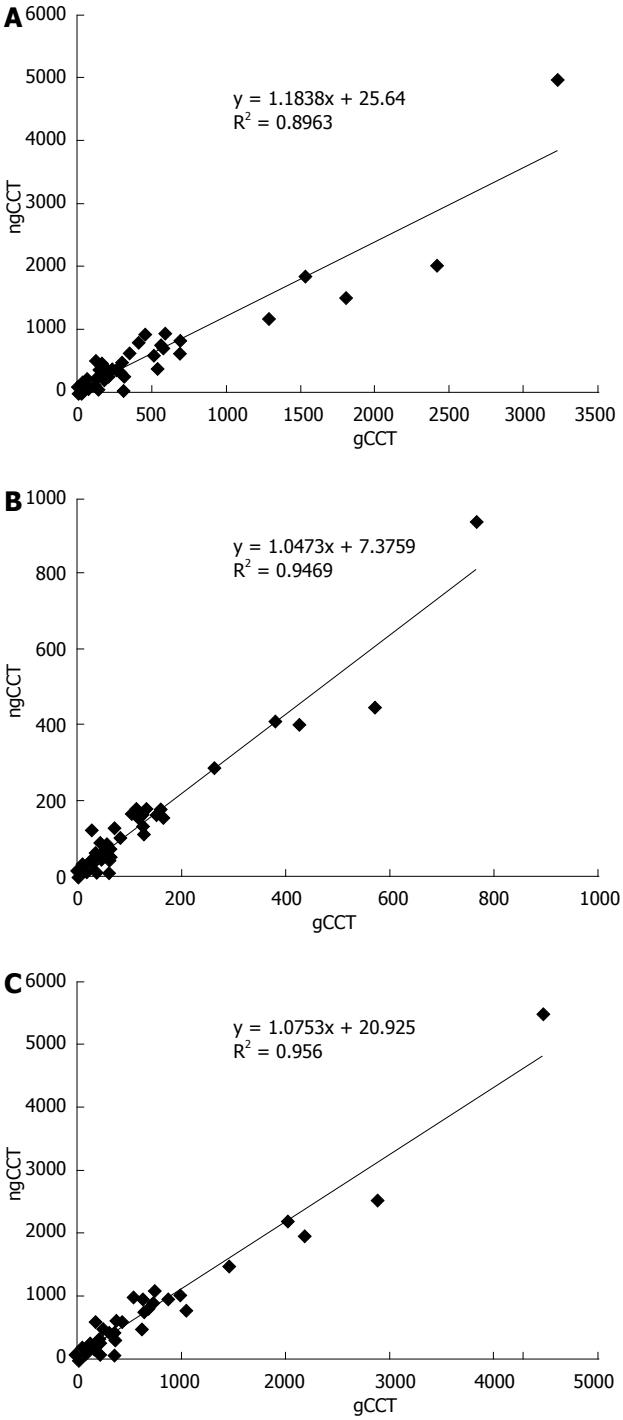

Figure 2 Scatter plots coronary artery calcium score values. The scatter plots show the high correlation of Volume (A), Mass (B), and Agatston (C) scores obtained with gCCT and ngCCT. gCCT: ECG gated cardiac computed tomography; ngCCT: Non-gated chest computed tomography.

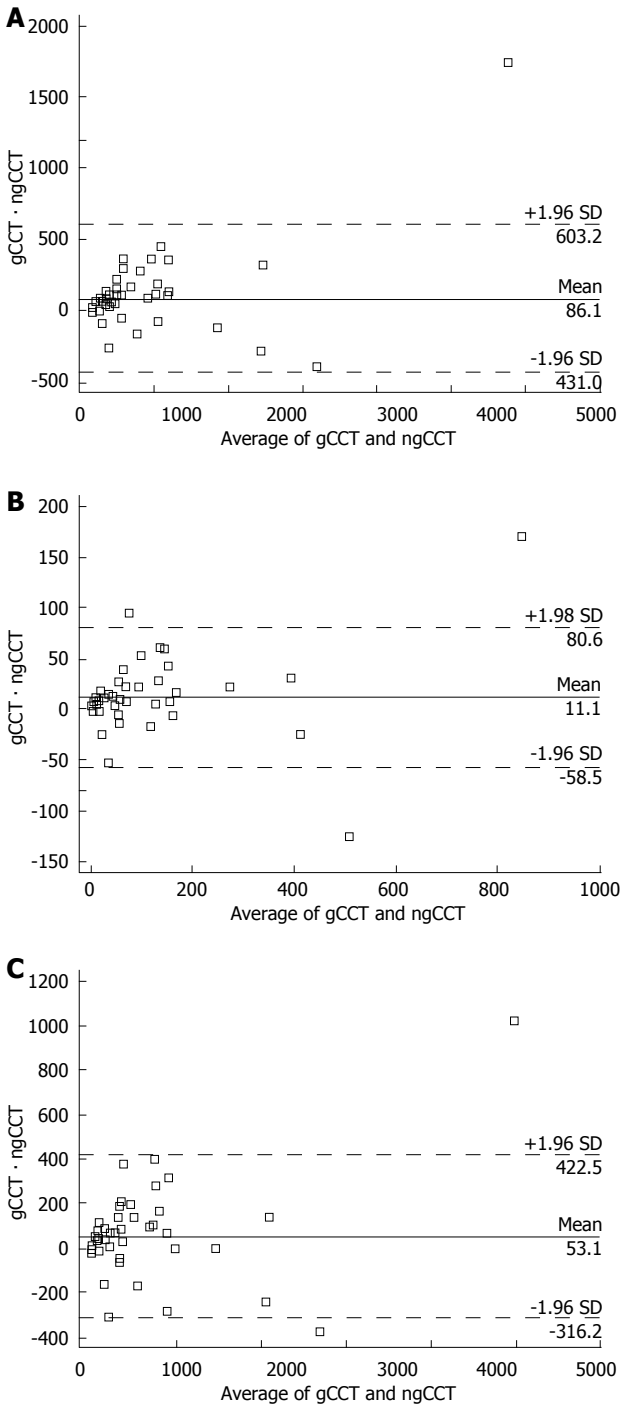

Figure 3 Bland-Altman plots of coronary artery calcium score values. The Bland-Altman plots show the slight but significant tendency to overestimate Volume (A), Mass (B), and Agatston (C) scores of ngCCT as compared to gCCT. There are 2 patients with values far off in ngCCT *vs* gCCT. However, they are both with very high values and this does not affect significantly further reclassification. gCCT: ECG gated cardiac computed tomography; ngCCT: Non-gated chest computed tomography.

quire any additional reconstruction as suggested by other studies previously published (from 1 mm to 3 mm slice thickness)[3,4,9,10]. CACS assessment can be done using the same data routinely reconstructed for the purpose of lung cancer screening, resulting easily applicable in daily clinical practice.

Clinical implications

From our observation and the observation of Jacobs *et al*[3,4] we can suggest that individuals undergoing HRCT for lung cancer screening should be assessed for CACS. CACS assessment is a relatively simple procedure that requires a dedicated software application (currently available on all CT scanners able to perform Cardiac Imaging) and a basic training. It is not time consuming (it requires few minutes) but it has a very important prognostic value

Table 4 Cardio vascular risk stratification based on absolute coronary artery calcium score classes *n* (%)

CACS class	gCCT	ngCCT
0	6 (10)	10 (16.7)
1-10	6 (10)	7 (11.7)
11-100	14 (23.3)	10 (16.7)
101-400	14 (23.3)	17 (28.3)
400-1000	14 (23.3)	10 (16.7)
> 1000	6 (10)	6 (10)

The Table shows how the total Agatston score distributed using the Mayo Clinic Classification (Rumberger *et al*[17]) with gCCT and ngCCT within the same population. In total 23 (38.3%) patients shifted to a different cardiovascular risk group. gCCT: ECG gated cardiac computed tomography; ngCCT: Non-gated chest computed tomography.

which is independent from conventional cardiovascular risk factors[1,2,15].

Limitations

Study has several limitations: The first is the relatively low number of patients. This also limits the sub-analysis of the CACS groups. However, this is the first study that prospectively tests in a cross-over design the hypothesis that ngCCT could be used for CACS purposes. Enrolling more patients would have exposed more individuals to un-necessary additional radiation.

The second limitation is the additional radiation dose delivered to the patients which is consistent with the design of the study and has been minimized by using available hardware and software solutions.

The third limitation is related to the absence of prospective ECG triggering protocol for gCCT. This feature was available but we decided not to use it due to the higher reproducibility of spiral CT scanning for CACS[16]. The use of prospective ECG triggering would have further reduced the radiation dose of gCCT. The fourth limitation is the lack of outcome data. However, this was beyond the aim of the study and the number of patients enrolled is not adequate for this purpose anyway. This aspect has been showed in other studies[4]. Recently another substudy of the MILD trial provided insight into this aspect and showed that individuals with > 400 modified Agatston score performed on non-gated chest CT scans have a worse prognosis in terms of mortality and cardiovascular events[8]. Actually, with this study we wanted to demonstrate the feasibility of CACS in ngCCT scans.

CACS assessment is feasible on unenhanced chest CT, however the variability of CACS values and the associated re-stratification of patients in cardiovascular risk groups should be taken into account.

COMMENTS

Background

Lung cancer screening is a long standing topic. Low dose high resolution computed tomography (CT) is becoming the preferred mean for this purpose in high risk smoker population. Meanwhile, coronary artery calcium score by means of CT has become a strong and reliable method for cardiovascular risk stratification in asymptomatic individuals.

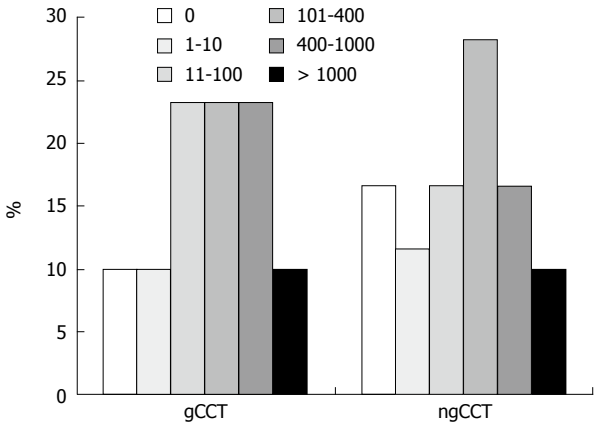

Figure 4 Restratification. The Figure shows the pattern of reclassification of cardiovascular risk categories using the Mayo Clinic Classification (Rumberger *et al*) with gCCT and ngCCT within the same population (CACS score according to Agatston). ngCCT determines a shift in the ranges between 1 and 400 Agatston score. Some of these patients shift to a lower category (in particular the ones with Agatston score between 1 and 10), while some of the patients shifts towards higher risk categories (in particular the ones with Agatston score between 11 and 100). In total 23 patients shifted to another cardiovascular risk category in ngCCT. gCCT: ECG gated cardiac computed tomography; ngCCT: Non-gated chest computed tomography; CACS: Coronary artery calcium score.

Research frontiers

This study demonstrates that coronary artery calcium score for cardiovascular risk stratification can be performed in the context of lung cancer screening by means of low dose CT.

Innovations and breakthroughs

There are no studies in literature performed as cross-over and prospective in such a population.

Applications

This study provides the clue on the feasibility of coronary calcium score in individuals undergoing low dose CT for lung cancer screening.

Terminology

Low dose computed tomography: it is a diagnostic method by which it is possible to detect small pulmonary nodules before they become larger tumors. Coronary artery calcium score: it is a test performed with CT that allows the quantification of coronary artery calcium as a surrogate and independent marker of cardiovascular risk.

Peer review

This is a well written manuscript that compares quantification of coronary artery calcium scoring by non-gated techniques with traditional thick slice reconstructions as used in lung screening exams with calcium scoring by traditional gated techniques with thin slice reconstructions.

REFERENCES

1 **Shaw LJ**, Raggi P, Schisterman E, Berman DS, Callister TQ. Prognostic value of cardiac risk factors and coronary artery calcium screening for all-cause mortality. *Radiology* 2003; **228**: 826-833 [PMID: 12869688 DOI: 10.1148/radiol.2283021006]

2 **Greenland P**, LaBree L, Azen SP, Doherty TM, Detrano RC. Coronary artery calcium score combined with Framingham score for risk prediction in asymptomatic individuals. *JAMA* 2004; **291**: 210-215 [PMID: 14722147 DOI: 10.1001/jama.291.2.210]

3 **Jacobs PC**, Gondrie MJ, van der Graaf Y, de Koning HJ, Isgum I, van Ginneken B, Mali WP. Coronary artery calcium can predict all-cause mortality and cardiovascular events on low-dose CT screening for lung cancer. *AJR Am J Roentgenol* 2012; **198**: 505-511 [PMID: 22357989 DOI: 10.2214/AJR.10.5577]

4 **Jacobs PC**, Prokop M, van der Graaf Y, Gondrie MJ, Janssen

KJ, de Koning HJ, Isgum I, van Klaveren RJ, Oudkerk M, van Ginneken B, Mali WP. Comparing coronary artery calcium and thoracic aorta calcium for prediction of all-cause mortality and cardiovascular events on low-dose non-gated computed tomography in a high-risk population of heavy smokers. *Atherosclerosis* 2010; **209**: 455-462 [PMID: 19875116 DOI: 10.1016/j.atherosclerosis.2009.09.031]

5 **Ashar BH**, Hughes MT, Marinopoulos SS, Prokopowicz GP, Berkenblit GV, Sisson SD, Simonson LA, Miller RG. Current evidence for the use of emerging radiologic technologies for disease screening. *Am J Manag Care* 2005; **11**: 385-392 [PMID: 15974558]

6 **Greenland P**, Bonow RO, Brundage BH, Budoff MJ, Eisenberg MJ, Grundy SM, Lauer MS, Post WS, Raggi P, Redberg RF, Rodgers GP, Shaw LJ, Taylor AJ, Weintraub WS. ACCF/AHA 2007 clinical expert consensus document on coronary artery calcium scoring by computed tomography in global cardiovascular risk assessment and in evaluation of patients with chest pain: a report of the American College of Cardiology Foundation Clinical Expert Consensus Task Force (ACCF/AHA Writing Committee to Update the 2000 Expert Consensus Document on Electron Beam Computed Tomography) developed in collaboration with the Society of Atherosclerosis Imaging and Prevention and the Society of Cardiovascular Computed Tomography. *J Am Coll Cardiol* 2007; **49**: 378-402 [PMID: 17239724 DOI: 10.1016/j.jacc.2006.10.001]

7 **Greenland P**, Alpert JS, Beller GA, Benjamin EJ, Budoff MJ, Fayad ZA, Foster E, Hlatky MA, Hodgson JM, Kushner FG, Lauer MS, Shaw LJ, Smith SC, Taylor AJ, Weintraub WS, Wenger NK, Jacobs AK, Smith SC, Anderson JL, Albert N, Buller CE, Creager MA, Ettinger SM, Guyton RA, Halperin JL, Hochman JS, Kushner FG, Nishimura R, Ohman EM, Page RL, Stevenson WG, Tarkington LG, Yancy CW. 2010 ACCF/AHA guideline for assessment of cardiovascular risk in asymptomatic adults: a report of the American College of Cardiology Foundation/American Heart Association Task Force on Practice Guidelines. *J Am Coll Cardiol* 2010; **56**: e50-103 [PMID: 21144964 DOI: 10.1016/j.jacc.2010.09.001]

8 **Sverzellati N**, Cademartiri F, Bravi F, Martini C, Gira FA, Maffei E, Marchianò A, La Vecchia C, De Filippo M, Kuhnigk JM, Rossi C, Pastorino U. Relationship and prognostic value of modified coronary artery calcium score, FEV1, and emphysema in lung cancer screening population: the MILD trial. *Radiology* 2012; **262**: 460-467 [PMID: 22114241]

9 **Budoff MJ**, Nasir K, Kinney GL, Hokanson JE, Barr RG, Steiner R, Nath H, Lopez-Garcia C, Black-Shinn J, Casaburi R. Coronary artery and thoracic calcium on noncontrast thoracic CT scans: comparison of ungated and gated examinations in patients from the COPD Gene cohort. *J Cardiovasc Comput Tomogr* 2011; **5**: 113-118 [PMID: 21167806 DOI: 10.1016/j.jcct.2010.11.002]

10 **Wu MT**, Yang P, Huang YL, Chen JS, Chuo CC, Yeh C, Chang RS. Coronary arterial calcification on low-dose ungated MDCT for lung cancer screening: concordance study with dedicated cardiac CT. *AJR Am J Roentgenol* 2008; **190**: 923-928 [PMID: 18356438 DOI: 10.2214/AJR.07.2974]

11 **Bongartz G**, Golding SJ. 2004 CT quality criteria. Luxembourg, Luxembourg. European Commission, 2004. Available from: URL: http://www.msct.eu/CT_Quality_Criteria.htm

12 **Bach PB**, Mirkin JN, Oliver TK, Azzoli CG, Berry DA, Brawley OW, Byers T, Colditz GA, Gould MK, Jett JR, Sabichi AL, Smith-Bindman R, Wood DE, Qaseem A, Detterbeck FC. Benefits and harms of CT screening for lung cancer: a systematic review. *JAMA* 2012; **307**: 2418-2429 [PMID: 22610500 DOI: 10.1001/jama.2012.5521]

13 **Budoff MJ**, Gul KM. Expert review on coronary calcium. *Vasc Health Risk Manag* 2008; **4**: 315-324 [PMID: 18561507]

14 **Shemesh J**, Henschke CI, Farooqi A, Yip R, Yankelevitz DF, Shaham D, Miettinen OS. Frequency of coronary artery calcification on low-dose computed tomography screening for lung cancer. *Clin Imaging* 2006; **30**: 181-185 [PMID: 16632153 DOI: 10.1016/j.clinimag.2005.11.002]

15 **Shemesh J**, Henschke CI, Shaham D, Yip R, Farooqi AO, Cham MD, McCauley DI, Chen M, Smith JP, Libby DM, Pasmantier MW, Yankelevitz DF. Ordinal scoring of coronary artery calcifications on low-dose CT scans of the chest is predictive of death from cardiovascular disease. *Radiology* 2010; **257**: 541-548 [PMID: 20829542 DOI: 10.1148/radiol.10100383]

16 **Ohnesorge B**, Flohr T, Fischbach R, Kopp AF, Knez A, Schröder S, Schöpf UJ, Crispin A, Klotz E, Reiser MF, Becker CR. Reproducibility of coronary calcium quantification in repeat examinations with retrospectively ECG-gated multisection spiral CT. *Eur Radiol* 2002; **12**: 1532-1540 [PMID: 12042964 DOI: 10.1007/s00330-002-1394-2]

17 **Rumberger JA**, Brundage BH, Rader DJ, Kondos G. Electron beam computed tomographic coronary calcium scanning: a review and guidelines for use in asymptomatic persons. *Mayo Clin Proc* 1999; **74**: 243-252 [PMID: 10089993]

P- Reviewers: Biondi-Zoccai G, Srichai-Parsia M
S- Editor: Ma YJ **L- Editor**: A **E- Editor**: Zhang DN

World Journal of Radiology

Submit a Manuscript: http://www.wjgnet.com/esps/
Help Desk: http://www.wjgnet.com/esps/helpdesk.aspx
DOI: 10.4329/wjr.v6.i6.388

World J Radiol 2014 June 28; 6(6): 388-391
ISSN 1949-8470 (online)
© 2014 Baishideng Publishing Group Inc. All rights reserved.

CASE REPORT

Myotendinous rupture of temporalis muscle: A rare injury following seizure

Lena N Naffaa, Yasmeen K Tandon, Michael Rubin

Lena N Naffaa, Michael Rubin, Department of Radiology, Akron Children's Hospital, Akron, OH 44308, United States
Yasmeen K Tandon, Department of Radiology, Case Western Reserve University-Metro Health Medical Center, Cleveland, OH 44109, United States
Author contributions: Naffaa LN, Tandon YK and Rubin M contributed equally to this work; Naffaa LN and Rubin M interpreted images in this study; Tandon YK and Naffaa LN collected the patient's clinical data; Naffaa LN, Tandon YK and Rubin M analyzed the data and wrote the paper; Naffaa LN, Tandon YK and Rubin M gave final approval of the version to be published.
Correspondence to: Lena N Naffaa, MD, Radiologist, Department of Radiology, Akron Children's Hospital, 1 Perkins Square, Akron, OH 44308, United States. lnaffaa@chmca.org
Telephone: +1-330-5438275 Fax: +1-330-5433760
Received: March 23, 2014 Revised: April 14, 2014
Accepted: May 8, 2014
Published online: June 28, 2014

Abstract

Seizures are one of the most common pediatric neurologic disorders. Many complications secondary to seizures have been described in the literature including head trauma, fractures, drowning and burns. However, to the best of our knowledge, rupture of the myotendinous insertion of the temporalis muscle on the mandible secondary to a seizure has never been described in the literature. We report the case of a unilateral temporalis muscle rupture in a 16-year-old boy who developed unilateral facial swelling following new onset tonic-clonic seizures. We emphasize on the computed tomography and magnetic resonance imaging findings in this case report. Two mechanisms have been proposed to explain such an injury. The favored mechanism in our patient is a pull on the temporalis myotendinous insertion on the mandible following vigorous and brisk deviation of the head and neck during seizure. Radiologists should be familiar with this type of injury following seizures in order to prevent misdiagnosis and subsequently mistreatment.

© 2014 Baishideng Publishing Group Inc. All rights reserved.

Key words: Seizure; Rupture; Temporalis; Muscle; Pediatric

Core tip: We report the unique case of a unilateral temporalis muscle rupture following new onset tonic-clonic seizures in a 16-year-old boy. The favored mechanism in our patient is a pull on the temporalis myotendinous insertion on the mandible following vigorous and brisk deviation of the head and neck during seizure. Although this is a rare entity, it is important to be familiar with such type of injury in a patient who develops unilateral facial swelling and pain following tonic-clonic seizures in order to prevent misdiagnosis and mistreatment.

Naffaa LN, Tandon YK, Rubin M. Myotendinous rupture of temporalis muscle: A rare injury following seizure. *World J Radiol* 2014; 6(6): 388-391 Available from: URL: http://www.wjgnet.com/1949-8470/full/v6/i6/388.htm DOI: http://dx.doi.org/10.4329/wjr.v6.i6.388

INTRODUCTION

Seizures are one of the most common pediatric neurologic disorders. It is estimated that 4% to 10% of children will have at least one seizure in the first 16 years of life[1]. Many complications have been described in the literature secondary to seizures, such as head trauma, fractures, drowning and burns[2-4]. However, to the best of our knowledge, this is the first reported case of myotendinous rupture of the temporalis muscle after seizures. We report the computed tomography (CT) and magnetic resonance imaging (MRI) findings of rupture of the myotendinous insertion of the right temporalis muscle on the coronoid process of the mandible following generalized tonic-clonic seizures. Two mechanisms have been proposed to explain such an injury: significant pull on the

myotendinous insertion following brisk and forceful deviation of the head and neck toward the contolateral side during seizures or direct fall on the face. In our patient, the first mechanism is favored as there was no witnessed fall nor signs of facial trauma on physical exam.

CASE REPORT

Patient is a 16-year-old male with a past medical history of Attention Deficit Hyperactivity Disorder (ADHD) who was admitted for new onset seizures. Approximately 12 h prior to his presentation to our institution, he had a sudden witnessed episode of violent bilateral shaking of his arms and legs that lasted approximately 2 min associated with foaming at the mouth. He was taken to an outside hospital emergency department (ED) where a basic metabolic panel including glucose and calcium levels was normal. His urine toxicology was negative and urine analysis was also within normal limits. Head CT was performed and was reportedly normal. Just prior to discharge from the ED, his mother noticed a small bump that had developed over his right temple.

He was discharged home after he returned to his neurological baseline. At home, the patient continued to have increasing facial swelling that was spreading down to his cheek. Patient also began to complain of pain and noted difficulty opening his mouth secondary to pain. At home, a few hours after returning from the ED, the patient's mother again witnessed him having another seizure that lasted approximately 2 min where he was noted to have bilateral arm and leg shaking with foaming at the mouth. He was taken back to the outside hospital ED. He returned to his neurological baseline and was transferred to our institution for further management.

Shortly after arrival to our institution, he had another seizure witnessed by nursing staff where he had full body stiffening followed by bilateral jerking of his arms and legs with his eyes and head deviated to the left. This episode lasted 1.5 min. The patient's mother and the providing physicians noted that the right sided facial swelling continued to worsen and the patient continued to experience worsening right sided facial pain. On physical exam, there was diffuse swelling over the right temporal region extending all the way down to reach the right ear and right jaw. This region was extremely tender to palpation. There were no external signs of trauma such as bruising or laceration. Laboratory tests including CBC demonstrates a high WBC of 17.8 (Normal range: 4.5-13.0 10E9/L), elevated CPK of 762(Normal range: 24-195 U/L), normal blood amylase, negative blood culture at 24 h and normal coagulation profile. The initial differential diagnosis for the facial swelling included a dental abscess, parotitis, or non specific myositis. Patient was empirically started on Clindamycin to treat any potential underlying infectious etiology.

A CT scan of the face with intravenous contrast was performed in our institution for further evaluation using the following technique: GE Medical Systems,

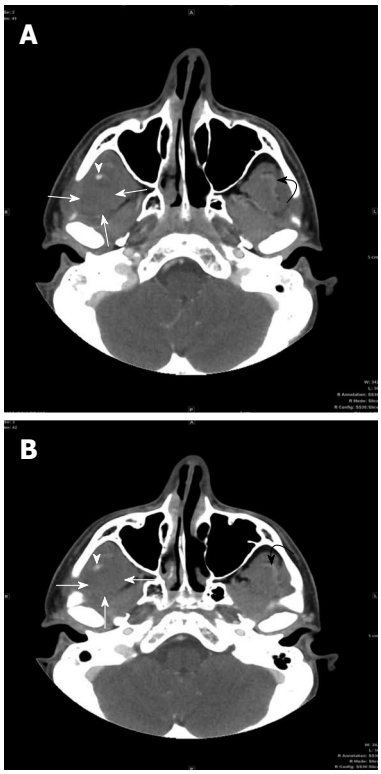

Figure 1 Axial contrast enhanced computed tomography images of the face with soft tissue settings demonstrate swelling (A) and subtle hypoattenuation (B) of myotendinous portion of right Temporalis muscle (straight arrows) as it passes medial to the zygomatic bone just prior to its insertion to the coronoid process and anterior ramus of the right mandible. It contains a small high density material which may represent hemorrhage (arrowhead). Note the normal appearance of contralateral temporalis muscle (curved arrows).

Pitch:0.562:1, Pixel spacing: 0.361 mm/0.361 mm, Kvp 120, mA 129, rotate time: 0.8, ST 2.5 mm, FOV 18 cm, Tilt 0, W:342, L:56, Contrast: 98 cc of Isovue 300. The CT images (Figures 1 and 2) demonstrate swelling and diminished attenuation of right temporalis muscle most prominent near its myotendinous portion as it passes medial to the zygomatic bone just prior to its insertion to the coronoid process and anterior ramus of the right mandible. A small high density is identified just prior to its insertion to the mandible which may represent hemorrhage. The CT findings were in favor of a non specific myositis, possibly infectious in nature. The subtle hypoattenuation near the insertion to the mandible was felt to represent a possible phlegmon without a mature abscess seen.

An MRI of the face prior and following intravenous contrast administration was performed the next day for better characterization. The following pulse sequences were obtained on a 3 Tesla magnet(Siemens/Skyra): T2 coronal SPIR(repetition time/echo time = 6580/91, Number of excitations (NEX) = 2, matrix = 320 × 240, slice thickness = 2.5 mm), T2 axial fat sat (6070/98, NEX = 2, 4 mm, 256 × 256, 2 mm), T1 coronal (600/8.4, NEX =1, 256 × 205, 2.5 mm), T2 axial GRE (627/19.9, NEX = 1, 320 × 240, 4 mm), T1 axial fat sat pre and post intravenous administration of 5.7 mL of Gadavist

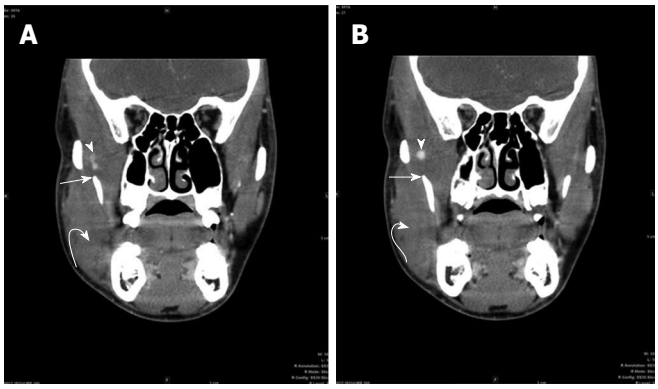

Figure 2 Three millimeter reconstructed contrast enhanced coronal computed tomography images of the face with soft tissue settings demonstrate swelling of the entire right temporalis muscle more prominent at its myotendinous insertion to the mandible (straight arrow). There is also swelling of right masseter muscle (curved arrow). Small high density material is again seen in region of myotendinous insertion of right temporalis muscle suggesting hemorrhage (arrowhead).

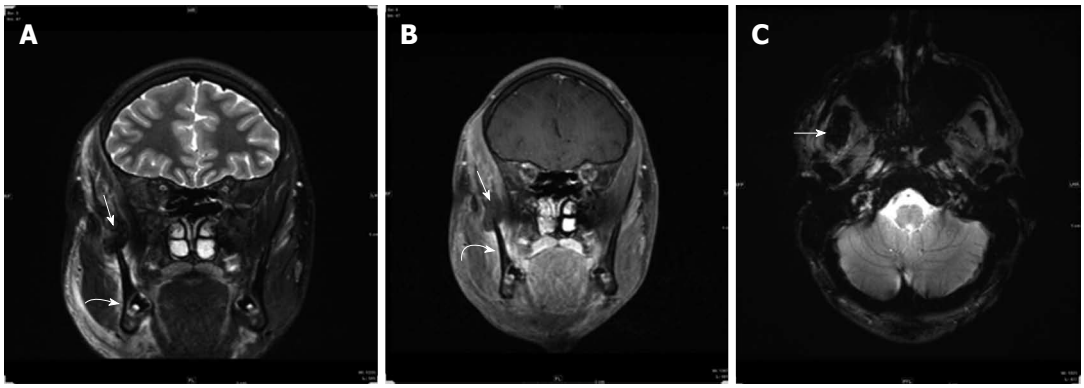

Figure 3 T2 Coronal SPIR (A) and T1 Coronal SPIR post contrast images (B) through the face demonstrate rupture of myotendinous insertion of right temporalis muscle with a 2.5 cm × 1.5 cm collection surrounding the coronoid region of right mandible at the site of temporalis muscle insertion (straight arrows), the collection demonstrates low signal on T2 weighted imaging (A) and susceptibility artifact/blooming on the T2 axial GRE image (C) consistent with hematoma. Additionally, there is mild swelling, increased T2 signal and mild enhancement in the right masseter muscle notably near its insertion to the anterior mandible as demonstrated on figures A and B suggesting a sprain (curved arrow). Swelling and edema of overlying subcutaneous soft tissues is noted as well.

(661/8.4, NEX = 1, 256 × 205, 4 mm), T1 coronal fat sat post contrast (899/8.4, NEX = 1, 256 × 205, 2.5 mm). The MRI findings (Figure 3) are consistent with rupture of the right temporalis myotendinous junction with a small hematoma formation at its insertion onto the coronoid process of the mandible. There was swelling and mild inflammatory changes in the entire right temporalis muscle over the temporal calvarium. Swelling and mild inflammatory changes were also seen in the right masseter muscle especially at its attachment to the anterior ramus and angle of the mandible consistent with sprain.

Plastic surgery was consulted and after examining the patient decided to treat conservatively with pain medication and physical therapy.

DISCUSSION

The temporalis muscle is a broad, fan shaped muscle that fills the temporal fossa, superior to the zygomatic arch. The muscle originates from the temporal fossa and the deep surface of the temporal fascia. As the muscle fibers descend, they form a tendon which passes medial to the zygomatic arch and inserts into the medial surface, apex, and anterior border of the coronoid process, and the anterior border of the mandibular ramus[5,6]. Its function is to elevate and retract the mandible[5,6].

Thorough review of the literature reveals that not much has been written about rupture of the temporalis muscle insertion. Etiologies that have been described as a potential cause for injury include direct injury to the muscle fibers caused by inappropriate intra operative dissection or retraction[7-10]. Direct trauma such as a blow to the side of the head or a motor vehicle accident can also cause injury to the temporalis muscle. Sleep bruxism is a common sleep-related motor disorder characterized by tooth grinding and clenching in which there can be strain of the temporalis muscle[11]. However, frank rupture of the myotendinous insertion of the temporalis muscle has not been reported especially in the context of seizure related injuries.

We describe the CT and MRI findings of rupture of myotendinous insertion of right temporalis muscle on the mandible in a 16-year-old male following multiple witnessed generalized tonic-clonic seizures. Two mechanisms have been proposed to explain such an injury: significant pull on the myotendinous insertion following violent jerking of his head and neck to the controlateral side during seizures or a direct fall on the face. In our patient, the first mechanism is favored as no facial bruising or laceration were identified on physical exam and no direct trauma or fall to the head or face was witnessed by parents or medical staff.

Rupture of the myotendinous junction of temporalis muscle is extremely rare. It is important to be familiar

with such type of injury in a patient who developed unilateral facial swelling and pain following tonic-clonic seizures in order to prevent misdiagnosis and mistreatment.

COMMENTS

Case characteristics

Sixty-year-old boy who developed unilateral facial swelling and pain following new onset tonic-clonic seizures.

Clinical diagnosis

Diffuse swelling over the right temporal region extending all the way down to reach the right ear and right jaw which was tender to palpation.

Differential diagnosis

Dental abscess, parotitis, non specific myositis, rupture of the myotendinous junction of temporalis muscle.

Laboratory diagnosis

WBC 17.8; CPK of 762; normal blood amylase; negative blood culture at 24 h; negative urine toxicology; normal coagulation profile; normal basic metabolic panel and urine analysis.

Imaging diagnosis

Computed tomography finding: Swelling and diminished attenuation of right temporalis muscle most prominent near its myotendinous portion as it passes medial to the zygomatic bone just prior to its insertion to the coronoid process and anterior ramus of the right mandible. A small high density is identified just prior to its insertion to the mandible which may represent hemorrhage; Magnetic resonance findings: Rupture of the right temporalis myotendinous junction with a small hematoma formation at its insertion onto the coronoid process of the mandible. Swelling and sprain of the right masseter muscle especially at its attachment to the anterior ramus and angle of the mandible.

Treatment

Conservative treatment with pain medication and physical therapy.

Related reports

The literature regarding rupture of the temporalis muscle insertion is sparse. Potential etiologies described in the literature include direct injury to the muscle fibers caused by inappropriate intra operative dissection or retraction or direct trauma such as a blow to the side of the head or a motor vehicle accident.

Experiences and lessons

This case reports a rare case of temporalis muscle rupture following seizure. Although this is a rare entity, it is important to be familiar with such type of injury in a patient who develops unilateral facial swelling and pain following a tonic-clonic seizure in order to prevent misdiagnosis and mistreatment.

Peer review

The authors present an interesting and well done clinical note and describe the neuroimaging findings of rupture of myotendinous insertion of right temporalis muscle of the mandible in a 16-year-old male following multiple witnessed generalized tonic-clonic seizures. This is the first reported case of myotendinous rupture of the temporalis muscle after seizure. This information is interesting from a clinical point of view.

REFERENCES

1 **McAbee GN**, Wark JE. A practical approach to uncomplicated seizures in children. *Am Fam Physician* 2000; **62**: 1109-1116 [PMID: 10997534]

2 **Tan M**, D'Souza W. Seizure-related injuries, drowning and vehicular crashes -- a critical review of the literature. *Curr Neurol Neurosci Rep* 2013; **13**: 361 [PMID: 23690025 DOI: 10.1007/s11910-013-0361-4]

3 **Ting YW**, Kwong KL. Seizure-related injuries in newly diagnosed childhood epilepsy. *Pediatr Neurol* 2010; **42**: 417-421 [PMID: 20472194 DOI: 10.1016/j.pediatrneurol.2010.02.010]

4 **Asadi-Pooya AA**, Nikseresht A, Yaghoubi E, Nei M. Physical injuries in patients with epilepsy and their associated risk factors. *Seizure* 2012; **21**: 165-168 [PMID: 22130005 DOI: 10.1016/j.seizure.2011.10.009]

5 **Fehrenbach MJ**, Herring SW. Illustrated Anatomy of the Head and Neck and Herring. 4th ed. St. Louis: Elsevier, 2012: 98

6 **Jacob S**. Human Anatomy: A Clinically-Orientated Approach. 1st ed. New York: Elsevier, 2008: 194

7 **Oikawa S**, Mizuno M, Muraoka S, Kobayashi S. Retrograde dissection of the temporalis muscle preventing muscle atrophy for pterional craniotomy. Technical note. *J Neurosurg* 1996; **84**: 297-299 [PMID: 8592239 DOI: 10.3171/jns.1996.84.2.0297]

8 **Spetzler RF**, Lee KS. Reconstruction of the temporalis muscle for the pterional craniotomy. Technical note. *J Neurosurg* 1990; **73**: 636-637 [PMID: 2398396 DOI: 10.3171/jns.1990.73.4.0636]

9 **Kadri PA**, Al-Mefty O. The anatomical basis for surgical preservation of temporal muscle. *J Neurosurg* 2004; **100**: 517-522 [PMID: 15035289 DOI: 10.3171/jns.2004.100.3.0517]

10 **Abdulazim A**, Filis A, Sadr-Eshkevari P, Schulte F, Sandu N, Schaller B. Postcraniotomy function of the temporal muscle in skull base surgery: technical note based on a preliminary study. *ScientificWorldJournal* 2012; **2012**: 427081 [PMID: 22536141 DOI: 10.1100/2012/427081]

11 **Carra MC**, Huynh N, Lavigne G. Sleep bruxism: a comprehensive overview for the dental clinician interested in sleep medicine. *Dent Clin North Am* 2012; **56**: 387-413 [PMID: 22480810 DOI: 10.1016/j.cden.2012.01.003]

P- Reviewers: Arboix A, Gumustas OG **S- Editor**: Song XX
L- Editor: A **E- Editor**: Zhang DN

World Journal of Radiology

Submit a Manuscript: http://www.wjgnet.com/esps/
Help Desk: http://www.wjgnet.com/esps/helpdesk.aspx
www.wjgnet.com

World J Radiol 2014 June 28; 6(6): I-V
ISSN 1949-8470 (online)
© 2014 Baishideng Publishing Group Inc. All rights reserved.

INSTRUCTIONS TO AUTHORS

GENERAL INFORMATION

World Journal of Radiology (*World J Radiol*, *WJR*, online ISSN 1949-8470, DOI: 10.4329) is a peer-reviewed open access (OA) academic journal that aims to guide clinical practice and improve diagnostic and therapeutic skills of clinicians.

Aim and scope

WJR covers topics concerning diagnostic radiology, radiation oncology, radiologic physics, neuroradiology, nuclear radiology, pediatric radiology, vascular/interventional radiology, medical imaging achieved by various modalities and related methods analysis. The current columns of *WJR* include editorial, frontier, diagnostic advances, therapeutics advances, field of vision, mini-reviews, review, topic highlight, medical ethics, original articles, case report, clinical case conference (clinicopathological conference), and autobiography.

We encourage authors to submit their manuscripts to *WJR*. We will give priority to manuscripts that are supported by major national and international foundations and those that are of great basic and clinical significance.

WJR is edited and published by Baishideng Publishing Group (BPG). BPG has a strong professional editorial team composed of science editors, language editors and electronic editors. BPG currently publishes 43 OA clinical medical journals, including 42 in English, has a total of 15471 editorial board members or peer reviewers, and is a world first-class publisher.

Columns

The columns in the issues of *WJR* will include: (1) Editorial: The editorial board members are invited to make comments on an important topic in their field in terms of its current research status and future directions to lead the development of this discipline; (2) Frontier: The editorial board members are invited to select a highly cited cutting-edge original paper of his/her own to summarize major findings, the problems that have been resolved and remain to be resolved, and future research directions to help readers understand his/her important academic point of view and future research directions in the field; (3) Diagnostic Advances: The editorial board members are invited to write high-quality diagnostic advances in their field to improve the diagnostic skills of readers. The topic covers general clinical diagnosis, differential diagnosis, pathological diagnosis, laboratory diagnosis, imaging diagnosis, endoscopic diagnosis, biotechnological diagnosis, functional diagnosis, and physical diagnosis; (4) Therapeutics Advances: The editorial board members are invited to write high-quality therapeutic advances in their field to help improve the therapeutic skills of readers. The topic covers medication therapy, psychotherapy, physical therapy, replacement therapy, interventional therapy, minimally invasive therapy, endoscopic therapy, transplantation therapy, and surgical therapy; (5) Field of Vision: The editorial board members are invited to write commentaries on classic articles, hot topic articles, or latest articles to keep readers at the forefront of research and increase their levels of clinical research. Classic articles refer to papers that are included in Web of Knowledge and have received a large number of citations (ranking in the top 1%) after being published for more than years, reflecting the quality and impact of papers. Hot topic articles refer to papers that are included in Web of Knowledge and have received a large number of citations after being published for no more than 2 years, reflecting cutting-edge trends in scientific research. Latest articles refer to the latest published high-quality papers that are included in PubMed, reflecting the latest research trends. These commentary articles should focus on the status quo of research, the most important research topics, the problems that have now been resolved and remain to be resolved, and future research directions. Basic information about the article to be commented (including authors, article title, journal name, year, volume, and inclusive page numbers); (6) Minireviews: The editorial board members are invited to write short reviews on recent advances and trends in research of molecular biology, genomics, and related cutting-edge technologies to provide readers with the latest knowledge and help improve their diagnostic and therapeutic skills; (7) Review: To make a systematic review to focus on the status quo of research, the most important research topics, the problems that have now been resolved and remain to be resolved, and future research directions; (8) Topic Highlight: The editorial board members are invited to write a series of articles (7-10 articles) to comment and discuss a hot topic to help improve the diagnostic and therapeutic skills of readers; (9) Medical Ethics: The editorial board members are invited to write articles about medical ethics to increase readers' knowledge of medical ethics. The topic covers international ethics guidelines, animal studies, clinical trials, organ transplantation, *etc.*; (10) Clinical Case Conference or Clinicopathological Conference: The editorial board members are invited to contribute high-quality clinical case conference; (11) Original Articles: To report innovative and original findings in radiology; (12) Brief Articles: To briefly report the novel and innovative findings in radiology; (13) Meta-Analysis: Covers the systematic review, mixedtreatment comparison, meta-regression, and overview of reviews, in order to summarize a given quantitative effect, *e.g.*, the clinical effectiveness and safety of clinical treatments by combining data from two or more randomized controlled trials, thereby providing more precise and externally valid estimates than those which would stem from each individual dataset if analyzed separately from the others; (15) Letters to the Editor: To discuss and make reply to the contributions published in *WJR*, or to introduce and comment on a controversial issue of general interest; (16) Book Reviews: To introduce and comment on quality monographs of radiology; and (17) Autobiography: The editorial board members are invited to write their autobiography to provide readers with stories of success or failure in their scientific research career. The topic covers their basic personal information and information about when they started doing research work, where and how they did research work, what they have achieved, and their lessons from success or failure.

Name of journal

World Journal of Radiology

ISSN

ISSN 1949-8470 (online)

Launch date

December 31, 2009

Frequency

Monthly

Editor-in-Chief

Kai U Juergens, MD, Associate Professor, MRT und PET/CT, Nuklearmedizin Bremen Mitte, ZEMODI - Zentrum für morpholo-

gische und molekulare Diagnostik, Bremen 28177, Germany

Edwin JR van Beek, MD, PhD, Professor, Clinical Research Imaging Centre and Department of Medical Radiology, University of Edinburgh, Edinburgh EH16 4TJ, United Kingdom

Thomas J Vogl, MD, Professor, Reader in Health Technology Assessment, Department of Diagnostic and Interventional Radiology, Johann Wolfgang Goethe University of Frankfurt, Frankfurt 60590, Germany

Editorial office
Jin-Lei Wang, Director
Xiu-Xia Song, Vice Director
World Journal of Radiology
Room 903, Building D, Ocean International Center,
No. 62 Dongsihuan Zhonglu, Chaoyang District,
Beijing 100025, China
Telephone: +86-10-85381891
Fax: +86-10-85381893
E-mail: editorialoffice@wjgnet.com
Help Desk: http://www.wjgnet.com/esps/helpdesk.aspx
http://www.wjgnet.com

Publisher
Baishideng Publishing Group Inc
8226 Regency Drive,
Pleasanton, CA 94588, USA
Telephone: +1-925-223-8242
Fax: +1-925-223-8243
E-mail: bpgoffice@wjgnet.com
Help Desk: http://www.wjgnet.com/esps/helpdesk.aspx
http://www.wjgnet.com

Instructions to authors
Full instructions are available online at http://www.wjgnet.com/1948-5204/g_info_20100312180518.htm.

Indexed and Abstracted in
PubMed Central, PubMed, Digital Object Identifier, and Directory of Open Access Journals.

SPECIAL STATEMENT

All articles published in journals owned by the BPG represent the views and opinions of their authors, and not the views, opinions or policies of the BPG, except where otherwise explicitly indicated.

Biostatistical editing
Statisital review is performed after peer review. We invite an expert in Biomedical Statistics to evaluate the statistical method used in the paper, including *t*-test (group or paired comparisons), chi-squared test, Ridit, probit, logit, regression (linear, curvilinear, or stepwise), correlation, analysis of variance, analysis of covariance, *etc*. The reviewing points include: (1) Statistical methods should be described when they are used to verify the results; (2) Whether the statistical techniques are suitable or correct; (3) Only homogeneous data can be averaged. Standard deviations are preferred to standard errors. Give the number of observations and subjects (*n*). Losses in observations, such as drop-outs from the study should be reported; (4) Values such as ED50, LD50, IC50 should have their 95% confidence limits calculated and compared by weighted probit analysis (Bliss and Finney); and (5) The word 'significantly' should be replaced by its synonyms (if it indicates extent) or the *P* value (if it indicates statistical significance).

Conflict-of-interest statement
In the interests of transparency and to help reviewers assess any potential bias, *WJR* requires authors of all papers to declare any competing commercial, personal, political, intellectual, or religious interests in relation to the submitted work. Referees are also asked to indicate any potential conflict they might have reviewing a particular paper. Before submitting, authors are suggested to read "Uniform Requirements for Manuscripts Submitted to Biomedical Journals: Ethical Considerations in the Conduct and Reporting of Research: Conflicts of Interest" from International Committee of Medical Journal Editors (ICMJE), which is available at: http://www.icmje.org/ethical_4conflicts.html.

Sample wording: [Name of individual] has received fees for serving as a speaker, a consultant and an advisory board member for [names of organizations], and has received research funding from [names of organization]. [Name of individual] is an employee of [name of organization]. [Name of individual] owns stocks and shares in [name of organization]. [Name of individual] owns patent [patent identification and brief description].

Statement of informed consent
Manuscripts should contain a statement to the effect that all human studies have been reviewed by the appropriate ethics committee or it should be stated clearly in the text that all persons gave their informed consent prior to their inclusion in the study. Details that might disclose the identity of the subjects under study should be omitted. Authors should also draw attention to the Code of Ethics of the World Medical Association (Declaration of Helsinki, 1964, as revised in 2004).

Statement of human and animal rights
When reporting the results from experiments, authors should follow the highest standards and the trial should conform to Good Clinical Practice (for example, US Food and Drug Administration Good Clinical Practice in FDA-Regulated Clinical Trials; UK Medicines Research Council Guidelines for Good Clinical Practice in Clinical Trials) and/or the World Medical Association Declaration of Helsinki. Generally, we suggest authors follow the lead investigator's national standard. If doubt exists whether the research was conducted in accordance with the above standards, the authors must explain the rationale for their approach and demonstrate that the institutional review body explicitly approved the doubtful aspects of the study.

Before submitting, authors should make their study approved by the relevant research ethics committee or institutional review board. If human participants were involved, manuscripts must be accompanied by a statement that the experiments were undertaken with the understanding and appropriate informed consent of each. Any personal item or information will not be published without explicit consents from the involved patients. If experimental animals were used, the materials and methods (experimental procedures) section must clearly indicate that appropriate measures were taken to minimize pain or discomfort, and details of animal care should be provided.

SUBMISSION OF MANUSCRIPTS

Manuscripts should be typed in 1.5 line spacing and 12 pt. Book Antiqua with ample margins. Number all pages consecutively, and start each of the following sections on a new page: Title Page, Abstract, Introduction, Materials and Methods, Results, Discussion, Acknowledgements, References, Tables, Figures, and Figure Legends. Neither the editors nor the publisher are responsible for the opinions expressed by contributors. Manuscripts formally accepted for publication become the permanent property of Baishideng Publishing Group Co., Limited, and may not be reproduced by any means, in whole or in part, without the written permission of both the authors and the publisher. We reserve the right to copy-edit and put onto our website accepted manuscripts. Authors should follow the relevant guidelines for the care and use of laboratory animals of their institution or national animal welfare committee. For the sake of transparency in regard to the performance and reporting of clinical trials, we endorse the policy of the ICMJE to refuse to publish papers on clinical trial results if the trial was not recorded in a publicly-accessible registry at its outset. The only register now available, to our knowledge, is http://www.clinicaltrials.gov sponsored by the United States National Library of Medicine and we encourage all potential contributors to register with it. However, in the case

that other registers become available you will be duly notified. A letter of recommendation from each author's organization should be provided with the contributed article to ensure the privacy and secrecy of research is protected.

Authors should retain one copy of the text, tables, photographs and illustrations because rejected manuscripts will not be returned to the author(s) and the editors will not be responsible for loss or damage to photographs and illustrations sustained during mailing.

Online submissions

Manuscripts should be submitted through the Online Submission System at: http://www.wjgnet.com/esps/. Authors are highly recommended to consult the ONLINE INSTRUCTIONS TO AUTHORS (http://www.wjgnet.com/1948-5204/g_info_20100312180518.htm) before attempting to submit online. For assistance, authors encountering problems with the Online Submission System may send an email describing the problem to bpgoffice@wjgnet.com, or by telephone: +86-10-85381891. If you submit your manuscript online, do not make a postal contribution. Repeated online submission for the same manuscript is strictly prohibited.

MANUSCRIPT PREPARATION

All contributions should be written in English. All articles must be submitted using word-processing software. All submissions must be typed in 1.5 line spacing and 12 pt. Book Antiqua with ample margins. Style should conform to our house format. Required information for each of the manuscript sections is as follows:

Title page

Title: Title should be less than 12 words.

Running title: A short running title of less than 6 words should be provided.

Authorship: Authorship credit should be in accordance with the standard proposed by International Committee of Medical Journal Editors, based on (1) substantial contributions to conception and design, acquisition of data, or analysis and interpretation of data; (2) drafting the article or revising it critically for important intellectual content; and (3) final approval of the version to be published. Authors should meet conditions 1, 2, and 3.

Institution: Author names should be given first, then the complete name of institution, city, province and postcode. For example, Xu-Chen Zhang, Li-Xin Mei, Department of Pathology, Chengde Medical College, Chengde 067000, Hebei Province, China. One author may be represented from two institutions, for example, George Sgourakis, Department of General, Visceral, and Transplantation Surgery, Essen 45122, Germany; George Sgourakis, 2nd Surgical Department, Korgialenio-Benakio Red Cross Hospital, Athens 15451, Greece

Author contributions: The format of this section should be: Author contributions: Wang CL and Liang L contributed equally to this work; Wang CL, Liang L, Fu JF, Zou CC, Hong F and Wu XM designed the research; Wang CL, Zou CC, Hong F and Wu XM performed the research; Xue JZ and Lu JR contributed new reagents/analytic tools; Wang CL, Liang L and Fu JF analyzed the data; and Wang CL, Liang L and Fu JF wrote the paper.

Supportive foundations: The complete name and number of supportive foundations should be provided, e.g. Supported by National Natural Science Foundation of China, No. 30224801

Correspondence to: Only one corresponding address should be provided. Author names should be given first, then author title, affiliation, the complete name of institution, city, postcode, province, country, and email. All the letters in the email should be in lower case. A space interval should be inserted between country name and email address. For example, Montgomery Bissell, MD, Professor of Medicine, Chief, Liver Center, Gastroenterology Division, University of California, Box 0538, San Francisco, CA 94143, United States. montgomery.bissell@ucsf.edu

Telephone and fax: Telephone and fax should consist of +, country number, district number and telephone or fax number, e.g. Telephone: +86-10-85381891 Fax: +86-10-85381893

Peer reviewers: All articles received are subject to peer review. Normally, three experts are invited for each article. Decision on acceptance is made only when at least two experts recommend publication of an article. All peer-reviewers are acknowledged on Express Submission and Peer-review System website.

Abstract

There are unstructured abstracts (no less than 200 words) and structured abstracts. The specific requirements for structured abstracts are as follows:

An informative, structured abstract should accompany each manuscript. Abstracts of original contributions should be structured into the following sections: AIM (no more than 20 words; Only the purpose of the study should be included. Please write the Aim in the form of "To investigate/study/…"), METHODS (no less than 140 words for Original Articles; and no less than 80 words for Brief Articles), RESULTS (no less than 150 words for Original Articles and no less than 120 words for Brief Articles; You should present *P* values where appropriate and must provide relevant data to illustrate how they were obtained, e.g. 6.92 ± 3.86 *vs* 3.61 ± 1.67, $P < 0.001$), and CONCLUSION (no more than 26 words).

Key words

Please list 5-10 key words, selected mainly from *Index Medicus*, which reflect the content of the study.

Core tip

Please write a summary of less than 100 words to outline the most innovative and important arguments and core contents in your paper to attract readers.

Text

For articles of these sections, original articles and brief articles, the main text should be structured into the following sections: INTRODUCTION, MATERIALS AND METHODS, RESULTS and DISCUSSION, and should include appropriate Figures and Tables. Data should be presented in the main text or in Figures and Tables, but not in both. The main text format of these sections, editorial, topic highlight, case report, letters to the editors, can be found at: http://www.wjgnet.com/1948-5204/g_info_list.htm.

Illustrations

Figures should be numbered as 1, 2, 3, *etc*., and mentioned clearly in the main text. Provide a brief title for each figure on a separate page. Detailed legends should not be provided under the figures. This part should be added into the text where the figures are applicable. Keeping all elements compiled is necessary in line-art image. Scale bars should be used rather than magnification factors, with the length of the bar defined in the legend rather than on the bar itself. File names should identify the figure and panel. Avoid layering type directly over shaded or textured areas. Please use uniform legends for the same subjects. For example: Figure 1 Pathological changes in atrophic gastritis after treatment. A: ...; B: ...; C: ...; D: ...; E: ...; F: ...; G: …*etc*. It is our principle to publish high resolution-figures for the E-versions.

Tables

Three-line tables should be numbered 1, 2, 3, *etc*., and mentioned clearly in the main text. Provide a brief title for each table. Detailed legends should not be included under tables, but rather added into the text where applicable. The information should complement, but not duplicate the text. Use one horizontal line under the title, a second under column heads, and a third below the Table, above any footnotes. Vertical and italic lines should be omitted.

Notes in tables and illustrations

Data that are not statistically significant should not be noted. $^{a}P < 0.05$, $^{b}P < 0.01$ should be noted ($P > 0.05$ should not be noted). If there are other series of P values, $^{c}P < 0.05$ and $^{d}P < 0.01$ are used. A third series of P values can be expressed as $^{e}P < 0.05$ and $^{f}P < 0.01$. Other notes in tables or under illustrations should be expressed as ^{1}F, ^{2}F, ^{3}F; or sometimes as other symbols with a superscript (Arabic numerals) in the upper left corner. In a multi-curve illustration, each curve should be labeled with ●, ○, ■, □, ▲, △, *etc.*, in a certain sequence.

Acknowledgments

Brief acknowledgments of persons who have made genuine contributions to the manuscript and who endorse the data and conclusions should be included. Authors are responsible for obtaining written permission to use any copyrighted text and/or illustrations.

REFERENCES

Coding system

The author should number the references in Arabic numerals according to the citation order in the text. Put reference numbers in square brackets in superscript at the end of citation content or after the cited author's name. For citation content which is part of the narration, the coding number and square brackets should be typeset normally. For example, "Crohn's disease (CD) is associated with increased intestinal permeability[1,2]". If references are cited directly in the text, they should be put together within the text, for example, "From references[19,22-24], we know that..."

When the authors write the references, please ensure that the order in text is the same as in the references section, and also ensure the spelling accuracy of the first author's name. Do not list the same citation twice.

PMID and DOI

Pleased provide PubMed citation numbers to the reference list, e.g. PMID and DOI, which can be found at http://www.ncbi.nlm.nih.gov/sites/entrez?db=pubmed and http://www.crossref.org/SimpleTextQuery/, respectively. The numbers will be used in E-version of this journal.

Style for journal references

Authors: the name of the first author should be typed in bold-faced letters. The family name of all authors should be typed with the initial letter capitalized, followed by their abbreviated first and middle initials. (For example, Lian-Sheng Ma is abbreviated as Ma LS, Bo-Rong Pan as Pan BR). The title of the cited article and italicized journal title (journal title should be in its abbreviated form as shown in PubMed), publication date, volume number (in black), start page, and end page [PMID: 11819634 DOI: 10.3748/wjg.13.5396].

Style for book references

Authors: the name of the first author should be typed in bold-faced letters. The surname of all authors should be typed with the initial letter capitalized, followed by their abbreviated middle and first initials. (For example, Lian-Sheng Ma is abbreviated as Ma LS, Bo-Rong Pan as Pan BR) Book title. Publication number. Publication place: Publication press, Year: start page and end page.

Format

Journals

English journal article (list all authors and include the PMID where applicable)

1 **Jung EM**, Clevert DA, Schreyer AG, Schmitt S, Rennert J, Kubale R, Feuerbach S, Jung F. Evaluation of quantitative contrast harmonic imaging to assess malignancy of liver tumors: A prospective controlled two-center study. *World J Gastroenterol* 2007; **13**: 6356-6364 [PMID: 18081224 DOI: 10.3748/wjg.13.6356]

Chinese journal article (list all authors and include the PMID where applicable)

2 **Lin GZ**, Wang XZ, Wang P, Lin J, Yang FD. Immunologic effect of Jianpi Yishen decoction in treatment of Pixu-diarrhoea. *Shijie Huaren Xiaohua Zazhi* 1999; **7**: 285-287

In press

3 **Tian D**, Araki H, Stahl E, Bergelson J, Kreitman M. Signature of balancing selection in Arabidopsis. *Proc Natl Acad Sci USA* 2006; In press

Organization as author

4 **Diabetes Prevention Program Research Group**. Hypertension, insulin, and proinsulin in participants with impaired glucose tolerance. *Hypertension* 2002; **40**: 679-686 [PMID: 12411462 DOI:10.1161/01.HYP.0000035706.28494.09]

Both personal authors and an organization as author

5 **Vallancien G**, Emberton M, Harving N, van Moorselaar RJ; Alf-One Study Group. Sexual dysfunction in 1, 274 European men suffering from lower urinary tract symptoms. *J Urol* 2003; **169**: 2257-2261 [PMID: 12771764 DOI:10.1097/01.ju.0000067940.76090.73]

No author given

6 21st century heart solution may have a sting in the tail. *BMJ* 2002; **325**: 184 [PMID: 12142303 DOI:10.1136/bmj.325.7357.184]

Volume with supplement

7 **Geraud G**, Spierings EL, Keywood C. Tolerability and safety of frovatriptan with short- and long-term use for treatment of migraine and in comparison with sumatriptan. *Headache* 2002; **42** Suppl 2: S93-99 [PMID: 12028325 DOI:10.1046/j.1526-4610.42.s2.7.x]

Issue with no volume

8 **Banit DM**, Kaufer H, Hartford JM. Intraoperative frozen section analysis in revision total joint arthroplasty. *Clin Orthop Relat Res* 2002; (**401**): 230-238 [PMID: 12151900 DOI:10.1097/00003086-200208000-00026]

No volume or issue

9 Outreach: Bringing HIV-positive individuals into care. *HRSA Careaction* 2002; 1-6 [PMID: 12154804]

Books

Personal author(s)

10 **Sherlock S**, Dooley J. Diseases of the liver and billiary system. 9th ed. Oxford: Blackwell Sci Pub, 1993: 258-296

Chapter in a book (list all authors)

11 **Lam SK**. Academic investigator's perspectives of medical treatment for peptic ulcer. In: Swabb EA, Azabo S. Ulcer disease: investigation and basis for therapy. New York: Marcel Dekker, 1991: 431-450

Author(s) and editor(s)

12 **Breedlove GK**, Schorfheide AM. Adolescent pregnancy. 2nd ed. Wieczorek RR, editor. White Plains (NY): March of Dimes Education Services, 2001: 20-34

Conference proceedings

13 **Harnden P**, Joffe JK, Jones WG, editors. Germ cell tumours V. Proceedings of the 5th Germ cell tumours Conference; 2001 Sep 13-15; Leeds, UK. New York: Springer, 2002: 30-56

Conference paper

14 **Christensen S**, Oppacher F. An analysis of Koza's computational effort statistic for genetic programming. In: Foster JA, Lutton E, Miller J, Ryan C, Tettamanzi AG, editors. Genetic programming. EuroGP 2002: Proceedings of the 5th European Conference on Genetic Programming; 2002 Apr 3-5; Kinsdale, Ireland. Berlin: Springer, 2002: 182-191

Electronic journal (list all authors)

15 Morse SS. Factors in the emergence of infectious diseases. Emerg Infect Dis serial online, 1995-01-03, cited 1996-06-05; 1(1): 24 screens. Available from: URL: http://www.cdc.gov/ncidod/eid/index.htm

Patent (list all authors)

16 **Pagedas AC**, inventor; Ancel Surgical R&D Inc., assignee. Flexible endoscopic grasping and cutting device and positioning tool assembly. United States patent US 20020103498. 2002 Aug 1

Statistical data
Write as mean ± SD or mean ± SE.

Statistical expression
Express *t* test as *t* (in italics), *F* test as *F* (in italics), chi square test as χ^2 (in Greek), related coefficient as *r* (in italics), degree of freedom as υ (in Greek), sample number as *n* (in italics), and probability as *P* (in italics).

Units
Use SI units. For example: body mass, m (B) = 78 kg; blood pressure, p (B) = 16.2/12.3 kPa; incubation time, t (incubation) = 96 h, blood glucose concentration, c (glucose) 6.4 ± 2.1 mmol/L; blood CEA mass concentration, p (CEA) = 8.6 24.5 μg/L; CO_2 volume fraction, 50 mL/L CO_2, not 5% CO_2; likewise for 40 g/L formaldehyde, not 10% formalin; and mass fraction, 8 ng/g, *etc*. Arabic numerals such as 23, 243, 641 should be read 23243641.

The format for how to accurately write common units and quantums can be found at: http://www.wjgnet.com/1948-5204/g_info_20100312183048.htm.

Abbreviations
Standard abbreviations should be defined in the abstract and on first mention in the text. In general, terms should not be abbreviated unless they are used repeatedly and the abbreviation is helpful to the reader. Permissible abbreviations are listed in Units, Symbols and Abbreviations: A Guide for Biological and Medical Editors and Authors (Ed. Baron DN, 1988) published by The Royal Society of Medicine, London. Certain commonly used abbreviations, such as DNA, RNA, HIV, LD50, PCR, HBV, ECG, WBC, RBC, CT, ESR, CSF, IgG, ELISA, PBS, ATP, EDTA, mAb, can be used directly without further explanation.

Italics
Quantities: *t* time or temperature, *c* concentration, *A* area, *l* length, *m* mass, *V* volume.
Genotypes: *gyrA*, *arg* 1, *c myc*, *c fos*, *etc*.
Restriction enzymes: *Eco*RI, *Hin*dI, *Bam*HI, *Kbo* I, *Kpn* I, *etc*.
Biology: *H. pylori*, *E coli*, *etc*.

Examples for paper writing
All types of articles' writing style and requirement will be found in the link: http://www.wjgnet.com/esps/NavigationInfo.aspx?id=15

SUBMISSION OF THE REVISED MANUSCRIPTS AFTER ACCEPTED

Authors must revise their manuscript carefully according to the revision policies of Baishideng Publishing Group Co., Limited. The revised version, along with the signed copyright transfer agreement, responses to the reviewers, and English language Grade B certificate (for non-native speakers of English), should be submitted to the online system via the link contained in the e-mail sent by the editor. If you have any questions about the revision, please send e-mail to esps@wjgnet.com.

Language evaluation
The language of a manuscript will be graded before it is sent for revision. (1) Grade A: priority publishing; (2) Grade B: minor language polishing; (3) Grade C: a great deal of language polishing needed; and (4) Grade D: rejected. Revised articles should reach Grade A or B.

Copyright assignment form
Please download a Copyright assignment form from http://www.wjgnet.com/1948-5204/g_info_20100312182928.htm.

Responses to reviewers
Please revise your article according to the comments/suggestions provided by the reviewers. The format for responses to the reviewers' comments can be found at: http://www.wjgnet.com/1948-5204/g_info_20100312182841.htm.

Proof of financial support
For papers supported by a foundation, authors should provide a copy of the approval document and serial number of the foundation.

STATEMENT ABOUT ANONYMOUS PUBLICATION OF THE PEER REVIEWERS' COMMENTS

In order to increase the quality of peer review, push authors to carefully revise their manuscripts based on the peer reviewers' comments, and promote academic interactions among peer reviewers, authors and readers, we decide to anonymously publish the reviewers' comments and author's responses at the same time the manuscript is published online.

PUBLICATION FEE

WJR is an international, peer-reviewed, OA online journal. Articles published by this journal are distributed under the terms of the Creative Commons Attribution Non-commercial License, which permits use, distribution, and reproduction in any medium and format, provided the original work is properly cited. The use is non-commercial and is otherwise in compliance with the license. Authors of accepted articles must pay a publication fee. Publication fee: 698 USD per article. All invited articles are published free of charge.

Published by **Baishideng Publishing Group Inc**
8226 Regency Drive, Pleasanton, CA 94588, USA
Telephone: +1-925-223-8242
Fax: +1-925-223-8243
E-mail: bpgoffice@wjgnet.com
Help Desk: http://www.wjgnet.com/esps/helpdesk.aspx
http://www.wjgnet.com

© 2014 Baishideng Publishing Group Inc. All rights reserved.